



UiT The Arctic University of Norway

Faculty of Science and Technology

Exploring the Potential of CO₂: Enantioselective C-C Bond Formation

An experimental study on enantioselective Rh- and Cu-catalyzed carboxylation reactions using carbon dioxide.

Martin Pettersen

A dissertation for the degree of Philosophiae Doctor

January 2024



Acknowledgements

With the PhD finished, I would finally like to say that this journey has been an experience and, up to now, the best time of my life. I have developed myself a lot as a person, made many new friends and experienced memories that I will remember for the rest of my life. Now it is time for me to finally leave the nest and start my life.

First and foremost, I would like to express my gratitude to my main PhD supervisor prof. Annette Bayer for presenting me with the opportunity to work under her supervision. I am very thankful for the professional guidance she provided throughout this journey. Always making time for me, even with the busy time schedule as the institute leader. I am grateful for the professional guidance she provided me throughout this journey, both practical and with scientific writing. I am also grateful for the opportunity she presented me to be a part of the NordCO₂ network, further expanding my research knowledge and connections. I would also like to thank my co-supervisor Ashot Gevorgyan for the supervision provided, both practical and with scientific writing. I would also like to thank him for all the conversations in the lab and always being available for both supervision and just a chat if needed.

A special thanks goes to my friends Aleksii Kosonen, Bente Barge, Harald Magnussen, Magnus Burkow and Unni Mette Nordang for all the social activities and for cheering me on, hope we can stay connected for many years forward. Additionally, I would also like to thank all my friends from TSI PLASK for the trainings and social activities hosted throughout my PhD period.

I would like to thank my friends at the chemistry department Cuong Dat Do, Ryan Wilkins, Sahil Gahlawat, Gabriel Gerez, Tonje Reinholdt Haugen, Karoline Nordli, Krister Engedal Johannessen, Marc Joosten and Quentin Pitteloud. The time we spent engaging in social activities outside of work was a lot of fun and at the same time contributed to making the workspace a more social and engaging environment. I will cherish these memories forever.

I would also like to thank all my lab mates throughout the years, Roman Damm, Danielle van der Westhuizen, Lúcia Gonçalves Gameiro and Raju Yalla for all the enjoyable conversations and for making the lab space a more social and overall fun experience.

I also would like to thank Manuel Langer for all the help and guidance with the SFC. The department engineers, Truls Eirik Ingebriksen and Jostein Johansen, who maintains our equipment and make the work we do easier. I also want to thank Annette Bayer, Ashot Gevorgyan, Roman Damm, Anggi E. Putra, Kathrin H. Hopmann, Ljiljana Pavlovic, Cuong Dat Do, Marc F. Obst, and Janakiram Vaitla for collaborating on the work presented in this

thesis. Additionally, I would like to thank entirety of the CHOCO group for all the meetings, ideas and good feedback to my research.

Lastly, I want to thank my family, especially my mother Randi Lisbeth Larsen, brother Torkild Pettersen, and stepfather Pål Wabnig for all the support throughout the years of my PhD. A special thanks also goes to my aunt Solveig Larsen Klevstad for taking the time to come and support me for my PhD defense.

Abstract

CO₂ is a renewable source of carbon that has not yet been properly utilized. The reason for this is mostly due to its kinetic and thermodynamic stability. The potential renewability of CO₂, coupled with environmental concerns, has motivated scientists worldwide to develop new artificial carbon cycles for chemical fixation of CO₂. Unfortunately, the pronounced inertness of CO₂ allows only the synthesis of a range of C₁ molecules, often with poor selectivity. These limitations also make enantioselective *carbon-carbon* (C-C) bond-forming utilizing *carbon dioxide* (CO₂) difficult to achieve. Therefore, there has been relatively few examples of enantioselective C-C bondforming reactions reported in the literature.

The primary objective of my work is to develop enantioselective C-C bond-forming reactions using CO₂, with a particular focus on metal-catalyzed enantioselective incorporation of CO₂.

The first catalytic enantioselective hydrocarboxylation was reported in 2016 by Mikami and colleagues. We became interested in the mechanistic details of this transformation and set out to provide computational and experimental insights, on the transformation.

The enantioselective boracarboxylation has not yet been explored and is an interesting transformation to produce novel drug precursors. With an interest in enantioselective carboxylations, our group set out to develop an enantioselective method for boracarboxylation of styrenes.

As of writing this thesis, the boracarboxylation is currently restricted to alkynes and styrenes. We therefore aimed to expand the applicability of the boracarboxylation to allenes. With the boracarboxylation being similar to hydroboration, we started our study optimizing from known to work hydroboration conditions with CO₂ instead of a proton source.

List of Publications

Paper I. Computational and experimental insights into asymmetric Rh-catalyzed hydrocarboxylation with CO₂

Eur. J. Org. Chem., **2021**, 4, 663-670, DOI: <http://doi.org/10.1002/ejoc.202001469>

Ljiljana Pavlovic, **Martin Pettersen**, Ashot Gevorgyan, Janakiram Vaitla, Annette Bayer and Kathrin H. Hopmann

Paper II. Asymmetric boracarboxylation of styrenes using carbon dioxide

(manuscript under revision)

Martin Pettersen, Cuong Dat Do, Marc Ferry Obst, Roman Damm, Anggi Eka Putra, Ashot Gevorgyan, Ljiljana Pavlovic, Kathrin H. Hopmann and Annette Bayer

Summary of papers and Author contributions

Paper I – Computational and experimental insights into asymmetric Rh-catalyzed hydrocarboxylation with CO₂

Eur. J. Org. Chem., **2021**, issue 4, 663 – 670.

Ljiljana Pavlovic, **Martin Pettersen**, Ashot Gevorgyan, Janakiram Vaitla, Annette Bayer and Kathrin H. Hopmann

Paper Summary

In paper I we performed both an experimentally and computationally study on how different chiral bidentate ligands perform in the enantioselective Rh-catalyzed hydrocarboxylation of acrylates.

My Contribution:

I synthesized all substrates and Rh-complexes used in this study, I also carried out all the carboxylation reactions, measurements of e.e. values and the collection of other spectral data. I contributed to the writing of the experimental notes and parts of the manuscript. I did not carry out the computational part of this study.

Paper II – Asymmetric boracarboxylation of styrenes using carbon dioxide

Manuscript under revision

Martin Pettersen, Cuong D. Do, Marc F. Obst, Roman Damm, Ashot Gevorgyan, Ljiljana Pavlovic, Kathrin H. Hopmann and Annette Bayer.

Paper Summary

In paper II we developed an enantioselective method for boracarboxylation of styrene's and tried to explain the selectivity of the reaction for (S,S)-BDPP and (S,S)-QuinoxP* computationally.

My Contribution:

I planned and carried out the optimization of the reaction conditions, synthesis of chiral products and most racemates. I also developed the methods for resolution for SFC measuring equipped with a chiral column to determine the enantiomeric ratio (e.r.) and collection of other data (NMR, HRMS and Optical rotation). I supervised a bachelor student who carried out the

synthesis of selected racemic boracarboxylation products from styrenes. I have written the experimental part of the manuscript, the experimental supporting information and processing of spectral data for use in the SI. I did not do the computational work of this study.

Table of Contents

Acknowledgements	i
Abstract	iii
List of Publications.....	v
Summary of papers and Author contributions.....	vii
Paper I – Computational and experimental insights into asymmetric Rh-catalyzed hydrocarboxylation with CO ₂	vii
Paper II – Asymmetric boracarboxylation of styrenes using carbon dioxide.....	vii
Table of Contents	ix
Abbreviations	xi
1 Introduction	1
1.1 CO ₂ as a source of carbon	1
1.2 Focus and aims of the thesis.....	5
2 Background.....	7
2.1 CO ₂ -converting reactions.	7
2.1.1 Examples of relevant 1,2-addition reactions incorporating CO ₂	9
2.1.2 Examples of other relevant carboxylation reactions.....	20
2.1.3 Enantioselective C-C bond-forming reactions with CO ₂ and related transformations..	22
3 Results and Discussion	37
3.1 Rh-catalyzed enantioselective hydrocarboxylation (Paper I).....	37
3.1.1 Introduction	37
3.1.2 Results and discussion.....	37
3.1.3 Conclusion paper I.....	39
3.2 Enantioselective Boracarboxylation (Paper II)	40
3.2.1 Introduction	40
3.2.2 Optimization of reaction conditions	40
3.2.3 Substrate scope	43
3.2.4 Additional results not included in paper II.	46
3.2.5 Conclusion paper II	47
3.3 Preliminary results on boracarboxylation of allenes	48
3.3.1 Introduction	48
3.3.2 Initial determination of reaction conditions.....	48
3.3.3 First optimization attempt for the boracarboxylation of allenes.....	49
3.3.4 Second optimization attempt for boracarboxylation of allenes.	51

3.3.5	Conclusion for boracarboxylation of allenes.....	54
4	Conclusion and Outlook	57
5	Experimental Details	59
5.1	General methods.....	59
5.2	General procedures.....	60
5.2.1	General procedure for the synthesis of QuinoxPCy ₄	60
5.2.2	General procedure A for the synthesis of 1,1-dibromocyclopropanes	61
5.2.3	General procedure B for the synthesis of allenes	62
5.2.4	General procedure C for boracarboxylation of allenes.....	64
6	References	67
7	Appendix	87
7.1	NMR Spectra.....	87

Abbreviations

Abbreviation	Meaning
(3 <i>S</i> ,3' <i>S</i>)-BABIBOP	(3 <i>S</i> ,3' <i>S</i>)-3,3'-di-tert-butyl-2,2',3,3'-tetrahydro-4,4'-bibenzo[d][1,3]oxaphosphole
(<i>R</i>)-BINAP	(<i>R</i>)-2,2'-bis(diphenylphosphaneyl)-1,1'-binaphthalene
(<i>R</i>)-DTBM-SEGPPOS	(<i>R</i>)-(-)-5,5'-Bis[di(3,5-di-tert-butyl-4-methoxyphenyl)phosphino]-4,4'-bi-1,3-benzodioxole,[(4 <i>R</i>)-(4,4'-bi-1,3-benzodioxole)-5,5'-diyl]bis[bis(3,5-di-tert-butyl-4-methoxyphenyl)phosphine]
(<i>R</i>)-Walphos	(<i>R</i>)-(+)-1-[(<i>R</i>)-2-(2'-Dicyclohexylphosphinophenyl)ferrocenyl]ethylbis(3,5-trifluoromethylphenyl)phosphine
(<i>R,R</i>)-BenzP*	1,2-bis((<i>R</i>)-tert-butyl(methyl)phosphaneyl)benzene
(<i>R,R,R,R</i>)-BIBOP	(<i>R,R,R,R</i>)-BIBOP(2 <i>R</i> ,2' <i>R</i> ,3 <i>R</i> ,3' <i>R</i>)-3,3'-di-tert-butyl-2,2',3,3'-tetrahydro-2,2'-bibenzo[d][1,3]oxaphosphole
(<i>S</i>)-SEGPPOS	(<i>S</i>)-(-)-5,5'-Bis(diphenylphosphino)-4,4'-bi-1,3-benzodioxole
(<i>S,S</i>)-BDPP	(2 <i>S</i> ,4 <i>S</i>)-2,4-Bis(diphenylphosphino)pentane
(<i>S,S</i>)-Box- <i>i</i> Pr	(4 <i>S</i> ,4' <i>S</i>)-2,2'-(propane-2,2'-diyl)bis(4-isopropyl-4,5-dihydrooxazole)
(<i>S,S</i>)-Ph-BPE	(+)-1,2-Bis((2 <i>S</i> ,5 <i>S</i>)-2,5-diphenylphospholano)ethane
(<i>S,S</i>)-QuinoxP*	(<i>S,S</i>)-2,3-Bis(tert-butylmethylphosphino)quinoxaline
(<i>S,S</i>)- <i>t</i> Bu-BOX	(<i>S,S</i>)-2,2'-isopropylidenebis(4-tert-butyl-2-oxazoline)
(<i>S_{Fc}</i> , <i>R_C</i>)-Mandyphos	(<i>S,S</i>)-(-)-2,2'-Bis[(<i>R</i>)-(N,N-dimethylamino)(phenyl)methyl]-1,1'-bis(di(3,5dimethylphenyl)phosphino)ferrocene
18-Crown-6	1,4,7,10,13,16-Hexaoxacyclooctadecane
2-MeTHF	2-Methyltetrahydrofuran
4CzBnBN	3-benzyl-2,4,5,6-tetra(9H-carbazol-9-yl)benzotrile
4CzIPN	1,2,3,5-Tetrakis(carbazol-9-yl)-4,6-dicyanobenzene
9-BBN	9-Borabicyclo(3.3.1)nonane
ADP	Adenosine diphosphate
ATP	Adenosine triphosphate
B ₂ pin ₂	Bis(pinacolato)diboron
BI(OH)H	2-(1,3-dimethyl-2,3-dihydro-1H-benzo[d]imidazol-2-yl)phenol
BINAP	(2,2'-bis(diphenylphosphino)-1,1'-binaphthyl)
Boc	Tert-butyloxycarbonyl
BOX	Bis(oxazoline)

CCS	Carbon capture and storage
CCU	Carbon capture and utilization
cod	1,5-Cyclooctadiene
CRI	Carbon Recycling international
CTC	Charge transfer complex
Cy	Cyclohexyl
DCM	Dichloromethane
dcpe	1,2-Bis(dicyclohexylphosphino)ethane
DFT	Density Functional Theory
DIBAL-H	Diisobutylaluminium hydride
DiPAMP	(Ethane-1,2-diyl)bis[(2-methoxyphenyl)(phenyl)phosphane]
DMA	Dimethylacetamide
DME	Dimethoxyethane
DMF	Dimethylformamide
DMF-TBABF ₄	Dimethylformamide tetrabutylammonium tetrafluoroborate
dppbz	1,2-Bis(diphenylphosphino)benzene
dppe	1,2-Bis(diphenylphosphino)ethane
dppp	1,3-Bis(diphenylphosphino)propane
dtbpf	1,1'-Bis(di-tert-butylphosphino)ferrocene
<i>e.e.</i>	Enantiomeric excess
<i>e.r.</i>	Enantiomeric ratio
ESI	Electron spray ionization
HRMS	Mass Spectrometry
ICy HCl	1,3-Dicyclohexylimidazolium chloride
IMes HCl	1,3-Bis(2,4,6-trimethylphenyl)imidazolium chloride
IPr HCl	<i>N,N'</i> -Bis(2,6-bis(diphenylmethyl)-4-methylphenyl)imidazolium chloride
IR	Infrared
LED	Light emitting diode
LSF-x	La _{1-x} Sr _x FeO ₃
MOF	Metal organic framework
n.d.	Not determined
NADPH	Nicotinamide Adenine Dinucleotide Phosphate Hydrogen

NHC	N-heterocyclic carbene
NMR	Nuclear Magnetic Resonance
PE	Polyethylene
PEC	Polyethylene carbonate
PMP reductant	1,2,2,6,6-pentamethylpiperidine
PPC	Polypropylene carbonate
PU	Polyurethane
QuinoxPCy ₄	2,3-bis(dicyclohexylphosphaneyl)quinoxaline
SFC	Supercritical fluid chromatography
SIMes BF ₄	1,3-Bis(2,4,6-trimethylphenyl)imidazolium tetrafluoroborate
SIMes HCl	1,3-Bis(2,4,6-trimethylphenyl)imidazolium chloride
SIPr BF ₄	1,3-Bis(2,6-diisopropylphenyl)imidazolium tetrafluoroborate
SIPr HCl	1,3-Bis(2,6-diisopropylphenyl)imidazolium chloride
TBAB	Tetrabutylammonium bromide
TBAI	Tetrabutylammonium iodine
<i>t</i> -Bu-Xantphos	9,9-Dimethyl-4,5-bis(di- <i>tert</i> -butylphosphino)xanthene
TEA	Triethylamide
TEMPO	(2,2,6,6-tetramethylpiperidin-1-yl)oxidanyl
TFE	Tetrafluoroethylene
THF	Tetrahydrofuran
TLC	Thin layer chromatography
TMS	Trimethylsilyl
XantPhos	4,5-Bis(diphenylphosphino)-9,9-dimethylxanthene
Xphos	2-Dicyclohexylphosphino-2',4',6'-triisopropylbiphenyl

1 Introduction

1.1 CO₂ as a source of carbon

Carbon dioxide (CO₂), an often overlooked and undervalued source of carbon that is primarily considered a waste product from natural, and human made processes, such as respiration, agriculture and the burning of fossil fuels. For many CO₂ is known as the reason behind fizzy soft drinks or as dry ice for transporting perishable goods. While for chemists, CO₂ is seen as a promising future carbon source to produce a vast array of chemicals needed in today's society.

Over the last few decades, CO₂ has gained a lot of attention in the scientific community and the public. This traction is mainly caused by the rapidly increasing emissions prompted by the growing consumption of fossil fuels every year.^[1] It is estimated that about 37Gt of CO₂ is emitted from human activity each year and plants and phytoplankton contribute to the removal of about 30% via photosynthesis (See **Figure 1**) leaving a net surplus.^[2,3] The average concentration of CO₂ in the atmosphere as of 2023 is roughly 420 ppm and is growing with approximately 2.4 ppm every year.^[4] However, given the ever increasing supply of CO₂ it still remains mostly underutilized.

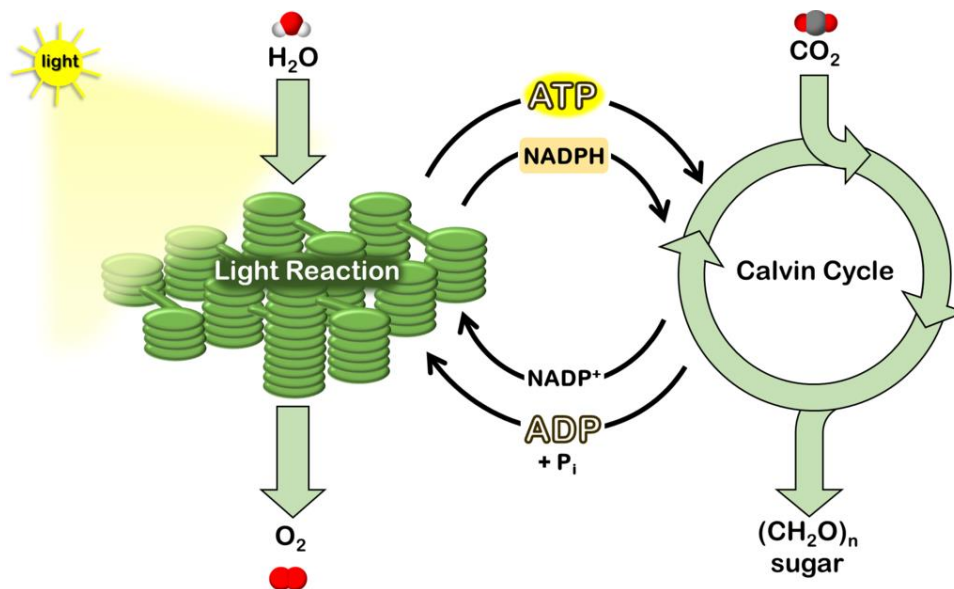


Figure 1: Picture of photosynthesis taken from Wikimedia Commons.^[5]

As of writing, newer technologies for handling CO₂ such as *Carbon Capture and Storage* (CCS) and *Carbon Capture and Utilization* (CCU) are being widely discussed and developed.^[6] CCS involves the capture of CO₂ emissions and storing them underground. While promising and scale able, it is prone to leaks which requires constant surveillance and is an energy heavy

solution.^[6-9] CCU is the more feasible of the two, it involves using CO₂ to generate useful higher value products.^[10,11] While CCU shows promise, currently, it cannot transform enough CO₂ alone to fully mitigate the effects of climate change and the available technologies for CO₂ conversion is limited.^[10,12] As of now, few well-established processes such as the production of methanol, urea and carbonates have been industrially developed and commercialized.^[13] However, these processes only make up about 1% of the available CO₂ on the planet and only account for a handful of the chemicals that are needed in today's society.^[14]

Given the untapped potential of CO₂ as a carbon feedstock, it does not come without its own set of challenges. As of now, even when considering the endless potential of CO₂ as our new future carbon source, the field of CO₂ conversion remains underdeveloped. The lack of CO₂-converting reactions is mainly due to its chemical inertness and thermodynamic stability, which in return makes the energy cost of CO₂ conversion high.^[15] Additionally, the requirement for a new CO₂-converting catalyst to be efficient and selective while also minimizing unwanted waste products makes the development of new catalysts challenging.^[16-19] As of now, methods for both capture, storage, and transport of CO₂, and scalability of industrial methods, are at the moment too expensive to be widely applied in industry.^[20] Furthermore, CO₂-converting technologies also needs to be either built or properly incorporated into the existing infrastructure before being widely applied in industry.^[21] Even though the abundance of available CO₂ in the atmosphere is high, the concentration compared to the other atmospheric gasses is low.^[22] In return, the low concentration of CO₂ in the atmosphere could also make capture and extraction less efficient.^[23]

With these challenges in mind, the question arises: why should we invest in CO₂ conversion in addition to CO₂ storage? While natural gas and fossil fuel are already deeply integrated into our infrastructure and provide a significant portion of the world's supply of carbon-based chemicals, they are finite and will eventually be depleted.^[24] The steadily decreasing fossil fuels reservoirs have made scientists look towards CO₂ as a potential candidate to replace traditional fossil sources. Compared to fossil fuels, CO₂ has a unique advantage and does not face the same depletion issue, since all chemicals being derived from CO₂ will eventually be converted back, effectively creating an artificial carbon cycle.^[24,25] Expanding from artificial carbon cycles, renewable energy sources like solar and wind power can efficiently convert CO₂ into high-energy fuels, providing a promising energy storage solution.^[26] In addition, the sheer abundance of CO₂ could also make it a cheap and valuable precursor for the production of fuels, polymers,

bulk chemicals and finer chemicals such as pharmaceuticals.^[27] Furthermore, as new CO₂ conversion methods are developed and optimized, there is the potential to show a significant impact on both the polymer and pharmaceutical industry.^[28,29] From a long term sustainable perspective, investing in CO₂ conversion could also help mitigate today's environmental challenges, while being more resource efficient and also meeting industrial needs for an efficient CO₂ conversion method.^[30] Therefore, the need for new efficient and selective catalysts for CO₂ conversion is essential in order to bring down the high energy cost.

While some efforts have been made towards the development of new C-C bond-forming reactions utilizing CO₂, progress towards an efficient CO₂-converting reaction remains limited.^[31] This challenge is particularly pronounced in relation to bulk chemical production. While bulk chemicals that do not require C-C bond formation from CO₂, such as *methanol* (CH₃OH), *methane* (CH₄), and *formic acid* (HCOOH) has seen emerging implementation in industry. Other chemicals that do require C-C bond formation (benzoic acid, ethanol, ethylene, polymers, etc.) that can be derived from CO₂ are still in the very early research stages.

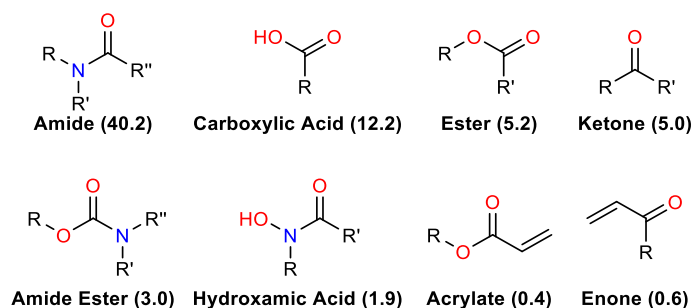


Figure 2: Examples of functional groups in pharmaceuticals that can be derived from CO₂ and their abundance (%) in pharmaceuticals.^[32]

Furthermore, the majority of research dedicated to the conversion of CO₂ into fine chemicals has centered around transition metal catalyzed C-C bond formation.^[33-35] The emphasis on C-C bond formation is particularly relevant because many of the functional groups that can be derived from CO₂ are commonly found in pharmaceutical drugs (See **Figure 2**), making up an abundance of approximately 68% of functional groups in all pharmaceuticals.^[32] This alone could make CO₂ a very important precursor in medicinal chemistry for the preparation of commercial drugs. Functional groups such as carboxylic acids,^[33] esters,^[36] and acrylates,^[37] can be prepared in one-step reactions, while amides,^[38] ketones,^[39] enones,^[40] amide esters,^[41] and hydroxamic acids,^[42] with follow-up transformations. For instance, drugs such as naproxen,

ibuprofen and fenoprofen (See **Figure 3**) all can be synthesized from CO₂ via a carboxylation reaction.^[43] These drugs are also unique in the sense that the carboxylation of their precursors generates a stereocenter at the carbon bound to the carboxyl group. The generated stereocenter results in two stereoisomers of the drug, each with different activity profiles. When entering the patient, the two conformers of the drug interact differently with the chiral environment of the body, potentially resulting in effects ranging from none to devastating for the patient.^[44] Naproxen, for example has two mirror images; the (*R*) conformer has a sedative effect, while the (*S*) is toxic to the liver.^[45] Therefore, for CO₂ to become a viable carbon source for the production of everyday pharmaceuticals an enantioselective conversion method must be developed. As of writing this thesis, the field of enantioselective carboxylations using CO₂ remains challenging and only a limited amount of successful chiral carboxylations utilizing CO₂ has been reported. The reasons for so few chiral reactions are mainly due to the high stability of CO₂, resulting in a restricted amount of reaction partners, highly reactive/unstable metalorganic catalysts are needed. Additionally, the harsh conditions required in order to transform CO₂, which in return makes low selectivity expected.^[46]

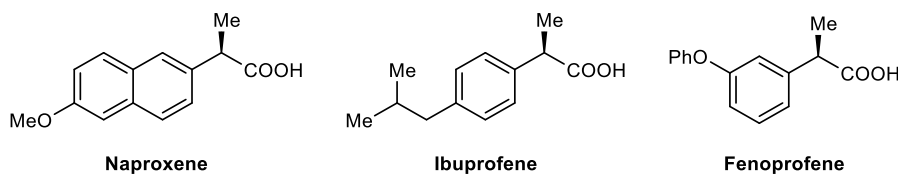


Figure 3: Structures of the chiral pharmaceuticals naproxene, ibuprofen and fenoprofen that can be derived from CO₂.

1.2 Focus and aims of the thesis.

The overarching aim of this thesis work was to contribute to the development of metal-catalyzed enantioselective carboxylation reactions using CO₂ for C-C bond formation. The aim was two parted with focus both on developing new methodology, but also on gaining increased understanding of mechanistic aspects of CO₂-converting catalytic systems.

To address these aims, we focused on three sub-goals:

1. to provide experimental support to computational mechanistic studies of the Rh-catalyzed hydrocarboxylation of acrylates (**paper I**, chapter **3.1**).
2. to develop an enantioselective Cu-catalyzed boracarboxylation of styrenes starting from a previously described non-enantioselective method (**paper II**, chapter **3.2**).
3. to extend the scope of the boracarboxylation from styrenes to allenes with the potential to develop an enantioselective method for boracarboxylation of allenes (chapter **3.3**).

2 Background

2.1 CO₂-converting reactions.

While CO₂-converting reactions remain a subject of ongoing research, certain processes have already found successful applications in industry (See **Figure 4**).^[47] One type of CO₂ converting reaction is the reduction of CO₂ to products such as methanol or methane.^[21] These processes typically use H₂ as a reductant and are facilitated by metal-based catalysts such as Ni, Ru and Rh.^[48-53] For instance, the methanol synthesis was commercialized in 2012 by *Carbon Recycling International* (CRI) in Iceland. CRI converts approximately 5600 tons of CO₂ yearly into methanol using hydrogen gas produced from geothermal energy.^[21] Electrochemical reduction of CO₂ can produce carbon monoxide,^[54] which is used for isolation of nickel in the metallurgy industry,^[55] or as a starting material in the Fischer-Tropsch process to produce hydrocarbon fuels.^[48,56-58] The electrochemical reduction of CO₂ to ethylene has been reported using heterogeneous Fe or CuAg containing catalysts.^[31,59,60] As of now, we have CO₂-based sustainable alternatives for most oil-based industrial processes. The main limitation preventing us from fully transitioning to CO₂-based industrial processes is that the technologies, including CO₂, are still more energy demanding than oil-based processes.^[61]

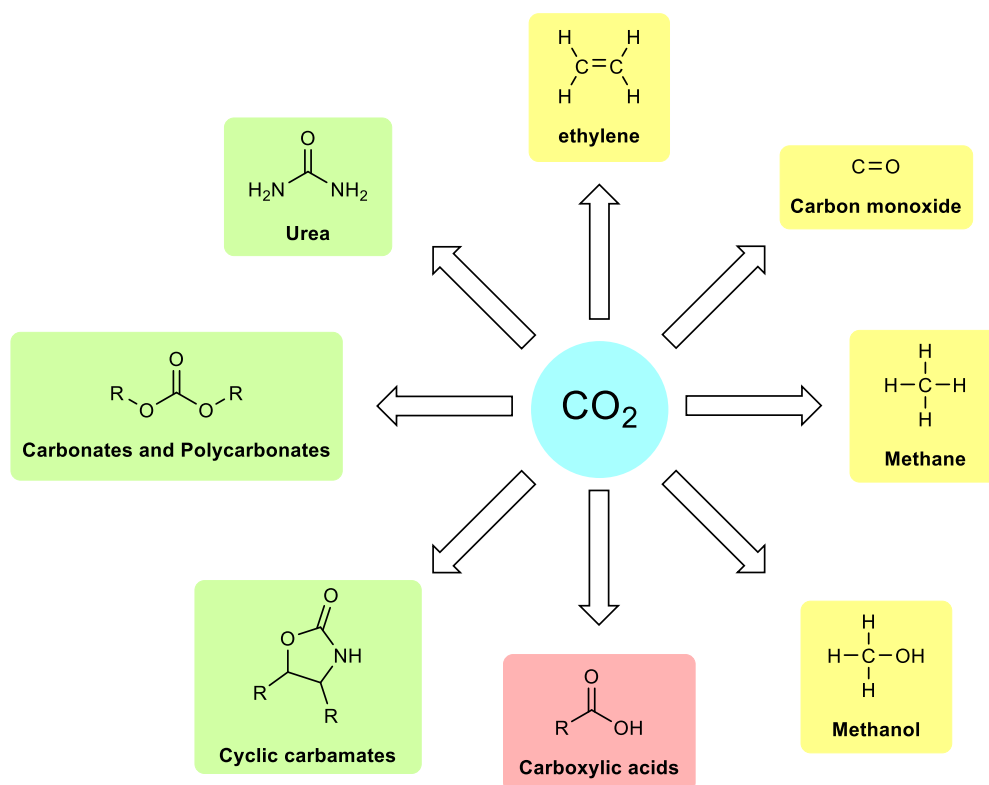
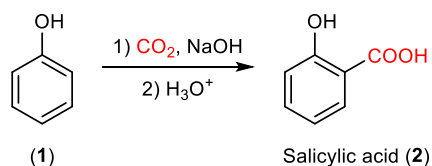


Figure 4: Selected basic transformations including CO₂, CO₂ reductions (yellow), addition of N/O-nucleophiles to CO₂ (green), C-C bond forming products from CO₂ (red).^[62]

Another group of CO₂ converting reactions are based on the reactivity of CO₂ with N/O-nucleophiles (See **Figure 4**, green). Typically used nucleophiles are amino alcohols, amines, epoxides, and alcohols.^[63] In the fertilizer industry, CO₂ reacts with ammonia to produce urea via the Bazarov reaction.^[54,55] This reaction converts CO₂ and ammonia to ammonium carbamate, followed by dehydration to urea.^[64,65] Currently, more than 90% of urea produced from the Bazarov reaction is used as fertilizer.^[30,66] Moreover, CO₂ can be used to produce important industrial polymer precursors, such as polycarbonates and polycarbamates.^[30,67,68] For example, the industrialized Asahi-Kasei process utilizes ethylene oxide and CO₂, for the production of polycarbonate (PC).^[69] CO₂ easily combines with amines to form the corresponding carbamic acid. However, when introducing alcohols to perform a subsequent dehydrative hydrogenation, the carbamate production is limited.^[70] Few reports on the direct conversion of CO₂, amines and alcohols to carbamates exist. The two known catalytic systems utilizes a homogeneous Sn or a Ni catalyst and are performed under high pressures.^[71,72] To the best of my knowledge, there are no commercial processes that utilize CO₂ for carbamates production. However, few relevant catalytic transformations are close to being industrialized.^[31]

The third group of reactions are C-C bond-forming reactions using CO₂ as C₁-synthon. Typical products are carboxylic acids, which have a wide range of applications such as food additives, cosmetics, pharmaceuticals, and polymers.^[73] The estimated market value of carboxylic acids is likely to reach 16 billion euros by 2024.^[74] To my knowledge, the only industrialized C-C bond-forming reaction including CO₂ to carboxylic acids is the Kolbe-Schmitt reaction (See **Scheme 1**), which produces salicylic acid (**2**), a precursor for aspirin.^[75]



Scheme 1: Reaction scheme for the the Kolbe-Schmitt reaction.^[75]

Recent methods for C-C bond formation using CO₂ are based on transition metal catalysis, photocatalysis, and electrochemical processes.^[76] Known transformations using metal catalyzed systems involve numerous different transition metals, such as Ni, Rh, Ir, Ti, Ru, Co, Fe, Zr, Cu, Pd, Au and Rh.^[77-79] These transformations include addition reactions, which CO₂ and another substituent is incorporated into a double bond.^[80] C-H carboxylations, that involve

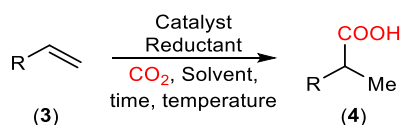
the direct functionalization of C-H bonds, typically facilitated by C-H activation, followed by carboxylation with CO₂.³³ The Cross-coupling C-C bond formation with CO₂, which typically couples an alkyl halide or organoboronate with CO₂ to form carboxylic acids.^[81] The electrochemical carboxylation, which relies on electrons from an external source in the form of an electric current to catalyze the reaction.^[82-84] Photoredox carboxylation utilizes a light source to excite the substrate, initiating a reaction that facilitates the incorporation of CO₂ to form carboxylic acids.^[85]

In this thesis, the focus will be primarily on the 1,2-addition reactions utilizing CO₂, specifically to saturated C-C bonds since they are the most relevant to the work conducted. While exploring this area extensively, the next sections will touch upon enantioselective carboxylations with emphasis on C-C bond formation. The conducted research on CO₂ addition reactions has paved the way for the development of many different transformations. Among these reactions the hydrocarboxylation, boracarboxylation, silacarboxylation, thiocarboxylation, carbocarboxylation, phosphonocarboxylation, photoredox carboxylative addition, electrochemical carboxylative addition.^[78,80-82,85-90]

2.1.1 Examples of relevant 1,2-addition reactions incorporating CO₂

2.1.1.1 Hydrocarboxylation

Hydrocarboxylation is a 1,2-addition reaction that introduces a carboxylic group and a hydrogen to an unsaturated bond (See **Scheme 2**). This reaction is useful in the way that it gives access to a wide range of different carboxylic acid derivatives. An ideal hydrocarboxylation would require only three components, which includes CO₂, H₂, and an olefin. As of now, these conditions are only considered a dream reaction since most hydrocarboxylations require stoichiometric amounts of base and a metallic or organic reductant.^[78] Many different examples of hydrocarboxylation of olefins using CO₂ have been developed, utilizing different transition metal catalysts such as Cu, Rh, Ni, Ti, Fe, Ru, Co, Pd and Zr.^[78]

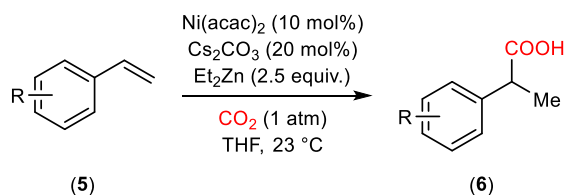


Scheme 2: General reaction scheme for a hydrocarboxylation reaction.

To the best of my knowledge, the first hydrocarboxylation dates back to 1978 and was reported by Lapidus and co-workers.^[91] They described the hydrocarboxylation of ethylene to propionic

acid, utilizing both homogeneous and heterogeneous Pd and Rh catalysts. The carboxylation of ethylene with CO₂ was successfully achieved under high temperature and pressure in an aqueous HCl solution (180 °C and 700 atm). Under these conditions, propionic acid was isolated in yields of 38% contaminated with ethanol, and ethyl propionate side products. After Lapidus discovery, Höberg and colleagues showed that Ni⁰ complexes could form nickel lactones, CO₂, and alkynes. Then, after acidification, gave the corresponding α,β-unsaturated carboxylic acid.^[92] In the early 1990s, the group of Duñach expanded the hydrocarboxylation to a broader scope of alkynes,^[93] including 1,3-diynes,^[94] 1,3-enynes,^[95] and α,ω-diynes.^[96]

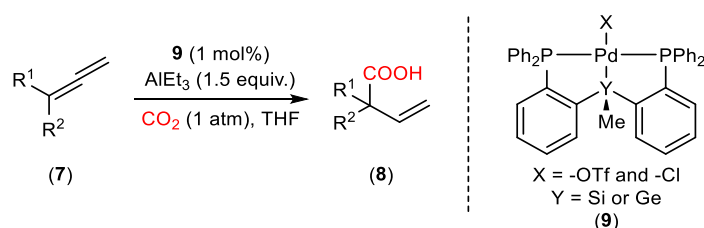
In 2008, Rovis and co-workers, developed the first hydrocarboxylation of styrenes (See **Scheme 3**). They employed a nickel catalyst, cesium carbonate as an additive, and diethyl zinc as the reductant and synthesized various carboxylic acid derivatives (**6**).^[97] Later in 2011 Ma and colleagues applied the same method to alkynes,^[98] and to 2-alkynylanilines in 2017.^[99] In 2015, the Martin group reported a hydrocarboxylation of alkynes using Mn as a reductant with alcohols as a proton source.^[100] Further, a similar system with styrenes, using an iron based catalyst and EtMgBr as a reductant was reported by the Thomas group in 2012.^[101] Subsequently, these conditions were also applied to alkynes in 2016 by the Cheng group.^[102] In the same year, the Xi group reported a hydrocarboxylation of styrenes using a titanium catalyst and *i*PrMgCl as a reductant.^[103] The following year, the same group also applied these conditions to alkynes.^[104] Another system utilizing DIBAL-H and a nickel catalyst for the hydrocarboxylation of 1,3-dienes was studied by the team of Kimura in 2021.^[105] Then, in 2023, the group of Lee reported a hydrocarboxylation of allenes with diisobutylaluminum hydride as the reducing agent and a NHC-CuCl catalyst.^[106]



Scheme 3: Shows the reaction conditions of Rovis and co-worker's hydrocarboxylation of styrenes reported in 2008.^[97]

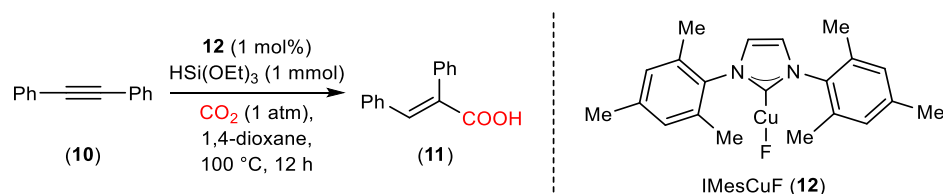
Not long after Rovis, in 2011, Iwasawa and co-workers expanded the scope of the reaction for allenes (See **Scheme 4**).^[107] By employing a Pd-pincer complex with a diphosphine silyl ligand (**9**) as a catalyst and AlEt₃ as a reductant, they facilitated the hydrocarboxylation of allenes (**7**) in the internal double bond. The same year they expanded the scope to include 1,3-dienes using

the same Pd-pincer complex (**9**).^[108] In 2015, they further developed the scope of allenes using HCOONBnMe₃ as a CO₂ source and reducing agent, with a Pd-pincer complex utilizing a diphosphine germanium ligand (**9**).^[109] Two years later, they further expanded the scope to also include terminal alkenes, and cesium formate as a CO₂ source and reducing agent.^[110]



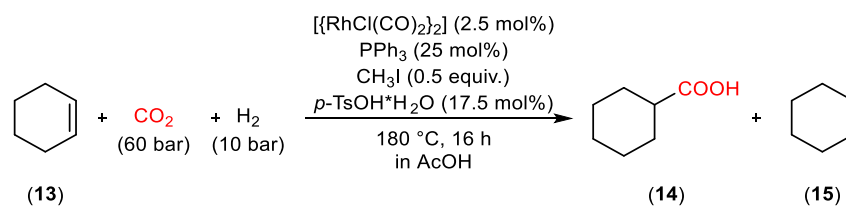
Scheme 4: Shows the conditions Iwasawa and coworkers utilized for the hydrocarboxylation of allenes in 2011.^[107]

In 2011, the research team of Tsuji showed a hydrocarboxylation of internal and terminal alkynes (**10**). By employing a Cu-NHC catalyst (**12**) in conjunction with hydrosilanes as a reductant (see **Scheme 5**), they obtained valuable carboxylic acids (**11**) in good yields.^[111] Later in 2020, the Jiang group published a similar hydrocarboxylation of alkynes, with tetrakis palladium and BINAP.^[112] The year after, the team of Li used catalytic amounts of water in conjunction with hydrosilanes to initiate the hydrocarboxylation of alkynes.^[113]



Scheme 5: Reaction scheme of Tsuji and co-worker's main conditions for the hydrocarboxylation of alkynes.^[111]

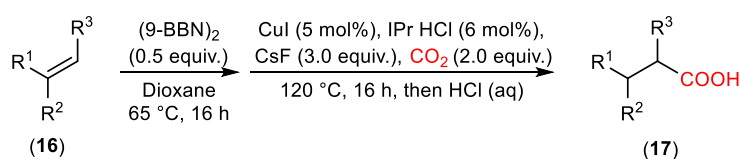
In 2013, Leitner and his team of researchers were inspired by Simonato's use of formic acid as a hydrocarboxylation reagent.^[114,115] They envisioned the direct conversion of CO₂, H₂, and olefins into carboxylic acids. After identifying optimal conditions (See **Scheme 6**), they achieved selective hydrocarboxylation for cyclohexene and cyclopentene, while the other substrates resulted in regioisomeric mixtures. Interestingly, by adding CH₃I as a promoter in 0.5 equiv. and *p*-TsOH·H₂O as a water source, the activity of the catalyst increased, resulting in higher yields. They also reduced the hydrogenation product (**15**) to only 5% and obtained the main product (**14**) in an excellent yield of 92%.^[114]



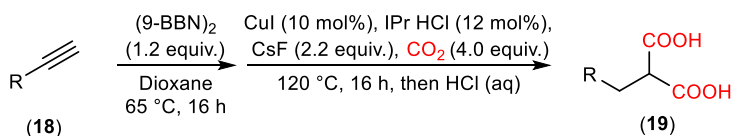
Scheme 6: General reaction conditions for Leitner and co-worker's hydrocarboxylation of olefins reported in 2013.^[116]

In 2011, Hou^[117] and Sawamura^[118] independently reported a hydroboration-carboxylation of terminal olefins using CO₂, copper catalysis, and alkoxides as additives to form carboxylic acids. Building on their findings, in 2017, Skrydstrup and colleagues set out to extend their two-step hydrocarboxylation to internal alkenes and terminal alkynes (See **Scheme 7**, a). Their conditions showed a viable alkoxide-free method to access carboxylic acids from cyclohexenes, stilbenes, and styrenes. The reaction is initiated by a hydroboration step with (9-BBN)₂ in dioxane. Then, in sequence, a carboxylation using CO₂ in the presence of a copper catalyst and CsF. Interestingly, for terminal alkynes (**18**), they found a double hydrocarboxylation, forming derivatives of malonic acid (See **Scheme 7**, b).^[119] Later in 2019, Bayer and colleagues discovered that the catalyst was not needed for substrates such as stilbenes, β-substituted styrenes, and allenes (See **Scheme 7**, c). Their approach showed a hydroboration of alkenes and allenes, followed by a CsF-mediated hydrocarboxylation.^[35] The year after, in 2020, a similar system using a copper catalyst, B₂pin₂, and KO^tBu for a selective 1,2-hydrocarboxylation of 1,3-dienes was reported by the Zhang group.^[120]

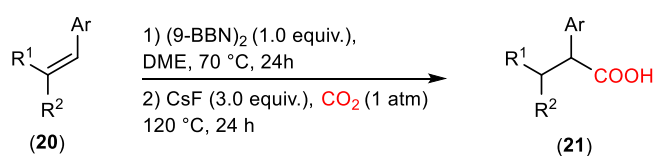
(a) Hydrocarboxylation of alkenes



(b) Hydrocarboxylation of terminal alkynes

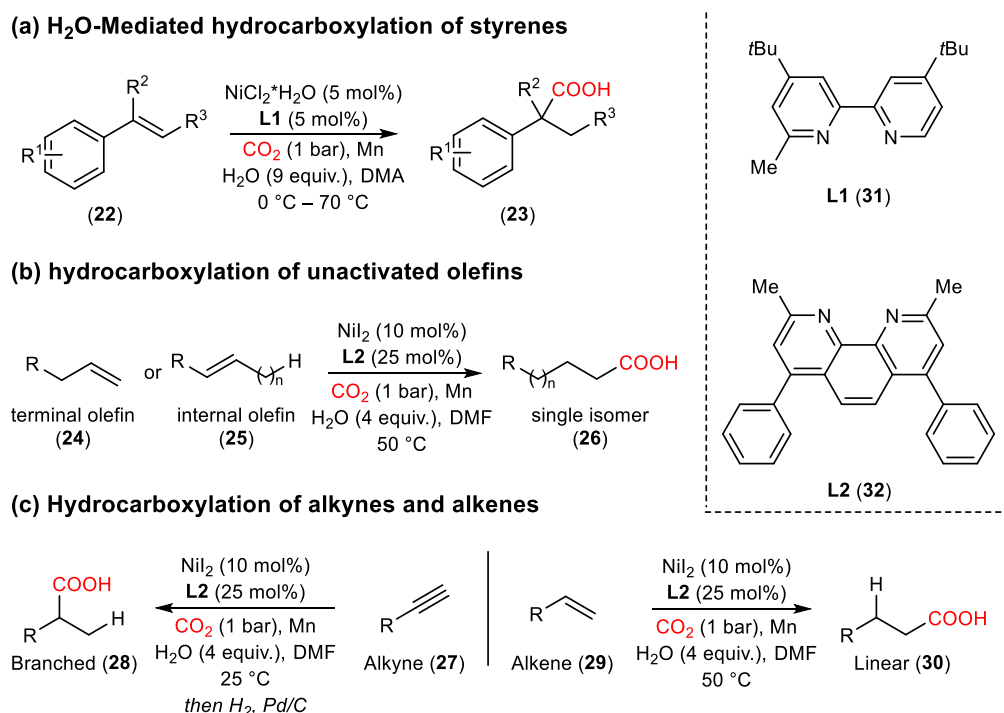


(c) CsF-Mediated hydrocarboxylation of alkenes



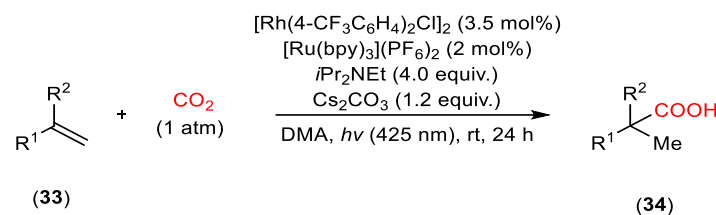
Scheme 7: Shows (a) Skrydstrup and co-worker's general conditions for hydrocarboxylation of alkenes, (b) terminal alkynes and (c) the group of Bayer's hydrocarboxylation of alkenes.^[35,121]

Martin and co-workers aimed to combine three abundant chemical feedstocks (water, CO₂, and olefins) under mild conditions. Screening styrenes (**22**) under optimal conditions with Mn as the reducing agent (See **Scheme 8**, a), the hydrocarboxylation products (**23**) were obtained in good to excellent yields. Also, by changing their conditions (See **Scheme 8**, b), they also found that unactivated olefins, both terminal (**24**), internal (**25**), and even as a mixture of regioisomers yielded the same product (**26**). For alkynes (**27**), they obtained the branched product (**28**) in moderate to good yields (See **Scheme 8**, c).^[119] The same year Sato and co-workers reported a similar system, using Zn as the reductant and water as a proton source for the hydrocarboxylation of ynamides.^[122]



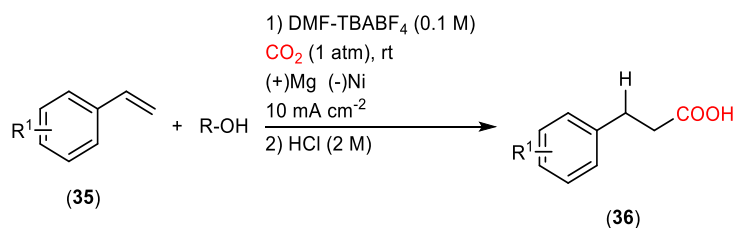
Scheme 8: Shows the optimal conditions for hydrocarboxylation of styrenes (a), hydrocarboxylation of terminal and internal olefins (b), hydrocarboxylation of alkenes and alkynes (c) all developed in the group of Martin.^[119]

To the best of my knowledge, the first hydrocarboxylation enabled by photoredox catalysis was reported by Iwasawa and colleagues in 2017 (See **Scheme 9**). By combination of a Rh-catalyst, with a Ru-photocatalyst, *i*Pr₂NEt as an electron donor, and Cs₂CO₃ as additive, they obtained carboxylic acids (**34**) in moderate yields.^[123] Later in 2019, they improved their method with the use of BI(OH)H as an electron donor, and an Ir-phocatalyst.^[124] In 2022, the same group reported a system based on a Rh-catalyst, Ru-photocatalyst, and H₂ gas as both a reductant and proton source.^[78] In 2017, the group of Jamison reported a similar hydrocarboxylation in continuous flow, with *p*-terphenyl as a photocatalyst, PMP as an electron donor, and water as an additive.^[125] In 2021, team of Romo reported a similar photocatalyzed hydrocarboxylation of acrylates under continuous flow. Their method used hydrosilanes as a hydrogen source, *p*-terphenyl as the photocatalyst, and a tetramethyl piperidine analogue as the reductant.^[126] Following the works of Jamison, the group of Wu reported the hydrocarboxylation of alkynes enabled by a combination of Co-catalysis and Iridium based photocatalyst.^[127] The same year the group of König reported a light driven hydrocarboxylation of styrenes, with a nickel-based catalyst, and 4CzIPN as a photocatalyst.^[128]



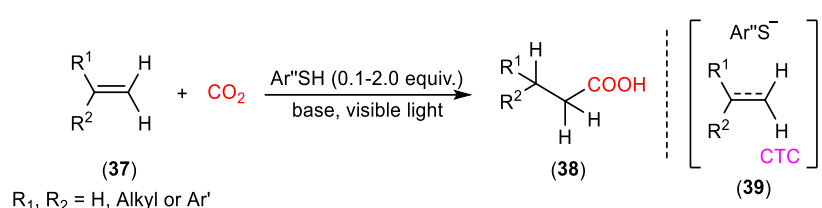
Scheme 9: Hydrocarboxylation of olefins enabled by photoredox catalysis developed in the group of Iwasawa.^[123]

Nam and colleagues investigated an electrochemical β -selective carboxylation of styrenes (See **Scheme 10**). By using a Mg-based cathode and Ni-based anode and a DMF-TBABF₄ electrolyte mixture, they were able to perform a 1,2-addition of styrenes generating carboxylic acids (**36**) with faradaic efficiencies reaching 65%.^[129] Using a similar system, Buckley and colleagues expanded the electrochemical carboxylative 1,2-addition to substituted olefins,^[130] and acrylates.^[131] In 2023, Mellah and co-workers reported an electrochemical Sm-catalyzed β -hydrocarboxylation of styrenes.^[132] During the same year, the team of Ye reported the electrochemical hydrocarboxylation of allenes.^[133]



Scheme 10: Electrochemical hydrocarboxylation of styrenes studied by Nam and co-workers.^[129]

In 2020, Yu and colleagues envisioned that electron rich thiolates, and electron-deficient acrylates/styrenes might form a *charge-transfer complex* (CTC) (**39**). The CTC prompts a single-electron reduction of acrylates/styrene or CO₂ to generate radical anions, which, in return, could facilitate hydrocarboxylation of both styrenes and acrylates (See **Scheme 11**). The reaction performed well for tetrasubstituted acrylates (**37**) and allowed the hydrocarboxylation of bioactive molecules, such as isborneol, L-(–)-menthol, α -terpineol, 4-carvomenthenol, and β -cholesterol.^[134]



Scheme 11: Shows the general procedure for light-activated hydrocarboxylation of styrenes and acrylates (**37**) using a CTC complex (**39**) performed by Yu and coworkers.^[134]

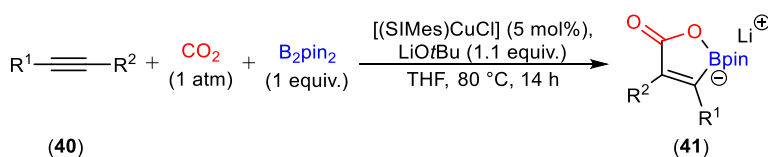
While the hydrocarboxylation is a well-studied and notable reaction that has seen a lot of progress since Lapidus original publication,^[91] it is crucial to acknowledge the persisting issues. The challenges related to kinetics, selectivity, and CO₂ activation, still persist.^[80]

2.1.1.2 Boracarboxylation

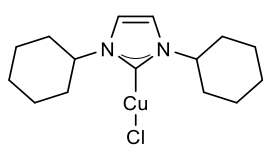
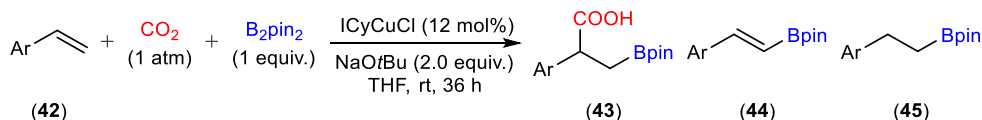
The boracarboxylation is an addition that introduces a carboxylic acid and a boronic ester to an unsaturated carbon-carbon bond (See **Scheme 12**). The boracarboxylation was first reported by the group of Hou in 2012. In their study, they demonstrated a reaction that is similar to a hydroboration; however, instead of a proton source as an electrophile, CO₂ was tested. The introduction of CO₂ resulted in a cyclic adduct in the form of lithium salt (**41**).^[135] Their substrate scope consisted of symmetric- and asymmetrically substituted alkynes (See **Scheme 12**). To their surprise, CO₂ would always insert into the benzylic position of the substrate. With further synthesis from **41**, they performed a Suzuki-Miyaura cross-coupling to obtain *trans* acrylic acid derivatives in moderate yields.^[135]

Later in 2016, Popp and coworkers reported a set of milder conditions that effectively could perform a regioselective boracarboxylation of styrenes (See **Scheme 12**). With an acidic workup, they were able to obtain the product (**43**) in the free acid form. During their investigations, they characterized three major products: The boracarboxylation product (**43**), the β-hydride elimination product (**44**), and the hydroboration product (**45**) (See **Scheme 12**). Like Hou, Popp also saw a clear trend that CO₂ would always insert into to the benzylic position of the styrene.^[87]

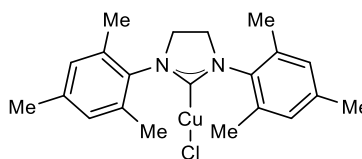
(a) Boracarboxylation of unsaturated systems



(b) Boracarboxylation of styrenes



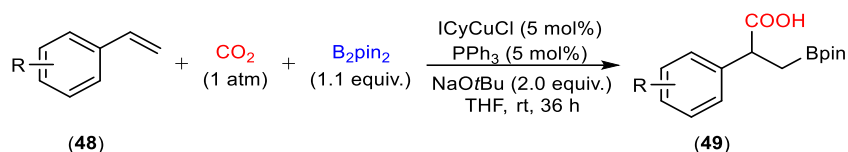
ICyCuCl (46)



[(SIMes)CuCl] (47)

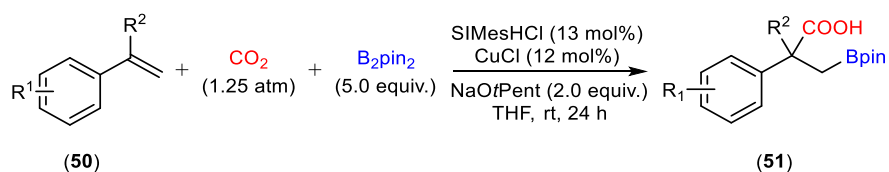
Scheme 12: (a) first boracarboxylation of unsaturated systems by Hou and co-workers.^[135] (b) Boracarboxylation of styrenes reported by the group of Popp.^[87]

In 2019, Popp and coworkers published a follow-up study (See **Scheme 13**) addressing the limitations regarding high catalyst loading (12 mol%) and poor yield for electron-deficient styrenes. Initially, when reducing the catalyst loading (5 mol%), they observed an increase in β -hydride elimination product (**44**). The increasing side product made them consider a decomposition of or inactive NHC-Cu complex at lower catalyst loading.^[136] Inspired by previous studies on the addition of *triphenylphosphine* (PPh₃) to Cu based catalytic systems,^[137-140] they hypothesized its introduction could improve their reaction yields. Their hypothesis was that PPh₃ served a dual role, by coordinating to and slowing down the decomposition of the NHC-Cu species. By reducing the catalyst (to 5 mol%) and adding PPh₃ (5 mol%), they obtained comparable and or elevated yields with the same substrates. In addition, the amount of β -hydride elimination product (**44**) was reduced, while also expanding the substrate scope.^[136]



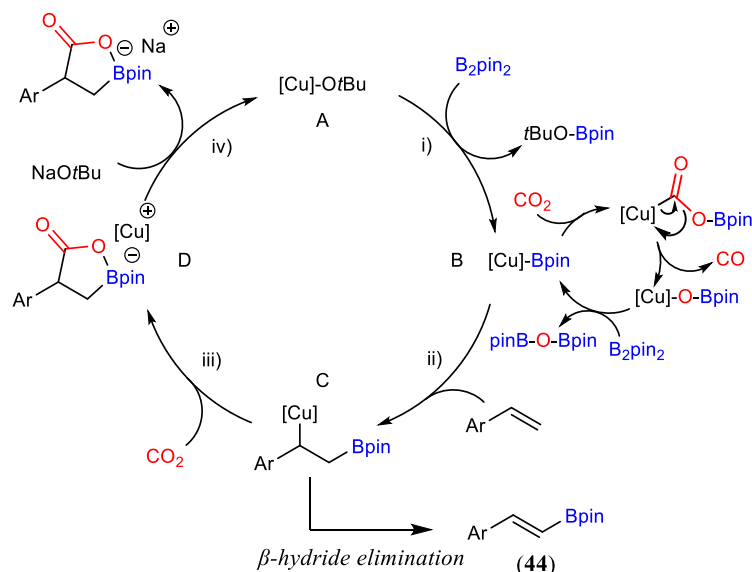
Scheme 13: Popp and co-workers study on phosphine-facilitated boracarboxylation of styrenes in 2019.^[136]

Later in 2022, the Popp group also investigated the boracarboxylation of α -substituted styrenes (See **Scheme 14**). To their surprise, when applying higher CO₂ pressure, the yields dropped drastically. With further testing, they managed to reproduce the best yields observed in the previous studies by increasing the B₂pin₂ loading. The observed lower yield could be the reason of CO₂ being consumption before the insertion of styrene into the copper carbene complex.^[88] From the accepted boracarboxylation mechanism, they suggested an alternative reaction pathway including the reduction of CO₂ to CO mediated by the intermediate Cu-Bpin complex and pinB-O-Bpin (See **Scheme 15**).^[141-143] Their conducted 13B NMR studies also revealed that elevated pressures of CO₂ resulted in the formation of large quantities of pinB-O-Bpin.^[88] Additionally, they suspected electron-deficient substrates to give better yields, since they are known for faster insertion into (NHC)Cu-boryl complexes.^[144] Indeed, after screening of styrenes, they observed higher yields at elevated pressures of CO₂ for electron-deficient systems. Overall, showing that a higher pressure could both benefit and pose a disadvantage depending on substrate type.^[88]



Scheme 14: General reaction conditions for Popp and co-workers study on boracarboxylation of α -substituted styrenes in 2022.^[88]

The first in-depth study of the boracarboxylation mechanism was conducted by Lu's group in 2017. Their investigation primarily explored the ligand effects. However, they also determined the observed regioselectivity was likely a result of the high stability of the benzylic copper intermediate (See **Scheme 15, C**). Additionally, they found that the β -hydride elimination of C to be less kinetically and thermodynamically favorable than the CO₂ insertion (See **Scheme 15, step iii**), which they also identified as the rate-determining step.^[142]



Scheme 15: Accepted mechanism of the Copper-catalyzed boracarboxylation with the reduction of CO_2 as a competitive side reaction.^[88, 135, 141-143]

In 2019 the group of Popp conducted a computational study on the mechanism of the boracarboxylation. They found that the formation of the Cu-boryl species **B** (See **Scheme 15**) occurs at a very low energy barrier and happens almost instantly. The Cu-boryl complex prefers insertion of the styrene according to the pathway ii to generate **C**, over the diverging CO_2 reduction pathway. From **C** they saw a clear preference for the CO_2 insertion step iii over β -hydride elimination to **44** (See **Scheme 15**) and other competing side reactions such as polymerization, hydroboration and decupration. Their study also determined the CO_2 insertion to be the likely rate-determining step,^[141] which aligns with Lu and coworkers previous report.^[142] In 2020, Popp and co-workers also considered the role of the organoboron reagent in the reaction mechanism. From calculations, they suggested that boron participates as a Lewis acid in the CO_2 insertion and promotes it (See **Figure 5, C**). The study demonstrated a correlation between the activation energy of CO_2 insertion and the electron deficiency at the boron center in organoboron reagents. As boron becomes more electron-deficient, the energy barrier decreases. This results in a more electrophilic carbon, enhancing its reactivity for the subsequent metalation by copper (See **Scheme 15, ii**).^[145]

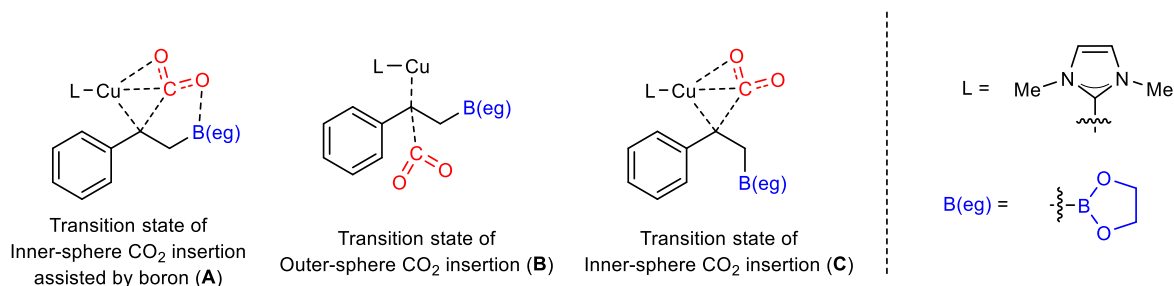


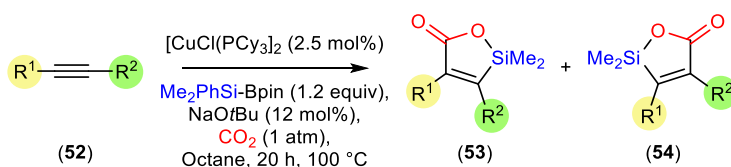
Figure 5: Figure of the boron assisted transition state **A**, outer-sphere transition state **B**, and inner-sphere transition state **C**.^[145]

2.1.2 Examples of other relevant carboxylation reactions

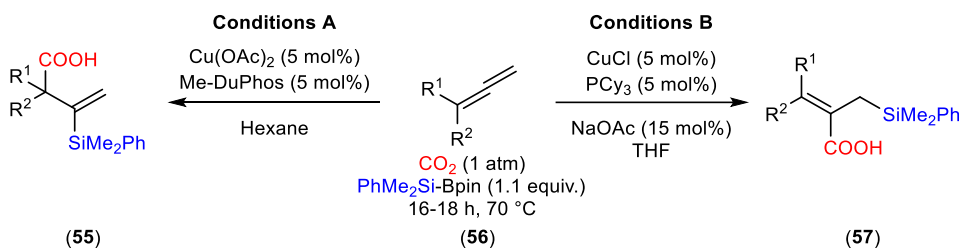
2.1.2.1 Silicarboxylation

The silicarboxylation was studied by the group of Tsuji in 2012, they demonstrated a copper-catalyzed reaction employing a silylboronate and CO₂ for 1,2-addition to an unsaturated system. They first studied the reaction using internal alkynes (**52**),^[89] but also later in 2014 expanded the substrate scope to include allenes (**56**).^[90] By employing two sets of conditions achieving excellent regioselectivities in both the internal (**55**) and terminal (**57**) double bond of the allene (See **Scheme 16, A and B**).

(a) Silicarboxylation of internal alkynes



(b) Silicarboxylation of allenes

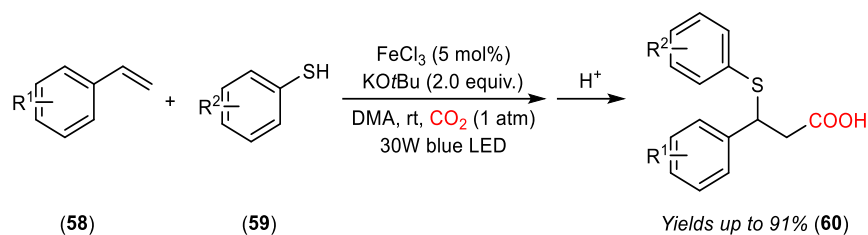


Scheme 16: Silicarboxylation of internal alkynes and allenes.^[89,90]

2.1.2.2 Thiocarboxylation

The thiocarboxylation was published in 2017 by Yu and co-workers (See **Scheme 17**), in their study they utilized visible light and catalytic amounts of FeCl₃ to drive their reaction forward. With this innovative approach, they were able to thiocarboxylate styrenes (**58**) under mild reaction conditions. They produced a wide range β -thioacids (**60**) with excellent yields, up to

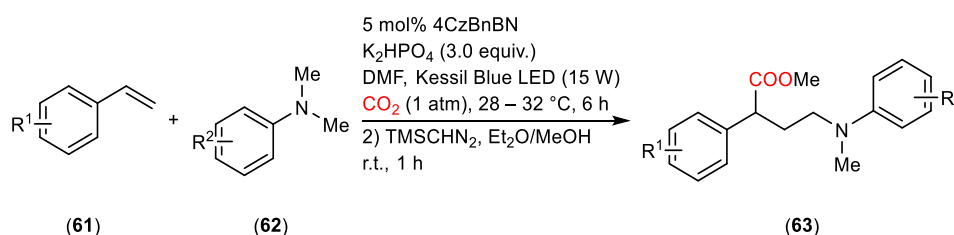
91%.^[86] In 2022, Jain and colleagues further developed the thiocarboxylation of styrenes using photocatalysis and an iron-based *metal-organic framework* (MOF).^[146]



Scheme 17: Thiocarboxylation of styrenes (58) using an iron based catalyst and 30W blue LED light.^[86]

2.1.2.3 Carbocarboxylation

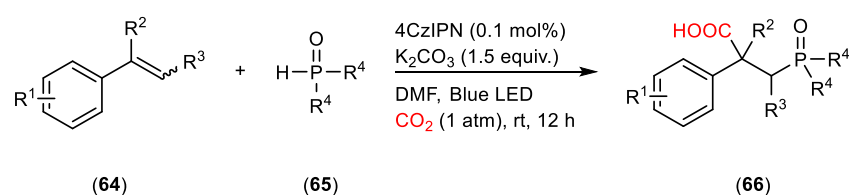
The carbocarboxylation enabled by photoredox catalysis was reported by the group of Hong in 2021 (See **Scheme 18**). In this study they combined 4CzBnBN as a photocatalyst, styrenes (61), substituted anilines (62), blue LED light and TMSCHN₂ as a methylation agent. With these conditions they were able to produce γ -aminobutyric esters (63) in yields of up to 91%.^[147]



Scheme 18: Metal-free photoredox-catalyzed carbocarboxylation of styrenes (61).^[147]

2.1.2.4 Phosphonocarboxylation

In 2019, Yu and colleagues published the first phosphinocarboxylation operating under photoredox catalysis. By utilizing 4CzIPN as a photocatalyst, disubstituted phosphine oxides (65), K₂CO₃ as a base, and blue LED (See **Scheme 19**) they performed a 1,2-addition that incorporates CO₂ and disubstituted phosphine oxides into the double bond of styrenes, with yields reaching 93%.^[148]



Scheme 19: Phosphonocarboxylation of styrenes enabled by photoredox catalysis (64).^[148]

2.1.3 Enantioselective C-C bond-forming reactions with CO₂ and related transformations.

Enantioselective reactions transform a prochiral starting material into a chiral product and produce an excess of one of the two enantiomeric forms of the product. The development of enantioselective reactions has been an important topic in modern organic chemistry.^[149] Which also was recognized by the Nobel prizes in chemistry for the development of enantioselective hydrogenations, oxidations (2001) and organocatalytic transformations.^[150,151] The first catalytic enantioselective reaction using a chiral transition metal complex was reported in 1966 by Noyori and colleagues. After Noyori and co-worker's discovery, a modern era of transition metal-catalyzed enantioselective reactions was born and paved the way for the development of important chiral ligands (See **Figure 6**), such as (*R*)-BINAP,^[152] (*S,S*)-DiPAMP,^[153] (*S,S*)-*t*Bu-BOX,^[154] (*S,S*)-Me-DuPhos,^[155] and more.^[150,151,156]

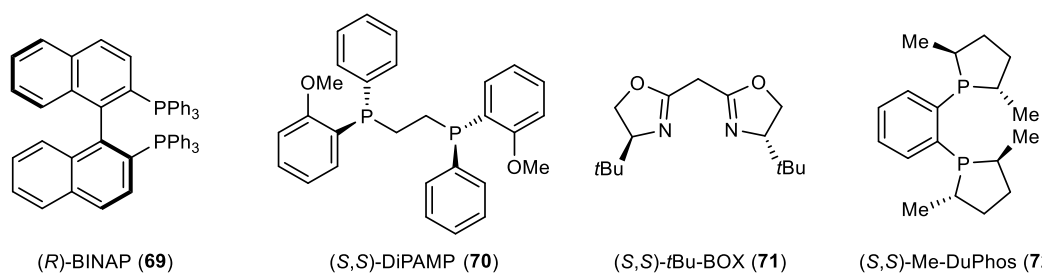
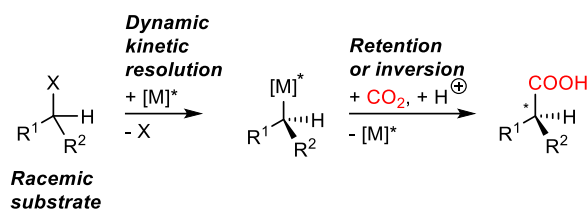


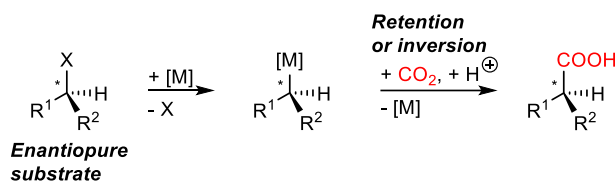
Figure 6: Structures of (*R*)-BINAP (69), (*S,S*)-DiPAMP (70), (*S,S*)-*t*Bu-BOX (71) and (*S,S*)-Me-DuPhos (72).

Enantioselective C-C bond-forming reactions that utilize CO₂ are still a relatively new research area. Therefore, little progress has been made to form enantioenriched molecules with CO₂ as a carbon feedstock. So far, there are three main strategies to obtain chiral molecules incorporating CO₂. The first strategy, *deracemization* (See **Scheme 20**, a) starts with a racemic starting material that is transformed to an enantiomerically enriched product using enantioconvergent processes such; dynamic kinetic resolution or enantioconvergent synthesis. The second approach involves *chirality transfer* (See **Scheme 20**, b) from an enantiopure substrate, without a chiral catalyst or additive. In this method, the formed chiral center depends on the absolute configuration of the starting material. The third strategy involves *enantioselective synthesis* (See **Scheme 20**, c). This method involves the formation of a chiral product from a prochiral substrate with the use of an enantiopure chiral catalyst or additive.^[157]

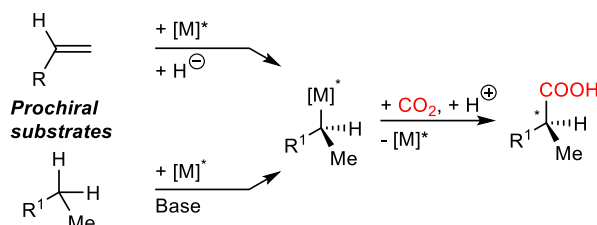
(a). Deracemization



(b). Chirality transfer

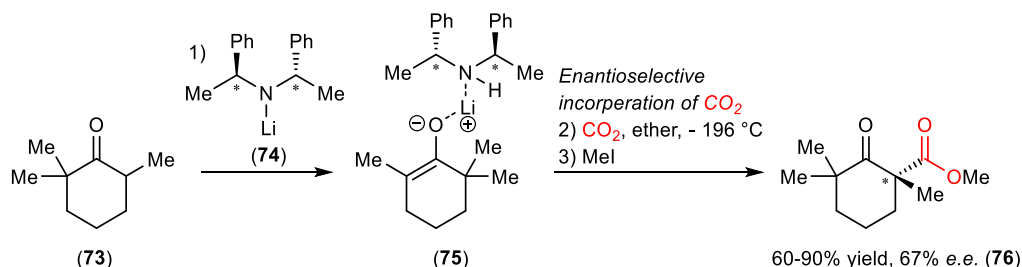


(c) Enantioselective synthesis



Scheme 20: The main strategies for enantioselective C-C incorporation of CO₂ (a) deracemization (b) chiral transfer and, (c) enantioselective synthesis.^[157]

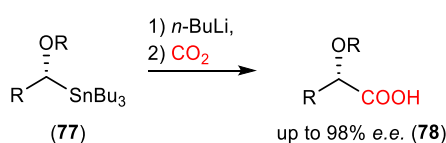
To the best of my knowledge, it was not until 1986 that the first enantioselective C-C bond-forming reaction with CO₂ was reported (See **Scheme 21**). The Hogeveen group investigated an enantioselective carboxylation of a lithium enolate (**75**), which was formed by the deprotonation of **73** with a chiral base, (*S,S*)- α,α' -dimethyldibenzylamide lithium (**74**). Carboxylation of the enolate and methylation of the acid formed an ester (**76**) in up to 67% *e.e.*, and yields ranging from 60 to 90%.^[158] This reaction marked a significant step forward in the field of enantioselective C-C bond-forming reactions with CO₂.



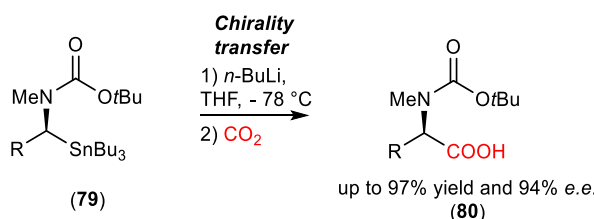
Scheme 21: Enantioconvergent carboxylation of (**73**) using the chiral base (*S,S*)- α,α' -dimethyldibenzylamide lithium (**74**).^[158]

In 1990, Chong and co-workers reported a chirality transfer of enantiopure α -alkoxyorganostannanes to α -hydroxy acid derivatives (See **Scheme 22**, a). By first using *n*-BuLi to perform a Sn-Li exchange, they generated an α -alkoxyorganolithium intermediate. Then, followed by the introduction of CO₂, resulted in enantioenriched α -hydroxy acid derivatives (**78**, up to 98% *e.e.*).^[159] In 1992, the same group reported that α -aminoorganostannanes (**79**) could also undergo chirality transfer to generate secondary α -amino organolithiums (See **Scheme 22**, b). Further, introducing CO₂ to their reaction mixture resulted in amino acid derivatives (**80**) with up to 94% *e.e.*^[160]

(a) Chong and co-workers chirality transfer 1990



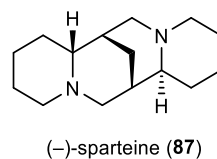
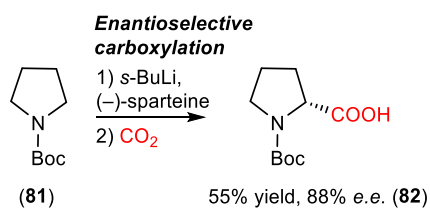
(b) Chong and co-workers followup study 1992



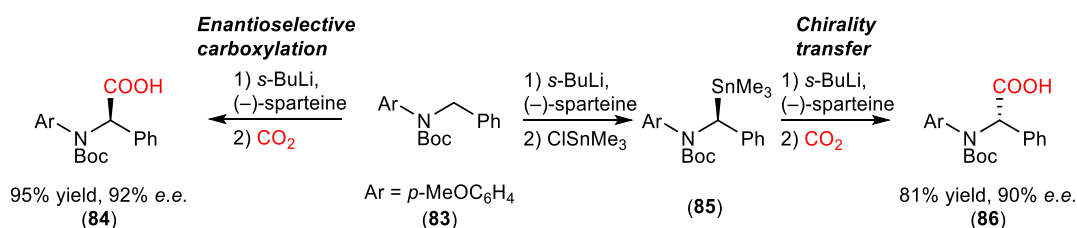
Scheme 22: Chong and colleagues chirality transfer of (a) α -hydroxy acid derivatives (**77**),^[159] and (b) α -aminoorganostannanes (**79**) to synthesize amino acid derivatives (**80**).^[160]

In 1991, the Beak group conducted an enantioselective carboxylation of Boc-pyrrolidine (**81**) using *s*-BuLi in the presence of (–)-sparteine (**87**). This was followed by CO₂ addition, affording (*R*)-proline (**82**) with 88% *e.e.* (See **Scheme 23**, a).^[161] In 1997, the group compared the outcome of the enantioselective carboxylation with the carboxylation via stannylation/chirality transfer (See **Scheme 23**, b), to synthesize amino acids (**84** and **86**) using (–)-sparteine (**87**) and *s*-BuLi.^[162] With the enantioselective carboxylation, they observed excellent yields of up to 95% for the amino acid derivatives (**84**), with *e.e.* reaching 92%. Additionally, the chirality transfer reached yields of up to 81% and *e.e.* values of 90% for (**86**).

(a) Beak and colleagues 1991 study



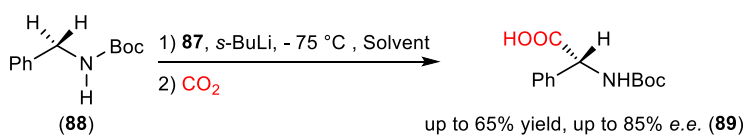
(b) Beak and colleagues 1997 study



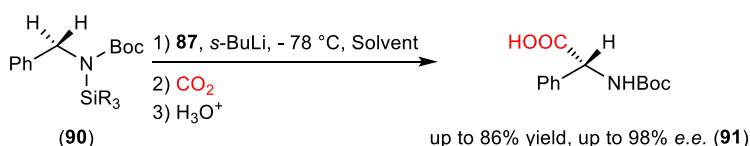
Scheme 23: Beak and colleagues 1991 study on (a) enantioselective carboxylation and (b) comparison of enantioselective carboxylation and chirality transfer.^[161,162]

Schlosser and co-workers reported an enantioselective deprotonation of **88** in the presence of (-)-sparteine (**87**) and *s*-BuLi (See **Scheme 24**, a). This transformation allowed for the synthesis of *N*-Boc-protected phenyl glycine derivatives (**89**) in yields up to 65% and *e.e.*'s reaching 85%.^[163] In 2001, Voyer and colleagues reported an analogous approach (See **Scheme 24**, b) using a substrate with a silyl protecting group combined with a Boc group (**90**). This way, they were able to obtain the *N*-Boc-protected phenyl glycine derivatives (**91**) in yields reaching 86% and *e.e.* values of 98%.^[164]

(a) Schlosser and co-workers (1995)



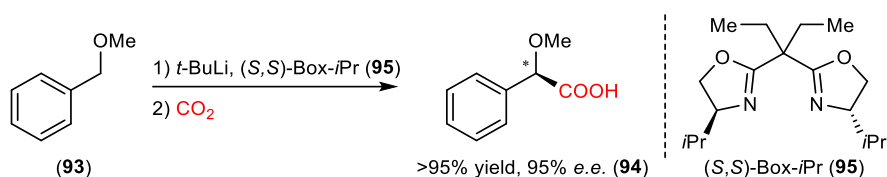
(b) Voyer and co-workers alternative approach (2001)



Scheme 24: The Schlosser (1995) and Voyer (2001) groups' enantioselective carboxylation to synthesize *N*-Boc-protected phenyl glycine derivatives (**89** and **91**).^[163,164]

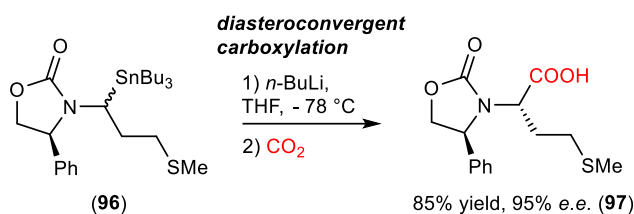
In 1999, a study conducted by the group of Nakai (See **Scheme 25**) showed a related enantioselective carboxylation of (methoxymethyl)benzene (**93**). By exposing their substrate to

t-BuLi in the presence of a (*S,S*)-Box-*i*Pr ligand (**95**) followed by the addition of CO₂, they were able to perform an enantioselective carboxylation with *e.e.* and yields of up to 95%.^[165]



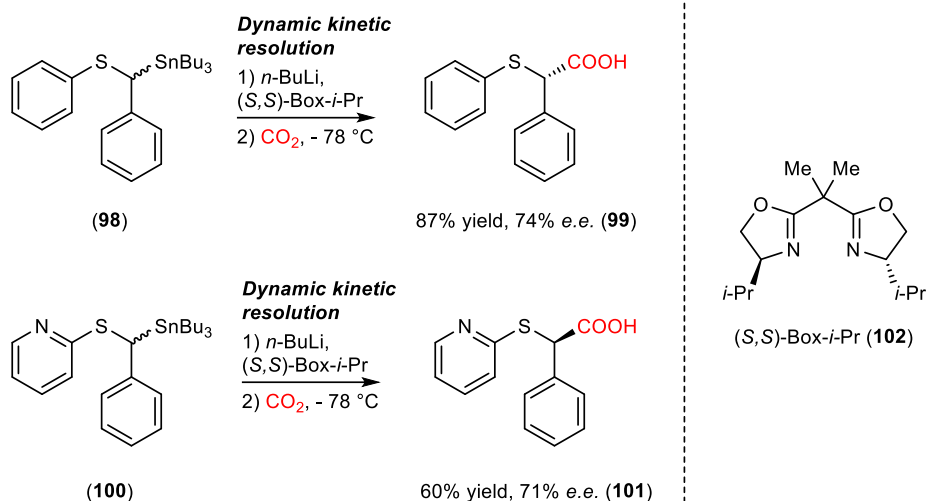
Scheme 25: Enantioselective carboxylation of benzyl methyl ethers reported by the group of Nakai.^[165]

A year later, in 2000, Fournet and co-workers presented an interesting diastereoconvergent carboxylation approach (See **Scheme 26**). By the treatment of *N*-(α -stannylalkyl) oxazolidinones (**96**) with *n*-BuLi, followed by the addition of CO₂, they managed to prepare protected amino acids with good yields and *e.e.* values up to 95%.^[166]



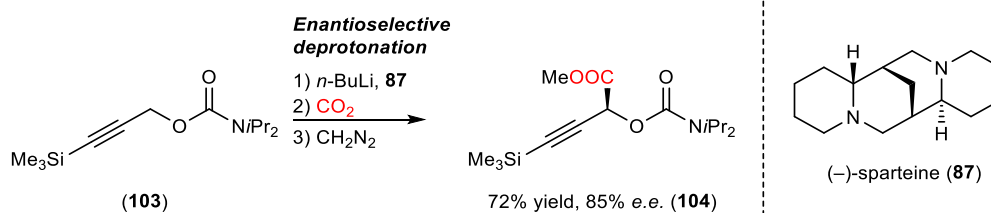
Scheme 26: Diastereoconvergent carboxylation of *N*-(α -stannylalkyl)oxazolidinones (**96**).^[166]

The same year, the group of Toru reported an enantioconvergent carboxylation of thioorganostannyls (See **Scheme 27**, **98** and **100**). By combining *n*-BuLi, with (*S,S*)-Box-*i*-Pr (**102**) followed by CO₂ addition, they obtained a range of α -thiocarboxylic acids (**99** and **101**) with *e.e.* values of up to 74%.^[167]



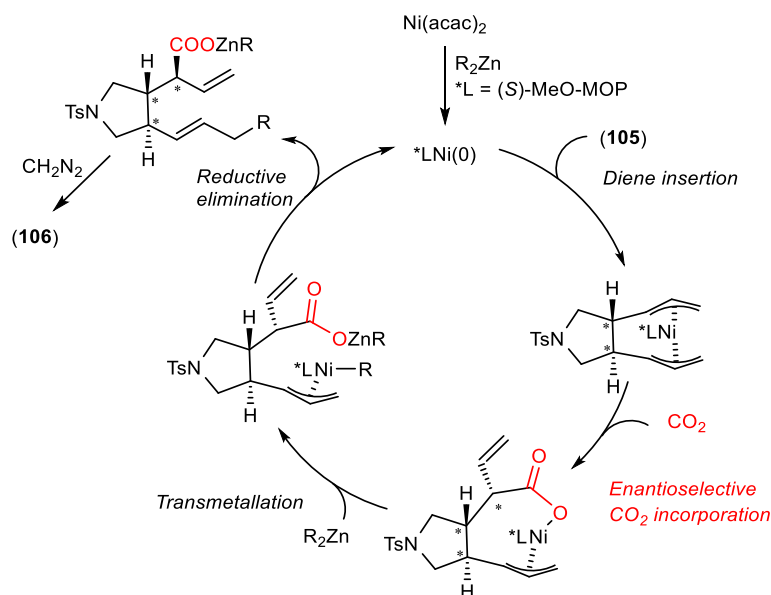
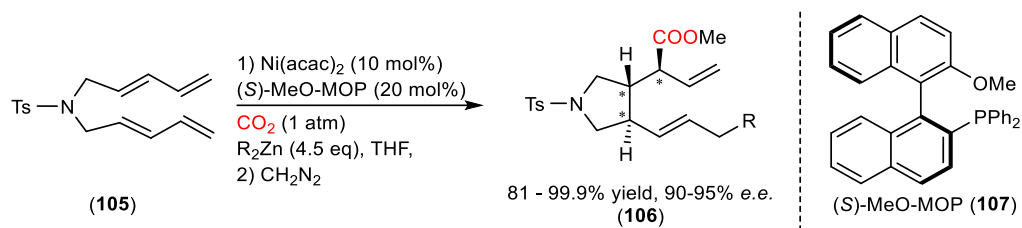
Scheme 27: Enantioconvergent carboxylation of thioorganostannyls reported by Toru and co-workers.^[167]

In 2001, Hoppe and co-workers reported an enantioselective carboxylation approach for propargylic carbamates (**103**) enabled by the combination of (–)-sparteine, *n*-BuLi at -78 °C, followed by addition of CO₂ (See **Scheme 28**). The chiral acid derivative (**104**) was obtained with *e.e.* values of up to 85%.^[168]



Scheme 28: Enantioselective carboxylation of propargylic carbamates (**103**).^[168]

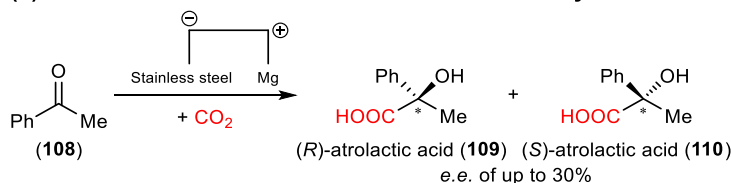
A few years later, in 2002,^[169] and 2004,^[170] Mori and colleagues published two consecutive studies (See **Scheme 29**) regarding a nickel catalyzed ring closing carboxylation of bis-1,3-dienes (**105**). Their study was interesting in the sense that it could generate three consecutive chiral centers in a single operation. Using Ni(acac)₂ and (*S*)-MeO-MOP (**107**) as a chiral catalyst with diethylzinc as a reductant, they observed (**106**) with 95% *e.e.* and yields up to 99.9%. The generated active Ni(0) species react with the diene to give a bis-allyl species, which then enantioselectively inserts CO₂ into the substrate. Transmetalation of the generated nickel carboxylate with R₂Zn, and then a reductive elimination followed by the addition of CH₂N₂ yields the methyl carboxylate (See **Scheme 29**).^[157]



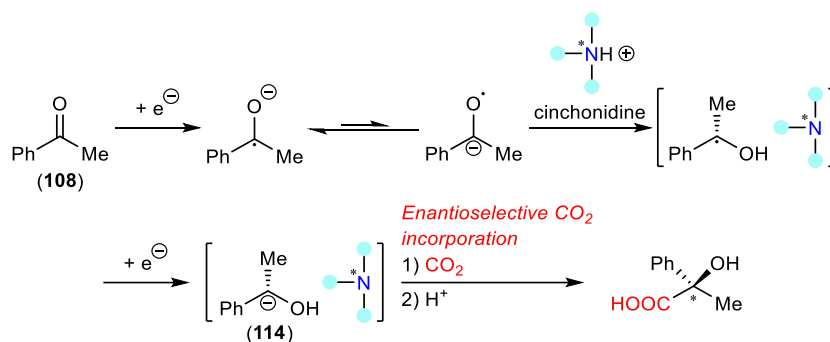
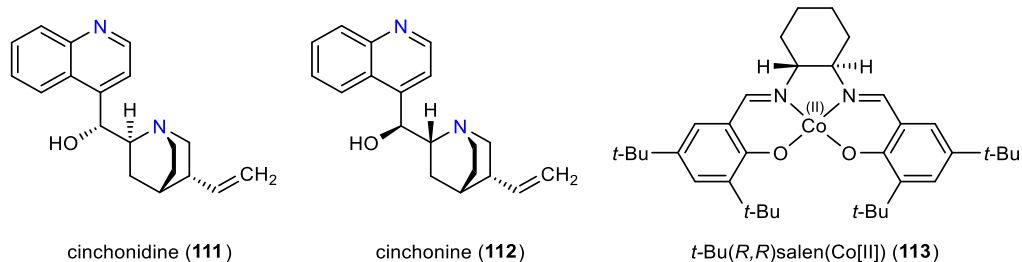
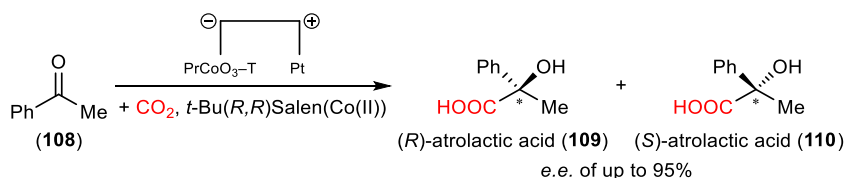
Scheme 29: Ni-catalyzed enantioselective carboxylation of dienes (**105**).^[169,170]

In 2009, Lu and colleagues took a different approach and decided to explore enantioselective electrocarboxylation (See **Scheme 30**, a). Their method employed a stainless steel or palladium electrode in the presence of a chiral ligand (**111** or **112**), to synthesize the pharmaceutical intermediate atrolactic acid (**109** and **110**). By generating an α -hydroxy anion (**114**) via electrochemical reduction of acetophenone (**108**), followed by incorporation of CO₂ in an enantioselective manner. This way, they were able to synthesize atrolactic acid (**109** and **110**) in *e.e.* up to 30%.^[171] Lu also expanded the substrate scope to include benzylic halides using **113**, both and heterogeneous catalysis in 2014 (*e.e.* up to 83%),^[172] homogeneous catalysis in 2015 (*e.e.* up to 73%).^[173] Recently, in 2021, they improved this method by using **113**, and LSF-x and Pt electrodes,^[174] and further in 2022 with PrCoO₃-T and Pt electrodes, giving *e.e.* values up to 95% (See **Scheme 30**, b).^[175] A year later, they also experimented with analogues of **113** reaching *e.e.* up to 83%.^[176]

(a) 2009 Enantioselective electrochemical carboxylation



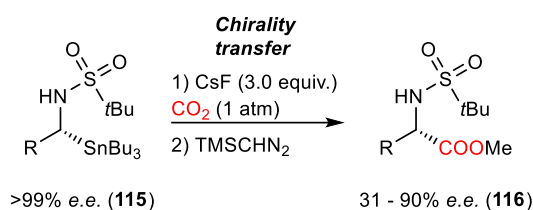
(b) 2022 improved Enantioselective electrochemical carboxylation



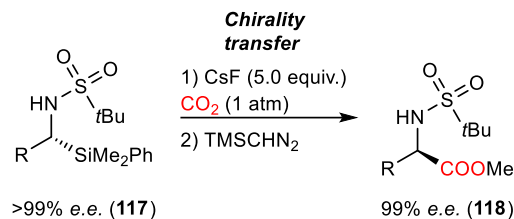
Scheme 30: Electrocarboxylation of acetophenone (**108**) using a (a) stainless steel Mg electrode,^[171] and (b) PrCoO₃-T Pt electrode,^[175] for the enantioselective synthesis of atrolactic acid (**109** and **110**).

Sato and colleagues reported an enantioselective carboxylation approach of chiral α -amido stannans (**115**) mediated by CsF for the activation of tin (See **Scheme 31**, a). The product resulted in *N*-sulfonyl amino acids (**116**) with *e.e.* values reaching 90%.^[177] Later in 2014, the group of Sato published a follow-up study using chiral α -amido silanes (**117**), with CsF as an activator, (See **Scheme 31**, b) to obtain α -amino acid derivatives (**118**) with *e.e.* values of 99%.^[178]

(a) Sato and co-workers 2012 study

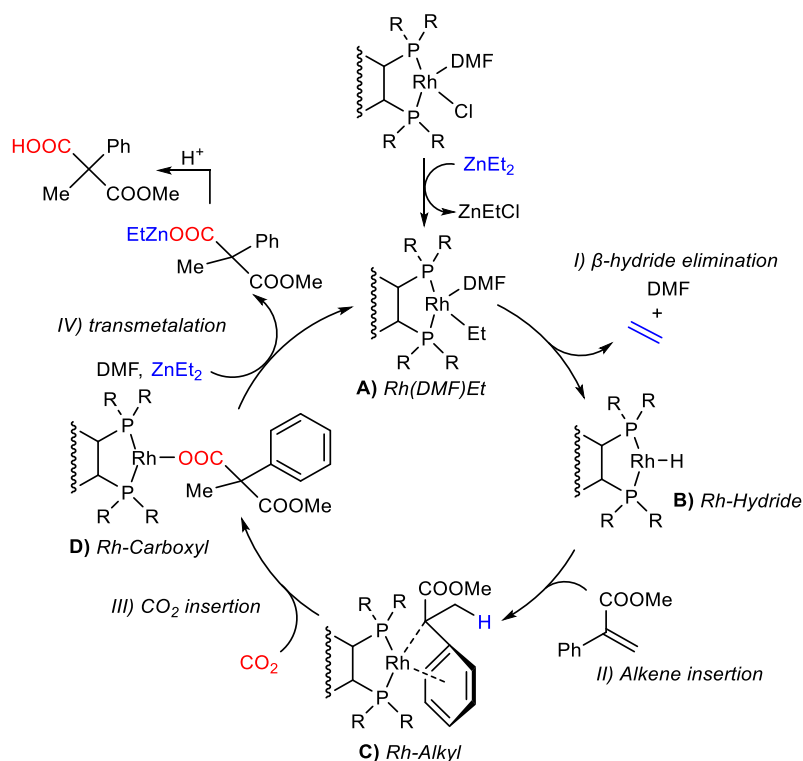
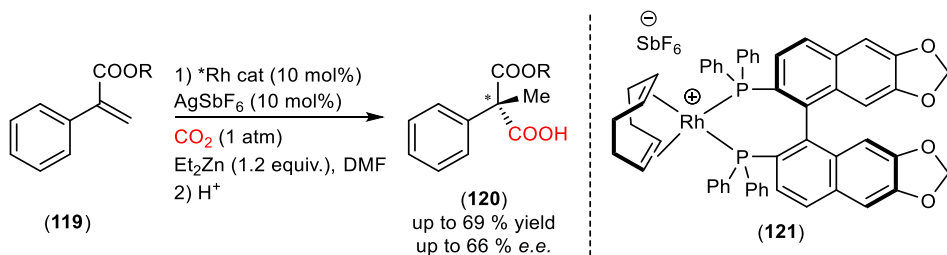


(b) Sato and co-workers follow-up 2014 study



Scheme 31: Chirality transfer in α -amido stannanas (**115**) (a) and α -amido silanes (**117**) (b).^[177,178]

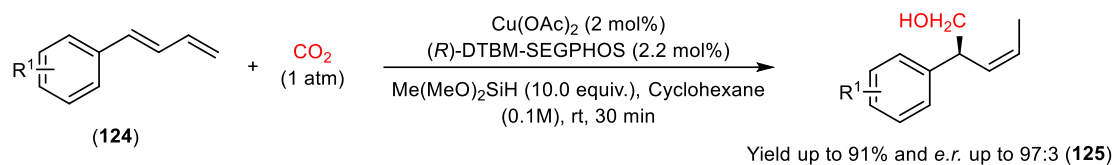
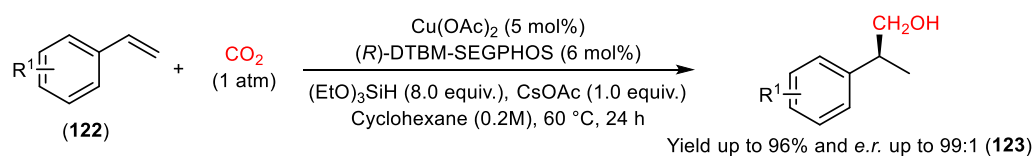
In 2016, the group of Mikami reported the first enantioselective hydrocarboxylation of acrylates (**119**) with CO_2 .^[179] Their method utilized a chiral Rh-phosphine complex (**121**) with diethylzinc as a reducing agent and CO_2 as a carbon source. They obtained their product (**120**) with *e.e.* as high as 66% and yields up to 69%. A mechanistic study conducted by Hopmann and co-workers in 2018 (See **Scheme 32**) gave important insight to the mechanism. They proposed a transmetalation between an ethyl group from diethylzinc and the Rh-complex, followed by β -hydride elimination to generate an active Rh-H species. Then, the acrylate (**119**) inserts into the Rh-H species to form a Rh-alkyl species C. The resulting complex has enough nucleophilicity to attack CO_2 , giving a rhodium carboxylate complex. Finally, a transmetalation between the rhodium complex and diethylzinc to reform the $\text{Rh}^{(1)}$ -Et complex, releasing the product (**120**). Hopmann also suggested an explanation for the moderate *e.e.* observed by Mikami's group. They proposed that Rh coordinates to the aryl ring of the substrate in a η^6 fashion during CO_2 insertion (See **scheme 32**). Additionally, the study presented a unique C- CO_2 bond formation step, showing that CO_2 does not interacting with either the Rh-complex or the organozinc reagent.^[180]



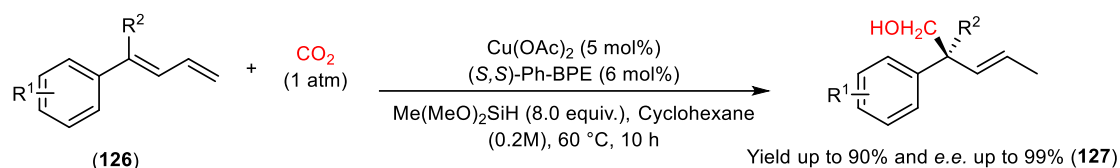
Scheme 32: Rh-catalyzed enantioselective hydrocarboxylation of acrylates (**119**) performed by Mikami and co-workers.^[179] Also shows the possible mechanism for the hydrocarboxylation of acrylates.^[180]

The year after, the group of Yu published a study on Cu-catalyzed hydroxymethylation of styrenes and 1,3-dienes (See **Scheme 33**, a and b).^[181] Their study describes a reaction including an addition of CO₂ followed by the reduction of the intermediate carboxylate. Using a chiral copper catalyst, with silanes as the reducing agent, and a base, they obtained corresponding alcohols (**123** and **125**) with excellent *e.e.* (up to 98%) and yields (up to 96%). In 2019, the reaction was extended to 1,1-disubstituted-1,3-dienes (See **Scheme 33**, b),^[182] and 1,1-disubstituted allenes (See **Scheme 33**, c),^[183] yielding chiral alcohols (**127** and **129**) with excellent *e.e.* values (up to 99%). Later in 2021, Ma and colleagues demonstrated the utility of this approach for terminal alkynes, reaching *e.e.* values up to 99%.^[184]

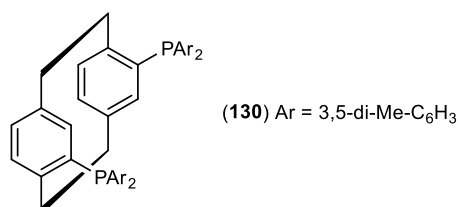
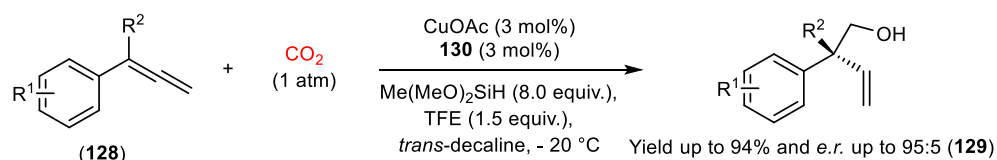
(a) Hydroxymethylation of styrenes and 1,3-dienes



(b) Hydroxymethylation of 1,1-disubstituted 1,3-dienes

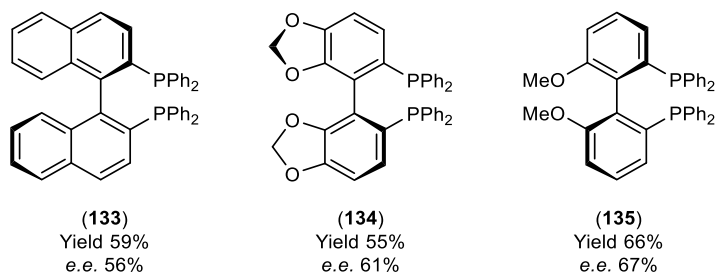
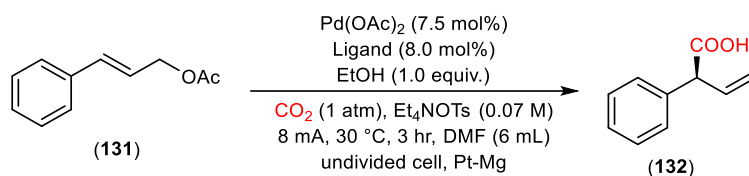


(c) Hydroxymethylation of 1,1-disubstituted allenes



Scheme 33: Enantioselective hydroxymethylation of (a) styrenes and 1,3-dienes (**122** and **124**), (b) 1,1-disubstituted 1,3-dienes (**126**) and (c) 1,1-disubstituted allenes (**128**).^[181-183]

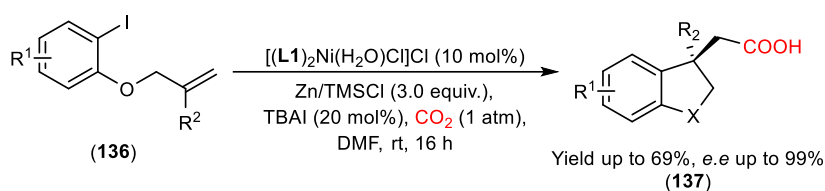
A few years later in 2018, Mei and colleagues experimented with enantioselective palladium-catalyzed reductive electrocarboxylation of allyl esters using CO₂. They raised the question if electric currents could be used for the catalytic reduction of allyl acetates (**131**). Their innovative method used chiral bidentate phosphines (**133** – **135**), Pd(OAc)₂, with Pt-Mg electrodes in an undivided cell (See **Scheme 34**).^[185] Chiral bidentate phosphines are typically inactive in the allylation of aldehydes,^[186-188] but were discovered to be efficient for catalytic conversions, including CO₂. Depending on the phosphine, they were able to obtain corresponding allyl carboxylic acid (**132**) products with a moderate *e.e.* of 56 – 67% (See **Scheme 34**).^[185]



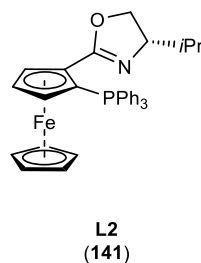
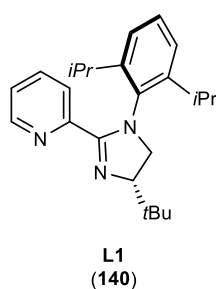
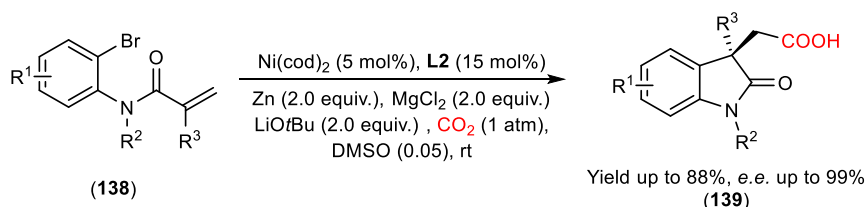
Scheme 34: Pd-catalyzed enantioselective electrocarboxylation of allylic acetates (**131**).^[185]

In 2021, the Bandini group reported an enantioselective carbocarboxylation of alkenes (**136**) with CO_2 (See **Scheme 35, a**).^[189] Their reaction was facilitated by a nickel catalyst equipped with a chiral ligand (**140**), Zn as a reductant, TMSCl and TBAI as additives. With these conditions, they obtained corresponding acids with an excellent *e.e.* of 99%. The same year, Yu's team reported a similar system based on the combination of Ni(cod)_2 with a chiral ligand (**141**), Zn as a reductant, with MgCl_2 and LiOtBu as additives (See **Scheme 35, b**).^[190] They also acquired their product with an excellent *e.e.* of 99%.

(a) Carbo-Carboxylation reported the team of Bandini

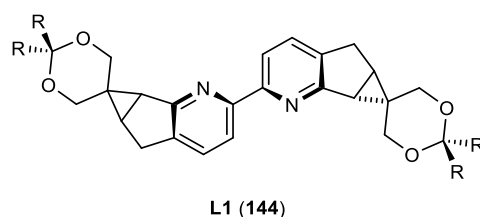
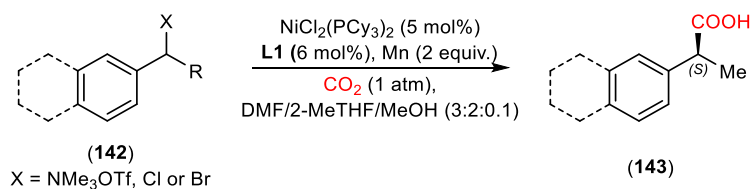


(a) Carbo-Carboxylation reported by Yu and co-workers



Scheme 35: Enantioselective carbocarboxylation reported by a) the Bandini group and b) the group of Yu.^[189,190]

In 2022, Li and co-workers (See **Scheme 36**) published a study on a nickel-catalyzed enantioconvergent carboxylation. The reaction was facilitated by $Ni(PCy_3)_2$, Mn as a reductant, and a chiral bipyridine ligand (144) in the presence of CO_2 . They were able to synthesize pharmaceuticals such as naproxen, ketoprofen, and fenoprofen in excellent *e.e.* of up to 98%. This transformation demonstrates the potential of catalytic C-C bond-forming reactions involving CO_2 to produce relevant enantiomerically pure compounds.^[191]



Scheme 36: Ni-catalyzed enantioconvergent carboxylation of benzylic(pseudo)halides (142).^[191]

3 Results and Discussion

3.1 Rh-catalyzed enantioselective hydrocarboxylation (Paper I)

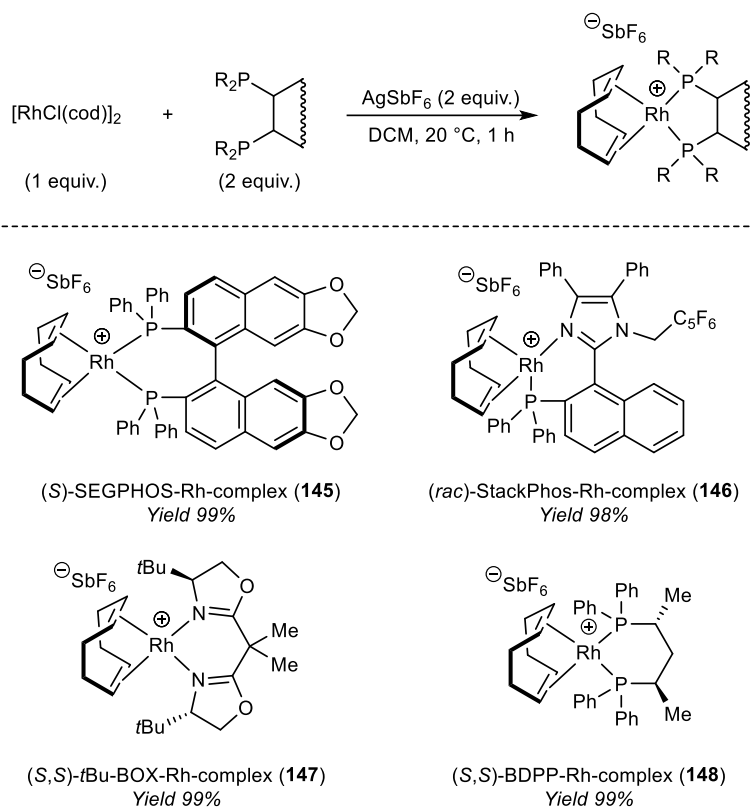
3.1.1 Introduction

To the best of my knowledge, the first hydrocarboxylation of acrylates was performed by Mikami and co-workers. They developed a hydrocarboxylation that utilized a chiral rhodium complex equipped with a chiral bidentate phosphine ligand. However, their conditions could only achieve moderate *e.e.*^[179] Shortly after the original report, our group conducted an experimental and computational study on the mechanism of the reaction.^[180] The goal of **Paper I** was gain a deeper understanding of what factors determine the enantioselectivity of the hydrocarboxylation. My task was to synthesize and determine the performance of four chiral Rh complexes, where three of them have not been studied before. The goal of my work was to experimentally validate the computational results and *e.e.* predictions. As I only carried out the experimental work, the computational results of **Paper I** will not be discussed in detail in my thesis.^[192]

3.1.2 Results and discussion

3.1.2.1 Synthesis of Rh complexes.

The synthesis for the Rh complexes **145** – **148** (See **Scheme 37**) was carried out using a slightly modified version of Mikami's procedure (See **Paper I SI**). Mikami separated AgSbF₆ and [Rh(cod)Cl]₂ in two Schlenk tubes, followed by canula addition of AgSbF₆ to [Rh(cod)Cl]₂. For the sake of ease, by combining [Rh(cod)Cl]₂ and AgSbF₆ into one round bottom flask, the canula step was avoided. The complexes **145**, **146** and **147** formed without any problem, all in quantitative yields. However, the synthesis of complex **148** was not done without a challenge. For the first attempt, a complex with two (*S,S*)-BDPP coordinated to the Rh-metal center was observed. To solve the issue of *1,5-cyclooctadiene* (cod) not coordinating to rhodium, Mikami's approach was tested (see **Paper I SI**). By first generating [Rh(cod)₂]SbF₆ in situ, followed by addition of a solution containing (*S,S*)-BDPP, complex **148** was obtained in a quantitative yield.

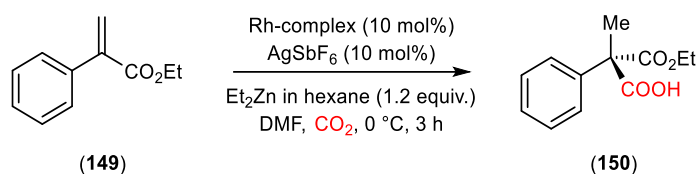


Scheme 37: General synthesis and structures of Rh complexes studied in **paper I**.^[192]

3.1.2.2 Hydrocarboxylation of model acrylate

When conducting the hydrocarboxylation of **149** with Rh complexes **145** – **148** (See **Scheme 37**), the product (**150**) was isolated in moderate to excellent yields (**Table 1**, entries 1 – 3). The corresponding experimental *e.e.* values varied from racemic to low. Comparing the experimental to the computed *e.e.*, a general trend was observed. When performing the hydrocarboxylation of **149** using complex **148**, propionic acid was the major product, and **150** was not observed. We hypothesized that the formation of the side product is a result of CO₂ inserting into the Rh-Et intermediate prior to the β-hydride elimination (See **Scheme 32, A**), leading to the release of propionic acid. The main suspicion was that the β-hydride elimination was slow, possibly due to the wide bite angle of (*S,S*)-BDPP.^[193-195] Therefore, CO₂ was introduced to the reaction while the contents of the reaction flask was under an argon atmosphere. This way, the concentration of CO₂ would be lower, and there would be time for the β-hydride elimination to occur before CO₂ could be incorporated into the Rh-complex. When applying a lower CO₂ concentration, the product (**150**) was obtained in a yield of 94% and *e.e.* of 4%.

Table 1: Hydrocarboxylation of model acrylate with tested Rh complexes, showing the obtained experimental and computational *e.e.* values for entries 1 – 4.^[192]



Entry	Rh complex	Isolated yield	<i>e.e.</i> exp. (%)	<i>e.e.</i> comp. (%)
1	(<i>S</i>)-SEGPPOS-Rh complex (145)	48 %	32.0 ^a	53.8
2	(<i>rac</i>)-StackPhos-Rh complex (146)	74 %	n.d.	47.0
3	(<i>S,S</i>)- <i>t</i> Bu-BOX-Rh complex (147)	99 %	0.0	6.4
4	(<i>S,S</i>)-BDPP-Rh complex (148)	94 %	4.0	24.3

a) Experiment reported by Mikami and colleagues to have 60% *e.e.*

While the experimental *e.e.* are low, the values were in agreement with the computationally predicted *e.e.*, and thus could be used to strengthen the computational mechanistic suggestions.

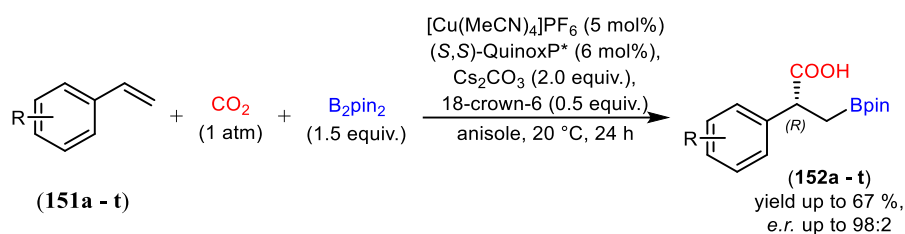
3.1.3 Conclusion paper I

Experiments using complexes **145** – **148** as catalysts revealed that all can catalyze the hydrocarboxylation, with **145**, **146**, and **147** providing good to excellent yields (74 – 99 %) for substrate **149**. The experimentally obtained *e.e.* values were used to validate and support the accuracy of the computational protocol, demonstrating the ability of DFT-D to model the enantioselective Rh-catalyzed hydrocarboxylation reactions. The joint experimental and computational results shown in **paper I**, suggest that the enantioselectivity of the hydrocarboxylation might be difficult to control.

3.2 Enantioselective Boracarboxylation (Paper II)

3.2.1 Introduction

The enantioselective boracarboxylation of styrenes have not been reported. This transformation is interesting in the sense that it gives an attractive method to produce enantioenriched pharmaceutical precursors with mild reaction conditions. Here, I present the work conducted towards an enantioselective method for the boracarboxylation of styrenes, reaching good yields and up to very good *e.r.* (See **Scheme 38**). Detailed computational studies of the reaction mechanism were also carried out, to further understand mechanistic factors determining the enantioselectivity. however, the computational results will not be further discussed in my thesis.

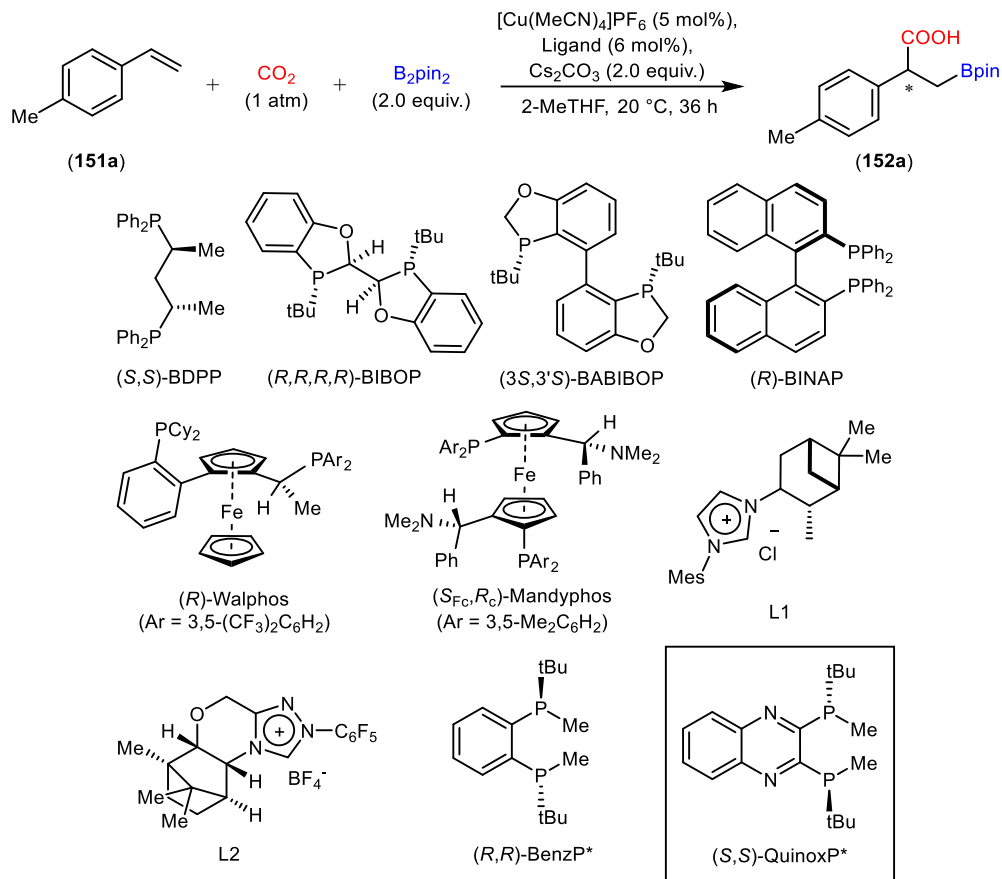


Scheme 38: Enantioselective boracarboxylation of styrenes with CO₂ presented in **paper II**.

3.2.2 Optimization of reaction conditions

My initial investigations showed that phosphine-based Cu-catalysts can be as effective as NHC-Cu-systems for regioselective boracarboxylation of styrenes (for further details, see **Paper II SI, Table S1 – S3**). Specifically, a catalytic system formed from [Cu(MeCN)₄]PF₆ and (*S,S*)-BDPP in the presence of Cs₂CO₃ as a base, and 2-MeTHF as solvent led to the formation of the boracarboxylation product of 4-methylstyrene in 84% isolated yield (See **Table 2**, entry 1).

Table 2: The performance of chiral phosphines for the borocarboxylation of 4-methylstyrene (**151a**).

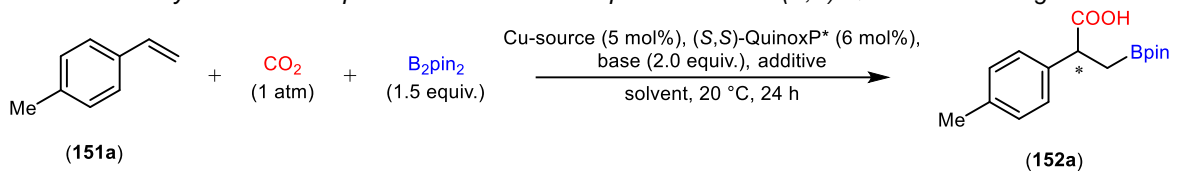


Entry	Ligand	<i>e.r.</i> ^{a)}	Isolated yield
1	(<i>S,S</i>)-BDPP	48:52	84%
2	(<i>R,R,R,R</i>)-BIBOP	43:57	46%
3	(<i>R</i>)-Walphos	39:61	44%
4	(<i>3S,3'S</i>)-BABIBOP	23:77	45%
5	(<i>R</i>)-BINAP	30:70	22%
6	(<i>SFC,RC</i>)-Mandyphos	23:77	23%
7	L1	35:65	71%
8	L2	48:52	72%
9	(<i>R,R</i>)-BenzP*	23:77	23%
10	(<i>S,S</i>)-QuinoxP*	92:8	26%

a) The *e.r.* of the product was determined by super critical fluid chromatography (SFC) with a chiral column.

Further, I examined a range of commercially available chiral ligands (See **Table 2**; for complete overview, see **Paper II SI Table S4**). The best yields were obtained with (*S,S*)-BDPP followed by the chiral phosphines (*R,R,R,R*)-BIBOP, (*R*)-Walphos and (*3S,3'S*)-BABIBOP though the enantioselectivity of the reactions was poor (44 – 46%; see **Table 2**, entries 2 – 4). (*3S,3'S*)-BABIBOP showed moderate enantioselectivity (*e.r.* 23:77), with similar *e.r.* attained for the well-established ligands (*R*)-BINAP (*e.r.* 30:70; see **Table 2**, entry 5) and (*S_{Fc},R_c*)-Mandyphos (*e.r.* 23:77; see **Table 2**, entry 6). In comparison, chiral NHC-ligands granted significantly better yields (71 – 72%), but lower selectivities (**L1** *e.r.* 35:65, **L2** *e.r.* 48:52; see **Table 2**, entries 7 and 8).^[87,88] The promising results obtained for (*3S,3'S*)-BABIBOP directed us towards extending the study to other P-chiral phosphines, such as (*R,R*)-BenzP* (See **Table 2**, entry 9) and (*S,S*)-QuinoxP* (See **Table 2**, entry 10). While both exhibited lower yields, (*S,S*)-QuinoxP* showed very good enantioselectivity, resulting in the boracarboxylation product in 92:8 *e.r.*, and we decided to optimize the reaction conditions with (*S,S*)-QuinoxP* as ligand (See **Table 3**).

The optimization of the reaction conditions for (*S,S*)-QuinoxP* was initiated with the screening of solvents (for a full overview; see **Paper II SI Table S5 – S9**). I focused mainly on ether-type solvents, as they were shown to give the best yields in the previous experiments. Nevertheless, ethers did not provide significantly better results, with a notable exception for anisole that somewhat improved the yields to 40% (See **Table 3**, entry 2), which could be increased even further to 76% by doubling the catalyst loading to 10 mol% (See **Table 3**, entry 8). The increased ligand loading decreased the *e.r.* to 84:16. Altering the base to alkoxides, such as NaOtBu (See **Table 3**, entry 4), which have been shown to work well for NHC-ligands,^[87,88] did not show improvement in yields for phosphines. Different copper sources resulted in a reduction in yields to 18 – 26% (See **Table 3**, entries 5 – 7). Advancing forward, I tested a range of additives; among these, phase transfer catalysts and weakly coordinating anions (See **Table 3**, entries 11 – 14) were included, with no observed improvement. A notable exception was 18-crown-6 ether (See **Table 3**, entry 9), which gave an improved yield from 40% to 58% at a catalyst loading of 5 mol%. In combination with the increased yield, 18-crown-6 ether also slightly improved the observed *e.r.* from 92:8 to 96:4. Increasing the catalyst loading to 10 mol% with 18-crown-6 ether as an additive did not enhance the yield further (See **Table 3**, entry 10).

Table 3: Summary of the most important results from the optimization with (*S,S*)-QuinoxP* as the ligand.

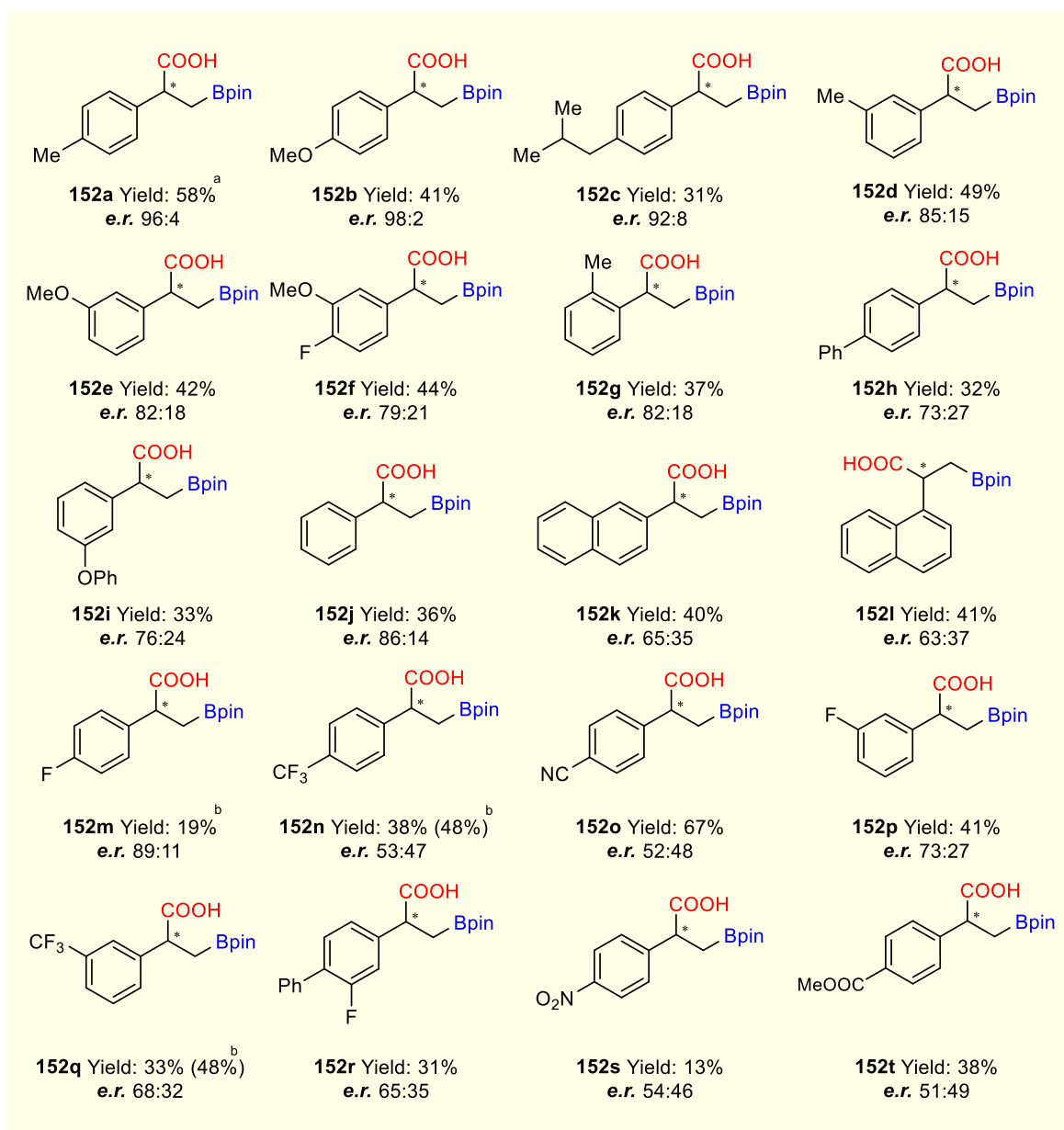
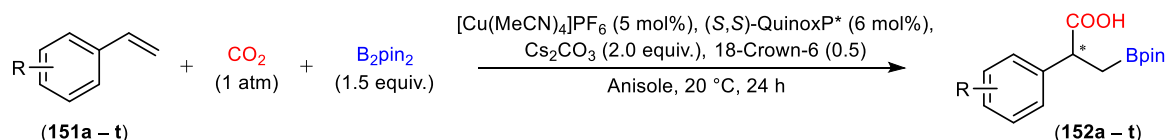
Entry	Cu-source	Base	Additive (mol%)	Solvent	<i>e.r.</i>	Yield ^{a)}
1	[Cu(MeCN) ₄]PF ₆	Cs ₂ CO ₃	-	Dioxane	n.d.	25%
2	[Cu(MeCN) ₄]PF ₆	Cs ₂ CO ₃	-	Anisole	92:8	40%
3	[Cu(MeCN) ₄]PF ₆	Cs ₂ CO ₃	-	Triglyme	n.d.	19%
4	[Cu(MeCN) ₄]PF ₆	NaOtBu	-	Anisole	n.d.	26%
5	[Cu(MeCN) ₄]BF ₄	Cs ₂ CO ₃	-	Anisole	n.d.	18%
6	[Cu(MeCN) ₄]SbF ₆	Cs ₂ CO ₃	-	Anisole	n.d.	20%
7	[Cu(MeCN) ₄]BArF	Cs ₂ CO ₃	-	Anisole	n.d.	26%
8	[Cu(MeCN) ₄]PF ₆	Cs ₂ CO ₃	-	Anisole	84:16	76% ^{b)}
9	[Cu(MeCN) ₄]PF ₆	Cs ₂ CO ₃	18-crown-6 (50)	Anisole	96:4	58% ^{c)}
10	[Cu(MeCN) ₄]PF ₆	Cs ₂ CO ₃	18-crown-6 (50)	Anisole	93:7	60% ^{b)}
11	[Cu(MeCN) ₄]PF ₆	Cs ₂ CO ₃	TBAB (50)	Anisole	95:5	42%
12	[Cu(MeCN) ₄]PF ₆	Cs ₂ CO ₃	PPh ₃ (20)	Anisole	91:9	32%
13	[Cu(MeCN) ₄]PF ₆	Cs ₂ CO ₃	monolaurin (20)	Anisole	87:13	37%
14	[Cu(MeCN) ₄]PF ₆	Cs ₂ CO ₃	palmitic acid (20)	Anisole	94:6	33%

a) Isolated yields. b) 10 mol% of Cu-source and 12 mol% of the ligand was used. c) Average yield of two experiments.

3.2.3 Substrate scope

Continuing the study, I tested the optimal conditions on a wide range of electron-rich, electron-deficient, and electron-neutral styrenes (See **Scheme 39**). Styrenes functionalized with a methyl group in the para, meta or ortho position (**151a**, **151d** and **151g**) were selectively transformed with yields ranging from 37 – 58% and *e.r.* varying from good to excellent (up to 96:4). When changing the substituent for a more electron donating group, such as methoxy (**151b** and **151e**), alkyl (**151c**) and phenoxy (**151i**), only fair yields were observed (33 – 42%). However, the products associated to the fair yields were obtained with high *e.r.* (up to 98:2 *e.r.*). Unfunctionalized styrene (**151j**) and naphthalene analogues (**151k** and **151l**) also exhibited fair yields (36 – 41%), whereas the observed *e.r.* values for these substrates had diminished (up to 86:14). Styrenes with electron-withdrawing groups including fluorine (**151m** and **151p**), trifluoromethyl (**151n** and **151q**), cyano (**151o**), nitro (**151s**) and ester (**151t**) resulted in similar yields to the electron-neutral and -rich styrenes (13 – 67%). However, the observed lower *e.r.*

in the electron-deficient systems suggest that electronic effects from the substrate could play a decisive role for the level of enantioselectivity of boracarboxylations. To further investigate this hypothesis, we decided to test two analogues of the electron-rich substrates **151e** and **151h** with a fluorine substituent (**151f** and **151r**). This led to a significant decrease in enantiomeric ratios for the products **152f** and **152r**.

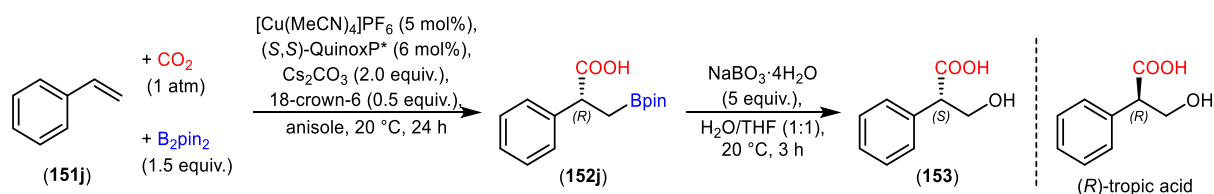


Scheme 39: The substrate scope for the enantioselective boracarboxylation of styrenes. a) Average yield of two experiments. b) Yield obtained at 5 atm of CO₂.

Also, we investigated the impact of CO₂ pressure on the enantioselectivity of the boracarboxylation. In a recent publication, the research group of Popp showed that a higher pressure of CO₂ is beneficial in terms of yield for the electron-deficient styrenes.^[88] When applying 5 atm of CO₂ pressure for the electron-deficient substrates (**151m**, **151n**, **151p** and **151q**), the observed yield increased for **152m** (from <5% to 19%), **152n** (from 38 to 48%) and **152q** (from 33 to 48%), while the *e.r.* remained unchanged.

Benzylic protons are known to be fairly acidic depending on the substituents.^[196] As the enantiomeric ratio for most of the electron deficient products were low, we were concerned the boracarboxylation product could racemize under our basic conditions. Therefore, compound **152p** and **152q**, respectively, were dissolved in anisole and left vigorously stirring in the presence of Cs₂CO₃ (2.0 equiv.), B₂pin₂ (1.5 equiv.) and CO₂. When analyzing **152p** and **152q** with SFC after 24 hours, the *e.r.* values were unchanged. However, in the presence of in presence of Cs₂CO₃ (2.0 equiv.) alone, there was notable racemization.

To determine the absolute configuration of the major enantiomer of the boracarboxylation product, we utilized sodium perborate tetrahydrate to transform **152j** to tropic acid **153** (See **Scheme 40**). The generated tropic acid was obtained in a quantitative yield, with the *e.r.* of **153** retained and shown to have the (*S*)-configuration (**Paper II SI**, Chromatogram S21). This means that the absolute configuration of the obtained boracarboxylation product is the (*R*)-configuration. Noteworthy, tropic acid is a key intermediate in asymmetric synthesis of atropine and tropicamide related alkaloids.^[197]



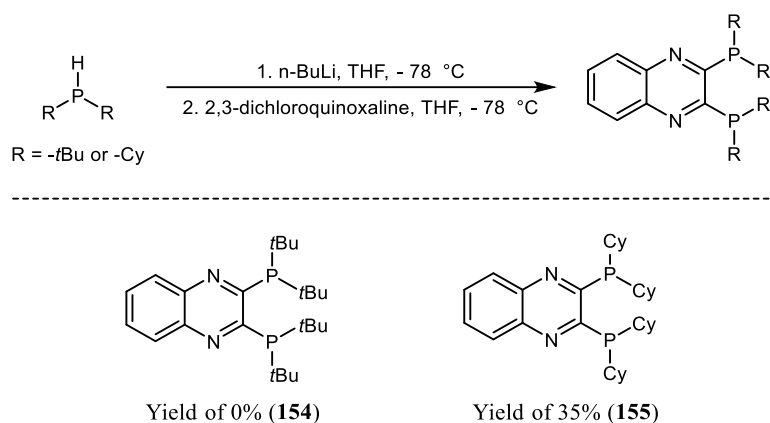
Scheme 40: Determination of the absolute configuration of the boracarboxylation product **152j** via synthesis of tropic acid.

3.2.4 Additional results not included in paper II.

3.2.4.1 Analogue of (*S,S*)-QuinoxP* for optimization of reaction conditions.

After screening multiple commercially available chiral ligands, (*S,S*)-QuinoxP* was identified as the best ligand in terms of enantioselectivity. We had some concerns about proceeding with further optimization using (*S,S*)-QuinoxP*, due to its high cost. For a cost-effective optimization, a none-chiral analogue of (*S,S*)-QuinoxP* was prepared.

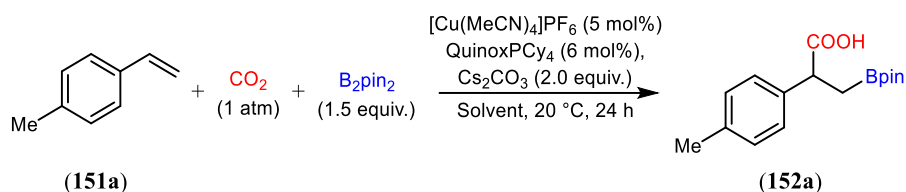
Following the general procedure reported by Yoshida and co-workers, an attempt to synthesize QuinoxPtBu₄ (**154**) and QuinoxPCy₄ (**155**) (See **Scheme 41**) was made.^[198] Firstly, the aim was to synthesize **154**; however the reaction gave 0% yield. So, I proceeded to the synthesis of **155** and obtained the ligand in a yield of 35% (462 mg).



Scheme 41: General conditions for the synthesis of the none-chiral (*S,S*)-QuinoxP* analogue **154** and **155**.^[198]

A solvent screen was performed with ligand (**155**) showing the best yields when using THF (51%) (**Table 4**, entry 1). Unfortunately, upon switching ligand **155** to (*S,S*)-QuinoxP*, the observed yield for the boracarboxylation at otherwise identical conditions (**Table 4**, entry 1) did not persist. This disappointing result prompted us to use (*S,S*)-QuinoxP* as the ligand for optimizing the enantioselective boracarboxylation.

Table 4: Screening of solvents for the boracarboxylation with the nonchiral (*S,S*)-QuinoxP* analogue QuinoxPCy₄ (**155**).



Entry	Solvent	Isolated yield
1	THF	51%
2	2-MeTHF	9%
3	Dioxane	37%
4	DME	36%
5	Eucalyptol	30%
6	Acetal	24%
7	Diglyme	29%
8	Triglyme	33%
9	Methylal	39%
10	Isosorbide	0%
11	Anisole	0%
12	DMF	22%
13	Acetonitrile	0%
14	Chloroform	12%
15	Tetraethyl Orthosilicate	0%

3.2.5 Conclusion paper II

Through optimization and testing of substrates, we have designed an enantioselective boracarboxylation including addition of CO₂ to styrenes. The developed method involves a chiral copper catalyst derived from the *P*-chiral ligand (*S,S*)-QuinoxP* and [Cu(MeCN)₄]PF₆. The method ensures high regioselectivity with yields reaching up to 58%. The enantioselectivity of the reaction is potentially influenced by the electronic structure of the styrene, with electron-rich styrenes delivering the best enantiomeric ratios. The synthetic protocol achieves *e.r.* values of up to 98:2, comparable to the highest enantioselectivities reported thus far for other CO₂-based carboxylations. The chiral β-boronated carboxylic acids synthesized in this way could potentially serve as valuable building blocks for synthesis of natural products and analogues of pharmaceutical.

3.3 Preliminary results on boracarboxylation of allenes

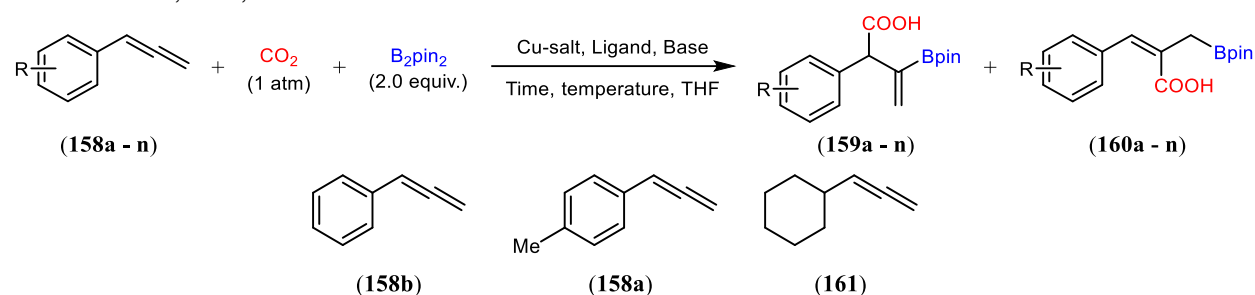
3.3.1 Introduction

During the work on the enantioselective boracarboxylation of styrenes, we became interested in expanding the boracarboxylation to other types of substrates. While alkynes and styrenes as substrates for boracarboxylation were described,^[87,135] allenes had not been reported at the time this study was conducted. However, the hydroboration of allenes, a reaction that is quite similar to the boracarboxylation in terms of reaction conditions, has been reported.^[199-203] We therefore decided to look closer at the potential boracarboxylation of allenes with CO₂.

3.3.2 Initial determination of reaction conditions

To find working reaction conditions for the boracarboxylation of allenes, we tested modified reaction conditions used for Cu-catalyzed hydroborations of allenes^[203,204] (See **Table 5**, entries 1-2), and some of the reaction conditions identified during our work with boracarboxylation of styrenes (See **Table 5**, entries 3-10). The best result was obtained using the conditions for enantioselective boracarboxylation in 2-MeTHF (See **Table 5**, entry 3). Starting with aryl allene **158a**, one major product (**159a**) with a yield of 55% was obtained. For alkyl allene **161**, the boracarboxylation resulted in a mixture of several regioisomers in 35% yield (See **Table 5**, entry 4). Using the optimal conditions for enantioselective boracarboxylation in anisole with several achiral ligands such as dcpe, dtbpf, *t*-Bu-Xantphos, PPh₃, and dppbz resulted in poor yields (0% – 25%; See **Table 5**, entries 5 – 10). We therefore decided to focus the further optimization on aryl allenes using a catalytic system based on Cu(MeCN)₄PF₆ and (*S,S*)-BDPP.

Table 5: The performance of selected test reaction conditions and chosen test substrates for the boracarboxylation of allenes **157b**, **157a**, and **160**.



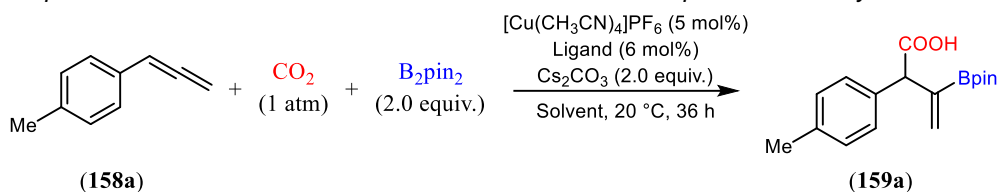
Entry	Substrate	Catalyst (mol%)	Ligand (mol%)	Base (equiv.)	Solvent	°C/h	Yield
1	158b	CuI (5)	ICy HCl (6)	NaOtBu (2.0)	THF	20/24	0%
2	158b	CuI (5)	IPr HCl (6)	NaOtBu (2.0)	THF	20/24	0%
3	158a	Cu(MeCN) ₄ PF ₆ (5)	(<i>S,S</i>)-BDPP (6)	Cs ₂ CO ₃ (2.0)	2-MeTHF	20/36	55% ^a
4	161	Cu(MeCN) ₄ PF ₆ (5)	(<i>S,S</i>)-BDPP (6)	Cs ₂ CO ₃ (2.0)	2-MeTHF	20/36	35% ^b
5	158a	Cu(MeCN) ₄ PF ₆ (5)	dcpe	Cs ₂ CO ₃ (2.0)	Anisole	20/36	10%
6	158a	Cu(MeCN) ₄ PF ₆ (5)	dtbpf	Cs ₂ CO ₃ (2.0)	Anisole	20/36	0%
7	158a	Cu(MeCN) ₄ PF ₆ (5)	<i>t</i> -Bu-Xantphos	Cs ₂ CO ₃ (2.0)	Anisole	20/36	0%
8	158a	Cu(MeCN) ₄ PF ₆ (5)	ICy HCl	Cs ₂ CO ₃ (2.0)	Anisole	20/36	10%
9	158a	Cu(MeCN) ₄ PF ₆ (5)	PPh ₃	Cs ₂ CO ₃ (2.0)	Anisole	20/36	27% ^c
10	158a	Cu(MeCN) ₄ PF ₆ (5)	dppbz	Cs ₂ CO ₃ (2.0)	Anisole	20/36	25%

a) Resulted in one major product (**159a**), b) Product resulted in complex mixture of regioisomers c) For this experiment 12 mol% of PPh₃ was used.

3.3.3 First optimization attempt for the boracarboxylation of allenes.

Screening of solvents (See **Table 6**, entries 1 – 12) pointed at DME as a good solvent with 74% yields (See **Table 6**, entry 4). Next, achiral phosphine ligands were tested (See **Table 6**, entries 13 – 15) and we were pleased to see that dppbz provided the corresponding acid in 89% yield (See **Table 6**, entry 15). The first goal for this project was to develop a boracarboxylation of allenes not focusing particularly on enantioselectivity. However, a control experiment without ligand (See **Table 6**, entry 16) showed that the ligand was essential for product formation, a prerequisite for the future development of an enantioselective method.

Table 6: The performance of selected reaction conditions for the 1st attempt to boracarboxylate allenes.



Entry	Ligand (mol%)	Solvent	Isolated yield
1	(<i>S,S</i>)-BDPP	THF	40%
2	(<i>S,S</i>)-BDPP	2-MeTHF	55%
3	(<i>S,S</i>)-BDPP	Dioxane	46%
4	(<i>S,S</i>)-BDPP	DME	74% ^a
5	(<i>S,S</i>)-BDPP	Eucalyptol	12%
6	(<i>S,S</i>)-BDPP	Acetal	31%
7	(<i>S,S</i>)-BDPP	Diglyme	30%
8	(<i>S,S</i>)-BDPP	Methylal	46%
9	(<i>S,S</i>)-BDPP	Anisole	25%
10	(<i>S,S</i>)-BDPP	DMF	54%
11	(<i>S,S</i>)-BDPP	Toluene	0%
12	(<i>S,S</i>)-BDPP	DME	71% ^b
13	dppp	DME	43%
14	PPh ₃	DME	49% ^c
15	dppbz	DME	89% ^a
16	None	DME	0%

a) Average yield from two experiments. b) For this experiment 10 mol% of the copper salt and 12 mol% of the ligand was used. c) For this experiment 12 mol% of PPh₃ was used.

With satisfying conditions using $[\text{Cu}(\text{CH}_3\text{CN})]\text{PF}_6$ (5 mol%), dppbz (6 mol%), Cs_2CO_3 (2.0 equiv.), and DME (See **Table 6**, entry 15) in hand, we planned to investigate the substrate scope of the reaction (See **Figure 7**). When conducting experiments for substrate **158b** – **158d** (See **Figure 7**), a significant drop in reaction yields was observed. Alarmed by the sudden low yields the optimized reaction with **158a** was re-examined (See **Table 6**, entry 15). The yield was not reproducible and had dropped from 89 to 5%. The same result was found when re-examining the experiments described in **Table 6**, entries 4 and 12 giving 74% and 71% yield.

Several reagents were identified as potential sources for the reproducibility problems: new batches of $[\text{Cu}(\text{CH}_3\text{CN})_4]\text{PF}_6$, B_2pin_2 , dppbz and Cs_2CO_3 were used in the low-yielding reactions. To rule out that we used reagents of bad quality, new reagents ($[\text{Cu}(\text{CH}_3\text{CN})]\text{PF}_6$ from TCI and Sigma Aldrich), Cs_2CO_3 (>99.9% purity from Sigma Aldrich), dppbz (from Sigma Aldrich) were tested. We also tested solvents of different quality (DME both anhydrous

>99.5% inhibitor-free and reagent plus >99% from Sigma Aldrich) to make sure that the solvent did not contain an unidentified component, which negatively impacts the yields. None of these reactions were successful. Currently, our working hypothesis is that either one of the reagents used during optimization contained an impurity crucial for optimal reaction yields. Unfortunately, we did not have the batch information for the previous chemicals, therefore pursuing new optimized conditions seemed more productive than identifying the missing component.

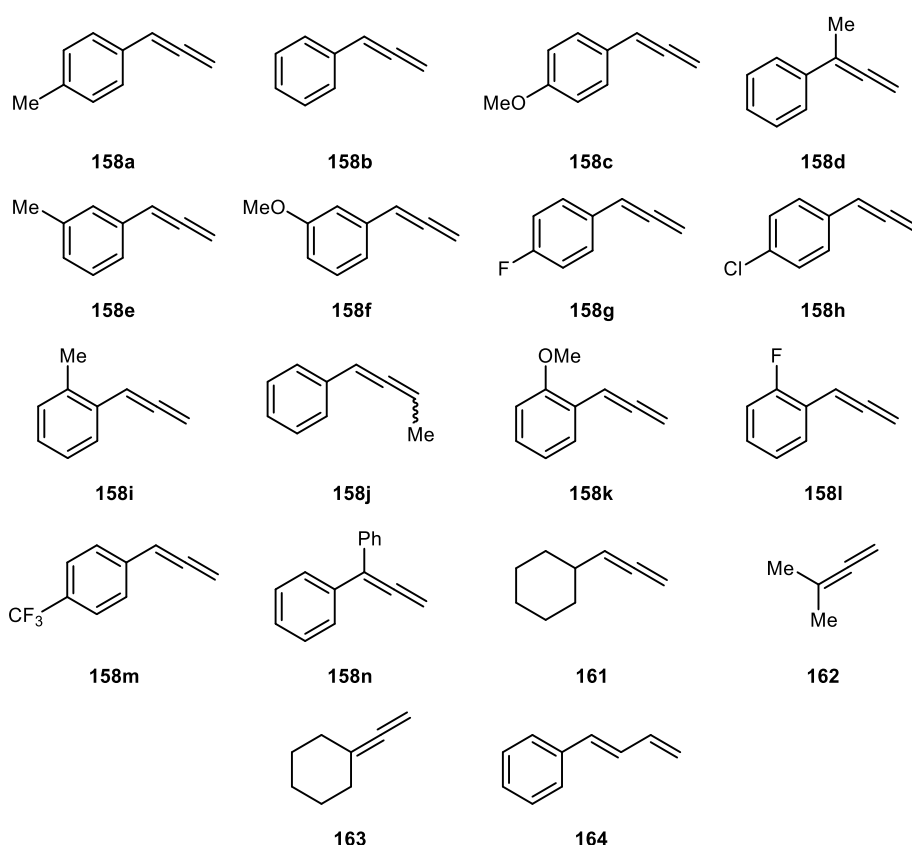


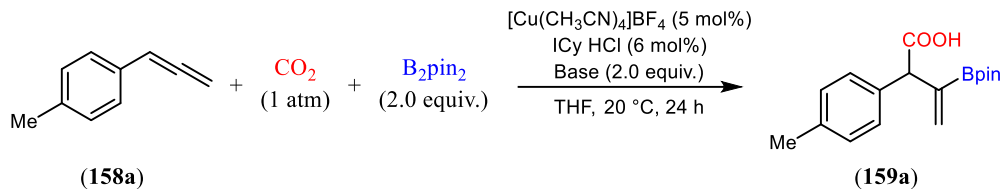
Figure 7: Planned substrate scope for the boracarboxylation of allenes.

3.3.4 Second optimization attempt for boracarboxylation of allenes.

Starting over again, the decision to change the Cu-salt to $[\text{Cu}(\text{CH}_3\text{CN})]\text{BF}_4$, which showed promise in our previous optimization with styrenes using (*S,S*)-BDPP. The ligand and solvent were changed to ICy HCl and THF, based on their promising results in boracarboxylation of styrenes.^[87,88] The reaction time was shortened from 36 to 24 hours for time conservation and yields were recorded with quantitative NMR analysis. Starting with the screening of bases, common alkoxides proved to be ineffective, resulting in 0 – 3% yield (See **Table 4**, entries 1 –

3). The best base for the new screening was Cs₂CO₃ (See **Table 4**, entry 4), and additional analysis of CsF and TEA did not result in further improvement (See **Table 4**, entries 5 and 6).

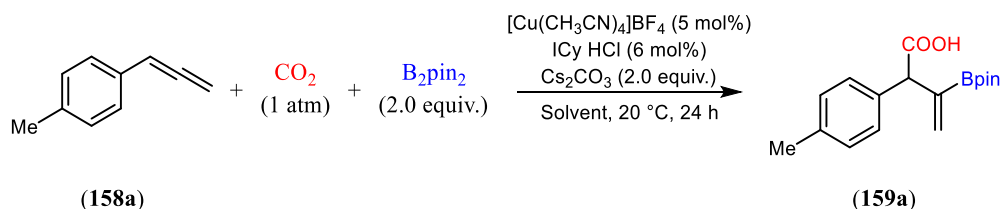
Table 4: Tested bases for the second attempt to optimize for the boracarboxylation of allenes.



Entry	Base (2.0 equiv.)	NMR yield
1	NaOtBu	3%
2	KOtBu	0%
3	LiOMe	0%
4	Cs ₂ CO ₃	30%
5	CsF	3%
6	TEA	0%

Further solvent screening of ethers and more polar solvents gave yields ranging from 6 – 31% (See **Table 5**, entries 1 – 6). Here among others I examined different solvent mixtures and was pleased to find that a mixture of DME and DMF (4:1) resulted in a higher yield of 32% (See **Table 5**, entry 7).

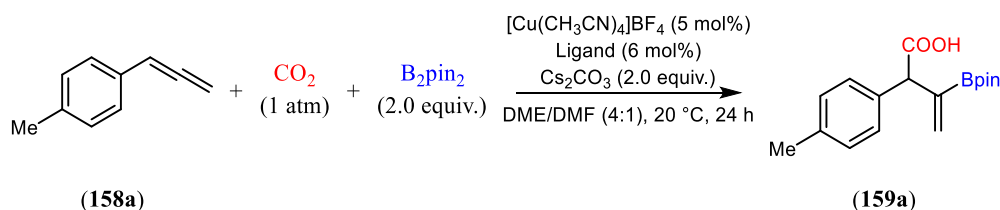
Table 5: Screening of solvents for the 2nd attempt to optimize the boracarboxylation of allenes.



Entry	Solvent	NMR yield
1	THF	31%
2	2-MeTHF	15%
3	Dioxane	18%
4	DME	31%
5	Anisole	6%
6	DMF	29%
7	DME/DMF (4:1)	32%
8	DME/Dioxane (1:1)	26%
9	DME/MeCN (4:1)	5%
10	DME/Toluene (4:1)	31%

Screening of ligands revealed that phosphine ligands, which performed well in the previous optimization, resulted in very poor yields of 0 – 7% (See **Table 6**, entries 2 – 9). NHC ligands were a better choice, with SIMes HCl providing the product in 46% yield (See **Table 6**, entry 12). More carbene ligands were therefore tested after the optimization of the Cu-source but did not result in further reaction improvement (See **Table 6**, entries 12 – 15).

Table 6: Screening of selected ligands for the second optimization.

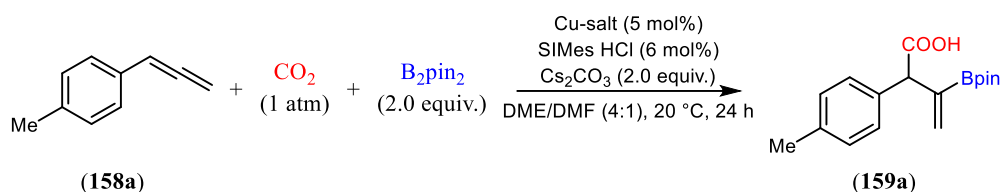


Entry	Ligand (6 mol%)	NMR yield
1	ICy HCl	31%
2	PPh ₃ (12 mol%)	5%
3	Xphos (12 mol%)	7%
4	XantPhos	4%
5	Cy ₃ PHBF ₄ (12 mol%)	0%
6	dppbz	0%
7	BINAP(rac)	0%
8	dppp	0%
9	dppe	0%
10	SIMes HCl	46%
11	IPr HCl	0%
12	IMes HCl	42% ^a
13	SIPr HCl	0% ^a
14	SIMes BF ₄	40% ^a
15	SIPr BF ₄	0% ^a
16	SIMes HCl (12 mol%)	43%

a) The reaction was conducted with CuCl as the Cu-salt in 5 mol%

Both gold and silver catalysts have been described for hydroboration,^[205,206] and can form similar NHC-complexes to copper.^[207,208] However, silver or gold salts (AgSbF₆ and (CH₃)₂SAuCl) (See **Table 7**, entries 1 and 2) as catalyst precursors were not successful. Copper halides provided the best yields, ranging from 35 – 54% (See **Table 7**, entries 3 – 5). Further testing of other copper sources did not lead to further improvement of the reaction.

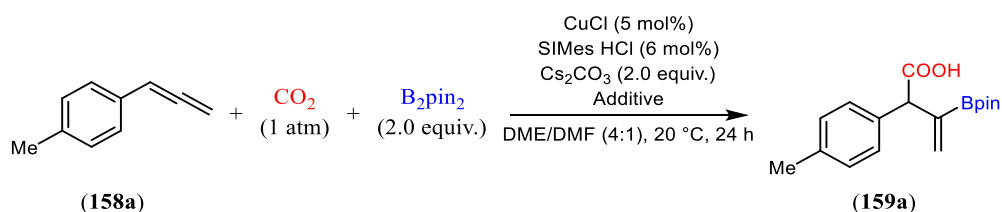
Table 7: Screening of different Cu-sources including a silver and a gold complex for the boracarboxylation of allenes.



Entry	Cu-salt (5 mol%)	NMR yield
1	AgSbF ₆	0%
2	(CH ₃) ₂ SAuCl	0%
3	CuCl	54%
4	CuBr	45%
5	CuI	35%
6	[Cu(COD)Cl] ₂	23%
7	Cu(MeCN) ₄ PF ₆	36%
8	Mesitylcopper(I)	20%

For now, due to time constraints resulting from the new optimization and writing this thesis, only five additives for the boracarboxylation of allenes have been tested (See **Table 8**, entries 1 – 5); however, no further improvement in yield was observed.

Table 8: Selected additives for testing for the boracarboxylation of allenes.



Entry	Additive	NMR yield
1	Phenylalanine (20 mol%)	36%
2	Pyridine (20 mol%)	49%
3	PPh ₃ (12 mol%)	41%
4	Cy ₃ PHBF ₄ (12 mol%)	28%
5	XantPhos (6 mol%)	0%

3.3.5 Conclusion for boracarboxylation of allenes

In conclusion, the study aimed to explore boracarboxylation of allenes, a substrate that has previously unexplored for this reaction. Initially, we were able to identify promising conditions including, [Cu(CH₃CN)]PF₆ (5 mol%), dppbz (6 mol%), Cs₂CO₃ (2.0 equiv.), B₂pin₂ (2.0 equiv.), and DME as the solvent, resulting in 89% yield. Unfortunately, we were not able to reproduce these results over time. We hypothesize that this relates to changes in the quality of

the used reagents or solvents. A second attempt to optimize the reaction conditions resulted in the best boracarboxylation of allene **158a** in 54% yield using CuCl (5 mol%), SIMes HCl (6 mol%), B₂pin₂ (2.0 equiv.), Cs₂CO₃ (2.0 equiv.), DME:DMF (4:1) as the solvent.

In summary, the study illustrates the challenges in achieving consistent boracarboxylation of allenes. As of now, due to complications related to the reproducibility of the first developed conditions, the project has halted in favor of writing this thesis. Despite the obstacles, the boracarboxylation of allenes is possible to develop and this study has laid the groundwork for future exploration of the reaction.

4 Conclusion and Outlook

In this thesis I successfully developed and broadened the scope of available enantioselective C-C bond forming reactions utilizing CO₂.

I supported the mechanistic studies conducted within our group with experimental studies. Three new chiral Rh-complexes were synthesized (**145** – **148**) and tested as catalyst in the enantioselective hydrocarboxylation of the model acrylate (**149**). The experimental *e.e.* was used to verify the accuracy of the computational protocol and was in agreement with the *e.e.* predicted computationally. This joint computational and experimental study strengthens understanding of the mechanism of the enantioselective hydrocarboxylation reported by Mikami and co-workers.

An enantioselective method for the boracarboxylation of styrenes using CO₂ was developed. We were able to obtain the boracarboxylation products of electron-rich styrenes with very good *e.r.* values (up to 98:2). In addition, we found the absolute configuration of the boracarboxylation product with (*S,S*)-QuinoxP* as the ligand to be the (*R*)-enantiomer. We also extended the boracarboxylation to include five new styrenes.

A study to extend the boracarboxylation to allenes and other related unsaturated systems has started. Despite the challenges related to reproducibility of the reaction yields, a solid groundwork for the continuation of the investigation has been laid. Currently, we can reach yields of 54% with the optimization substrate (**158a**) and obtain one major product (**159a**) with excellent regioselectivity. As of now, the goal to develop an enantioselective method for boracarboxylation of allenes was not reached, primarily due to complications with reproducibility.

Future work should include the development of a new catalytic system, allowing for the enantioselective boracarboxylation for electron-poor substrates. Also, expansion of the strategy to other substrate types, such as stilbenes, 1,3-dienes and imines is an interesting topic to address in the future. Additionally, exploration of applications for the chiral boracarboxylation products, in the form of natural products or pharmaceuticals, such as β -amino acids and atropine and tropicamide related alkaloids.

I believe this thesis contributes to advancing synthetic methodologies and enhancing our fundamental understanding of catalytic processes, including C-C bond formation with CO₂. As we move forward, the exploration of new catalytic systems for C-C bond-forming reactions using CO₂ will remain important. The challenges encountered also present an exciting opportunity for future studies.

5 Experimental Details

This chapter includes experimental details not included in the manuscript for paper II and the experimental procedures and analytical data for the boracarboxylation of allenes.

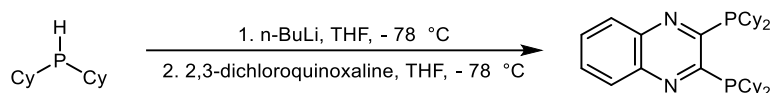
5.1 General methods

Commercially available starting materials, reagents, catalysts, ligands, solvents, and anhydrous solvents were used without further purification. Non-anhydrous solvents were dried using activated 4Å molecular sieves. Flash column chromatography was performed with Merck silica gel 60 (230-400 mesh). Thin layer chromatography was carried out using Merck TLC Silica gel 60 F254 and visualized by short-wavelength ultraviolet light. ^1H , ^{13}C and ^{19}F NMR spectra were recorded on a Bruker Avance 400 MHz at 20 °C. All ^1H NMR spectra were reported in parts per million (ppm) downfield of TMS and were measured relative to the signals for residual CHCl_3 (7.26 ppm). All ^{13}C NMR spectra were reported in ppm relative to residual CDCl_3 (77.20 ppm) and were obtained with ^1H decoupling. Coupling constants, J , were reported in Hertz (Hz).

5.2 General procedures

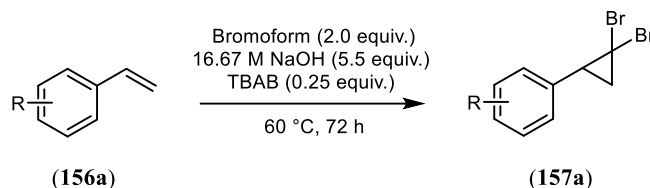
5.2.1 General procedure for the synthesis of QuinoxPCy₄

5.2.1.1 2,3-bis(dicyclohexylphosphaneyl)quinoxaline (155).^[209]



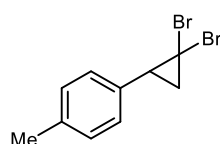
In a glove box, a 100 mL round bottom flask was charged with dicyclohexylphosphine (2.20 equiv.) and sealed using a rubber septa and electrical tape. In sequence, another 100 mL round bottom flask was charged with 2,3-dichloroquinoxaline (1 equiv.) and sealed with a rubber septa and electrical tape. To both round bottom flasks 10 mL of dry THF were added via a 20 mL syringe. The round bottom flask containing the phosphine was then put on a cold bath and cooled down to -78 °C. When the desired temperature of -78 °C was reached, *n*-BuLi (2.5 M, 2.1 equiv.) was slowly dripped via a 20 mL syringe to round bottom flask containing the phosphine. The reaction mixture was then allowed to stir at -78 °C for 1h before being warmed up to room temperature. Next, the reaction mixture was again cooled down to -78 °C and the mixture containing the 2,3-dichloroquinoxaline was transferred via a 20 mL syringe and slowly dropped to the reaction mixture containing the phosphine. After addition, the reaction mixture was then stirred for 4h at -78 °C, followed by letting the mixture slowly warm up to room temperature. Further, the mixture was quenched using 20mL of water and then extracted with Heptane (3 x 30mL). The organic extract was then washed with 20 mL of water and transferred to a 500mL round bottom flask and added 5g of silica gel. The heptane was then evaporated, and the product was purified using column chromatography (1 part DCM : 3 parts heptane). the fractions containing the product were combined and evaporated to dryness yielding 462 mg or an orange powder (yield 35%). ¹H NMR (400 MHz, CDCl₃) δ 8.13 – 8.01 (m, 2H), 7.75 – 7.64 (m, 2H), 2.42 – 2.28 (m, 4H), 2.01 – 1.90 (m, 4H), 1.80 – 1.70 (m, 10H), 1.66 – 1.58 (m, 12H), 1.35 – 1.08 (m, 29H). ¹³C NMR (101 MHz, CDCl₃) δ 166.1 – 165.9 (m), 141.1, 129.5 (d, *J* = 32.1 Hz), 34.6 (t, *J* = 4.6 Hz), 33.2 (d, *J* = 4.1 Hz), 32.3 (d, *J* = 18.3 Hz), 30.4, 30.1 (t, *J* = 5.7 Hz), 29.9 (t, *J* = 7.0 Hz), 29.8, 29.7, 27.43 (q, *J* = 5.4 Hz), 27.3, 27.2, 27.1, 26.6, 26.4. ³¹P NMR (162 MHz, CDCl₃) δ -5.48.

5.2.2 General procedure A for the synthesis of 1,1-dibromocyclopropanes



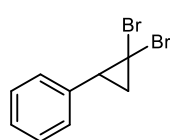
Tetrabutylammonium bromide (0.25 equiv.) and a stirring bar was added to a 100mL round bottom flask. The flask was then sealed with a rubber septum and an electric tape. Then styrene (1 equiv.) and bromoform (2.0 equiv.) were transferred to the flask via syringe. A solution of 16.7 M sodium hydroxide in water (5.5 equiv.) was then slowly added using a syringe while stirring at 50 °C. The mixture was then left stirring for 3 days at 60 °C. After, the reaction was quenched by the addition of 6 M HCl solution (40 mL). The aqueous mixture was then extracted with diethyl ether (3 x 50 mL). The combined organic extracts were washed with 6M HCl solution (50 mL), then saturated sodium bicarbonate solution (50 mL) and finally with distilled water (50 mL). The organic solvent was then removed using a rotary evaporator. The leftover brown organic residue was then purified using silica gel column chromatography (eluent was mixture of heptane and ethyl acetate). For some systems we removed the leftover styrene using evaporation with azeotrope of water.

5.2.2.1 1-(2,2-dibromocyclopropyl)-4-methylbenzene, (157a).^[210]



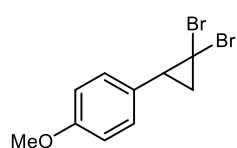
Following the general procedure A, **156a** (5.909 g, 50 mmol) was transformed to the target compound **157a** (4.789 g, 16.514 mmol) as a colorless oil in 33% yield. ¹H NMR (400 MHz, CDCl₃) δ 7.23 – 7.13 (m, 4H), 2.94 (dd, *J* = 10.5, 8.3 Hz, 1H), 2.38 (s, 3H), 2.13 (t, *J* = 10.5, 7.6 Hz, 1H), 2.00 (t, *J* = 9.0, 7.1 Hz, 1H). ¹³C NMR (101 MHz, CDCl₃) δ 137.5, 133.1, 129.1, 128.9, 35.8, 29.0, 27.3, 21.4, 21.3.

5.2.2.2 (2,2-dibromocyclopropyl)benzene, (157b).^[210]



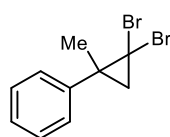
Following the general procedure A, **156b** (2.600 g, 25 mmol) was transformed to the target compound **157b** (0.808 g, 2.928 mmol), as a colorless oil in 12% yield. ¹H NMR (400 MHz, CDCl₃) δ 7.41 – 7.24 (m, 5H), 2.98 (dd, *J* = 10.5, 8.3 Hz, 1H), 2.15 (dd, *J* = 10.5, 7.8 Hz, 1H), 2.03 (t, *J* = 8.0 Hz, 1H). ¹³C NMR (101 MHz, CDCl₃) δ 136.1, 129.0, 128.4, 127.8, 36.1, 28.6, 27.3.

5.2.2.3 1-(2,2-dibromocyclopropyl)-4-methoxybenzene, (157c).^[210]



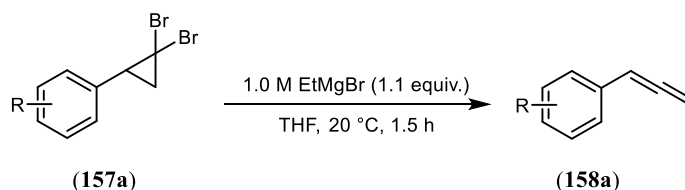
Following the general procedure **A**, **156c** (3.350 g, 25 mmol) was transformed to the target compound **157c** (3.071 g, 10.036 mmol), as a yellow oil in 40% yield. ¹H NMR (400 MHz, CDCl₃) δ 7.23 – 7.14 (m, 2H), 6.94 – 6.86 (m, 2H), 3.82 (s, 3H), 2.91 (dd, *J* = 10.8, 8.1 Hz, 1H), 2.11 (dd, *J* = 10.6, 7.7 Hz, 1H), 1.96 (t, *J* = 8.0 Hz, 1H). ¹³C NMR (101 MHz, CDCl₃) δ 159.1, 130.1, 128.3, 113.8, 55.4, 35.4, 29.4, 27.4.

5.2.2.4 (2,2-dibromo-1-methylcyclopropyl)benzene, (157d).^[211]



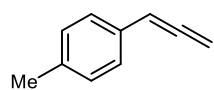
Following the general procedure **A**, **156d** (2.950 g, 25 mmol) was transformed to the target compound **157d** (3.083 g, 10.631 mmol), as a white solid in 43% yield. ¹H NMR (400 MHz, CDCl₃) δ 7.40 – 7.27 (m, 5H), 2.17 (d, *J* = 7.5 Hz, 1H), 1.79 (d, *J* = 7.6 Hz, 1H), 1.72 (s, 3H). ¹³C NMR (101 MHz, CDCl₃) δ 142.5, 128.6, 128.5, 127.4, 36.9, 35.9, 33.8, 27.9.

5.2.3 General procedure B for the synthesis of allenes



To a vigorously stirred solution of a 1,1-dibromocyclopropane in dry THF (40 mL), EtMgBr (1.1 equiv, 1 M solution in THF) was added at 20 °C. The reaction mixture was stirred at room temperature for 1.5 h. Afterwards, the reaction mixture was quenched by adding saturated aq. NH₄Cl solution (20 mL) followed by extraction with Et₂O (3 x 30 mL). The combined organic fractions were dried by filtering through a silica plug and concentrated on a rotary evaporator to give the corresponding allene.

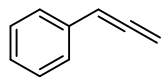
5.2.3.1 1-methyl-4-(propa-1,2-dien-1-yl)benzene (158a).^[210]



Following the general procedure **B**, **157a** (4.785 g, 16.500 mmol) was transformed to the target compound **158a** (2.140 g, 16.438 mmol), as a yellow oil in 99% yield. ¹H NMR (400 MHz, CDCl₃) δ 7.24 (d, *J* = 8.2 Hz, 2H), 7.16 (d, *J* =

8.0 Hz, 2H), 6.19 (t, $J = 6.8$ Hz, 1H), 5.17 (d, $J = 6.8$ Hz, 2H), 2.38 (s, 3H). ^{13}C NMR (101 MHz, CDCl_3) δ 209.7, 136.7, 131.0, 129.5, 126.7, 93.9, 78.8, 21.3.

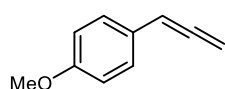
5.2.3.2 propa-1,2-dien-1-ylbenzene, (158b).^[210]



Following the general procedure **B**, **157b** (0.808 g, 2.928 mmol) was transformed to the target compound **158b** (0.253 g, 2.178 mmol), as a yellow oil in 74% yield.

^1H NMR (400 MHz, CDCl_3) δ 7.27 – 7.07 (m, 5H), 6.08 (t, $J = 6.8$ Hz, 1H), 5.06 (d, $J = 6.8$ Hz, 2H). ^{13}C NMR (101 MHz, CDCl_3) δ 209.9, 134.0, 128.7, 127.0, 126.8, 94.1, 78.9.

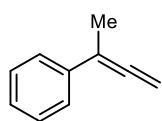
5.2.3.3 1-methoxy-4-(propa-1,2-dien-1-yl)benzene, (158c).^[210]



Following the general procedure **B**, **157c** (3.071 g, 10.036 mmol) was transformed to the target compound **158c** (1.284 g, 8.783 mmol), as a brown oil in 86% yield.

^1H NMR (400 MHz, CDCl_3) δ 7.27 – 7.20 (m, 2H), 6.90 – 6.82 (m, 2H), 6.14 (t, $J = 6.8$ Hz, 1H), 5.13 (d, $J = 6.8$ Hz, 2H), 3.81 (s, 3H). ^{13}C NMR (101 MHz, CDCl_3) δ 209.4, 158.7, 127.8, 126.1, 114.2, 93.4, 78.8, 55.3.

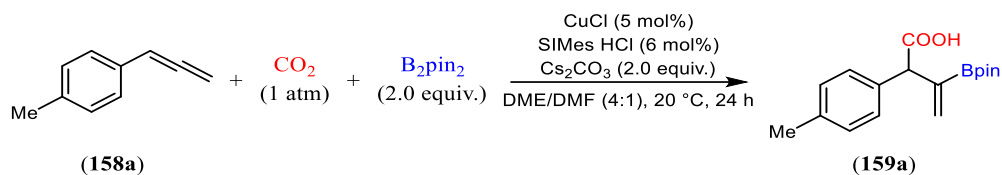
5.2.3.4 buta-2,3-dien-2-ylbenzene, (158d).^[212]



Following the general procedure **B**, **157d** (3.083 g, 10.631 mmol) was transformed to the target compound **158d** (1.237 g, 9.502 mmol), as a yellow oil in 99% yield.

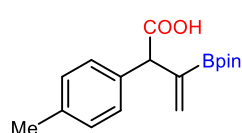
^1H NMR (400 MHz, CDCl_3) δ 7.47 – 7.18 (m, 5H), 5.04 (q, $J = 3.2$ Hz, 2H), 2.12 (t, $J = 3.2$ Hz, 3H). ^{13}C NMR (101 MHz, CDCl_3) δ 209.1, 136.8, 128.5, 126.7, 125.8, 99.9, 77.0, 16.8.

5.2.4 General procedure C for borocarboxylation of allenes



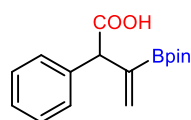
An oven dried 100 mL round bottom flask equipped with a stirring bar was introduced to the glove box. The round bottom flask was charged with B_2pin_2 (2 equiv.), base (2.0 equiv.), ligand (6 mol%) and Cu-salt (5 mol%), closed with a septum and sealed tight using electric tape. The round bottom flask was then evacuated, and a CO_2 atmosphere was applied. Solvent (20 mL) was added, and the mixture was left stirring for 30 minutes. Then, allene (1 equiv.) was added via a syringe, and a balloon filled with dry CO_2 was attached to the flask. The reaction mixture was left stirring for 24 hours at 20 °C. Afterwards, the flask was opened to air and diluted with Et_2O (20 mL). The organic mixture was extracted using aq. saturated Na_2CO_3 (3 x 30 mL). The combined aq. phases were slowly acidified with aq. 6M HCl (60 mL) and extracted using Et_2O (3 x 30 mL). The combined organic fractions were washed using distilled water (30 mL) and evaporated to dryness to give the product.

5.2.4.1 3-(4,4,5,5-tetramethyl-1,3,2-dioxaborolan-2-yl)-2-(p-tolyl)but-3-enoic acid (159a).



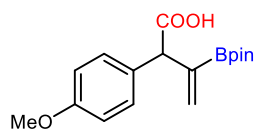
Following the general procedure C, **158a** (0.150 g, 1.152 mmol) was transformed to the target compound **159a** (0.311 g, 1.029 mmol), as a faint yellow oil in 89% yield. $^1\text{H NMR}$ (400 MHz, CDCl_3) δ 7.20 – 7.11 (m, 4H), 6.04 – 5.95 (m, 1H), 5.51 – 5.41 (m, 1H), 4.62 – 4.52 (m, 1H), 2.34 (s, 3H), 1.23 (d, $J = 3.0$ Hz, 12H). $^{13}\text{C NMR}$ (101 MHz, CDCl_3) δ 179.4, 137.0, 133.8, 130.8, 129.2, 129.2, 84.0, 55.3, 24.7, 24.5, 21.2. **HRMS** calculated m/z for $[\text{C}_{17}\text{H}_{22}\text{BO}_4]^-$: 301.1606, found 301.1617.

5.2.4.2 2-phenyl-3-(4,4,5,5-tetramethyl-1,3,2-dioxaborolan-2-yl)but-3-enoic acid (159b).



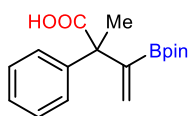
Following the general procedure C, **158b** (0.134 g, 1.152 mmol) was transformed to the target compound **159b** (0.190 g, 0.6594 mmol), as a faint orange oil in 57% yield (crude). $^1\text{H NMR}$ (400 MHz, CDCl_3) δ 7.31 – 7.24 (m, 5H), 6.02 – 5.97 (m, 1H), 5.49 – 5.44 (m, 1H), 4.62 – 4.56 (m, 1H), 1.21 (d, $J = 4.4$ Hz, 12H). $^{13}\text{C NMR}$ (101 MHz, CDCl_3) δ 178.8, 144.9, 136.9, 130.9, 129.4, 128.6, 127.4, 84.1, 55.7, 24.6. **HRMS** calculated m/z for $[\text{C}_{16}\text{H}_{20}\text{BO}_4]^-$: 287.1449, found 287.1461.

5.2.4.3 2-(4-methoxyphenyl)-3-(4,4,5,5-tetramethyl-1,3,2-dioxaborolan-2-yl)but-3-enoic acid (159c).



Following the general procedure **C**, **158c** (0.168 g, 1.149 mmol) was transformed to the target compound **159c** (0.03 g, 0.0920 mmol), as a brown oil in 8% yield (crude). **¹H NMR** (400 MHz, CDCl₃) δ 7.21 – 7.16 (m, 2H), 6.88 – 6.82 (m, 2H), 5.99 – 5.93 (m, 1H), 5.50 – 5.45 (m, 1H), 4.56 – 4.50 (m, 1H), 3.78 (s, 3H), 1.23 (s, 12H). **¹³C NMR** (101 MHz, CDCl₃) δ 178.5, 158.9, 131.4, 130.6, 130.4, 129.1, 114.0, 114.0, 84.0, 55.3, 24.6. **HRMS** calculated m/z for [C₁₇H₂₂BO₅]⁻: 317.1555, found 317.1556.

5.2.4.4 2-methyl-2-phenyl-3-(4,4,5,5-tetramethyl-1,3,2-dioxaborolan-2-yl)but-3-enoic acid (159d).



Following the general procedure **C**, **158d** (0.150 g, 1.152 mmol) was not transformed to the target compound **159d**.

6 References

- [1] Maslin, M. The climate change debate; *Oxford University Press*, **2014**. DOI: <https://doi.org/10.1093/actrade/9780198719045.003.0002>.
- [2] Mas, M.; Cardona, M.; Fernández de Guevara, J.; Righi, R.; De Prato, G.; Robledo, J.; López-Cobo, M.; Samoili, S. **2018**, The 2018 PREDICT key facts report: an analysis of ICT R&D in the EU and beyond, *Publications Office of the European Union*, Luxembourg. DOI: <https://doi.org/10.2760/984658>. (accessed 22.01.2024).
- [3] Terrer, C.; Phillips, R. P.; Hungate, B. A.; Rosende, J.; Pett-Ridge, J.; Craig, M. E.; Van groenigen, K. J.; Keenan, T. F.; Sulman, B. N.; Stocker, B. D.; Reich, P. B.; Pellegrini, A. F. A.; Pendall, E.; Zhang, H.; Evans, R. D.; Carrillo, Y.; Fisher, J. B.; Van Sundert, K.; Vicca, S.; Jackson, R. B. A trade-off between plant and soil carbon storage under elevated CO₂. *Nature* **2021**, *591*, 599-603,603A-603M. DOI: <https://doi.org/10.1038/s41586-021-03306-8>.
- [4] Trends in Atmospheric Carbon Dioxide. *Earth System Research Laboratory (NOAA)*: <https://gml.noaa.gov/ccgg/trends/> (accessed 13/02/2023).
- [5] Laurent, E. *Wikimedia commons*: https://commons.wikimedia.org/wiki/File:Photosynthesis_overview.png (accessed 08/02/2023).
- [6] Atsbha, T. A.; Yoon, T.; Seongho, P.; Lee, C.-J. A review on the catalytic conversion of CO₂ using H₂ for synthesis of CO, methanol, and hydrocarbons. *J. CO₂ Util.* **2021**, *44*, 101413. DOI: <https://doi.org/10.1016/j.jcou.2020.101413>.
- [7] Romeo, L. M.; Lara, Y.; González, A. Reducing energy penalties in carbon capture with Organic Rankine Cycles. *Appl. Therm. Eng.* **2011**, *31*, 2928-2935. DOI: <https://doi.org/10.1016/j.applthermaleng.2011.05.022>.
- [8] Tapia, J. F. D.; Lee, J.-Y.; Ooi, R. E. H.; Foo, D. C. Y.; Tan, R. R. A review of optimization and decision-making models for the planning of CO₂ capture, utilization and storage (CCUS) systems. *Sustain. Prod. Consum.* **2018**, *13*, 1-15. DOI: <https://doi.org/10.1016/j.spc.2017.10.001>.
- [9] Aresta, M.; Dibenedetto, A. Utilisation of CO₂ as a chemical feedstock: opportunities and challenges. *Dalton Trans.* **2007**, 2975-2992. DOI: <https://doi.org/10.1039/B700658F>.
- [10] Cuéllar-Franca, R. M.; Azapagic, A. Carbon capture, storage and utilisation technologies: A critical analysis and comparison of their life cycle environmental impacts. *J. CO₂ Util.* **2015**, *9*, 82-102. DOI: <https://doi.org/10.1016/j.jcou.2014.12.001>.
- [11] P. Styring, D. J., H. de Coninck, H. Reith, K. Armstrong. **2011**, Carbon Capture and Utilisation in the green economy, *Centre for Low Carbon Futures*, <http://co2chem.co.uk/wp-content/uploads/2012/06/CCU%20in%20the%20green%20economy%20report.pdf>. (accessed 06/06/2023).

- [12] Van Peteghem, L.; Sakarika, M.; Matassa, S.; Pikaar, I.; Ganigué, R.; Rabaey, K. Towards new carbon-neutral food systems: Combining carbon capture and utilization with microbial protein production. *Bioresour. Technol.* **2022**, *349*, 126853. DOI: <https://doi.org/10.1016/j.biortech.2022.126853>.
- [13] Aresta, M. Carbon dioxide as chemical feedstock; *Wiley-VCH*: Weinheim, **2010**. DOI: <https://doi.org/h10.1002/9783527629916>.
- [14] Cokoja, M.; Bruckmeier, C.; Rieger, B.; Herrmann, W. A.; Kühn, F. E. Transformation of Carbon Dioxide with Homogeneous Transition-Metal Catalysts: A Molecular Solution to a Global Challenge? *Angew. Chem. Int. Ed.* **2011**, *50*, 8510-8537. DOI: <https://doi.org/10.1002/anie.201102010>.
- [15] Kafi, M.; Sanaeepur, H.; Ebadi Amooghin, A. Grand Challenges in CO₂ Capture and Conversion. *JRR* **2023**, *1*. DOI: <https://doi.org/10.52547/jrr.2302-1007>.
- [16] Alvarez-Hernandez, J. L.; Salamatian, A. A.; Han, J. W.; Bren, K. L. Potential- and Buffer-Dependent Selectivity for the Conversion of CO₂ to CO by a Cobalt Porphyrin-Peptide Electrocatalyst in Water. *ACS Catal.* **2022**, *12*, 14689-14697. DOI: <https://doi.org/10.1021/acscatal.2c03297>.
- [17] Whang, H. S.; Lim, J.; Choi, M. S.; Lee, J.; Lee, H. Heterogeneous catalysts for catalytic CO₂ conversion into value-added chemicals. *BMC Chem. Eng.* **2019**, *1*, 9. DOI: <https://doi.org/10.1186/s42480-019-0007-7>.
- [18] Melián-Cabrera, I. Catalytic Materials: Concepts to Understand the Pathway to Implementation. *Ind. Eng. Chem. Res.* **2021**, *60*, 18545-18559. DOI: <https://doi.org/10.1021/acs.iecr.1c02681>.
- [19] Zheng, R.; Liu, Z.; Wang, Y.; Xie, Z. Industrial catalysis: Strategies to enhance selectivity. *Chinese J. Catal.* **2020**, *41*, 1032-1038. DOI: [https://doi.org/10.1016/S1872-2067\(20\)63578-1](https://doi.org/10.1016/S1872-2067(20)63578-1).
- [20] Pan, S.-Y.; Chung, T.-C.; Ho, C.-C.; Hou, C.-J.; Chen, Y.-H.; Chiang, P.-C. CO₂ Mineralization and Utilization using Steel Slag for Establishing a Waste-to-Resource Supply Chain. *Scientific Reports* **2017**, *7*, 17227. DOI: <https://doi.org/10.1038/s41598-017-17648-9>.
- [21] IEA. **2019**, Putting CO₂ to Use, *International Energy Agency*, Paris, <https://www.iea.org/reports/putting-co2-to-use>. (accessed 12/06/2023).
- [22] Buis, A. The Atmosphere: Getting a Handle on Carbon Dioxide. *National Aeronautics and Space Administration*: <https://climate.nasa.gov/news/2915/the-atmosphere-getting-a-handle-on-carbon-dioxide/> (accessed 19/09/2023).
- [23] Ma, J.; Li, L.; Wang, H.; Du, Y.; Ma, J.; Zhang, X.; Wang, Z. Carbon Capture and Storage: History and the Road Ahead. *Engineering* **2022**, *14*, 33-43. DOI: <https://doi.org/10.1016/j.eng.2021.11.024>.
- [24] Olah, G. A.; Prakash, G. K. S.; Goepfert, A. Anthropogenic Chemical Carbon Cycle for a Sustainable Future. *J. Am. Chem. Soc.* **2011**, *133*, 12881-12898. DOI: <https://doi.org/10.1021/ja202642y>.

- [25] Zhang, Z.; Yi, P.; Hu, S.; Jin, Y. Achieving artificial carbon cycle via integrated system of high-emitting industries and CCU technology: Case of China. *J. Environ. Manage.* **2023**, *340*, 118010. DOI: <https://doi.org/10.1016/j.jenvman.2023.118010>.
- [26] Esmailirad, M.; Jiang, Z.; Harzandi, A. M.; Kondori, A.; Tamadoni Saray, M.; Segre, C. U.; Shahbazian-Yassar, R.; Rappe, A. M.; Asadi, M. Imidazolium-functionalized Mo₃P nanoparticles with an ionomer coating for electrocatalytic reduction of CO₂ to propane. *Nat. Energy* **2023**, *8*, 891-900. DOI: <https://doi.org/10.1038/s41560-023-01314-8>.
- [27] Abderrahmane Ballamine; Abdellah Kotni; Jean-Pierre Llored; Caillol, S. Valuing CO₂ in the development of polymer materials. *Sci. Tech. Energ. Transition* **2022**, *77*, 5. DOI: <https://doi.org/10.2516/stet/2021001>.
- [28] Sun, L.-B.; Kang, Y.-H.; Shi, Y.-Q.; Jiang, Y.; Liu, X.-Q. Highly Selective Capture of the Greenhouse Gas CO₂ in Polymers. *ACS Sustain. Chem. Eng.* **2015**, *3*, 3077-3085. DOI: <https://doi.org/10.1021/acssuschemeng.5b00544>.
- [29] Sahoo, P. K.; Zhang, Y.; Das, S. CO₂-Promoted Reactions: An Emerging Concept for the Synthesis of Fine Chemicals and Pharmaceuticals. *ACS Catal.* **2021**, *11*, 3414-3442. DOI: <https://doi.org/10.1021/acscatal.0c05681>.
- [30] Huang, C.-H.; Tan, C.-S. A Review: CO₂ Utilization. *AAQR* **2014**, *14*, 480-499. DOI: <https://doi.org/10.4209/aaqr.2013.10.0326>.
- [31] Burkart, M. D.; Hazari, N.; Tway, C. L.; Zeitler, E. L. Opportunities and Challenges for Catalysis in Carbon Dioxide Utilization. *ACS Catal.* **2019**, *9*, 7937-7956. DOI: <https://doi.org/10.1021/acscatal.9b02113>.
- [32] Ertl, P.; Altmann, E.; McKenna, J. M. The Most Common Functional Groups in Bioactive Molecules and How Their Popularity Has Evolved over Time. *J. Med. Chem.* **2020**, *63*, 8408-8418. DOI: <https://doi.org/10.1021/acs.jmedchem.0c00754>.
- [33] Gevorgyan, A.; Hopmann, K. H.; Bayer, A. Exploration of New Biomass-Derived Solvents: Application to Carboxylation Reactions. *ChemSusChem* **2020**, *13*, 2080-2088. DOI: <https://doi.org/10.1002/cssc.201903224>.
- [34] Gevorgyan, A.; Hopmann, K. H.; Bayer, A. Formal C-H Carboxylation of Unactivated Arenes. *Chem. Eur. J.* **2020**, *26*, 6064-6069. DOI: <https://doi.org/10.1002/chem.202000515>.
- [35] Gevorgyan, A.; Obst, M. F.; Guttormsen, Y.; Maseras, F.; Hopmann, K. H.; Bayer, A. Caesium fluoride-mediated hydrocarboxylation of alkenes and allenes: scope and mechanistic insights. *Chem. Sci.* **2019**, *10*, 10072-10078. DOI: <https://doi.org/10.1039/C9SC02467K>.
- [36] Wu, X.-F.; Zheng, F. Synthesis of Carboxylic Acids and Esters from CO₂. *Top. Curr. Chem.* **2016**, *375*, 4. DOI: <https://doi.org/10.1007/s41061-016-0091-6>.
- [37] Lejkowski, M. L.; Lindner, R.; Kageyama, T.; Bódizs, G. É.; Plessow, P. N.; Müller, I. B.; Schäfer, A.; Rominger, F.; Hofmann, P.; Fütter, C.; Schunk, S. A.; Limbach, M. The First Catalytic Synthesis of an Acrylate from CO₂ and an Alkene—A Rational

- Approach. *Chem. Eur. J.* **2012**, *18*, 14017-14025. DOI: <https://doi.org/10.1002/chem.201201757>.
- [38] Lanigan, R. M.; Starkov, P.; Sheppard, T. D. Direct Synthesis of Amides from Carboxylic Acids and Amines Using B(OCH₂CF₃)₃. *J. Org. Chem.* **2013**, *78*, 4512-4523. DOI: <https://doi.org/10.1021/jo400509n>.
- [39] Ismael, A.; Skrydstrup, T.; Bayer, A. Carbonylative Suzuki–Miyaura couplings of sterically hindered aryl halides: synthesis of 2-aryloxybenzoate derivatives. *Org. Biomol. Chem.* **2020**, *18*, 1754-1759. DOI: <https://doi.org/10.1039/D0OB00044B>.
- [40] Sims, H. S.; Dai, M. Palladium-Catalyzed Carbonylations: Application in Complex Natural Product Total Synthesis and Recent Developments. *J. Org. Chem.* **2023**, *88*, 4925-4941. DOI: <https://doi.org/10.1021/acs.joc.2c02746>.
- [41] Sirviö, J. A.; Heiskanen, J. P. Carbamation of Starch with Amine Using Dimethyl Carbonate as Coupling Agent. *ACS Omega* **2019**, *4*, 15702-15710. DOI: <https://doi.org/10.1021/acsomega.9b02350>.
- [42] Citarella, A.; Moi, D.; Pinzi, L.; Bonanni, D.; Rastelli, G. Hydroxamic Acid Derivatives: From Synthetic Strategies to Medicinal Chemistry Applications. *ACS Omega* **2021**, *6*, 21843-21849. DOI: <https://doi.org/10.1021/acsomega.1c03628>.
- [43] Ha, M. W.; Paek, S. M. Recent Advances in the Synthesis of Ibuprofen and Naproxen. *Molecules* **2021**, *26*. DOI: <https://doi.org/10.3390/molecules26164792>.
- [44] Petrie, B.; Camacho-Muñoz, D. Analysis, fate and toxicity of chiral non-steroidal anti-inflammatory drugs in wastewaters and the environment: a review. *Environ. Chem. Lett.* **2021**, *19*, 43-75. DOI: <https://doi.org/10.1007/s10311-020-01065-y>.
- [45] Chhabra, N.; Aseri, M. L.; Padmanabhan, D. A review of drug isomerism and its significance. *Int. J. Appl. Basic Med. Res.* **2013**, *3*, 16-18. DOI: <https://doi.org/10.4103/2229-516x.112233>.
- [46] Yang, Y.; Lee, J.-W. Toward ideal carbon dioxide functionalization. *Chem. Sci.* **2019**, *10*, 3905-3926. DOI: <https://doi.org/10.1039/C8SC05539D>.
- [47] Yusuf, N.; Almomani, F.; Qiblawey, H. Catalytic CO₂ conversion to C₁ value-added products: Review on latest catalytic and process developments. *Fuel* **2023**, *345*, 128178. DOI: <https://doi.org/10.1016/j.fuel.2023.128178>.
- [48] Liu, W.-C.; Baek, J.; Somorjai, G. A. The Methanol Economy: Methane and Carbon Dioxide Conversion. *Top. Catal.* **2018**, *61*, 530-541. DOI: <https://doi.org/10.1007/s11244-018-0907-4>.
- [49] Borisut, P.; Nuchitprasittichai, A. Methanol Production via CO₂ Hydrogenation: Sensitivity Analysis and Simulation—Based Optimization. *Front. Energy Res.* **2019**, *7*. DOI: <https://doi.org/10.3389/fenrg.2019.00081>.
- [50] Khojasteh-Salkuyeh, Y.; Ashrafi, O.; Mostafavi, E.; Navarri, P. CO₂ utilization for methanol production; Part I: Process design and life cycle GHG assessment of different

- pathways. *J. CO₂ Util.* **2021**, *50*, 101608. DOI: <https://doi.org/10.1016/j.jcou.2021.101608>.
- [51] Xavier, K. O.; Sreekala, R.; Rashid, K. K. A.; Yusuff, K. K. M.; Sen, B. Doping effects of cerium oxide on Ni/Al₂O₃ catalysts for methanation. *Catal. Today* **1999**, *49*, 17-21. DOI: [https://doi.org/10.1016/S0920-5861\(98\)00403-9](https://doi.org/10.1016/S0920-5861(98)00403-9).
- [52] Utaka, T.; Takeguchi, T.; Kikuchi, R.; Eguchi, K. CO removal from reformed fuels over Cu and precious metal catalysts. *Appl. Catal. A: Gen.* **2003**, *246*, 117-124. DOI: [https://doi.org/10.1016/S0926-860X\(03\)00048-6](https://doi.org/10.1016/S0926-860X(03)00048-6).
- [53] Panagiotopoulou, P.; Kondarides, D. I.; Verykios, X. E. Selective methanation of CO over supported noble metal catalysts: Effects of the nature of the metallic phase on catalytic performance. *Appl. Catal. A: Gen.* **2008**, *344*, 45-54. DOI: <https://doi.org/10.1016/j.apcata.2008.03.039>.
- [54] Liang, S.; Huang, L.; Gao, Y.; Wang, Q.; Liu, B. Electrochemical Reduction of CO₂ to CO over Transition Metal/N-Doped Carbon Catalysts: The Active Sites and Reaction Mechanism. *Adv. Sci.* **2021**, *8*, 2102886. DOI: <https://doi.org/10.1002/advs.202102886>.
- [55] The Extraction of Nickel from its Ores by the Mond Process. *Nature* **1898**, *59*, 63-64. DOI: <https://doi.org/10.1038/059063a0>.
- [56] Wentrup, J.; Pesch, G. R.; Thöming, J. Dynamic operation of Fischer-Tropsch reactors for power-to-liquid concepts: A review. *Renew. Sust. Energ. Rev.* **2022**, *162*, 112454. DOI: <https://doi.org/10.1016/j.rser.2022.112454>.
- [57] Carbon monoxide. *Department of Climate Change, Energy, the Environment and Water*: <https://www.dccew.gov.au/environment/protection/npi/substances/factsheets/carbon-monoxide-0> (accessed 13/06/2023).
- [58] Fujimori, S.; Inoue, S. Carbon Monoxide in Main-Group Chemistry. *J. Am. Chem. Soc.* **2022**, *144*, 2034-2050. DOI: <https://doi.org/10.1021/jacs.1c13152>.
- [59] Wang, J.; You, Z.; Zhang, Q.; Deng, W.; Wang, Y. Synthesis of lower olefins by hydrogenation of carbon dioxide over supported iron catalysts. *Catal. Today* **2013**, *215*, 186-193. DOI: <https://doi.org/10.1016/j.cattod.2013.03.031>.
- [60] Hoang, T. T. H.; Verma, S.; Ma, S.; Fister, T. T.; Timoshenko, J.; Frenkel, A. I.; Kenis, P. J. A.; Gewirth, A. A. Nanoporous Copper-Silver Alloys by Additive-Controlled Electrodeposition for the Selective Electroreduction of CO₂ to Ethylene and Ethanol. *J. Am. Chem. Soc.* **2018**, *140*, 5791-5797. DOI: <https://doi.org/10.1021/jacs.8b01868>.
- [61] Liu, Q.; Wu, L.; Jackstell, R.; Beller, M. Using carbon dioxide as a building block in organic synthesis. *Nat. Commun.* **2015**, *6*, 5933. DOI: <https://doi.org/10.1038/ncomms6933>.
- [62] Kwawu, C. R.; Aniagyei, A. A review on the computational studies of the reaction mechanisms of CO₂ conversion on pure and bimetals of late 3d metals. *J. Mol. Model.* **2021**, *27*, 200. DOI: <https://doi.org/10.1007/s00894-021-04811-3>.

- [63] Wang, L.; Qi, C.; Xiong, W.; Jiang, H. Recent advances in fixation of CO₂ into organic carbamates through multicomponent reaction strategies. *Chinese J. Catal.* **2022**, *43*, 1598-1617. DOI: [https://doi.org/10.1016/S1872-2067\(21\)64029-9](https://doi.org/10.1016/S1872-2067(21)64029-9).
- [64] Ding, J.; Ye, R.; Fu, Y.; He, Y.; Wu, Y.; Zhang, Y.; Zhong, Q.; Kung, H. H.; Fan, M. Direct synthesis of urea from carbon dioxide and ammonia. *Nat. Commun.* **2023**, *14*, 4586. DOI: <https://doi.org/10.1038/s41467-023-40351-5>.
- [65] Wang, H.; Xin, Z.; Li, Y. Synthesis of Ureas from CO₂. *Top. Curr. Chem.* **2017**, *375*, 49. DOI: <https://doi.org/10.1007/s41061-017-0137-4>.
- [66] Urea. *ACS Chemistry for Life*: <https://www.acs.org/molecule-of-the-week/archive/u/urea.html> (accessed 13/6/2023).
- [67] Chen, X.; Chen, J.; Alghoraibi, N. M.; Henckel, D. A.; Zhang, R.; Nwabara, U. O.; Madsen, K. E.; Kenis, P. J. A.; Zimmerman, S. C.; Gewirth, A. A. Electrochemical CO₂-to-ethylene conversion on polyamine-incorporated Cu electrodes. *Nat. Catal.* **2021**, *4*, 20-27. DOI: <https://doi.org/10.1038/s41929-020-00547-0>.
- [68] Dai, W.-L.; Luo, S.-L.; Yin, S.-F.; Au, C.-T. The direct transformation of carbon dioxide to organic carbonates over heterogeneous catalysts. *Appl. Catal. A: Gen.* **2009**, *366*, 2-12. DOI: <https://doi.org/10.1016/j.apcata.2009.06.045>.
- [69] Fukuoka, S.; Fukawa, I.; Adachi, T.; Fujita, H.; Sugiyama, N.; Sawa, T. Industrialization and Expansion of Green Sustainable Chemical Process: A Review of Non-phosgene Polycarbonate from CO₂. *Org. Process Res. Dev.* **2019**, *23*, 145-169. DOI: <https://doi.org/10.1021/acs.oprd.8b00391>.
- [70] Ion, A.; Doorslaer, C. V.; Parvulescu, V.; Jacobs, P.; Vos, D. D. Green synthesis of carbamates from CO₂, amines and alcohols. *Green Chem.* **2008**, *10*, 111-116. DOI: <https://doi.org/10.1039/B711197E>.
- [71] Abila, M.; Choi, J.-C.; Sakakura, T. Halogen-free process for the conversion of carbon dioxide to urethanes by homogeneous catalysis. *Chem. Commun.* **2001**, 2238-2239. DOI: <https://doi.org/10.1039/B106201H>.
- [72] Abila, M.; Choi, J.-C.; Sakakura, T. Nickel-catalyzed dehydrative transformation of CO₂ to urethanes. *Green Chem.* **2004**, *6*, 524-525. DOI: <https://doi.org/10.1039/B408429B>.
- [73] Georgiana Ileana, B. Carboxylic Acid: Key Role in Life Sciences; *IntechOpen*: London, **2018**. DOI: <http://dx.doi.org/10.5772/intechopen.68350>.
- [74] Davies, J.; Lyonnet, J. R.; Zimin, D. P.; Martin, R. The road to industrialization of fine chemical carboxylation reactions. *Chem* **2021**, *7*, 2927-2942. DOI: <https://doi.org/10.1016/j.chempr.2021.10.016>.
- [75] Calvo-Castañera, F.; Álvarez-Rodríguez, J.; Candela, N.; Maroto-Valiente, Á. First Phenol Carboxylation with CO₂ on Carbon Nanostructured C@Fe-Al₂O₃ Hybrids in Aqueous Media under Mild Conditions. **2021**, *11*. DOI: <https://doi.org/10.3390/nano11010190>.

- [76] Börjesson, M.; Moragas, T.; Gallego, D.; Martin, R. Metal-Catalyzed Carboxylation of Organic (Pseudo)halides with CO₂. *ACS Catal.* **2016**, *6*, 6739-6749. DOI: <https://doi.org/10.1021/acscatal.6b02124>.
- [77] Yan, S.-S.; Fu, Q.; Liao, L.-L.; Sun, G.-Q.; Ye, J.-H.; Gong, L.; Bo-Xue, Y.-Z.; Yu, D.-G. Transition metal-catalyzed carboxylation of unsaturated substrates with CO₂. *Coord. Chem. Rev.* **2018**, *374*, 439-463. DOI: <https://doi.org/10.1016/j.ccr.2018.07.011>.
- [78] Jin, Y.; Caner, J.; Nishikawa, S.; Toriumi, N.; Iwasawa, N. Catalytic direct hydrocarboxylation of styrenes with CO₂ and H₂. *Nat. Commun.* **2022**, *13*, 7584. DOI: <https://doi.org/10.1038/s41467-022-35293-3>.
- [79] Tortajada, A.; Juliá-Hernández, F.; Börjesson, M.; Moragas, T.; Martin, R. Transition-Metal-Catalyzed Carboxylation Reactions with Carbon Dioxide. *Angew. Chem. Int. Ed.* **2018**, *57*, 15948-15982. DOI: <https://doi.org/10.1002/anie.201803186>.
- [80] Ran, C.-K.; Liao, L.-L.; Gao, T.-Y.; Gui, Y.-Y.; Yu, D.-G. Recent progress and challenges in carboxylation with CO₂. *Curr. Opin. Green Sustain. Chem.* **2021**, *32*, 100525. DOI: <https://doi.org/10.1016/j.cogsc.2021.100525>.
- [81] Cao, Y.; A. Dhahad, H.; Hussen, H. M.; E. Anqi, A.; Farouk, N.; Issakhov, A.; Heravi, M. R. P. Alkylative/aryllative carboxylation of unsaturated hydrocarbons utilizing CO₂ as C1 synthon: An update. *J. CO₂ Util.* **2021**, *52*, 101664. DOI: <https://doi.org/10.1016/j.jcou.2021.101664>.
- [82] Wang, S.; Feng, T.; Wang, Y.; Qiu, Y. Recent Advances in Electrocarboxylation with CO₂. *Chem. Asian J.* **2022**, *17*, e202200543. DOI: <https://doi.org/10.1002/asia.202200543>.
- [83] Yu, Z.; Shi, M. Recent advances in the electrochemically mediated chemical transformation of carbon dioxide. *Chem. Commun.* **2022**, *58*, 13539-13555. DOI: <https://doi.org/10.1039/D2CC05242C>.
- [84] Liu, X.-F.; Zhang, K.; Tao, L.; Lu, X.-B.; Zhang, W.-Z. Recent advances in electrochemical carboxylation reactions using carbon dioxide. *Green Chem. Eng.* **2022**, *3*, 125-137. DOI: <https://doi.org/10.1016/j.gce.2021.12.001>.
- [85] Nandi, S.; Jana, R. Toward Sustainable Photo-/Electrocatalytic Carboxylation of Organic Substrates with CO₂. *Asian J. Org. Chem.* **2022**, *11*, e202200356. DOI: <https://doi.org/10.1002/ajoc.202200356>.
- [86] Ye, J.-H.; Miao, M.; Huang, H.; Yan, S.-S.; Yin, Z.-B.; Zhou, W.-J.; Yu, D.-G. Visible-Light-Driven Iron-Promoted Thiocarboxylation of Styrenes and Acrylates with CO₂. *Angew. Chem.* **2017**, *129*, 15618-15622. DOI: <https://doi.org/10.1002/ange.201707862>.
- [87] Butcher, T. W.; McClain, E. J.; Hamilton, T. G.; Perrone, T. M.; Kroner, K. M.; Donohoe, G. C.; Akhmedov, N. G.; Petersen, J. L.; Popp, B. V. Regioselective Copper-Catalyzed Borocarboxylation of Vinyl Arenes. *Org. Lett.* **2016**, *18*, 6428-6431. DOI: <https://doi.org/10.1021/acs.orglett.6b03326>.

- [88] Knowlden, S. W.; Popp, B. V. Regioselective Boracarboxylation of α -Substituted Vinyl Arenes. *Organometallics* **2022**, *41*, 1883-1891. DOI: <https://doi.org/10.1021/acs.organomet.2c00184>.
- [89] Fujihara, T.; Tani, Y.; Semba, K.; Terao, J.; Tsuji, Y. Copper-Catalyzed Silacarboxylation of Internal Alkynes by Employing Carbon Dioxide and Silylboranes. *Angew. Chem. Int. Ed.* **2012**, *51*, 11487-11490. DOI: <https://doi.org/10.1002/anie.201207148>.
- [90] Tani, Y.; Fujihara, T.; Terao, J.; Tsuji, Y. Copper-Catalyzed Regiodivergent Silacarboxylation of Allenes with Carbon Dioxide and a Silylborane. *J. Am. Chem. Soc.* **2014**, *136*, 17706-17709. DOI: <https://doi.org/10.1021/ja512040c>.
- [91] Lapidus, A. L.; Pirozhkov, S. D.; Koryakin, A. A. Catalytic synthesis of propionic acid by carboxylation of ethylene with carbon dioxide. *Bull. Acad. Sci. USSR, Div. Chem. Sci.* **1978**, *27*, 2513-2515. DOI: <https://doi.org/10.1007/BF00941114>.
- [92] Burkhart, G.; Hoberg, H. Oxanickelacyclopentene Derivatives from Nickel(0), Carbon Dioxide, and Alkynes. *Angew. Chem., Int. Ed. Engl.* **1982**, *21*, 76-76. DOI: <https://doi.org/10.1002/anie.198200762>.
- [93] Dérien, S.; Duñach, E.; Périchon, J. From Stoichiometry to Catalysis: Electroreductive Coupling of Alkynes and Carbon Dioxide with Nickel-Bipyridine Complexes. Magnesium Ions as the Key for Catalysis. *J. Am. Chem. Soc.* **1991**, *113*, 8447-8454. DOI: <https://doi.org/10.1021/ja00022a037>.
- [94] Dérien, S.; Clinet, J.-C.; Duñach, E.; Périchon, J. First example of direct carbon dioxide incorporation into 1,3-diynes: a highly regio- and stereo-selective nickel-catalysed electrochemical reaction. *J. Chem. Soc., Chem. Commun.* **1991**, 549-550. DOI: <https://doi.org/10.1039/C39910000549>.
- [95] Dérien, S.; Clinet, J.-C.; Duñach, E.; Périchon, J. New C-C bond formation through the nickel-catalysed electrochemical coupling of 1,3-enynes and carbon dioxide. *J. Organomet. Chem.* **1992**, *424*, 213-224. DOI: [https://doi.org/10.1016/0022-328X\(92\)83151-7](https://doi.org/10.1016/0022-328X(92)83151-7).
- [96] Dérien, S.; Duñach, E.; Périchon, J. Electrogenated nickel(0) catalyzed carbon dioxide incorporation into α,ω -diynes. *J. Organomet. Chem.* **1990**, *385*, C43-C46. DOI: [https://doi.org/10.1016/0022-328X\(90\)85018-T](https://doi.org/10.1016/0022-328X(90)85018-T).
- [97] Williams, C. M.; Johnson, J. B.; Rovis, T. Nickel-Catalyzed Reductive Carboxylation of Styrenes Using CO₂. *J. Am. Chem. Soc.* **2008**, *130*, 14936-14937. DOI: <https://doi.org/10.1021/ja8062925>.
- [98] Li, S.; Yuan, W.; Ma, S. Highly Regio- and Stereoselective Three-Component Nickel-Catalyzed syn-Hydrocarboxylation of Alkynes with Diethyl Zinc and Carbon Dioxide. *Angew. Chem. Int. Ed.* **2011**, *50*, 2578-2582. DOI: <https://doi.org/10.1002/anie.201007128>.
- [99] Miao, B.; Zheng, Y.; Wu, P.; Li, S.; Ma, S. Bis(cycloocta-1,5-diene)nickel-Catalyzed Carbon Dioxide Fixation for the Stereoselective Synthesis of 3-Alkylidene-2-

- indolinones. *Adv. Synth. Catal.* **2017**, *359*, 1691-1707. DOI: <https://doi.org/10.1002/adsc.201700086>.
- [100] Wang, X.; Nakajima, M.; Martin, R. Ni-Catalyzed Regioselective Hydrocarboxylation of Alkynes with CO₂ by Using Simple Alcohols as Proton Sources. *J. Am. Chem. Soc.* **2015**, *137*, 8924-8927. DOI: <https://doi.org/10.1021/jacs.5b05513>.
- [101] Greenhalgh, M. D.; Thomas, S. P. Iron-Catalyzed, Highly Regioselective Synthesis of α -Aryl Carboxylic Acids from Styrene Derivatives and CO₂. *J. Am. Chem. Soc.* **2012**, *134*, 11900-11903. DOI: <https://doi.org/10.1021/ja3045053>.
- [102] Santhoshkumar, R.; Hong, Y.-C.; Luo, C.-Z.; Wu, Y.-C.; Hung, C.-H.; Hwang, K.-Y.; Tu, A.-P.; Cheng, C.-H. Synthesis of Vinyl Carboxylic Acids using Carbon Dioxide as a Carbon Source by Iron-Catalyzed Hydromagnesiation. *ChemCatChem* **2016**, *8*, 2210-2213. DOI: <https://doi.org/10.1002/cctc.201600279>.
- [103] Shao, P.; Wang, S.; Chen, C.; Xi, C. Cp₂TiCl₂-Catalyzed Regioselective Hydrocarboxylation of Alkenes with CO₂. *Org. Lett.* **2016**, *18*, 2050-2053. DOI: <https://doi.org/10.1021/acs.orglett.6b00665>.
- [104] Shao, P.; Wang, S.; Du, G.; Xi, C. Cp₂TiCl₂-catalyzed hydrocarboxylation of alkynes with CO₂: formation of α,β -unsaturated carboxylic acids. *RSC Adv.* **2017**, *7*, 3534-3539. DOI: <https://doi.org/10.1039/C6RA25003C>.
- [105] Luo, Y.; Chan, B.; Fukuda, T.; Onodera, G.; Kimura, M. Nickel-Catalyzed Carboxylation of Conjugated Dienes with Carbon Dioxide and DIBAL-H for the Synthesis of β,γ -Unsaturated Carboxylic Acids. *Synlett* **2021**, *32*, 1551-1554. DOI: <https://doi.org/10.1055/a-1336-8034>.
- [106] Lee, S.; Lee, Y. Synthesis of α -Quaternary Carboxylic Acids through Cu-Catalyzed Hydrocarboxylation of Allenes with Diisobutylaluminum Hydride and Carbon Dioxide. *Adv. Synth. Catal.* **2023**, *365*, 4641-4646. DOI: <https://doi.org/10.1002/adsc.202300825>.
- [107] Takaya, J.; Iwasawa, N. Hydrocarboxylation of Allenes with CO₂ Catalyzed by Silyl Pincer-Type Palladium Complex. *J. Am. Chem. Soc.* **2008**, *130*, 15254-15255. DOI: <https://doi.org/10.1021/ja806677w>.
- [108] Takaya, J.; Sasano, K.; Iwasawa, N. Efficient One-to-One Coupling of Easily Available 1,3-Dienes with Carbon Dioxide. *Org. Lett.* **2011**, *13*, 1698-1701. DOI: <https://doi.org/10.1021/ol2002094>.
- [109] Zhu, C.; Takaya, J.; Iwasawa, N. Use of Formate Salts as a Hydride and a CO₂ Source in PGeP-Palladium Complex-Catalyzed Hydrocarboxylation of Allenes. *Org. Lett.* **2015**, *17*, 1814-1817. DOI: <https://doi.org/10.1021/acs.orglett.5b00692>.
- [110] Takaya, J.; Miyama, K.; Zhu, C.; Iwasawa, N. Metallic reductant-free synthesis of α -substituted propionic acid derivatives through hydrocarboxylation of alkenes with a formate salt. *Chem. Commun.* **2017**, *53*, 3982-3985. DOI: <https://doi.org/10.1039/C7CC01377A>.

- [111] Fujihara, T.; Xu, T.; Semba, K.; Terao, J.; Tsuji, Y. Copper-Catalyzed Hydrocarboxylation of Alkynes Using Carbon Dioxide and Hydrosilanes. *Angew. Chem. Int. Ed.* **2011**, *50*, 523-527. DOI: <https://doi.org/10.1002/anie.201006292>.
- [112] Xiong, W.; Shi, F.; Cheng, R.; Zhu, B.; Wang, L.; Chen, P.; Lou, H.; Wu, W.; Qi, C.; Lei, M.; Jiang, H. Palladium-Catalyzed Highly Regioselective Hydrocarboxylation of Alkynes with Carbon Dioxide. *ACS Catal.* **2020**, *10*, 7968-7978. DOI: <https://doi.org/10.1021/acscatal.0c01687>.
- [113] Wang, M.-M.; Lu, S.-M.; Paridala, K.; Li, C. Water-initiated hydrocarboxylation of terminal alkynes with CO₂ and hydrosilane. *Chem. Commun.* **2021**, *57*, 1230-1233. DOI: <https://doi.org/10.1039/D0CC06320G>.
- [114] Simonato, J.-P.; Walter, T.; Métivier, P. Iridium–formic acid based system for hydroxycarbonylation without CO gas. *J. Mol. Catal. A Chem.* **2001**, *171*, 91-94. DOI: [https://doi.org/10.1016/S1381-1169\(01\)00114-5](https://doi.org/10.1016/S1381-1169(01)00114-5).
- [115] Simonato, J.-P. New efficient catalytic system for hydroxycarbonylation without CO gas. *J. Mol. Catal. A Chem.* **2003**, *197*, 61-64. DOI: [https://doi.org/10.1016/S1381-1169\(02\)00676-3](https://doi.org/10.1016/S1381-1169(02)00676-3).
- [116] Ostapowicz, T. G.; Schmitz, M.; Krystof, M.; Klankermayer, J.; Leitner, W. Carbon Dioxide as a C1 Building Block for the Formation of Carboxylic Acids by Formal Catalytic Hydrocarboxylation. *Angew. Chem. Int. Ed.* **2013**, *52*, 12119-12123. DOI: <https://doi.org/10.1002/anie.201304529>.
- [117] Ohishi, T.; Zhang, L.; Nishiura, M.; Hou, Z. Carboxylation of Alkylboranes by N-Heterocyclic Carbene Copper Catalysts: Synthesis of Carboxylic Acids from Terminal Alkenes and Carbon Dioxide. *Angew. Chem. Int. Ed.* **2011**, *50*, 8114-8117. DOI: <https://doi.org/10.1002/anie.201101769>.
- [118] Ohmiya, H.; Tanabe, M.; Sawamura, M. Copper-Catalyzed Carboxylation of Alkylboranes with Carbon Dioxide: Formal Reductive Carboxylation of Terminal Alkenes. *Org. Lett.* **2011**, *13*, 1086-1088. DOI: <https://doi.org/10.1021/ol103128x>.
- [119] Gaydou, M.; Moragas, T.; Juliá-Hernández, F.; Martin, R. Site-Selective Catalytic Carboxylation of Unsaturated Hydrocarbons with CO₂ and Water. *J. Am. Chem. Soc.* **2017**, *139*, 12161-12164. DOI: <https://doi.org/10.1021/jacs.7b07637>.
- [120] Zhang, P.; Zhou, Z.; Zhang, R.; Zhao, Q.; Zhang, C. Cu-Catalyzed highly regioselective 1,2-hydrocarboxylation of 1,3-dienes with CO₂. *Chem. Commun.* **2020**, *56*, 11469-11472. DOI: <https://doi.org/10.1039/D0CC05056C>.
- [121] Cao, T.; Yang, Z.; Ma, S. Selectivities in Nickel-Catalyzed Hydrocarboxylation of Enynes with Carbon Dioxide. *ACS Catal.* **2017**, *7*, 4504-4508. DOI: <https://doi.org/10.1021/acscatal.7b00556>.
- [122] Doi, R.; Abdullah, I.; Taniguchi, T.; Saito, N.; Sato, Y. Nickel-catalyzed hydrocarboxylation of ynamides with CO₂ and H₂O: observation of unexpected regioselectivity. *Chem. Commun.* **2017**, *53*, 7720-7723. DOI: <https://doi.org/10.1039/C7CC03127K>.

- [123] Murata, K.; Numasawa, N.; Shimomaki, K.; Takaya, J.; Iwasawa, N. Construction of a visible light-driven hydrocarboxylation cycle of alkenes by the combined use of Rh(i) and photoredox catalysts. *Chem. Commun.* **2017**, *53*, 3098-3101. DOI: <https://doi.org/10.1039/C7CC00678K>.
- [124] Murata, K.; Numasawa, N.; Shimomaki, K.; Takaya, J.; Iwasawa, N. Improved Conditions for the Visible-Light Driven Hydrocarboxylation by Rh(I) and Photoredox Dual Catalysts Based on the Mechanistic Analyses. *Front. Chem.* **2019**, *7*. DOI: <https://doi.org/10.3389/fchem.2019.00371>.
- [125] Seo, H.; Liu, A.; Jamison, T. F. Direct β -Selective Hydrocarboxylation of Styrenes with CO₂ Enabled by Continuous Flow Photoredox Catalysis. *J. Am. Chem. Soc.* **2017**, *139*, 13969-13972. DOI: <https://doi.org/10.1021/jacs.7b05942>.
- [126] Kang, G.; Romo, D. Photocatalyzed, β -Selective Hydrocarboxylation of α,β -Unsaturated Esters with CO₂ under Flow for β -Lactone Synthesis. *ACS Catal.* **2021**, *11*, 1309-1315. DOI: <https://doi.org/10.1021/acscatal.0c05050>.
- [127] Hou, J.; Ee, A.; Feng, W.; Xu, J.-H.; Zhao, Y.; Wu, J. Visible-Light-Driven Alkyne Hydro-/Carboxylation Using CO₂ via Iridium/Cobalt Dual Catalysis for Divergent Heterocycle Synthesis. *J. Am. Chem. Soc.* **2018**, *140*, 5257-5263. DOI: <https://doi.org/10.1021/jacs.8b01561>.
- [128] Meng, Q.-Y.; Wang, S.; Huff, G. S.; König, B. Ligand-Controlled Regioselective Hydrocarboxylation of Styrenes with CO₂ by Combining Visible Light and Nickel Catalysis. *J. Am. Chem. Soc.* **2018**, *140*, 3198-3201. DOI: <https://doi.org/10.1021/jacs.7b13448>.
- [129] Kim, Y.; Park, G. D.; Balamurugan, M.; Seo, J.; Min, B. K.; Nam, K. T. Electrochemical β -Selective Hydrocarboxylation of Styrene Using CO₂ and Water. *Adv. Sci.* **2020**, *7*, 1900137. DOI: <https://doi.org/10.1002/advs.201900137>.
- [130] Alkayal, A.; Tabas, V.; Montanaro, S.; Wright, I. A.; Malkov, A. V.; Buckley, B. R. Harnessing Applied Potential: Selective β -Hydrocarboxylation of Substituted Olefins. *J. Am. Chem. Soc.* **2020**, *142*, 1780-1785. DOI: <https://doi.org/10.1021/jacs.9b13305>.
- [131] Sheta, A. M.; Alkayal, A.; Mashaly, M. A.; Said, S. B.; Elmorsy, S. S.; Malkov, A. V.; Buckley, B. R. Selective Electrosynthetic Hydrocarboxylation of α,β -Unsaturated Esters with Carbon Dioxide**. *Angew. Chem. Int. Ed.* **2021**, *60*, 21832-21837. DOI: <https://doi.org/10.1002/anie.202105490>.
- [132] Bazzi, S.; Hu, L.; Schulz, E.; Mellah, M. Electrogenated Sm(II)-Catalyzed Carbon Dioxide Reduction for β -Hydrocarboxylation of Styrenes. *Organometallics* **2023**, *42*, 1425-1431. DOI: <https://doi.org/10.1021/acs.organomet.3c00076>.
- [133] Ding, C.-L.; Zhong, J.-S.; Yan, H.; Ye, K.-Y. Electrochemical Hydro- and Deuterocarboxylation of Allenes. *Synthesis* **2023**. DOI: <https://doi.org/10.1055/a-2200-5332>.
- [134] Huang, H.; Ye, J.-H.; Zhu, L.; Ran, C.-K.; Miao, M.; Wang, W.; Chen, H.; Zhou, W.-J.; Lan, Y.; Yu, B.; Yu, D.-G. Visible-Light-Driven Anti-Markovnikov

- Hydrocarboxylation of Acrylates and Styrenes with CO₂. *CCS Chem.* **2020**, *3*, 1746-1756. DOI: <https://doi.org/10.31635/ccschem.020.202000374>.
- [135] Zhang, L.; Cheng, J.; Carry, B.; Hou, Z. Catalytic Boracarboxylation of Alkynes with Diborane and Carbon Dioxide by an N-Heterocyclic Carbene Copper Catalyst. *J. Am. Chem. Soc.* **2012**, *134*, 14314-14317. DOI: <https://doi.org/10.1021/ja3063474>.
- [136] Perrone, T. M.; Gregory, A. S.; Knowlton, S. W.; Ziemer, N. R.; Alsulami, R. N.; Petersen, J. L.; Popp, B. V. Beneficial Effect of a Secondary Ligand on the Catalytic Difunctionalization of Vinyl Arenes with Boron and CO₂. *ChemCatChem* **2019**, *11*, 5814-5820. DOI: <https://doi.org/10.1002/cctc.201901197>.
- [137] Bandar, J. S.; Ascic, E.; Buchwald, S. L. Enantioselective CuH-Catalyzed Reductive Coupling of Aryl Alkenes and Activated Carboxylic Acids. *J. Am. Chem. Soc.* **2016**, *138*, 5821-5824. DOI: <https://doi.org/10.1021/jacs.6b03086>.
- [138] Ascic, E.; Buchwald, S. L. Highly Diastereo- and Enantioselective CuH-Catalyzed Synthesis of 2,3-Disubstituted Indolines. *J. Am. Chem. Soc.* **2015**, *137*, 4666-4669. DOI: <https://doi.org/10.1021/jacs.5b02316>.
- [139] Zhu, S.; Buchwald, S. L. Enantioselective CuH-Catalyzed Anti-Markovnikov Hydroamination of 1,1-Disubstituted Alkenes. *J. Am. Chem. Soc.* **2014**, *136*, 15913-15916. DOI: <https://doi.org/10.1021/ja509786v>.
- [140] Lipshutz, B. H.; Noson, K.; Chrisman, W.; Lower, A. Asymmetric Hydrosilylation of Aryl Ketones Catalyzed by Copper Hydride Complexed by Nonracemic Biphenyl Bisphosphine Ligands. *J. Am. Chem. Soc.* **2003**, *125*, 8779-8789. DOI: <https://doi.org/10.1021/ja021391f>.
- [141] Lin, S.; Lin, Z. DFT Studies on the Mechanism of Copper-Catalyzed Boracarboxylation of Alkene with CO₂ and Diboron. *Organometallics* **2019**, *38*, 240-247. DOI: <https://doi.org/10.1021/acs.organomet.8b00680>.
- [142] Lv, X.; Wu, Y.-B.; Lu, G. Computational exploration of ligand effects in copper-catalyzed boracarboxylation of styrene with CO₂. *Catal. Sci. Technol.* **2017**, *7*, 5049-5054. DOI: <https://doi.org/10.1039/C7CY01637A>.
- [143] Baughman, N. N.; Akhmedov, N. G.; Petersen, J. L.; Popp, B. V. Experimental and Computational Analysis of CO₂ Addition Reactions Relevant to Copper-Catalyzed Boracarboxylation of Vinyl Arenes: Evidence for a Phosphine-Promoted Mechanism. *Organometallics* **2021**, *40*, 23-37. DOI: <https://doi.org/10.1021/acs.organomet.0c00488>.
- [144] Laitar, D. S.; Tsui, E. Y.; Sadighi, J. P. Copper(I) β -Boroalkyls from Alkene Insertion: Isolation and Rearrangement. *Organometallics* **2006**, *25*, 2405-2408. DOI: <https://doi.org/10.1021/om060131u>.
- [145] Baughman, N. N.; Popp, B. V. Evidence of Boron Assistance for CO₂ Activation during Copper-Catalyzed Boracarboxylation of Vinyl Arenes: A Synthetic Model for Cooperative Fixation of CO₂. *Comments Inorg. Chem.* **2020**, *40*, 159-175. DOI: <https://doi.org/10.1080/02603594.2020.1726328>.

- [146] Saini, S.; Chakraborty, D.; Erakulan, E. S.; Thapa, R.; Bal, R.; Bhaumik, A.; Jain, S. L. Visible Light-Driven Metal–Organic Framework-Mediated Activation and Utilization of CO₂ for the Thiocarboxylation of Olefins. *ACS Appl. Mater. Interfaces* **2022**, *14*, 50913-50922. DOI: <https://doi.org/10.1021/acsami.2c14462>.
- [147] Hahm, H.; Kim, J.; Ryoo, J. Y.; Han, M. S.; Hong, S. Photocatalytic carbocarboxylation of styrenes with CO₂ for the synthesis of γ -aminobutyric esters. *Org. Biomol. Chem.* **2021**, *19*, 6301-6312. DOI: <https://doi.org/10.1039/D1OB00866H>.
- [148] Fu, Q.; Bo, Z.-Y.; Ye, J.-H.; Ju, T.; Huang, H.; Liao, L.-L.; Yu, D.-G. Transition metal-free phosphonocarboxylation of alkenes with carbon dioxide via visible-light photoredox catalysis. *Nat. Commun.* **2019**, *10*, 3592. DOI: <https://doi.org/10.1038/s41467-019-11528-8>.
- [149] Moss, G. P. Basic terminology of stereochemistry (IUPAC Recommendations 1996). **1996**, *68*, 2193-2222. DOI: <https://doi.org/10.1351/pac199668122193>.
- [150] Knowles, W. S. Asymmetric Hydrogenations (Nobel Lecture). *Angew. Chem. Int. Ed.* **2002**, *41*, 1998-2007. DOI: [https://doi.org/10.1002/1521-3773\(20020617\)41:12<1998::AID-ANIE1998>3.0.CO;2-8](https://doi.org/10.1002/1521-3773(20020617)41:12<1998::AID-ANIE1998>3.0.CO;2-8).
- [151] Noyori, R. Asymmetric Catalysis: Science and Opportunities (Nobel Lecture). *Angew. Chem. Int. Ed.* **2002**, *41*, 2008-2022. DOI: [https://doi.org/10.1002/1521-3773\(20020617\)41:12<2008::AID-ANIE2008>3.0.CO;2-4](https://doi.org/10.1002/1521-3773(20020617)41:12<2008::AID-ANIE2008>3.0.CO;2-4).
- [152] Miyashita, A.; Yasuda, A.; Takaya, H.; Toriumi, K.; Ito, T.; Souchi, T.; Noyori, R. Synthesis of 2,2'-bis(diphenylphosphino)-1,1'-binaphthyl (BINAP), an atropisomeric chiral bis(triaryl)phosphine, and its use in the rhodium(I)-catalyzed asymmetric hydrogenation of α -(acylamino)acrylic acids. *J. Am. Chem. Soc.* **1980**, *102*, 7932-7934. DOI: <https://doi.org/10.1021/ja00547a020>.
- [153] Knowles, W. S. Asymmetric hydrogenation. *Acc. Chem. Res.* **1983**, *16*, 106-112. DOI: <https://doi.org/10.1021/ar00087a006>.
- [154] Lowenthal, R. E.; Abiko, A.; Masamune, S. Asymmetric catalytic cyclopropanation of olefins: bis-oxazoline copper complexes. *Tetrahedron Lett.* **1990**, *31*, 6005-6008. DOI: [https://doi.org/10.1016/S0040-4039\(00\)98014-6](https://doi.org/10.1016/S0040-4039(00)98014-6).
- [155] Burk, M. J.; Feaster, J. E.; Nugent, W. A.; Harlow, R. L. Preparation and use of C₂-symmetric bis(phospholanes): production of α -amino acid derivatives via highly enantioselective hydrogenation reactions. *J. Am. Chem. Soc.* **1993**, *115*, 10125-10138. DOI: <https://doi.org/10.1021/ja00075a031>.
- [156] Pfaltz, A.; Drury, W. J. Design of chiral ligands for asymmetric catalysis: From C₂-symmetric P,P- and N,N-ligands to sterically and electronically nonsymmetrical P,N-ligands. *PNAS* **2004**, *101*, 5723-5726. DOI: <https://doi.org/10.1073/pnas.0307152101>.
- [157] Vaitla, J.; Guttormsen, Y.; Mannisto, J. K.; Nova, A.; Repo, T.; Bayer, A.; Hopmann, K. H. Enantioselective Incorporation of CO₂: Status and Potential. *ACS Catal.* **2017**, *7*, 7231-7244. DOI: <https://doi.org/10.1021/acscatal.7b02306>.

- [158] Hogeveen, H.; Menge, W. M. P. B. Enantioselective carboxylation of a prochiral enolate in the presence of a chiral lithium amide. *Tetrahedron Lett.* **1986**, *27*, 2767-2770. DOI: [https://doi.org/10.1016/S0040-4039\(00\)84639-0](https://doi.org/10.1016/S0040-4039(00)84639-0).
- [159] Chan, P. C. M.; Michael Chong, J. Preparation of enantiomerically enriched α -hydroxy acid derivatives from α -alkoxyorganostannanes. *Tetrahedron Lett.* **1990**, *31*, 1985-1988. DOI: [https://doi.org/10.1016/S0040-4039\(00\)88895-4](https://doi.org/10.1016/S0040-4039(00)88895-4).
- [160] Chong, J. M.; Park, S. B. Enantiomerically enriched tert-BOC-protected α -aminoorganolithiums: preparation and configurational stability. *J. Org. Chem.* **1992**, *57*, 2220-2222. DOI: <https://doi.org/10.1021/jo00034a007>.
- [161] Kerrick, S. T.; Beak, P. Asymmetric deprotonations: enantioselective syntheses of 2-substituted tert-(butoxycarbonyl)pyrrolidines. *J. Am. Chem. Soc.* **1991**, *113*, 9708-9710. DOI: <https://doi.org/10.1021/ja00025a066>.
- [162] Park, Y. S.; Beak, P. Enantioselective Syntheses of α -, β -, and γ -Aryl Amino Acids and Esters. *J. Org. Chem.* **1997**, *62*, 1574-1575. DOI: <https://doi.org/10.1021/jo9700080>.
- [163] Schlosser, M.; Limat, D. Sparteine-mediated α -lithiation of N-BOC-N-methylbenzylamine: Rapid racemization and subsequent deracemization. *J. Am. Chem. Soc.* **1995**, *117*, 12342-12343. DOI: <https://doi.org/10.1021/ja00154a040>.
- [164] Barberis, C.; Voyer, N.; Roby, J.; Chénard, S.; Tremblay, M.; Labrie, P. Rapid access to N-Boc phenylglycine derivatives via benzylic lithiation reactions. *Tetrahedron* **2001**, *57*, 2965-2972. DOI: [https://doi.org/10.1016/S0040-4020\(01\)00159-4](https://doi.org/10.1016/S0040-4020(01)00159-4).
- [165] Komine, N.; Wang, L.-F.; Tomooka, K.; Nakai, T. Enantioselective carboxylation of α -methoxybenzyl lithium generated via asymmetric lithiation with a t-BuLi/chiral bis(oxazoline) complex. *Tetrahedron Lett.* **1999**, *40*, 6809-6812. DOI: [https://doi.org/10.1016/S0040-4039\(99\)01364-7](https://doi.org/10.1016/S0040-4039(99)01364-7).
- [166] Jeanjean, F.; Fournet, G.; Bars, Didier L.; Goré, J. Synthesis of Highly Enantio-Enriched α -Amino Acids by Carboxylation of N-(α -Lithioalkyl)oxazolidinones. *Eur. J. Org. Chem.* **2000**, *2000*, 1297-1305. DOI: [https://doi.org/10.1002/1099-0690\(200004\)2000:7<1297::AID-EJOC1297>3.0.CO;2-L](https://doi.org/10.1002/1099-0690(200004)2000:7<1297::AID-EJOC1297>3.0.CO;2-L).
- [167] Nakamura, S.; Nakagawa, R.; Watanabe, Y.; Toru, T. Highly Enantioselective Reactions of Configurationally Labile α -Thioorganolithiums Using Chiral Bis(oxazoline)s via Two Different Enantiodetermining Steps. *J. Am. Chem. Soc.* **2000**, *122*, 11340-11347. DOI: <https://doi.org/10.1021/ja0025191>.
- [168] Schultz-Fademrecht, C.; Wibbeling, B.; Fröhlich, R.; Hoppe, D. Synthesis of Enantiomerically Enriched Allenes by (-)-Sparteine-Mediated Lithiation of Alkynyl Carbamates. *Org. Lett.* **2001**, *3*, 1221-1224. DOI: <https://doi.org/10.1021/ol0157104>.
- [169] Takimoto, M.; Mori, M. Novel Catalytic CO₂ Incorporation Reaction: Nickel-Catalyzed Regio- and Stereoselective Ring-Closing Carboxylation of Bis-1,3-dienes. *J. Am. Chem. Soc.* **2002**, *124*, 10008-10009. DOI: <https://doi.org/10.1021/ja026620c>.
- [170] Takimoto, M.; Nakamura, Y.; Kimura, K.; Mori, M. Highly Enantioselective Catalytic Carbon Dioxide Incorporation Reaction: Nickel-Catalyzed Asymmetric Carboxylative

- Cyclization of Bis-1,3-dienes. *J. Am. Chem. Soc.* **2004**, *126*, 5956-5957. DOI: <https://doi.org/10.1021/ja049506y>.
- [171] Zhang, K.; Wang, H.; Zhao, S.-F.; Niu, D.-F.; Lu, J.-X. Asymmetric electrochemical carboxylation of prochiral acetophenone: An efficient route to optically active atrolactic acid via selective fixation of carbon dioxide. *J. Electroanal. Chem.* **2009**, *630*, 35-41. DOI: <https://doi.org/10.1016/j.jelechem.2009.02.013>.
- [172] Chen, B.-L.; Zhu, H.-W.; Xiao, Y.; Sun, Q.-L.; Wang, H.; Lu, J.-X. Asymmetric electrocarboxylation of 1-phenylethyl chloride catalyzed by electrogenerated chiral [CoI(salen)]⁻ complex. *Electrochem. Commun.* **2014**, *42*, 55-59. DOI: <https://doi.org/10.1016/j.elecom.2014.02.009>.
- [173] Yang, H.-P.; Yue, Y.-N.; Sun, Q.-L.; Feng, Q.; Wang, H.; Lu, J.-X. Entrapment of a chiral cobalt complex within silver: a novel heterogeneous catalyst for asymmetric carboxylation of benzyl bromides with CO₂. *Chem. Commun.* **2015**, *51*, 12216-12219. DOI: <https://doi.org/10.1039/C5CC04554A>.
- [174] Yang, L.-R.; Zhang, J.-J.; Zhao, Y.-J.; Wang, Z.-L.; Wang, H.; Lu, J.-X. La_{1-x}Sr_xFeO₃ perovskite electrocatalysts for asymmetric electrocarboxylation of acetophenone with CO₂. *Electrochim. Acta* **2021**, *398*, 139308. DOI: <https://doi.org/10.1016/j.electacta.2021.139308>.
- [175] Zhao, Y.-J.; Yang, L.-R.; Wang, L.-T.; Wang, Y.; Lu, J.-X.; Wang, H. Asymmetric electrocarboxylation of 4'-methylacetophenone over PrCoO₃ perovskites. *Catal. Sci. Technol.* **2022**, *12*, 2887-2893. DOI: <https://doi.org/10.1039/D2CY00116K>.
- [176] Xiong, R.; Wang, Y.; Zhu, J.-W.; Li, M.-H.; Lu, J.-X.; Wang, H. Chiral Metal Salen Complexes as Chiral Electrocatalysts for Asymmetric Electrochemical Carboxylation of Acetophenone. *ChemistrySelect* **2023**, *8*, e202301126. DOI: <https://doi.org/10.1002/slct.202301126>.
- [177] Mita, T.; Sugawara, M.; Hasegawa, H.; Sato, Y. Synthesis of Arylglycine and Mandelic Acid Derivatives through Carboxylations of α -Amido and α -Acetoxy Stannanes with Carbon Dioxide. *J. Org. Chem.* **2012**, *77*, 2159-2168. DOI: <https://doi.org/10.1021/jo202597p>.
- [178] Mita, T.; Sugawara, M.; Saito, K.; Sato, Y. Catalytic Enantioselective Silylation of N-Sulfonylimines: Asymmetric Synthesis of α -Amino Acids from CO₂ via Stereospecific Carboxylation of α -Amino Silanes. *Org. Lett.* **2014**, *16*, 3028-3031. DOI: <https://doi.org/10.1021/ol501143c>.
- [179] Kawashima, S.; Aikawa, K.; Mikami, K. Rhodium-Catalyzed Hydrocarboxylation of Olefins with Carbon Dioxide. *Eur. J. Org. Chem.* **2016**, *2016*, 3166-3170. DOI: <https://doi.org/10.1002/ejoc.201600338>.
- [180] Pavlovic, L.; Vaitla, J.; Bayer, A.; Hopmann, K. H. Rhodium-Catalyzed Hydrocarboxylation: Mechanistic Analysis Reveals Unusual Transition State for Carbon-Carbon Bond Formation. *Organometallics* **2018**, *37*, 941-948. DOI: <https://doi.org/10.1021/acs.organomet.7b00899>.

- [181] Gui, Y.-Y.; Hu, N.; Chen, X.-W.; Liao, L. L.; Ju, T.; Ye, J.-H.; Zhang, Z.; Li, J.; Yu, D.-G. Highly Regio- and Enantioselective Copper-Catalyzed Reductive Hydroxymethylation of Styrenes and 1,3-Dienes with CO₂. *J. Am. Chem. Soc.* **2017**, *139*, 17011-17014. DOI: <https://doi.org/10.1021/jacs.7b10149>.
- [182] Chen, X.-W.; Zhu, L.; Gui, Y.-Y.; Jing, K.; Jiang, Y.-X.; Bo, Z.-Y.; Lan, Y.; Li, J.; Yu, D.-G. Highly Selective and Catalytic Generation of Acyclic Quaternary Carbon Stereocenters via Functionalization of 1,3-Dienes with CO₂. *J. Am. Chem. Soc.* **2019**, *141*, 18825-18835. DOI: <https://doi.org/10.1021/jacs.9b09721>.
- [183] Qiu, J.; Gao, S.; Li, C.; Zhang, L.; Wang, Z.; Wang, X.; Ding, K. Construction of All-Carbon Chiral Quaternary Centers through CuI-Catalyzed Enantioselective Reductive Hydroxymethylation of 1,1-Disubstituted Allenes with CO₂. *Chem. Eur. J.* **2019**, *25*, 13874-13878. DOI: <https://doi.org/10.1002/chem.201903906>.
- [184] Wang, M.-Y.; Jin, X.; Wang, X.; Xia, S.; Wang, Y.; Huang, S.; Li, Y.; He, L.-N.; Ma, X. Copper-Catalyzed and Proton-Directed Selective Hydroxymethylation of Alkynes with CO₂. *Angew. Chem. Int. Ed.* **2021**, *60*, 3984-3988. DOI: <https://doi.org/10.1002/anie.202012768>.
- [185] Jiao, K.-J.; Li, Z.-M.; Xu, X.-T.; Zhang, L.-P.; Li, Y.-Q.; Zhang, K.; Mei, T.-S. Palladium-catalyzed reductive electrocarboxylation of allyl esters with carbon dioxide. *Org. Chem. Front.* **2018**, *5*, 2244-2248. DOI: <https://doi.org/10.1039/C8QO00507A>.
- [186] Zhu, S.-F.; Qiao, X.-C.; Zhang, Y.-Z.; Wang, L.-X.; Zhou, Q.-L. Highly enantioselective palladium-catalyzed umpolung allylation of aldehydes. *Chem. Sci.* **2011**, *2*, 1135-1140. DOI: <https://doi.org/10.1039/C0SC00645A>.
- [187] Howell, G. P.; Minnaard, A. J.; Feringa, B. L. Asymmetric allylation of aryl aldehydes: studies on the scope and mechanism of the palladium catalysed diethylzinc mediated umpolung using phosphoramidite ligands. *Org. Biomol. Chem.* **2006**, *4*, 1278-1283. DOI: <https://doi.org/10.1039/B518165H>.
- [188] Zanoni, G.; Gladiali, S.; Marchetti, A.; Piccinini, P.; Tredici, I.; Vidari, G. Enantioselective Catalytic Allylation of Carbonyl Groups by Umpolung of π -Allyl Palladium Complexes. *Angew. Chem. Int. Ed.* **2004**, *43*, 846-849. DOI: <https://doi.org/10.1002/anie.200352743>.
- [189] Cerveri, A.; Giovanelli, R.; Sella, D.; Pedrazzani, R.; Monari, M.; Nieto Faza, O.; López, C. S.; Bandini, M. Enantioselective CO₂ Fixation Via a Heck-Coupling/Carboxylation Cascade Catalyzed by Nickel. *Chem. Eur. J.* **2021**, *27*, 7657-7662. DOI: <https://doi.org/10.1002/chem.202101082>.
- [190] Chen, X.-W.; Yue, J.-P.; Wang, K.; Gui, Y.-Y.; Niu, Y.-N.; Liu, J.; Ran, C.-K.; Kong, W.; Zhou, W.-J.; Yu, D.-G. Nickel-Catalyzed Asymmetric Reductive Carbo-Carboxylation of Alkenes with CO₂. *Angew. Chem. Int. Ed.* **2021**, *60*, 14068-14075. DOI: <https://doi.org/10.1002/anie.202102769>.
- [191] Wang, L.; Li, T.; Perveen, S.; Zhang, S.; Wang, X.; Ouyang, Y.; Li, P. Nickel-Catalyzed Enantioconvergent Carboxylation Enabled by a Chiral 2,2'-Bipyridine Ligand.

- Angew. Chem. Int. Ed.* **2022**, *61*, e202213943. DOI: <https://doi.org/10.1002/anie.202213943>.
- [192] Pavlovic, L.; Pettersen, M.; Gevorgyan, A.; Vaitla, J.; Bayer, A.; Hopmann, K. H. Computational and Experimental Insights into Asymmetric Rh-Catalyzed Hydrocarboxylation with CO₂. *Eur. J. Org. Chem.* **2021**, *2021*, 663-670. DOI: <https://doi.org/10.1002/ejoc.202001469>.
- [193] Hartwig, J. F. Organotransition metal chemistry: from bonding to catalysis, *University Science Books*, Sausalito, California, **2010**.
- [194] Hartwig, J. F.; Richards, S.; Barañano, D.; Paul, F. Influences on the Relative Rates for C–N Bond-Forming Reductive Elimination and β -Hydrogen Elimination of Amides. A Case Study on the Origins of Competing Reduction in the Palladium-Catalyzed Amination of Aryl Halides. *J. Am. Chem. Soc.* **1996**, *118*, 3626-3633. DOI: <https://doi.org/10.1021/ja954121o>.
- [195] Joy, M. N.; Bodke, Y. D.; Khader, K. K. A.; Sajith, A. M.; Venkatesh, T.; Kumar, A. K. A. Simultaneous exploration of TBAF·3H₂O as a base as well as a solvating agent for the palladium catalyzed Suzuki cross-coupling of 4-methyl-7-nonafluorobutylsulfonyloxy coumarins under microwave irradiation. *J. Fluorine Chem.* **2016**, *182*, 109-120. DOI: <https://doi.org/10.1016/j.jfluchem.2016.01.002>.
- [196] Hans Reich's Collection. Bordwell pKa Table. *ACS Division of Organic Chemistry*: <https://organicchemistrydata.org/hansreich/resources/pka/> (accessed 16/01/2024).
- [197] Zhang, K.; Ren, B.-H.; Liu, X.-F.; Wang, L.-L.; Zhang, M.; Ren, W.-M.; Lu, X.-B.; Zhang, W.-Z. Direct and Selective Electrocarboxylation of Styrene Oxides with CO₂ for Accessing β -Hydroxy Acids. *Angew. Chem. Int. Ed.* **2022**, *61*, e202207660. DOI: <https://doi.org/10.1002/anie.202207660>.
- [198] Imamoto, T.; Sugita, K.; Yoshida, K. An Air-Stable P-Chiral Phosphine Ligand for Highly Enantioselective Transition-Metal-Catalyzed Reactions. *J. Am. Chem. Soc.* **2005**, *127*, 11934-11935. DOI: <https://doi.org/10.1021/ja053458f>.
- [199] Semba, K.; Shinomiya, M.; Fujihara, T.; Terao, J.; Tsuji, Y. Highly Selective Copper-Catalyzed Hydroboration of Allenes and 1,3-Dienes. *Chem. Eur. J.* **2013**, *19*, 7125-7132. DOI: <https://doi.org/10.1002/chem.201300443>.
- [200] Jung, B.; Hoveyda, A. H. Site- and Enantioselective Formation of Allene-Bearing Tertiary or Quaternary Carbon Stereogenic Centers through NHC–Cu-Catalyzed Allylic Substitution. *J. Am. Chem. Soc.* **2012**, *134*, 1490-1493. DOI: <https://doi.org/10.1021/ja211269w>.
- [201] Yuan, W.; Ma, S. Ligand Controlled Highly Selective Copper-Catalyzed Borylcuprations of Allenes with Bis(pinacolato)diboron. *Adv. Synth. Catal.* **2012**, *354*, 1867-1872. DOI: <https://doi.org/10.1002/adsc.201100929>.
- [202] Meng, F.; Jung, B.; Haeffner, F.; Hoveyda, A. H. NHC–Cu-Catalyzed Protoboration of Monosubstituted Allenes. Ligand-Controlled Site Selectivity, Application to Synthesis and Mechanism. *Org. Lett.* **2013**, *15*, 1414-1417. DOI: <https://doi.org/10.1021/ol4004178>.

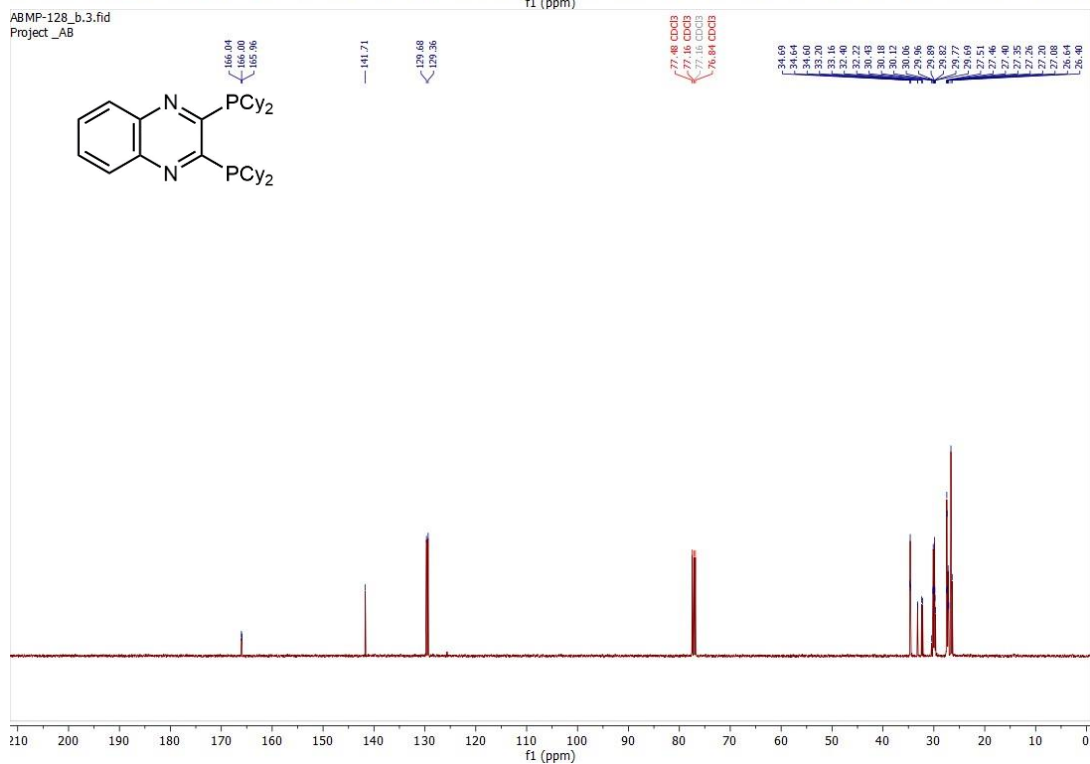
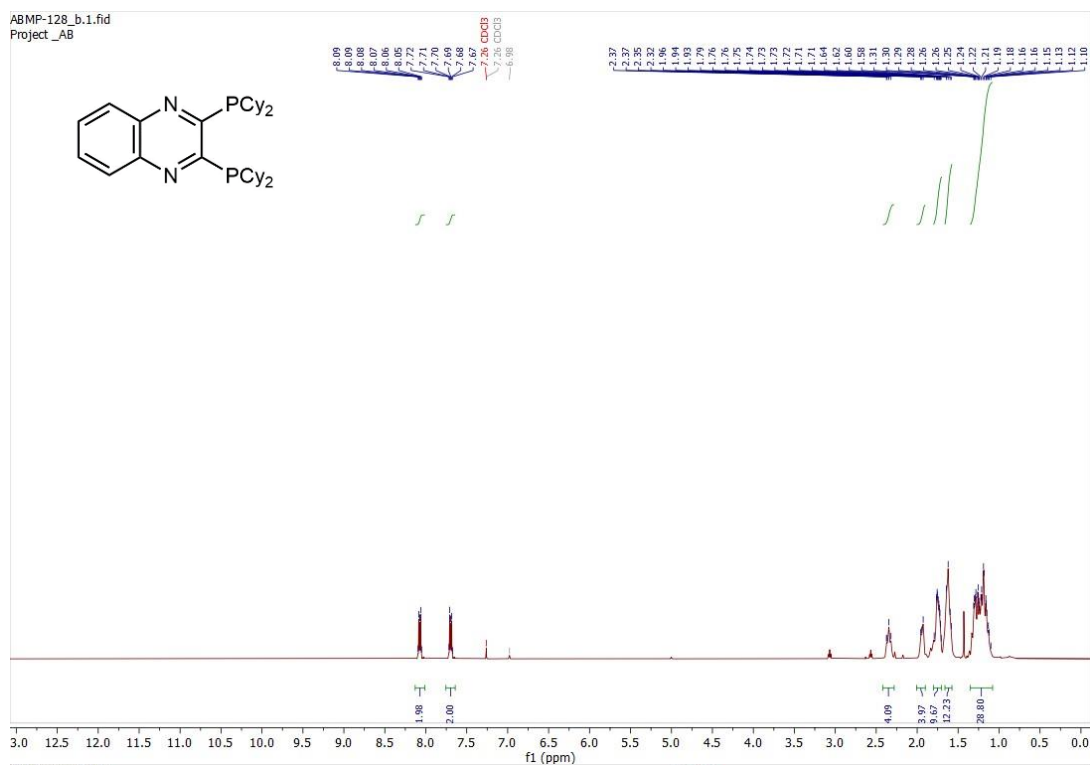
- [203] Jang, H.; Jung, B.; Hoveyda, A. H. Catalytic Enantioselective Protoboration of Disubstituted Allenes. Access to Alkenylboron Compounds in High Enantiomeric Purity. *Org. Lett.* **2014**, *16*, 4658-4661. DOI: <https://doi.org/10.1021/ol5022417>.
- [204] Pulis, A. P.; Yeung, K.; Procter, D. J. Enantioselective copper catalysed, direct functionalisation of allenes via allyl copper intermediates. *Chem. Sci.* **2017**, *8*, 5240-5247. DOI: <https://doi.org/10.1039/C7SC01968H>.
- [205] Wang, Y.; Guan, R.; Sivaguru, P.; Cong, X.; Bi, X. Silver-Catalyzed anti-Markovnikov Hydroboration of C–C Multiple Bonds. *Org. Lett.* **2019**, *21*, 4035-4038. DOI: <https://doi.org/10.1021/acs.orglett.9b01217>.
- [206] Leyva, A.; Zhang, X.; Corma, A. Chemoselective hydroboration of alkynes vs. alkenes over gold catalysts. *Chem. Commun.* **2009**, 4947-4949. DOI: <https://doi.org/10.1039/B901953G>.
- [207] Nahra, F.; Tzouras, N. V.; Collado, A.; Nolan, S. P. Synthesis of N-heterocyclic carbene gold(I) complexes. *Nat. Protoc.* **2021**, *16*, 1476-1493. DOI: <https://doi.org/10.1038/s41596-020-00461-6>.
- [208] Gürbüz, N.; Kaloğlu, N.; Kızrak, Ü.; Özdemir, İ.; Türkmen, N. B.; Çiftçi, O.; Özdemir, İ.; Mansour, L.; Naceur, H. Silver(I) N-heterocyclic carbene complexes: Synthesis, characterization and cytotoxic properties. *J. Organomet. Chem.* **2020**, *923*, 121434. DOI: <https://doi.org/10.1016/j.jorganchem.2020.121434>.
- [209] Hou, J.; Yuan, M.-L.; Xie, J.-H.; Zhou, Q.-L. Nickel-catalyzed hydrocarboxylation of alkynes with formic acid. *Green Chem.* **2016**, *18*, 2981-2984. DOI: <https://doi.org/10.1039/C6GC00549G>.
- [210] Lin, F.; Liu, Z.; Wang, T.; Cui, D. Highly 2,3-Selective Polymerization of Phenylallene and Its Derivatives with Rare-Earth Metal Catalysts: From Amorphous to Crystalline Products. *Angew. Chem. Int. Ed.* **2017**, *56*, 14653-14657. DOI: <https://doi.org/10.1002/anie.201707601>.
- [211] Léonel, E.; Lejaye, M.; Oudeyer, S.; Paul Paugam, J.; Nédélec, J.-Y. gem-Dihalocyclopropane formation by iron/copper activation of tetrahalomethanes in the presence of nucleophilic olefins. Evidence for a carbene pathway. *Tetrahedron Lett.* **2004**, *45*, 2635-2638. DOI: <https://doi.org/10.1016/j.tetlet.2004.01.124>.
- [212] Liu, J.; Nie, M.; Zhou, Q.; Gao, S.; Jiang, W.; Chung, L. W.; Tang, W.; Ding, K. Enantioselective palladium-catalyzed diboration of 1,1-disubstituted allenes. *Chem. Sci.* **2017**, *8*, 5161-5165. DOI: <https://doi.org/10.1039/C7SC01254C>.

7 Appendix

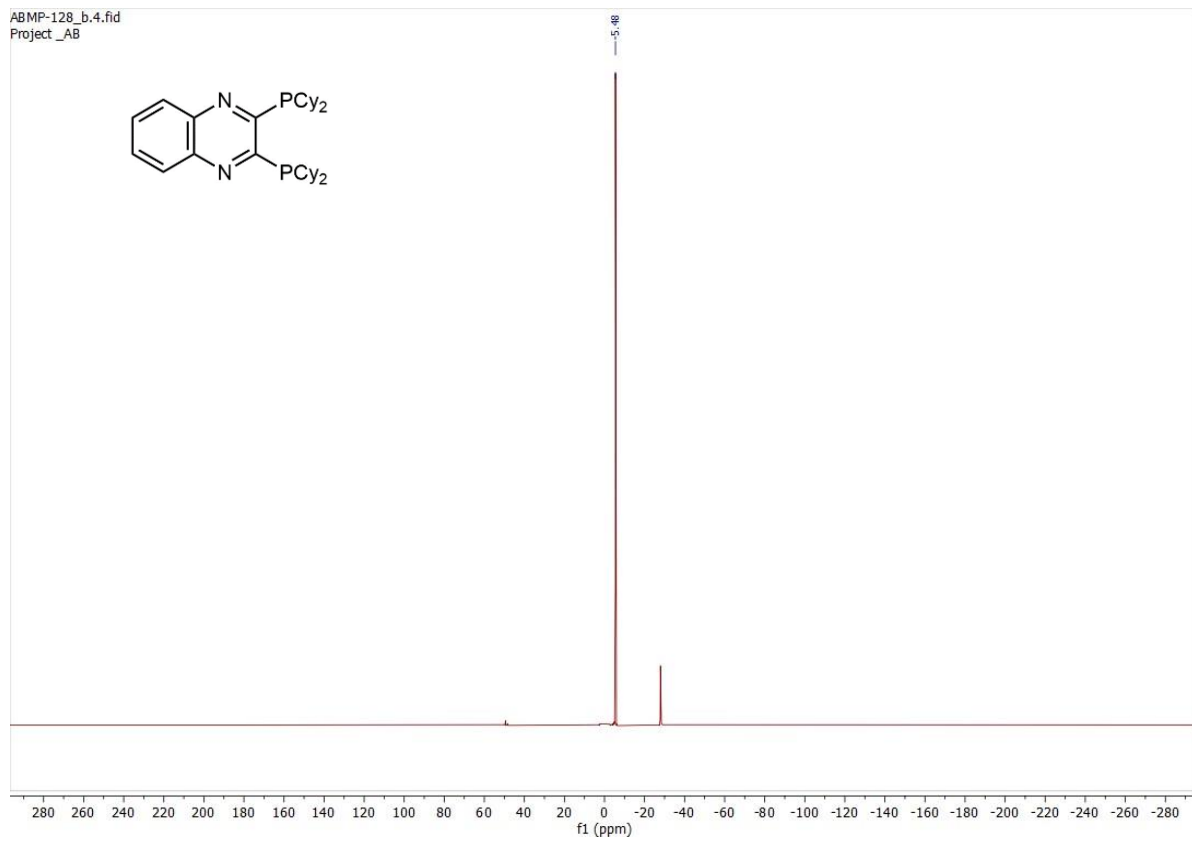
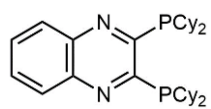
This chapter includes additional spectroscopic data for the compounds described in chapter 5.

7.1 NMR Spectra

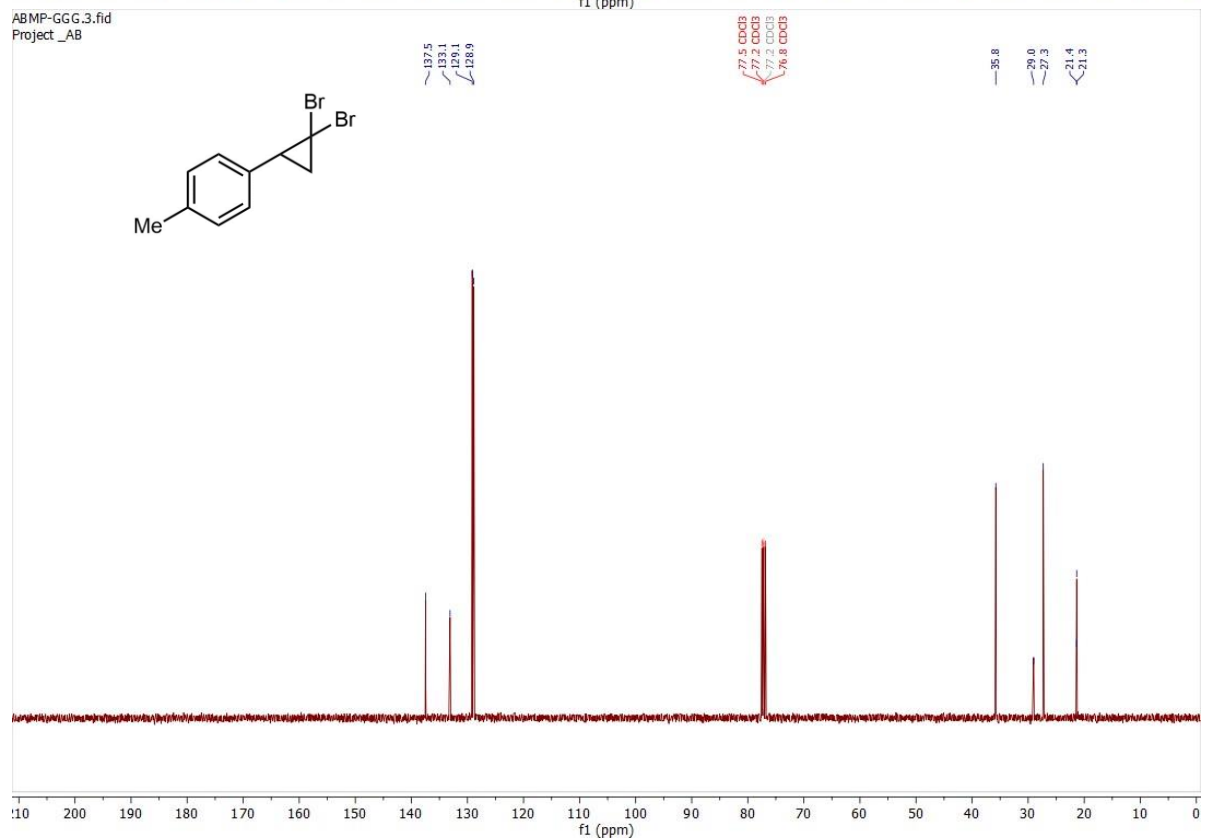
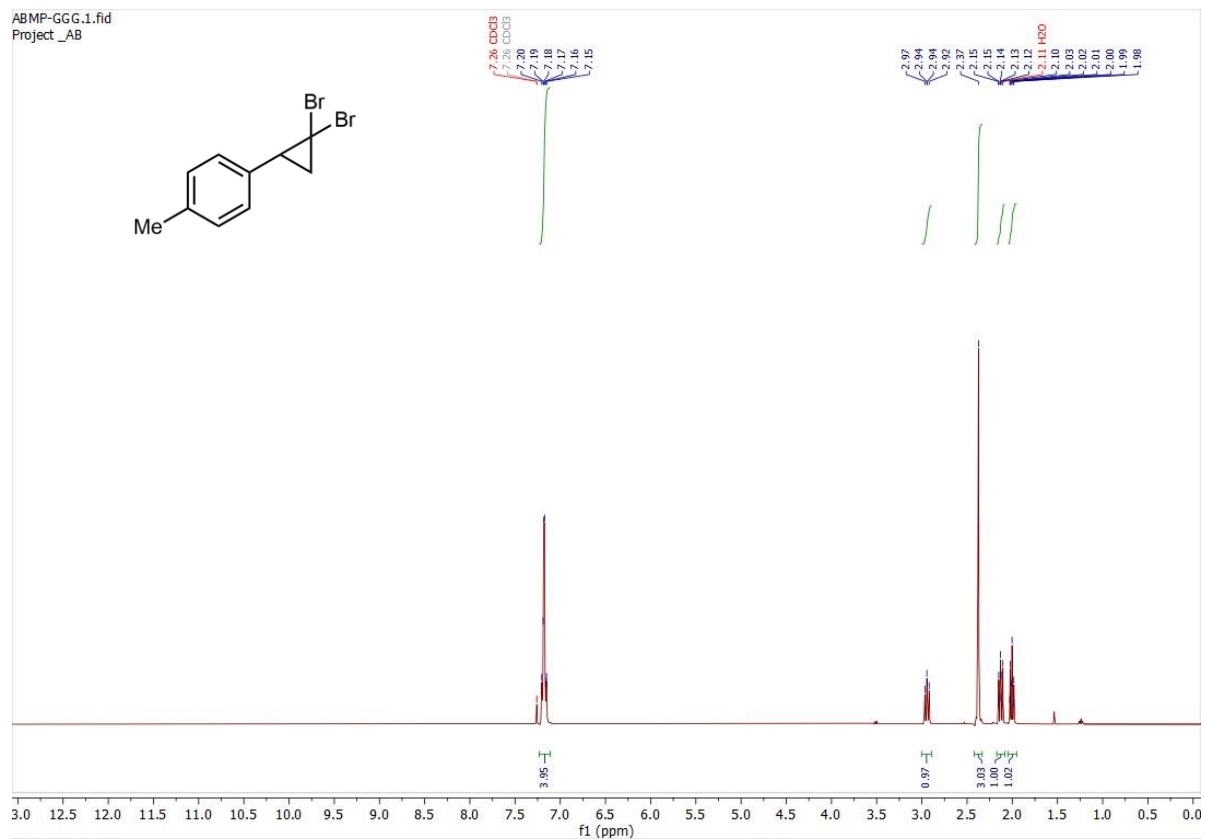
2,3-bis(dicyclohexylphosphaneyl)quinoxaline (155).



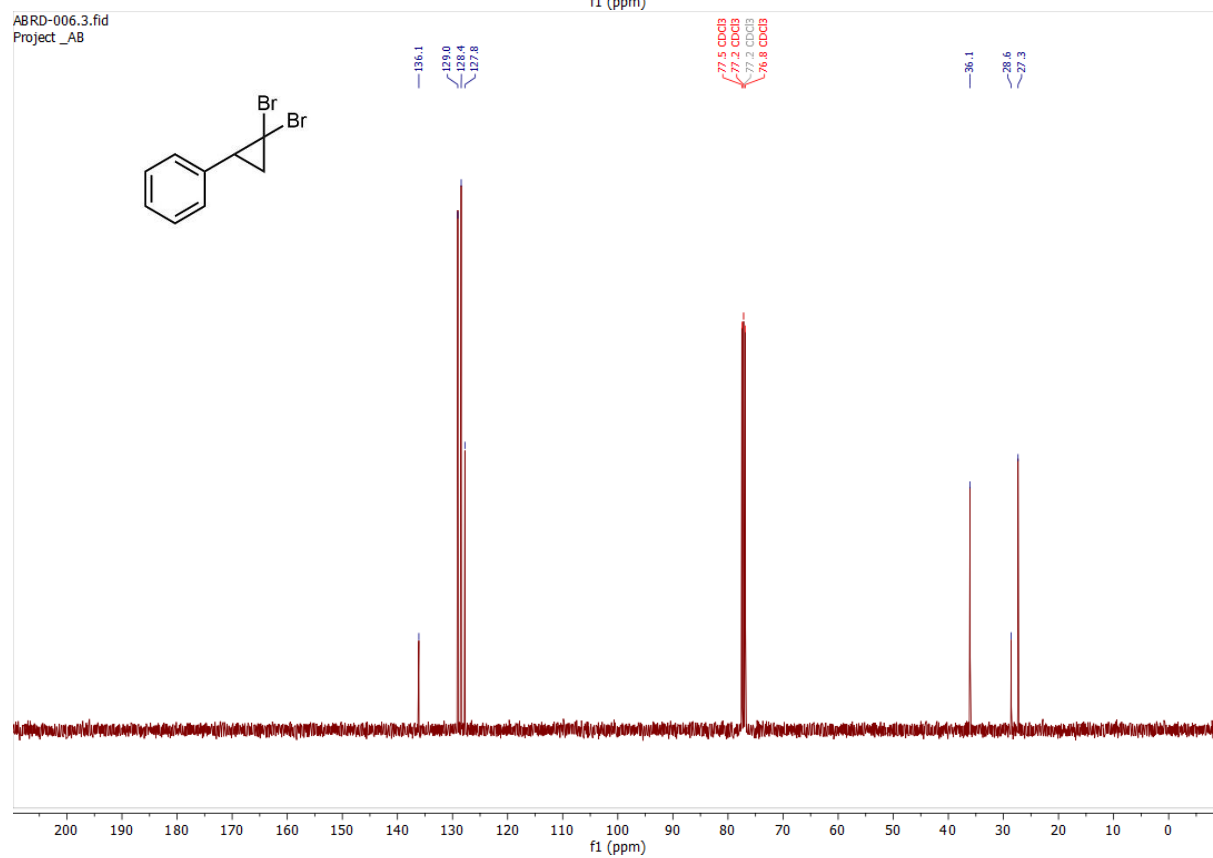
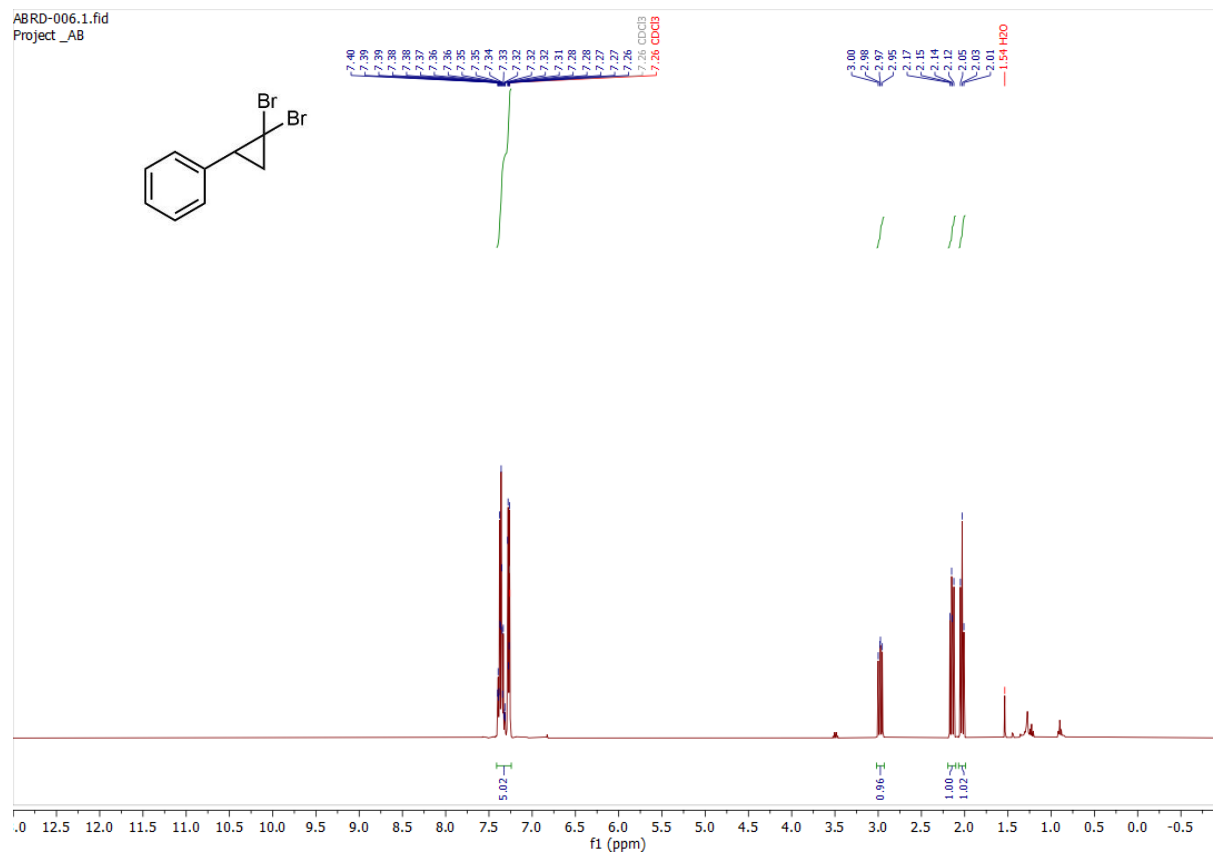
ABMP-128_b.4.fid
Project_AB



1-(2,2-dibromocyclopropyl)-4-methylbenzene (157a)

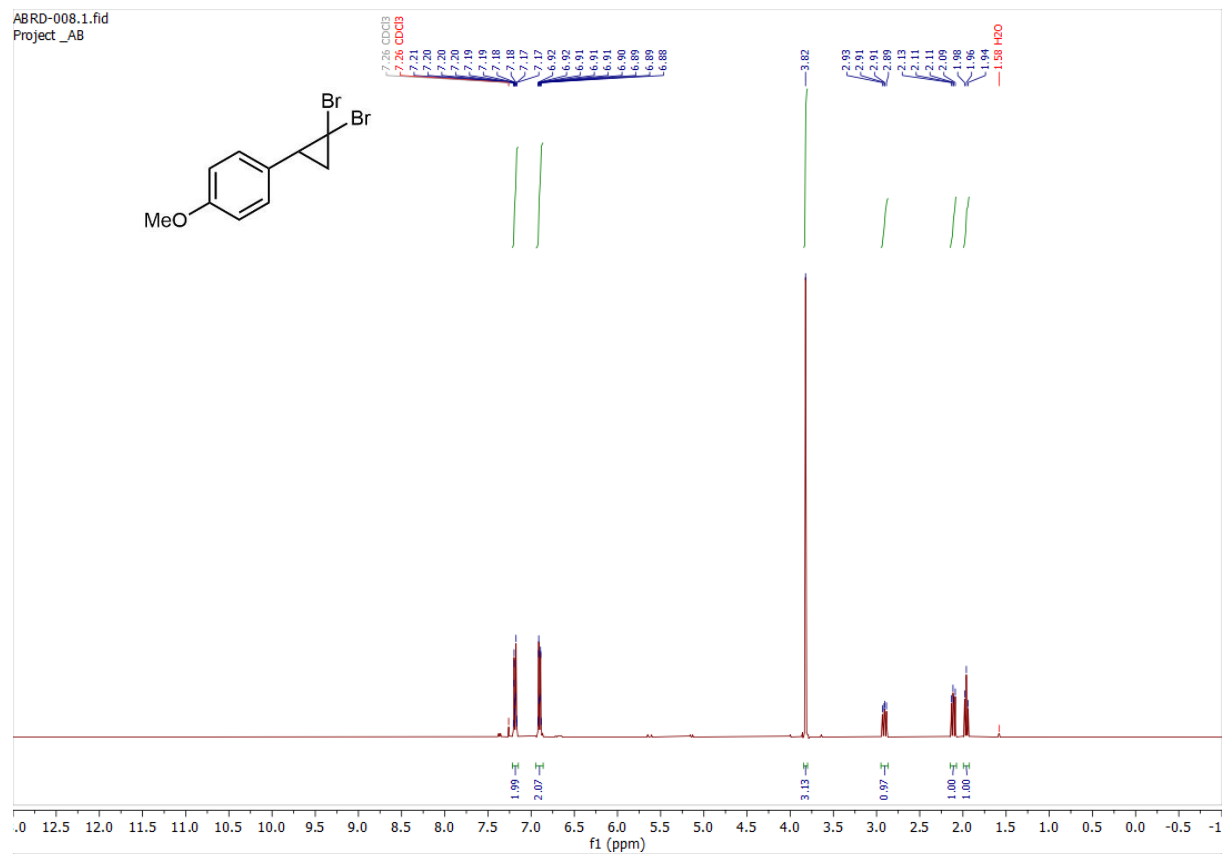


(2,2-dibromocyclopropyl)benzene (157b)

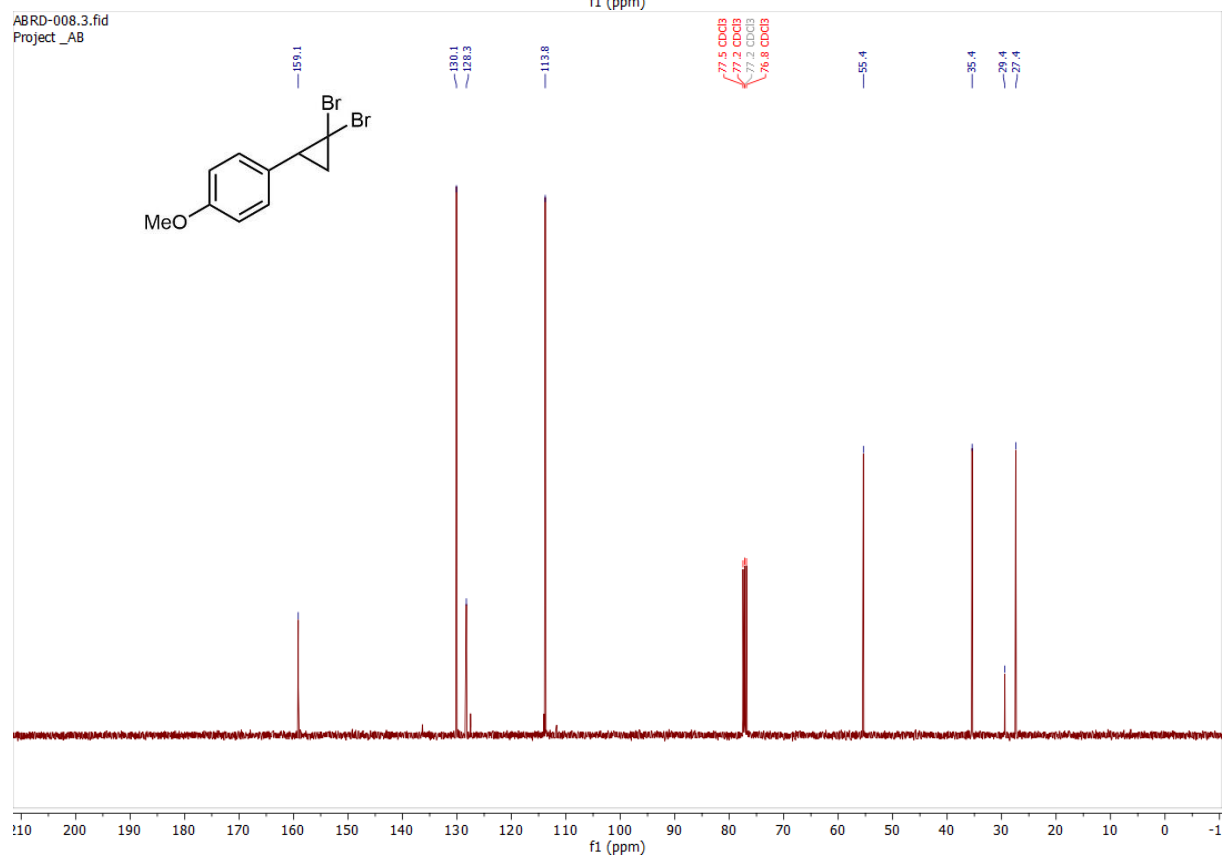


1-(2,2-dibromocyclopropyl)-4-methoxybenzene (157c)

ABRD-008.1.fid
Project_AB

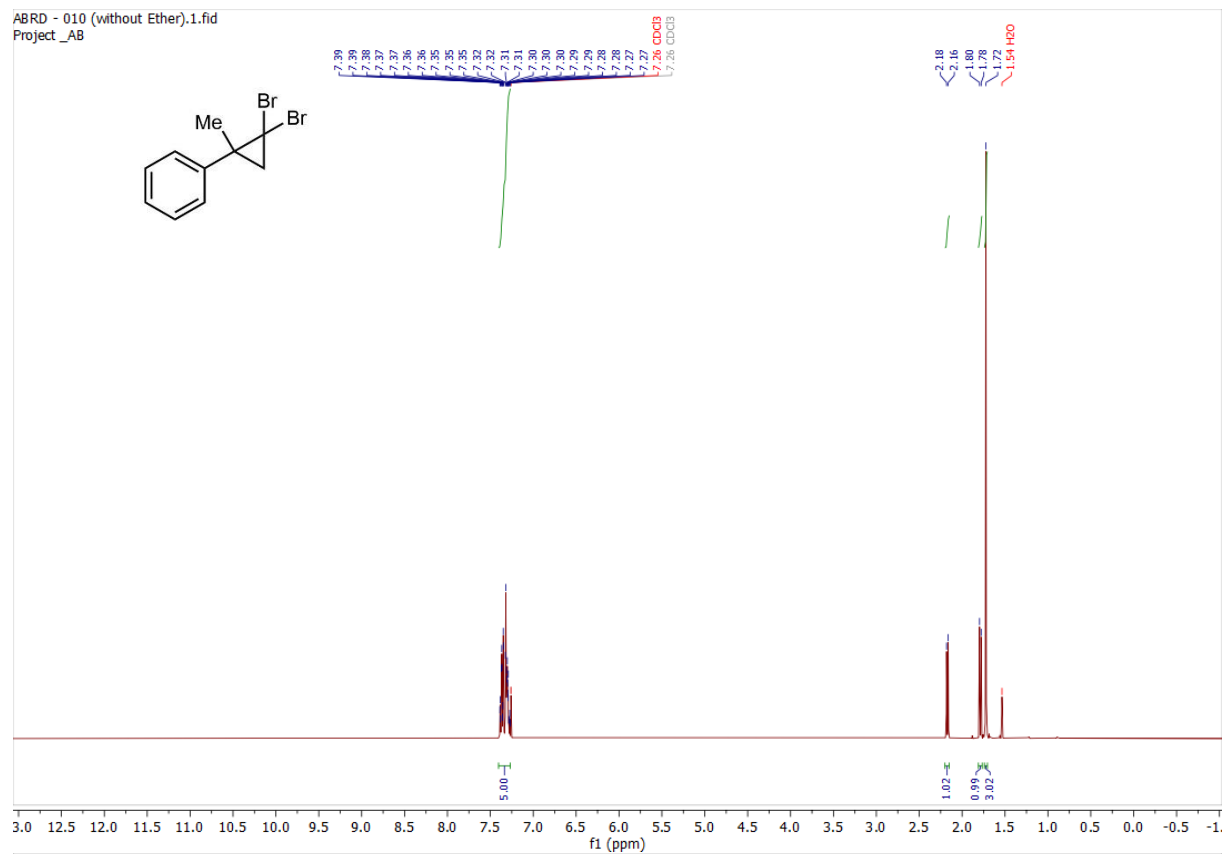


ABRD-008.3.fid
Project_AB

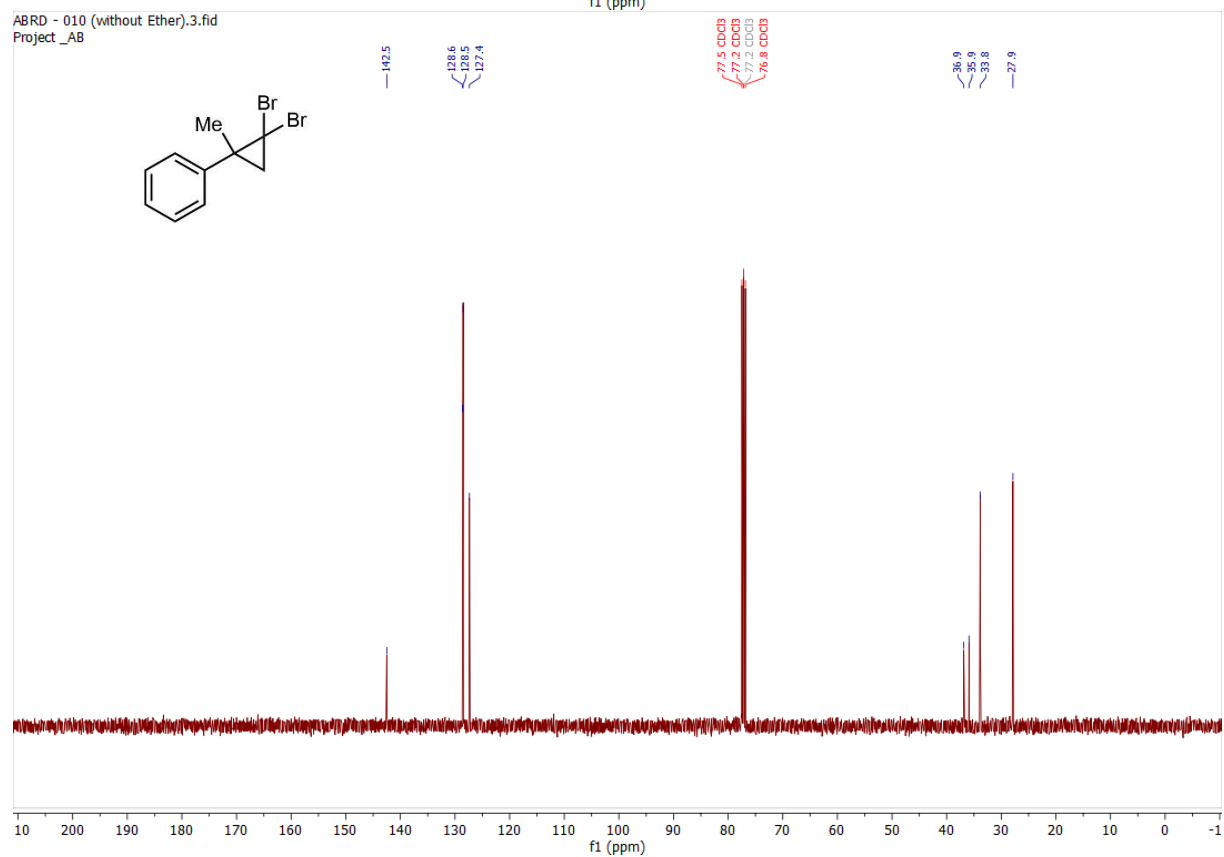


(2,2-dibromo-1-methylcyclopropyl)benzene (157d)

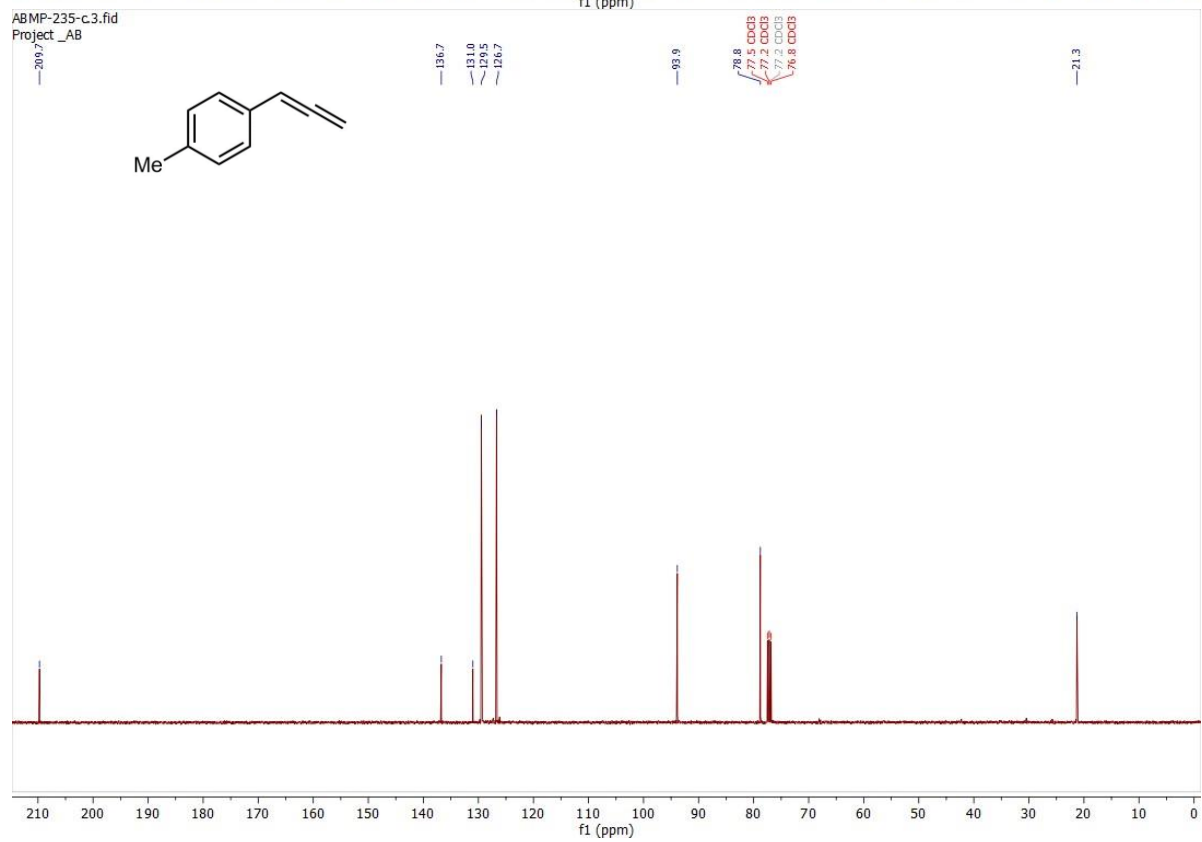
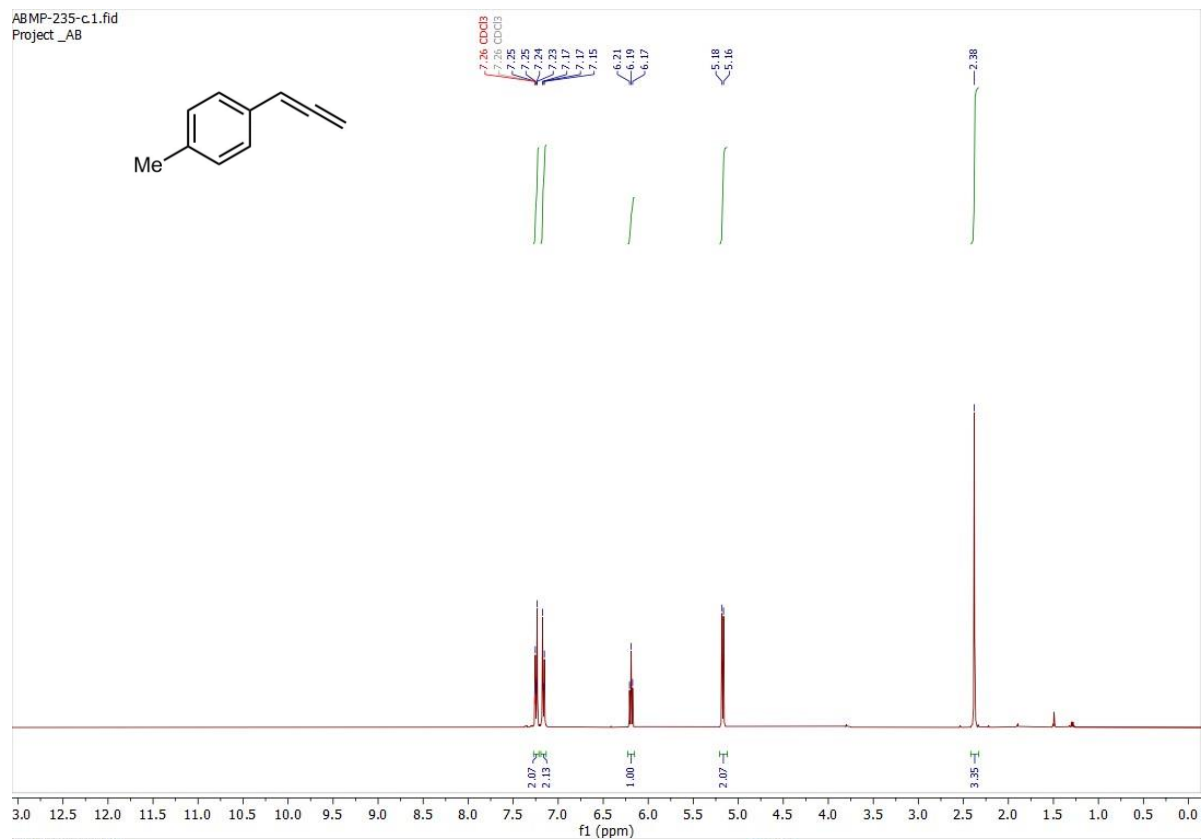
ABRD - 010 (without Ether).1.fid
Project_AB



ABRD - 010 (without Ether).3.fid
Project_AB

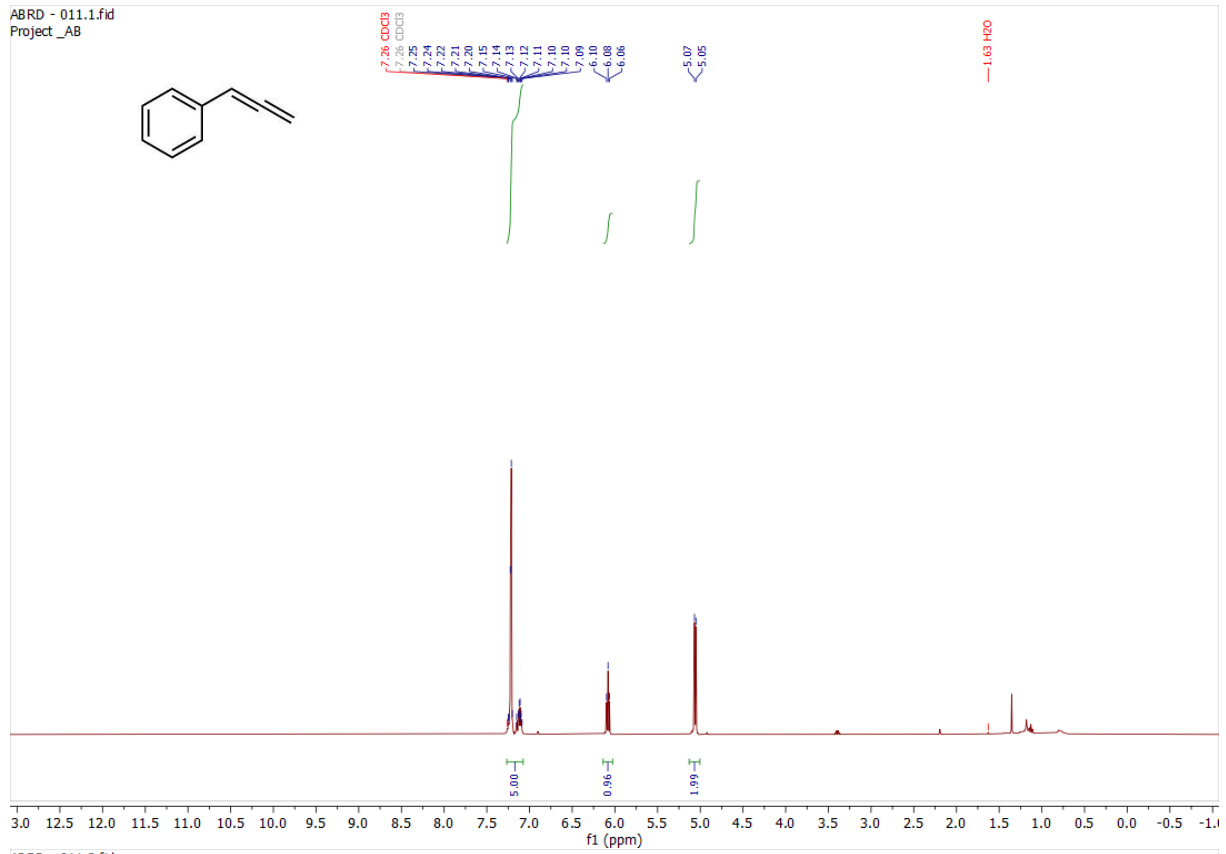


1-methyl-4-(propa-1,2-dien-1-yl)benzene (158a).

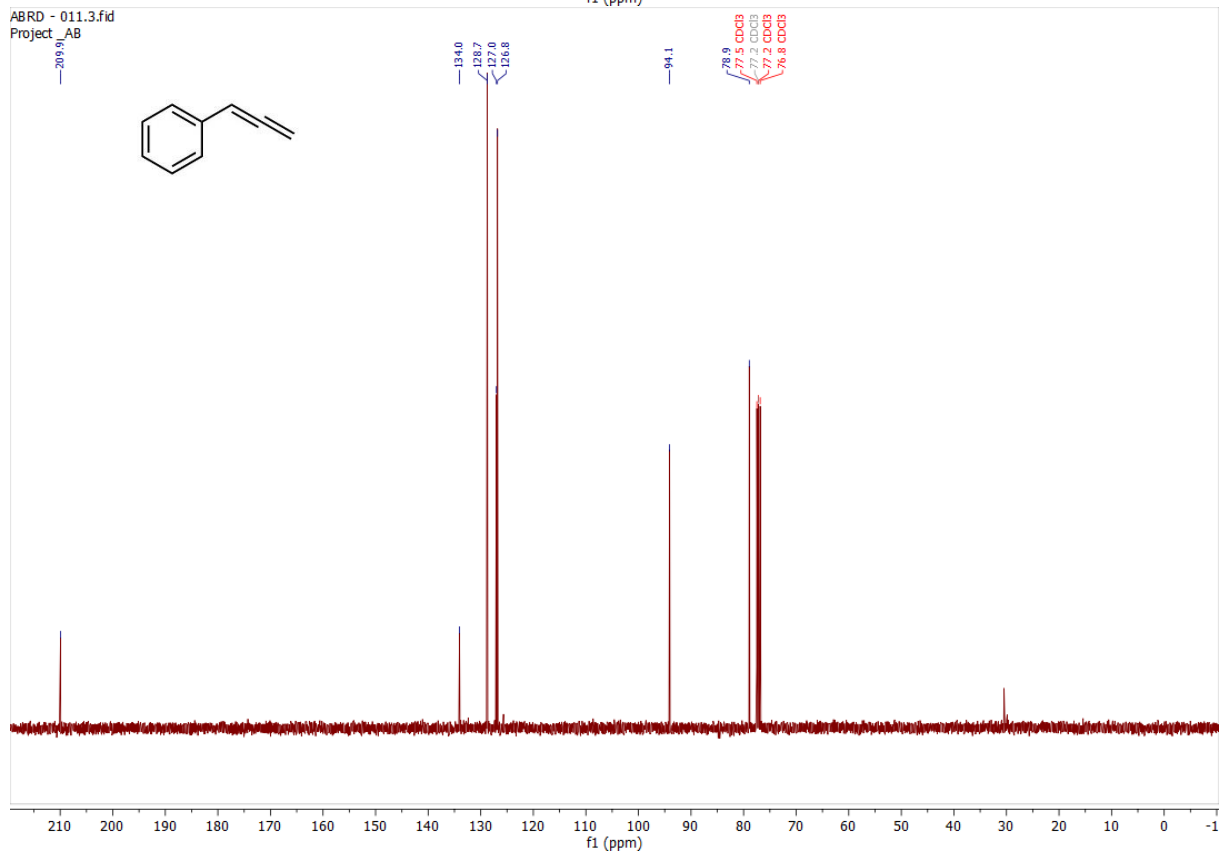


propa-1,2-dien-1-ylbenzene (**158b**)

ABRD - 011.1.fid
Project_AB

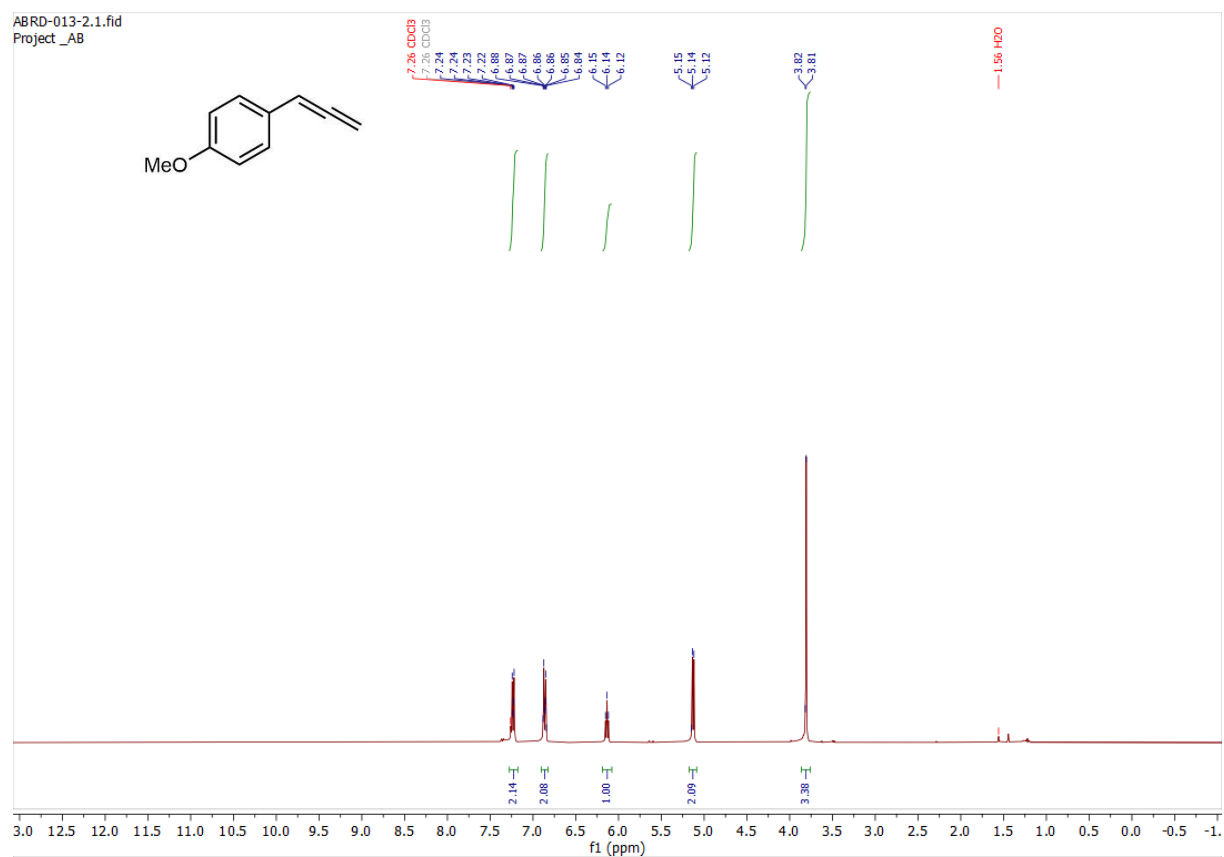


ABRD - 011.3.fid
Project_AB

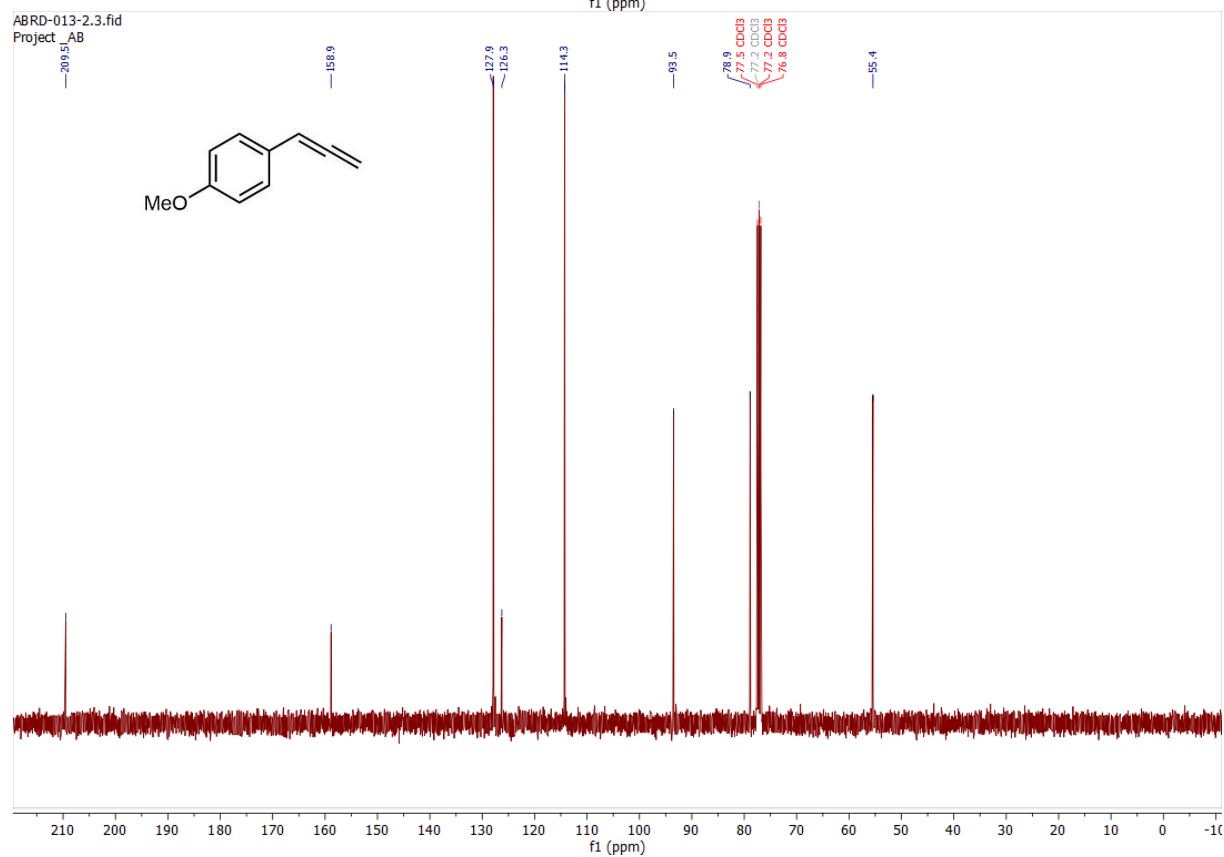


1-methoxy-4-(propa-1,2-dien-1-yl)benzene (158c)

ABRD-013-2.1.fid
Project_AB

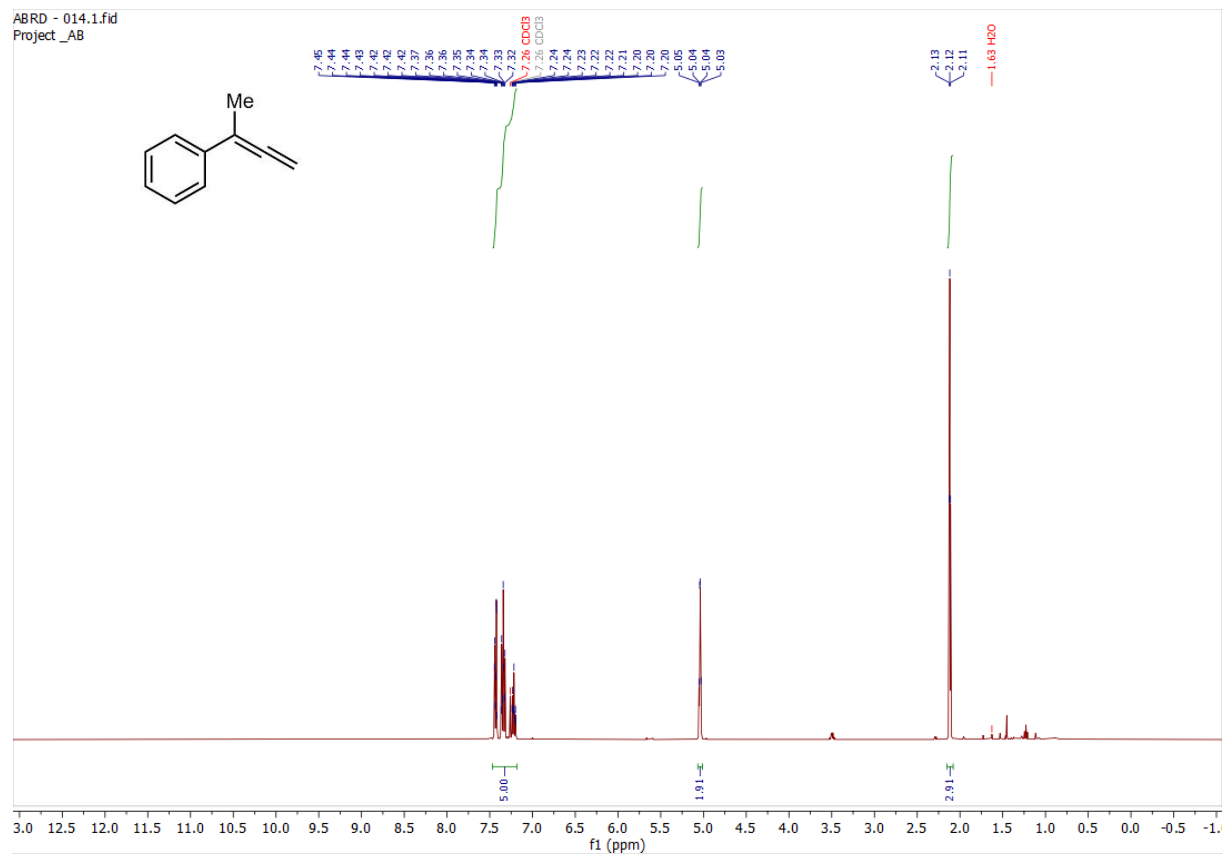


ABRD-013-2.3.fid
Project_AB

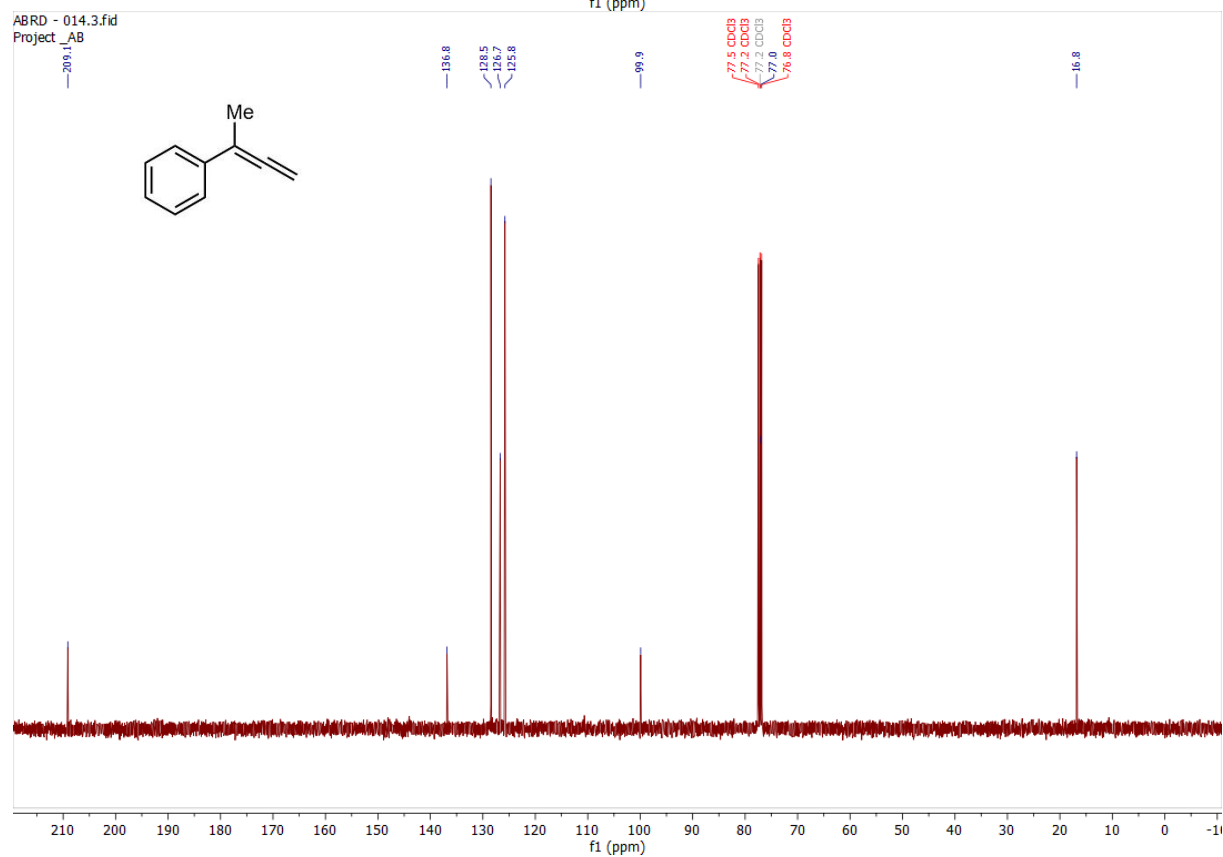


buta-2,3-dien-2-ylbenzene (158d)

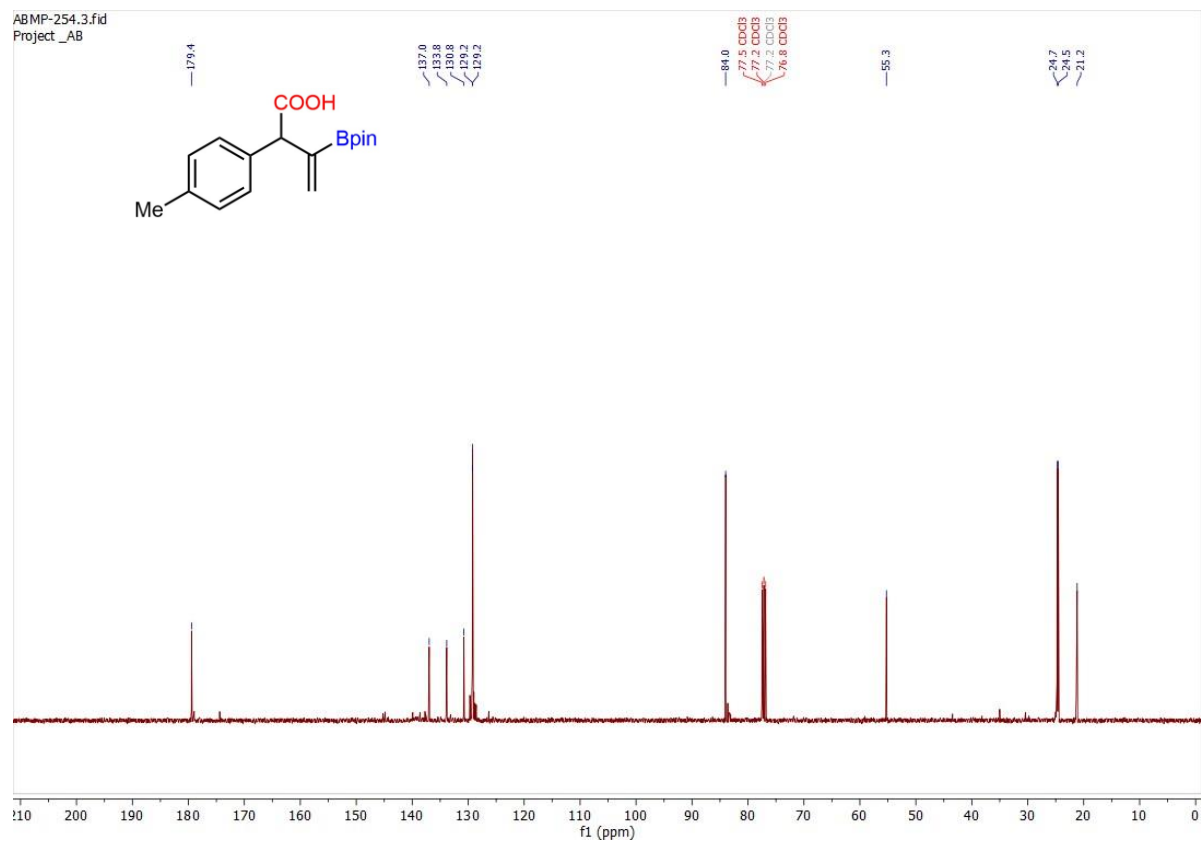
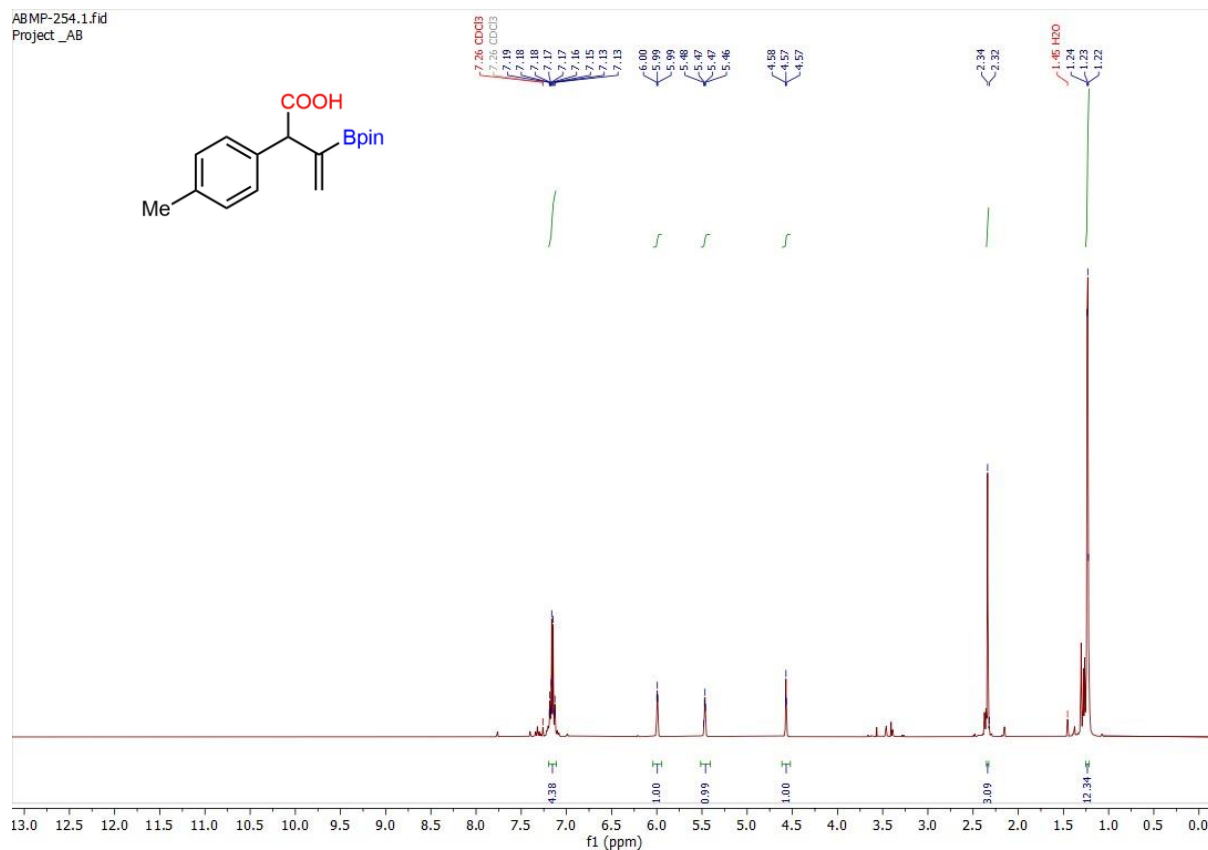
ABRD - 014.1.fid
Project_AB



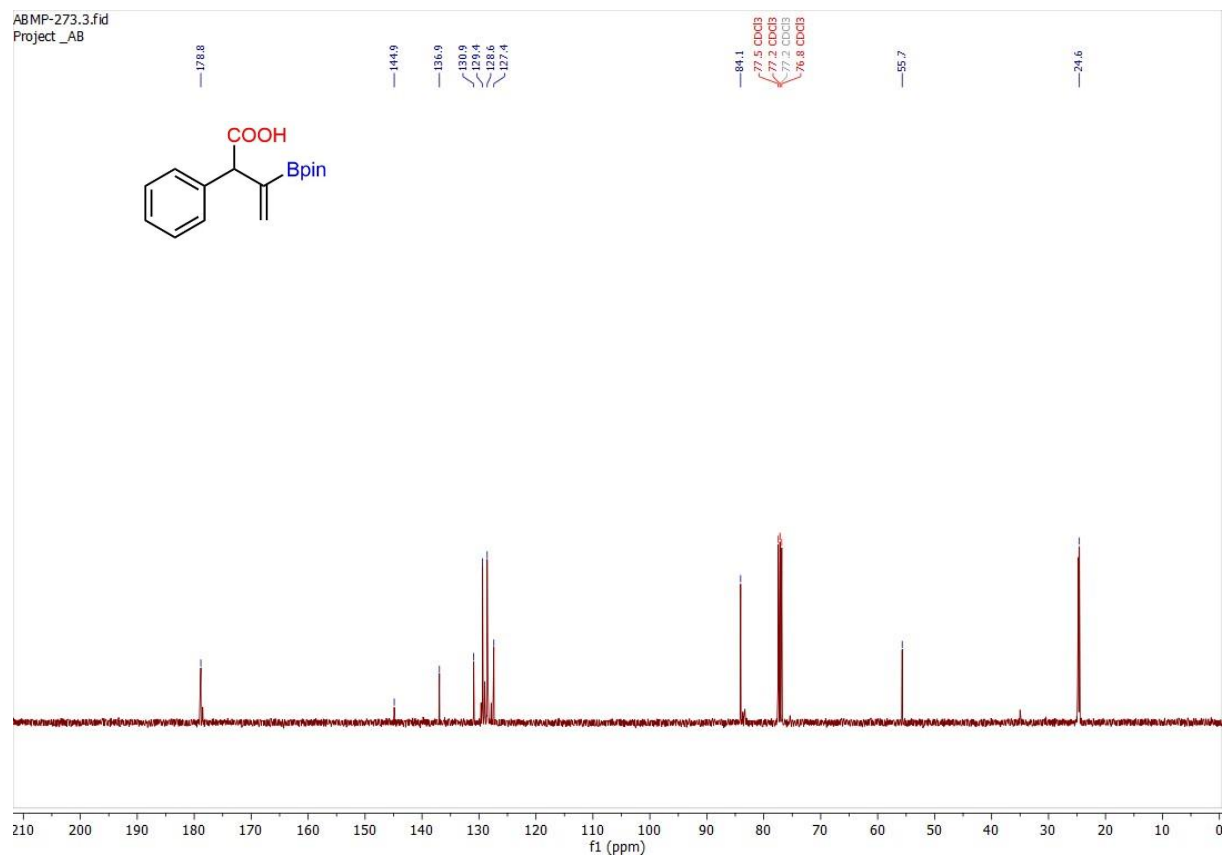
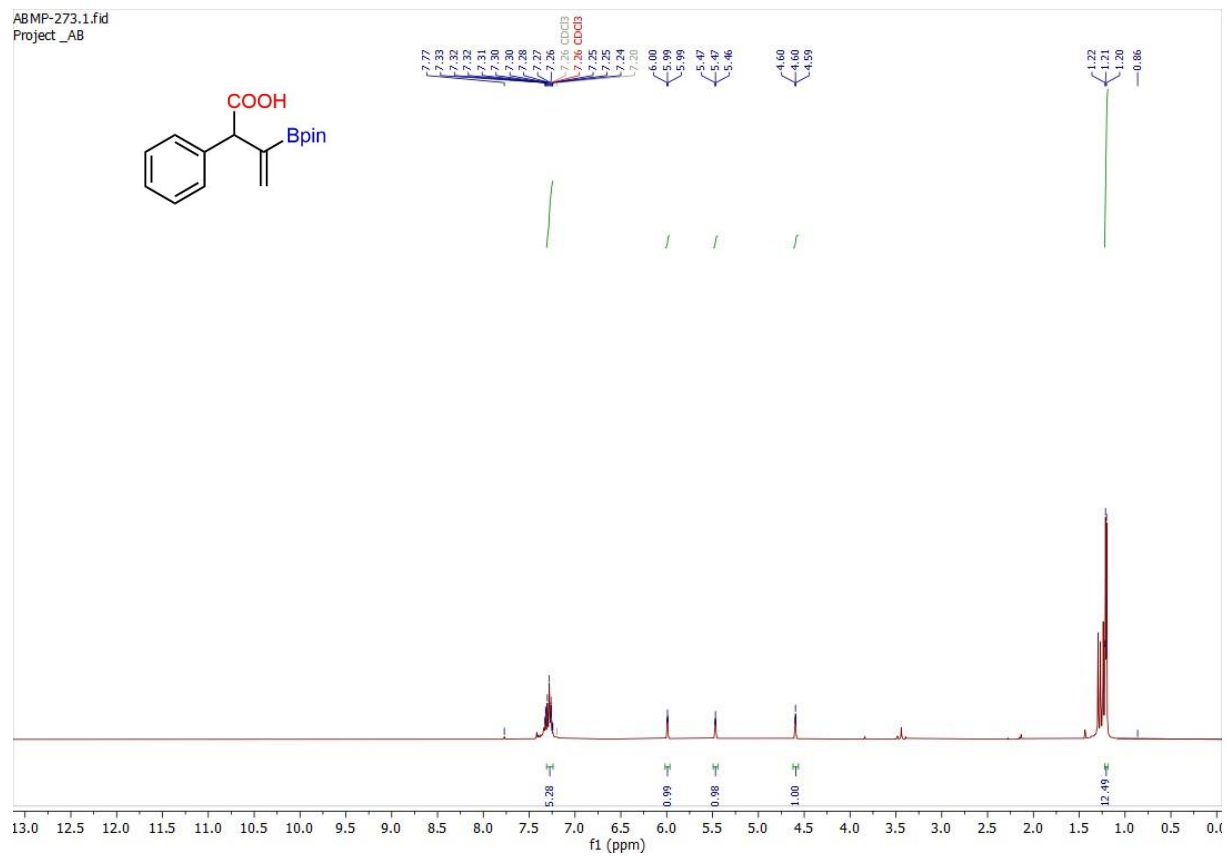
ABRD - 014.3.fid
Project_AB



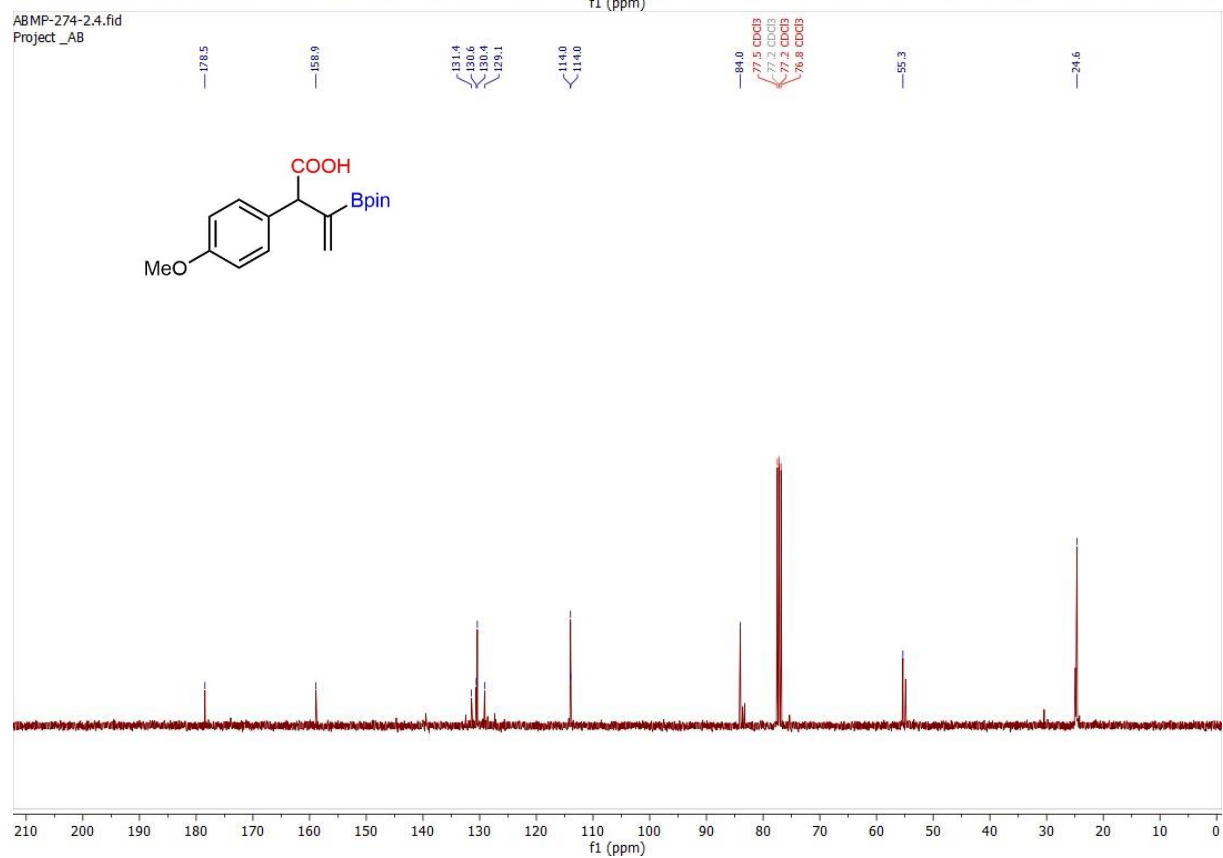
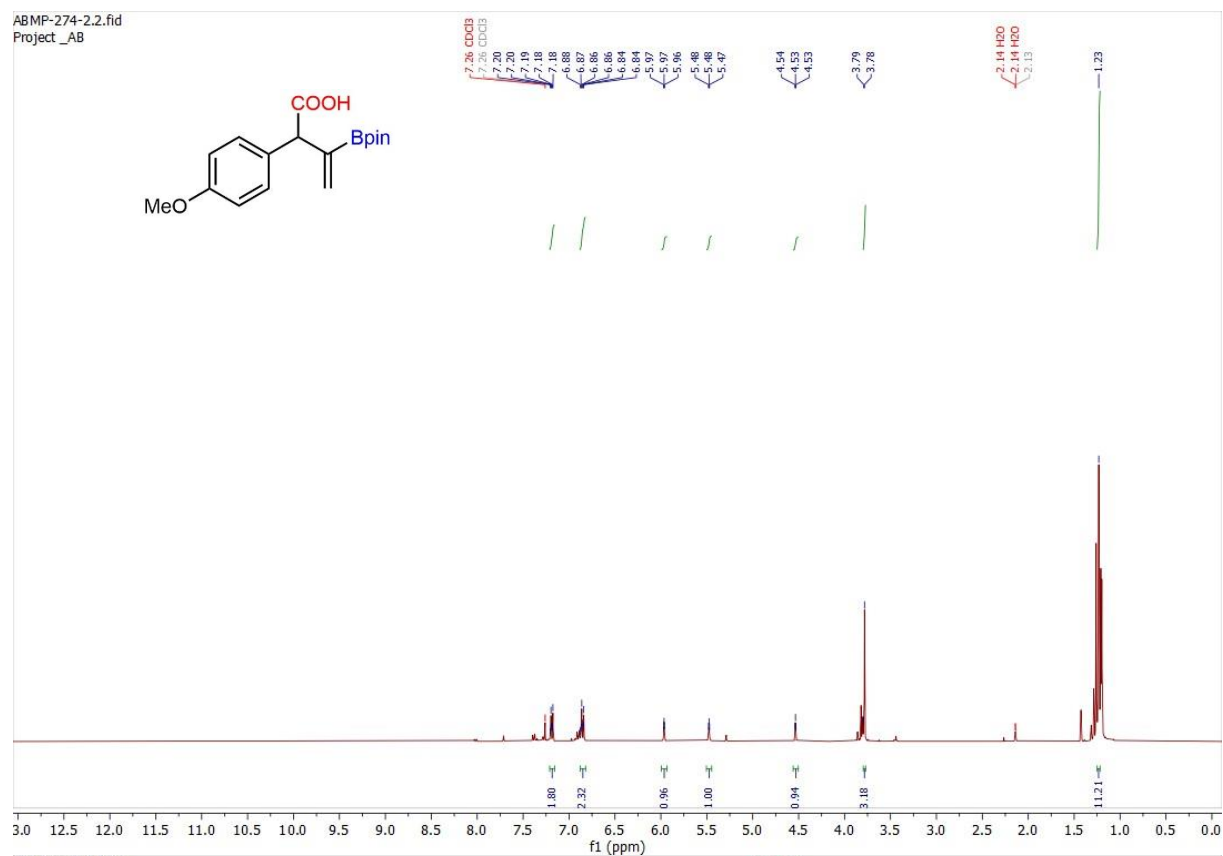
3-(4,4,5,5-tetramethyl-1,3,2-dioxaborolan-2-yl)-2-(p-tolyl)but-3-enoic acid (**159a**)



2-phenyl-3-(4,4,5,5-tetramethyl-1,3,2-dioxaborolan-2-yl)but-3-enoic acid (**159b**).



2-(4-methoxyphenyl)-3-(4,4,5,5-tetramethyl-1,3,2-dioxaborolan-2-yl)but-3-enoic acid (**159c**).



Paper I

Computational and experimental insights into asymmetric Rh-catalyzed hydrocarboxylation with CO₂

Eur. J. Org. Chem. **2021**, 4, 663-670

DOI: <https://doi.org/10.1002/ejoc.202001469>

Computational and Experimental Insights into Asymmetric Rh-Catalyzed Hydrocarboxylation with CO₂

Ljiljana Pavlovic,^[a] Martin Pettersen,^[b] Ashot Gevorgyan,^[b] Janakiram Vaitla,^[b] Annette Bayer,^{*[b]} and Kathrin H. Hopmann^{*[a]}

The asymmetric Rh-catalyzed hydrocarboxylation of α,β -unsaturated carbonyl compounds was originally developed by Mikami and co-workers but gives only moderate enantiomeric excesses. In order to understand the factors controlling the enantioselectivity and to propose novel ligands for this reaction, we have used computational and experimental methods to study the Rh-catalyzed hydrocarboxylation with different bidentate ligands. The analysis of the C–CO₂ bond formation transition states with DFT methods shows a preference for outer-sphere

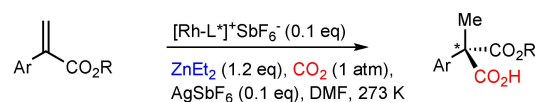
CO₂ insertion, where CO₂ can undergo a backside or frontside reaction with the nucleophile. The two ligands that prefer a frontside reaction, StackPhos and ^tBu-BOX, display an intriguing stacking interaction between CO₂ and an N-heterocyclic ring of the ligand (imidazole or oxazoline). Our experimental results support the computationally predicted low enantiomeric excesses and highlight the difficulty in developing a highly selective version of this reaction.

Introduction

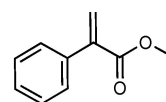
Widespread efforts are currently devoted to the search of catalysts, which can fixate CO₂ into organic molecules.^[1] A significant part of this activity is focused on metal-catalyzed carbon-carbon bond formation with CO₂.^[2] For the metal-catalyzed formation of saturated carboxylic acids, different protocols have been reported, including carboxylation of halides (C–X bonds)^[2a,b] and reductive carboxylation of unsaturated compounds such as alkenes.^[2c–h] An example of the carboxylation of Csp³–X bonds has been reported by Martin and co-workers, who developed a mild Ni(I)-catalyzed protocol for converting benzyl halides and CO₂ to phenylacetic acids.^[2b] The catalytic reductive carboxylation of alkenes is a challenging area, which has witnessed some progress in recent years. For example, Greenhalgh and Thomas reported a Fe(II)-catalyzed synthesis of α -aryl carboxylic acids from styrene derivatives and CO₂.^[2e] A Cu(I)/CsF-based protocol for the incorporation of CO₂ into disubstituted alkenes was reported by Skrydstrup, Nielsen, and co-workers.^[2h]

Interestingly, many of the known C–CO₂ bond formations result in generation of *chiral* carboxylic acids, but as racemic mixtures only.^[2b,e,h] Indeed, the design of enantioselective C–CO₂ bond formation reactions remains a major challenge. This is demonstrated by the fact that only very few studies on asymmetric C–CO₂ bond formation have been reported.^[1f,2c,3] In order to broaden the usefulness of CO₂ as a carbon synthon in the chemical and pharmaceutical industry, it is essential that novel enantioselective carboxylation protocols are developed, for example for the preparation of chiral carboxylic acids, which are important intermediates in many synthetic processes.^[4]

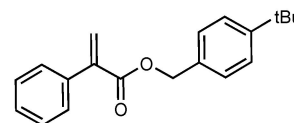
A promising asymmetric C–CO₂ bond formation protocol has been reported by Mikami and co-workers in 2016, involving the first enantioselective hydrocarboxylation of α,β -unsaturated carbonyl compounds (Figure 1).^[2c] The rhodium-based reaction involved the use of (S)-SEGPHOS as a chiral ligand, but only moderate enantiomeric excesses (*e.e.*'s) of up to 66% could be



sub1: methyl 2-phenylacrylate
L* = (S)-SEGPHOS
59% yield, 60% (S) *e.e.*



sub2: 4-(^tBu)benzyl 2-phenylacrylate
L* = (S)-SEGPHOS
60% yield, 66% (S) *e.e.*



sub3: ethyl 2-phenylacrylate
L* = (S)-SEGPHOS
46% yield, 66% (S) *e.e.*

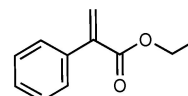


Figure 1. Enantioselective hydrocarboxylation reaction reported by Mikami and coworkers.^[2c]

[a] Dr. L. Pavlovic, Prof. Dr. K. H. Hopmann
Hylleraas Center for Quantum Molecular Sciences
Department of Chemistry, UiT The Arctic University of Norway
9037 Tromsø, Norway
E-mail: kathrin.hopmann@uit.no
https://site.uit.no/choco

[b] M. Pettersen, Dr. A. Gevorgyan, Dr. J. Vaitla, Prof. Dr. A. Bayer
Department of Chemistry, UiT The Arctic University of Norway
9037 Tromsø, Norway
E-mail: annette.bayer@uit.no
https://site.uit.no/bayerlab/

Supporting information for this article is available on the WWW under
https://doi.org/10.1002/ejoc.202001469

© 2020 The Authors. European Journal of Organic Chemistry published by Wiley-VCH GmbH. This is an open access article under the terms of the Creative Commons Attribution License, which permits use, distribution and reproduction in any medium, provided the original work is properly cited.

achieved.^[2c] The (S)-BINAP ligand gave similar results to (S)-SEGPPOS whereas other ligands, such as (S)-SynPhos or (R,R)-Pr-DuPhos, provided significantly lower *e.e.*'s.^[2c]

A computational analysis of the related non-enantioselective Rh-COD-catalyzed hydrocarboxylation reaction showed that during C–CO₂ bond formation, the CO₂ molecule does not interact with rhodium.^[5] Moreover, it was shown that benzylic substrates display an unusual η^6 -coordination mode, with the nucleophilic carbon positioned up to 3.6 Å away from rhodium.^[5] The same substrate binding mode and preference for an outer sphere CO₂ insertion were found computationally for the chiral Rh-(S)-SEGPPOS catalyst.^[6] This raises the question how the enantioselectivity is controlled in systems where CO₂ is not constrained through interactions with the metal. Although CO₂ preferably is positioned in the outer sphere, it may still be affected by repulsive and attractive nonbonding interactions with the ligand. A better understanding of the factors that govern the preferred positions and orientations of CO₂ may help to design catalysts with higher enantioselectivities.

Modern computational methods are sufficiently advanced to provide insights into the factors that control the enantioselectivity in metal-catalyzed reactions.^[7] For example, the selectivity may be influenced by the presence of specific interactions between the chiral catalyst and the substrate, and in particular, nonbonding forces may contribute significantly to the preferred formation of one product enantiomer.^[7–8] The identification of the selectivity-determining interactions typically relies on the computational optimization of the involved diastereomeric transition states. Such structures are generally built manually, followed by DFT optimizations, using different optimization algorithms.^[9] However, approaches to speed-up the computational analysis through automatized techniques have been put forward,^[10] with one example being the open-source toolkit AARON (An Automated Reaction Optimizer for New catalysts) designed by Wheeler and co-workers.^[10a] AARON employs TS templates provided by the user, but can automatically swap the ligands to build new geometries.

Herein, we perform a computational analysis of the selectivity-determining factors in the Rh-catalyzed hydrocarboxylation for four chiral rhodium complexes, of which three ligands have not previously been tested in this reaction. Ligand swapping is performed with AARON, followed by DFT optimizations. To validate the enantioselectivities predicted by the computations, an experimental analysis of all systems is performed.

Results and Discussion

Our study of the Rh-catalyzed asymmetric hydrocarboxylation reaction consists of three parts. Initially, we validated the computational protocol through analysis of the Rh-(S)-SEGPPOS-catalyzed hydrocarboxylation of two experimentally known substrates.^[2c] Next, we expanded our computational study to include the CO₂ insertion TSs for three additional chiral ligands, which have not been used in experiments on this reaction. Finally, we conducted an experimental evaluation of the corresponding Rh-complexes for hydrocarboxylation of ethyl 2-phenylacrylate.

For the analysis of the chiral ligands, 10 outer sphere CO₂ insertion TSs were built for each ligand, with different ligand-substrate orientations (Figure 2). Five of them were pro-(S)-TSs, and five the corresponding pro-(R) TSs. In the conformations **TS1a** and **TS1b**, the phenyl ring of the substrate interacts with the Rh-center in an η^6 fashion, whereas CO₂ is in the outer sphere, leading to a *backside* C–CO₂ bond formation (reminiscent of a S_E2(back) reaction). The difference between **TS1a** and **TS1b** is the orientation of the ester moiety (Figure 2). At **TS2a** and **TS2b**, the substrate is still bound in an η^6 fashion, but the CO₂ is positioned closer to metal, leading to a *frontside* reaction (reminiscent of a S_E2(front) reaction). At **TS3**, both the phenyl group and the carbonyl oxygen of the substrate interact with the Rh-center. It is important to highlight that for the comparative analysis of the four ligands, only *outer sphere* CO₂ insertion was considered,^[5] because the TS conformations, where interactions between Rh and CO₂ take place (referred to as *inner sphere* CO₂ insertion), show very high barriers (TS4_S and TS4_R, Supporting Information, Table S1). The four studied chiral ligands are given in Figure 3.

Computational analysis of Rh-(S)-SEGPPOS: The Rh-SEGPPOS-catalyzed hydrocarboxylation was here investigated computationally with the styrene-type α,β -unsaturated carbonyl substrates **sub1** and **sub2** (Figure 1), which previously have been studied experimentally by Mikami and co-workers.^[2c] The overall hydrocarboxylation mechanism for substrates of this type has been reported with [Rh(cod)Cl]₂ (S), Figure S1).^[5] We have here studied the full mechanism with Rh-(S)-SEGPPOS as the catalyst and methyl 2-phenylacrylate (**sub1**) as the substrate, with the energy profile shown in Figure S2 (Supporting Information). The mechanistic steps include a transmetalation of an ethyl from diethylzinc to the precatalyst, followed by a β -hydride elimination to give an Rh-H-Et intermediate. Insertion

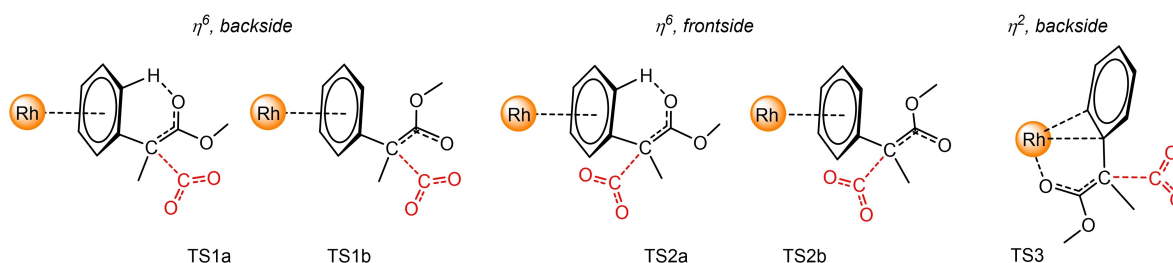


Figure 2. Five TS orientations considered here. For each of these, both pro-(R) and pro-(S) conformations were included.

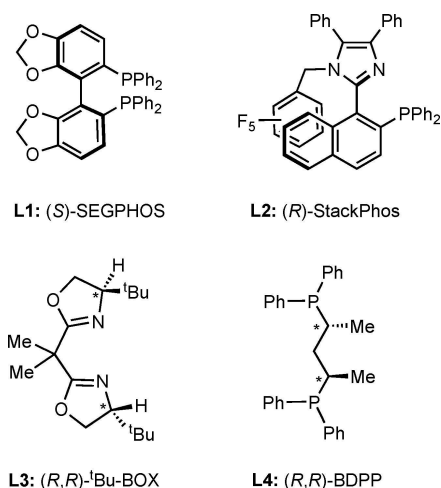


Figure 3. Four chiral ligands studied here in Rh-catalyzed hydrocarboxylation.

of the substrate leads to an energetically low-lying Rh-benzyl species that can attack CO₂.^[5] The CO₂ insertion is rate- and enantioselectivity-determining.^[5] At the carboxylation TS, the benzyl group prefers to coordinate in an η⁶ mode to rhodium, with the formally negative charge on the substrate delocalized between the nucleophilic carbon and the ester group, yielding an intermediate enolate (Figure 4). The enolate can attack CO₂ from its *re* or *si* face, and with a chiral ligand, unequal amounts of the (*R*)- and (*S*)-enantiomer of the product can be formed.

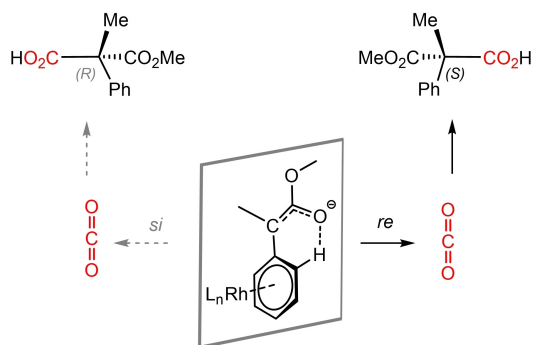


Figure 4. Illustration of the enolate intermediate of **sub1** and its attack on CO₂.

Carboxylation of methyl 2-phenylacrylate: In order to validate our computational protocol and our mechanistic understanding of this reaction, we first analyzed the Rh-(*S*)-SEGPHOS-catalyzed C–CO₂ bond formation with **sub1** (Figure 1). The results support our previous observation that CO₂ prefers to be in the outer sphere during C–CO₂ bond formation,^[5] as the inner and outer sphere TSs with Rh-(*S*)-SEGPHOS show an energy difference of 17.3 kcal/mol in favor of outer-sphere insertion (SI, Table S1, Figure S3).

At the lowest-lying outer sphere transition state **TS1a**_{S_{sub1/L1}}, the η⁶-coordinated enolate attacks CO₂ via its *re* face (Δ*G*[‡] = 12.1 kcal/mol relative to the Rh-benzyl intermediate, Figure S4, SI) and the experimentally observed (*S*)-product is obtained. At **TS1a**_{R_{sub1/L1}}, which is higher in energy by 0.7 kcal/mol, CO₂ is attacked by the enolate *si* face, giving the (*R*)-product (Figure 5). Other outer sphere conformations (Figure 2) were significantly higher in energy (Table 1). On the basis of all computed TS energies, we evaluated the *e.e.* for the Rh-(*S*)-SEGPHOS-catalyzed hydrocarboxylation of **sub1**, providing a computed *e.e.* of 53.8% (*S*), in very good agreement with the experimentally reported *e.e.* of 60.0% (*S*).^[2c]

Various noncovalent interactions between the ligand and **sub1** can be identified at the two energetically lowest-lying SEGPHOS TSs, **TS1a**_{S_{sub1/L1}} and **TS1a**_{R_{sub1/L1}} (Figure 5). At **TS1a**_{S_{sub1/L1}}, the phenyl rings of SEGPHOS form two C–H⋯π interactions (2.95, 3.10 Å) with the phenyl of the substrate. At the energetically higher lying **TS1a**_{R_{sub1/L1}}, SEGPHOS forms three C–H⋯π interactions with **sub1**, two with the substrate phenyl (2.97 and 3.14 Å), and one with the methyl group of the ester moiety (3.16 Å, Figure 5). As the strength of these C–H⋯π interactions appear similar at the two diastereomeric TSs, they do not seem to determine the selectivity. An analysis of C–H⋯O attractions at the two TSs shows comparable distances for interactions within the substrate (**TS1a**_{S_{sub1/L1}}: 2.16 Å, **TS1a**_{R_{sub1/L1}}: 2.11 Å), but significant differences in the *intermolecular* C–H⋯O interaction between the **sub1** carbonyl and the SEGPHOS phenyl (**TS1a**_{S_{sub1/L1}}: 2.46 Å, **TS1a**_{R_{sub1/L1}}: 3.00 Å). We speculate that this C–H⋯O interaction may be an essential factor in determining the enantioselectivity in the Rh-(*S*)-SEGPHOS-catalyzed hydrocarboxylation of methyl 2-phenylacrylate.

If CO₂ is placed closer to rhodium, here referred to as *frontside* insertion (TS2, Figure 2), the barriers increase by several kcal/mol (Figure 5). Interestingly, the *frontside* attack provides an incorrect enantioselectivity, as the **TS2a**_{R_{sub1/L1}}

Table 1. Barrier differences (ΔΔ*G*[‡], kcal/mol, 273 K) for different TS conformations (Figure 2) in Rh-catalyzed hydrocarboxylation of **sub1**.

Ligand	η ⁶ , backside				η ⁶ , frontside				η ² , backside		e.e. _{comp} [%]	e.e. _{exp} [%]
	TS1a _S	TS1a _R	TS1b _S	TS1b _R	TS2a _S	TS2a _R	TS2b _S	TS2b _R	TS3 _S	TS3 _R		
L1 (SEGPHOS)	0.0	0.7	3.1	2.0	6.5	4.0	7.3	4.9	8.3	7.9	53.8 (<i>S</i>)	60.0 (<i>S</i>) ^[c]
L2 (StackPhos)	2.2	2.8	2.1	3.0	0.0 ^[a]	0.6 ^[a]	0.8	1.0	15.2	10.8	47.0 (<i>S</i>)	n.d. ^[d]
					0.8 ^[b]	1.9 ^[b]						
L3 (t-Bu-BOX)	1.9	0.7	3.1	0.8	0.0	0.5	3.6	2.5	3.2	5.3	6.4 (<i>S</i>)	(0) ^[e]
L4 (BDPP)	0.5	0.0	0.8	1.9	5.8	5.5	8.6	6.4	9.7	12.1	24.3 (<i>R</i>)	(4) ^[e]

[a] TS2a structures as given in Figure 8 (TS2a_{S_{sub1/L2}}/TS2a_{R_{sub1/L2}}). [b] TS2a structures with stacking of pentafluorophenyl and phenyl as given in the SI, Figure S6 (TS2a_{stack}_{S_{sub1/L2}}/TS2a_{stack}_{R_{sub1/L2}}). [c] From ref.^[2c]. [d] Only racemic StackPhos could be tested, and the *e.e.* could thus not be determined. [e] Experimental results obtained here with **sub3**, which has an ethyl group instead of the methyl in **sub1** (Figure 1).

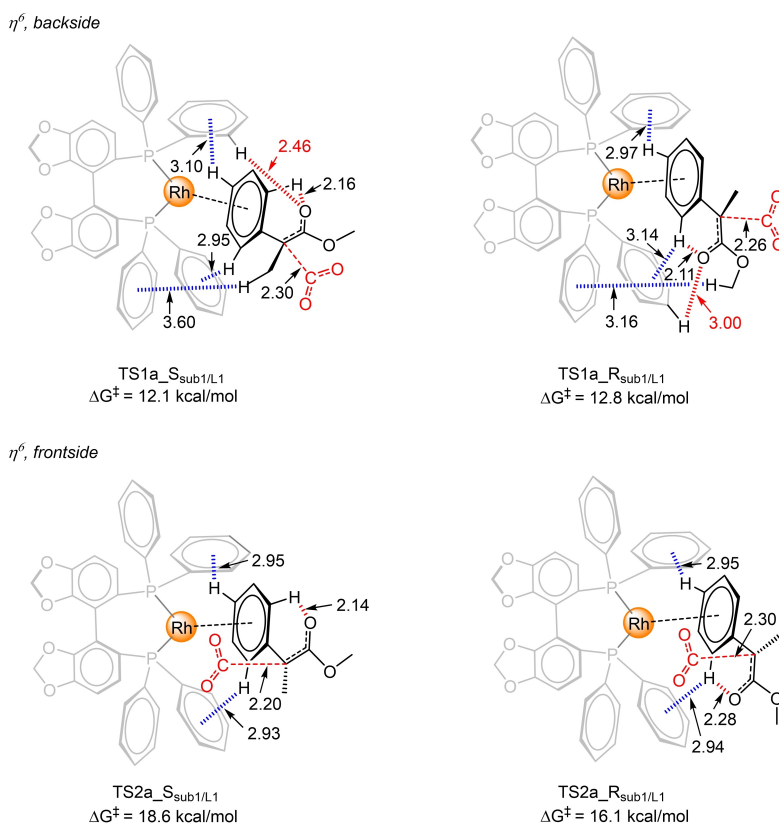


Figure 5. Illustration of the noncovalent interactions at four of the optimized CO₂ insertion TSs for Rh-(S)-SEGPPOS-catalyzed hydrocarboxylation of methyl 2-phenylacrylate (**sub1**). Only some of the hydrogens are shown for clarity. Distances in Å.

structure is 2.5 kcal/mol lower in energy than **TS2a** **S**_{sub1/L1}. The experimentally observed (*S*)-selectivity^[2c] is thus dominated by the *backside* structures. These findings highlight the need to compare computationally predicted TSs with experimental selectivities to evaluate if appropriate TS conformations were located.

The TS3 conformations, where the ester of the substrate interacts with rhodium (Figure 2), are ~8 kcal/mol higher in energy than TS1 and are not considered relevant (Table 1).

Carboxylation of 4-(tert-butyl)benzyl 2-phenylacrylate: We proceeded to analyze **sub2**, which contains two phenyl rings (Figure 1), leading to several favorable C–H... π interactions during C–CO₂ bond formation (Figure 6). A similar pattern as for **sub1** is observed, where at the lowest-lying transition state **TS1a**_{sub2/L1} ($\Delta G^\ddagger = 12.0$ kcal/mol), the Rh-benzyl (*SI*, Figure S4) attacks CO₂ from its *re* face, resulting in the (*S*)-product. A favorable C–H...O (2.47 Å) interaction is seen at **TS1a**_{sub2/L1} but lacks at **TS1a**_{sub2/L1}, which is higher in energy by 1.0 kcal/mol. The computed *e.e.* of 73% (*S*) is in good agreement with the experimental value of 66% (*S*).^[2c]

The combined results for **sub1** and **sub2** indicate that the enantioselectivity of Rh-(*S*)-SEGPPOS-catalyzed hydrocarboxylation appears to be a result of favorable C–H...O interactions between the substrate and the SEGPPOS ligand. At the preferred TS1a conformations (Figure 5 and Figure 6), the CO₂ molecule is placed away from the metal center (> 5 Å) and thus

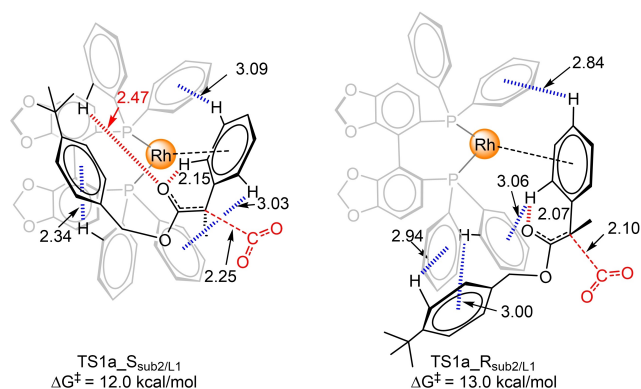


Figure 6. Illustration of the preferred TSs for Rh-(*S*)-SEGPPOS-catalyzed carboxylation of **sub2**. Only some of the hydrogens are shown for clarity. Distances in Å.

the chiral catalyst is promoting the enantioselectivity through the positioning of the alkene substrate, not through interactions with CO₂.

Potential of other ligands in the Rh-catalyzed asymmetric hydrocarboxylation: We selected a set of ligands structurally different from SEGPPOS from the library of AARON^[10a] (**L2–L4**, Figure 3) and investigated their predicted enantioselectivities with DFT. The set includes one *P,N* ligand (**L2**: StackPhos),^[11] an *N,N* ligand (**L3**: ^tBu-BOX)^[12] and a *P,P* ligand (**L4**: BDPP).^[13] These

ligands have shown good performance in other asymmetric transformations (allylation, aziridination, hydrovinylation),^[14] and to our knowledge, they have not previously been used for Rh-catalyzed hydrocarboxylation.

The outer sphere TS conformations depicted in Figure 2 were evaluated for L2–L4 and **sub1** through manual DFT calculations, with the energies summarized in Table 1 (geometric parameters are shown in Figure 7, Figure 8 and Tables S1–4, SI). For BDPP (L4), we see a similar behaviour as for SEGPHOS, with a preference for *backside* insertion (Table 1). However, the StackPhos (L2) and ^tBu-BOX (L3) ligands show a computed preference for *frontside* insertion. Both ligands display an intriguing stacking interaction between CO₂ and the N-heterocyclic ring of the ligand (imidazole or oxazoline, Figure 7, SI, Figure S7).

It can be noted that related attractive stacking interactions have been predicted in computational studies focusing on the binding of CO₂ to N-heterocyclic compounds,^[15] and in experimental and computational studies on the solvation of aromatic compounds in supercritical CO₂.^[16] However, to our knowledge, the heterocycle-CO₂ stacking interaction has not been described in the context of an organometallic ligand or a CO₂ insertion reaction.

The heterocycle-CO₂ interaction appears strongest at the StackPhos TS geometries, with a nitrogen-C_{CO2} distance of 3.22 Å (Figure 7). The StackPhos TS geometries with **sub1** are

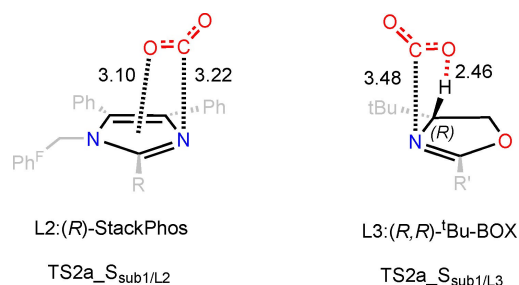


Figure 7. Stacking of CO₂ above the N-heterocyclic ring of L2 and L3 at the *frontside* TSs. Distances in Å.

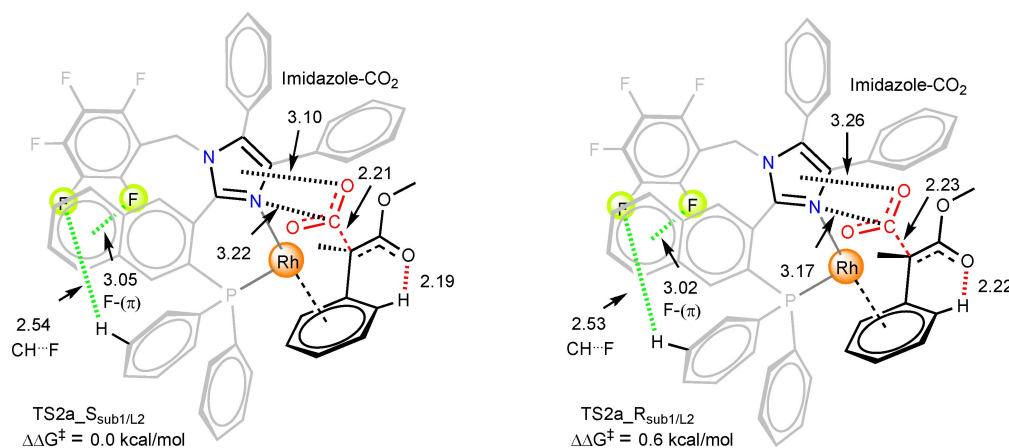


Figure 8. Illustration of the preferred TSs for Rh-(*R*)-StackPhos-catalyzed carboxylation of **sub1**. Distances in Å

therefore discussed in further detail here. Besides the CO₂-imidazole stacking, the lowest lying TS2a_*S*_{sub1/L2} also displays an intriguing F- π attraction between a fluoro group of the pentafluoro-phenyl and the naphthalene ring (3.05 Å), alongside a C–H...F interaction (2.53 Å, Figure 8). Similar F- π interactions to phenantrene-like aromatic systems have been reported in the literature.^[17] Interestingly, this F- π interaction is not seen in the X ray structure of the StackPhos ligand,^[11a] which instead displays π - π stacking between pentafluorophenyl and naphthalene subunits (3.38 Å). In our computations, this π - π stacking increases the TS energy by 2.5 kcal/mol (SI, Figure S5).

An alternative π - π interaction between pentafluorophenyl and another phenyl substituent increases the CO₂ insertion barrier slightly by 0.8 kcal/mol (TS2a_*stack_S*_{sub1/L2} SI, Figure S6). In the case of *backside* insertion with StackPhos, the imidazole-CO₂ interactions are absent, which increases the barriers by 2 to 3 kcal/mol (Table 1). The TS3 structures, where the ester carbonyl interacts with rhodium, are more than 11 kcal/mol above the TS2 structures and therefore are not relevant.

The best (*R*)-pathway obtained for **sub1** with StackPhos proceeds via *frontside* insertion and is 0.6 kcal/mol above the best (*S*)-structure (TS2a_*R*_{sub1/L2}, Figure 8). This TS also displays stacking of CO₂ above the imidazole moiety and an F- π interaction between pentafluorophenyl and the naphthalene subunits (Figure 8). The *e.e.* computed on the basis of all obtained StackPhos TS structures is 47% (*S*) (Table 1), which indicates that this ligand is not expected to perform significantly better than SEGPHOS.

The other studied ligands are predicted to give low *e.e.*'s. Our calculations show that with the (*R,R*)-^tBu-BOX chiral ligand, at the lowest-lying TS2a_*S*_{sub1/L3}, the *frontside* CO₂ insertion is preferred (SI, Figure S7). The opposite enantiomer TS2a_*R*_{sub1/L3} is higher in energy by only 0.5 kcal/mol. The predicted *e.e.* on the basis of all optimized TS conformations is only 6.4% (Table 1).

With the (*R,R*)-BDPP ligand, at the lowest-lying TS1a_*R*_{sub1/L4}, the CO₂ prefers *backside* insertion (SI, Figure S7). TS1a_*S*_{sub1/L4} has a barrier that is only 0.5 kcal/mol higher than TS1a_*R*_{sub1/L4}.

The TSs for the *frontside* CO₂ insertion are higher in energy by more than 5 kcal/mol (Table S4). This scenario is reminiscent of the biphosphine ligand (*S*)-SEGPPOS. These observations may be a consequence of the bulky phenyl groups of the ligands, which restrict CO₂, making the *backside* insertion more preferable. The computed *e.e.* for this ligand is 24% (*R*) (Table 1).

Experimental analysis of Rh-catalyzed hydrocarboxylation of L1 to L4: We analyzed the ability of L1 to L4 to mediate the CO₂ insertion reaction with **sub3** (Figure 1), which is closely related to the computationally studied substrate **sub1**, but which has an ethyl instead of a methyl ester. In the work by Mikami and co-workers, **sub3** and **sub1** behaved similarly, providing respectively 66% and 60% *e.e.*'s for Rh-SEGPPOS catalyzed hydrocarboxylation.^[2c]

In our work, we obtained a product yield of 48% and an *e.e.* of 32% with L1 and **sub3** (Table 2). Although the yield is similar as previously reported, the *e.e.* is somewhat lower than the reported 66%.^[2c] For L2, only a racemic mixture of the ligand could be tested,^[18] providing a yield of 74% for carboxylation of **sub3** (Table 2). Thus, L2 may provide reasonable yields, and may be a relevant starting point for future development of ligands for this reaction.

For L3, experimental hydrocarboxylation of **sub3** gave the acid in as much as 99% yield but with 0% *e.e.* (Table 2), in good agreement with our predictions for **sub1** of 6.4% *e.e.* (Table 1).

For L4, our experimental results on **sub3** showed 94% yield, but only 4% *e.e.* (Table 2), in line with the predicted low *e.e.* of 24% *e.e.* for **sub1** (Table 1).

We conclude that our experimental results are in good agreement with the low *e.e.*'s predicted by the computations. This validates the proposed outer sphere mechanisms presented here for ligands L1 to L4 and indicates that DFT-D methods can be employed to model the enantioselectivities of these kinds of systems. At the same time, it highlights the difficulty to make a selective version of the rhodium-catalyzed hydrocarboxylation of acrylates.

Conclusion

We have employed computational and experimental methods to study the potential of bidentate chiral ligands L1 to L4 for

the asymmetric rhodium-catalyzed hydrocarboxylation of acrylates.

Our DFT analysis of the mechanism supports a preference for an η⁶ coordination of benzylic substrates and an outer sphere insertion of CO₂ also with chiral ligands.^[5] The reported experimental enantioselectivity with SEGPPOS^[2c] is reproduced for substrates **sub1** and **sub2** in our calculations and is predicted to arise from the C–H...O interaction between a phenyl group of SEGPPOS and the carbonyl group of the substrate.

Our computations on the chiral *P,N* ligand StackPhos (L2), the *N,N* ligand ^tBu-BOX (L3) and the *P,P* ligand BDPP (L4) showed up to 47% *e.e.* for **sub1**. For StackPhos and ^tBu-BOX, the preferred transition state geometries display an intriguing stacking interaction of CO₂ with the N-heterocyclic ring (imidazole or oxazoline, Figure 7). Experimental analyses of ligands L1 to L4 showed that all are able to catalyze the hydrocarboxylation reaction, with L2, L3, and L4 providing good yields of 74 to 99% for carboxylation of **sub3**. Although the experimentally observed enantiomeric excesses are low, they are in good agreement with computations, underpinning the ability of DFT-D to adequately model complex enantioselective reactions.

Our combined results on Rh-catalyzed hydrocarboxylation indicate that the enantioselectivity of this reaction is difficult to control. A possible strategy to be considered is to steer CO₂ into a specific position to decrease its conformational freedom. The noncovalent stacking interactions observed between CO₂ and L2 or L3 (Figure 7) may be interesting in this sense and variants of these ligands may thus be a relevant starting point for future developments.

Computational section

Computational models: Calculations were performed with full substrates **sub1** and **sub2** (Figure 1) and with the full ligands (Figure 3). No molecular truncations or symmetry constraints were applied.

Computational methods: All calculations were performed at the DFT level of theory as implemented in the Gaussian09 package.^[19] For geometry optimizations, the DFT functional PBE^[20] was employed together with the Grimme empirical dispersion correction (D2^[21]) and the implicit polarizable continuum model using the integral equation formalism, IEFPCM^[22] (DMF solvent). The PBE functional has been found to be an adequate choice for rhodium-catalyzed hydrocarboxylation reactions in our previous study,^[5] where it provided a good agreement with experimental results.^[2c] The geometries of all intermediates and transition states were fully optimized and frequency calculations were performed in order to confirm the nature of the stationary points, where all transition states structures exhibited only one imaginary frequency.

In geometry optimizations, the BS1 basis set was employed, consisting of 6-311G(d,p)^[23] for C, H, O, N, F, and P, and the LANL2DZ^[24] basis set and pseudopotential for rhodium, including an extra f polarization function with exponent 1.35.^[25] A larger basis set, BS2, was employed for single-point energy calculations, consisting of 6-311+G(2d,2p) on all non-metal atoms and LANL2TZ (f) on rhodium.

Table 2. Experimental yields and *e.e.*'s with four chiral ligands employed in Rh-catalyzed hydrocarboxylation of **sub3**.

Ligand	Yields [%]	<i>e.e.</i> _{exp} [%]
L1 (SEGPPOS)	48.0	32.0
L2 (StackPhos)	74.0	n.d. ^[a]
L3 (^t Bu-BOX)	99.0	0.0
L4 (BDPP)	94.0	4.0

[a] n.d = Not detected.

In order to convert computed free energies (ΔG° , BS1) at 1 atm into a 1 M standard state, a standard state (SS) correction was included. At 273 K, this correction is -1.69 kcal/mol (for a reaction that goes from 2 moles to 1).^[26]

The final Gibbs free energy was determined with the following expression: $\Delta G^\circ_{1M,273K} = \Delta G^\circ_{1atm,BS1,273K} - \Delta E_{BS1} + \Delta E_{BS2} + SS_{273K}$.

The enantiomeric excess (e.e.) was computed using the formula Eq. (1):^[17,27]

$$e.e. (\%) = \frac{\sum_{i=1}^n k_{Ri} - \sum_{i=1}^n k_{Si}}{\sum_{i=1}^n k_{Ri} + \sum_{i=1}^n k_{Si}}$$

where k_{ri} are the computed rate constants of TS structures with (*R*) configuration, which are summed from $i=1$ to $i=n$, where n is equal to the number of TSs within 3 kcal/mol from the best TS. k_{si} is the equivalent for (*S*)-TSs.

AARON ligand swapping: The TS library used for AARON^[10a] was based on the SEGPHOS structures obtained in the manual DFT analysis. Three ligands present in the AARON ligand library (**L2**, **L3**, **L4**) were then specified to be swapped with SEGPHOS. We preoptimized the conformations with the swapped ligands with AARON in two steps, using HF/6-31 in the first step and PBE-D2/BS1_{mod} in the second step, where BS1_{mod} is as BS1 but lacks the additional *f* polarization function on rhodium, as AARON did not allow the addition of basis functions. The obtained geometries for all ligands were then used as input for further manual DFT investigations, with the protocol as described above for manual DFT calculations. Note that for **L4**, the (*R,R*) ligand was computed, but the (*S,S*) ligand was used in experiments (which should give opposite enantioselectivity).

Experimental Section

Experimental Details: Commercially available starting materials, reagents, catalysts, and anhydrous and degassed solvents were used without further purification. Thin-layer chromatography was carried out using Merck TLC Silica gel 60 F₂₅₄ and visualized by short-wavelength ultraviolet light or by treatment with potassium permanganate (KMnO₄) stain. ¹H, ¹³C, ¹⁹F, and ³¹P NMR spectra were recorded on a Bruker Avance 400 MHz at 20 °C. All ¹H NMR spectra are reported in parts per million (ppm) downfield of TMS and were measured relative to the signals for CHCl₃ (7.26 ppm). All ¹³C NMR spectra were reported in ppm relative to residual CDCl₃ (77.20 ppm) and were obtained with ¹H decoupling. Coupling constants, *J*, are reported in Hertz (Hz). High-resolution mass spectra (HRMS) were recorded from methanol solutions on an LTQ Orbitrap XL (Thermo Scientific) in positive electrospray ionization (ESI) mode.

(*S*)-SEGPHOS, (*S,S*)-^tBu-BOX, and (*S,S*)-BDPP ligands are commercially available. Ethyl 2-phenylacrylate, StackPhos, and corresponding Rh complexes were prepared according to slightly modified literature procedures. For more details, see Electronic Supporting Information.

General experimental procedure for the preparation of Rh-complexes (Figure 9): Inside of the glove box an oven-dried 25 mL round bottom flask was charged with [Rh(cod)Cl]₂ (100.0 mg, 1 equiv.) and AgSbF₆. The flask was sealed with a rubber septa, removed from the glove box, and equipped with an Ar balloon. Inside of the glove box, another oven dried 25 mL round bottom flask was charged with the corresponding chelating ligand (2 equiv.), sealed with a rubber septum, removed from the glove box, and equipped with an Ar balloon. Both flasks were charged with dry CHCl₃ (5 mL) and allowed to stir for 30 min at 20 °C. This was followed by the dropwise addition of CHCl₃ solution of the ligand to the stirring

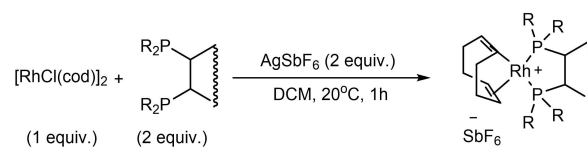


Figure 9. Experimental procedure for the preparation of Rh-complexes.

solution of [Rh(cod)Cl]₂, which was accompanied by precipitation of a white powder (AgCl/NaCl). The resulting mixture was stirred at 20 °C for 1 h. Afterward, the precipitate was filtered off and the solvent was evaporated to give the corresponding complex as an orange powder.

General experimental procedure for Rh-catalyzed hydrocarboxylation of ethyl 2-phenylacrylate (Table 2): Inside of the glove box an oven-dried 25 mL Schlenk flask was charged with corresponding Rh-complex (10 mol%) and AgSbF₆ (10 mol%). The flask was sealed with a rubber septum, removed from the glove box, evacuated, filled with CO₂, and equipped with a CO₂ balloon. This was followed by sequential addition of dry DMF (5 mL) and ethyl 2-phenylacrylate (150 mg, 1 equiv.) using syringes. The resulting mixture was transferred into an ice bath where under vigorous stirring 1 M solution of Et₂Zn in hexane (1.2 equiv.) was added dropwise using a syringe. The resulting mixture was allowed to stir at 0 °C for 3 h. Then the reaction mixture was diluted with Et₂O (5 mL) and carefully neutralized using 6 M HCl (5 mL). The acidic solution was diluted with water (5 mL) and removed using a separating funnel. The organic phase was then extracted using a solution of saturated NaHCO₃ (3 × 30 mL). The collected aqueous solution was carefully treated with 6 M HCl (60 mL) and extracted using Et₂O (3 × 30 mL). Collected Et₂O solution was washed with distilled water (30 mL) and evaporated to give the target acid as a faint orange oil. Enantiomers were separated using SFC on a chiral column (CEL-2), eluent *i*PrOH:EtOH:TFA – 70:30:2, and gradient 3–8, 10 min run.

Starting from 0.851 mmol of ethyl 2-phenylacrylate the product was obtained as a faint orange oil, yield 48%, e.e. 32% (0.091 g, [Rh(cod)((*S*)-SEGPHOS)]SbF₆), yield 74% (0.121 g, [Rh(cod)((*rac*)-StackPhos)]SbF₆), yield 99%, e.e. 0% (0.189 g, [Rh(cod)((*S,S*)-^tBu-BOX)]SbF₆), yield 94%, e.e. 4% (0.178 g, [Rh(cod)((*S,S*)-BDPP)]SbF₆). ¹H NMR (400 MHz, CDCl₃): δ = 10.38 (br s, 1H), 7.39–7.24 (m, 5H), 4.21 (q, *J* = 7.1 Hz, 2H), 1.87 (s, 3H), 1.22 (t, *J* = 7.1 Hz, 4H). ¹³C NMR (101 MHz, CDCl₃): δ = 177.0, 171.9, 137.7, 128.4, 128.0, 127.4, 62.3, 58.7, 22.0, 14.0.

Acknowledgements

This work has been supported by the Research Council of Norway (No. 262695, No. 300769), by the Tromsø Research Foundation (No. TFS2016KHH), by Notur – The Norwegian Metacenter for Computational Science through grants of computer time (No. nn9330k and nn4654k), and by NordForsk (No. 85378). We thank Manuel K. Langer for support with the SFC and Prof. Steven Wheeler, Victoria M. Ingman, Anthony J. Schaefer, and Stig Rune Jensen for advice and technical assistance in the implementation of AARON

Conflict of Interest

The authors declare no conflict of interest.

Keywords: Asymmetric catalysis · Carboxylation · Carbon dioxide fixation · Density functional calculations · Rhodium

- [1] a) M. Cokoja, C. Bruckmeier, B. Rieger, W. A. Herrmann, F. E. Kühn, *Angew. Chem. Int. Ed. Engl.* **2011**, *50*, 8510–8537; b) S. Dabral, T. Schaub, *Adv. Synth. Catal.* **2019**, *361*, 223–246; c) A. Tortajada, F. Julia-Hernandez, M. Borjesson, T. Moragas, R. Martin, *Angew. Chem. Int. Ed.* **2018**, *57*, 15948–15982; d) Y. Yang, J.-W. Lee, *Chem. Sci.* **2019**, *10*, 3905–3926; e) Y.-X. Luan, M. Ye, *Tetrahedron Lett.* **2018**, *59*, 853–861; f) J. Vaitla, Y. Guttormsen, J. K. Mannisto, A. Nova, T. Repo, A. Bayer, K. H. Hopmann, *ACS Catal.* **2017**, *7*, 7231–7244.
- [2] a) T. Fujihara, K. Nogi, T. Xu, J. Terao, Y. Tsuji, *J. Am. Chem. Soc.* **2012**, *134*, 9106–9109; b) T. León, A. Correa, R. Martin, *J. Am. Chem. Soc.* **2013**, *135*, 1221–1224; c) S. Kawashima, K. Aikawa, K. Mikami, *Eur. J. Org. Chem.* **2016**, 3166–3170; d) C. M. Williams, J. B. Johnson, T. Rovis, *J. Am. Chem. Soc.* **2008**, *130*, 14936–14937; e) M. D. Greenhalgh, S. P. Thomas, *J. Am. Chem. Soc.* **2012**, *134*, 11900–11903; f) P. Shao, S. Wang, C. Chen, C. Xi, *Org. Lett.* **2016**, *18*, 2050–2053; g) K. Murata, N. Numasawa, K. Shimomaki, J. Takaya, N. Iwasawa, *Chem. Commun.* **2017**, *53*, 3098–3101; h) M. Juhl, S. L. R. Laursen, Y. Huang, D. U. Nielsen, K. Daasbjerg, T. Skrydstrup, *ACS Catal.* **2017**, *7*, 1392–1396; i) K. Ukai, M. Aoki, J. Takaya, N. Iwasawa, *J. Am. Chem. Soc.* **2006**, *128*, 8706–8707; j) H. Mizuno, J. Takaya, N. Iwasawa, *J. Am. Chem. Soc.* **2011**, *133*, 1251–1253.
- [3] a) L. Dian, D. S. Müller, I. Marek, *Angew. Chem. Int. Ed.* **2017**, *56*, 6783–6787; *Angew. Chem.* **2017**, *129*, 6887–6891; b) Y.-Y. Gui, N. Hu, X.-W. Chen, L. L. Liao, T. Ju, J.-H. Ye, Z. Zhang, J. Li, D.-G. Yu, *J. Am. Chem. Soc.* **2017**, *139*, 17011–17014; c) X.-W. Chen, L. Zhu, Y.-Y. Gui, K. Jing, Y.-X. Jiang, Z.-Y. Bo, Y. Lan, J. Li, D.-G. Yu, *J. Am. Chem. Soc.* **2019**, *141*, 18825–18835; d) Y. Shi, B.-W. Pan, Y. Zhou, J. Zhou, Y.-L. Liu, F. Zhou, *Org. Biomol. Chem.* **2020**, *18*, 8597–8619; e) C.-K. Ran, X.-W. Chen, Y.-Y. Gui, J. Liu, L. Song, K. Ren, D.-G. Yu, *Sci. China Chem.* **2020**, *63*, 1336–1351.
- [4] Y. G. Liu, Q. Chen, C. L. Mou, L. T. Pan, X. Y. Duan, X. K. Chen, H. Z. Chen, Y. L. Zhao, Y. P. Lu, Z. C. Jin, Y. R. Chi, *Nat. Commun.* **2019**, *10*, 1675, 1–8.
- [5] Lj. Pavlovic, J. Vaitla, A. Bayer, K. H. Hopmann, *Organometallics* **2018**, *37*, 941–948.
- [6] D. García-López, Lj. Pavlovic, K. H. Hopmann, *Organometallics* **2020**, *39*, 1339–1347.
- [7] Q. Peng, F. Duarte, R. S. Paton, *Chem. Soc. Rev.* **2016**, *45*, 6093–6107.
- [8] a) K. H. Hopmann, *Int. J. Quantum Chem.* **2015**, *115*, 1232–1249; b) H. J. Davis, R. J. Phipps, *Chem. Sci.* **2017**, *8*, 864–877.
- [9] a) H. B. Schlegel, *J. Comput. Chem.* **1982**, *3*, 214–218; b) H. B. Schlegel, *Wiley Interdiscip. Rev.: Comput. Mol. Sci.* **2011**, *1*, 790–809; c) J. J. Zheng, M. J. Frisch, *J. Chem. Theory Comput.* **2017**, *13*, 6424–6432; d) C. Gonzalez, H. B. Schlegel, *J. Chem. Phys.* **1989**, *90*, 2154–2161.
- [10] a) Y. Guan, V. M. Ingman, B. J. Rooks, S. E. Wheeler, *J. Chem. Theory Comput.* **2018**, *14*, 5249–5261; b) A. R. Rosales, J. Wahlers, E. Limé, R. E. Meadows, K. W. Leslie, R. Savin, F. Bell, E. Hansen, P. Helquist, R. H. Munday, O. Wiest, P.-O. Norrby, *Nat. Can.* **2019**, *2*, 41–45.
- [11] a) F. S. P. Cardoso, K. A. Abboud, A. Aponick, *J. Am. Chem. Soc.* **2013**, *135*, 14548–14551; b) P. Braunstein, F. Naud, S. J. Rettig, *New J. Chem.* **2001**, *25*, 32–39; c) B. V. Rokade, P. J. Guiry, *ACS Catal.* **2018**, *8*, 624–643.
- [12] G. Desimoni, G. Faita, K. A. Jørgensen, *Chem. Rev.* **2006**, *106*, 3561–3651.
- [13] J. Bakos, Á. Orosz, S. Cserépi, I. Tóth, D. Sinou, *J. Mol. Catal. A* **1997**, *116*, 85–97.
- [14] a) B. M. Trost, D. L. Van Vranken, *Chem. Rev.* **1996**, *96*, 395–422; b) D. A. Evans, M. M. Faul, M. T. Bilodeau, B. A. Anderson, D. M. Barnes, *J. Am. Chem. Soc.* **1993**, *115*, 5328–5329; c) J. P. Page, T. V. RajanBabu, *J. Am. Chem. Soc.* **2012**, *134*, 6556–6559.
- [15] a) H. M. Lee, I. S. Youn, M. Saleh, J. W. Lee, K. S. Kim, *Phys. Chem. Chem. Phys.* **2015**, *17*, 10925–10933; b) E. Hernández-Marín, A. A. Lemus-Santana, *J. Mex. Chem. Soc.* **2015**, *59*, 36–42; c) M. Prakash, K. Mathivon, D. M. Benoit, G. Chambaud, M. Hochlaf, *Phys. Chem. Chem. Phys.* **2014**, *16*, 12503–12509.
- [16] D. Kajjiya, K.-i. Saitow, *J. Phys. Chem. B* **2010**, *114*, 16832–16837.
- [17] P. Li, J. M. Maier, E. C. Vik, C. J. Yehl, B. E. Dial, A. E. Rickher, M. D. Smith, P. J. Pellechia, K. D. Shimizu, *Angew. Chem. Int. Ed. Engl.* **2017**, *56*, 7209–7212.
- [18] The costly separation of enantiomers of the synthesized racemic mixture of L2 was not attempted, due to the computationally predicted low enantiomeric excess expected for this ligand in hydrocarboxylations.
- [19] M. J. Frisch, G. W. Trucks, H. B. Schlegel, G. E. Scuseria, M. A. Robb, J. R. Cheeseman, G. Scalmani, V. Barone, B. Mennucci, G. A. Peterson, H. Nakatsuji, M. Caricato, X. Li, H. P. Hratchian, A. F. Izmaylov, J. Bloino, G. Zheng, J. L. Sonnenberg, M. Hada, M. Ehara, K. Toyota, R. Fukuda, J. Hasegawa, M. Ishida, T. Nakajima, Y. Honda, O. Kitao, H. Nakai, T. Vreven, J. A. Jr Montgomery, J. E. Peralta, F. Ogliaro, M. Bearpark, J. J. Heyd, E. Brothers, K. N. Kudin, V. N. Staroverov, R. Kobayashi, J. Normand, K. Raghavachari, A. Rendell, J. C. Burant, S. S. Iyengar, J. Tomasi, M. Cossi, N. Raga, J. M. Millam, M. Klene, J. E. Knox, J. B. Cross, V. Bakken, C. Adamo, J. Jaramillo, R. Gomperts, R. E. Stratmann, O. Yazyev, A. J. Austin, R. Cammi, C. Pomelli, J. W. Ochterski, R. L. Martin, K. Morokuma, V. G. Zakrzewski, G. A. Voth, P. Salvador, J. J. Dannenberg, S. Dapprich, A. D. Daniels, O. Farkas, J. B. Foresman, J. V. Ortiz, J. Cioslowski, D. J. Fox, *Gaussian 09, rev. D.01*; Gaussian, Inc., Wallingford, CT, **2013**.
- [20] a) A. D. Becke, *Phys. Rev. A* **1988**, *38*, 3098–3100; b) C. Lee, W. Yang, R. G. Parr, *Phys. Rev. B* **1988**, *37*, 785–789.
- [21] S. Grimme, *J. Comput. Chem.* **2006**, *27*, 1787–1799.
- [22] a) E. Cancès, B. Mennucci, J. Tomasi, *J. Chem. Phys.* **1997**, *107*, 3032–3041; b) J. Tomasi, B. Mennucci, E. Cancès, *J. Mol. Struct.* **1999**, *464*, 211–226; c) J. Tomasi, B. Mennucci, R. Cammi, *Chem. Rev.* **2005**, *105*, 2999–3094.
- [23] R. Krishnan, J. S. Binkley, R. Seeger, J. A. Pople, *J. Chem. Phys.* **1980**, *72*, 650–654.
- [24] P. J. Hay, W. R. Wadt, *J. Chem. Phys.* **1985**, *82*, 299–310.
- [25] A. W. Ehlers, M. Böhme, S. Dapprich, A. Gobbi, A. Höllwarth, V. Jonas, K. F. Köhler, R. Stegmann, A. Veldkamp, G. Frenking, *Chem. Phys. Lett.* **1993**, *208*, 111–114.
- [26] a) C. J. Cramer, *Essentials of computational chemistry: theories and models*, J. Wiley, West Sussex, England; New York, **2002**; b) K. H. Hopmann, *Organometallics* **2016**, *35*, 3795–3807.
- [27] S. T. Schneebeli, M. L. Hall, R. Breslow, R. Friesner, *J. Am. Chem. Soc.* **2009**, *131*, 3965–3973.

Manuscript received: November 9, 2020
Revised manuscript received: December 14, 2020
Accepted manuscript online: December 18, 2020

European Journal of Organic Chemistry

Supporting Information

Computational and Experimental Insights into Asymmetric Rh-Catalyzed Hydrocarboxylation with CO₂

Ljiljana Pavlovic, Martin Pettersen, Ashot Gevorgyan, Janakiram Vaitla, Annette Bayer,* and
Kathrin H. Hopmann*

Contents

Computational part	2
Proposed mechanism for Rh-catalyzed hydrocarboxylation	2
Computed free energy profile for Rh-(S)-SEGPHOS catalyzed hydrocarboxylation of methyl 2-phenylacrylate	3
Computational results for Rh-(S)-SEGPHOS (L1)	4
The optimized TSs (C-CO₂) with Rh-CO₂ interactions	5
The optimized geometries of Rh-benzyl intermediates	6
Computational results for Rh-(R)-StackPhos (L2)	7
The optimized higher-energy TSs with StackPhos	8
Computational results for Rh-(R,R)-^tBu-BOX (L3)	9
Computational results for Rh-(R,R)-BDPP (L4)	10
Experimental part	11
General considerations	11
Experimental procedures and characterization of products	11
Copies of spectra	19
Copies of chromatograms	47

Computational part

Proposed mechanism for Rh-catalyzed hydrocarboxylation

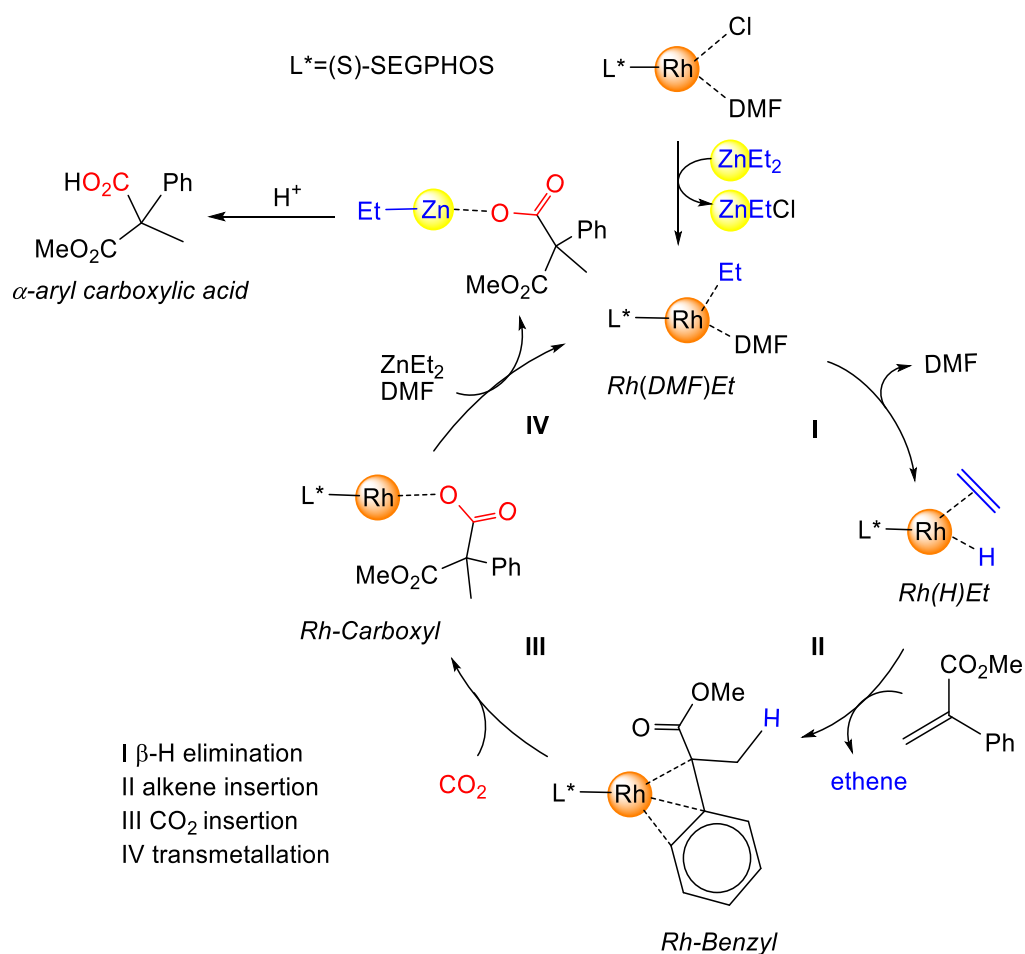


Figure S1. Mechanism for Rh-SEGPHOS-catalyzed hydrocarboxylation, based on the previous experimental proposal,¹ and computations performed in our computational study with COD ligand.² Rh-benzyl intermediate displays η^3 binding mode of the substrate to the metal.

¹ S. Kawashima, K. Aikawa, K. Mikami, *Eur. J. Org. Chem.* **2016**, 3166-3170.

² Lj. Pavlovic, J. Vaitla, A. Bayer, K. H. Hopmann, *Organometallics* **2018**, 37, 941-948.

Computed free energy profile for Rh-(S)-SEGPPOS catalyzed hydrocarboxylation of methyl 2-phenylacrylate

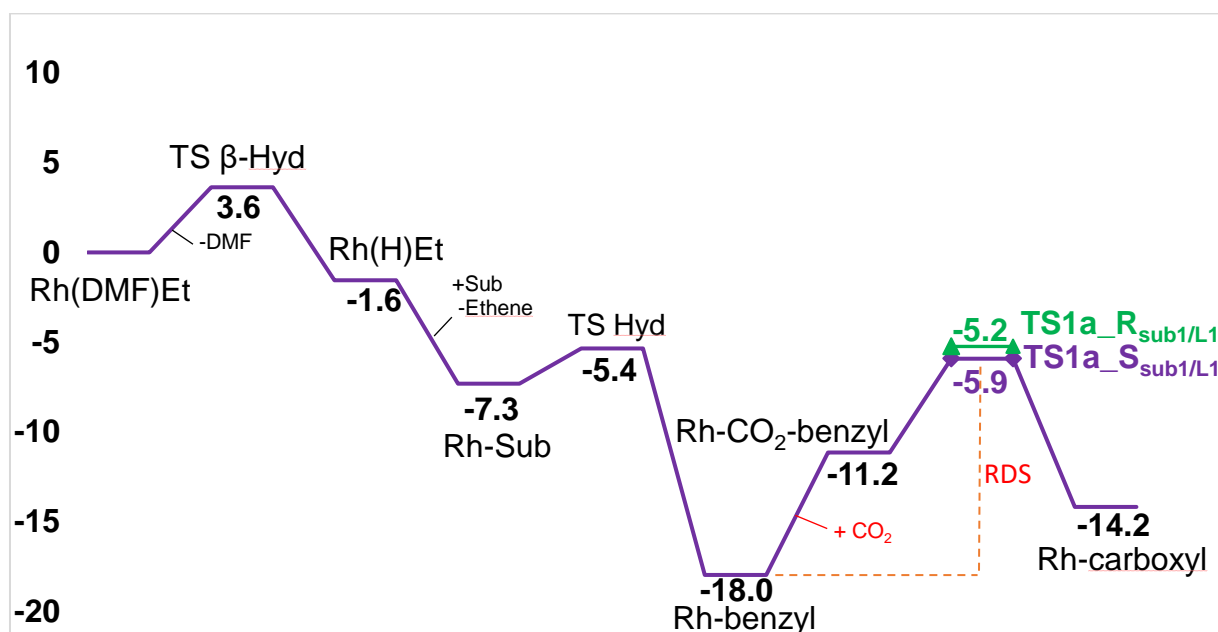


Figure S2. Computed free energy profile (kcal/mol, 273 K, PBE-D2/BS2[IEFPCM]//PBE-D2/BS1[IEFPCM] level of theory) for Rh-(S)-SEGPPOS-catalyzed hydrocarboxylation of methyl 2-phenylacrylate. The Rh(DMF)Et intermediate is the energetic reference. The last step, transmetalation is not included, as this TS could not be located. The rate and enantioselectivity-determining step is the CO₂ insertion into the Rh-benzyl intermediate.

Computational results for Rh-(S)-SEGPHOS (L1)

Table S1. Selected distances (Å) of noncovalent interactions at the TS conformations with Rh-(S)-SEGPHOS and methyl 2-phenylacrylate. The energy differences between pro-(S) and pro-(R) TSs ($\Delta\Delta G^\ddagger$) are given in kcal/mol. The computed e.e. is 53.8 % (Table 1, main text).

		TS	Stereo	CH..O (Cat-Sub)	CH... π (Sub-Cat)	C-H..O (within sub)	Rh-C (Nuc)	C-CO ₂	$\Delta\Delta G^\ddagger$	
Outer sphere insertion	Backside CO ₂ insertion	TS1a_S	pro-(S)	2.46	2.95; 3.08;3.60	2.16(Ph)	3.60	2.30	0.0	
		TS1b_S	pro-(S)	2.43	2.85; 3.20	2.40(Me)	3.70	2.20	3.1	
		TS1a_R	pro-(R)	2.97	3.16; 2.97;3.14	2.11(Ph)	3.64	2.26	0.7	
		TS1b_R	pro-(R)	3.32	3.24; 2.94	2.33(Me)	3.67	2.20	2.0	
	Frontside CO ₂ insertion	TS2a_S	pro-(S)	>4.00	2.93;2.95	2.14(Ph)	3.90	2.20	6.5	
		TS2b_S	pro-(S)	>4.00	3.00; 3.24	2.35(Me)	3.90	2.20	7.3	
		TS2a_R	pro-(R)	>4.00	2.95;2.94	2.28(Ph)	3.80	2.32	4.0	
		TS2b_R	pro-(R)	>4.00	2.90; 2.94	2.40(Me)	3.96	2.30	4.9	
	Rh-O=C (ester)	TS3_S	pro-(S)	Rh- O(Es) 2.17	2.71;3.16	2.47(Ph)	3.43	2.45	8.3	
		TS3_R	pro-(R)	2.17	2.64;3.24	2.53(Ph)	3.60	2.30	7.9	
	Inner sphere	Rh-CO ₂ interaction	TS 4_S	pro-(S)	Rh-CO ₂ 2.18	2.93; 4.02	2.21(Ph)	2.80	2.23	17.3
			TS 4_R	pro-(R)	2.60	2.82;3.06	2.21(Ph)	2.71	2.07	18.7

The optimized TSs (C-CO₂) with Rh-CO₂ interactions

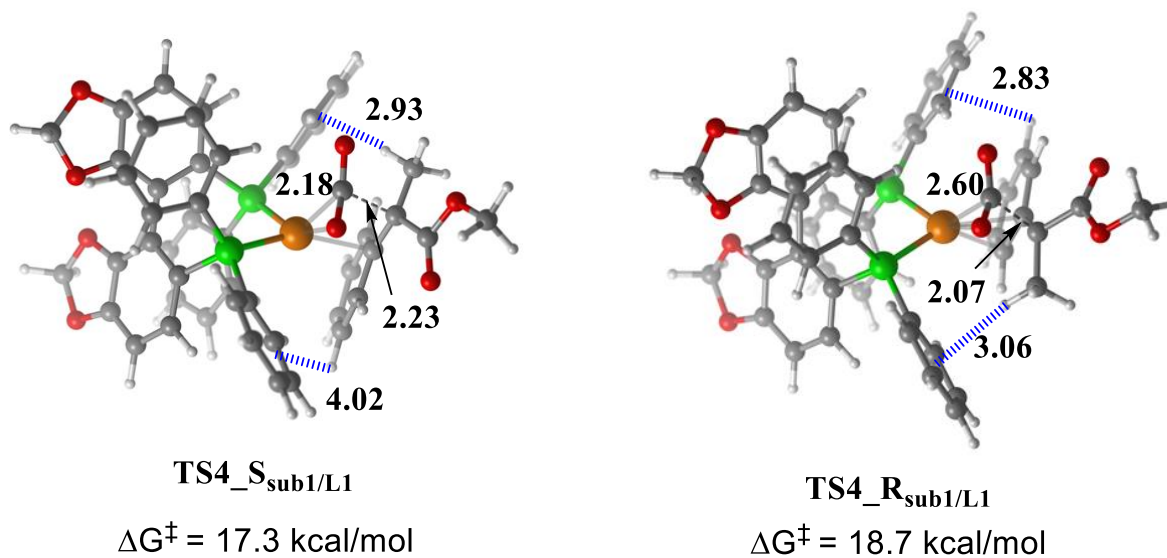
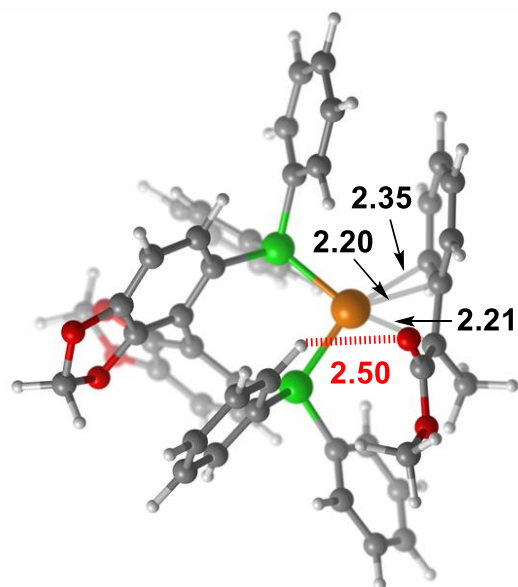


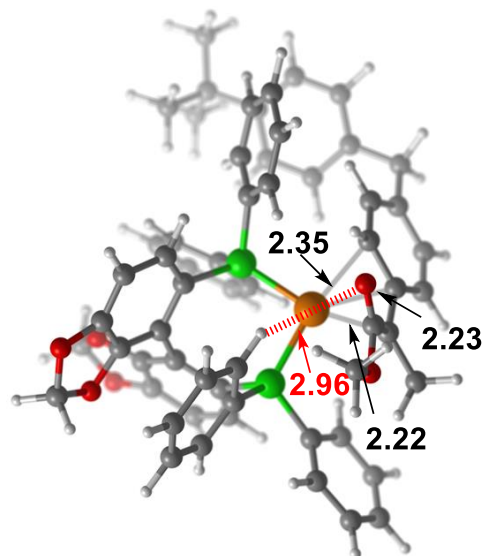
Figure S3. The optimized TSs for C-CO₂ bond formation step with Rh-CO₂ interaction present (inner sphere CO₂ insertion, **TS4_S_{sub1/L1}** and **TS4_R_{sub1/L1}**), with methyl 2-phenylacrylate and (S)-SEGPHOS (distances in Å). Structures given in SI are generated using CYLview.³

³CYLview, 1.0b; Legault, C. Y., Université de Sherbrooke, **2009** (<http://www.cylview.org>)

The optimized geometries of Rh-benzyl intermediates



*Rh-benzyl with methyl
2-phenylacrylate (Sub1)*



*Rh-benzyl with 4-(tert-butyl)benzyl
2-phenylacrylate (Sub2)*

Figure S4. The optimized Rh-benzyl structures. On the left side is given the Rh-benzyl intermediate with methyl 2-phenylacrylate substrate. On the right side is given Rh-benzyl intermediate with 4-(*tert*-butyl)benzyl 2-phenylacrylate substrate (distances in Å). Rh-benzyl intermediates display η^3 binding mode of the substrate to the metal.

Computational results for Rh-(R)-StackPhos (L2)

Table S2. Selected distances (Å) of noncovalent interactions at the TS conformations with Rh-(R)-StackPhos and methyl 2-phenylacrylate. The energy difference between pro-(S) and pro-(R) TSs ($\Delta\Delta G^\ddagger$) are given in kcal/mol. The computed e.e. is 47.0 % (Table 1, main text.) Only *frontside* TSs display Imidazole-CO₂ stacking interaction.

	TS	Stereo	C-CO ₂	Rh-C (Nuc)	Imidazole-CO ₂		CH... π (Sub-Cat)	F- π	CH...F	$\Delta\Delta G^\ddagger$
					C _{CO2} -N _{Im}	O _{CO2} -Imid.				
Backside CO ₂ insertion	TS1a_S ⁴	pro-(S)	2.26	3.68	-	-	2.53; 3.16	2.78	2.37	2.2
	TS1b_S ⁵	pro-(S)	2.24	3.78	-	-	3.33; 3.32, 2.80	2.78	2.37	2.1
	TS1a_R ⁶	pro-(R)	2.55	3.48	-	-	2.56; 3.46	2.90	2.45	2.8
	TS1b_R ⁷	pro-(R)	2.55	3.52	-	-	2.58; 3.31	2.94	2.47	3.0
Frontside CO ₂ insertion	TS2a_S	pro-(S)	2.21	3.73	3.22	3.10	2.64;3.28	3.05	2.54	0.0
	TS2b_S	pro-(S)	2.21	3.74	3.26	3.10	2.66; 3.26	3.03	2.53	0.8
	TS2_S tack_2_S	Pro-(S)	2.21	3.73	3.21	3.08	2.66;3.40	2.95	π - π 3.46	0.8
	TS2a_R ⁸	pro-(R)	2.23	3.85	3.17	3.26	2.84; 3.18	3.02	2.53	0.6
	TS2b_R	pro-(R)	2.20	3.85	3.16	3.28	2.73; 3.30	2.96	3.16	1.0
	TS2_S tack_2_R	pro-(R)	2.23	3.83	3.15	3.23	2.82, 3.28	2.91	π - π 3.48	1.9
Rh-O=C (ester)	TS3_S ⁹	pro-(S)	2.53	2.97	-	-	3.02; 3.50	2.77	2.31; 2.52	15.2
	TS3_R ¹⁰	pro-(R)	2.32	3.56	-	-	3.07	2.84	2.40; 2.55	10.8

⁴ There is one CH...O interaction at 2.54 Å. An intramolecular CH...O interaction is at 2.19 Å.

⁵ There is one weak CH...O interaction at 3.10 Å

⁶ There is one CH... π interaction between the Me of the ester and naphthalene ring (2.60 Å). A CH...O interaction is identified at 2.3 Å.

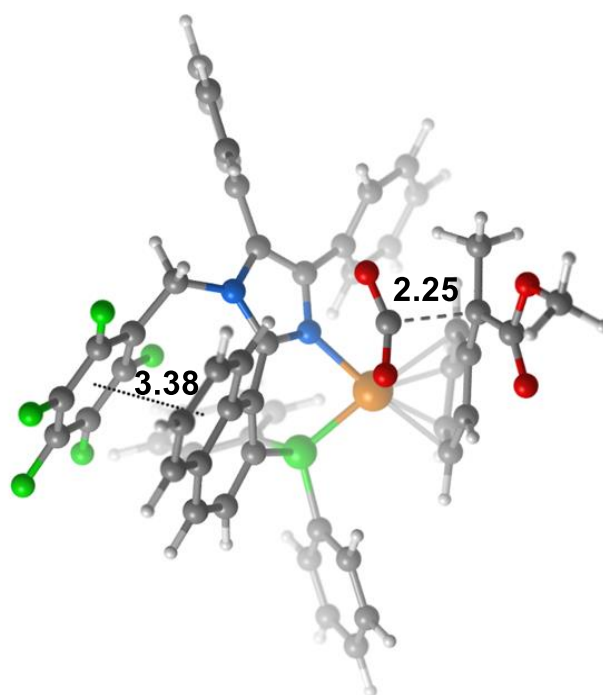
⁷ There is one CH... π interaction between the Me of the ester and naphthalene ring (2.60 Å).

⁸ An intramolecular CH...O interaction is at 2.22 Å.

⁹ A Rh-O=C(ester) interaction is at 2.16 Å.

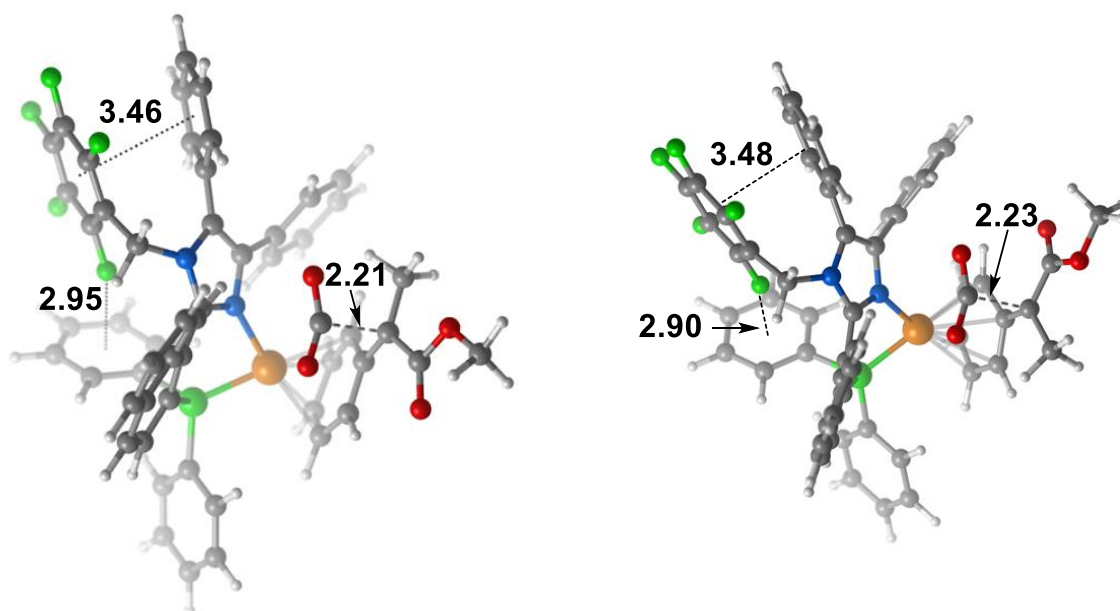
¹⁰ A Rh-O=C(ester) interaction is at 2.26 Å.

The optimized higher-energy TSs with StackPhos



TS2a_Stack_I_{sub1/L2}
 $\Delta G^\ddagger = 2.5$ kcal/mol

Figure S5. Illustration of stacking interaction between the the pentafluorophenyl group and naphthalene ring, at the **TS2a_Stack_I_{sub1/L2}** (distances are in Å).



TS2a_Stack_S_{sub1/L2}
 $\Delta G^\ddagger = 0.8$ kcal/mol

TS2a_Stack_R_{sub1/L2}
 $\Delta G^\ddagger = 1.9$ kcal/mol

Figure S6. Illustration of stacking interaction between the pentafluorophenyl group and the second phenyl group linked to imidazole ring, at the **TS2a_Stack_S_{sub1/L2}** and **TS2a_Stack_R_{sub1/L2}**. The pentafluorophenyl group also forms F- π interaction with the phenyl group, which is attached to the phosphorus (distances in Å).

Computational results for Rh-(*R,R*)-^tBu-BOX (L3)

Table S3. Selected distances (Å) of noncovalent interactions at the TS conformations with Rh-(*R,R*)-^tBu-BOX and methyl 2-phenylacrylate. The energy difference between pro-(*S*) and pro-(*R*) TSs ($\Delta\Delta G^\ddagger$) are given in kcal/mol. The computed e.e. is 6.4 % (*S*) (Table 1, main text). *Frontside* TSs display Oxazoline-CO₂ interaction.

	TS	Stereo	C-CO ₂	Rh-C (Nuc)	CH...O (Sub-Lig)	N...H(π)	$\Delta\Delta G^\ddagger$
Backside CO ₂ insertion	TS1a_S	pro-(<i>S</i>)	1.98	3.56	2.64	3.34	1.9
	TS1b_S	pro-(<i>S</i>)	2.23	3.90	-	3.40	3.1
	TS1a_R	pro-(<i>R</i>)	2.25	3.76	2.43, 2.72	2.91	0.7
	TS1b_R	pro-(<i>R</i>)	2.26	3.89	3.01	2.92	0.8
Frontside CO ₂ insertion	TS2a_S	pro-(<i>S</i>)	2.21	4.03	N_(ox)-C_(CO2) 3.48	H_(ox)-O_(CO2) 2.46	0.0
	TS2b_S	pro-(<i>S</i>)	2.26	4.05	3.87	2.35	3.6
	TS2a_R	pro-(<i>R</i>)	2.14	3.96	3.54	2.60	0.5
	TS2b_R	pro-(<i>R</i>)	2.13	3.92	3.61	2.43	2.5
Rh-Estar	TS3_S	pro-(<i>S</i>)	2.54	3.06	Rh-O(Est) 2.10	CH- π 2.50	3.2
	TS3_R	pro-(<i>R</i>)	2.39	3.08	2.11	2.53	5.3

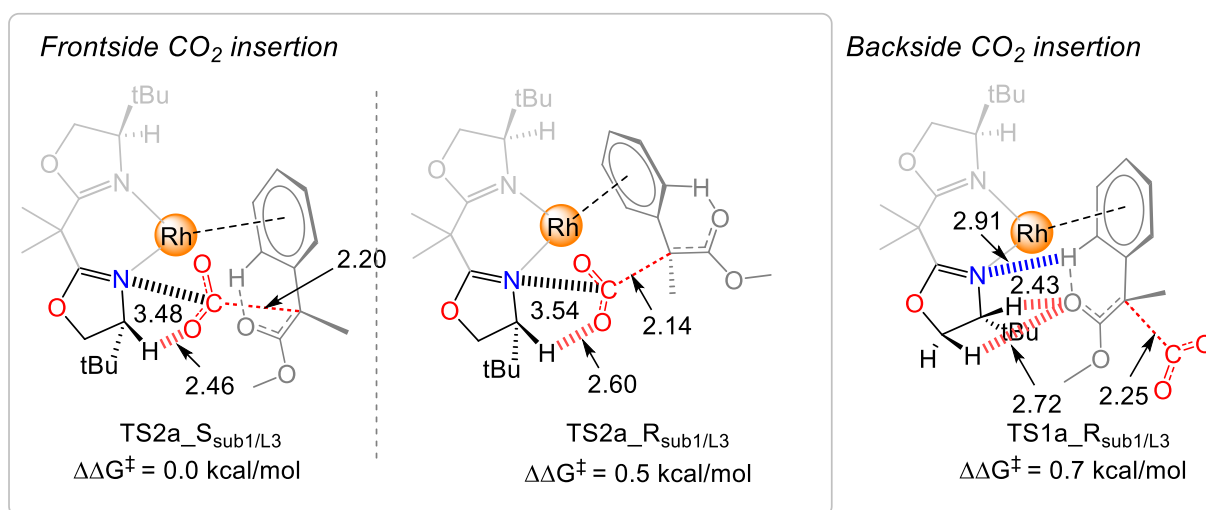


Figure S7. Illustration of the noncovalent interactions at the lowest lying pro-(*S*) and pro-(*R*) **TS2a_{sub1/L3}** carboxylation structures alongside **TS1a_{sub1/L3}** conformation with Rh-(*R,R*)-^tBu-BOX (distances are in Å). At the **TS1a_{sub1/L3}**, the oxygen atom of the ester group of the substrate forms two CH...O interactions with the oxazoline ring.

Computational results for Rh-(*R,R*)-BDPP (L4)

Table S4. Selected distances (Å) of noncovalent interactions at the TS conformations with Rh-(*R,R*)-BDPP and methyl 2-phenylacrylate. The energy difference between pro-(*S*) and pro-(*R*) TSs ($\Delta\Delta G^\ddagger$) are given in kcal/mol. The computed e.e. is 24.3 (*R*) % (Table 1, main text).

	TS	Stereo	C-CO ₂	Rh-C (Nuc)	CH...O (Sub-Lig)	CH... π (Sub-Lig)	$\Delta\Delta G^\ddagger$
Backside CO ₂ insertion	TS1a_S	pro-(<i>S</i>)	2.22	3.64	2.31	3.28; 3.40	0.5
	TS1b_S	pro-(<i>S</i>)	2.22	3.72	3.20	2.83; 3.13; 3.35	0.8
	TS1a_R	pro-(<i>R</i>)	2.21	3.64	2.46	3.00; 3.10; 3.40	0.0
	TS1b_R	pro-(<i>R</i>)	2.18	3.68	2.74	3.11; 3.36	1.9
Frontside CO ₂ insertion	TS2a_S	pro-(<i>S</i>)	2.38	3.82	-	3.38; 3.38	5.8
	TS2b_S	pro-(<i>S</i>)	2.31	3.86	-	3.53; 3.47	8.6
	TS2a_R	pro-(<i>R</i>)	2.45	3.85	-	3.30; 3.47	5.5
	TS2b_R	pro-(<i>R</i>)	2.42	3.82	-	3.36; 3.35	6.4
Rh-Estar	TS3_S	pro-(<i>S</i>)	2.45	3.40	Rh..O(Est) (2.20)	2.52; 3.23	9.7
	TS3_R	pro-(<i>R</i>)	2.28	3.28	Rh..O(Est) (2.22)	2.36; 3.58	12.1

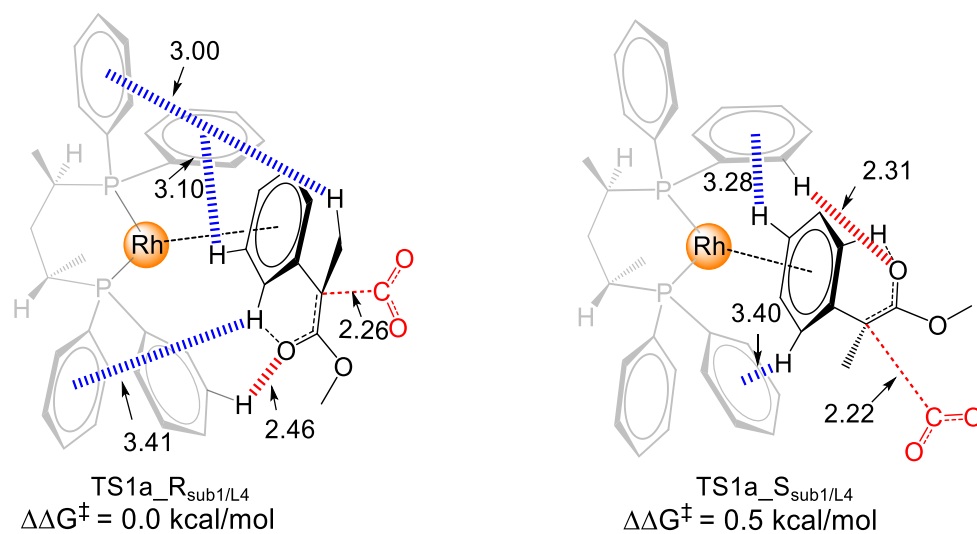


Figure S8. Illustration of the noncovalent interactions in the lowest lying pro-(*S*) and pro-(*R*) TS1a_{sub1/L4} carboxylation structures with Rh-(*R,R*)-BDPP (distances are in Å).

Experimental part

General considerations

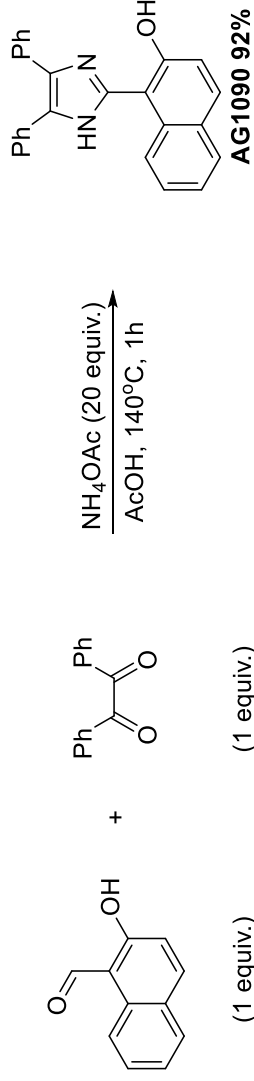
Commercially available starting materials, reagents, catalysts and anhydrous and degassed solvents were used without further purification. Thin layer chromatography was carried out using Merck TLC Silica gel 60 F₂₅₄ and visualized by short-wavelength ultraviolet light or by treatment with potassium permanganate (KMnO₄) stain. ¹H, ¹³C, ¹⁹F and ³¹P NMR spectra were recorded on a Bruker Avance 400 MHz at 20 °C. All ¹H NMR spectra are reported in parts per million (ppm) downfield of TMS and were measured relative to the signals for CHCl₃ (7.26 ppm). All ¹³C NMR spectra were reported in ppm relative to residual CDCl₃ (77.20 ppm) and were obtained with ¹H decoupling. Coupling constants, *J*, are reported in Hertz (Hz). High-resolution mass spectra (HRMS) were recorded from methanol solutions on an LTQ Orbitrap XL (Thermo Scientific) in positive electrospray ionization (ESI) mode.

(*S*)-SEPHOS, (*S,S*)-fBu-BOX and (*S,S*)-BDPP ligands are commercially available. Ethyl 2-phenylacrylate,¹¹ StackPhos¹² and corresponding Rh complexes^{1,13} were prepared according to slightly modified literature procedures.

Experimental procedures and characterization of products

General experimental procedure for preparation of *rac*-StackPhos.¹³

1-(4,5-Diphenyl-1H-imidazol-2-yl)naphthalen-2-ol.



Under the flow of Ar an oven dried 100 mL pressure tube was sequentially charged with benzyl (1 equiv.), 2-hydroxynaphthalene-1-carbaldehyde (5 g, 1 equiv.) and ammonium acetate (20 equiv.). This was followed by addition of glacial acetic acid (40 mL). The pressure tube was sealed and stirred at 140 °C for 1h. Formed yellow solid was treated with water (40 mL), filtered and thoroughly washed with water. The resulting yellow powder was recrystallized from ethanol to give 9.001 g (86%) of the title compound as a yellow solid.

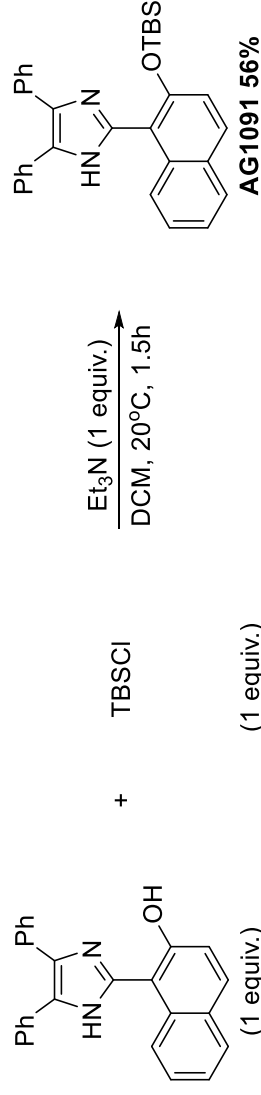
¹¹ H. Gong, R. S. Andrews, J. L. Zuccarello, S. J. Lee, M. R. Gagne, *Org. Lett.* **2009**, 11, 879-882.

¹² F. S. P. Cardoso, K. A. Abboud, A. Aponick, *J. Am. Chem. Soc.* **2013**, 135, 14548-14551.

¹³ K. Mikami, Y. Yusa, M. Hatano, K. Wakabayashi, K. Aikawa, *Tetrahedron* **2004**, 60, 4475-4480.

¹H NMR (400 MHz, CDCl₃): δ = 11.94 (br s, 2H, NH, OH), 8.21 (d, J = 8.5 Hz, 1H, Ar), 7.89 (t, J = 8.7 Hz, 2H, Ar), 7.60-7.57 (m, 4H, Ar), 7.52-7.48 (m, 1H, Ar), 7.41-7.29 (m, 8H, Ar). **¹³C NMR** (101 MHz, CDCl₃): δ = 154.5, 143.0, 135.5, 132.3, 130.6, 129.6, 129.5, 128.5, 128.1, 127.9, 127.7, 127.1, 126.9, 124.5, 123.0, 118.4, 109.2.

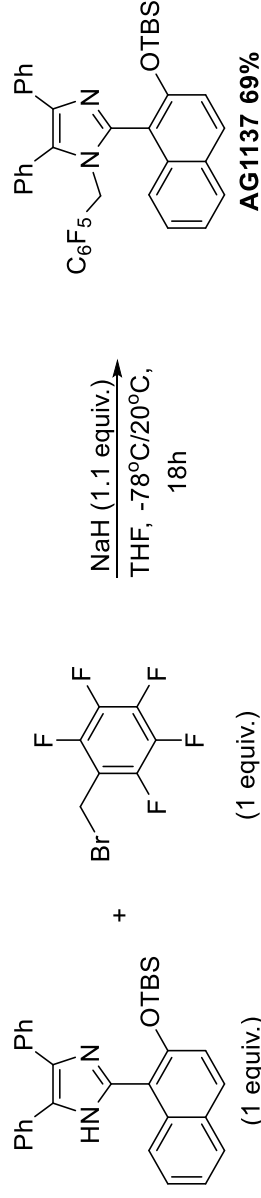
2-(2-((tert-Butyldimethylsilyl)oxy)naphthalen-1-yl)-4,5-diphenyl-1H-imidazole.



Under the flow of Ar an oven dried 250 mL round bottom flask was charged with the phenol (7.5 g, 1 equiv.), DCM (90 mL) and TEA (1 equiv.). The flask was sealed with a rubber septa and the resulting mixture was stirred at 20 °C for 30min. This was followed by addition of TBSCl (1 equiv.), under the flow of Ar. The flask was sealed with a rubber septa and the resulting mixture was stirred at 20 °C for 2h. Afterwards the volatiles were removed using rotary evaporator, the resulting crude mixture was purified by column chromatography to give 5.549 g (56%) of the title compound as a colorless solid.

¹H NMR (400 MHz, CDCl₃): δ = 9.59 (br s, 1H, NH), 8.83 (dd, J = 8.5, 1.2 Hz, 1H, Ar), 7.82-7.78 (m, 4H, Ar), 7.55-7.50 (m, 3H, Ar), 7.43-7.26 (m, 7H, Ar), 7.15 (d, J = 8.9 Hz, 1H, Ar), 0.86 (s, 9H, tBu), 0.11 (s, 6H, 2xMe). **¹³C NMR** (101 MHz, CDCl₃): δ = 151.9, 142.4, 135.3, 133.5, 131.5, 130.8, 130.0, 129.1, 128.4, 128.0, 127.9, 127.6, 126.9, 126.3, 124.6, 121.2, 116.3, 25.7, 18.3, 4.4.

2-(2-((tert-Butyldimethylsilyl)oxy)naphthalen-1-yl)-1-((perfluorophenyl)methyl)-4,5-diphenyl-1H-imidazole.

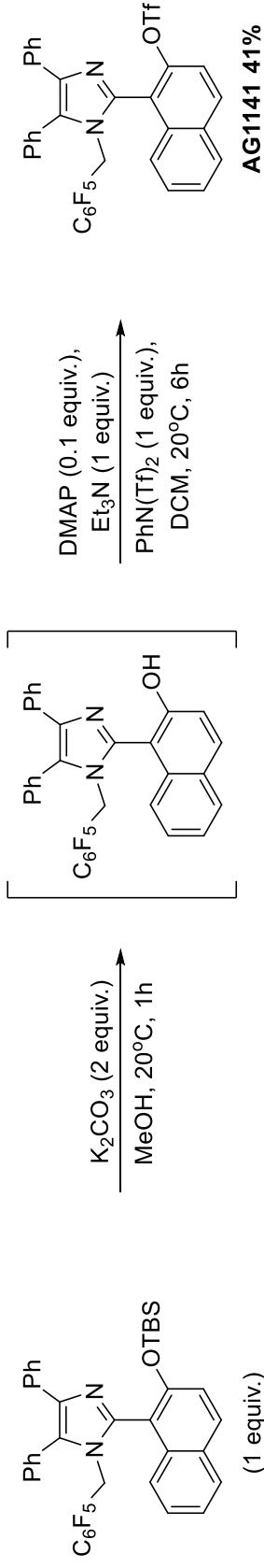


Inside of glove box an oven dried 100 mL round bottom flask was charged with NaH (1.1 equiv.). The flask was sealed with a rubber septa, removed from the glove box and equipped with an Ar balloon. This was followed by addition of dry THF (15 mL). The resulting suspension was

transferred into an isopropanol bath (-78 °C), which was followed by dropwise addition of previously prepared solution of the silyl ether (5.549 g, 1 equiv.) (an oven dried 100 mL round bottom flask was charged with the silyl ether, sealed with a rubber septa, equipped with an Ar balloon, evacuated and back filled with Ar (3 times) that was followed by addition of dry THF (30 mL)). The resulting mixture was stirred at -78 °C for 10min, which was followed by dropwise addition of previously prepared solution of pentafluorobenzyl bromide (1 equiv.) in dry THF (5 mL). The resulting mixture was allowed to reach 20 °C where it was stirred for 18h. The resulting mixture was evaporated to dryness and purified by column chromatography to give 5.263 g (69%) of the title compound as a colorless solid.

¹H NMR (400 MHz, CDCl₃): δ = 7.78 (d, J = 7.78 Hz, 1H, Ar), 7.71-7.69 (m, 1H, Ar), 7.61-7.59 (m, 2H, Ar), 7.52-7.48 (m, 6H, Ar), 7.32 (pd, J = 6.9, 1.5 Hz, 2H, Ar), 7.25-7.20 (m, 2H, Ar), 7.18-7.14 (m, 1H, Ar), 7.12 (d, J = 8.9 Hz, 1H, Ar), 5.07 (d, J = 15.3 Hz, 1H, CH₂), 4.85 (dd, J = 15.3, 1.6 Hz, 1H, CH₂), 0.95 (s, 9H, tBu), 0.31 (s, 3H, Me). **¹³C NMR** (101 MHz, CDCl₃): δ = 152.8, 142.9, 137.7, 134.9, 133.9, 131.4 (d, J = 21.3 Hz), 129.8, 129.4, 129.2, 129.1, 128.2, 127.6, 127.0, 126.4, 124.5 (d, J = 15.0 Hz), 120.8, 116.8, 110.2 (t, J = 15.7 Hz), 36.7, 25.7, 18.2, -3.9, -4.6.

1-(1-((Perfluorophenyl)methyl)-4,5-diphenyl-1H-imidazol-2-yl)naphthalen-2-yl trifluoromethanesulfonate.

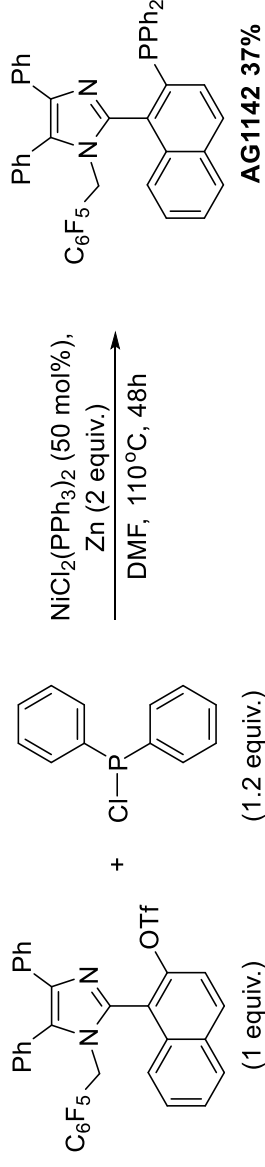


An oven dried 250 mL round bottom flask was charged with the TBS-ether (5.2 g, 1 equiv.), K₂CO₃ (2 equiv.) and MeOH (100 mL). Following the stirring for 1h at 20 °C, the mixture was concentrated under reduced pressure to ~10 mL. The residue was dissolved in EtOAc (50 mL) and poured into water (80 mL). The organic phase was separated and the water phase was extracted with EtOAc (2 x 50 mL). The combined organic layers were concentrated under reduced pressure to give the deprotected product as a white solid that was used in the next step without further purification.

An oven dried 250 mL round bottom flask was sequentially charged with the free phenol obtained above, DMAP (10 mol%) and *N*-phenyl-bis(trifluoromethanesulfonimide) (1 equiv.). The flask was sealed with a rubber septa, equipped with a balloon, evacuated and back filled with Ar (3 times). That was followed by addition of DCM (100 mL) and trimethylamine (1 equiv.). The resulting solution was stirred at 20 °C for 6h and concentrated under reduced pressure. The residue was purified by column chromatography to give 2.210 g (41%) of the title compound as a colorless solid.

¹H NMR (400 MHz, CDCl₃): δ = 7.80 (d, *J* = 9.1 Hz, 1H, Ar), 7.67-7.65 (m, 1H, Ar), 7.53 (d, *J* = 8.1 Hz, 1H, Ar), 7.39-7.24 (m, 10H, Ar), 7.03-6.99 (m, 2H, Ar), 6.98-6.93 (m, 1H, Ar), 4.80-4.71 (m, 2H, CH₂). **¹³C NMR** (101 MHz, CDCl₃): δ = 146.5, 146.1, 143.6, 142.0, 139.4, 139.2, 138.6, 138.1, 137.9, 135.7, 134.2, 134.0, 133.1, 132.6, 132.3, 131.3, 130.9, 130.5, 129.5, 129.3, 128.4, 128.3, 128.1, 127.7, 127.2, 127.0, 126.9, 126.1, 124.2, 123.4, 121.2, 120.2, 119.3, 117.1, 113.9, 109.9, 109.7, 109.5, 37.0.

2-(2-(Diphenylphosphaney)naphthalen-1-yl)-1-((perfluorophenyl)methyl)-4,5-diphenyl-1H-imidazole, rac-StackPhos.

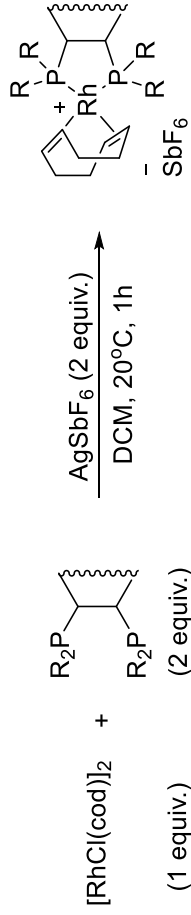


Inside of glove box an oven dried 100 mL round bottom flask was sequentially charged with corresponding triflate (2.1 g, 1 equiv.), NiCl₂(PPh₃)₂ (50 mol%) and activated Zn dust (2 equiv., 100 mesh).¹⁴ The resulting mixture was dissolved in dry DMF (14 mL), which was followed by dropwise addition of chlorodiphenylphosphine (1.2 equiv.). The flask was sealed with a rubber septa, removed from the glove box and stirred at 110 °C for 48h. The resulting mixture was evaporated to dryness and purified by column chromatography to give 0.822 g (37%) of the title compound as a colorless solid.

¹H NMR (400 MHz, CDCl₃): δ = 7.80 (d, *J* = 8.6 Hz, 1H, Ar), 7.75 (d, *J* = 8.2 Hz, 1H, Ar), 7.60-7.40 (m, 11H, Ar), 7.38-7.36 (m, 1H, Ar), 7.34-7.22 (m, 9H, Ar), 7.17-7.11 (m, 3H, Ar), 5.17 (dd, *J* = 15.4, 3.5 Hz, 1H, CH₂), 4.86 (d, *J* = 15.4 Hz, 1H, CH₂). **¹³C NMR** (101 MHz, CDCl₃): δ = 144.3 (d, *J* = 4.6 Hz), 138.6 (d, *J* = 14.0 Hz), 137.5, 136.5 (d, *J* = 10.5 Hz), 135.7 (d, *J* = 8.2 Hz), 134.7, 134.6, 134.4, 134.2, 133.1, 133.0, 132.4, 132.3, 132.2, 131.9, 131.3, 131.2, 129.9, 129.8, 129.3, 129.1, 129.0, 128.9, 128.8, 128.7, 128.6, 128.5, 128.1, 128.0, 127.8, 127.7, 127.3, 127.0, 126.8 (d, *J* = 8.1 Hz), 126.6, 126.3, 125.6 (d, *J* = 2.2 Hz), 110.0, 109.9, 37.2 (d, *J* = 10.8 Hz).

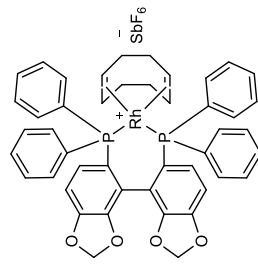
General experimental procedure for the preparation of Rh-complexes.¹

¹⁴ The activation of Zn was realized according to a literature procedure: P. Knochel, M. C. P. Yeh, S. C. Berk, J. Talbert, *J. Org. Chem.* **1988**, *53*, 2390-2392.

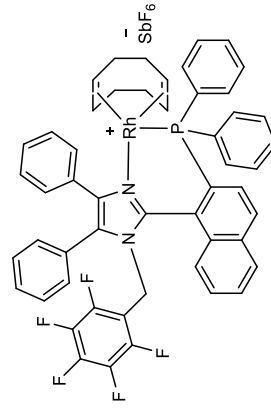


Inside of glove box an oven dried 25 mL round bottom flask was charged with $[\text{Rh}(\text{cod})\text{Cl}]_2$ (100.0 mg, 1 equiv.) and AgSbF_6 . The flask was sealed with a rubber septa, removed from the glove box and equipped with an Ar balloon. Inside of glove box another oven dried 25 mL round bottom flask was charged with the corresponding chelating ligand (2 equiv.), sealed with a rubber septa, removed from the glove box and equipped with an Ar balloon. Both flasks were charged with dry CHCl_3 (5 mL) and allowed to stir for 30 min at 20 °C. This was followed by dropwise addition of CHCl_3 solution of the ligand to the stirring solution of $[\text{Rh}(\text{cod})\text{Cl}]_2$, which was accompanied by precipitation of a white powder (AgCl/NaCl). The resulting mixture was stirred at 20 °C for 1h. Afterwards the precipitate was filtered off and the solvent was evaporated to give the corresponding complex as an orange powder.

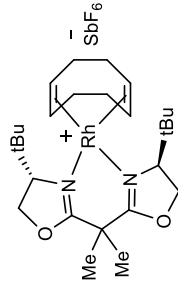
$[\text{Rh}(\text{cod})((\text{S})\text{-SEGPHOS})\text{SbF}_6$. Starting from 0.203 mmol of $[\text{Rh}(\text{cod})\text{Cl}]_2$ the product was obtained as an orange powder, yield 99% (0.214 g). **$^1\text{H NMR}$** (400 MHz, CDCl_3): δ = 7.66-7.54 (m, 4H), 7.39-7.14 (m, 16H), 7.06-6.94 (m, 2H), 6.28 (d, J = 8.3 Hz, 2H), 5.55 (s, 2H), 5.39 (s, 2H), 4.55-4.30 (m, 4H), 2.68-2.52 (m, 2H), 2.38-2.23 (m, 2H), 2.03-1.89 (m, 2H), 1.84-1.68 (m, 2H). **$^{13}\text{C NMR}$** (101 MHz, CDCl_3): δ = 149.5, 146.8, 136.0, 134.2, 131.5, 131.1, 129.0, 128.7, 127.4, 127.2, 126.6, 121.9, 121.6, 121.7, 117.6, 108.4, 102.7, 101.7, 98.7, 53.6, 34.1, 32.1, 30.2, 29.8, 29.5, 28.1, 26.9, 22.8, 19.9, 14.3. **HRMS-EI** (m/z) $[\text{M-SbF}_6]^+$ calcd. for $\text{C}_{46}\text{H}_{40}\text{O}_4\text{P}_2\text{Rh}$ 821.1451 found 821.1462.



$[\text{Rh}(\text{cod})(\text{rac})\text{-StackPhos}]\text{SbF}_6$. Starting from 0.203 mmol of $[\text{Rh}(\text{cod})\text{Cl}]_2$ the product was obtained as an orange powder, m.p. = 162-165°C, yield 98% (0.230 g). **$^1\text{H NMR}$** (400 MHz, CDCl_3): δ = 8.15-8.04 (m, 3H), 7.95 (t, J = 7.7 Hz, 1H), 7.89-7.84 (m, 2H), 7.82-7.63 (m, 5H), 7.60-7.36 (m, 10H), 7.22 (s, 3H), 7.06 (t, 2H), 5.26 (s, 2H), 4.93 (d, J = 15.7 Hz, 1H), 4.55 (d, J = 15.8 Hz, 1H), 4.21 (t, J = 6.9 Hz, 1H), 3.67-3.57 (m, 1H), 3.30-3.21 (m, 1H), 2.81-2.65 (m, 1H), 2.29-2.19 (m, 2H), 2.16-2.05 (m, 1H), 1.88-1.73 (m, 2H). **$^{13}\text{C NMR}$** (101 MHz, CDCl_3): δ = 145.6, 143.3, 143.2, 143.1, 142.2, 139.7, 139.0, 137.9, 137.7, 136.1, 135.5, 135.4, 134.5, 134.5, 134.2, 134.0, 133.6, 133.5, 132.4, 132.4, 132.4, 132.3, 132.1, 132.0, 131.9, 131.4, 131.4, 131.3, 130.7, 130.5, 130.4, 130.2, 130.1, 129.6, 129.5, 129.4, 129.3, 129.3, 129.2, 129.1, 129.0, 128.9, 128.8, 128.7, 127.5, 127.4, 127.3, 127.2, 127.0, 126.6, 126.1, 125.0, 124.9, 108.1, 108.0, 107.8, 106.4, 106.3, 106.2, 101.5, 101.5, 101.4, 101.3, 80.1, 79.9, 78.9, 78.8, 53.6, 40.4, 39.4, 37.5, 37.2, 35.8, 35.7, 32.8, 32.5, 32.0, 31.0, 30.2, 30.1, 29.8, 29.4, 28.0, 27.8, 27.2, 25.8, 25.8, 22.8,

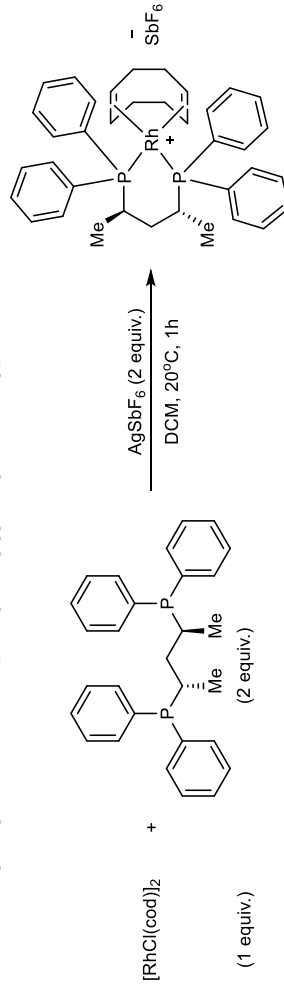


22.8, 22.7, 19.8, 14.5, 14.2, 11.5. **HRMS-EI** (m/z) [M-SbF₆]⁺ calcd. for C₅₂H₄₀F₅N₂PRh 921.1899 found 921.1914. IR (ATR, cm⁻¹) ν = 2933 (s), 1524 (s), 1470 (s), 1345 (m), 1125 (m), 1100 (m), 986 (m), 920 (m), 820 (m), 740 (m), 705 (s), 652 (s).



[Rh(cod)]((S,S)-tBu-BOX)]SbF₆. Starting from 0.203 mmol of [Rh(cod)Cl]₂ the product was obtained as an orange powder, m.p. over 200°C, yield 99% (0.298 g). **¹H NMR** (400 MHz, CDCl₃): δ = 4.60-4.53 (m, 2H), 4.37-4.21 (m, 6H), 3.60 (dd, J = 8.6, 2.6 Hz, 2H), 2.67-2.50 (m, 2H), 2.37-2.23 (m, 2H), 2.02 (s, 6H), 2.00-1.90 (m, 2H), 1.74-1.61 (m, 2H), 0.83 (s, 18H). **¹³C NMR** (101 MHz, CDCl₃): δ = 178.3, 82.7, 82.6, 80.4, 80.3, 73.1, 72.4, 53.6, 40.7, 34.1, 31.2, 29.1, 25.3, 25.2. **HRMS-EI** (m/z) [M-SbF₆]⁺ calcd. for C₂₅H₄₂N₂O₂Rh 505.2296 found 505.2294. IR (ATR, cm⁻¹) ν = 2959 (m), 1626 (s), 1473 (m), 1372 (m), 1253 (m), 1149 (s), 963 (m), 944 (m), 651 (s).

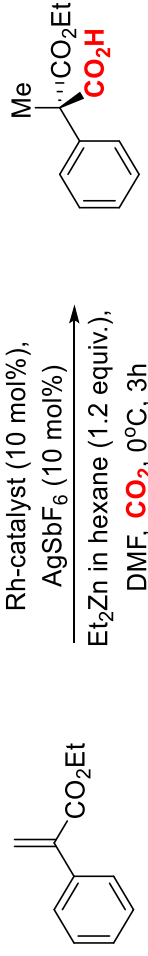
General experimental procedure for the preparation of [Rh(cod)((*S,S*)-BDPP)]SbF₆.¹⁴



Inside of glove box an oven dried 25 mL round bottom flask was charged with [Rh(cod)Cl]₂ (100.0 mg, 1 equiv.). The flask was sealed with a rubber septa, removed from the glove box and equipped with an Ar balloon. In a similar manner 2 other oven dried 25 mL round bottom flasks were charged with (*S,S*)-BDPP (2 equiv.) and AgSbF₆ (2 equiv.) respectively. The flasks were sealed with rubber septa, removed from the glove box and equipped with Ar balloons. All 3 flasks were then charged with dry CHCl₃ (5 mL each) and allowed to stir at 20 °C for 10 min. Afterwards the solution of AgSbF₆ was added (dropwise) to the solution of [Rh(cod)Cl]₂ using a syringe, which was accompanied by precipitation of AgCl. The resulting mixture was allowed to stir at 20 °C for 30 min. This was followed by dropwise addition of the solution of (*S,S*)-BDPP to the reaction mixture. The resulting mixture was allowed to stir at 20 °C for 1 h. Afterwards the precipitate was filtered off and the solvent was evaporated to give the corresponding complex (99%, 0.356 g, m.p. over 200°C) as an orange powder.

¹H NMR (400 MHz, CDCl₃): δ = 8.07-7.96 (m, 4H), 7.61-7.53 (m, 6H), 7.36-7.26 (m, 6H), 7.13-7.08 (m, 4H), 4.52 (t, *J* = 7.2 Hz, 2H), 3.80 (q, *J* = 7.5 Hz, 2H), 2.57 (dt, *J* = 9.7, 7.3 Hz, 2H), 2.50-2.37 (m, 2H), 2.37-2.27 (m, 2H), 1.90-1.69 (m, 4H), 1.59-1.41 (m, 2H), 1.07 (s, 1H), 0.84 (q, *J* = 6.7 Hz, 6H). **¹³C NMR** (101 MHz, CDCl₃): δ = 136.6, 136.5, 136.4, 133.1, 131.5, 131.5, 131.4, 131.1, 130.8, 130.0, 129.9, 129.9, 129.5, 129.4, 129.4, 129.2, 129.0, 128.8, 128.8, 128.2, 128.0, 127.8, 104.2, 104.2, 104.1, 104.1, 104.1, 104.1, 98.2, 98.2, 98.2, 98.1, 98.1, 53.6, 37.8, 33.2, 29.8, 28.1, 27.3, 27.3, 27.1, 26.9, 22.8, 18.9, 18.9, 18.8. **HRMS-EI** (*m/z*) [M-SbF₆]⁺ calcd. for C₃₇H₄₂P₂Rh 651.1811 found 651.1813. IR (ATR, cm⁻¹) *v* = 2925 (m), 1439 (s), 1316 (m), 1186 (m), 1100 (s), 914 (m), 754 (s), 702 (s), 655 (s).

General experimental procedure for Rh-catalyzed hydrocarboxylation of ethyl 2-phenylacrylate.¹

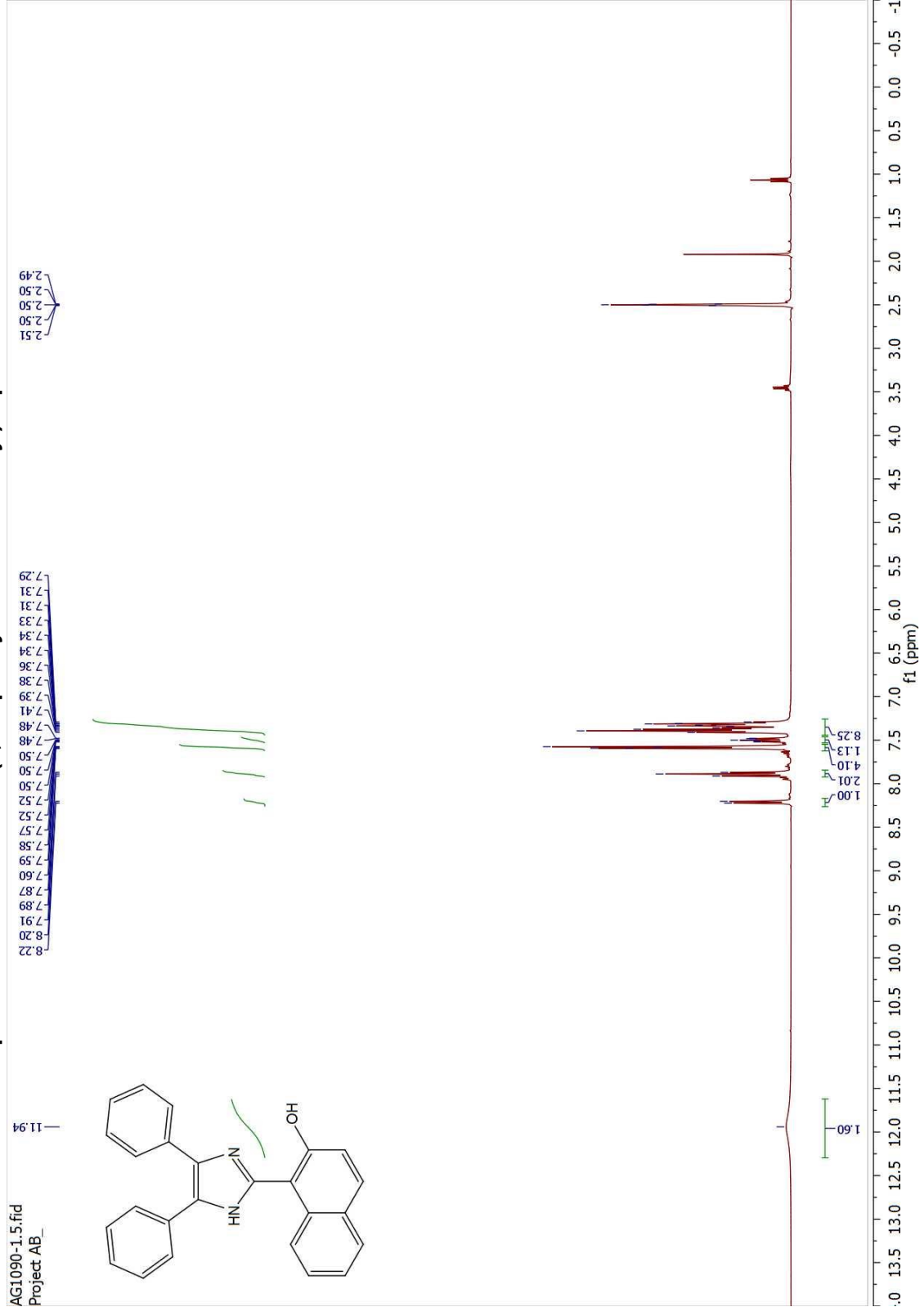


Inside of glove box an oven dried 25 mL Schlenk flask was charged with corresponding Rh-complex (10 mol%) and AgSbF₆ (10 mol%). The flask was sealed with a rubber septa, removed from the glove box, evacuated, filled with CO₂ and equipped with a CO₂ balloon. This was followed by

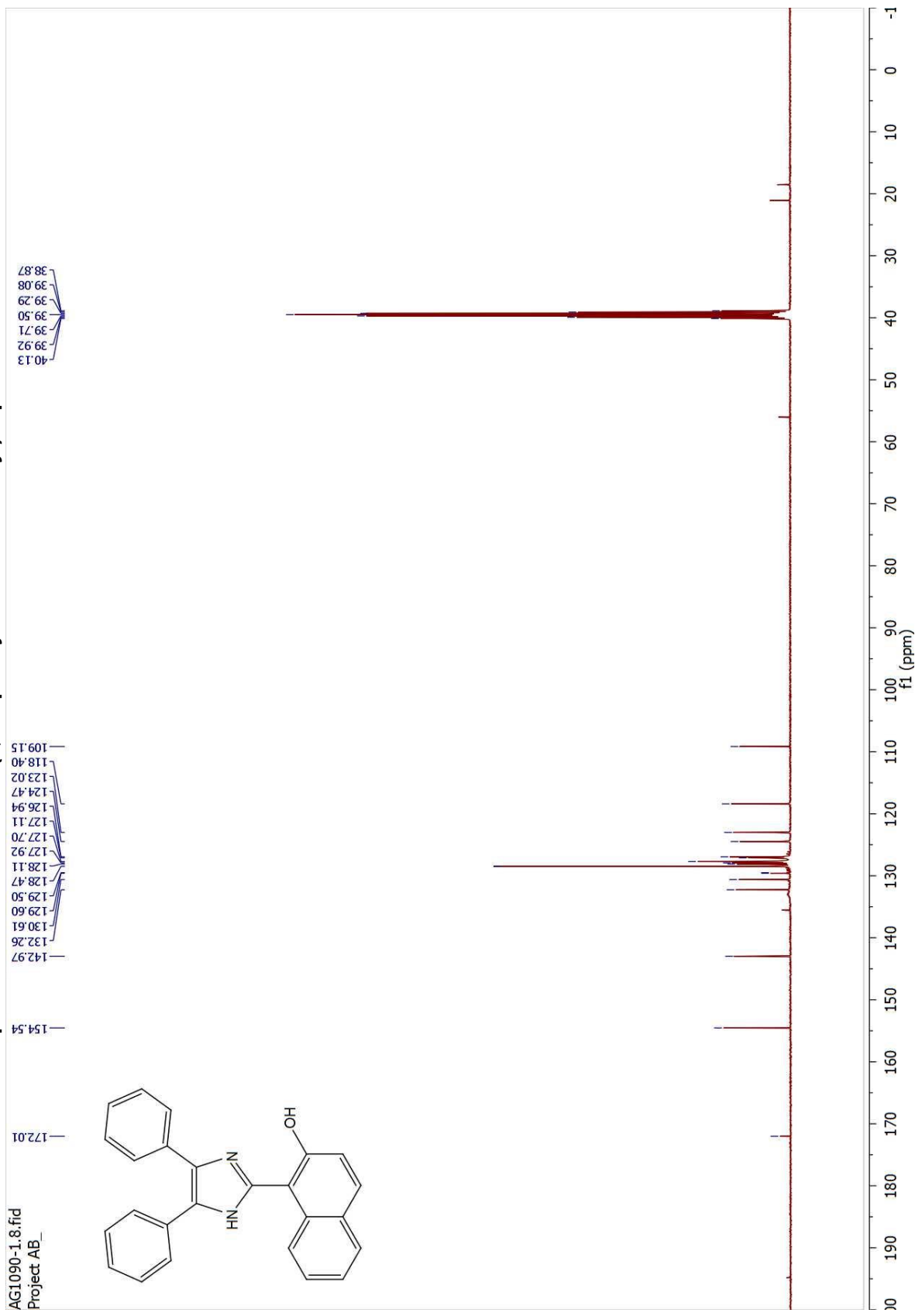
sequential addition of dry DMF (5 mL) and ethyl 2-phenylacrylate (150 mg, 1 equiv.) using syringes. The resulting mixture was transferred into an ice bath where under vigorous stirring 1 M solution of Et₂Zn in hexane (1.2 equiv.) was added dropwise using a syringe. The resulting mixture was allowed to stir at 0 °C for 3h. Then the reaction mixture was diluted with Et₂O (5 mL) and carefully neutralized using 6 M HCl (5 mL). The acidic solution was diluted with water (5 mL) and removed using a separating funnel. The organic phase was then extracted using a solution of saturated NaHCO₃ (3 x 30 mL). Collected aqueous solution was carefully treated with 6 M HCl (60 mL) and extracted using Et₂O (3 x 30 mL). Collected Et₂O solution was washed with distilled water (30 mL) and evaporated to give the target acid as a faint orange oil. Enantiomers were separated using SFC on chiral column (CEL-2), eluent *i*PrOH:EtOH:TFA - 70:30:2 and gradient 3-8, 10 min run. Starting from 0.851 mmol of 2-phenylacrylate the product was obtained as a faint orange oil, yield 48%, e.e. 32% (0.091 g, [Rh(cod)]((S)-SEGPPOS)]SbF₆), yield 74% (0.121 g, [Rh(cod)](*rac*)-StackPhos)]SbF₆), yield 99%, e.e. 0% (0.189 g, [Rh(cod)]((S,S)-*t*Bu-BOX)]SbF₆), yield 94%, e.e. 4% (0.178 g, [Rh(cod)]((S,S)-BDPPP)]SbF₆). **¹H NMR** (400 MHz, CDCl₃): δ = 10.38 (br s, 1H), 7.39-7.24 (m, 5H), 4.21 (q, J = 7.1 Hz, 2H), 1.87 (s, 3H), 1.22 (t, J = 7.1 Hz, 4H). **¹³C NMR** (101 MHz, CDCl₃): δ = 177.0, 171.9, 137.7, 128.4, 128.0, 127.4, 62.3, 58.7, 22.0, 14.0.

Copies of spectra

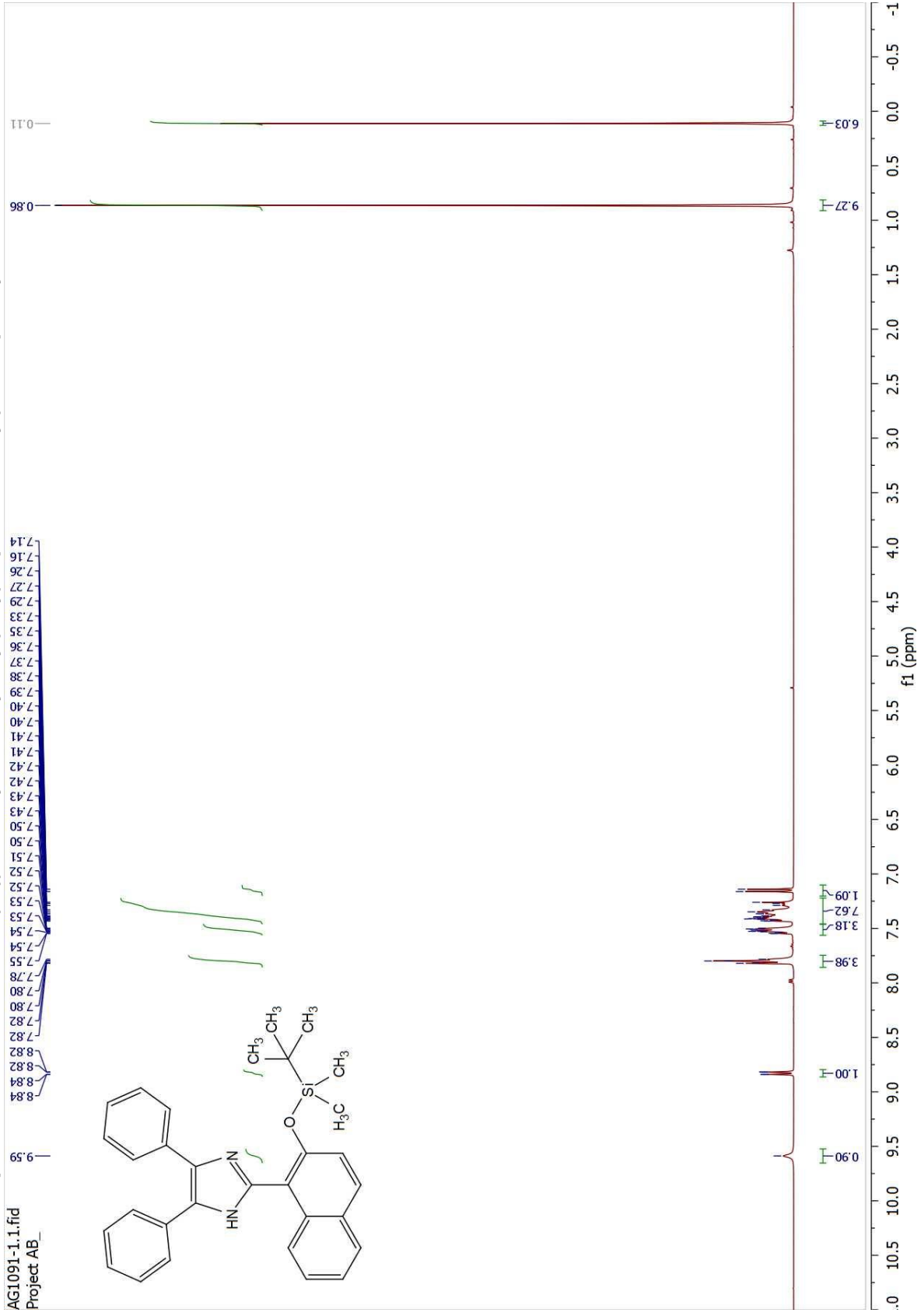
Spectrum 1: ¹H NMR of 1-(4,5-diphenyl-1H-imidazol-2-yl)naphthalen-2-ol



Spectrum 2: ¹³C NMR of 1-(4,5-diphenyl-1H-imidazol-2-yl)naphthalen-2-ol

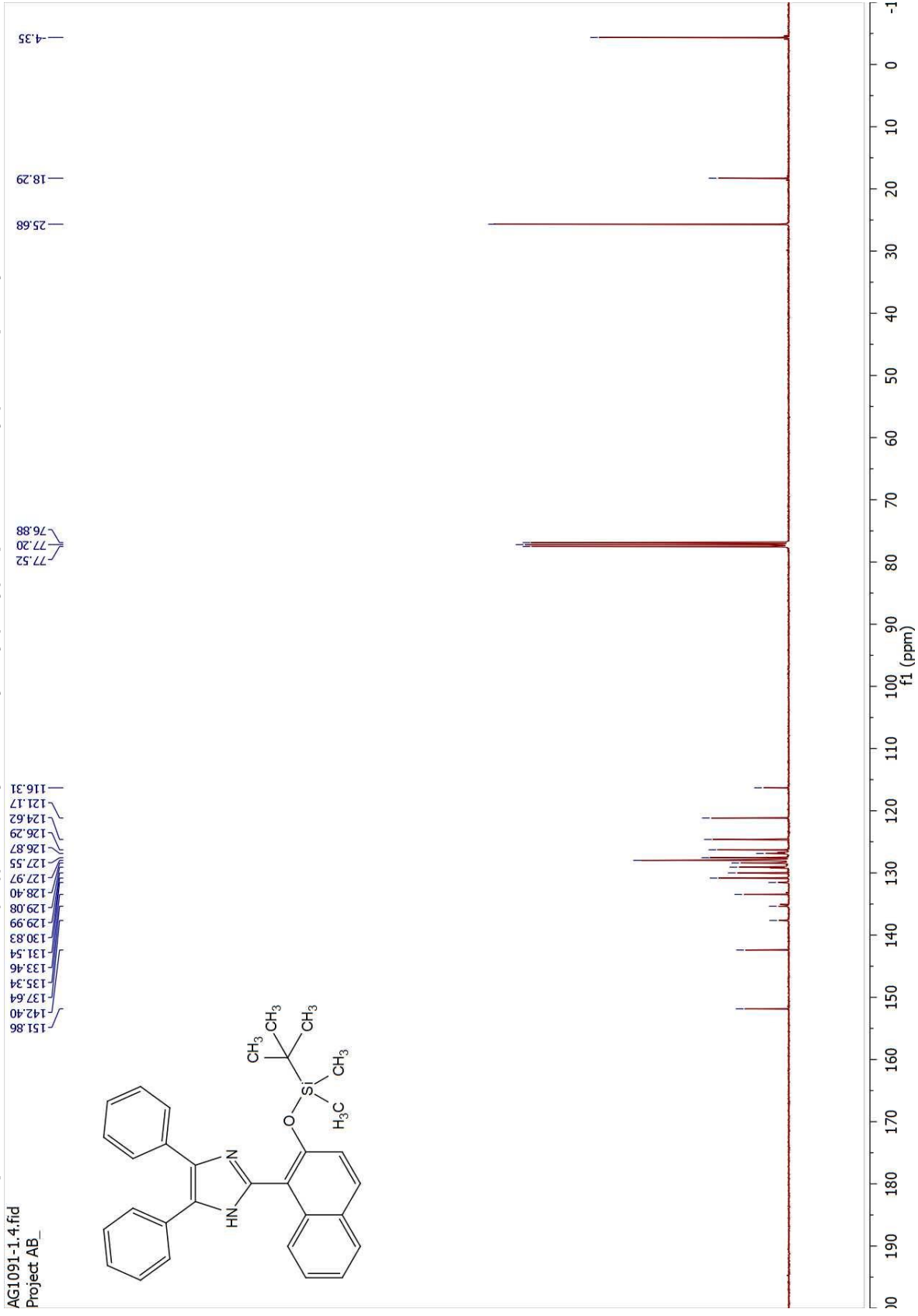


Spectrum 3: ¹H NMR of 2-(2-(*tert*-butyldimethylsilyloxy)naphthalen-1-yl)-4,5-diphenyl-1*H*-imidazole

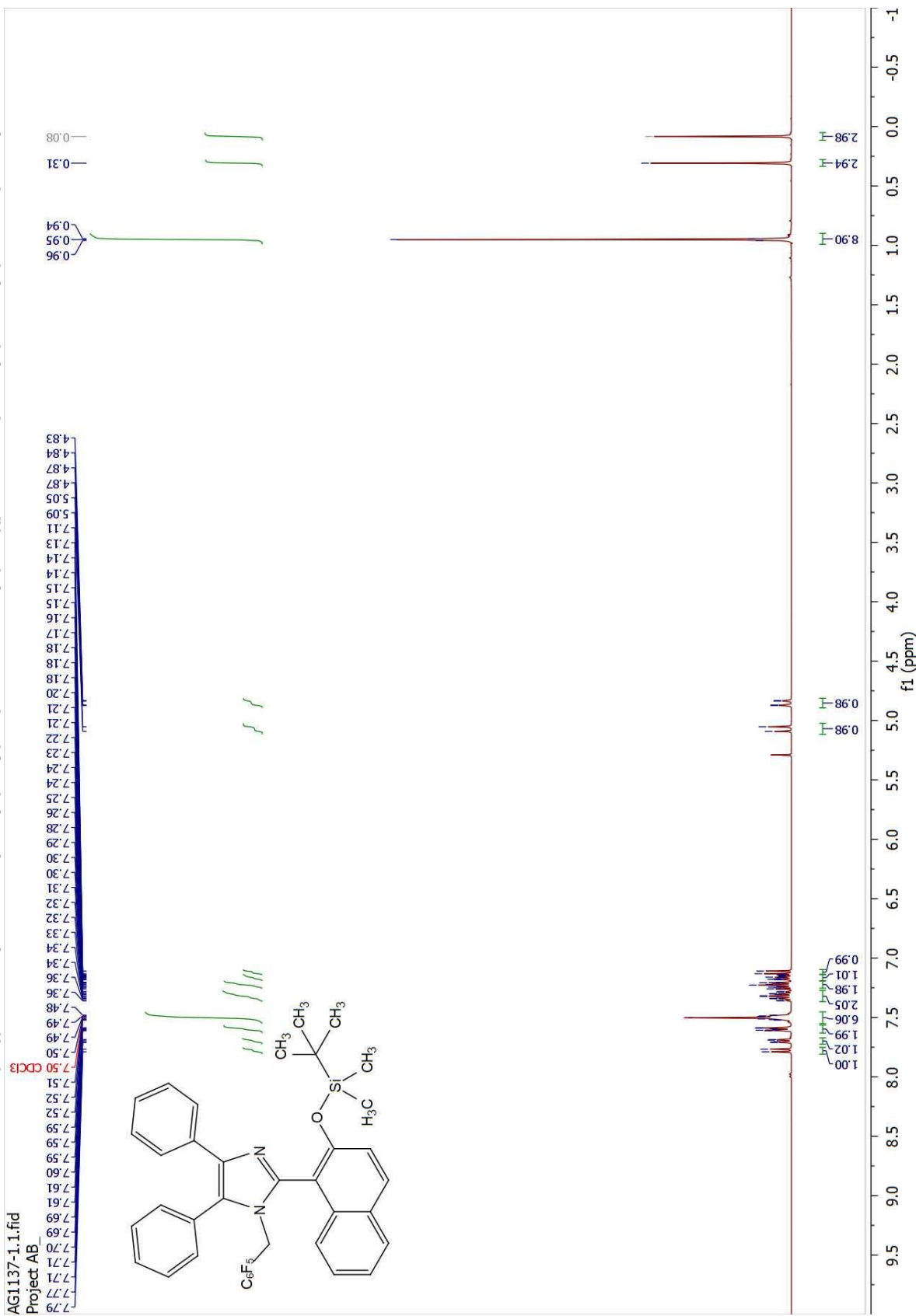


Spectrum 4: ¹³C NMR of 2-((*tert*-butyldimethylsilyloxy)naphthalen-1-yl)-4,5-diphenyl-1*H*-imidazole

AG1091-1-4.fid
Project AB

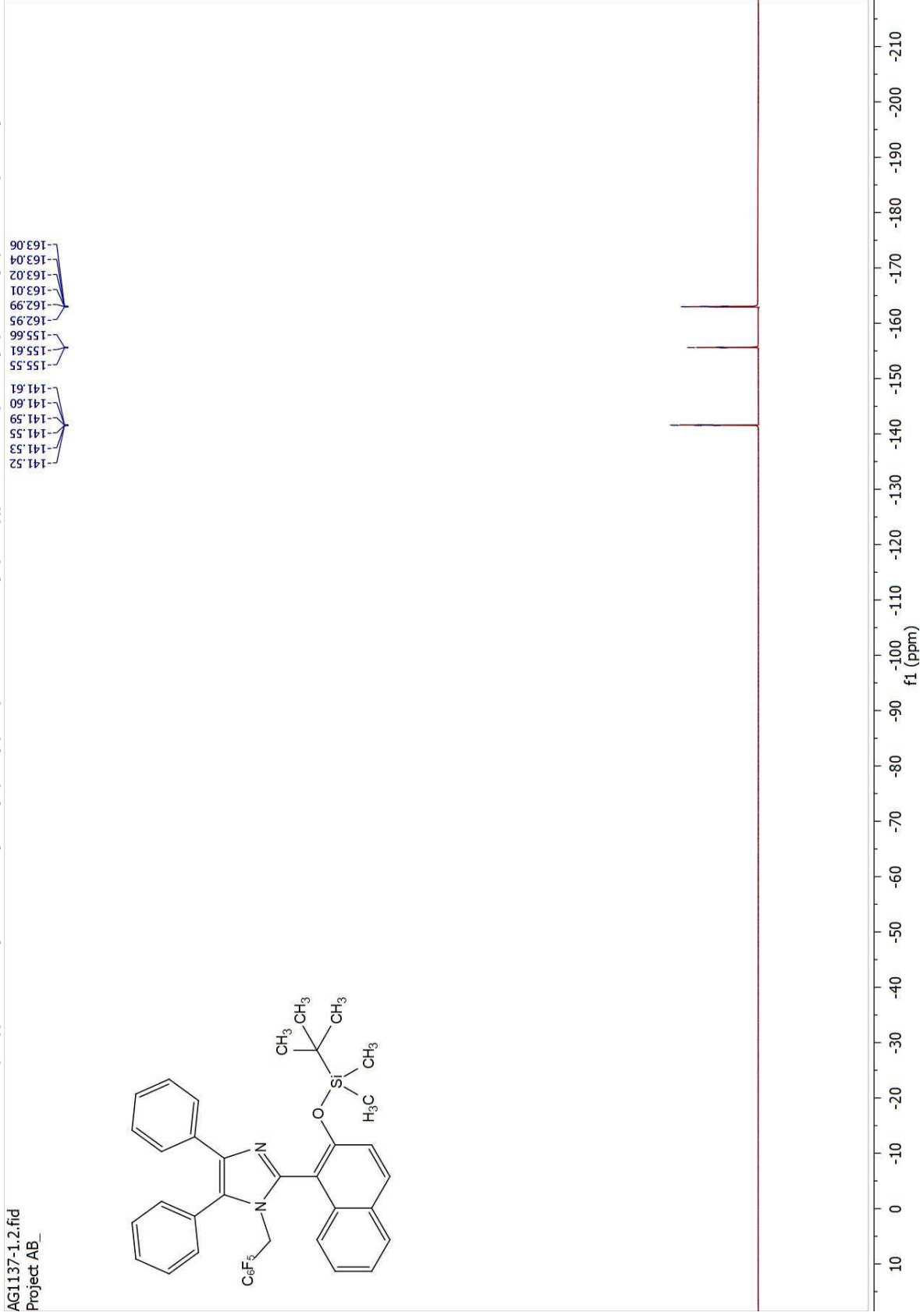


Spectrum 5: ¹H NMR of 2-(2-((tert-butyl(dimethylsilyl)oxy)naphthalen-1-yl)-1-((perfluorophenyl)methyl)-4,5-diphenyl-1H-imidazole



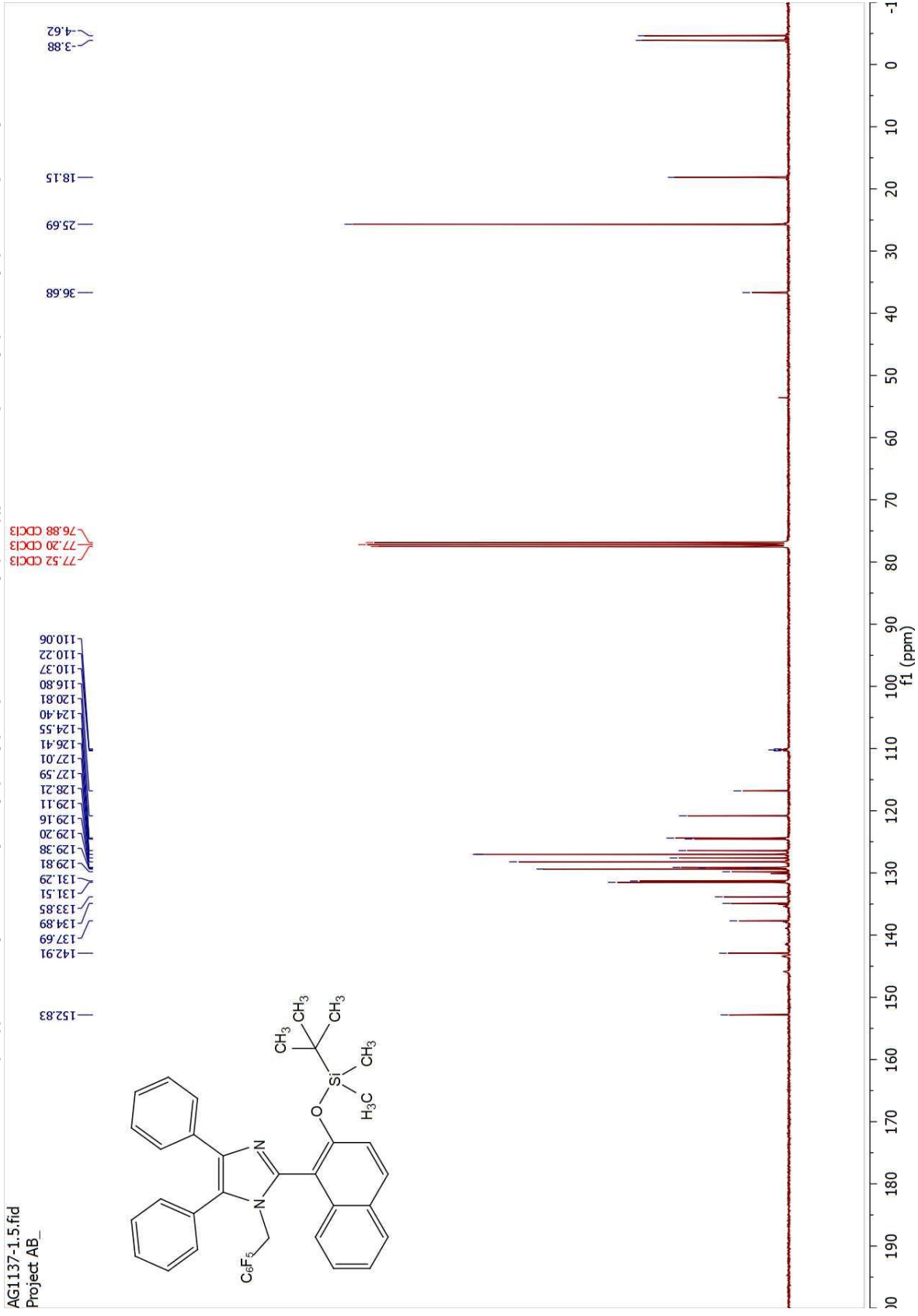
Spectrum 6: ^{19}F NMR of 2-(2-((tert-butylidimethylsilyl)oxy)naphthalen-1-yl)-1-((perfluorophenyl)methyl)-4,5-diphenyl-1H-imidazole

AG1137-1.2.fid
Project AB

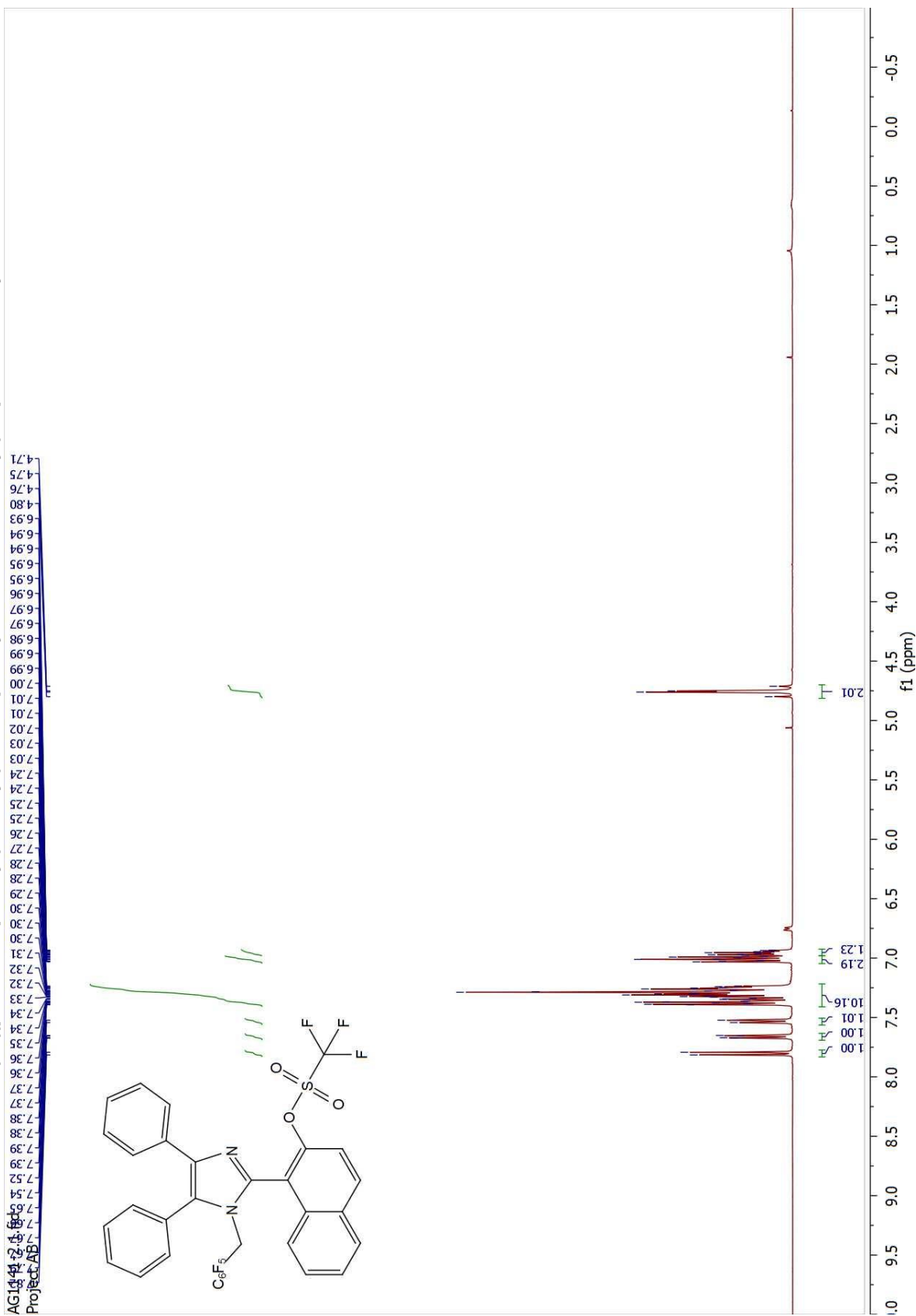


Spectrum 7: ¹³C NMR of 2-(2-(*tert*-butyldimethylsilyloxy)naphthalen-1-yl)-1-(perfluorophenyl)-1*H*-imidazole

AG1137-1.5.fid
Project AB

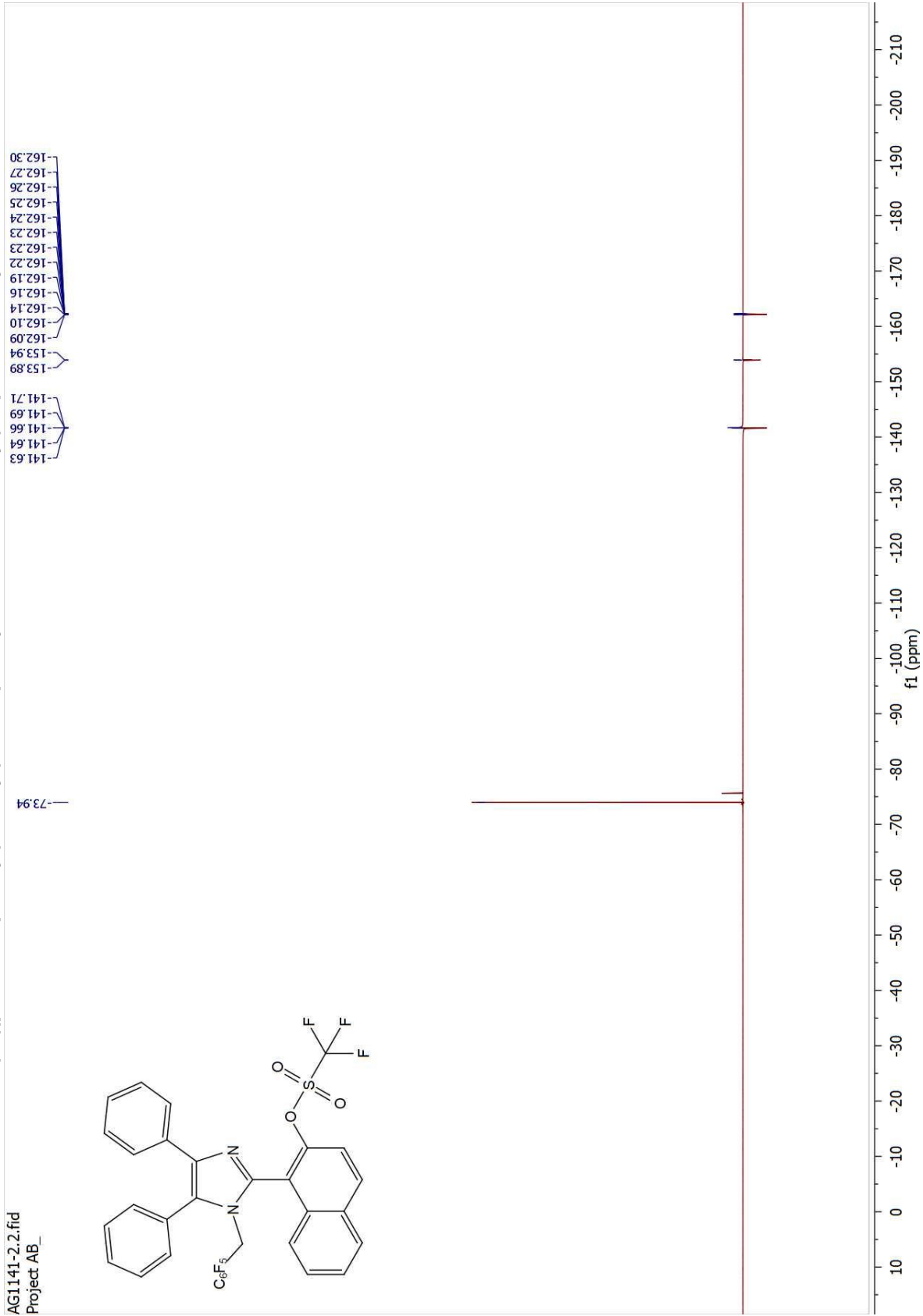


Spectrum 8: ¹H NMR of 1-(1-(perfluorophenyl)methyl)-4,5-diphenyl-1H-imidazol-2-yl)naphthalen-2-yl trifluoromethanesulfonate



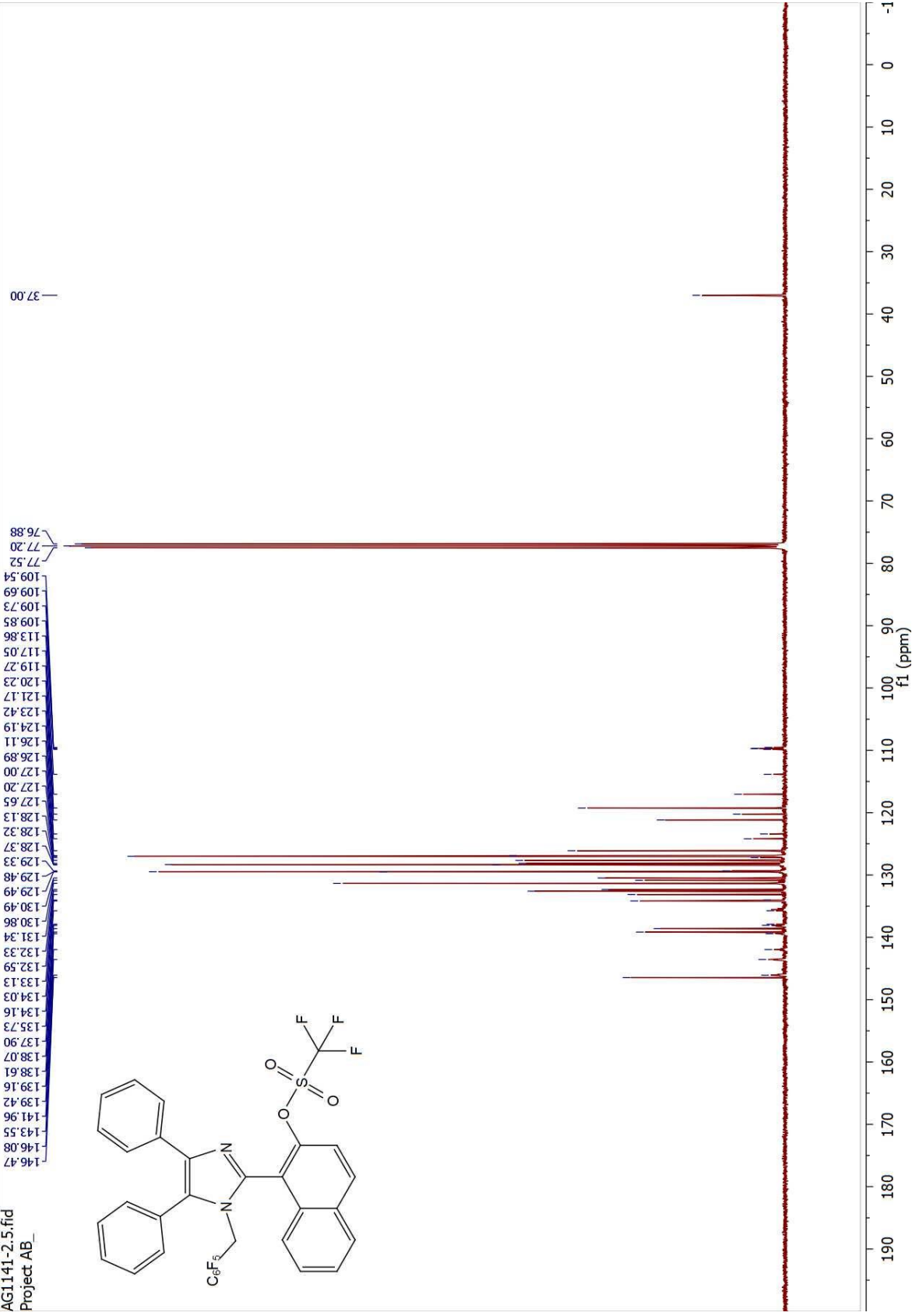
Spectrum 9: ¹⁹F NMR of 1-(1-((perfluorophenyl)methyl)-4,5-diphenyl-1H-imidazol-2-yl)naphthalen-2-yl trifluoromethanesulfonate

AG1141-2.2.fid
Project AB

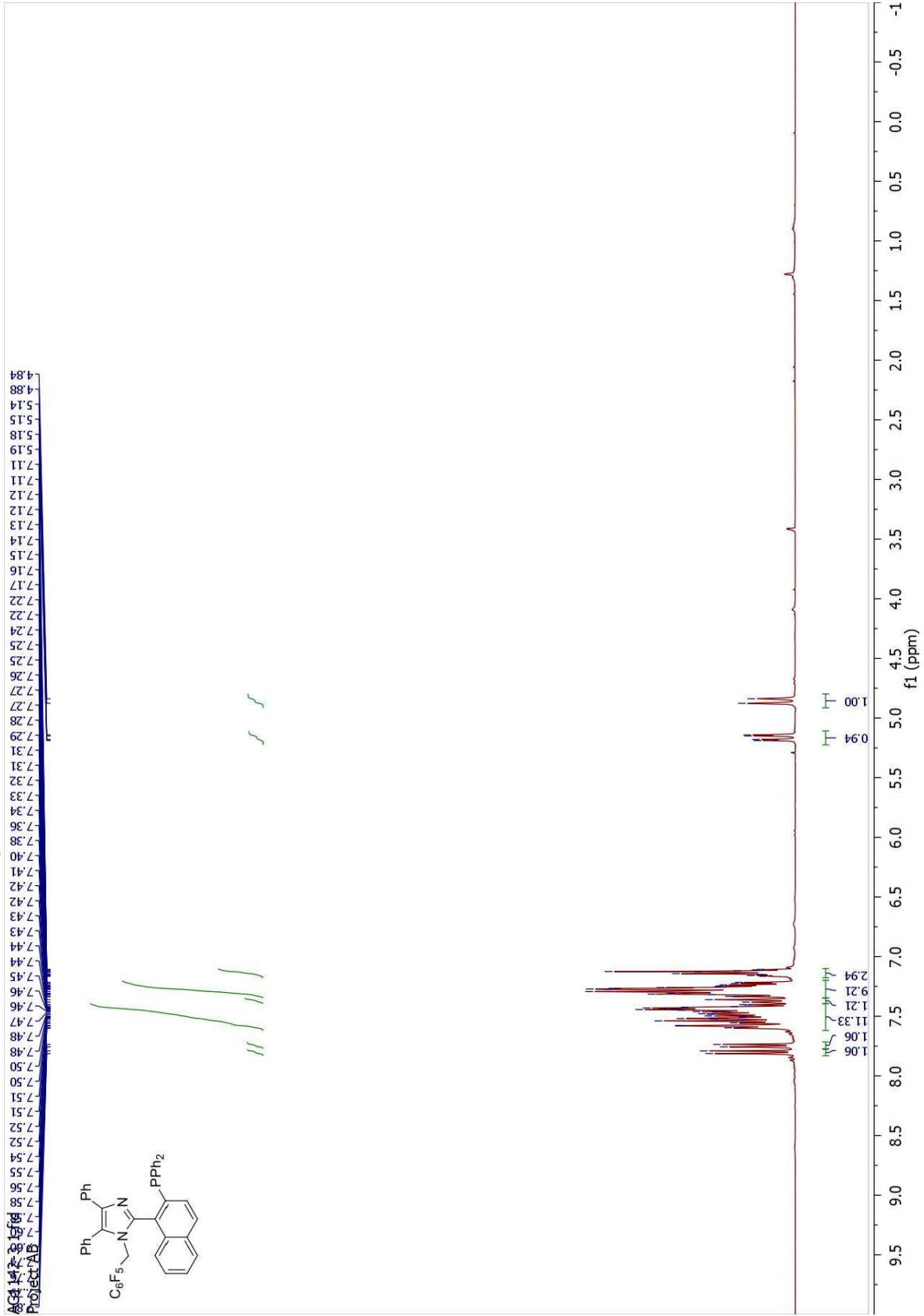


Spectrum 10: ^{13}C NMR of 1-(1-(perfluorophenyl)methyl)-4,5-diphenyl-1H-imidazol-2-yl)naphthalen-2-yl trifluoromethanesulfonate

AG1141-2.5.fid
Project AB

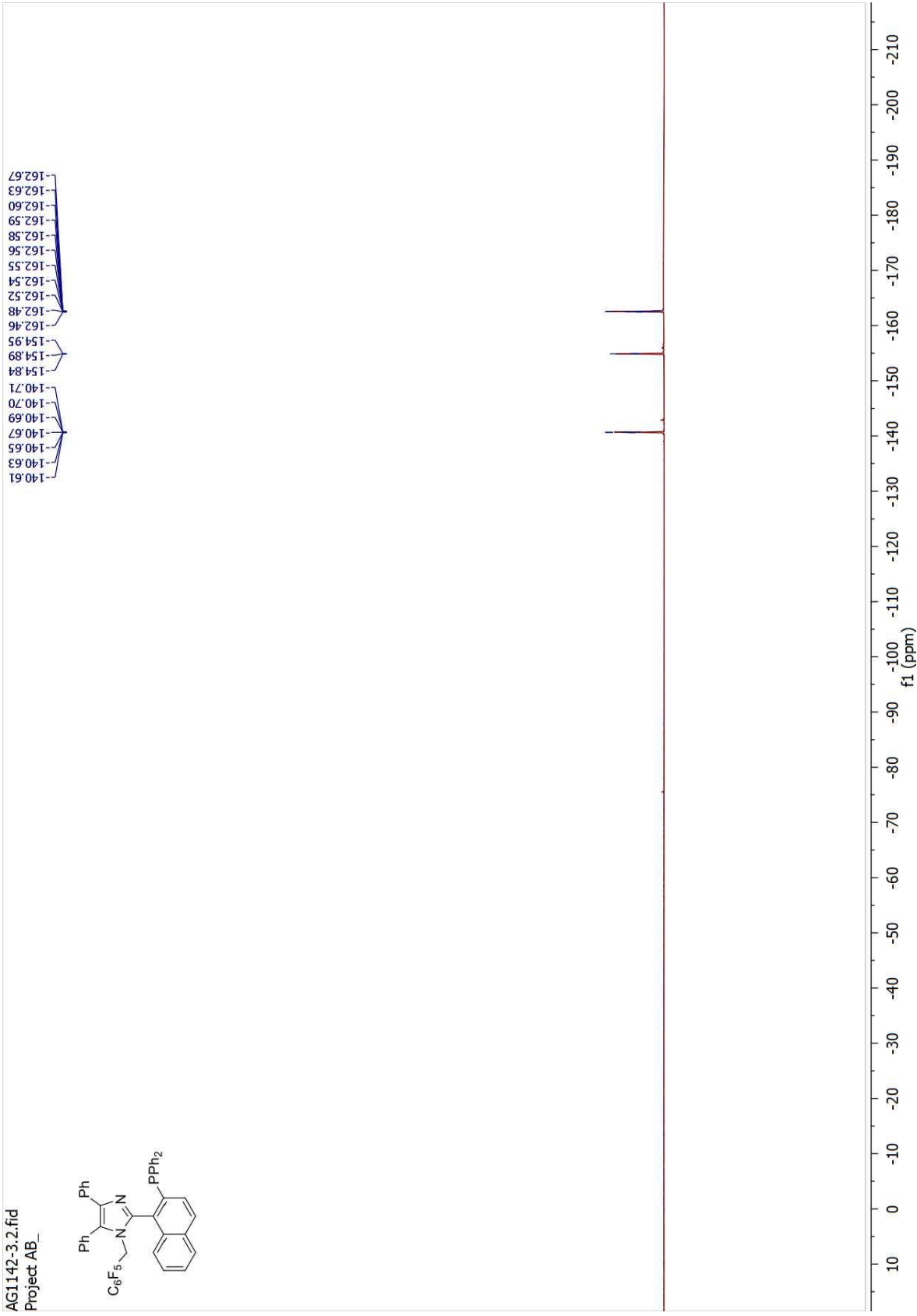
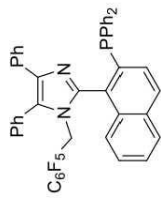


Spectrum 11: ¹H NMR of rac-StackPhos



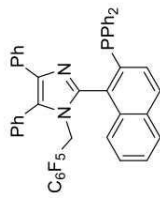
Spectrum 12: ¹⁹F NMR of *rac*-StackPhos

AG1142-3.2.fid
Project AB

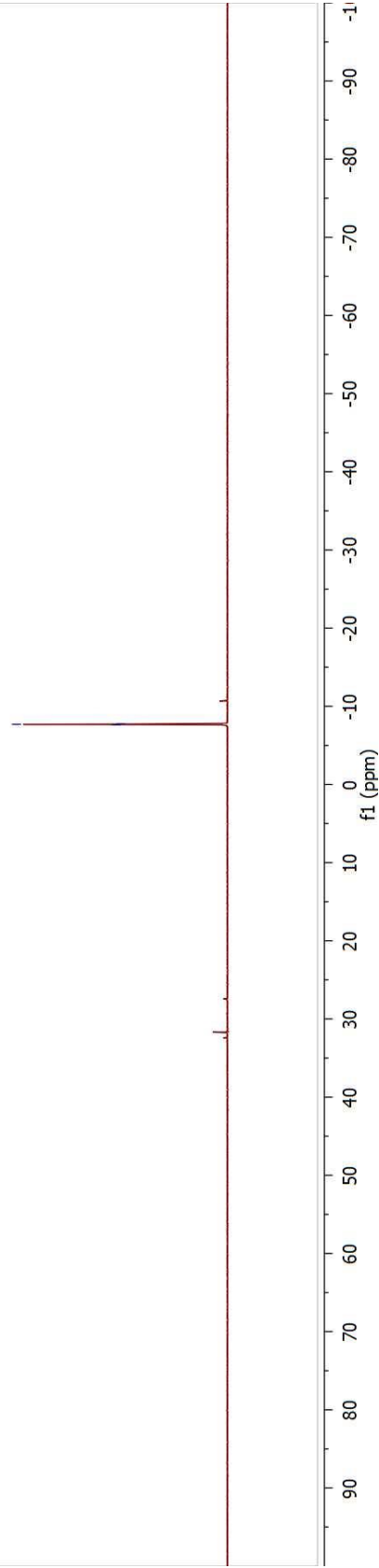


Spectrum 13: ^{31}P NMR of *rac*-StackPhos

AG1142-3.7.fid
Project AB

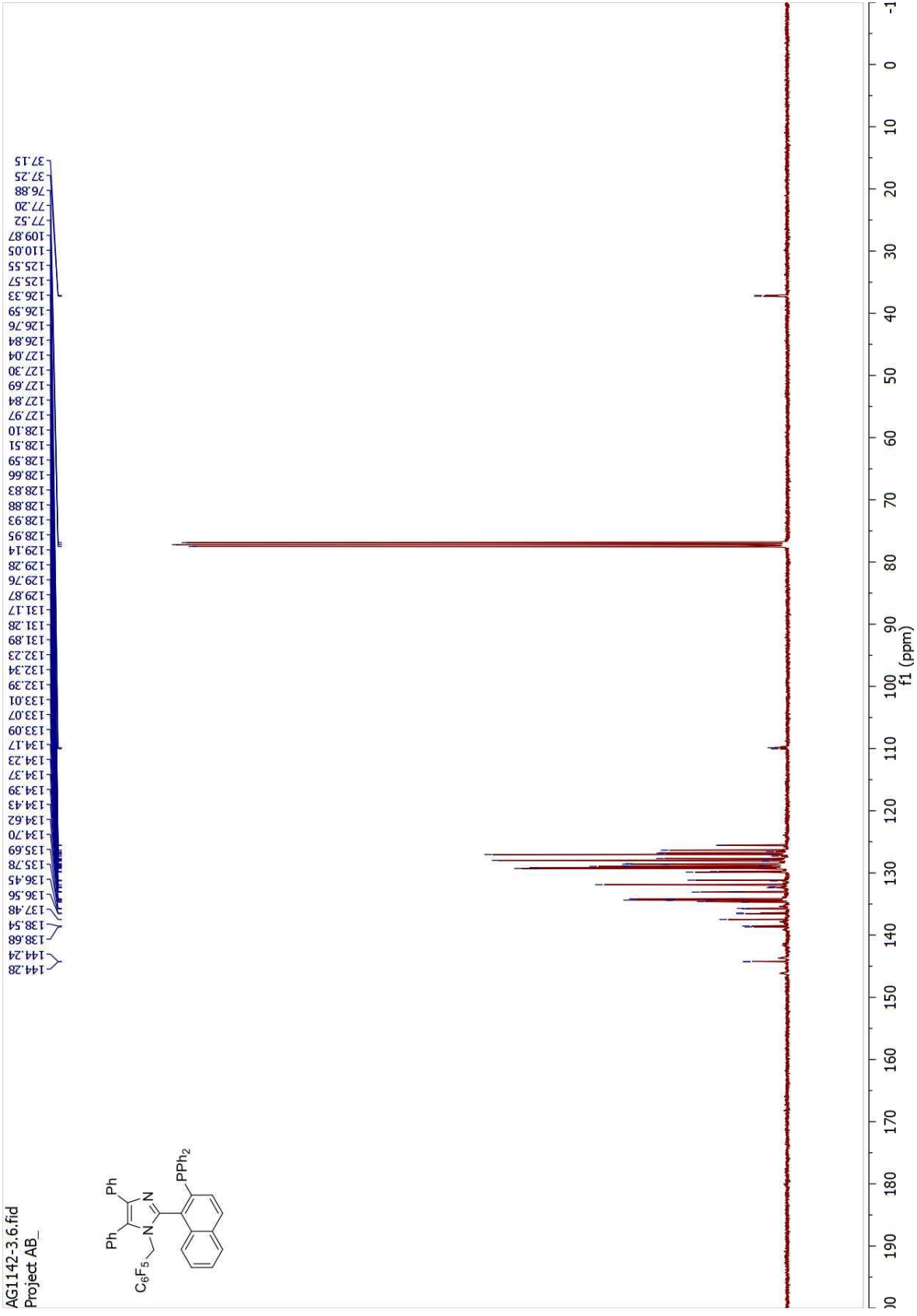
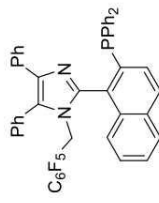


7.66
7.70
7.73

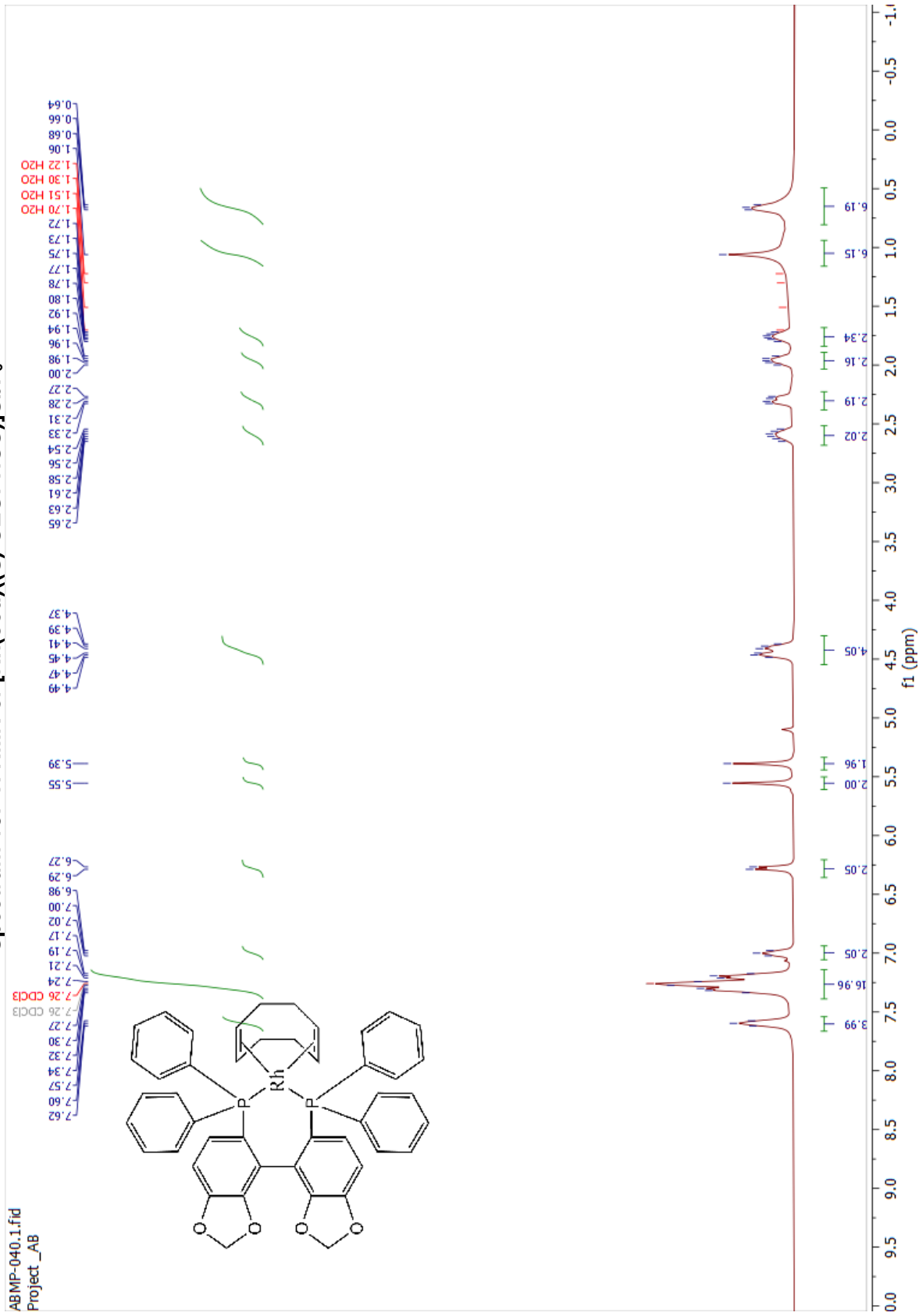


Spectrum 14: ^{13}C NMR of *rac*-StackPhos

AG1142-3.6.fid
Project AB

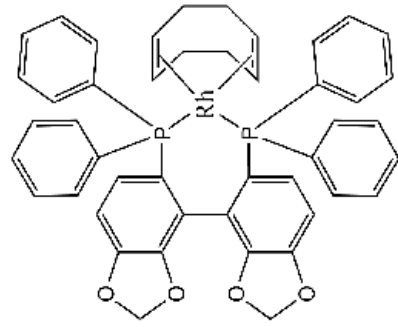


Spectrum 15: ^1H NMR of $[\text{Rh}(\text{cod})((S)\text{-SEGPHOS})]\text{SbF}_6$

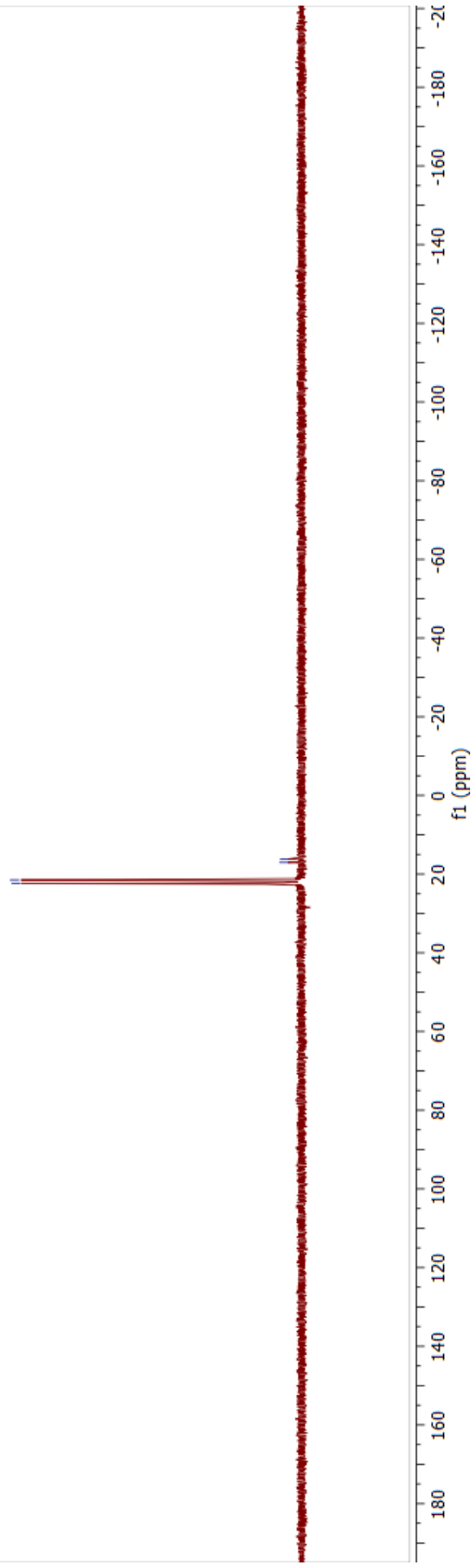


Spectrum 16: ^{31}P NMR of $[\text{Rh}(\text{cod})((S)\text{-SEGPHOS})]\text{SbF}_6$

ABMP-040.2.fid
Project_AB

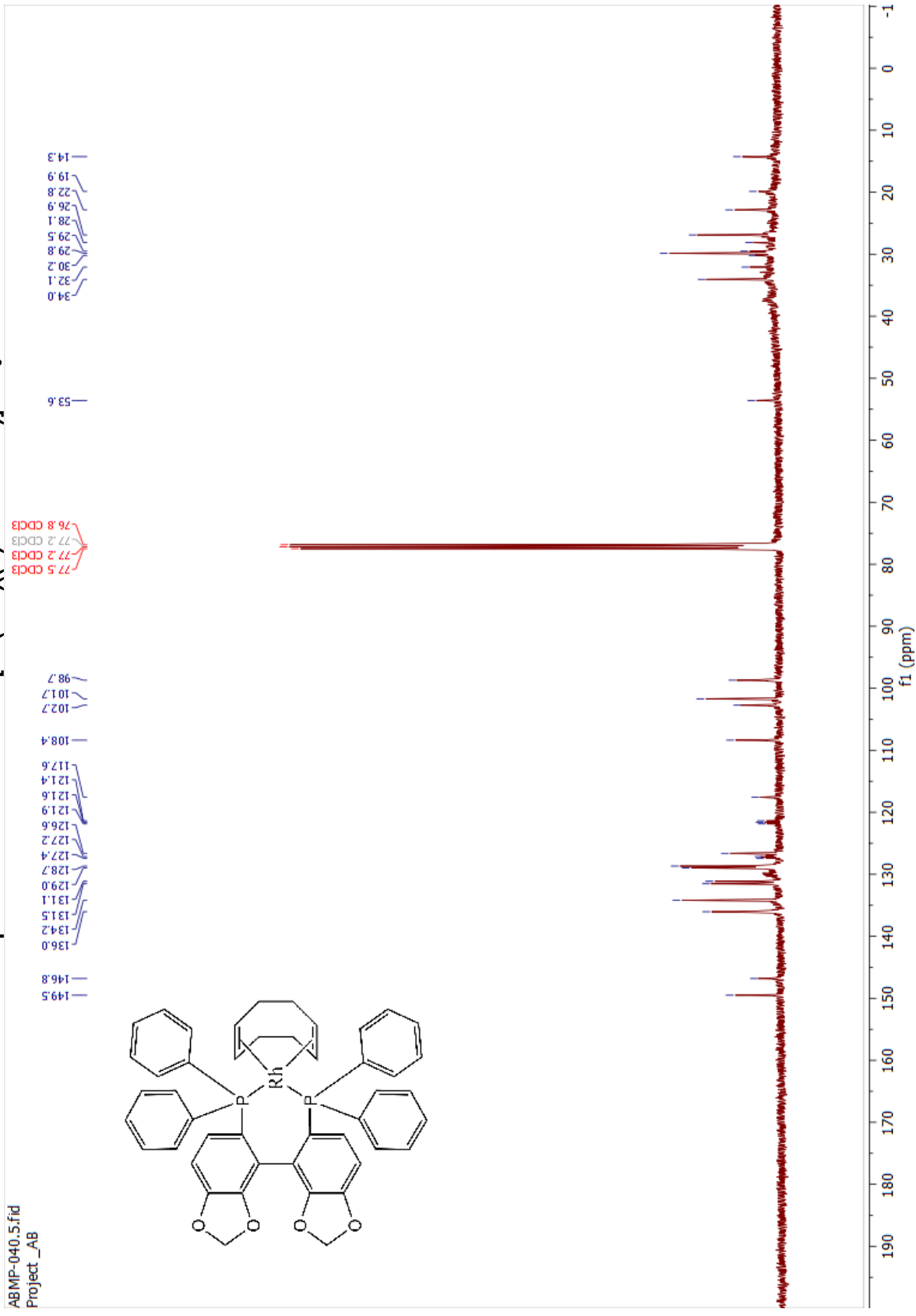


22.4
21.5
17.0
16.2

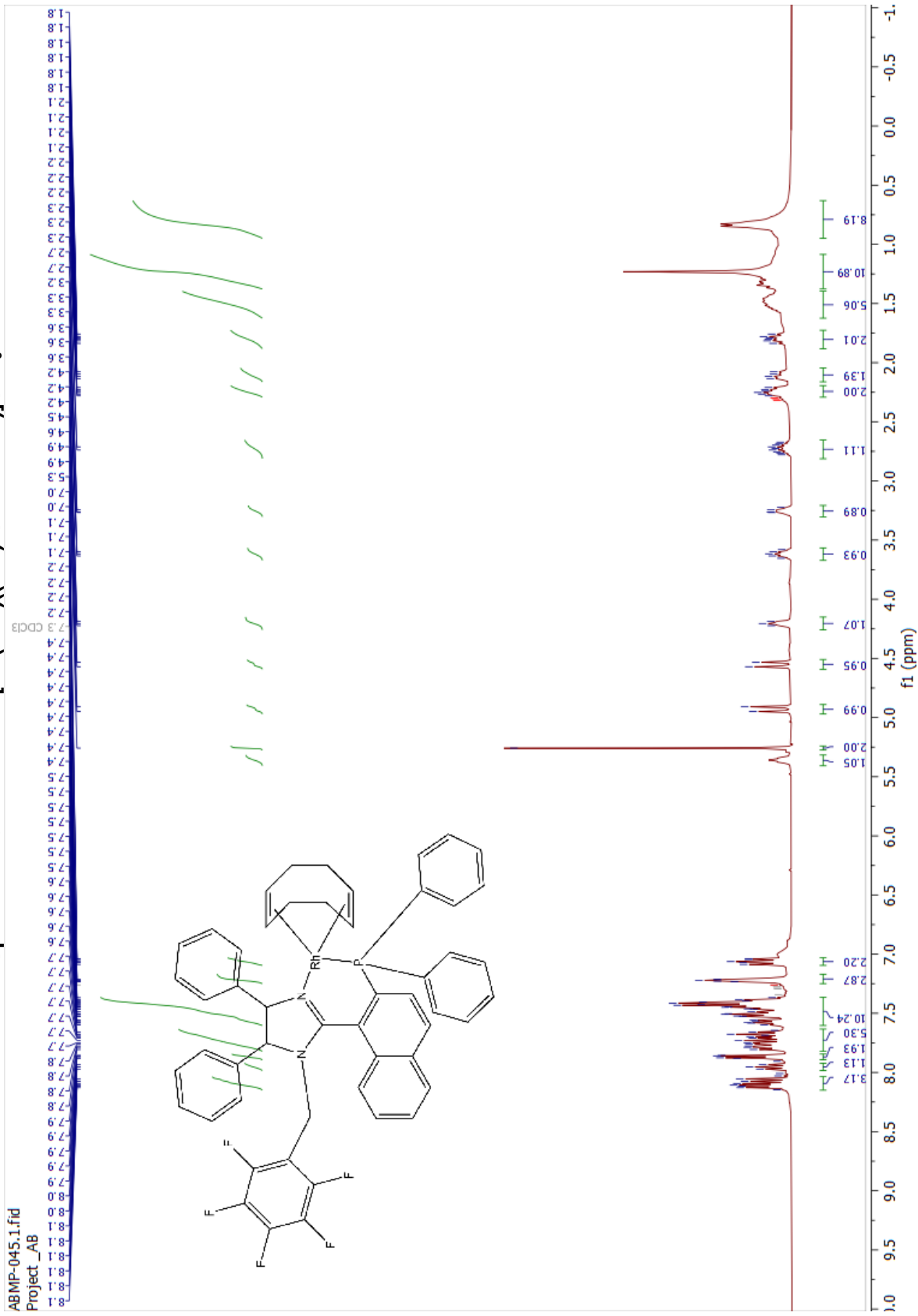


Spectrum 17: ^{13}C NMR of $[\text{Rh}(\text{cod})((S)\text{-SEGPHOS})]\text{SbF}_6$

ABMP-040.5.fid
Project_AB

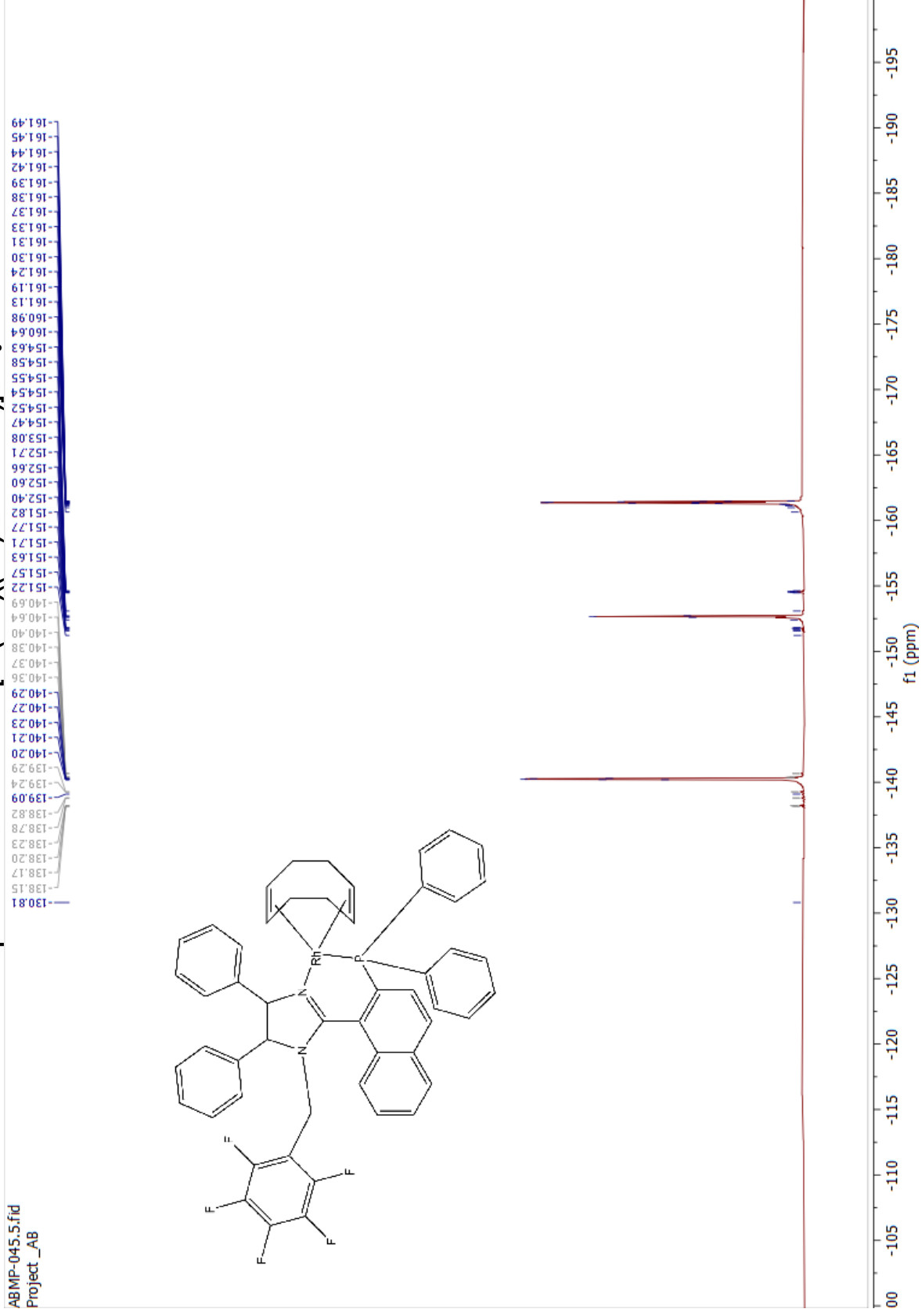


Spectrum 18: ^1H NMR of $[\text{Rh}(\text{cod})((\text{rac})\text{-StackPhos})]\text{SbF}_6$



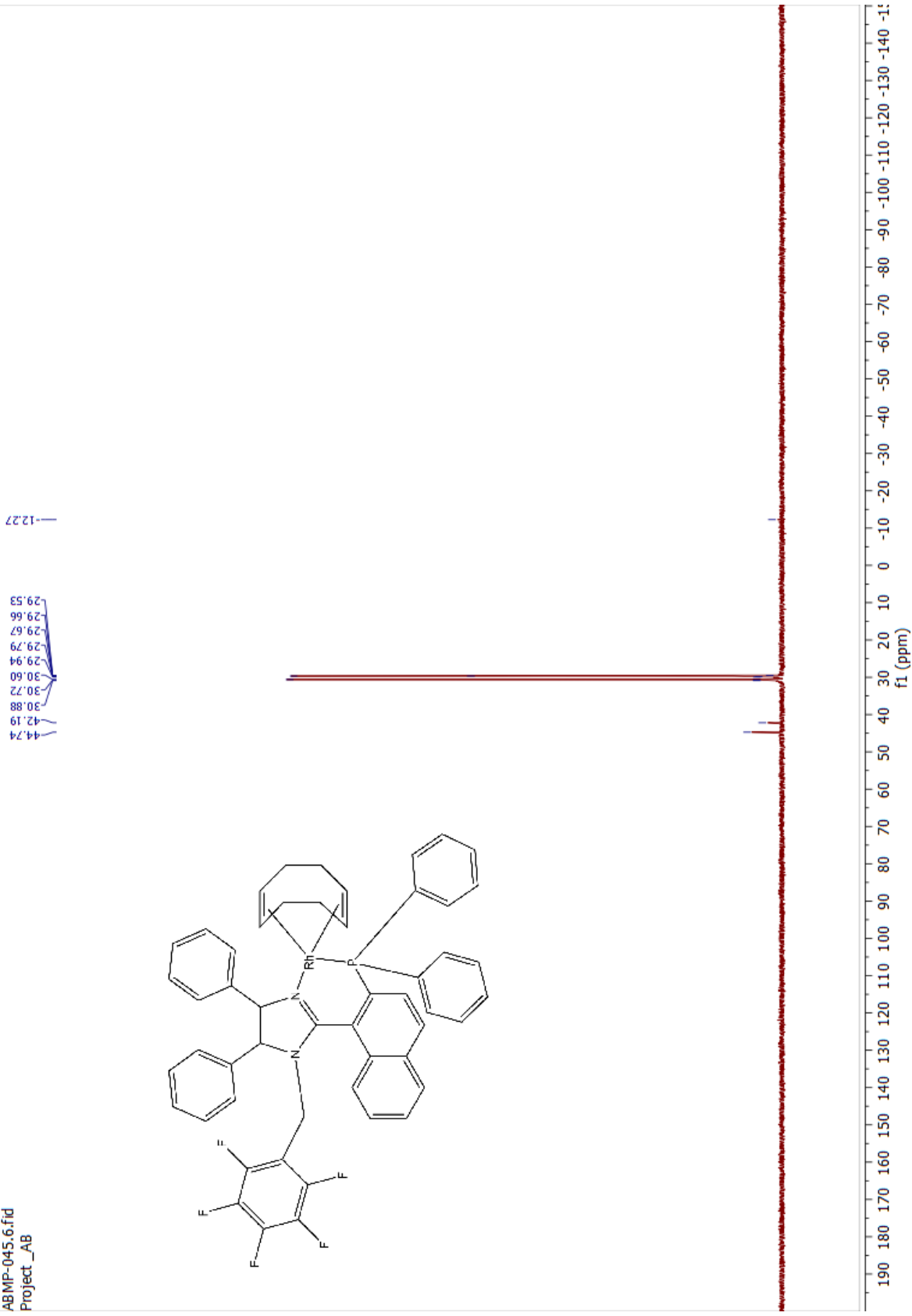
Spectrum 19: ^{19}F NMR of $[\text{Rh}(\text{cod})((\text{rac})\text{-StackPhos})]\text{SbF}_6$

ABMP-045.5.fid
Project _AB

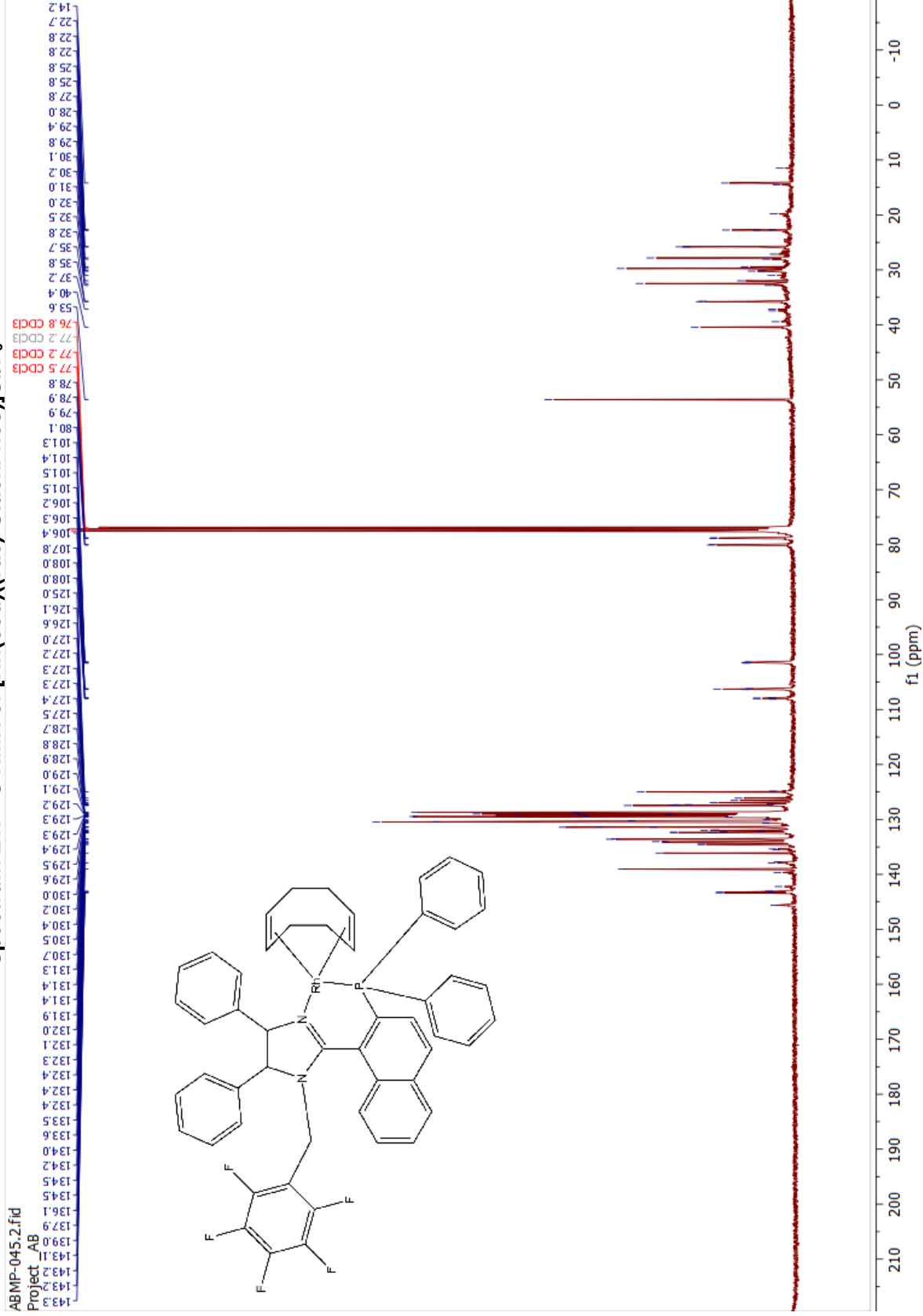


Spectrum 20: ^{31}P NMR of $[\text{Rh}(\text{cod})((\text{rac})\text{-StackPhos})]\text{SbF}_6$

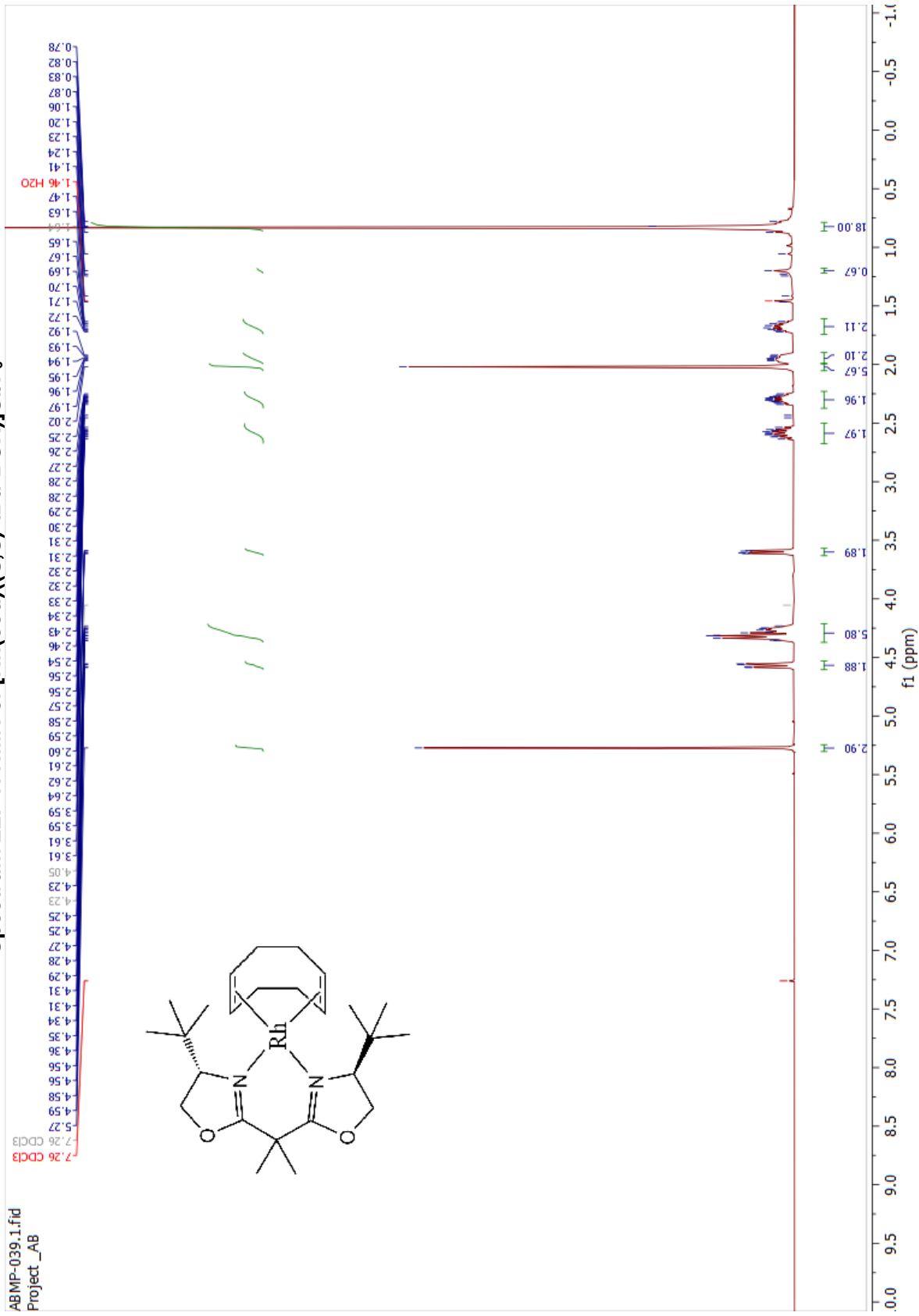
ABMP-045.6.fid
Project _AB



Spectrum 21: ^{13}C NMR of $[\text{Rh}(\text{cod})((\text{rac})\text{-StackPhos})]\text{SbF}_6$

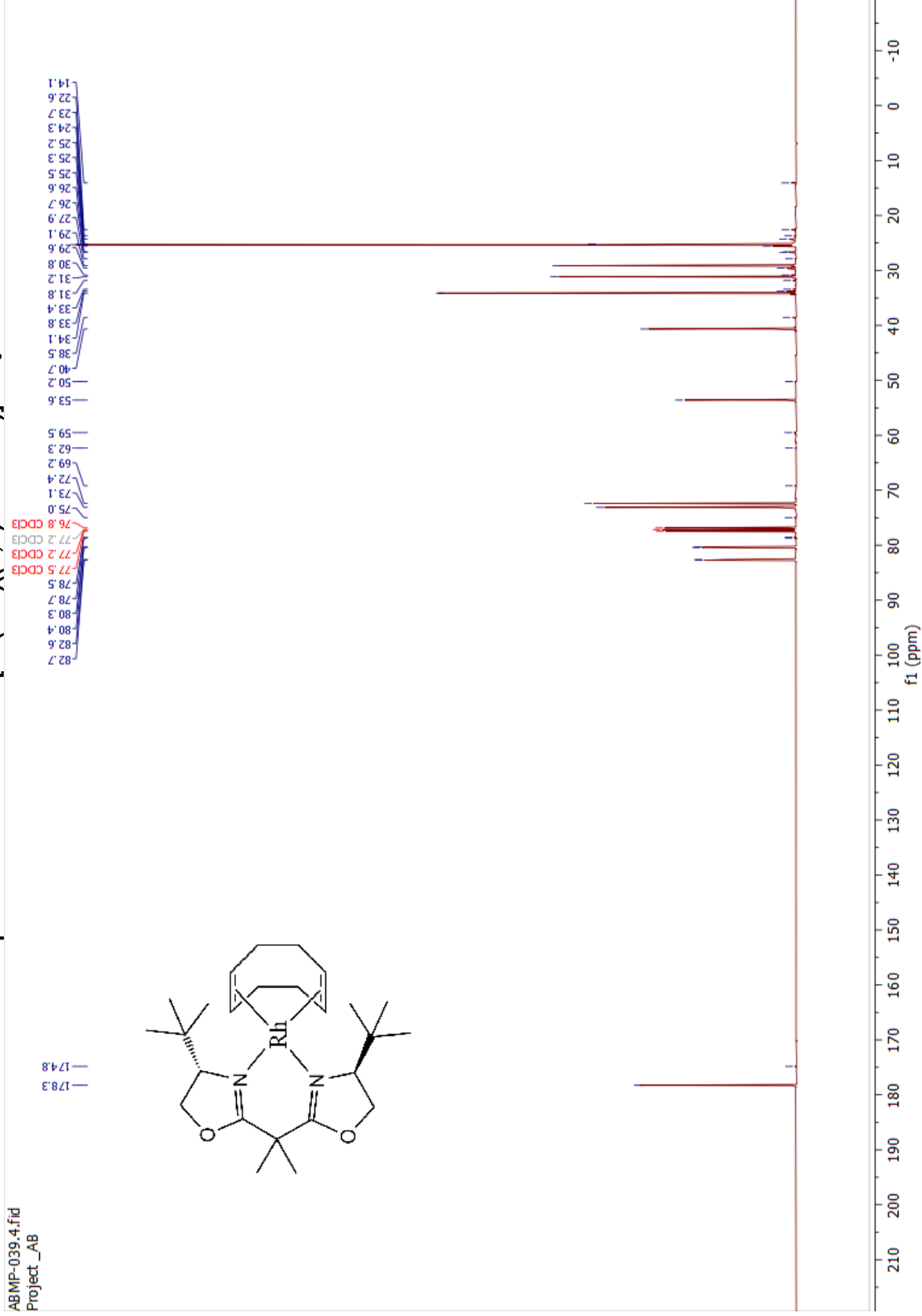


Spectrum 22: ^1H NMR of $[\text{Rh}(\text{cod})((S,S)\text{-tBu-BOX})]\text{SbF}_6$

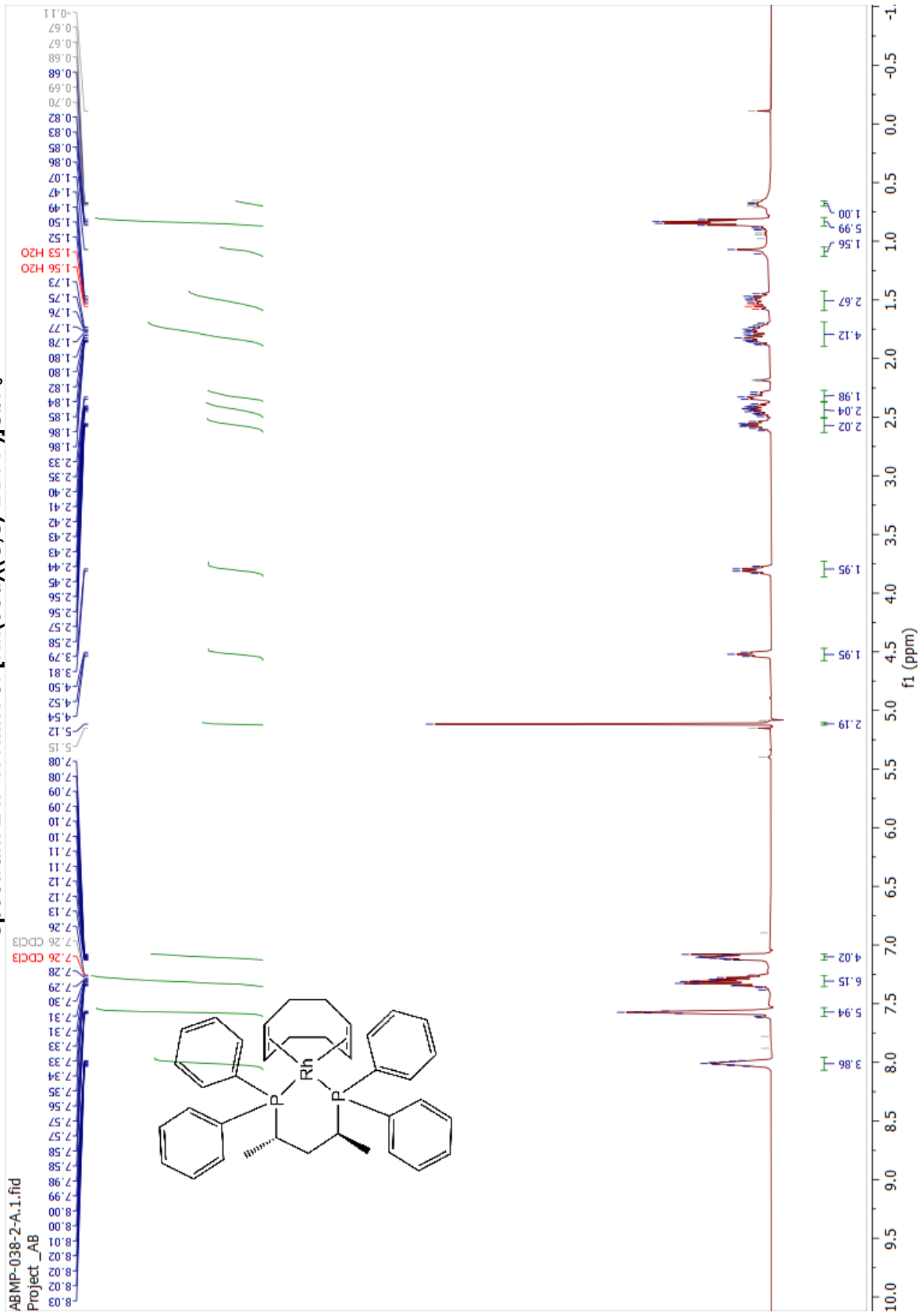


Spectrum 23: ^{13}C NMR of $[\text{Rh}(\text{cod})((S,S)\text{-}t\text{Bu-BOX})]\text{SbF}_6$

ABMP-039_4.fid
Project _AB

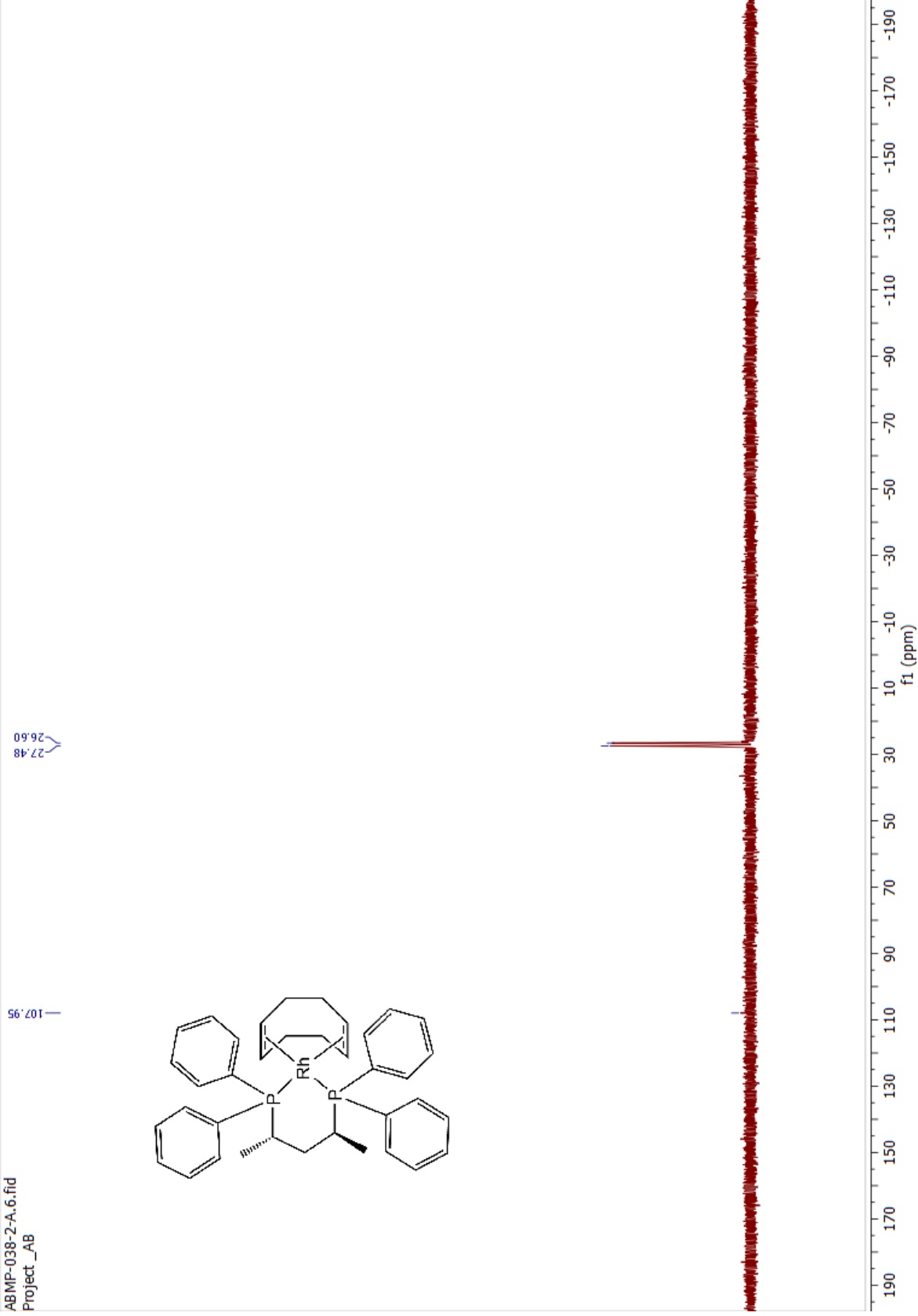


Spectrum 24: ^1H NMR of $[\text{Rh}(\text{cod})((S,S)\text{-BDPP})]\text{SbF}_6$



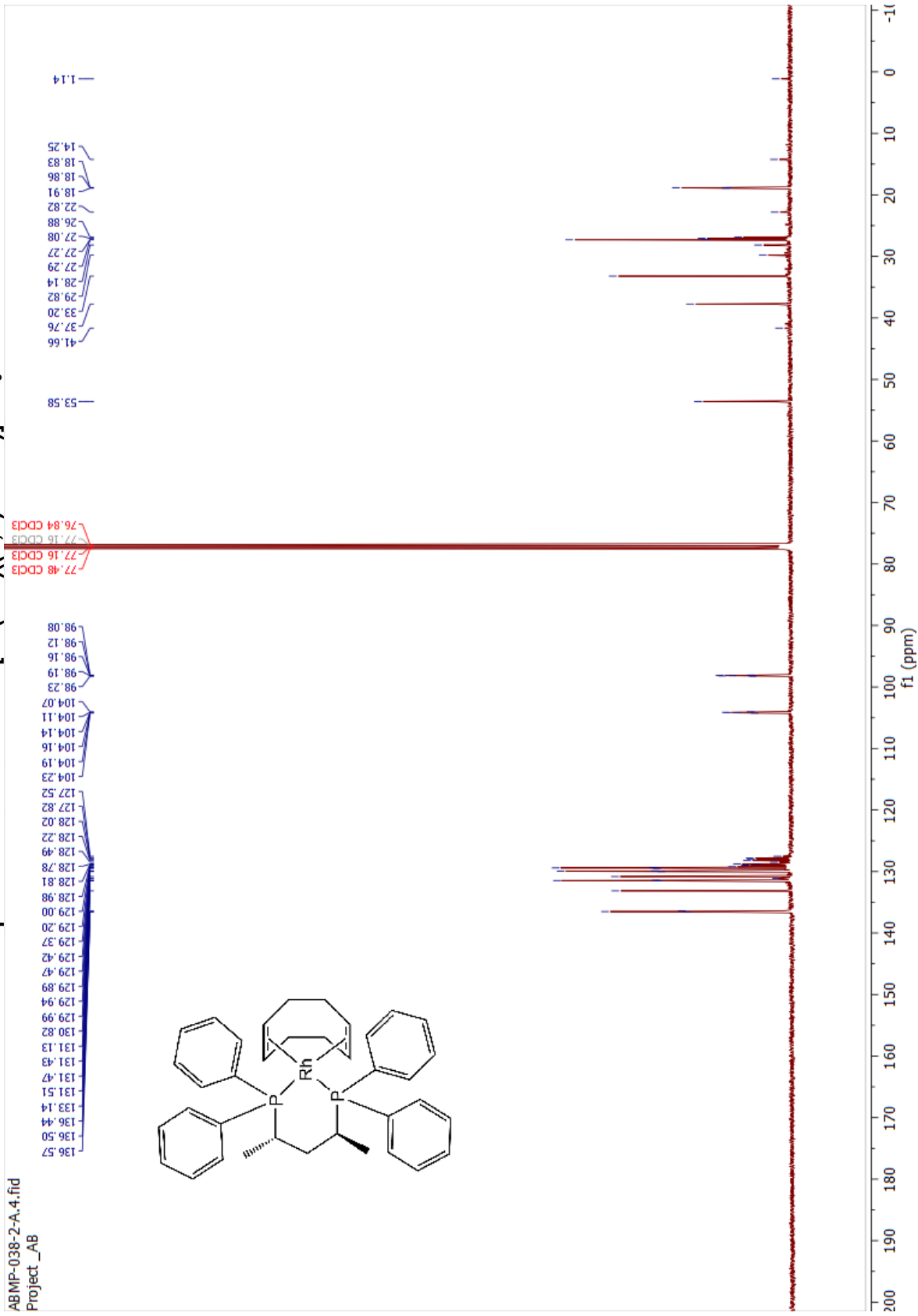
Spectrum 25: ^{31}P NMR of $[\text{Rh}(\text{cod})((S,S)\text{-BDPP})]\text{SbF}_6$

ABMP-038-2-A-6.fid
Project _AB

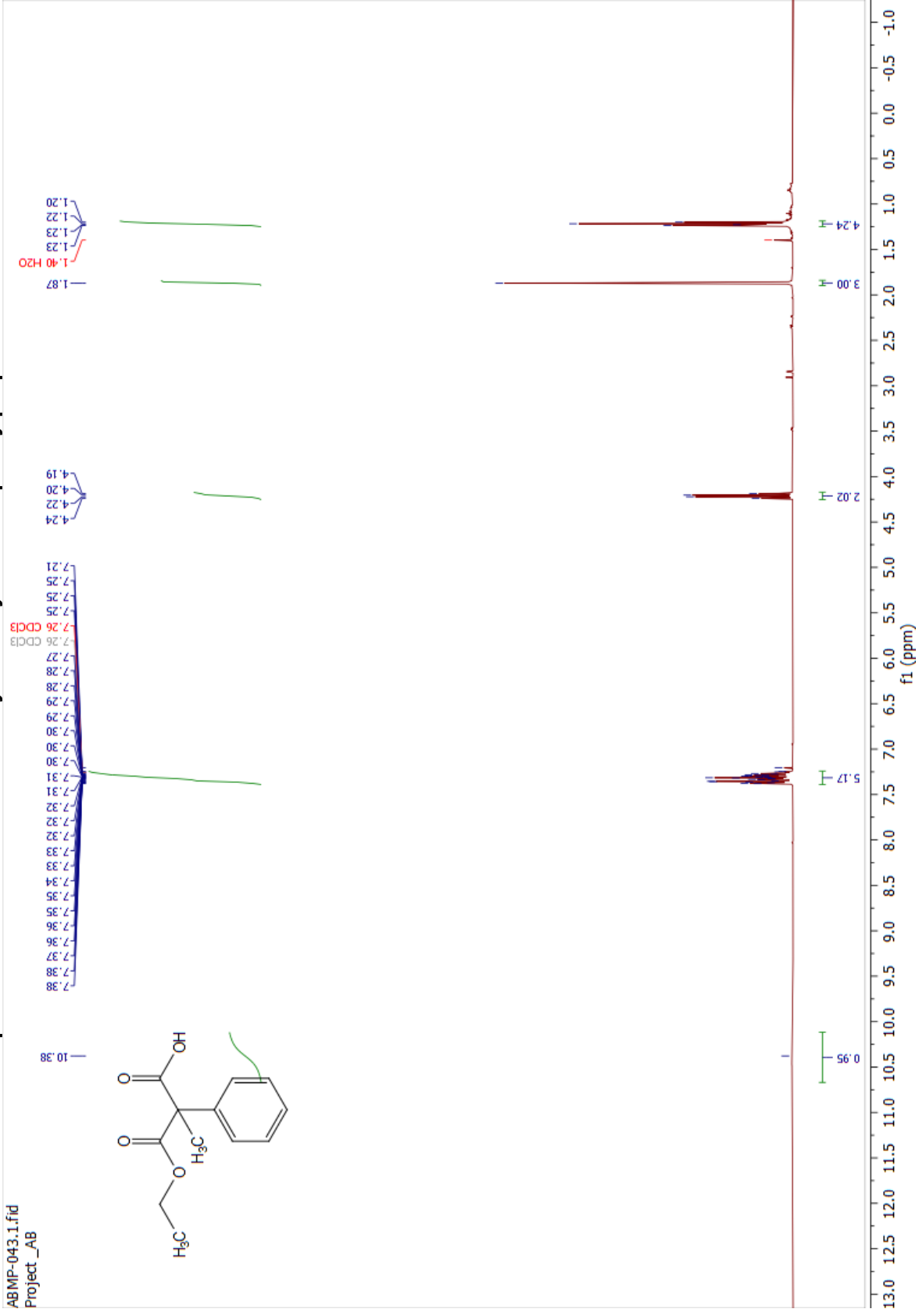


Spectrum 26: ^{13}C NMR of $[\text{Rh}(\text{cod})((S,S)\text{-BDPP})\text{SbF}_6$

ABMP-038-2-A_4.fid
Project_AB

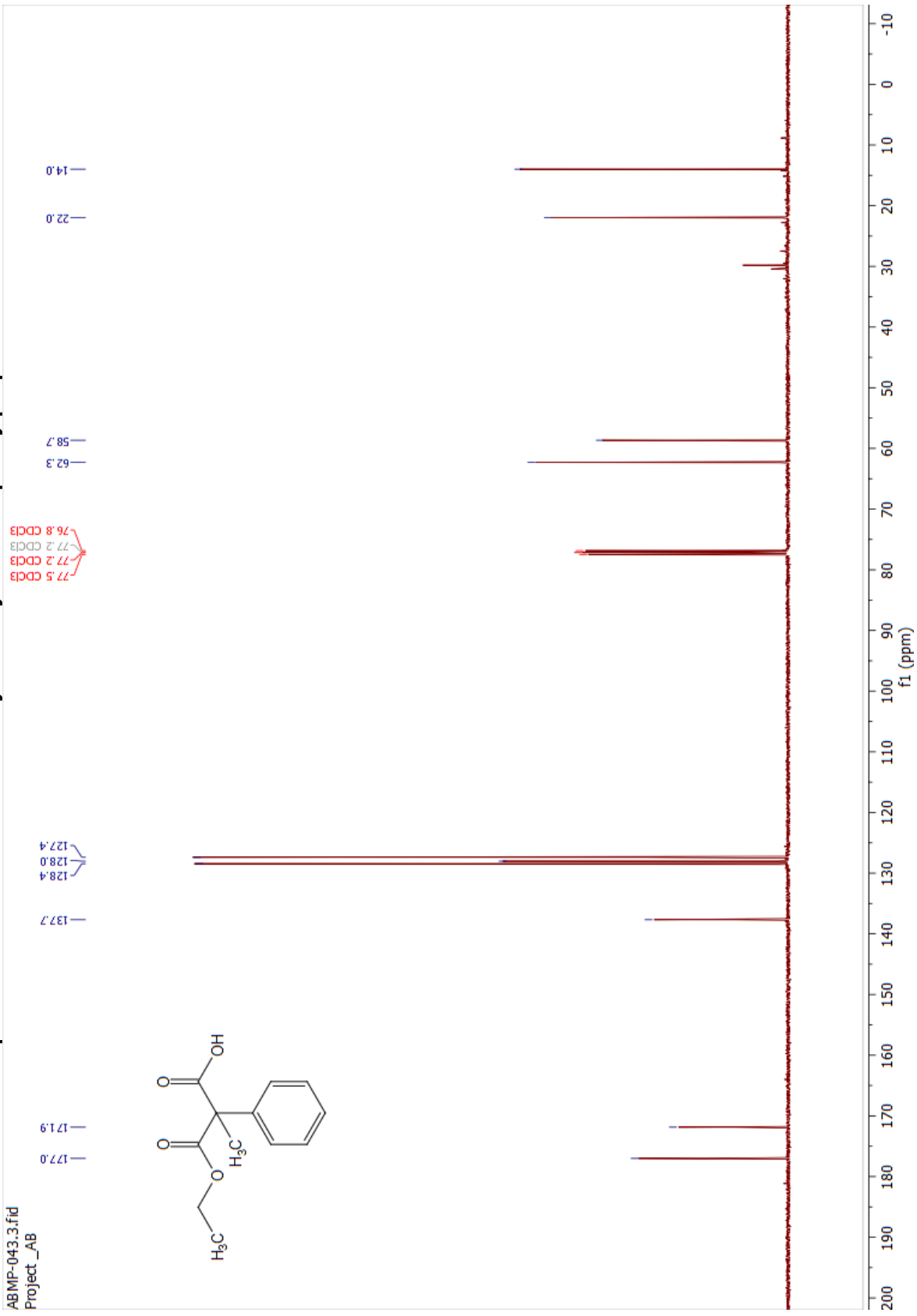


Spectrum 27: ¹H NMR of 3-ethoxy-2-methyl-3-oxo-2-phenylpropanoic acid



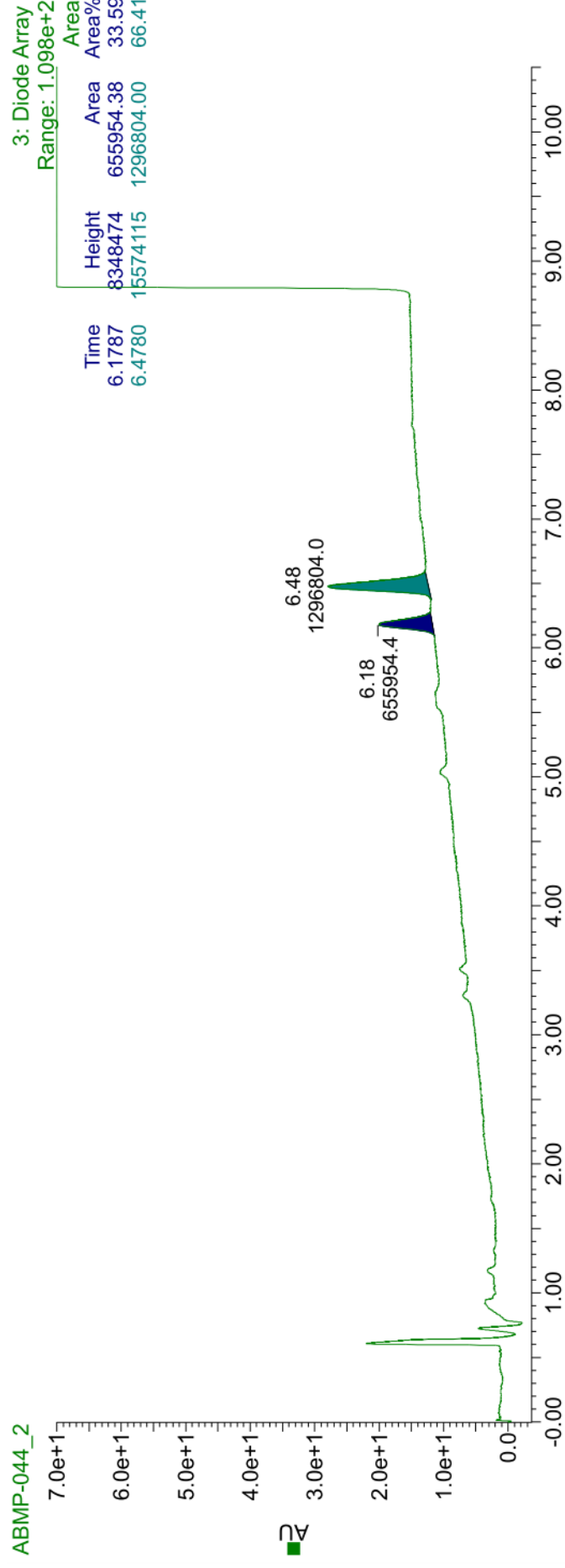
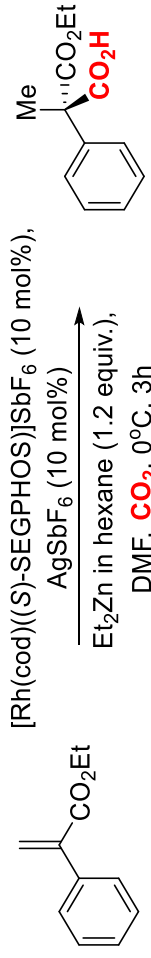
Spectrum 28: ¹³C NMR of 3-ethoxy-2-methyl-3-oxo-2-phenylpropanoic acid

ABMP-043.3.fid
Project_AB

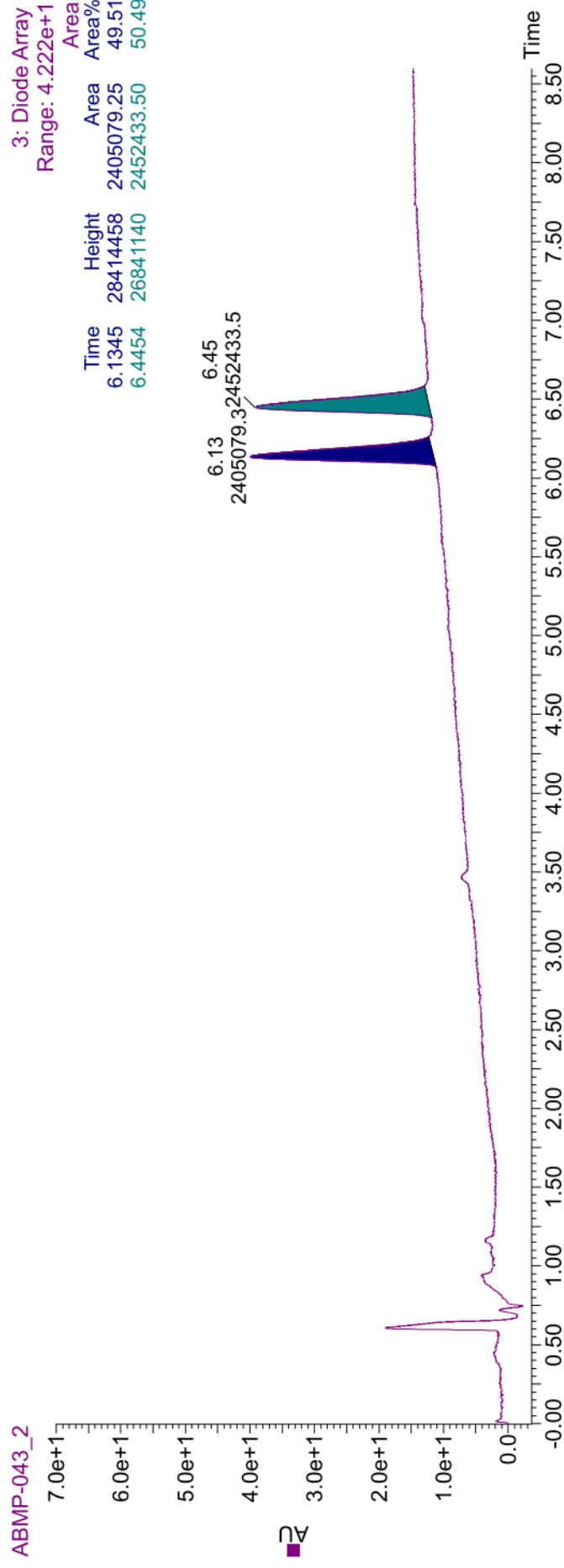
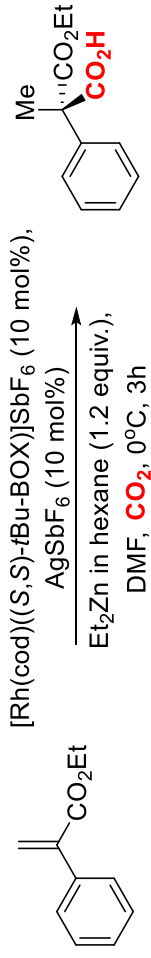


Copies of chromatograms

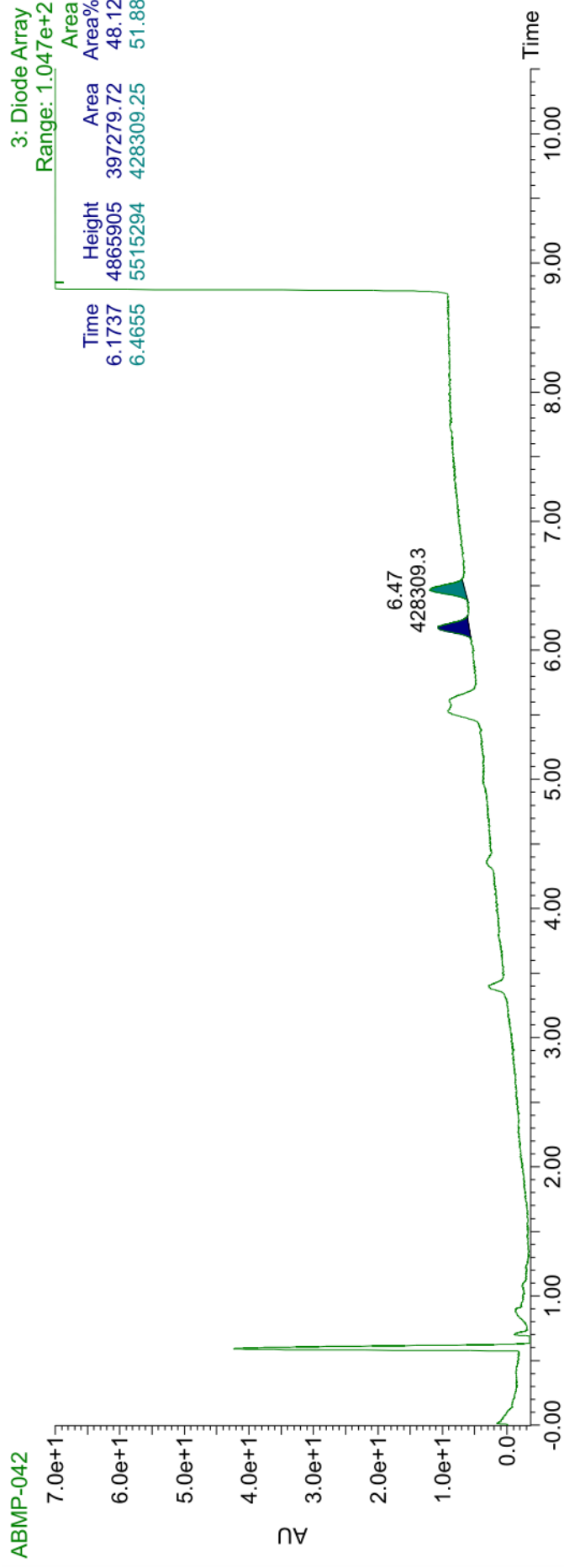
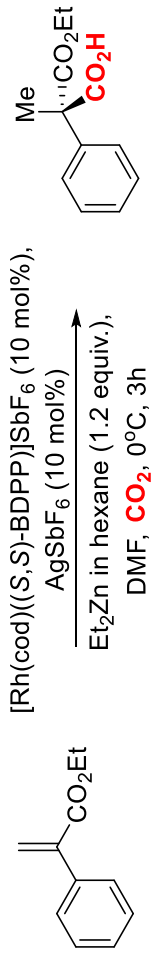
Chromatogram of hydrocarboxylation with [Rh(cod)((S)-SEGPBOS)]SbF₆



Chromatogram of hydrocarboxylation with [Rh(cod)((S,S)-tBu-BOX)]SbF₆



Chromatogram of hydrocarboxylation with $[\text{Rh}(\text{cod})((S,S)\text{-BDPP})\text{SbF}_6]$



Paper II

Asymmetric boracarboxylation of styrenes using carbon dioxide

Manuscript under revision

Asymmetric boracarboxylation of styrenes using carbon dioxide

Martin Pettersen,^{a,†} Cuong Dat Do,^{a,b,†} Marc F. Obst,^a Roman Damm,^a Anggi E. Putra,^a Ashot Gevorgyan,^a Ljiljana Pavlovic,^a Kathrin H. Hopmann^{*a,§} and Annette Bayer^{*a,§}

^a Department of Chemistry, UiT The Arctic University of Norway, N-9017 Tromsø, Norway. E-Mail: annette.bayer@uit.no; kathrin.hopmann@uit.no.

^b Hylleraas Center for Quantum Molecular Sciences, UiT The Arctic University of Norway, N-9017 Tromsø, Norway.

^{†,§} Have contributed equally.

Abstract. The boracarboxylation reaction has potential for production of new drug candidates, but the development of an asymmetric version of this transformation is challenging. We report an enantioselective boracarboxylation of styrenes, enabled by a copper catalyst containing chiral phosphines. Our experimental conditions provide yields of up to 76% and enantiomeric ratios reaching 98:2. A computational analysis of the mechanistic details shows a complex pattern

of competing reaction pathways explaining challenges encountered when developing asymmetric reactions using CO₂.

Keywords: Asymmetric catalysis; Carbon dioxide fixation; Carboxylation; Copper; Computational chemistry; Reaction mechanism.

Introduction

Carbon dioxide is a cheap and widely abundant waste gas that can serve as a source of carbon. One of its possible applications is as a building block for the formation of value-added chemicals.^[1] This requires efficient ways to form C-C bonds with CO₂. The use of CO₂ in carboxylation reactions is of large interest, given the abundance of carboxylic acid functional groups in natural and medicinal compounds.^[2] A review from 2020 concluded that over 60% of all bioactive molecules described in the medicinal chemistry literature contain at least one carboxylic acid moiety or another functional group that can be derived from a carboxylic acid.^[3]

Conventional methods for carboxylation using CO₂ such as the Grignard reaction and the Kolbe-Schmitt reaction are well developed, have been commercialized and can be used to prepare food additives such as benzoic and acetic acid or pharmaceutical products such as salicylic acid.^[4] In the last two decades, there has been increasing focus on developing catalytic and electrochemical methods for CO₂-based carboxylations broadening the scope of CO₂-based chemical transformations.^[5]

The ability to form chiral carboxylic acids plays a critical role in natural product synthesis and drug development. However, the number of catalytic asymmetric carboxylations employing CO₂ is limited.^[6] In 2004, the Mori group demonstrated the generation of three stereocenters through Ni-catalysed carboxylative cyclization of bis-1,3-dienes with enantiomer ratio (*e.r.*) up to 96:4 and yields up to 99%.^[7] A notable study was published in 2016 by Mikami's group, who applied a chiral Rh-based catalyst in the hydrocarboxylation of acrylates. In their study they achieved an *e.r.* of up to 83:17 and excellent yields.^[8] Another significant study in the field of asymmetric CO₂ utilization was published by the

group of Yu in 2017.^[9] Their study describes a Cu-catalyzed hydroxymethylation of styrenes and 1,3-dienes, achieved from addition of CO₂ and in-situ reduction of the intermediate carboxylate, with conditions obtaining excellent *e.r.* (up to 99:1) and yields (up to 96%). Later, this method was extended to the hydroxymethylation of 1,1-disubstituted-1,3-dienes^[10] and 1,1-disubstituted allenes^[11] producing quaternary stereocentres with good enantioselectivity.

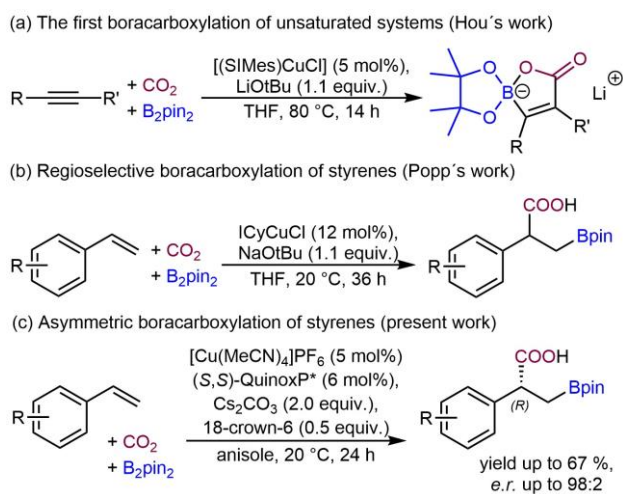
Also, in 2017 Marek and co-workers achieved a Cu-catalysed asymmetric carbomagnesiation of cyclopropene using CO₂ as electrophile in one example. The reaction exhibited good yields (up to 75%) and excellent *e.r.* values (up to 98:2).^[12] Recently, enantioselective carbo-carboxylations of alkenes via a Ni-catalysed Heck coupling/carboxylation cascade have been reported by the groups of Lopez and Bandini,^[13] and Kong and Yu.^[14] The first example of an enantioselective electrochemical carboxylation was reported by Lu and co-workers in 2009 transforming acetophenone to the corresponding α -hydroxyacid with an *e.r.* of 65:35.^[15] Recently, the method was modified to provide an *e.r.* of up to 97:3 for selected examples.^[16] The group of Lu also reported the electrochemical transformation of benzylic halides to the corresponding carboxylic acids with an *e.r.* up to 92:8 using either a chiral homogeneous^[17] or heterogeneous^[18] co-catalyst. Similarly, in 2018, Mei and co-workers reported the electrochemical carboxylation of allylic acetates with an *e.r.* of up to 84:16 using a chiral Pd-catalyst.^[19]

One reaction of interest in terms of asymmetric development is the boracarboxylation, which allows for direct carboxylation of an unsaturated C-C bond using CO₂ as a carbon source. The simultaneous addition of a boron moiety creates a reactive C-B bond that subsequently can be used for derivatization leading to potential drug precursors, for example of anti-inflammatory agents such as naproxen,

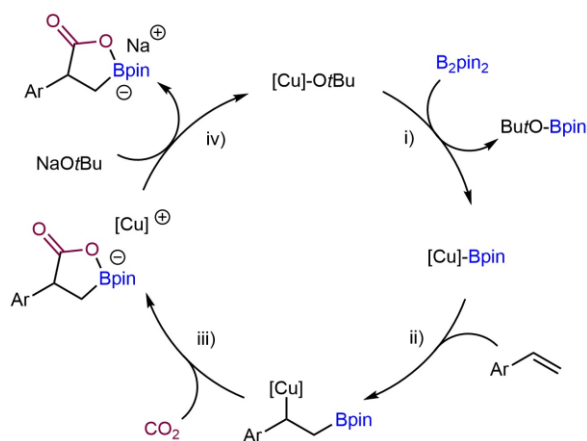
flurbiprofen or fenoprofen.^[20] The first reported catalytic boracarboxylation of unsaturated C-C bond dates from 2012. Hou and co-workers (**Scheme 1a**) described the boracarboxylation of various alkynes using carbon dioxide and bis(pinacolato)diboron (B_2pin_2), in the presence of a NHC-copper(I)-based catalyst.^[21] Popp and co-workers showed that similar reaction conditions could also be used for the regioselective boracarboxylation of substituted styrenes (**Scheme 1b**),^[22] as well as α -substituted vinyl arenes.^[23] However, to our knowledge, no enantioselective boracarboxylation of unsaturated C-C bonds has been reported so far.

Computational analyses of the regioselective boracarboxylation of unsaturated substrates^[24] have indicated a plausible reaction pathway, with elementary steps involving i) formation of the reactive copper(I) boronate species, ii) insertion of the unsaturated substrate into the copper-boron bond, and iii) carboxylation at the carbon bound to copper (**Scheme 2**).

Here, we present our work towards an asymmetric boracarboxylation method allowing for the enantioselective addition of CO_2 to styrenes, with good yields and excellent enantiomeric excesses (**Scheme 1c**). Detailed computational studies of the reaction mechanism reveal multiple competing carboxylation pathways, which impact the enantioselective outcome.



Scheme 1. Previously reported boracarboxylations of a) acetylenes,^[21] and b) styrenes,^[22a] and c) the present work on stereoselective boracarboxylation.



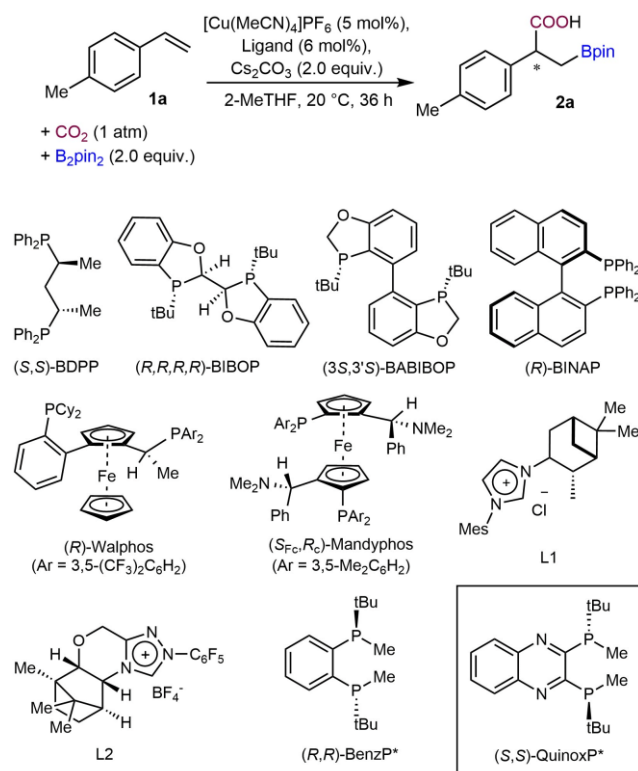
Scheme 2. Proposed mechanism for copper-catalyzed boracarboxylation of styrenes.^[21, 23-25]

Results and Discussion

Our investigation commenced with the development of a regioselective boracarboxylation protocol based on phosphine ligands. Our preliminary studies showed that phosphine-based copper catalysts can be very effective for boracarboxylation of styrenes (ESI, **Table S1-S3**). In particular the combination of $[Cu(MeCN)_4]PF_6$ and (*S,S*)-BDPP in the presence of Cs_2CO_3 as a base in 2-MeTHF leads to formation of the boracarboxylation product of 4-methylstyrene in 84% isolated yield, albeit with a close to racemic result (*e.r.* 48:52, **Table 1**, entry 1).

Based on the initial reaction conditions, we investigated a range of commercially available chiral phosphine ligands (**Table 1** and complete overview in ESI, **Table S4**). In addition, some chiral NHC-ligands were included in the screening (**Table 1**, entry 7 and 8).^[22a, 23] Relative to the results obtained for (*S,S*)-BDPP (84% yield), the yields of the reaction dropped for other chiral phosphines. The next best phosphine ligands in terms of yield (44-46%) were (*R,R,R*)-BIBOP, (*R*)-Walphos and (*3S,3'S*)-BABIBOP (entry 2-4). At this stage, (*3S,3'S*)-BABIBOP (entry 4) showed the best enantioselectivity (*e.r.* 23:77), with similar enantiomeric ratios obtained for the well-known ligands (*R*)-BINAP (*e.r.* 30:70; entry 5) and (*S_{Fc},R_c*)-Mandyphos (*e.r.* 23:77; entry 6). The chiral NHC-ligands L1 and L2 (entry 7-8) showed good yields (71% and 72%), but low selectivities (L1 *e.r.* 35:65 and L2 *e.r.* 48:52). The promising results obtained for (*3S,3'S*)-BABIBOP prompted us to extend our study towards other *P*-chiral phosphines, such as (*R,R*)-BenzP* (entry 9) and (*S,S*)-QuinoxP* (entry 10).^[26] While both resulted in poor yields (23-26%), (*S,S*)-QuinoxP* (entry 10) exhibited an excellent enantioselectivity, providing the boracarboxylation product with an *e.r.* of 92:8. With these results in hand, we proceeded to optimize reaction conditions using (*S,S*)-QuinoxP* as chiral ligand.

Table 1. The performance of selected chiral phosphines for the boracarboxylation of 4-methylstyrene (**1a**).



Entry	Ligand	<i>e.r.</i> ^{a)}	Yield ^{b)}
1	(<i>S,S</i>)-BDPP	48:52	84%
2	(<i>R,R,R,R</i>)-BIBOP	43:57	46%
3	(<i>R</i>)-Walphos	39:61	44%
4	(<i>3S,3'S</i>)-BABIBOP	23:77	45%
5	(<i>R</i>)-BINAP	30:70	22%
6	(<i>S</i> _{F_C} , <i>R</i> _C)-Mandyphos	39:61	44%
7	L1	35:65	71%
8	L2	48:52	72%
9	(<i>R,R</i>)-BenzP*	23:77	23%
10	(<i>S,S</i>)-QuinoxP*	92:8	26%

^{a)} The enantiomeric ratio of the product was determined by super critical fluid chromatography with a chiral column. ^{b)} Isolated yields.

Initially, we focused on altering the solvent. Although ethers did not provide better results, somewhat improved yields of 40% were obtained with anisole (**Table 2**, entry 2), which could be increased to 76% yield by doubling the catalyst loading to 10 mol% (**Table 2**, entry 8). This reaction showed a good enantiomeric ratio of 84:16. A change of the base to alkoxides such as NaOtBu, which worked well for carbene ligands,^[22a] did not improve yields (**Table 2**, entry 4). The copper source had critical impact on the yield, with a change in counterion resulting in a drop

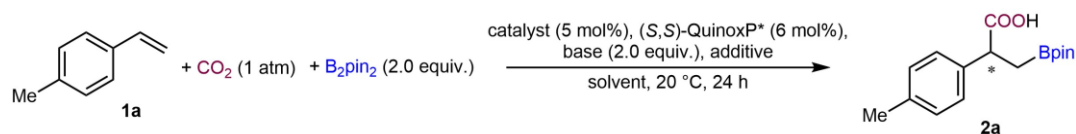
to 18-26% (**Table 2**, entry 5-7). Inclusion of different additives such as phase transfer catalysts and weakly coordinating anions did not provide any improvement (**Table 2**, entry 11-14), with the exception of 18-crown-6 ether (**Table 2**, entry 9), which demonstrated a significant enhancement from 40% to 58% yield at 5 mol% catalyst loading. The addition of 18-crown-6 did not only increase the yield, but also slightly improved the enantioselectivity from *e.r.* 92:8 to 96:4. Increased catalyst loading with 18-crown-6 as an additive did not result in further improvement (**Table 2**, entry 10).

We moved on to study the reaction for a range of electron-rich, electron-deficient, and electron-neutral styrenes (**Scheme 3**) using $[\text{Cu}(\text{MeCN})_4]\text{PF}_6$ /*(S,S)*-QuinoxP* as precatalyst, Cs_2CO_3 as base combined with 18-crown-6 as additive in anisole as solvent. Styrenes with a methyl substituent in para, meta or ortho position (**1a**, **1d** and **1g**) could be selectively functionalized in 37-58% yields with enantiomeric ratios ranging from good to excellent (up to 96:4). When changing to more electron donating substituents such as methoxy (**1b** and **1e**), alkyne (**1c**) and phenoxy (**1i**), the yields were fair (33-42%), but corresponding products were obtained with high enantioselectivity (up to 98:2 *e.r.*). Unsubstituted styrene (**1j**) and naphthalene derivatives (**1k** and **1l**) also resulted in fair yields (36-41%), but the enantioselectivity for these substrates went down. Electron-withdrawing substituents such as fluorine (**1m** and **1p**), trifluoromethyl (**1n** and **1q**), cyano (**1o**), nitro (**1s**) and ester (**1t**) resulted in comparable yields to those seen for electron-neutral and -rich systems (13-67%). However, the lower enantiomeric ratios suggest that electronic effects from the substrate impact the enantioselectivity of boracarboxylations. This hypothesis was investigated by adding a fluorine to the electron-rich substrates **1e** and **1h**, which resulted in a noticeable drop in *e.r.* for the products **2f** and **2r**.

We also explored the potential impact of the CO_2 pressure on the enantioselectivity of the reaction. In a recent study, the Popp group showed that higher pressures of CO_2 can benefit the yield of the reactions involving electron-deficient systems.^[23] Accordingly, we investigated the influence of the CO_2 pressure on the yield and enantioselectivity for electron-deficient substrates (**2m**, **2n**, **2p** and **2q**). While the yields for the reactions involving these substrates increased for **2m** (from <5% to 19%), **2n** (from 38% to 48%) and **2q** (from 33% to 48%), the enantiomeric ratio was practically unaffected.

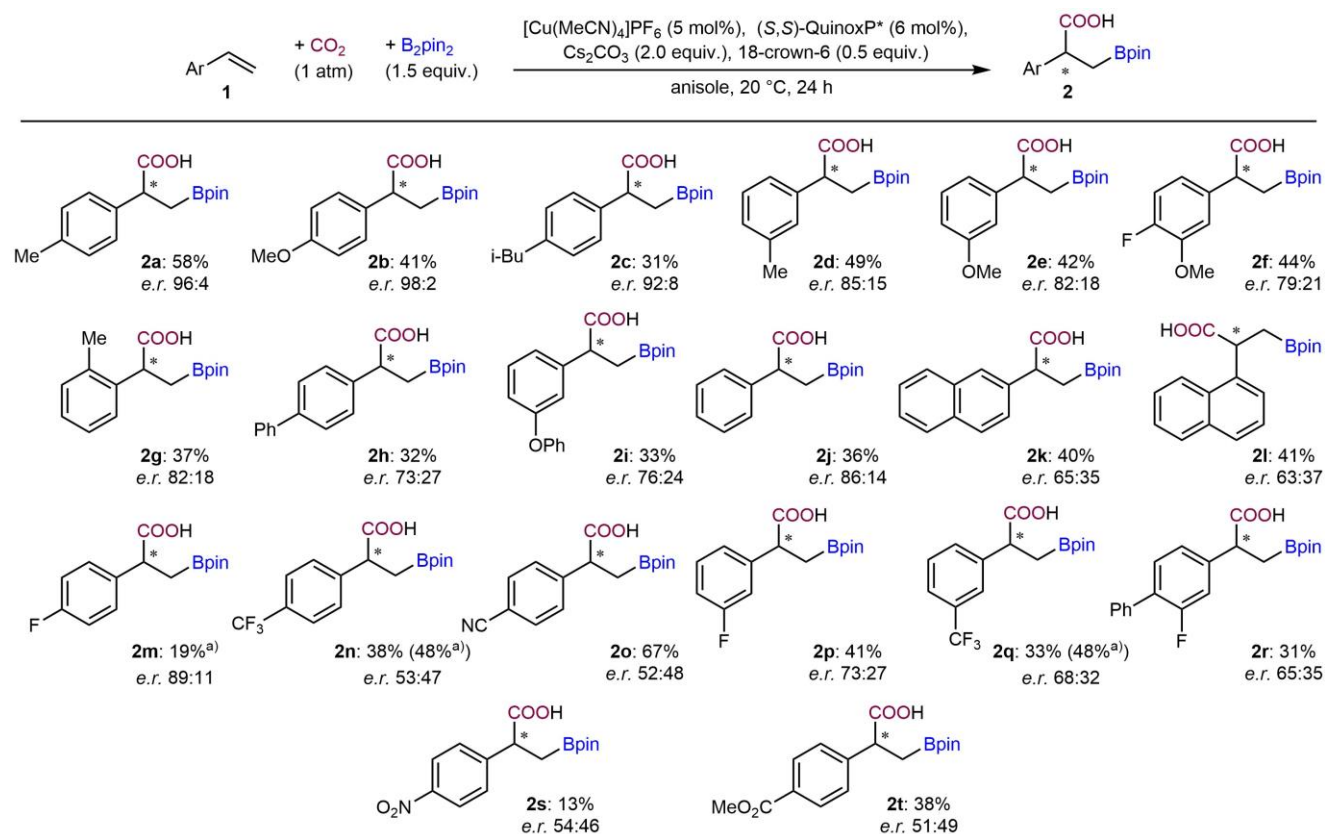
To establish the absolute configuration of the major boracarboxylation product, we employed sodium perborate tetrahydrate to convert **2j** to tropic acid **3j** (**Scheme 4**). The later was obtained in a quantitative yield, with the enantiomeric ratio of the product retained (ESI, **Chromatogram S21**). Comparing the chromatogram of **3j** to commercially available (*R*)-tropic acid, we concluded that the (*R*)-enantiomer of **2j** was formed upon boracarboxylation of **1j** with (*S,S*)-QuinoxP*

Table 2. Summary of the optimization of the reaction for (*S,S*)-QuinoxP*.

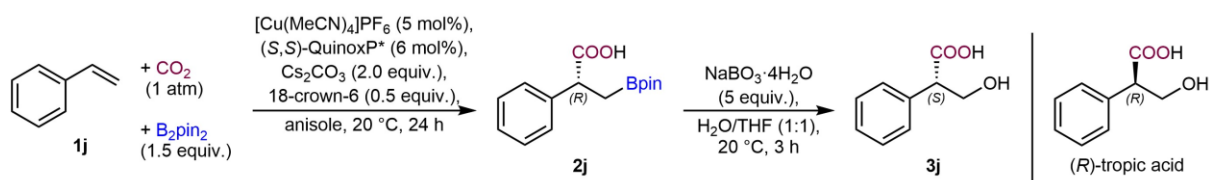


Entry	Cu source	Base	Additive (mol%)	Solvent	<i>e.r.</i>	Yield ^{a)}
1	[Cu(MeCN) ₄]PF ₆	Cs ₂ CO ₃	-	Dioxane	n.d.	25%
2	[Cu(MeCN) ₄]PF ₆	Cs ₂ CO ₃	-	Anisole	92:8	40%
3	[Cu(MeCN) ₄]PF ₆	Cs ₂ CO ₃	-	Triglyme	n.d.	19%
4	[Cu(MeCN) ₄]PF ₆	NaOtBu	-	Anisole	n.d.	26%
5	[Cu(MeCN) ₄]BF ₄	Cs ₂ CO ₃	-	Anisole	n.d.	18%
6	[Cu(MeCN) ₄]SbF ₆	Cs ₂ CO ₃	-	Anisole	n.d.	20%
7	[Cu(MeCN) ₄]BarF	Cs ₂ CO ₃	-	Anisole	n.d.	26%
8	[Cu(MeCN) ₄]PF ₆	Cs ₂ CO ₃	-	Anisole	84:16	76% ^{b)}
9	[Cu(MeCN) ₄]PF ₆	Cs ₂ CO ₃	18-crown-6 (50)	Anisole	96:4	58% ^{c)}
10	[Cu(MeCN) ₄]PF ₆	Cs ₂ CO ₃	18-crown-6 (50)	Anisole	93:7	60% ^{b)}
11	[Cu(MeCN) ₄]PF ₆	Cs ₂ CO ₃	TBAB (50)	Anisole	95:5	42%
12	[Cu(MeCN) ₄]PF ₆	Cs ₂ CO ₃	PPh ₃ (20)	Anisole	91:9	32%
13	[Cu(MeCN) ₄]PF ₆	Cs ₂ CO ₃	monolaurin (20)	Anisole	87:13	37%
14	[Cu(MeCN) ₄]PF ₆	Cs ₂ CO ₃	palmitic acid (20)	Anisole	94:6	33%

^{a)} Isolated yields. ^{b)} 10 mol% of Cu-source and 12 mol% of the ligand was used. ^{c)} Average yield of two experiments.



Scheme 3. The substrate scope of the asymmetric borocarboxylation. ^{a)} Yield obtained at 5 atm of CO₂.



Scheme 4. Boracarboxylation of **1j** into (*R*)-**2j** and oxidation of the boracarboxylation product (*R*)-**2j** to (*S*)-tropic acid **3j**.

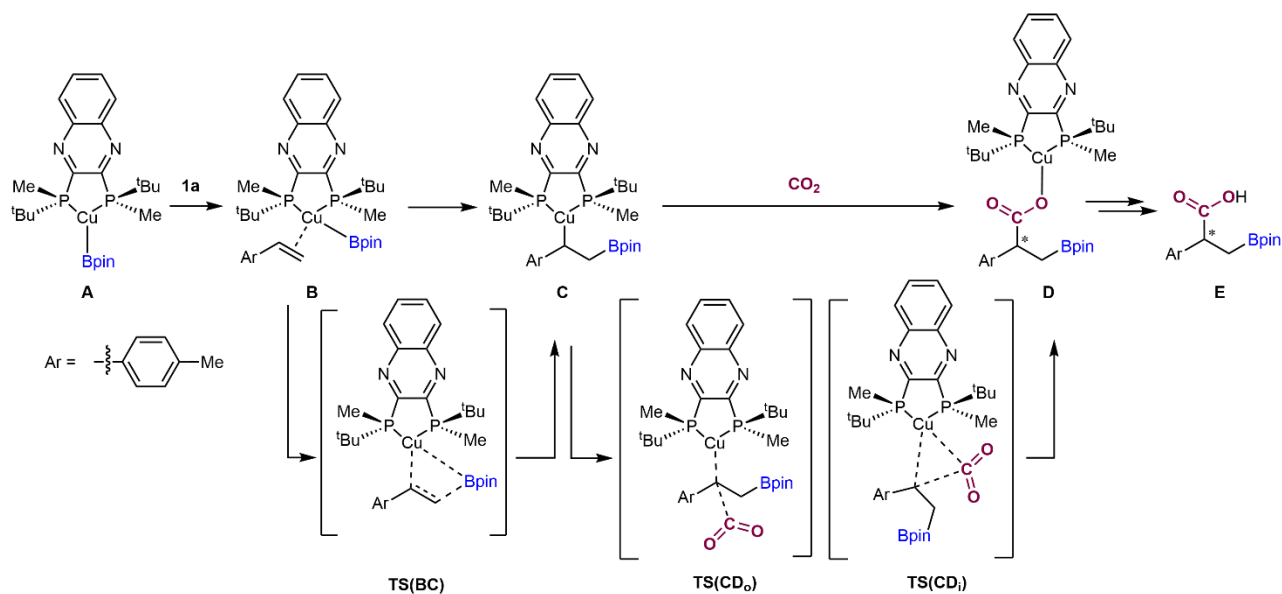
A computational analysis of the mechanistic details was performed, initially focusing on substrate **1a** and the (*S,S*)-BDPP ligand (see ESI **Figures S10, S11** and **Table S10**). The most relevant reaction pathways (see **Scheme 5**) were then studied with (*S,S*)-QuinoxP*. We hypothesized that the first step of the reaction would be the formation of the reactive copper borate **A** through the activation of B₂pin₂ with the base Cs₂CO₃,^[27] and the subsequent transmetalation between the activated diboron species and the copper complex (see ESI **Scheme S1** for details). Coordination of styrene **1a** to **A** leads to formation of intermediate **B**, followed by a 2,1-borocupration to form **C** (**Scheme 5** and **Figure 1**). The latter step involves transfer of the borate to the terminal position of the substrate, which in our calculations has a low barrier (2.3 to 3.1 kcal/mol relative to **B**, depending on the resulting stereoisomer). The alternative 1,2-borocupration displays a higher insertion barrier (9.8 kcal/mol relative to **B**), explaining the absence of the corresponding product in experiments.

Intermediate **C** exists as two diastereomeric forms (**C_R** and **C_S**) with either (*R*) or (*S*) configuration at the benzylic carbon. The formation of **C_R** and **C_S** is exergonic by 15.2 and 16.5 kcal/mol respectively, relative to **A** (**Figure 1**). Considering that the reverse barriers from **C_R** and **C_S** to **B** are less than 20 kcal/mol

at room temperature (**Figure 1**),^[28] we assume that the diastereomeric species can interconvert rapidly, implying Curtin Hammett conditions.^[29]

The subsequent CO₂ insertion into the diastereomeric intermediates **C_R** and **C_S** is rate-determining (**Figure 2**) and controls the enantioselectivity. We have previously shown that carboxylation at benzylic positions may occur through either inner or outer sphere CO₂ insertion, with the preferred pathway determined by the transition metal and, in particular, by the size of the ligand.^[30] Consequently, both **C_R** and **C_S** can independently form the carboxylated species **D_R** and **D_S**. If CO₂ insertion occurs in an inner sphere fashion (where CO₂ interacts with the copper centre), the stereochemistry at the benzylic carbon in **C** is retained, whereas outer sphere insertion (where CO₂ does not interact with copper) results in an inversion. Under Curtin-Hammett conditions, the *e.r.* of the final product will depend on the barriers of all energetically available CO₂ insertion pathways.^[29a]

Starting from **C_S**, the outer sphere carboxylation TS leading to the (*R*)-product is significantly lower in energy (13.7 kcal/mol) than the inner sphere TS (17.4 kcal/mol respectively, **Figure 2**). From **C_R**, both outer and inner sphere pathways have near-identical barriers (14.0 and 14.1 kcal/mol respectively).



Scheme 5. Proposed mechanism for the boracarboxylation of styrene **1a**.

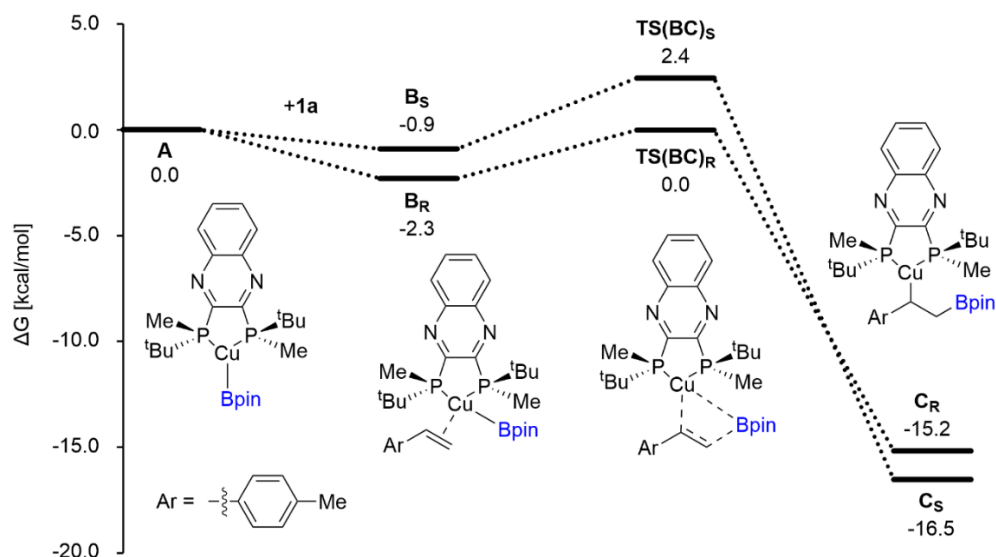


Figure 1. Gibbs free energy profile (kcal/mol, PBE-D3BJ/PC-2//PBE-D3BJ/6-31+G*(SDD for Cu), IEFPCM:THF, 298.15K) for the formation of intermediate C.

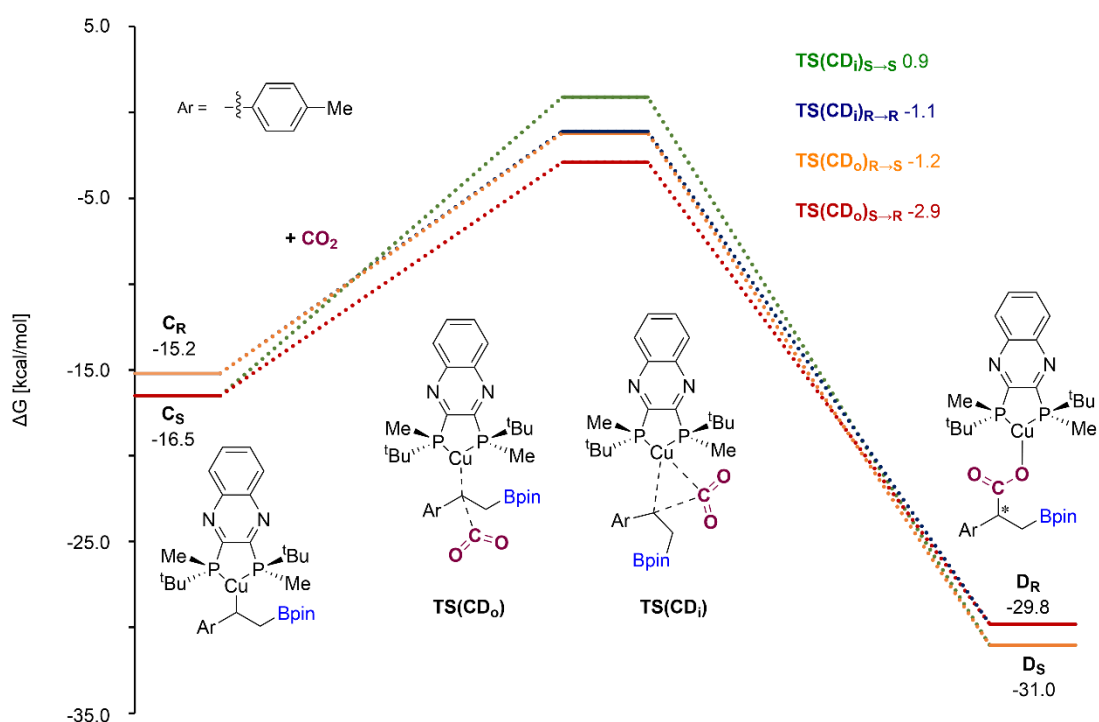


Figure 2. Gibbs free energy profile for the insertion of CO₂ into the diastereomeric C intermediates (kcal/mol, PBE-D3BJ/PC-2//PBE-D3BJ/6-31+G*(SDD for Cu), IEFPCM:THF, 298.15K, energies are given relative to A). TS(CD)_i refers to inner sphere TSs, and TS(CD)_o refers to outer sphere TSs.

The optimized geometries (**Figure 3**) show that in all four TSs, the CO₂ molecule is stabilized by CH/O interactions with the substrate. In the inner sphere TSs, a significant bending of the substrate occurs to accommodate the CO₂ molecule, which interacts with both the benzylic carbon and the copper atom. The distortion of the substrate requires a significant amount

of energy making the inner sphere TSs less favourable than the outer sphere TSs. In the latter, the CO₂ molecule approaches the substrate from the backside of the C_(benzylic)—Cu bond. Even though more unfavourable steric clashes are seen in the outer sphere TSs than in the inner sphere TSs, the outer sphere TSs remain preferred. Looking at TS(CD)_oS→R, we can see

a CH/O interaction (2.50Å) between one of the hydrogens of the copper complex and one of the oxygens in Bpin, which stabilizes the structure and makes this TS more favoured than $\text{TS}(\text{CD}_0)_{R \rightarrow S}$.

On the basis of all four transition states leading to **D** (Figure 2), we obtain a theoretical *e.r.* of 71:29 (in THF) in favour of the (*R*)-product, which is in line with the experimentally observed *e.r.* of 96:4 (in anisole). Changing the implicit solvent model from THF to anisole (ESI, Table S12) provides similar results, with a computed *e.r.* of 87:13. The reverse barriers from **D** to **C** are higher than 40 kcal/mol, which indicates that the CO₂ insertion is irreversible at room temperature. The overall thermodynamic driving force for the

formation of the free products **E_R** and **E_S** is -67.3 kcal/mol (see ESI for details).

When examining the crude reaction mixture of the boracarboxylation of **1j** by NMR, we see 23% of borated styrene (ESI, Spectrum S55), possibly formed through a competing β-hydride-elimination from **C**, in line with previous results.^[22a] We calculated the β-hydride elimination pathway using (*S,S*)-QuinoxP* as ligand, which shows a barrier of 17.1 kcal/mol (ESI, Scheme S2), thus being 3.4 kcal/mol higher than the CO₂ insertion step (13.7 kcal/mol). This energy difference rationalizes the formation of small amounts of borated styrene in experiments.

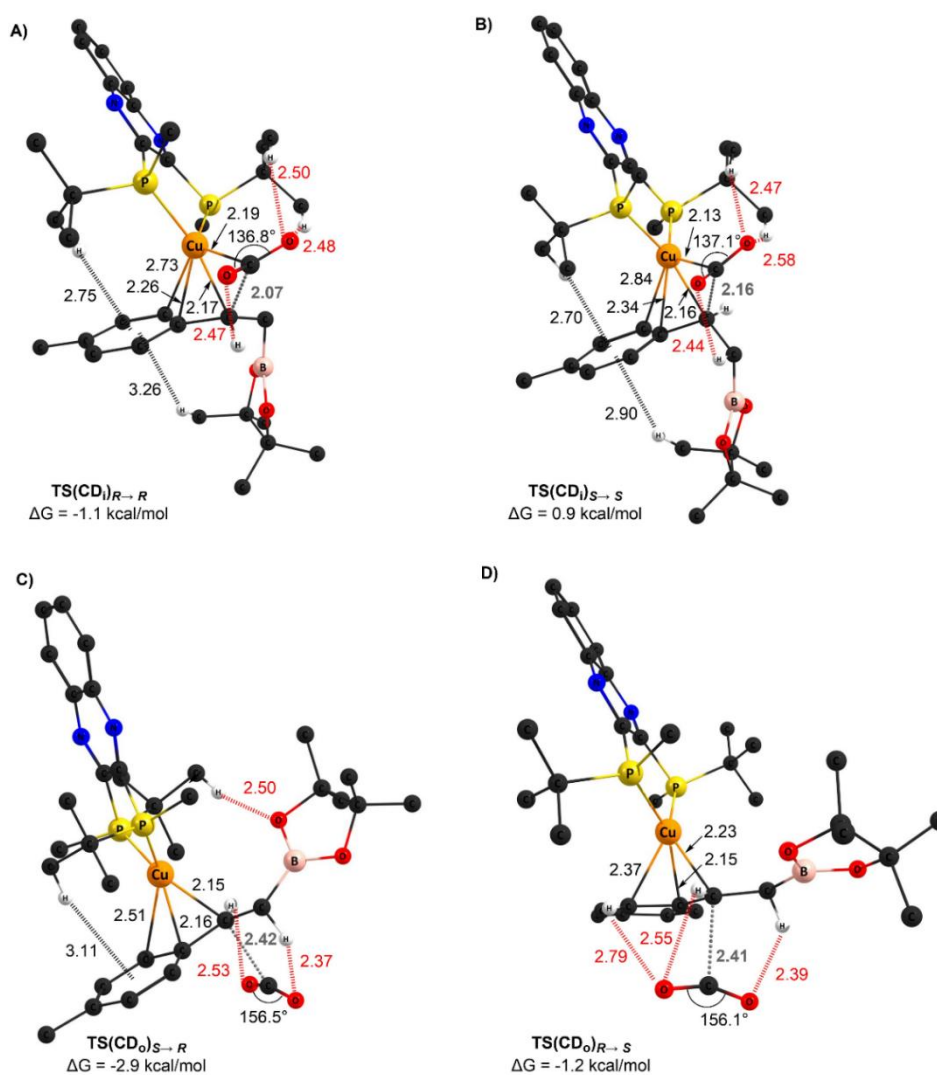


Figure 3. Optimized geometries of all four CO₂ insertion TSs, grey = C-C(CO₂) distances, red = attractive CH/O interactions, black = attractive CH/π interactions, distances in Å, energies relative to **A**, PBE-D3BJ/PC-2//PBE-D3BJ/6-31+G*(SDD for Cu), IEFPCM:THF, 298.15K. For clarity, only hydrogen atoms of interest are shown.

Conclusion

We have developed a boracarboxylation method for the enantioselective addition of CO₂ to styrenes, using a chiral copper catalyst derived from the *P*-chiral ligand (*S,S*)-QuinoxP* and [Cu(MeCN)₄]PF₆. Our

approach provides the boracarboxylation product with high regioselectivity and yields up to 76%. The enantioselectivity of the reaction clearly depends on the electronic structure of the styrene, with electron-rich styrenes providing the best enantiomeric ratios. Detailed computational studies of the mechanism show

that the reaction occurs through multiple competing pathways, which impacts the enantioselective outcome. For the studied copper precatalysts based on phosphine ligands, we find that inner and outer sphere carboxylations show similar barriers, indicating that both pathways will compete. This phenomenon significantly impacts the enantioselectivity and complicates the development of a robust enantioselective method. Nonetheless, our synthetic protocol provides enantiomeric ratios of up to 98:2, which are comparable to the best enantioselectivities reported so far for CO₂-based carboxylations. The chiral β -boronated carboxylic acids accessible in this way provide valuable building blocks for the synthesis of pharmaceuticals.

Experimental Section

Commercially available starting materials, reagents, catalysts, ligands, solvents, and anhydrous solvents were used without further purification. The chiral ligands were purchased from Sigma Aldrich and Stream chemicals. Racemates were prepared according to the literature procedure.^[22a] Non-anhydrous solvents were dried using activated 4Å molecular sieves. ¹H, ¹³C and ¹⁹F NMR spectra were recorded on a Bruker Avance 400 MHz at 20 °C. All ¹H NMR spectra were reported in parts per million (ppm) downfield of TMS and were measured relative to the signals for residual CHCl₃ (7.26 ppm). All ¹³C NMR spectra were reported in ppm relative to residual CDCl₃ (77.20 ppm) and were obtained with ¹H decoupling. Coupling constants, J, were reported in Hertz (Hz). High-resolution mass spectra (HRMS) were recorded from methanol solutions on an LTQ Orbitrap XL (Thermo Scientific) either in negative or in positive electrospray ionization (ESI) mode. Infrared spectra were recorded on an Agilent Cary 630 FT-IR spectrometer and absorptions are reported in wavenumber (cm⁻¹); br = broad, s = strong, m = medium, w = weak. Melting points were recorded using Stuart SMP50 automatic melting point detector. Optical rotation measurements were performed using a Polarimeter AA-10R from Optical Activity LTD. Determination of *e.r.* values were carried out on a Waters ACQUITY UPC2 system equipped with a Trefoil™ AMY1, 2.5µm 3.0 x 150mm column. Compounds were detected on a Waters ACQUITY PDA detector spanning wavelengths from 190 to 400 nm. The resolution of the products was performed with a mobile phase consisting of supercritical CO₂ and *i*-PrOH containing 0.5 % of TFA and a linear gradient of 2 – 20 % *i*-PrOH over 8 min followed by isocratic 1.5 min of 20 % *i*-PrOH with a flow rate of 1.0 mL/min (SFC method A) or a linear gradient of 2 – 30 % *i*-PrOH over 8 min followed by isocratic 1.5 min of 30 % *i*-PrOH with a flow rate of 1.5 mL/min (SFC method B).

Representative procedure for the asymmetric boracarboxylation: An oven dried 100 mL round bottom flask (see **Figure S1**) and a stir bar were introduced to the argon filled glove box. To the round bottom flask, a magnetic stir bar, B₂pin₂ (1.5 equiv.), base (2.0 equiv.), ligand (6 mol%) and Cu-salt (5 mol%) were added, closed with a septum, and sealed tight using electric tape. To the flask, 20 mL of solvent were added and left stirring for 30 minutes. Then the corresponding styrene (1 equiv.) was added, and a balloon filled with dry CO₂ was attached to the flask. The round bottom flask was then left stirring for 24 hours at 20° C (see **Figure S5**). Afterwards, the flask was opened to air and the content was diluted with 20 mL of Et₂O. The reaction mixture was transferred into a 250 mL separating funnel where the organic layer was extracted using a solution of saturated NaHCO₃ (3x30 mL). Then the separated aqueous solution was first washed with Et₂O (3x30 mL), acidified by slow addition of 60 mL 6M HCl and then extracted using Et₂O (3x30 mL). The organic solution was washed using 30 mL of distilled water. Afterwards the

organic solution was evaporated to dryness to give the product.

Computational details: All molecules were calculated with no truncations or symmetry constraints, using the Gaussian 16 program, revision B.01.^[31] Geometries were optimized at the PBE^[32] level of theory with the 6-31+G* basis set^[33] (using the SDD ECP for Cu), including the D3BJ dispersion correction by Grimme.^[34] The solvation effects were included implicitly using the polarizable continuum model (PCM) with the parameters for THF.^[35] Transition states and minima were confirmed through frequency calculations (no imaginary frequencies for minima, one imaginary frequency for transition states). Single point energies were computed with the PC-2^[36] basis set. All Gibbs free energies are given at 298.15K and 1atm. The theoretically predicted *e.r.* was determined using a modified version of the Eyring equation (see equation in ESI).^[37]

Acknowledgements

This work was supported by the Research Council of Norway (No. 300769 and 313462), Sigma2 (No. nn9330k and nn4654k), the Nordforsk NordCO₂ consortium (No. 85378) and UiT The Arctic University of Norway through funding of the iCCU-project.

References

- [1] a) J. Davies, J. R. Lyonnet, D. P. Zimin, R. Martin, *Chem* 2021, 7, 2927-2942; b) A. Otto, T. Grube, S. Schiebahn, D. Stolten, *Energy Environ. Sci.* 2015, 8, 3283-3297.
- [2] L. J. Gooßen, N. Rodríguez, K. Gooßen, *Angew. Chem. Int. Ed.* 2008, 47, 3100-3120.
- [3] P. Ertl, E. Altmann, J. M. McKenna, *J. Med. Chem.* 2020, 63, 8408-8418.
- [4] F. Calvo-Castañera, J. Álvarez-Rodríguez, N. Candela, Á. Maroto-Valiente, *Nanomaterials* 2021, 11, 190.
- [5] a) A. Tortajada, F. Juliá-Hernández, M. Börjesson, T. Moragas, R. Martin, *Angew. Chem. Int. Ed.* 2018, 57, 15948-15982; b) R. Cauwenbergh, V. Goyal, R. Maiti, K. Natte, S. Das, *Chem. Soc. Rev.* 2022, 51, 9371-9423; c) X.-F. Liu, K. Zhang, L. Tao, X.-B. Lu, W.-Z. Zhang, *Green Chem. Eng.* 2022, 3, 125-137.
- [6] a) F. Yan, J.-F. Bai, Y. Li, in *The Chemical Transformations of C1 Compounds*, John Wiley & Sons, Ltd, 2022, pp. 1265-1303; b) Y. Shi, B.-W. Pan, Y. Zhou, J. Zhou, Y.-L. Liu, F. Zhou, *Org. Biomol. Chem.* 2020, 18, 8597-8619; c) J. Vaitla, Y. Guttormsen, J. K. Mannisto, A. Nova, T. Repo, A. Bayer, K. H. Hopmann, *ACS Catalysis* 2017, 7, 7231-7244.
- [7] M. Takimoto, Y. Nakamura, K. Kimura, M. Mori, *J. Am. Chem. Soc.* 2004, 126, 5956-5957.
- [8] S. Kawashima, K. Aikawa, K. Mikami, *Eur. J. Org. Chem.* 2016, 2016, 3166-3170.
- [9] Y.-Y. Gui, N. Hu, X.-W. Chen, L. L. Liao, T. Ju, J.-H. Ye, Z. Zhang, J. Li, D.-G. Yu, *J. Am. Chem. Soc.* 2017, 139, 17011-17014.

- [10] X.-W. Chen, L. Zhu, Y.-Y. Gui, K. Jing, Y.-X. Jiang, Z.-Y. Bo, Y. Lan, J. Li, D.-G. Yu, *J. Am. Chem. Soc.* 2019, 141, 18825-18835.
- [11] J. Qiu, S. Gao, C. Li, L. Zhang, Z. Wang, X. Wang, K. Ding, *Chem. Eur. J.* 2019, 25, 13874-13878.
- [12] L. Dian, D. S. Müller, I. Marek, *Angew. Chem. Int. Ed.* 2017, 56, 6783-6787.
- [13] A. Cerveri, R. Giovanelli, D. Sella, R. Pedrazzani, M. Monari, O. Nieto Faza, C. S. López, M. Bandini, *Chem. Eur. J.* 2021, 27, 7657-7662.
- [14] X.-W. Chen, J.-P. Yue, K. Wang, Y.-Y. Gui, Y.-N. Niu, J. Liu, C.-K. Ran, W. Kong, W.-J. Zhou, D.-G. Yu, *Angew. Chem. Int. Ed.* 2021, 60, 14068-14075.
- [15] K. Zhang, H. Wang, S.-F. Zhao, D.-F. Niu, J.-X. Lu, *J. Electroanal. Chem.* 2009, 630, 35-41.
- [16] Y.-J. Zhao, L.-R. Yang, L.-T. Wang, Y. Wang, J.-X. Lu, H. Wang, *Catal. Sci. Technol.* 2022, 12, 2887-2893.
- [17] B.-L. Chen, H.-W. Zhu, Y. Xiao, Q.-L. Sun, H. Wang, J.-X. Lu, *Electrochem. Commun.* 2014, 42, 55-59.
- [18] H.-P. Yang, Y.-N. Yue, Q.-L. Sun, Q. Feng, H. Wang, J.-X. Lu, *Chem. Commun.* 2015, 51, 12216-12219.
- [19] K.-J. Jiao, Z.-M. Li, X.-T. Xu, L.-P. Zhang, Y.-Q. Li, K. Zhang, T.-S. Mei, *Org. Chem. Front.* 2018, 5, 2244-2248.
- [20] R. T. Abeyasinghe, A. C. Ravenscroft, S. W. Knowlden, N. G. Akhmedov, B. S. Dolinar, B. V. Popp, *Inorganics* 2023, 11.
- [21] L. Zhang, J. Cheng, B. Carry, Z. Hou, *J. Am. Chem. Soc.* 2012, 134, 14314-14317.
- [22] a) T. W. Butcher, E. J. McClain, T. G. Hamilton, T. M. Perrone, K. M. Kroner, G. C. Donohoe, N. G. Akhmedov, J. L. Petersen, B. V. Popp, *Org. Lett.* 2016, 18, 6428-6431; b) T. M. Perrone, A. S. Gregory, S. W. Knowlden, N. R. Ziemer, R. N. Alsulami, J. L. Petersen, B. V. Popp, *ChemCatChem* 2019, 11, 5814-5820; c) S. W. Knowlden, PhD thesis thesis, West Virginia University 2022.
- [23] S. W. Knowlden, B. V. Popp, *Organometallics* 2022, 41, 1883-1891.
- [24] a) S. Lin, Z. Lin, *Organometallics* 2019, 38, 240-247; b) X. Lv, Y.-B. Wu, G. Lu, *Catal. Sci. Technol.* 2017, 7, 5049-5054.
- [25] N. N. Baughman, N. G. Akhmedov, J. L. Petersen, B. V. Popp, *Organometallics* 2021, 40, 23-37.
- [26] T. Imamoto, K. Tamura, Z. Zhang, Y. Horiuchi, M. Sugiyama, K. Yoshida, A. Yanagisawa, I. D. Gridnev, *J. Am. Chem. Soc.* 2012, 134, 1754-1769.
- [27] a) C. Pubill-Ulldemolins, A. Bonet, C. Bo, H. Gulyás, E. Fernández, *Chem. Eur. J.* 2012, 18, 1121-1126; b) K. Takahashi, T. Ishiyama, N. Miyaoura, *J. Organomet. Chem.* 2001, 625, 47-53.
- [28] H. Ryu, J. Park, H. K. Kim, J. Y. Park, S.-T. Kim, M.-H. Baik, *Organometallics* 2018, 37, 3228-3239.
- [29] a) J. I. Seeman, *Chem. Rev.* 1983, 83, 83-134; b) J. I. Seeman, *J. Chem. Educ.* 1986, 63, 42-48.
- [30] a) M. F. Obst, A. Gevorgyan, A. Bayer, K. H. Hopmann, *Organometallics* 2020, 39, 1545-1552; b) M. Obst, L. Pavlovic, K. H. Hopmann, *J. Organomet. Chem.* 2018, 864, 115-127; c) L. Pavlovic, J. Vaitla, A. Bayer, K. H. Hopmann, *Organometallics* 2018, 37, 941-948; d) D. García-López, L. Pavlovic, K. H. Hopmann, *Organometallics* 2020, 39, 1339-1347; e) A. P. Deziel, M. R. Espinosa, L. Pavlovic, D. J. Charboneau, N. Hazari, K. H. Hopmann, B. Q. Mercado, *Chem Sci* 2022, 13, 2391-2404; f) L. Pavlovic, M. Pettersen, A. Gevorgyan, J. Vaitla, A. Bayer, K. H. Hopmann, *Eur. J. Org. Chem.* 2021, 2021, 663-670.
- [31] M. J. Frisch, G. W. Trucks, H. B. Schlegel, G. E. Scuseria, M. A. Robb, J. R. Cheeseman, G. Scalmani, V. Barone, G. A. Petersson, H. Nakatsuji, X. Li, M. Caricato, A. V. Marenich, J. Bloino, B. G. Janesko, R. Gomperts, B. Mennucci, H. P. Hratchian, J. V. Ortiz, A. F. Izmaylov, J. L. Sonnenberg, Williams, F. Ding, F. Lipparini, F. Egidi, J. Goings, B. Peng, A. Petrone, T. Henderson, D. Ranasinghe, V. G. Zakrzewski, J. Gao, N. Rega, G. Zheng, W. Liang, M. Hada, M. Ehara, K. Toyota, R. Fukuda, J. Hasegawa, M. Ishida, T. Nakajima, Y. Honda, O. Kitao, H. Nakai, T. Vreven, K. Throssell, J. A. Montgomery Jr., J. E. Peralta, F. Ogliaro, M. J. Bearpark, J. J. Heyd, E. N. Brothers, K. N. Kudin, V. N. Staroverov, T. A. Keith, R. Kobayashi, J. Normand, K. Raghavachari, A. P. Rendell, J. C. Burant, S. S. Iyengar, J. Tomasi, M. Cossi, J. M. Millam, M. Klene, C. Adamo, R. Cammi, J. W. Ochterski, R. L. Martin, K. Morokuma, O. Farkas, J. B. Foresman, D. J. Fox, *Gaussian 16 Rev. B.01*, Wallingford, CT, 2016.
- [32] J. P. Perdew, K. Burke, M. Ernzerhof, *Phys. Rev. Lett.* 1996, 77, 3865-3868.
- [33] a) G. A. Petersson, M. A. Al - Laham, *J. Chem. Phys.* 1991, 94, 6081-6090; b) G. A. Petersson, A. Bennett, T. G. Tensfeldt, M. A. Al - Laham, W. A. Shirley, J. Mantzaris, *J. Chem. Phys.* 1988, 89, 2193-2218; c) T. Clark, J. Chandrasekhar, G. W. Spitznagel, P. V. R. Schleyer, *J. Comput. Chem.* 1983, 4, 294-301.
- [34] S. Grimme, S. Ehrlich, L. Goerigk, *J. Comput. Chem.* 2011, 32, 1456-1465.
- [35] J. Tomasi, B. Mennucci, R. Cammi, *Chem. Rev.* 2005, 105, 2999-3094.
- [36] a) F. Jensen, *J. Chem. Phys.* 2013, 138, 014107; b) F. Jensen, *J. Chem. Phys.* 2001, 115, 9113-9125; c) F. Jensen, *J. Chem. Phys.* 2002, 116, 7372-7379; d) F. Jensen, *J. Phys. Chem. A* 2007, 111, 11198-11204; e) F. Jensen, T. Helgaker, *J. Chem. Phys.* 2004, 121, 3463-3470.
- [37] Q. Peng, F. Duarte, R. S. Paton, *Chem. Soc. Rev.* 2016, 45, 6093-6107.

Electronic Supplementary Information

Asymmetric boracarboxylation of styrenes using carbon dioxide

Martin Pettersen,^{a,†} Cuong Dat Do,^{a,b,†} Marc F. Obst,^a Roman Damm,^a Anggi E. Putra,^a Ashot Gevorgyan,^a Ljiljana Pavlovic,^a Kathrin H. Hopmann*^{a,§} and Annette Bayer*^{a,§}

^a Department of Chemistry, UiT The Arctic University of Norway, N-9307 Tromsø, Norway.

^b Hylleraas Center for Quantum Molecular Sciences, Department of Chemistry, UiT The Arctic University of Norway, N-9307 Tromsø, Norway.

E-mail: annette.bayer@uit.no, kathrin.hopmann@uit.no.

^{†,§} Have contributed equally.

Contents

1	Experimental procedures	2
1.1	General considerations	2
1.2	General procedures.....	2
1.2.1	Method A: General procedure for boracarboxylation of styrenes. Reactions performed at atmospheric pressure of CO ₂	2
1.2.2	Method B: General procedure for boracarboxylation of styrenes. Reactions performed at high pressure of CO ₂	3
1.2.3	Description of the used glassware and setup of the reactions	4
1.3	Overview of optimization tables	8
1.4	Characterization of products.....	15
2	Computational data.....	21
2.1	General considerations	21
2.2	Mechanistic studies of the boracarboxylation with (S,S)-BDPP as ligand	21
2.3	Mechanistic studies of the formation of the boracupration reagent	23
2.4	Evaluation of solvent effects on the boracarboxylation	24
2.5	Mechanistic study of the β-hydride side reaction.....	24
3	Documentation of analytical data	26
4	References.....	102

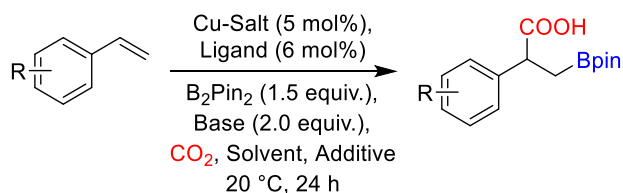
1 Experimental procedures

1.1 General considerations

Commercially available starting materials, reagents, catalysts, ligands, solvents, and anhydrous solvents were used without further purification. The chiral ligands were purchased from Sigma Aldrich and Stream chemicals. Racemates were prepared according to the literature procedure.^[1] Non-anhydrous solvents were dried using activated 4Å molecular sieves. ¹H, ¹³C and ¹⁹F NMR spectra were recorded on a Bruker Avance 400 MHz at 20 °C. All ¹H NMR spectra were reported in parts per million (ppm) downfield of TMS and were measured relative to the signals for residual CHCl₃ (7.26 ppm). All ¹³C NMR spectra were reported in ppm relative to residual CDCl₃ (77.20 ppm) and were obtained with ¹H decoupling. Coupling constants, J, were reported in Hertz (Hz). High-resolution mass spectra (HRMS) were recorded from methanol solutions on an LTQ Orbitrap XL (Thermo Scientific) either in negative or in positive electrospray ionization (ESI) mode. Infrared spectra were recorded on an Agilent Cary 630 FT-IR spectrometer and absorptions are reported in wavenumber (cm⁻¹); br = broad, s = strong, m = medium, w = weak. Melting points were recorded using Stuart SMP50 automatic melting point detector. Optical rotation measurements were performed using a Polarimeter AA-10R from Optical Activity LTD. Determination of the enantiomeric ratio (*e.r.*) were carried out on a Waters ACQUITY UPC2 system equipped with a Trefoil™ AMY1, 2.5µm 3.0 x 150mm column. Compounds were detected on a Waters ACQUITY PDA detector spanning wavelengths from 190 to 400 nm. The resolution of the products was performed with a mobile phase consisting of supercritical CO₂ and i-PrOH containing 0.5 % of TFA. Resolution was achieved using one of the two gradients: SFC method A - a linear gradient of 2 – 20 % i-PrOH over 8 min followed by isocratic 1.5 min of 20 % i-PrOH with a flow rate of 1.0 mL/min; SFC method B - a linear gradient of 2 – 30 % i-PrOH over 8 min followed by isocratic 1.5 min of 30 % i-PrOH with a flow rate of 1.5 mL/min.

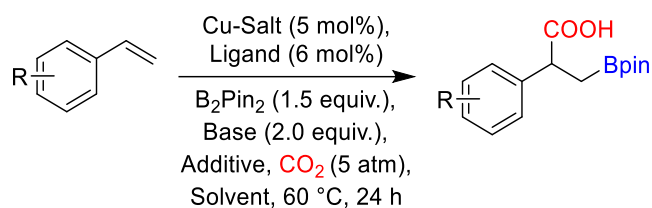
1.2 General procedures

1.2.1 Method A: General procedure for boracarboxylation of styrenes. Reactions performed at atmospheric pressure of CO₂.



An oven dried 100 mL round bottom flask and a stir bar were introduced to the argon filled glove box. To the round bottom flask, a magnetic stir bar, B₂pin₂ (1.5 equiv.), base (2.0 equiv.), ligand (6 mol%) and Cu-salt (5 mol%) were added, closed with a septum, and sealed tight using electric tape. To the flask, 20 mL of anhydrous solvent were added and left stirring for 30 minutes. Then the corresponding styrene (1 equiv.) was added, and a balloon filled with dry CO₂ was attached to the flask (see Figure S1). The round bottom flask was then left stirring for 24 hours at 20 °C. Afterwards, the flask was opened to air and the content was diluted with 20 mL of Et₂O. The reaction mixture was transferred into a 250 mL separating funnel where the organic layer was extracted using a solution of saturated NaHCO₃ (3x30 mL). Then the separated aqueous solution was first washed with Et₂O (3x30 mL), acidified by slow addition of 60 mL 6M HCl and then extracted using Et₂O (3x30 mL). The organic solution was washed using 30 mL of distilled water. Afterwards the organic solution was evaporated to dryness to give the product.

1.2.2 Method B: General procedure for boracarboxylation of styrenes. Reactions performed at high pressure of CO₂.



An oven dried 47 mL pressure vial (See Figure S2) and a stir bar were introduced to the argon filled glove box. To the pressure vial, a magnetic stir bar, B₂pin₂ (1.5 equiv.), base (2.0 equiv.), ligand (6 mol%) and Cu-salt (5 mol%) were added and the vial was sealed tight. Outside of the glove box to the pressure vial 10 mL of anhydrous solvent was added through the septum using a syringe. The vial was left stirring at 20 °C for 30 minutes. Then the corresponding styrene (1 equiv.) was added through the septum using a syringe, followed by injection of 120 mL CO₂ as it is shown in Figure S3. The reaction mixture was then left stirring for 3 hours at 60 °C (see Figure S4). Afterwards the reaction mixture was allowed to cool down to room temperature, the flask was opened to air and the reaction mixture was diluted with 10 mL of Et₂O. The reaction mixture was transferred into a 250 mL separating funnel where the organic layer was extracted using a solution of saturated NaHCO₃ (3x30 mL). Then the separated aqueous solution was first washed with Et₂O (3x30 mL), acidified by slow addition of 60 mL 6M HCl and then extracted using Et₂O (3x30 mL). The organic solution was washed using 30 mL of distilled water. Afterwards the organic solution was evaporated to dryness to give the product.

1.2.3 Description of the used glassware and setup of the reactions



Figure S1. Boracoxylation reactions under atmospheric pressure of CO₂. The balloons are filled with CO₂.

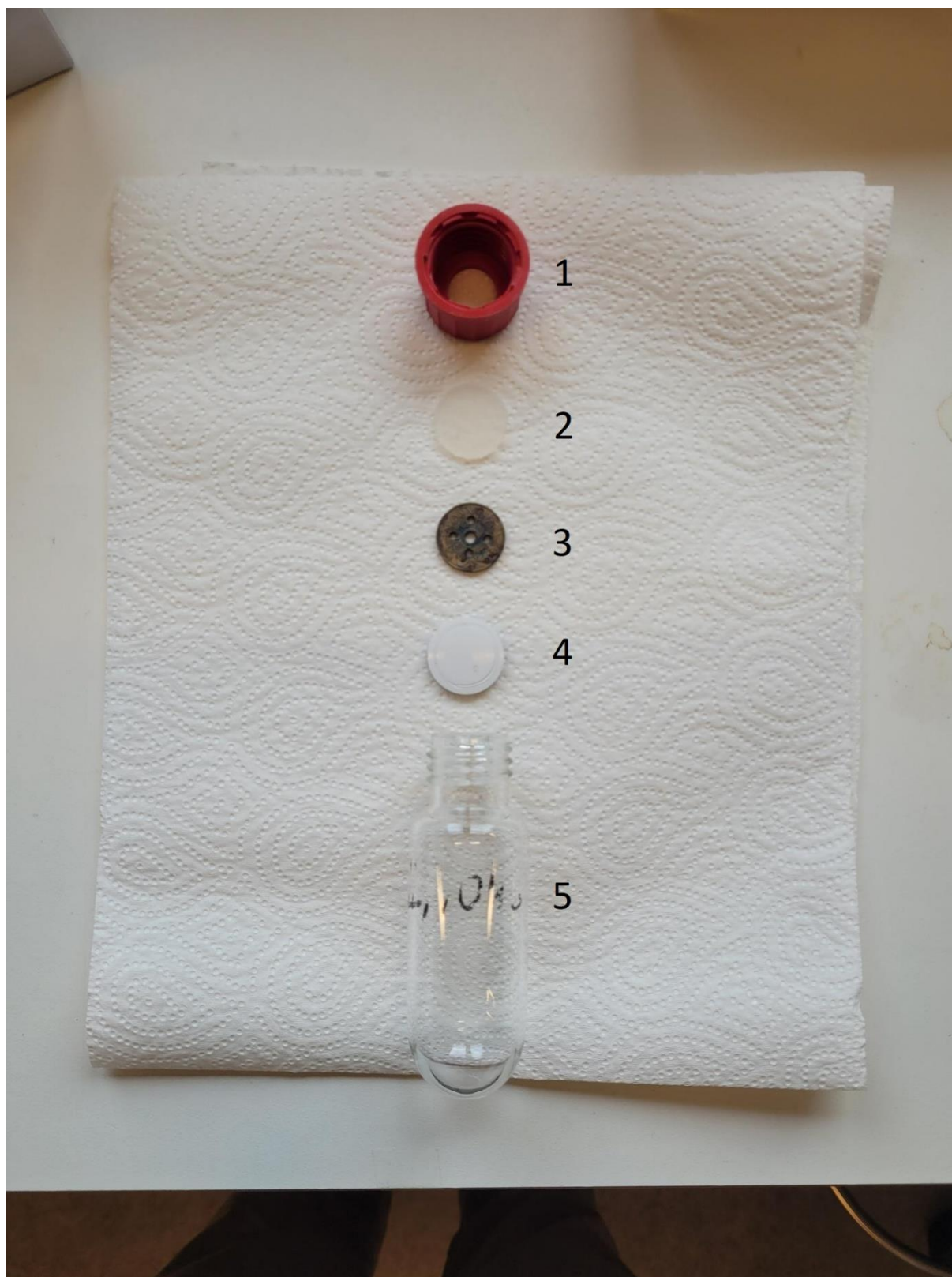


Figure S2. Shows the pressure vial used for the high-pressure experiments. The pressure vial is equipped with a screw cap (1), a silicon septum (2), a metallic stabilizer made from 1 NOK (3), a silicone septum with a protection layer made from Teflon (4) and a 47 mL vial (5).

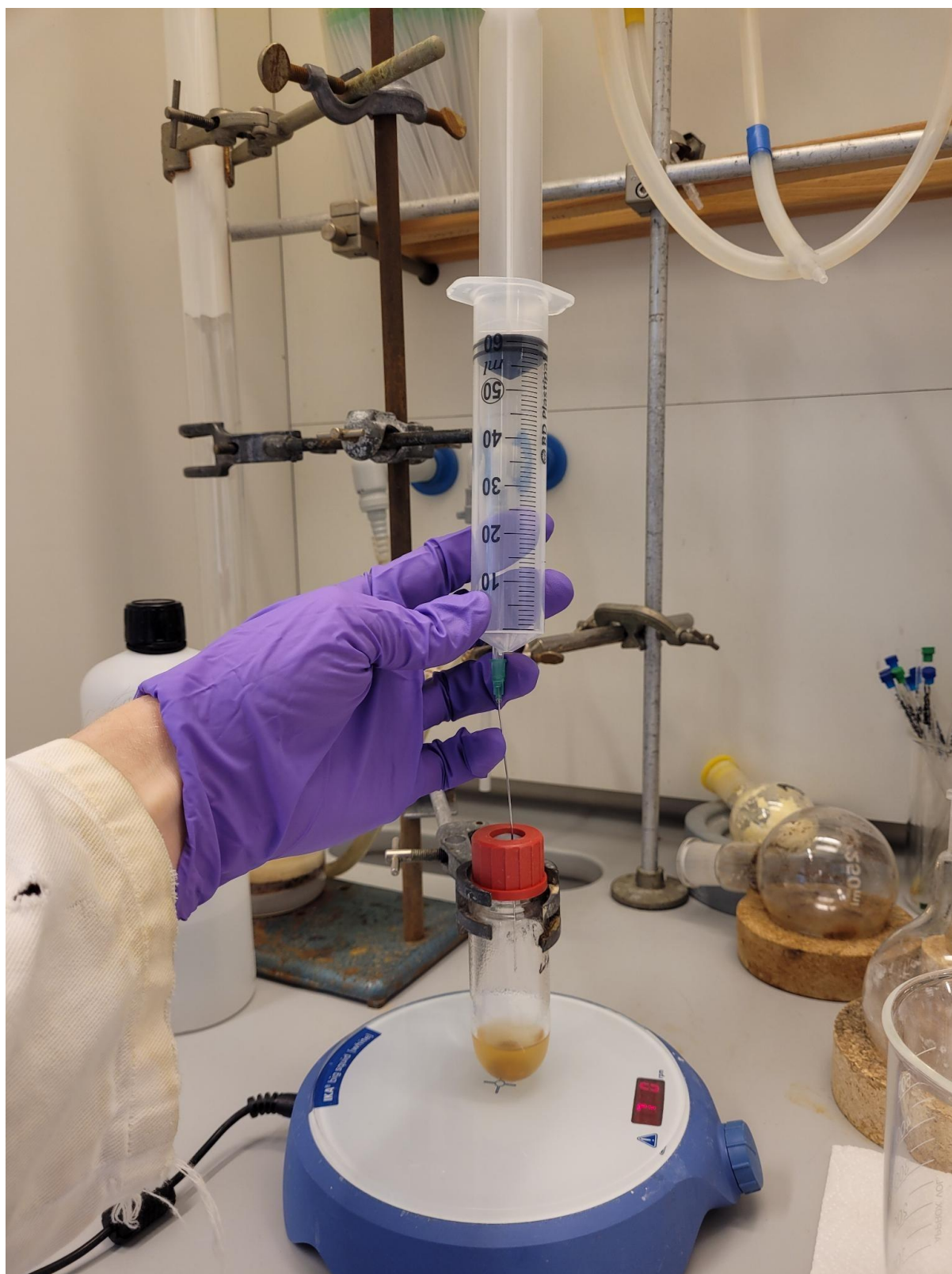


Figure S3. Injection of the first portion of CO₂ into the pressure vial.

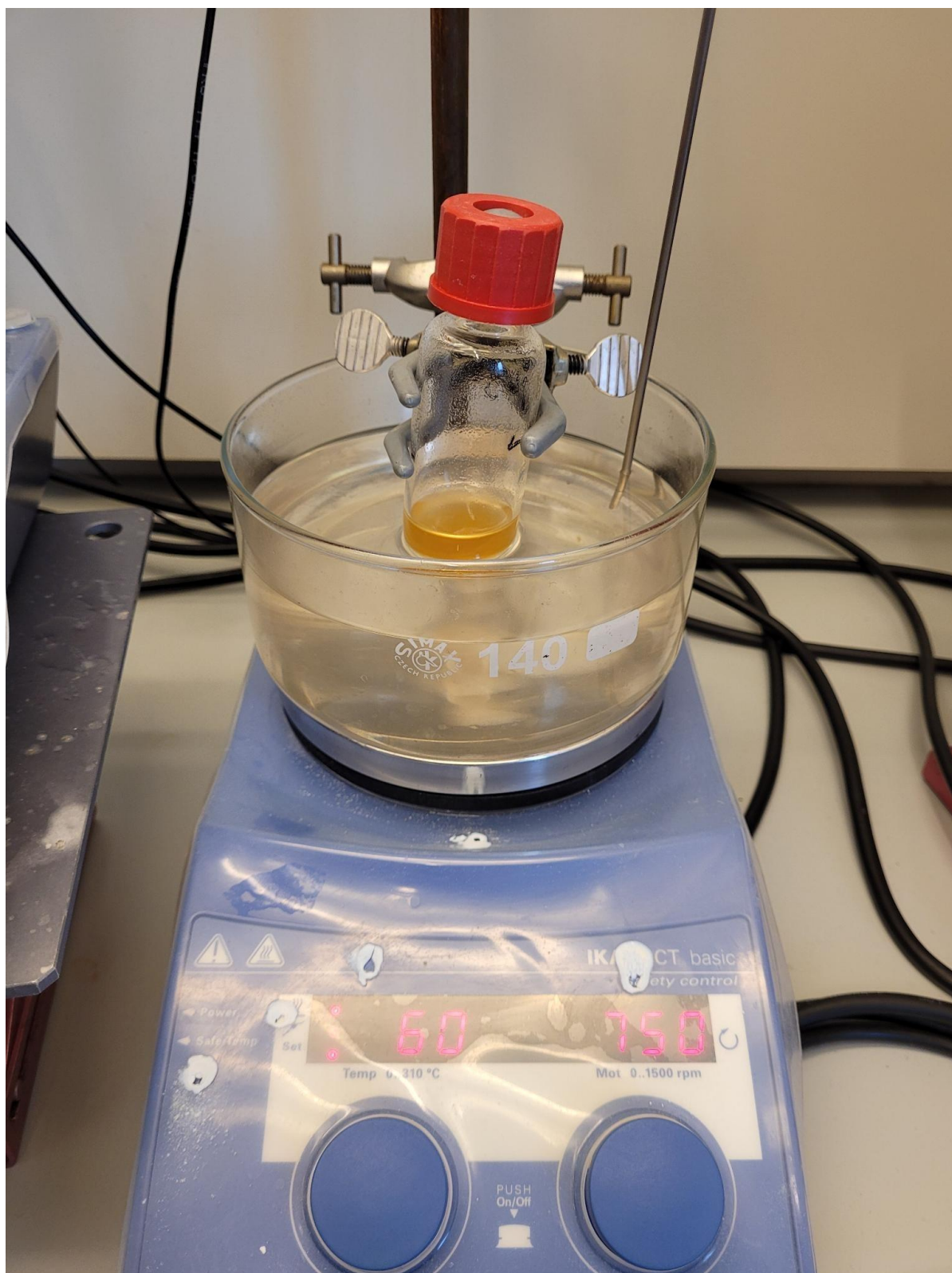
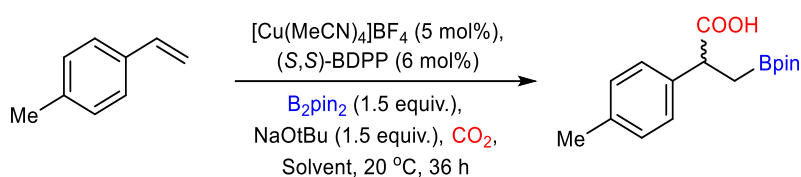


Figure S4. Shows the general setup for the experiments conducted with high pressure vials.

1.3 Overview of optimization tables

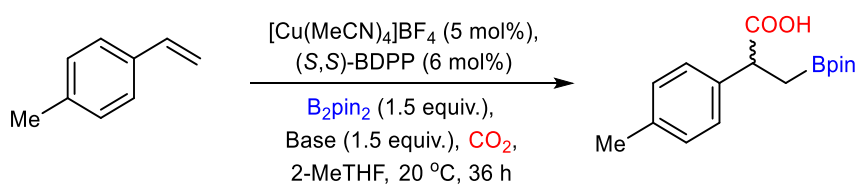
Table S1. Solvent screening for boracarboxylation of 4-methylstyrene.



Entry	Solvent	Yield ^a
1	THF	39%
2	2-MeTHF	45%
3	Dioxane	40%
4	DME	20%
5	Eucalyptol	35% ^b
6	Methylal	23% ^b
7	Toluene	0% ^b
8	Acetal	33% ^b

^a If not otherwise specified the yield refer to isolated products. ^b These experiments were done with $[\text{Cu}(\text{MeCN})_4]\text{PF}_6$ (5 mol%), Cs_2CO_3 (2 equiv.) and B_2Pin_2 (2 equiv.).

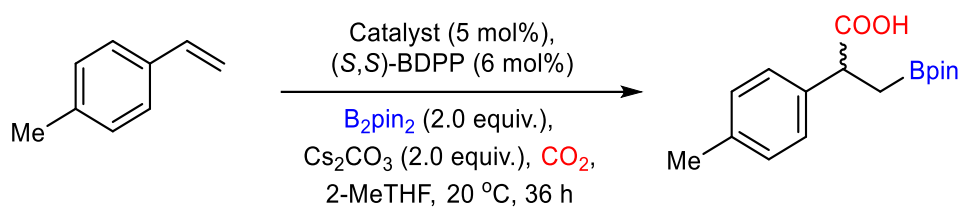
Table S2. The screening of bases for boracarboxylation of 4-methylstyrene.



Entry	Base (equiv.)	Yield ^a
1	LiOtBu (1.5)	48%
2	LiOMe (1.5)	43%
3	KOtBu (1.5)	5%
4	Cs_2CO_3 (1.5)	52%
5	CsF (1.5)	12%
6	Cs_2CO_3 (1.5)	28% ^b
7	CsOAc (1.5)	32%
8	Bu_4NOAc (1.5)	0%
9	Cs_2CO_3 (2.0)	73% ^{c,d}
10	Cs_2CO_3 (2.5)	60% ^e
11	Cs_2CO_3 (2.5)	20% ^c
12	Cs_2CO_3 (2.0)	0% ^{c,f}
13	Cs_2CO_3 (2.0)	60% ^e

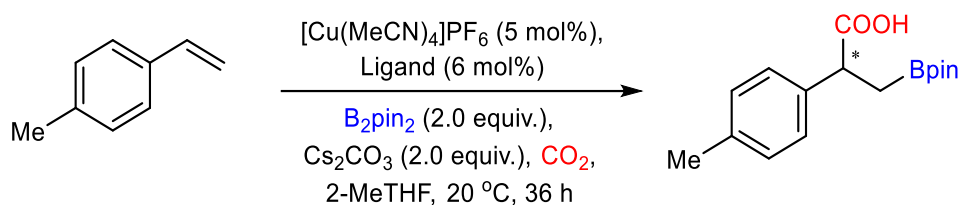
^a If not otherwise specified the yield refer to isolated products. ^b For this experiment the temperature was 60 °C. ^c For this experiment 2.0 equiv. of B_2pin_2 was used. ^d Average yield of two experiments. ^e For this experiment 2.5 equiv. of B_2pin_2 was used. ^f This experiment was done without the ligand.

Table S3. The screening of transition-metal complexes for boracarboxylation of 4-methylstyrene.



Entry	Catalyst (5 mol%)	Yield ^a
1	[Cu(MeCN) ₄]PF ₆	84%
2	Cu(TC)	62% ^b
3	CuI	0%
4	CuOAc	0%
5	CuF ₂	0%
6	[Cu(MeCN) ₄]PF ₆	65% ^c
7	[Cu(MeCN) ₄]PF ₆	0% ^d
8	Ni(cod) ₂	0%
9	NiCl ₂ glyme	0%
10	Co(acac) ₂	0%

^a If not otherwise specified the yield refer to isolated products. ^b Product was contaminated with thiophene-2-carboxylic acid (TC = thiophene-2-carboxylate). ^c For this experiment the reaction time was 24h. ^d For this experiment the reaction was done without the ligand.

Table S4. Screening of chiral ligands for the boracarboxylation reaction.

Entry	Ligand (6 mol%) ^a	<i>e.r.</i>	Yield ^b
1	(<i>S,S</i>)-BDPP	48:52	84%
2	(<i>S,S</i>)-Ph-BPE,BPE	68:32	23%
3	(<i>R</i>)-Josiphos	69:31	20%
4	(<i>S</i>)-MeOBIPHEP	75:25	21%
5	L1	35:65	71%
6	L2	48:52	72%
7	(1 <i>R</i> ,1' <i>R</i> ,2 <i>S</i> ,2' <i>S</i>)DuanPhos	40:60	30%
8	(<i>R,R</i>)- <i>i</i> -Pr-DUPHOS	45:55	24%
9	(<i>S,S</i>)-QuinoxP*	92:8	26%
10	(<i>S</i>)-DTBM-SEGPHOS [®]	-	0%
11	(<i>R</i>)-DTBM-Garphos [™]	58:41	25%
12	(<i>R</i>)-BINAP	30:70	22%
13	(<i>R</i>)-Josiphos	32:68	36%
14	(<i>R</i>)-Walphos	39:61	44%
15	(<i>S</i> _{Fc} , <i>R</i> _C)-Mandyphos	23:77	20%
16	(<i>R,S</i>)-O-pinap	60:40	28%
17	(<i>rac</i>)-StackPhos	-	27%
18	(<i>S</i>)-SEGPHOS	-	0%
19	(<i>S,S</i>)- <i>t</i> Bu-BOX	50:50	19%
20	L3	49:51	23%
21	(2 <i>R</i> ,3 <i>R</i>)-MeO-BoQPhos	31:69	19%
22	(<i>R,R,R,R</i>)-BIBOP	43:57	46%
23	(3 <i>S</i> ,3' <i>S</i>)-BABIBOP	23:77	45%
24	(<i>R,R</i>)-BenzP*	23:77	23%
25	L4	-	0%
26	(<i>S</i>)-BI-DIME	50:50	11%
27	Mandyphos SL-M002-1	-	0%
28	(<i>S</i>)-BINAPINE	-	0%

^a For the structure of ligands see Figures S5-S8. ^b If not otherwise specified the yield refer to isolated products.

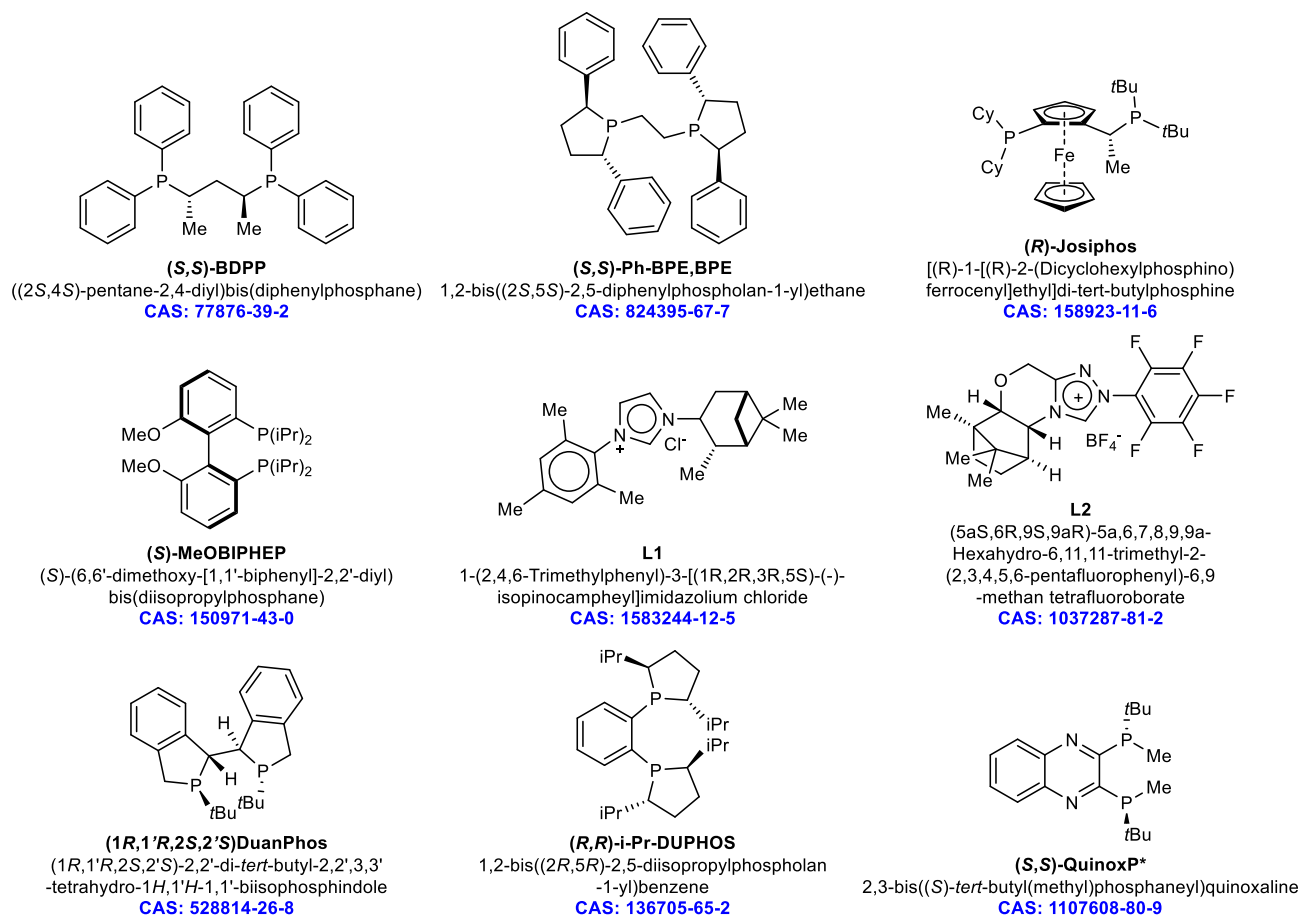


Figure S5. Shows the structures of the ligands for the entries 1-9 in Table S4.

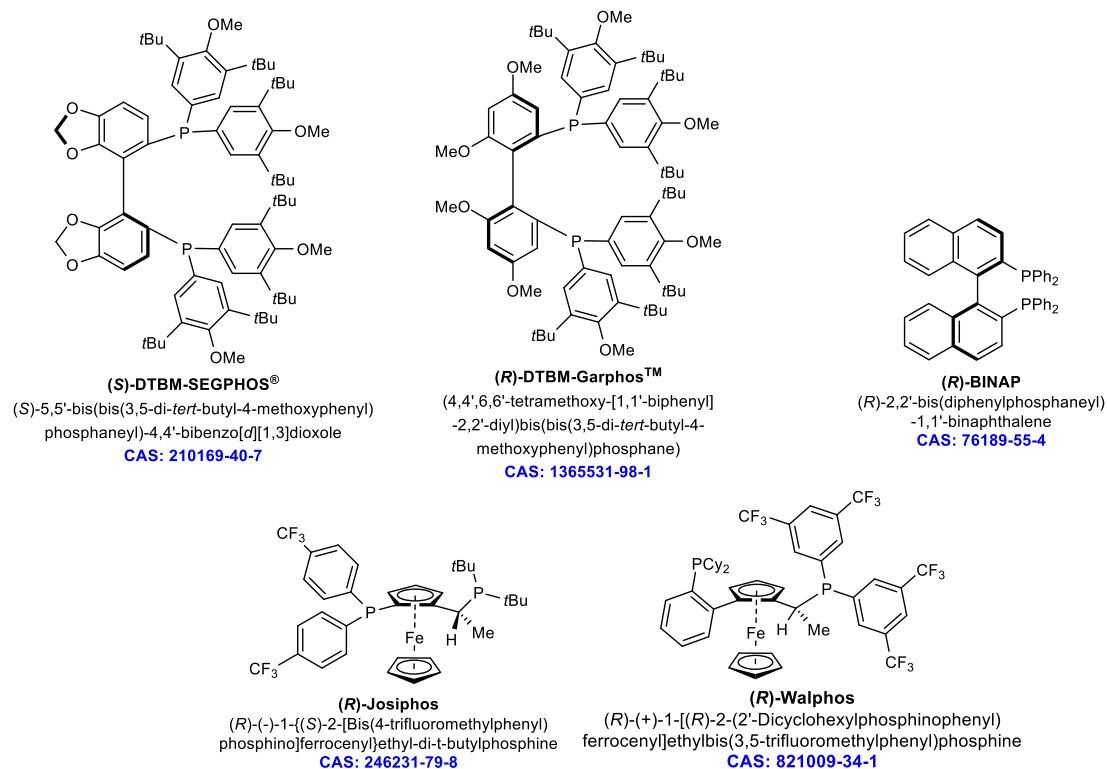


Figure S6. Shows the structures of the ligands for the entries 10-14 in Table S4.

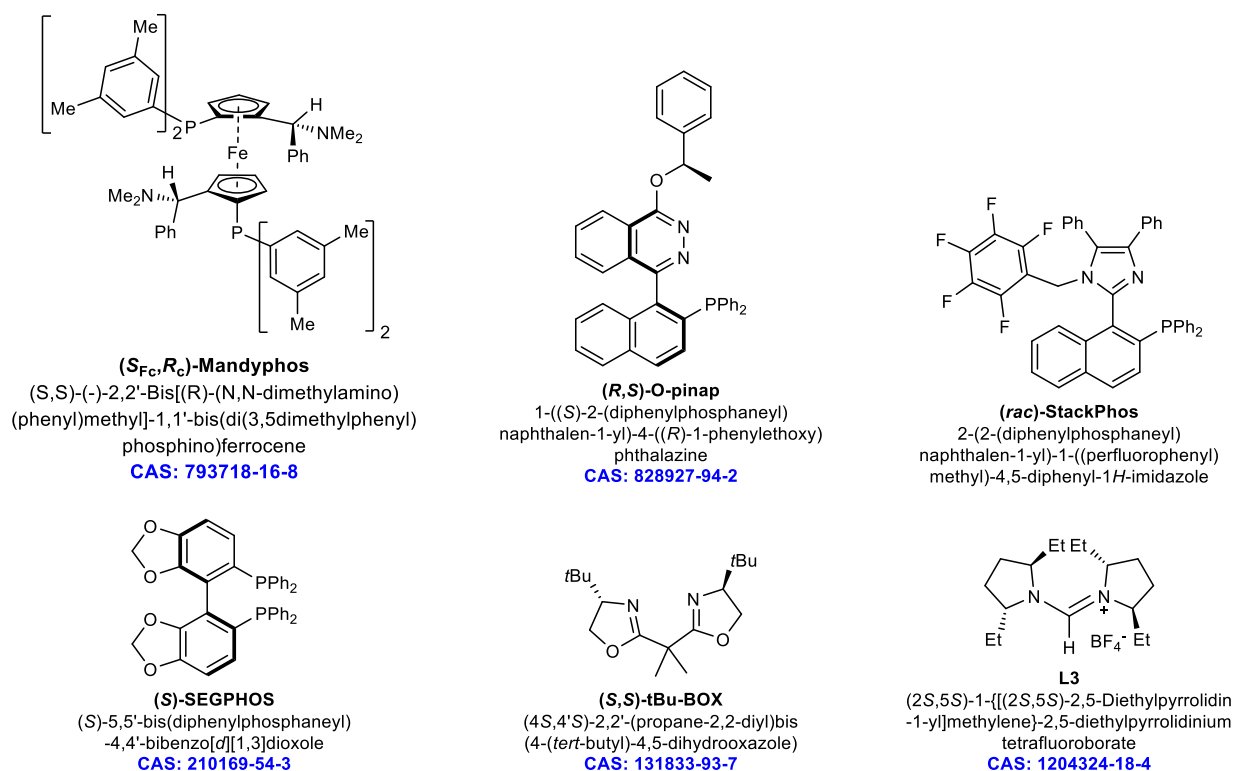


Figure S7. Shows the structures of the ligands for the entries 15-20 in Table S4.

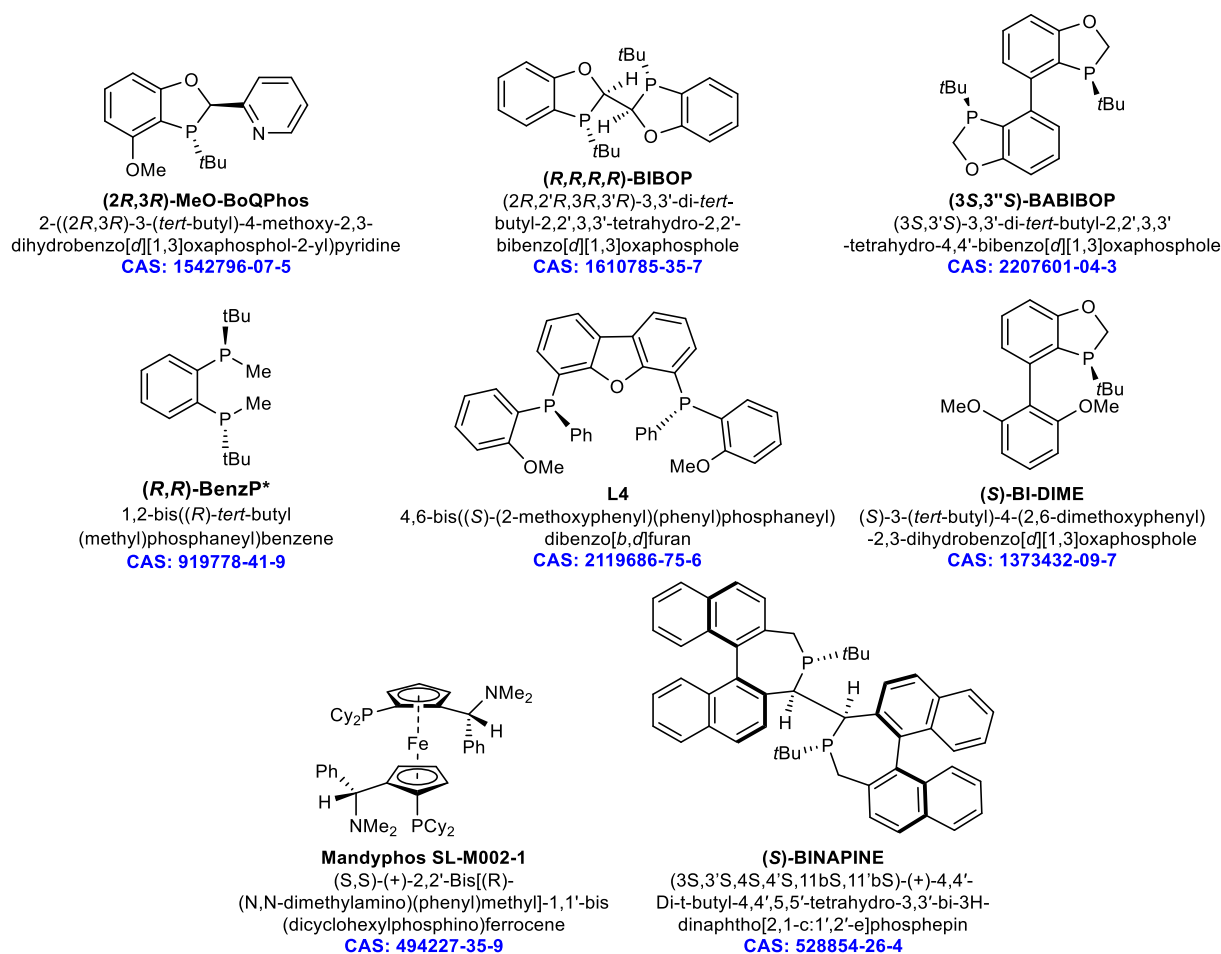
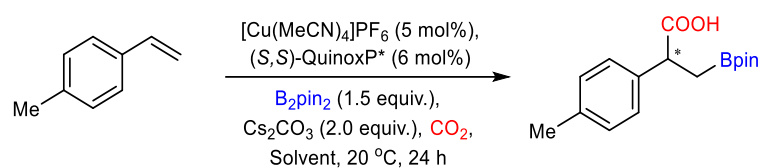


Figure S8. Shows the structures of the ligands for the entries 21-28 in Table S4.

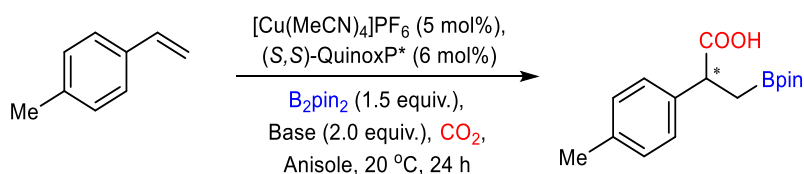
Table S5. Solvent screening for boracarboxylation of 4-methylstyrene enabled by (*S,S*)-QuinoxP* ligand.



Entry	Solvent	Yield ^a
1	THF	10%
2	2MeTHF	4%
3	Dioxane	25%
4	DME	10%
5	Eucalyptol	22%
6	Acetal	22%
7	Diglyme	13%
8	Triglyme	19%
9	Methylal	14%
10	Dimethyl Isosorbide	11%
11	Anisole	40%
12	DMF	11%
13	Acetonitrile	17%
14	1,2-Dimethoxybenzene	3%
15	Chloroform	12%
16	Tetraethyl Orthosilicate	13%
17	1,3-Dimethoxybenzene	23%

^a If not otherwise specified the yield refer to isolated products.

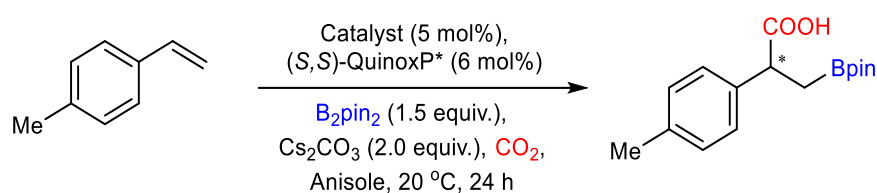
Table S6. The screening of bases for boracarboxylation of 4-methylstyrene enabled by (*S,S*)-QuinoxP* ligand.



Entry	Base (2 equiv.)	Yield ^a
1	Cs ₂ CO ₃	40%
2	Rb ₂ CO ₃	19%
3	CsOAc	0%
4	K ₃ PO ₄	0%
5	CsF	0%
6	RbF	0%
7	AgF	0%
8	LiOtBu	0%
9	LiOMe	0%
10	KOMe	0%
11	KOtBu	19%
12	NaOtBu	26%
13	NaOSiMe ₃	20%

^a If not otherwise specified the yield refer to isolated products.

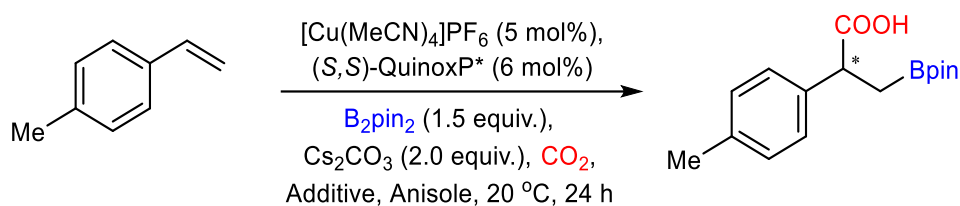
Table S7. The screening of Cu-complexes for boracarboxylation of 4-methylstyrene enabled by (*S,S*)-QuinoxP* ligand.



Entry	Cu-source (5 mol%)	Yield ^{a)}
1	[Cu(MeCN) ₄]PF ₆	40%
2	[Cu(MeCN) ₄]BF ₄	18%
3	[Cu(MeCN) ₄]SbF ₆	20%
4	[Cu(MeCN) ₄]BARf	26%
5	[Cu(MeCN) ₄]OTf	23%
6	[Cu(MeCN) ₄]ClO ₄	3%
7	Cu(TC)	42% ^{b)}
8	[Cu(cod)Cl] ₂	21% ^{c)}
9	[Cu(MeCN) ₄]PF ₆	76% ^{d),e)}

^{a)} If not otherwise specified the yield refer to isolated products. ^{b)} Product was contaminated with thiophene-2-carboxylic acid (TC = thiophene-2-carboxylate). ^{c)} for this experiment 2.5 mol% of the Cu-source was used. ^{d)} Amount of the used Cu source was 10 mol% and, while the ligand was 12 mol%. ^{e)} *e.r.* was measured to be 16:86.

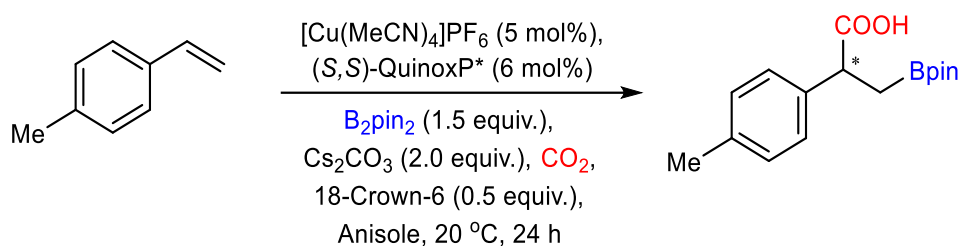
Table S8. The screening of additives for boracarboxylation of 4-methylstyrene enabled by (*S,S*)-QuinoxP* ligand.



Entry	Additive (mol%)	Yield ^{a)}
1	none	40%
2	NaBARf (20)	0%
3	18-Crown-6 (50)	58% ^{b),c)}
4	TBAB (50)	42%
5	PPh ₃ (20)	32%
6	ICy HCl (5)/NaOtBu (6)	12%
7	PCy ₃ HBF ₄ (5)/NaOtBu (6)	17%
8	DMAP (20)	23%
9	TBD (20)	38%
10	Monolautin (20)	37%
11	Palmitic Acid (20)	33%

^{a)} If not otherwise specified the yield refer to isolated products. ^{b)} Average yield of two experiments. ^{c)} *e.r.* was measured to be 96:4.

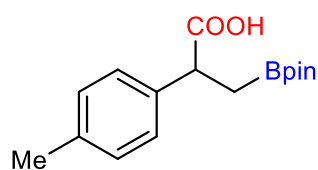
Table S9. Changing various parameters from the optimal conditions found for boracarboxylation of 4-methylstyrene enabled by (*S,S*)-QuinoxP* ligand.



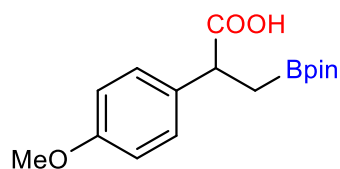
Entry	Change	<i>e.r.</i>	Yield ^a
1	none	96:4	58% ^b
2	[Cu(MeCN) ₄]PF ₆ (10 mol%) and (<i>S,S</i>)-QuinoxP* (12 mol%)	93:7	60%
3	18-Crown-6 (0.25 equiv.)	92:8	31%
4	18-Crown-6 (1 equiv.)	93:7	31%
5	B ₂ pin ₂ (2 equiv.)	93:7	48%
6	5 atm CO ₂ , 30 min, 3.0 equiv. B ₂ pin ₂ , 60 °C	92:8	34%
7	5 atm CO ₂ , 3 h, 3.0 equiv. B ₂ pin ₂ , 60 °C	91:9	50%
8	5 atm CO ₂ , 24h, 3.0 equiv. B ₂ pin ₂ , 60 °C	91:9	55%

^a If not otherwise specified the yield refer to isolated products. ^b Average yield of two experiments.

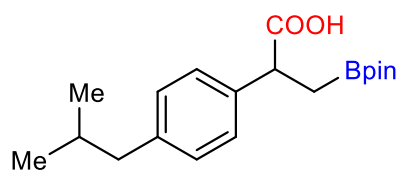
1.4 Characterization of products



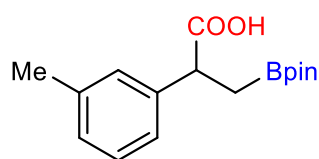
3-(4,4,5,5-tetramethyl-1,3,2-dioxaborolan-2-yl)-2-(p-tolyl)propanoic acid, 2a.^[1] Following the general procedure (method A) starting from 1.27 mmol of the corresponding styrene, the product was obtained as a faint yellow oil with average yield 58% (experiment 1: 184 mg; experiment 2: 243 mg). ¹H NMR (400 MHz, CDCl₃) δ 7.20 (d, 2H), 7.11 (d, *J* = 7.9 Hz, 2H), 3.84 (dd, *J* = 9.6, 7.0 Hz, 1H), 2.32 (s, 3H), 1.55 (dd, *J* = 16.0, 9.6 Hz, 1H), 1.26 (dd, *J* = 15.9, 7.0 Hz, 1H), 1.16 (d, *J* = 6.6 Hz, 12H). ¹³C NMR (101 MHz, CDCl₃) δ 180.9, 137.6, 136.8, 129.3, 127.8, 83.5, 67.1, 46.6, 24.8, 24.6, 21.1. HRMS: calculated *m/z* for [C₁₆H₂₂BO₄]⁻: 289.1620, found 289.1618. Enantioselective ratio = 94:6, determined by SFC method A, *t_R* = 6.99 min (major), *t_R* = 7.40 min (minor). [α]_D²⁰ = - 60.0 (c = 0.5 g/100mL, CHCl₃)



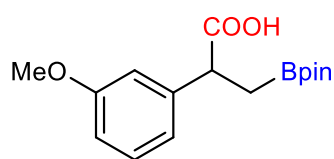
2-(4-methoxyphenyl)-3-(4,4,5,5-tetramethyl-1,3,2-dioxaborolan-2-yl)propanoic acid, 2b.^[1] Following the general procedure (method A) starting from 1.27 mmol of corresponding styrene the product was obtained as a faint yellow oil, yield 41% (0.158 g). ¹H NMR (400 MHz, CDCl₃) δ 7.24 – 7.19 (m, 2H), 6.85 – 6.79 (m, 2H), 3.80 (dd, *J* = 9.2, 7.4 Hz, 1H), 3.77 (s, 3H), 1.52 (dd, *J* = 15.9, 9.2 Hz, 1H), 1.30 – 1.23 (m, 1H), 1.14 (d, *J* = 4.1 Hz, 12H). ¹³C NMR (101 MHz, CDCl₃) δ 180.9, 158.8, 132.6, 129.0, 114.0, 83.5, 55.4, 46.1, 24.8, 24.7. HRMS: calculated *m/z* for [C₁₆H₂₂BO₅]⁻: 305.1569, found 305.1567. Enantioselective ratio = 98:2, determined by SFC method A, *t_R* = 4.99 min (major), *t_R* = 5.2 min (minor). [α]_D²⁰ = - 46.0 (c = 0.5 g/100mL, CHCl₃)



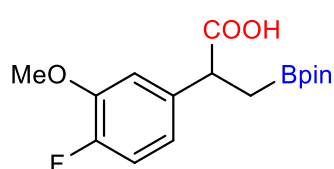
2-(4-isobutylphenyl)-3-(4,4,5,5-tetramethyl-1,3,2-dioxaborolan-2-yl)propanoic acid, 2c.^[1] Following the general procedure (method A) starting from 1.27 mmol of corresponding styrene the product was obtained as a faint yellow oil, yield 31% (0.132 g). ¹H NMR (400 MHz, CDCl₃) δ 7.21 (d, *J* = 7.8 Hz, 2H), 7.06 (d, *J* = 7.8 Hz, 2H), 3.83 (t, *J* = 8.3 Hz, 1H), 2.43 (d, *J* = 7.2 Hz, 2H), 1.83 (hept, *J* = 6.8 Hz, 1H), 1.53 (dd, *J* = 15.9, 9.1 Hz, 1H), 1.36 – 1.24 (m, 2H), 1.13 (d, *J* = 4.3 Hz, 12H), 0.88 (d, *J* = 6.6 Hz, 6H). ¹³C NMR (101 MHz, CDCl₃) δ 181.0, 140.7, 137.7, 129.4, 127.7, 83.5, 46.6, 45.2, 30.3, 24.8, 24.7, 22.5, 22.5. HRMS: calculated *m/z* for [C₁₉H₂₈BO₄]⁻: 331.2090, found 331.2089. Enantioselective ratio = 92:8, determined by SFC method A, *t_R* = 7.11 min (major), *t_R* = 7.65 min (minor). [α]_D²⁰ = - 56.0 (c = 0.5 g/100mL, CHCl₃)



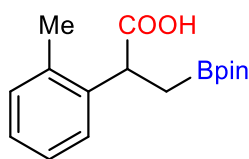
3-(4,4,5,5-tetramethyl-1,3,2-dioxaborolan-2-yl)-2-(m-tolyl)propanoic acid, 2d.^[1] Following the general procedure (method A) starting from 1.27 mmol of corresponding styrene the product was obtained as faint yellow crystals, yield 49% (0.182 g, 0.627 mmol). ¹H NMR (400 MHz, CDCl₃) δ 7.19 (t, *J* = 7.5 Hz, 1H), 7.14 – 7.03 (m, 3H), 3.84 (dd, *J* = 9.4, 7.1 Hz, 1H), 2.33 (s, 3H), 1.55 (dd, *J* = 16.0, 9.4 Hz, 1H), 1.31 – 1.24 (m, 1H), 1.16 (d, *J* = 5.1 Hz, 12H). ¹³C NMR (101 MHz, CDCl₃) δ 181.1, 140.5, 138.2, 128.7, 128.6, 128.1, 125.0, 83.5, 46.9, 24.8, 24.7, 21.5. HRMS: calculated *m/z* for [C₁₆H₂₂BO₄]⁻: 289.1620, found 289.1616. Enantioselective ratio = 85:15, determined by SFC method B, *t_R* = 4.24 min (major), *t_R* = 4.46 min (minor). [α]_D²⁰ = - 32.0 (c = 0.5 g/100mL, CHCl₃)



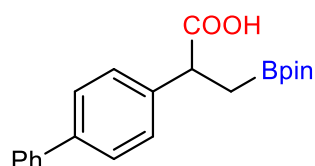
2-(3-methoxyphenyl)-3-(4,4,5,5-tetramethyl-1,3,2-dioxaborolan-2-yl)propanoic acid, 2e.^[1] Following the general procedure (method A) starting from 1.27 mmol of corresponding styrene the product was obtained as a colorless oil, yield 42% (0.164 g, 0.538 mmol). ¹H NMR (400 MHz, CDCl₃) δ 7.20 (t, *J* = 7.9 Hz, 1H), 6.92 – 6.83 (m, 2H), 6.78 (ddd, *J* = 8.3, 2.6, 0.9 Hz, 1H), 3.83 (dd, *J* = 9.5, 7.0 Hz, 1H), 3.77 (s, 3H), 1.54 (dd, *J* = 16.0, 9.5 Hz, 1H), 1.31 – 1.23 (m, 2H), 1.15 (d, *J* = 5.4 Hz, 12H). ¹³C NMR (101 MHz, CDCl₃) δ 180.8, 159.8, 142.0, 129.6, 120.3, 113.5, 112.9, 83.6, 55.3, 47.0, 24.8, 24.6. HRMS: calculated *m/z* for [C₁₆H₂₂BO₅]⁻: 305.1569, found 305.1566. Enantioselective ratio = 82:18, determined by SFC method A, *t_R* = 6.37 min (major), *t_R* = 6.54 min (minor). [α]_D²⁰ = - 36.0 (c = 0.5 g/100mL, CHCl₃)



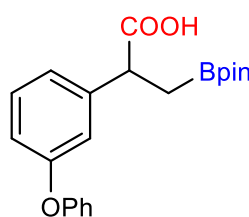
2-(4-fluoro-3-methoxyphenyl)-3-(4,4,5,5-tetramethyl-1,3,2-dioxaborolan-2-yl)propanoic acid, 2f. Following the general procedure (method A) starting from 1.27 mmol of corresponding styrene the product was obtained as a colorless oil, yield 44% (0.183 g). ¹H NMR (400 MHz, CDCl₃) δ 6.97 (dd, *J* = 11.1, 8.3 Hz, 1H), 6.92 (dd, *J* = 8.1, 2.1 Hz, 1H), 6.82 (ddd, *J* = 8.2, 4.2, 2.1 Hz, 1H), 3.85 (s, 3H), 3.81 (dd, *J* = 8.9, 7.6 Hz, 1H), 1.51 (dd, *J* = 16.0, 8.9 Hz, 1H), 1.28 (dd, *J* = 16.0, 7.7 Hz, 1H), 1.13 (d, *J* = 2.6 Hz, 12H). ¹³C NMR (101 MHz, CDCl₃) δ 180.7, 151.7 (d, *J* = 245.4 Hz), 147.5 (d, *J* = 10.8 Hz), 136.6 (d, *J* = 3.9 Hz), 120.3 (d, *J* = 6.9 Hz), 115.9 (d, *J* = 18.4 Hz), 113.2 (d, *J* = 1.9 Hz), 83.6, 56.3, 46.6, 24.7, 24.6. ¹⁹F NMR (377 MHz, CDCl₃) δ -137.4. IR (ATR): 3150 (br, w), 2979 (w), 1729 (s), 1612 (m), 1518 (s), 1377 (s), 1281 (s), 1141 (s), 1123 (s), 1033 (s), 851 (s), 814 (s) cm⁻¹. HRMS: calculated *m/z* for [C₁₆H₂₁BFO₅]⁻: 323.1475, found 323.1472. Enantioselective ratio = 79:21, determined by SFC method A, *t_R* = 6.04 min (major), *t_R* = 6.40 min (minor). [α]_D²⁰ = - 38.0 (c = 0.5 g/100mL, CHCl₃)



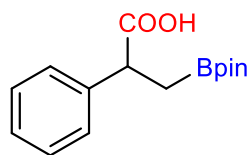
3-(4,4,5,5-tetramethyl-1,3,2-dioxaborolan-2-yl)-2-(o-tolyl)propanoic acid, 2g.^[1] Following the general procedure (method A) starting from 1.27 mmol of corresponding styrene the product was obtained as faint yellow crystals, yield 37% (0.137 g). ¹H NMR (400 MHz, CDCl₃) δ 7.37 – 7.32 (m, 1H), 7.26 – 7.18 (m, 3H), 4.21 (t, *J* = 8.3 Hz, 1H), 2.51 (s, 3H), 1.61 (dd, *J* = 16.0, 8.8 Hz, 1H), 1.40 (dd, *J* = 15.9, 7.8 Hz, 1H), 1.21 (s, 12H). ¹³C NMR (101 MHz, CDCl₃) δ 181.1, 139.0, 136.3, 130.4, 127.1, 126.4, 83.5, 42.6, 24.7, 24.6, 19.9. HRMS: calculated *m/z* for [C₁₆H₂₂BO₄]⁻: 289.1620, found 289.1617. Enantioselective ratio = 82:18, determined by SFC method A, *t_R* = 6.02 min (major), *t_R* = 6.37 min (minor). [α]_D²⁰ = -40.0 (c = 0.5 g/100mL, CHCl₃)



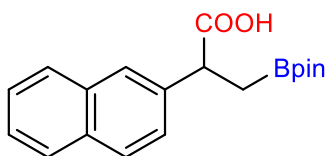
2-([1,1'-biphenyl]-4-yl)-3-(4,4,5,5-tetramethyl-1,3,2-dioxaborolan-2-yl)propanoic acid, 2h.^[1] Following the general procedure (method A) starting from 1.27 mmol of corresponding styrene the product was obtained as faint yellow crystals, yield 32% (0.143 g). ¹H NMR (400 MHz, CDCl₃) δ 7.55 (dd, *J* = 12.9, 7.8 Hz, 4H), 7.47 – 7.37 (m, 4H), 7.37 – 7.30 (m, 1H), 3.93 (t, *J* = 8.2 Hz, 1H), 1.61 (dd, *J* = 16.0, 9.3 Hz, 1H), 1.34 (dd, *J* = 16.0, 7.2 Hz, 1H), 1.16 (t, *J* = 4.5 Hz, 12H). ¹³C NMR (101 MHz, CDCl₃) δ 180.6, 141.0, 140.3, 139.5, 128.8, 128.4, 127.4, 127.3, 127.2, 83.6, 46.6, 24.8, 24.7. HRMS: calculated *m/z* for [C₂₁H₂₄BO₄]⁻: 351.1777, found 351.1773. Enantioselective ratio = 73:27, determined by SFC method B, *t_R* = 6.58 min (major), *t_R* = 6.96 min (minor). [α]_D²⁰ = -28.0 (c = 0.5 g/100mL, CHCl₃)



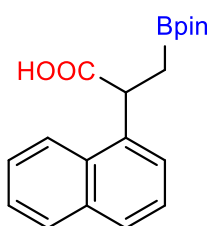
2-(3-phenoxyphenyl)-3-(4,4,5,5-tetramethyl-1,3,2-dioxaborolan-2-yl)propanoic acid, 2i.^[2] Following the general procedure (method A) starting from 1.27 mmol of corresponding styrene the product was obtained as a faint yellow oil, yield 33% (0.153 g). ¹H NMR (400 MHz, CDCl₃) δ 7.32 (t, *J* = 7.8 Hz, 2H), 7.25 (t, *J* = 7.9 Hz, 1H), 7.14 – 7.02 (m, 2H), 7.02 – 6.96 (m, 3H), 6.87 (dd, *J* = 8.2, 2.4 Hz, 1H), 3.84 (dd, *J* = 9.4, 7.1 Hz, 1H), 1.53 (dd, *J* = 16.0, 9.4 Hz, 1H), 1.32 – 1.22 (m, 1H), 1.16 (d, *J* = 4.3 Hz, 11H). ¹³C NMR (101 MHz, CDCl₃) δ 180.5, 157.5, 157.1, 142.4, 129.9, 129.8, 123.4, 122.7, 119.1, 118.6, 117.5, 83.6, 46.9, 24.8, 24.7. HRMS: calculated *m/z* for [C₂₁H₂₄BO₅]⁻: 367.1726, found 367.1721. Enantioselective ratio = 76:24, determined by SFC method A, *t_R* = 7.70 min (major), *t_R* = 8.42 min (minor). [α]_D²⁰ = -34.0 (c = 0.5 g/100mL, CHCl₃)



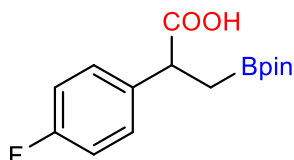
2-phenyl-3-(4,4,5,5-tetramethyl-1,3,2-dioxaborolan-2-yl)propanoic acid, 2j.^[1] Following the general procedure (method A) starting from 1.27 mmol of corresponding styrene the product was obtained as a white solid, yield 36% (0.125 g, 0.453 mmol). ¹H NMR (400 MHz, CDCl₃) δ 7.40 – 7.24 (m, 5H), 3.91 (dd, *J* = 9.3, 7.3 Hz, 1H), 1.61 (dd, *J* = 16.0, 9.3 Hz, 1H), 1.40 – 1.27 (m, 2H), 1.20 (d, *J* = 4.4 Hz, 11H). ¹³C NMR (101 MHz, CDCl₃) δ 180.6, 140.5, 128.6, 128.0, 127.3, 83.5, 47.0, 24.8, 24.6. HRMS: calculated *m/z* for [C₁₅H₂₀BO₄]⁻: 275.1463, found 275.1461. Enantioselective ratio = 86:14, determined by SFC method B, *t_R* = 5.10 min (major), *t_R* = 5.27 min (minor). [α]_D²⁰ = -46.0 (c = 0.5 g/100mL, CHCl₃)



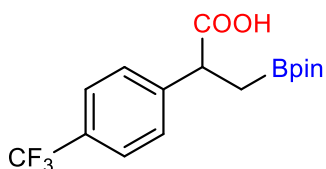
2-(naphthalen-2-yl)-3-(4,4,5,5-tetramethyl-1,3,2-dioxaborolan-2-yl)propanoic acid, 2k.^[1] Following the general procedure (method A) starting from 1.27 mmol of corresponding naphthalene the product was obtained as faint yellow crystals, yield 40% (0.168 g) ¹H NMR (400 MHz, CDCl₃) δ 7.78 (q, *J* = 5.5 Hz, 4H), 7.49 – 7.38 (m, 3H), 4.05 (t, *J* = 8.3 Hz, 1H), 1.66 (dd, *J* = 16.1, 9.3 Hz, 1H), 1.37 (dd, *J* = 16.1, 7.2 Hz, 1H), 1.12 (d, *J* = 4.6 Hz, 12H). ¹³C NMR (101 MHz, CDCl₃) δ 180.4, 138.0, 133.5, 132.8, 128.4, 128.0, 127.7, 126.7, 126.2, 126.1, 125.9, 83.6, 47.1, 24.8, 24.8, 24.7. HRMS: calculated *m/z* for [C₁₉H₂₂BO₄]⁻: 325.1620, found 325.1618. Enantioselective ratio = 69:31, determined by SFC method A, *t_R* = 9.61 min (major), *t_R* = 9.90 min (minor). [α]_D²⁰ = -34.0 (c = 0.5 g/100mL, CHCl₃)



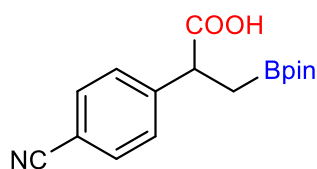
2-(naphthalen-1-yl)-3-(4,4,5,5-tetramethyl-1,3,2-dioxaborolan-2-yl)propanoic acid, 2l. Following the general procedure (method A) starting from 1.27 mmol of corresponding naphthalene the product was obtained as solid white crystals, m.p. = 129.3 – 131.7 °C, yield 41% (0.171 g) ¹H NMR (400 MHz, CDCl₃) δ 8.14 (d, *J* = 8.3 Hz, 1H), 7.84 (d, *J* = 7.9 Hz, 1H), 7.75 (d, *J* = 8.0 Hz, 1H), 7.56 – 7.38 (m, 4H), 4.67 (dd, *J* = 9.4, 6.9 Hz, 1H), 1.72 (dd, *J* = 16.0, 9.4 Hz, 1H), 1.46 – 1.37 (m, 1H), 1.13 – 1.06 (m, 12H). ¹³C NMR (101 MHz, CDCl₃) δ 180.5, 137.0, 134.1, 131.5, 129.0, 127.9, 126.3, 125.7, 125.6, 125.2, 123.7, 83.6, 24.8, 24.6. IR (ATR): 2974 (m), 2925 (br, m), 1702 (s), 1369 (s), 1322 (s), 1295 (s), 1138 (s), 846 (s), 788 (s) cm⁻¹. HRMS: calculated *m/z* for [C₁₉H₂₂BO₄]⁻: 325.1620, found 325.1618. Enantioselective ratio = 63:37, determined by SFC method A, *t_R* = 6.98 min (major), *t_R* = 7.22 min (minor). [α]_D²⁰ = 16.0 (c = 0.5 g/100mL, CHCl₃)



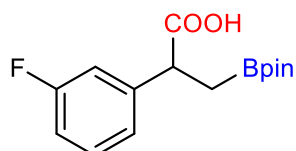
2-(4-fluorophenyl)-3-(4,4,5,5-tetramethyl-1,3,2-dioxaborolan-2-yl)propanoic acid, 2m.^[1] Following the general procedure (method B) starting from 0.63 mmol of corresponding styrene the product was obtained as a faint yellow oil, yield 19% (0.035 g). ¹H NMR (400 MHz, CDCl₃) δ 7.32 – 7.21 (m, 2H), 7.02 – 6.93 (m, 2H), 3.85 (dd, *J* = 8.9, 7.7 Hz, 1H), 1.53 (dd, *J* = 16.0, 8.9 Hz, 1H), 1.33 – 1.24 (m, 1H), 1.14 (d, *J* = 1.9 Hz, 12H). ¹³C NMR (101 MHz, CDCl₃) δ 180.2, 162.2 (d, *J* = 245.6 Hz), 136.1, 129.6 (d, *J* = 8.1 Hz), 115.5 (d, *J* = 21.3 Hz), 83.6, 46.1, 24.8, 24.7. ¹⁹F NMR (377 MHz, CDCl₃) δ -115.6. HRMS: calculated *m/z* for [C₁₅H₁₉BF₄O₄]⁻: 293.1369, found 293.1369. Enantioselective ratio = 89:11, determined by SFC method A, *t_R* = 5.80 min (major), *t_R* = 6.26 min (minor). [α]_D²⁰ = -28.0 (c = 0.5 g/100mL, CHCl₃)



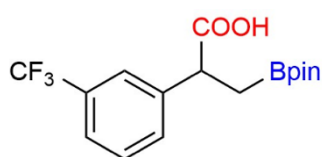
3-(4,4,5,5-tetramethyl-1,3,2-dioxaborolan-2-yl)-2-(4-(trifluoromethyl)phenyl)propanoic acid, 2n.^[2] Following the general procedure (method B) starting from 0.63 mmol of corresponding styrene the product was obtained as faint yellow crystals, yield 48% (0.104 g) ¹H NMR (400 MHz, CDCl₃) δ 7.55 (d, *J* = 8.1 Hz, 2H), 7.42 (d, *J* = 8.0 Hz, 2H), 3.92 (t, *J* = 8.2 Hz, 1H), 1.56 (dd, *J* = 16.1, 9.1 Hz, 1H), 1.29 (dd, *J* = 16.1, 7.5 Hz, 1H), 1.13 (d, *J* = 4.0 Hz, 12H). ¹³C NMR (101 MHz, CDCl₃) δ 179.8, 144.4, 129.7 (q, *J* = 32.4 Hz), 128.5, 125.6 (q, *J* = 3.9 Hz), 122.9, 83.8, 46.8, 24.7, 24.6. ¹⁹F NMR (377 MHz, CDCl₃) δ -62.6. HRMS: calculated *m/z* for [C₁₆H₁₉BF₃O₄]⁻: 343.1337, found 343.1332. Enantioselective ratio = 53:47, determined by SFC method A, *t_R* = 5.09 min (major), *t_R* = 5.41 min (minor). [α]_D²⁰ = -4.0 (c = 0.5 g/100mL, CHCl₃)



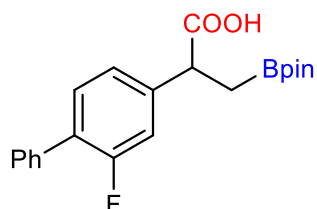
2-(4-cyanophenyl)-3-(4,4,5,5-tetramethyl-1,3,2-dioxaborolan-2-yl)propanoic acid, 2o.^[2] Following the general procedure (method A) starting from 1.27 mmol of corresponding styrene the product was obtained as a yellow powder, yield 67% (0.255 g) ¹H NMR (400 MHz, CDCl₃) δ 7.61 – 7.55 (m, 2H), 7.43 – 7.38 (m, 2H), 3.90 (dd, *J* = 8.8, 7.6 Hz, 1H), 1.53 (dd, *J* = 16.1, 8.8 Hz, 1H), 1.31 – 1.23 (m, 1H), 1.11 (s, 12H). ¹³C NMR (101 MHz, CDCl₃) δ 179.3, 145.7, 132.4, 128.9, 118.7, 111.2, 83.8, 47.0, 24.7, 24.6. HRMS: calculated *m/z* for [C₁₆H₁₉BNO₄]⁻: 300.1416, found 300.1441. Enantioselective ratio = 52:48, determined by SFC method A, *t_R* = 7.55 min (major), *t_R* = 7.74 min (minor). [α]_D²⁰ = 0.0 (*c* = 0.5 g/100mL, CHCl₃)



2-(3-fluorophenyl)-3-(4,4,5,5-tetramethyl-1,3,2-dioxaborolan-2-yl)propanoic acid, 2p.^[1] Following the general procedure (method A) starting from 1.27 mmol of corresponding styrene the product was obtained as a faint orange oil, yield 41% (0.154 g) ¹H NMR (400 MHz, CDCl₃) δ 7.47 – 7.35 (m, 1H), 7.24 (dt, *J* = 7.7, 1.3 Hz, 1H), 7.21 – 7.16 (m, 1H), 7.12 – 7.04 (m, 1H), 4.02 (dd, *J* = 9.1, 7.4 Hz, 1H), 1.69 (dd, *J* = 16.0, 9.2 Hz, 1H), 1.47 – 1.40 (m, 1H), 1.31 (d, *J* = 3.2 Hz, 12H). ¹³C NMR (101 MHz, CDCl₃) δ 180.1, 162.9 (d, *J* = 245.9 Hz), 142.8 (d, *J* = 7.3 Hz), 130.1 (d, *J* = 8.2 Hz), 123.7 (d, *J* = 2.9 Hz), 115.1 (d, *J* = 21.8 Hz), 114.2 (d, *J* = 20.9 Hz), 83.7, 46.7, 24.7, 24.6. ¹⁹F NMR (377 MHz, CDCl₃) δ -113.0. HRMS: calculated *m/z* for [C₁₅H₁₉BFO₄]⁻: 293.1369, found 293.1366. Enantioselective ratio = 73:27, determined by SFC method A, *t_R* = 5.57 min (major), *t_R* = 6.13 min (minor). [α]_D²⁰ = -26.0 (*c* = 0.5 g/100mL, CHCl₃)

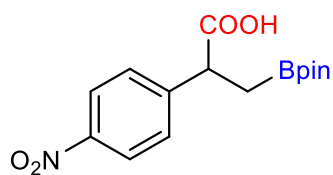


3-(4,4,5,5-tetramethyl-1,3,2-dioxaborolan-2-yl)-2-(3-(trifluoromethyl)phenyl)propanoic acid, 2q. Following the general procedure (method B) starting from 0.63 mmol of corresponding styrene the product was obtained as faint yellow crystals, m.p. = 81.0 – 84.0 °C, yield 48% (0.105 g) ¹H NMR (400 MHz, CDCl₃) δ 7.57 (d, *J* = 2.0 Hz, 1H), 7.53 – 7.48 (m, 2H), 7.41 (t, *J* = 7.7 Hz, 1H), 3.93 (t, *J* = 8.2 Hz, 1H), 1.57 (dd, *J* = 16.0, 8.6 Hz, 1H), 1.32 (dd, *J* = 16.0, 7.9 Hz, 1H), 1.12 (d, *J* = 1.2 Hz, 12H). ¹³C NMR (101 MHz, CDCl₃) δ 180.1, 141.3, 131.4, 130.7 (q, *J* = 32.3 Hz), 129.1, 125.5 (q, *J* = 272.2 Hz), 125.1 (q, *J* = 4.0 Hz), 124.2 (q, *J* = 4.0 Hz), 83.7, 46.8, 24.7, 24.6. ¹⁹F NMR (377 MHz, CDCl₃) δ -62.7. IR (ATR): 2983 (w), 2970 (br, w), 1705 (s), 1326 (s), 1168 (s), 1140 (s), 1121 (s), 1073 (s), 848 (m), 704 (w) cm⁻¹. HRMS: calculated *m/z* for [C₁₆H₁₉BF₃O₄]⁻: 343.1337, found 343.1334. Enantioselective ratio = 68:31, determined by SFC method A, *t_R* = 4.39 min (major), *t_R* = 4.84 min (minor). [α]_D²⁰ = -14.0 (*c* = 0.5 g/100mL, CHCl₃)

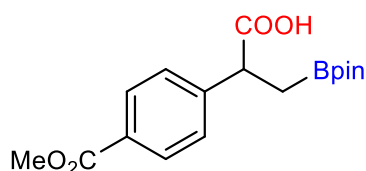


2-(2-fluoro-[1,1'-biphenyl]-4-yl)-3-(4,4,5,5-tetramethyl-1,3,2-dioxaborolan-2-yl)propanoic acid, 2r.^[2] Following the general procedure (method B) starting from 1.27 mmol of corresponding styrene the product was obtained as faint yellow crystals, yield 31% (0.145 g). ¹H NMR (400 MHz, CDCl₃) δ 7.55 – 7.49 (m, 2H), 7.43 (t, *J* = 7.5 Hz, 2H), 7.40 – 7.33 (m, 2H), 7.20 – 7.11 (m, 2H), 3.92 (dd, *J* = 9.2, 7.2 Hz, 1H), 1.59 (dd, *J* = 16.0, 9.2 Hz, 1H), 1.33 (dd, *J* = 16.0, 7.3 Hz, 1H), 1.17 (dd, *J* = 4.5, 2.2 Hz, 12H). ¹³C NMR (101 MHz, CDCl₃) δ 180.3, 159.7 (d, *J* = 248.3 Hz), 141.8 (d, *J* = 7.8 Hz), 135.7, 130.9 (d, *J* = 3.9 Hz), 129.1 (d, *J* = 2.9 Hz), 128.6, 128.0 (d, *J* = 13.6 Hz), 127.8, 124.0 (d, *J* = 3.3 Hz), 115.8 (d, *J* = 23.7 Hz), 83.7, 46.5, 24.8, 24.7. ¹⁹F NMR (377 MHz, CDCl₃) δ -117.73 (t, *J* = 9.7 Hz). HRMS: calculated *m/z* for [C₂₁H₂₃BFO₄]⁻:

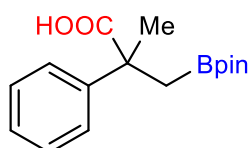
369.1683, found 369.1679. Enantioselective ratio = 65:35, determined by SFC method A, $t_R = 8.66$ min (major), $t_R = 9.46$ min (minor). $[\alpha]_D^{20} = -22.0$ ($c = 0.5$ g/100mL, CHCl_3)



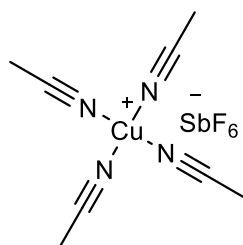
2-(4-nitrophenyl)-3-(4,4,5,5-tetramethyl-1,3,2-dioxaborolan-2-yl)propanoic acid, 2s. Following the general procedure (method A) starting from 1.27 mmol of corresponding styrene the product was obtained as a faint yellow powder, m.p. = 144.2 – 146.4 °C, yield 13% (0.054 g). $^1\text{H NMR}$ (400 MHz, CDCl_3) δ 8.16 (d, $J = 8.4$ Hz, 2H), 7.48 (d, $J = 8.4$ Hz, 2H), 3.98 (t, $J = 8.1$ Hz, 1H), 1.58 (dd, $J = 16.1, 8.8$ Hz, 1H), 1.30 (dd, $J = 16.2, 7.3$ Hz, 1H), 1.13 (s, 12H). $^{13}\text{C NMR}$ (101 MHz, CDCl_3) δ 179.0, 147.7, 147.3, 129.1, 123.9, 83.9, 46.8, 24.7, 24.7. IR (ATR): 2981 (m), 2920 (br, m), 1697 (s), 1600 (w), 1522 (s), 1371 (s), 1344 (s), 1329 (s), 1320 (s), 1141 (s), 848 (s), 839 (m) cm^{-1} . HRMS: calculated m/z for $[\text{C}_{15}\text{H}_{19}\text{BNO}_6]^-$: 320.1314, found 320.1307. Enantioselective ratio = 53:47, determined by SFC method B, $t_R = 5.53$ min (major), $t_R = 5.84$ min (minor). $[\alpha]_D^{20} = -2.0$ ($c = 0.5$ g/100mL, CHCl_3).



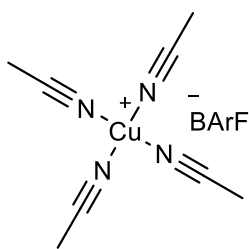
2-(4-(methoxycarbonyl)phenyl)-3-(4,4,5,5-tetramethyl-1,3,2-dioxaborolan-2-yl)propanoic acid, 2t. Following the general procedure (method A) starting from 1.27 mmol of corresponding styrene the product was obtained as faint white crystals, m.p. = 95.6 – 97.5 °C, yield 38% (0.160 g). $^1\text{H NMR}$ (400 MHz, CDCl_3) δ 7.97 (d, $J = 7.9$ Hz, 2H), 7.38 (d, $J = 8.1$ Hz, 2H), 3.96 – 3.91 (m, 1H), 3.90 (s, 3H), 1.56 (dd, $J = 16.1, 8.9$ Hz, 1H), 1.30 (dd, $J = 16.0, 7.6$ Hz, 1H), 1.13 (s, 12H). $^{13}\text{C NMR}$ (101 MHz, CDCl_3) δ 179.6, 167.0, 145.6, 130.0, 129.2, 128.1, 83.7, 52.2, 46.9, 24.8, 24.7. IR (ATR): 2975 (w), 2965 (br, w), 1721 (s), 1698 (s), 1369 (m), 1283 (s), 1189 (m), 1140 (m), 1108 (m), 1100 (m), 847 (w), 719 (w) cm^{-1} . HRMS: calculated m/z for $[\text{C}_{17}\text{H}_{22}\text{BO}_6]^-$: 333.1518, found 333.1515. Enantioselective ratio = 51:49, determined by SFC method A, $t_R = 7.56$ min (major), $t_R = 8.15$ min (minor). $[\alpha]_D^{20} = -2.0$ ($c = 0.5$ g/100mL, CHCl_3)



2-methyl-2-phenyl-3-(4,4,5,5-tetramethyl-1,3,2-dioxaborolan-2-yl)propanoic acid, 2u. Following the general procedure (method B) starting from 1.27 mmol of corresponding styrene no reaction was observed, yield 0%.

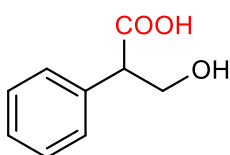


tetrakis(acetonitrile)copper(I)hexafluoroantimonate, 2ab.^[3] To a glovebox, two dried 50 mL round bottom flasks were introduced. One was charged with 1 mmol of CuCl and the other with 1 mmol of silver(I) hexafluoroantimonate. Both round bottom flasks were sealed in argon atmosphere using a rubber septa and tape. After that 10mL of dried acetonitrile was added to both round bottom flasks and they were left stirring for 30 minutes. Then the silver(I) hexafluoroantimonate solution was slowly dripped to the CuCl solution, and white AgCl precipitate was observed during the addition. After addition the solution was left stirring for 1h. After stirring the solution was filtered and the organic solution was then evaporated to give a white solid, yield of 99.5% (0.470 g) $^1\text{H NMR}$ (400 MHz, CD_3CN) δ 1.96 (s, 12H). $^{13}\text{C NMR}$ (101 MHz, CD_3CN) δ 235.4, 118.7. $^{19}\text{F NMR}$ (377 MHz, CD_3CN) δ -108.6 – 139.0 (m).



tetrakis(acetonitrile)copper(I)tetrakis[3,5-bis(trifluoromethyl)phenyl]borate, 2ac.^[3] To a glovebox two dry 50 mL round bottom flasks were introduced. One was charged with CuCl (0.060 g, 0.606 mmol) and the other with NaBARF (0.537 g, 0.606 mmol). Both flasks were sealed under argon atmosphere and added 10 mL of dry acetonitrile. The flask with the NaBARF mixture was heated to 60 degrees and the CuCl solution was slowly dripped to the solution using a syringe while stirring. After the addition of NaBARF, the reaction mixture was

left stirring for 24 h. When the reaction was finished the NaCl precipitate was filtered off and the organic mixture was evaporated to dryness giving a brown oil 99.9% yield (0.663 g) ¹H NMR (400 MHz, CD₃CN) δ 7.85 – 7.79 (m, 8H), 7.74 (s, 4H), 2.01 (s, 12H). ¹³C NMR (101 MHz, CD₃CN) δ 280.7 – 279.0 (m), 252.8, 247.7 – 246.5 (m), 242.6 (q, *J* = 271.9 Hz), 235.7 (hept, *J* = 3.9 Hz), 235.2. ¹⁹F NMR (377 MHz, CD₃CN) δ -63.3.



3-hydroxy-2-phenylpropanoic acid, 3j.^[1] To a 100mL round bottom flask **2j** (0.251 mg, 0.909 mmol) was added and dissolved in 20 mL of THF/water solution (1:1). The reaction mixture was added 5 equiv. of sodium perborate tetrahydrate (0.977 mg, 6.350 mmol) and left stirring for 3h. After stirring the flask was opened and diluted using 20 mL of Et₂O. The organic mixture was then

extracted using a solution of saturated NaHCO₂ (3x30 mL). Then the aqueous solution was first acidified by slow addition of 60 mL 6M HCl, then extracted using Et₂O (3x30 mL). The organic solution was then washed using 30 mL of distilled water. After washing the organic solution was evaporated to dryness yielding a crystalline white solid 80% yield (0.121 mg). ¹H NMR (400 MHz, MeOD) δ 7.29 (dd, *J* = 22.7, 4.9 Hz, 5H), 4.09 (q, *J* = 7.5, 6.6 Hz, 1H), 3.84 – 3.64 (m, 2H). ¹³C NMR (101 MHz, MeOD) δ 176.1, 137.9, 129.7, 129.2, 128.5, 65.1, 55.8. HRMS: calculated *m/z* for [C₉H₉O₃]⁻: 165.0557, found 165.0557. Enantioselective ratio = 80:20, determined by SFC method A, *t_R* = 5.25 min (major), *t_R* = 5.57 min (minor). [α]_D²⁰ = - 12 (c = 0.5, MeOH)

2 Computational data

2.1 General considerations

All molecules were calculated with no truncations or symmetry constraints, using the Gaussian 16 program, revision B.01.^[4] Geometries were optimized at the PBE^[5] level of theory with the 6-31+G* basis set^[6] (using the SDD ECP for Cu), including the D3BJ dispersion correction by Grimme.^[7] The solvation effects were included implicitly using the polarizable continuum model (PCM) with the parameters for THF.^[8] Transition states and minima were confirmed through frequency calculations (no imaginary frequencies for minima, one imaginary frequency for transition states). Single point energies were computed with the PC-2^[9] basis set. All Gibbs free energies are given at 298.15K and 1atm. The theoretical predicted e.r. was determined using a modified version of the Eyring equation.^[10] The equation is as follows:

$$ee_{theo}(\%) = \frac{1 - e\left(-\frac{\Delta\Delta G_{R/S}^{\ddagger}}{RT}\right)}{1 + e\left(-\frac{\Delta\Delta G_{R/S}^{\ddagger}}{RT}\right)} \cdot 100 \quad \text{Equation 1}$$

2.2 Mechanistic studies of the boracarboxylation with (*S,S*)-BDPP as ligand

The following figures and table (Figures S10, S11 and Table S10) show the calculations for the full mechanism using (*S,S*)-BDPP instead of (*S,S*)-QuinoxP*.

Similarly to the reaction with (*S,S*)-QuinoxP*, there is a very low barrier for the insertion of the substrate into the Cu-B bond (1.1 to 3.8 kcal/mol depending on the resulting stereoisomer (**Figure S10**). The interconversion barrier between intermediates C_R and C_S is also low enough to be reachable at room temperature, meaning that the two intermediates can interconvert.

For the CO₂ insertion step with (*S,S*)-BDPP as ligand (**Figure S11**), the lowest energy pathway seems to be the one going from intermediate C_R through an outer sphere pathway to product D_S .

The choice of solvent (THF or anisole) does not affect the final computed *e.r.* of the reaction (**Table S10**).

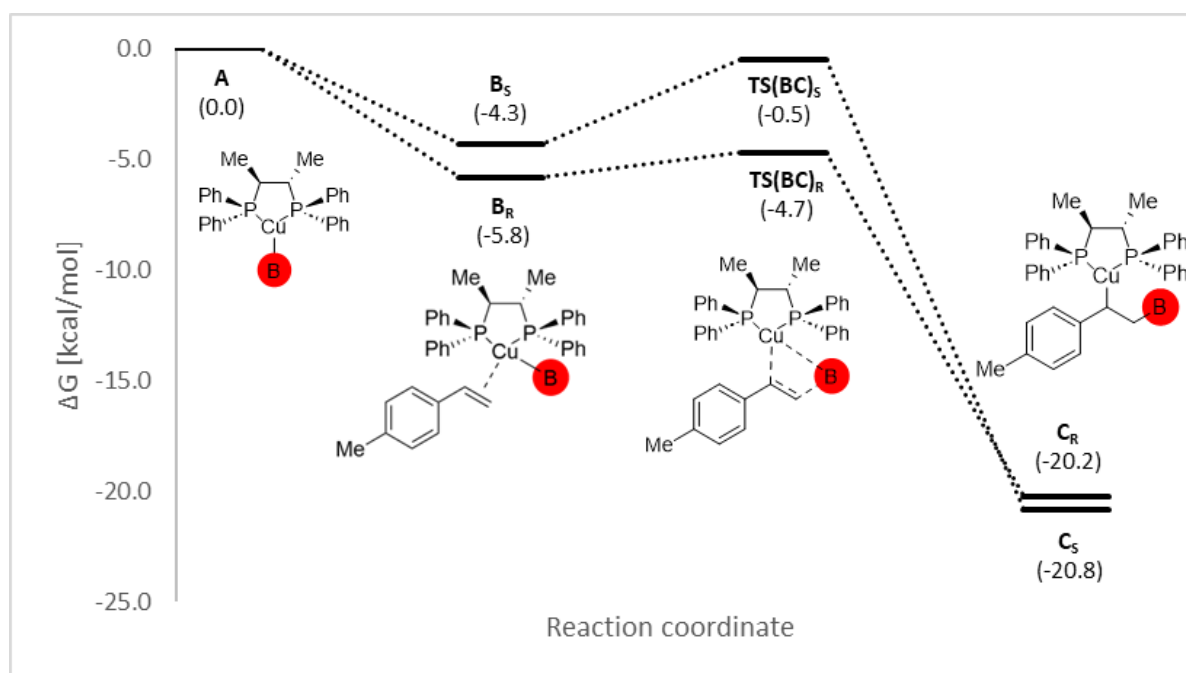


Figure S10. Gibbs free energy profile (PBE-D3BJ/PC-2//PBE-D3BJ/6-31+G*(SDD ECP and basis set for Cu), IEFPCM:THF, 298.15K) for the coordination of the p-methylstyrene to reagent A (with (*S,S*)-BDPP as ligand), followed by the formation of intermediate C. The calculated relative free energies (in kcal/mol) are in parentheses.

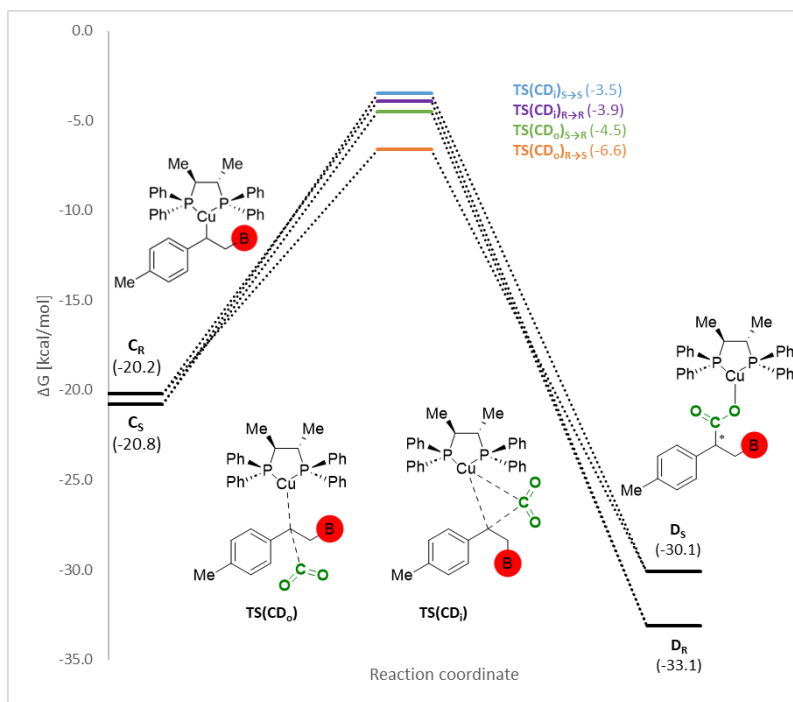
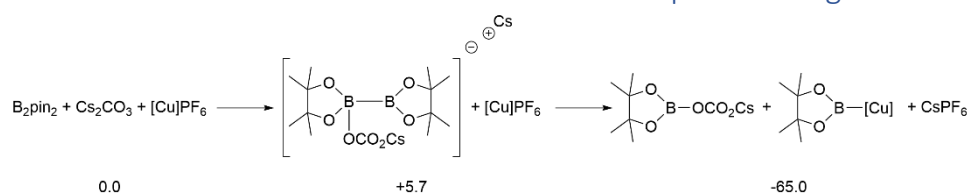


Figure S11. Gibbs free energy profile for the insertion of CO₂ into the diastereomeric C intermediates (kcal/mol, PBE-D3BJ/PC-2//PBE-D3BJ/6-31+G*(SDD ECP and basis set for Cu), IEFPCM:THF, 298.15K, energies are given relative to A), with (S,S)-BDPP as ligand. TS(CD_i) refers to inner sphere transition states, and TS(CD_o) refers to outer sphere transition states.

Table S10. Comparison of Gibbs free energies (kcal/mol) for the reaction (with (S,S)-BDPP as ligand), using THF or anisole as solvent (PBE-D3BJ/PC-2//PBE-D3BJ/6-31+G*(SDD ECP and basis set for Cu), IEFPCM, 298.15K).

	THF ($\epsilon = 7.4257$)	Anisole ($\epsilon = 4.2247$)
A	0.0	0.0
B_R	-5.8	-6.8
B_S	-4.3	-5.7
TS(BC)_R	-4.7	0.1
TS(BC)_S	-0.5	-1.1
C_R	-20.2	-21.1
C_S	-20.8	-21.5
TS(CD_i)_{R→R}	-3.9	-4.5
TS(CD_o)_{R→S}	-6.6	-7.4
TS(CD_o)_{S→R}	-4.5	-5.3
TS(CD_i)_{S→S}	-3.5	-3.1
D_R	-33.1	-32.6
D_S	-30.1	-31.7
Predicted e.r.	98:2 (S)	97:3 (S)

2.3 Mechanistic studies of the formation of the boracupration reagent



Scheme S1. Proposed formation of copper borate **A** (mechanism based on literature proposal^[11]) with calculated Gibbs free energies in kcal/mol relative to the starting reagents (PBE-D3BJ/PC-2//PBE-D3BJ/6-31+G*(SDD ECP and basis set for Cu), IEFPCM:THF, 298.15K).

2.4 Evaluation of solvent effects on the boracarboxylation

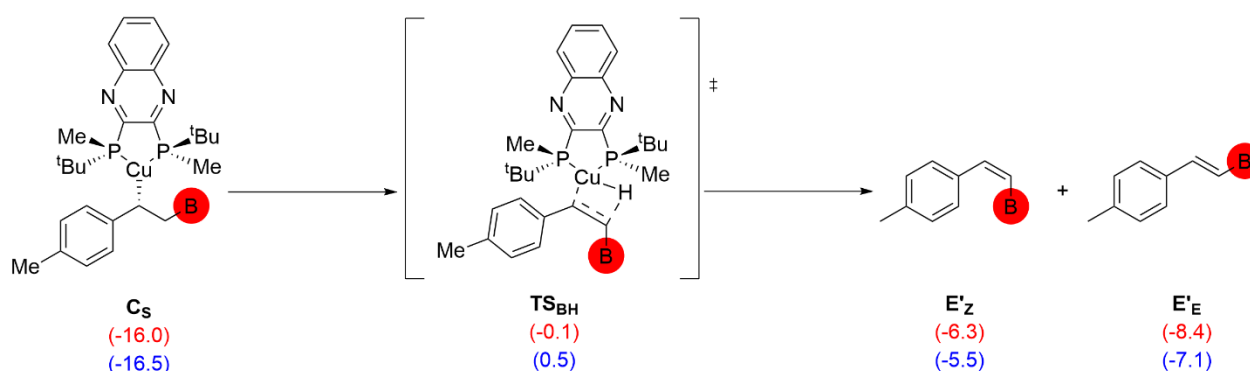
Table S11. Comparison of Gibbs free energies (kcal/mol, relative to **A**) for the reaction, using THF or anisole as solvent within the IEFPCM model (PBE-D3BJ/PC-2//PBE-D3BJ/6-31+G*(SDD ECP and basis set for Cu), IEFPCM:THF, 298.15K).

	THF ($\epsilon = 7.4257$)	Anisole ($\epsilon = 4.2247$)
A	0.0	0.0
B_R	-2.3	-3.2
B_S	-0.9	-1.6
TS(BC)_R	0.0	-0.9
TS(BC)_S	2.4	1.8
C_R	-15.2	-15.8
C_S	-16.5	-16.0
TS(CD_i)_{R→R}	-1.1	-1.5
TS(CD_o)_{R→S}	-1.2	-1.7
TS(CD_o)_{S→R}	-2.9	-3.1
TS(CD_i)_{S→S}	0.9	0.7
D_R	-29.8	-31.8
D_S	-31.0	-31.3

Table S12. Comparison of Gibbs free energy barriers (kcal/mol, relative to **C**) for the CO₂ insertion step and resulting theoretical enantiomeric ratio, using THF or anisole as solvent (PBE-D3BJ/PC-2//PBE-D3BJ/6-31+G*(SDD ECP and basis set for Cu), IEFPCM, 298.15K).

	THF ($\epsilon = 7.4257$)	Anisole ($\epsilon = 4.2247$)
C_R to TS(CD_i)_{R→R}	14.1	14.3
C_R to TS(CD_o)_{R→S}	14.0	14.0
C_R to TS(CD_o)_{S→R}	13.7	13.0
C_R to TS(CD_i)_{S→S}	17.4	16.7
Predicted e.r.	71:29 (R)	87:13 (R)

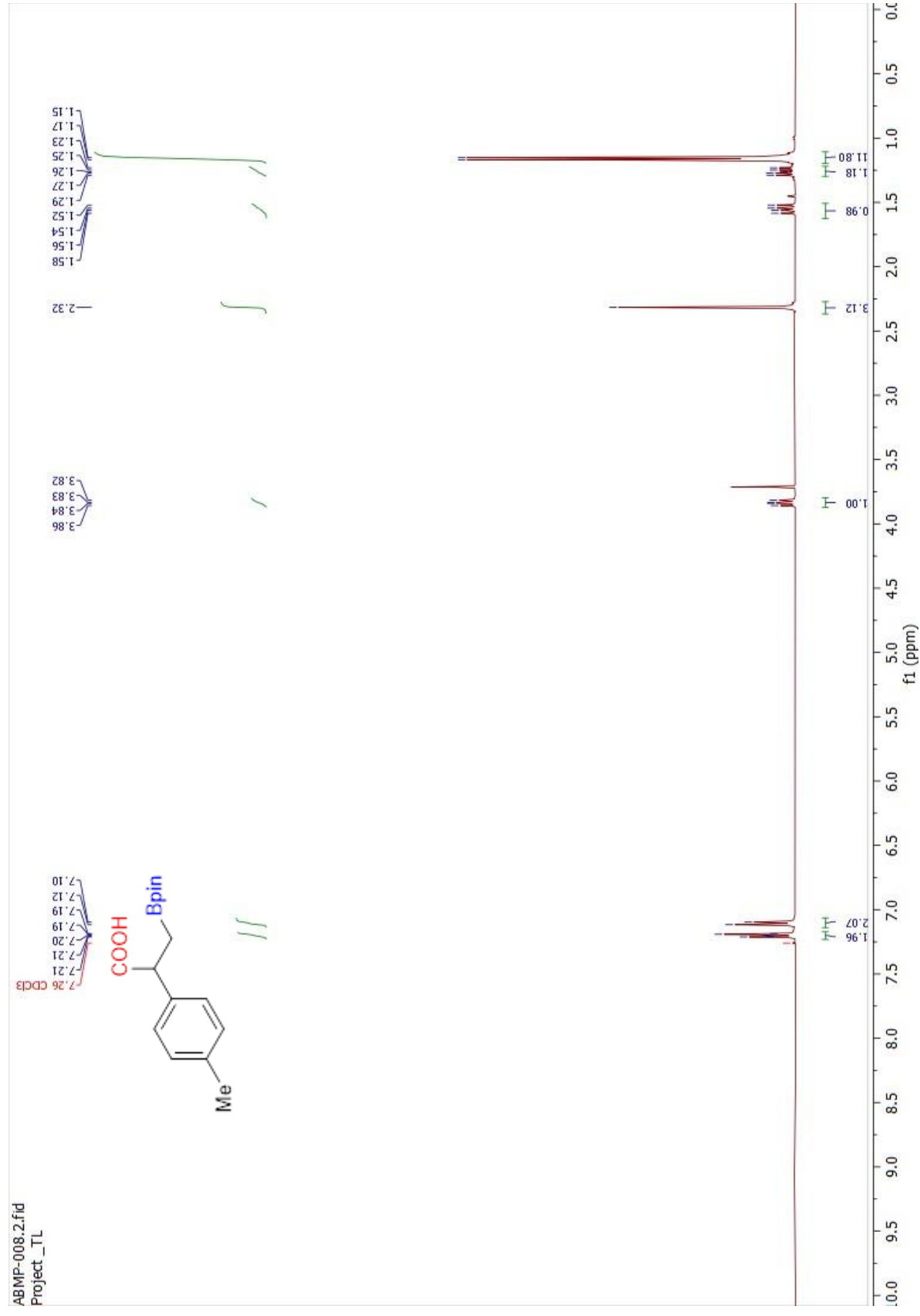
2.5 Mechanistic study of the β -hydride side reaction



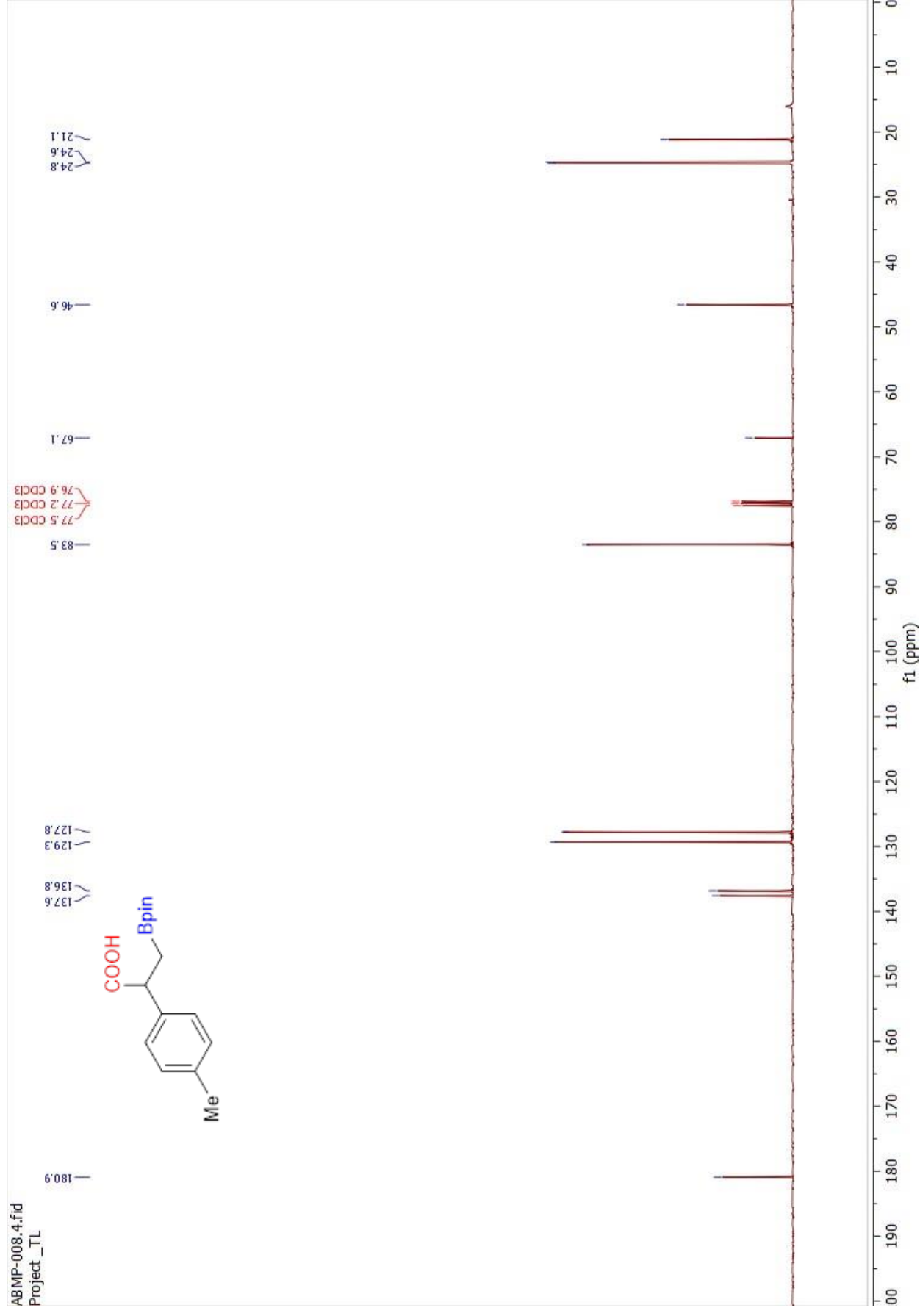
Scheme S2. Possible mechanism and calculated Gibbs free energies (kcal/mol, PBE-D3BJ/PC-2//PBE-D3BJ/6-31+G*(SDD ECP and basis set for Cu), IEFPCM, 298.15K, energies are given relative to **A**) for the β -H elimination pathway from intermediate **C_S**, leading to products **E'_Z** and **E'_E**. The Gibbs free energies in red are for IEFPCM:anisole, the ones in blue are for IEFPCM:THF.

3 Documentation of analytical data

Spectrum S1. ^1H NMR of compound **2a** in CDCl_3



Spectrum S2. ^{13}C NMR of compound **2a** in CDCl_3



Chromatogram S1. Compound 2a and its racemate.

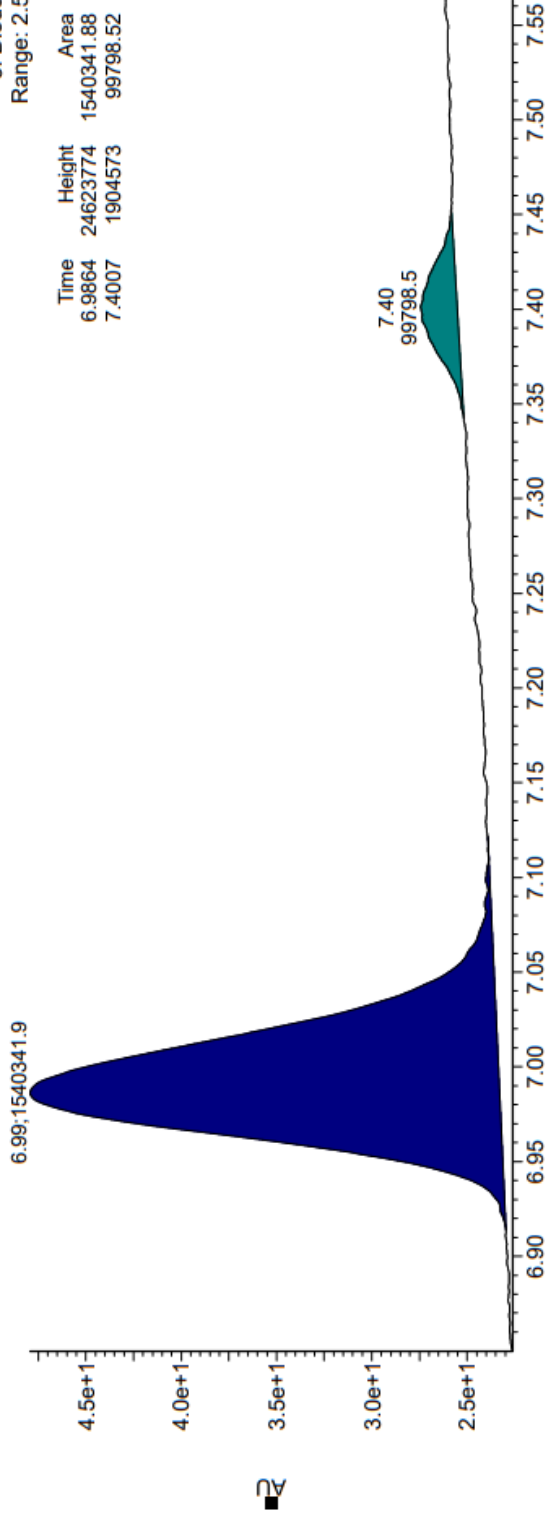
Amy1_iPrOH 0.5% TFA Chiral Separation

31-Mar-2023
14:06:27

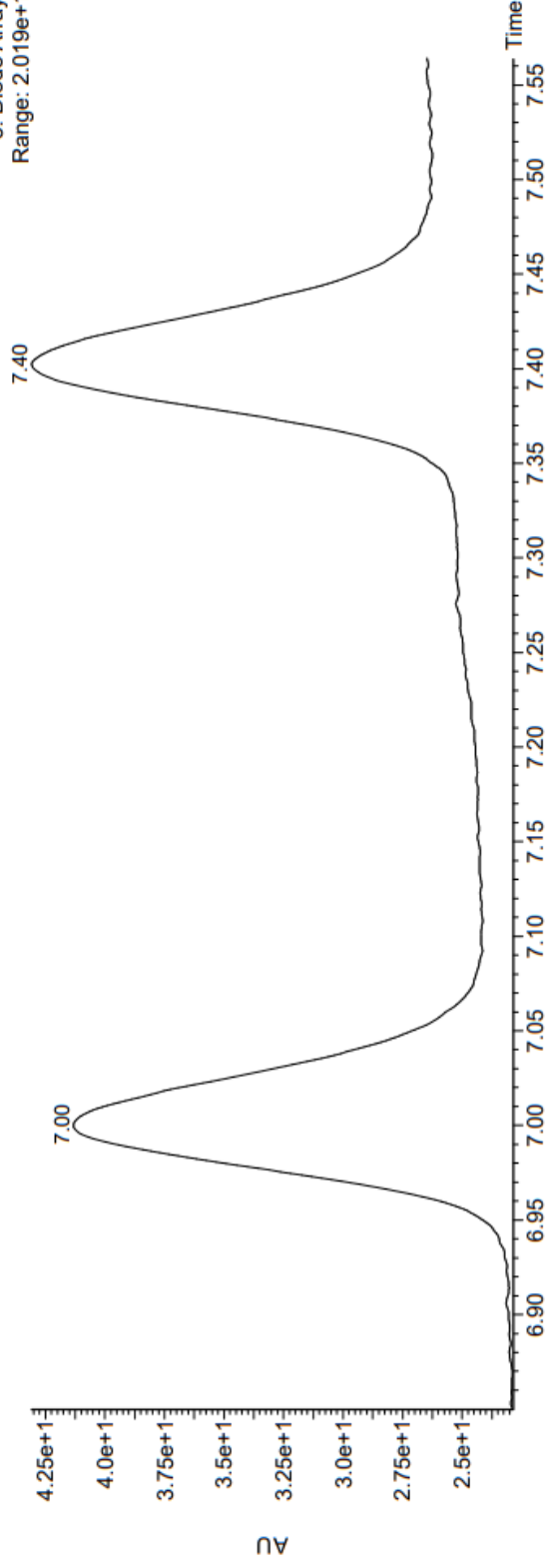
UPC2

3: Diode Array
Range: 2.526e+1

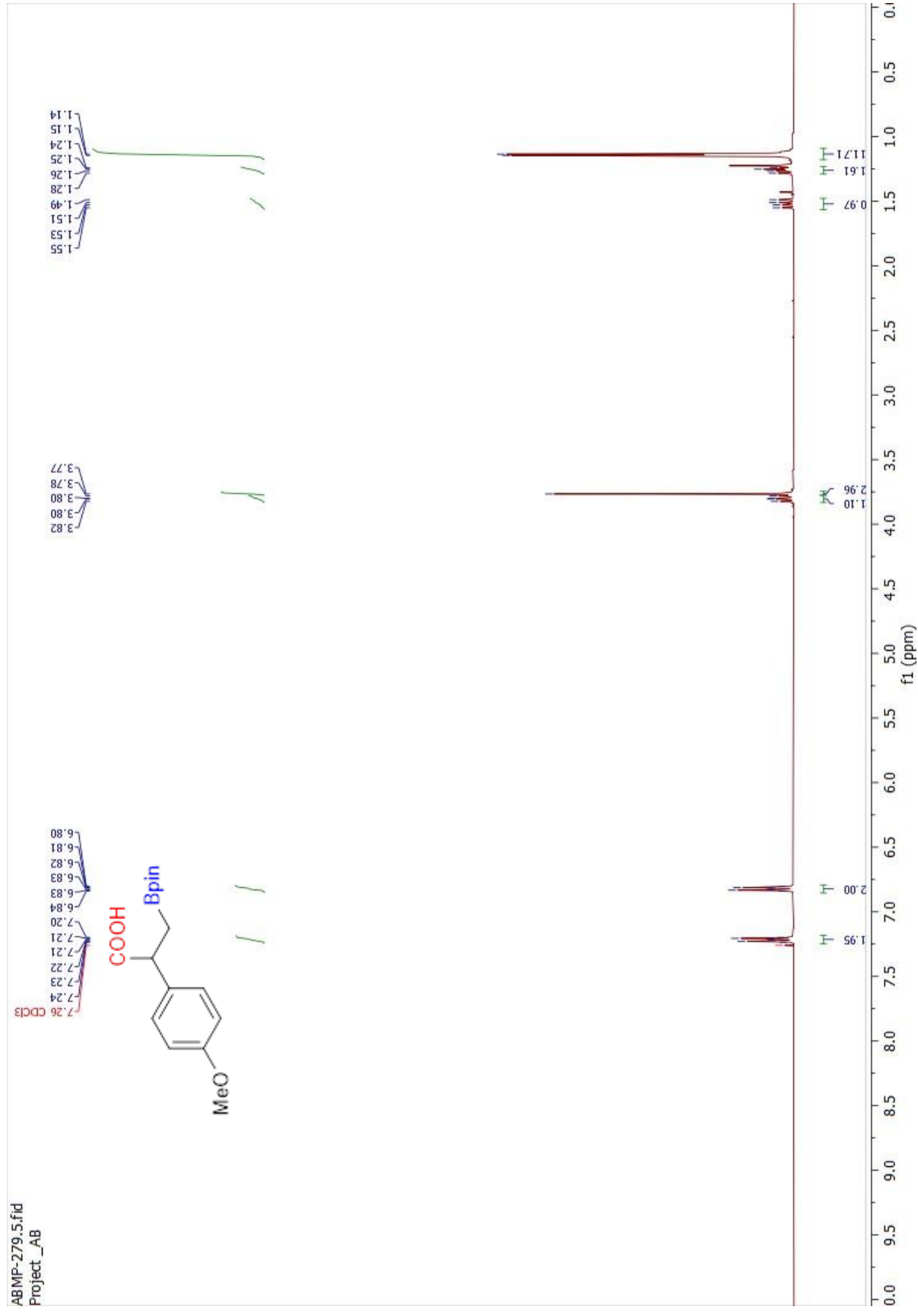
Time	Height	Area	Area%
6.9864	24623774	1540341.88	93.92
7.4007	1904573	99798.52	6.08



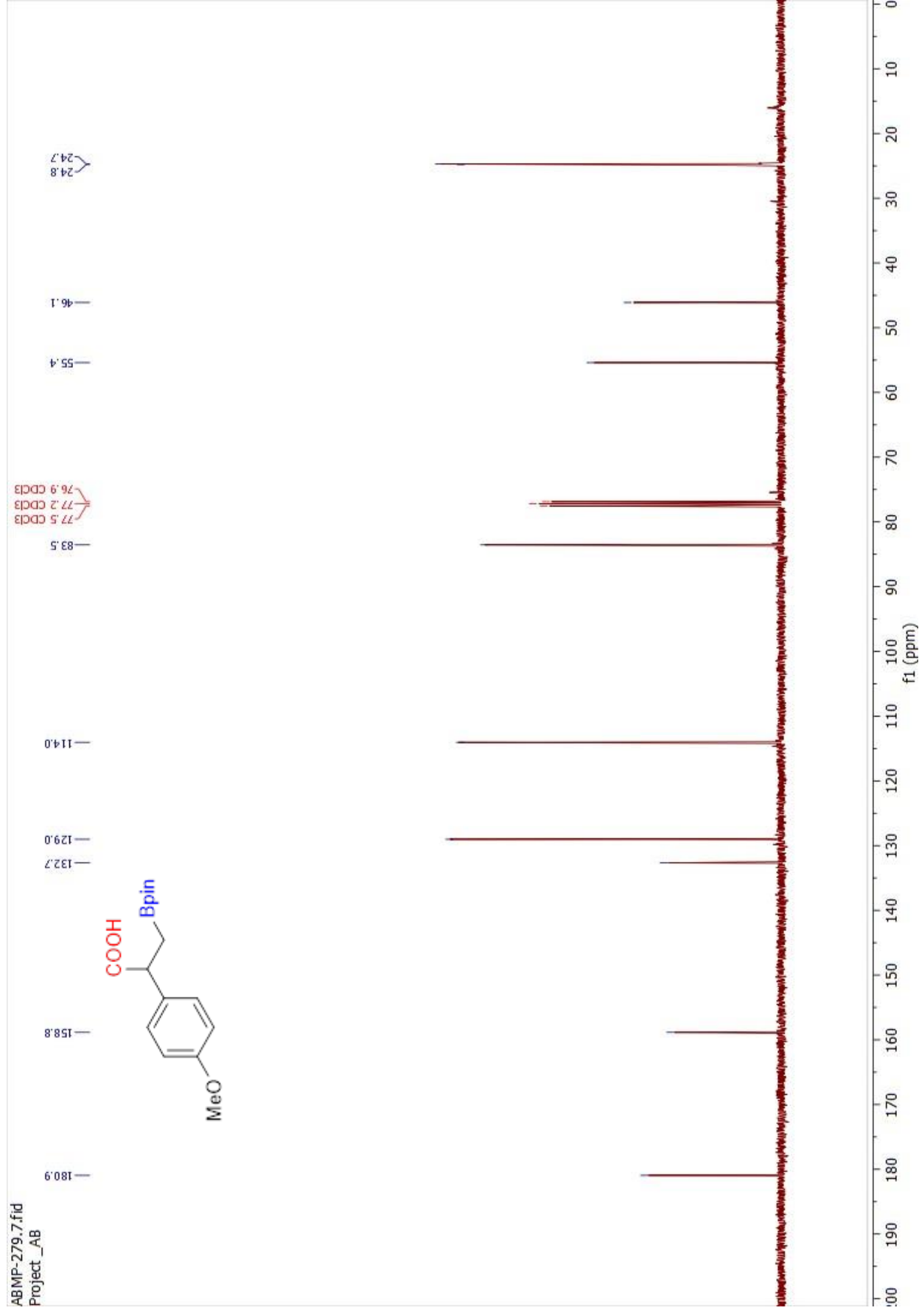
3: Diode Array
Range: 2.019e+1



Spectrum S3. ^1H NMR of compound **2b** in CDCl_3



Spectrum S4. ^{13}C NMR of compound **2b** in CDCl_3



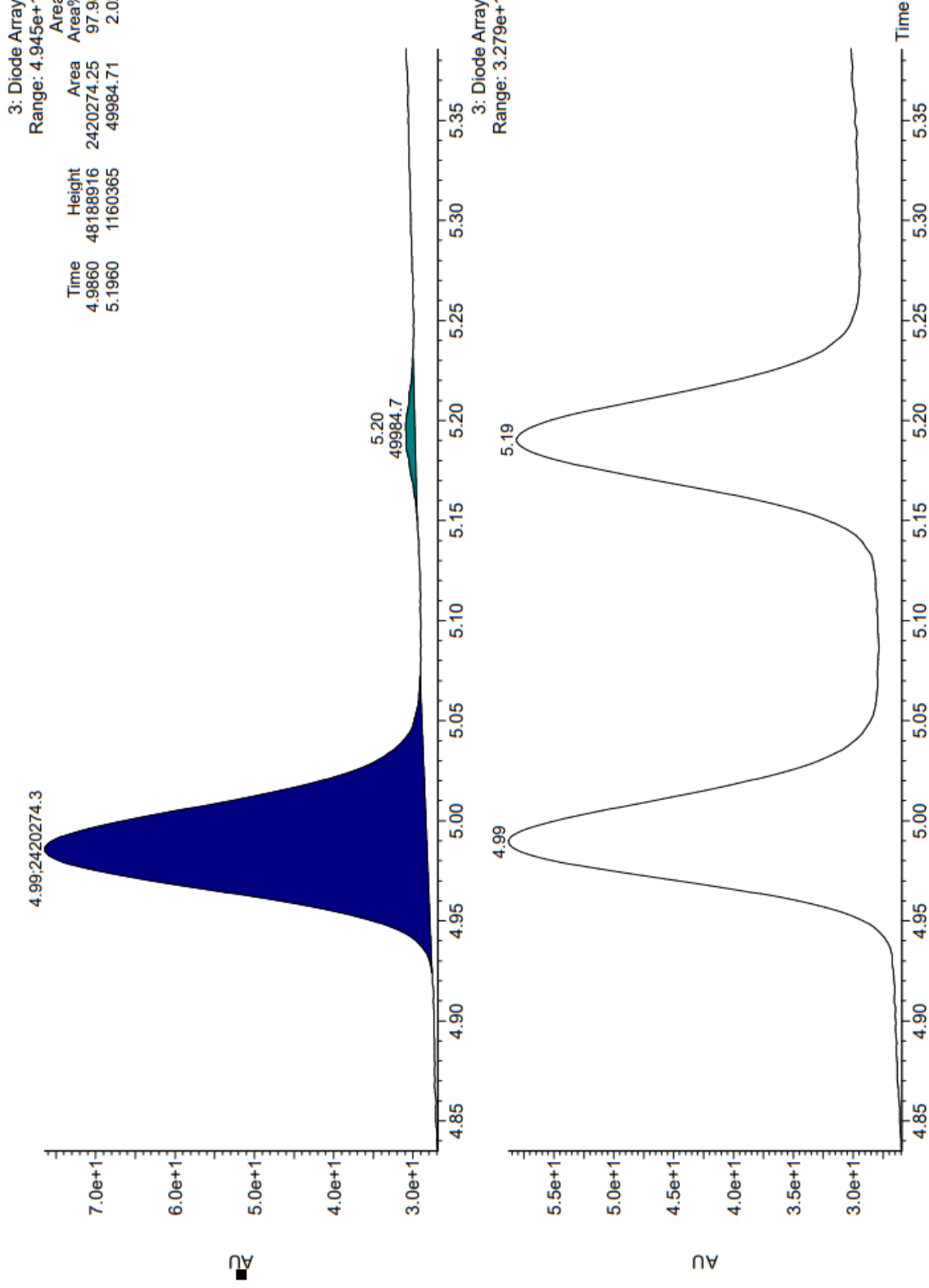
Chromatogram S2. Compound **2b** and its racemate.

Cel1_iPrOH 0.5% TFA Chiral Separation

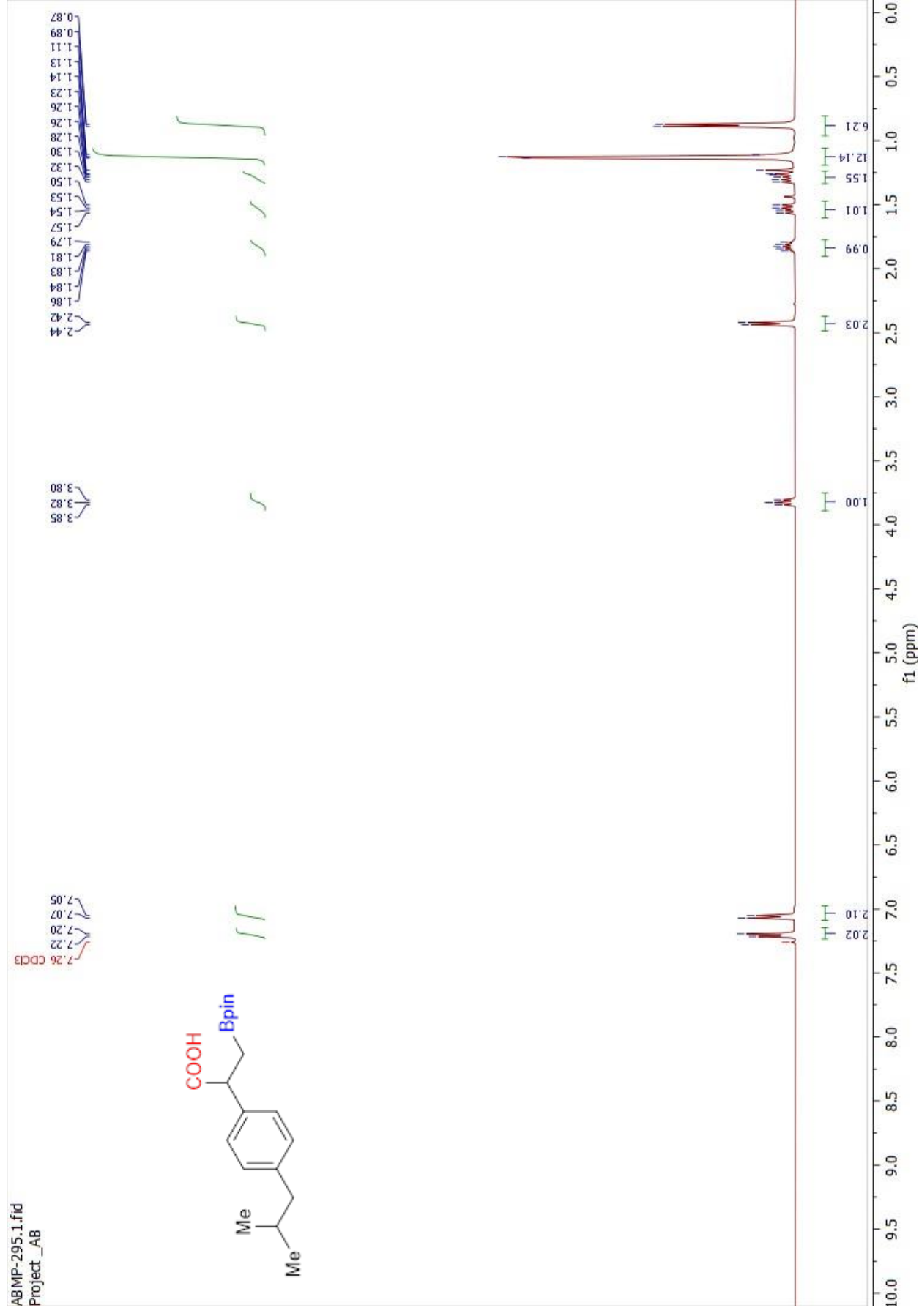
30-Mar-2023
09:52:29

UPC2

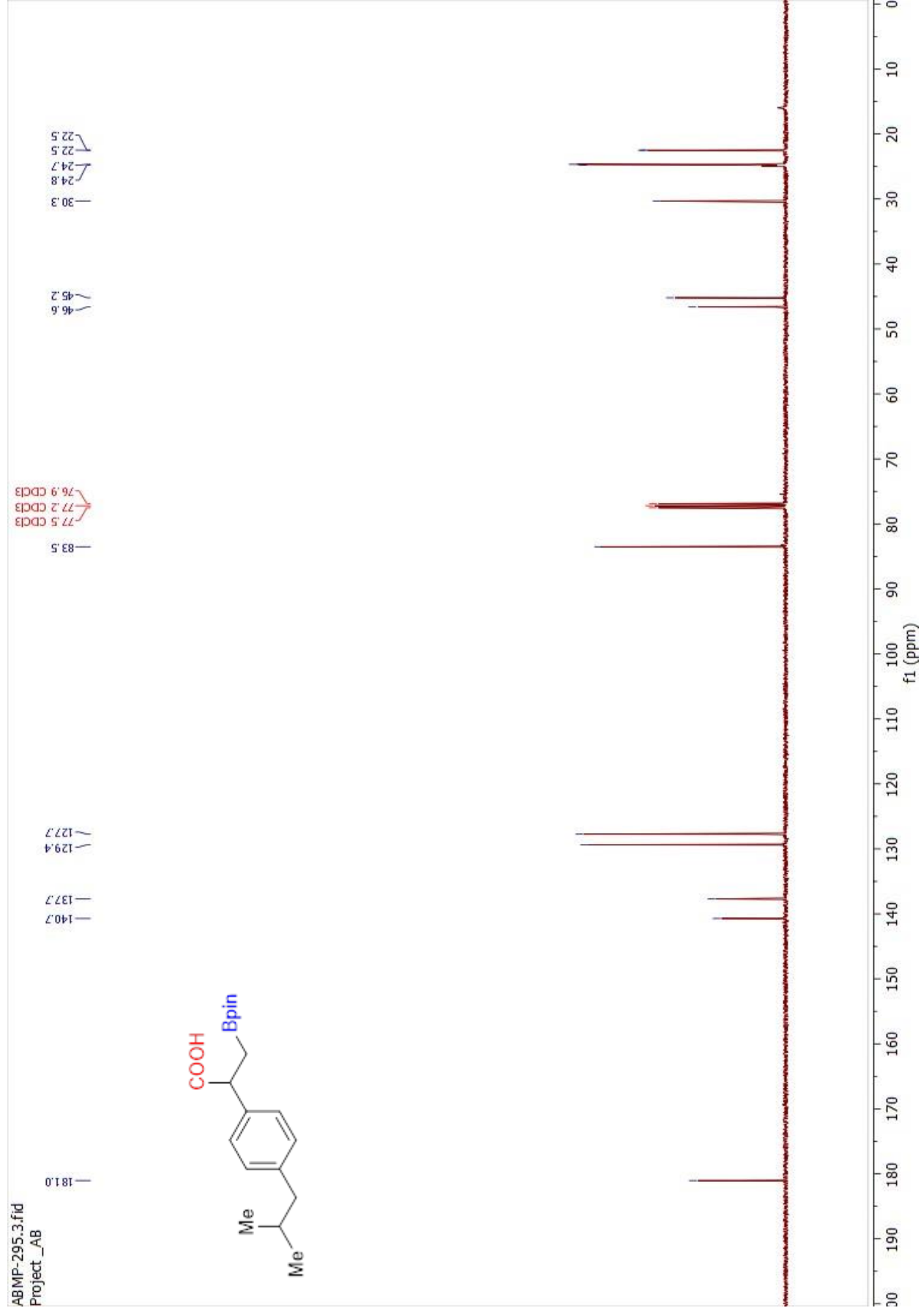
Time	Height	Area	Area%
4.9860	48188916	2420274.25	97.98
5.1960	1160365	49984.71	2.02



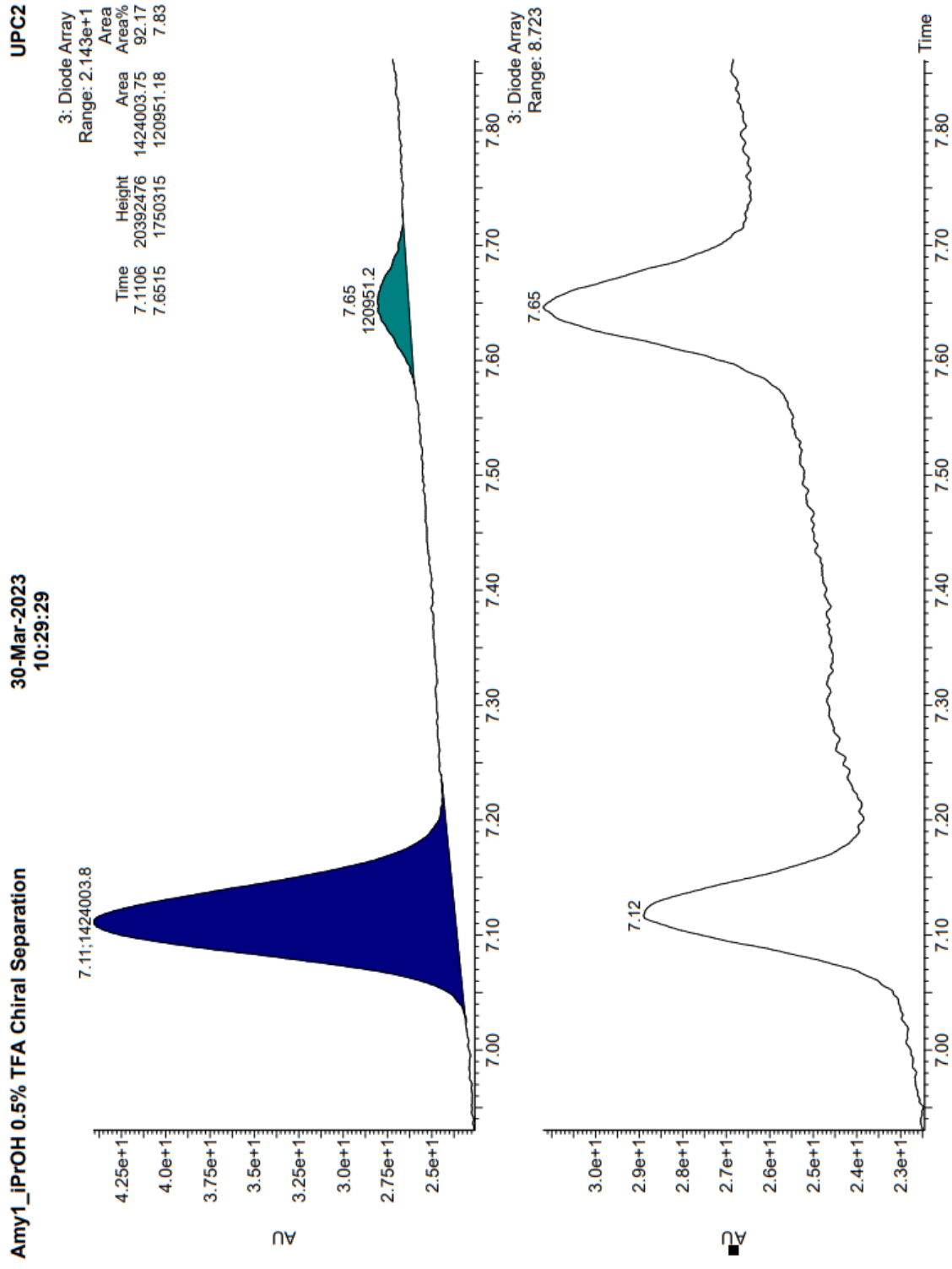
Spectrum S5. ¹H NMR of compound 2c in CDCl₃



Spectrum S6. ^{13}C NMR of compound **2c** in CDCl_3

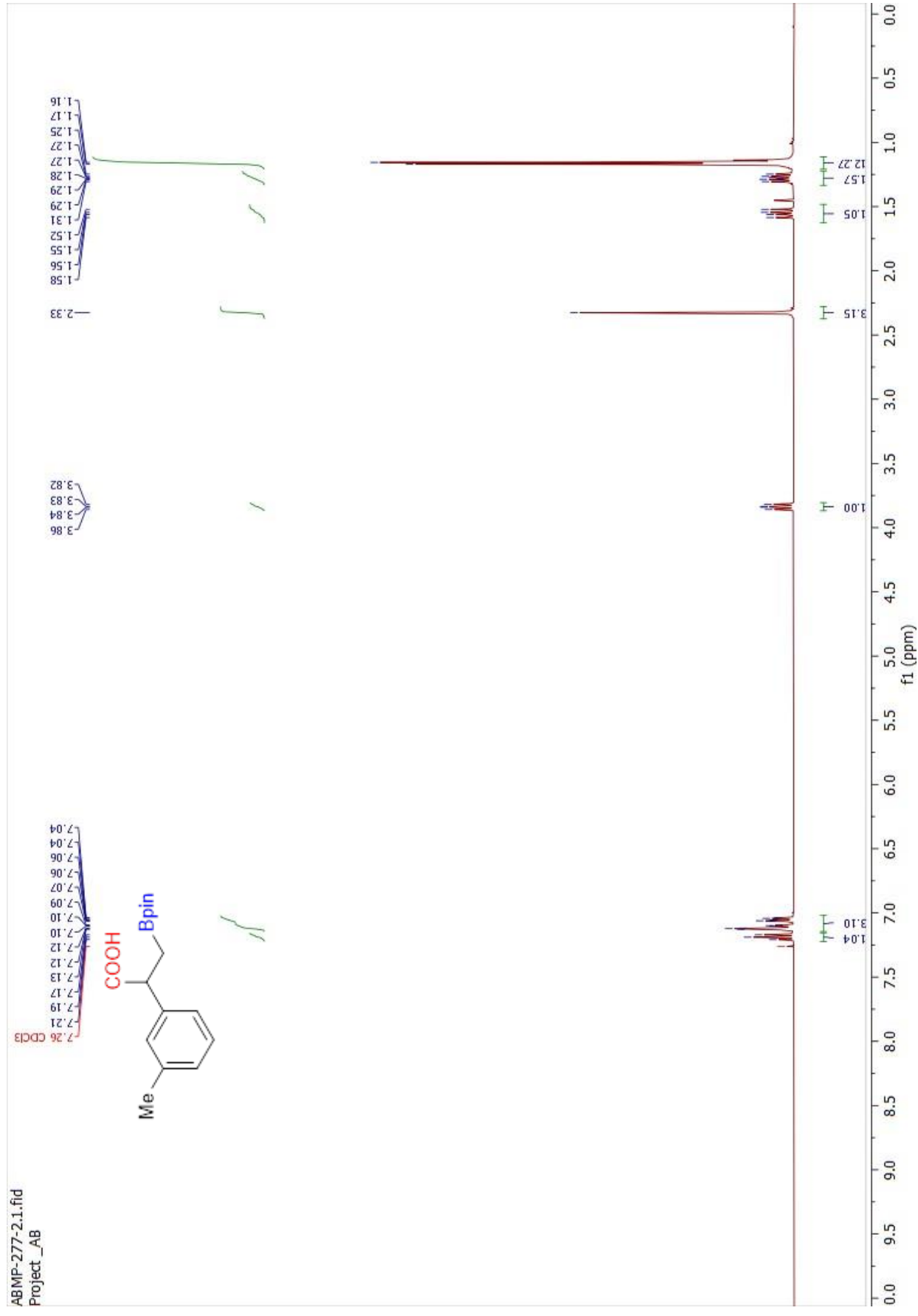


Chromatogram S3. Compound 2c and its racemate.

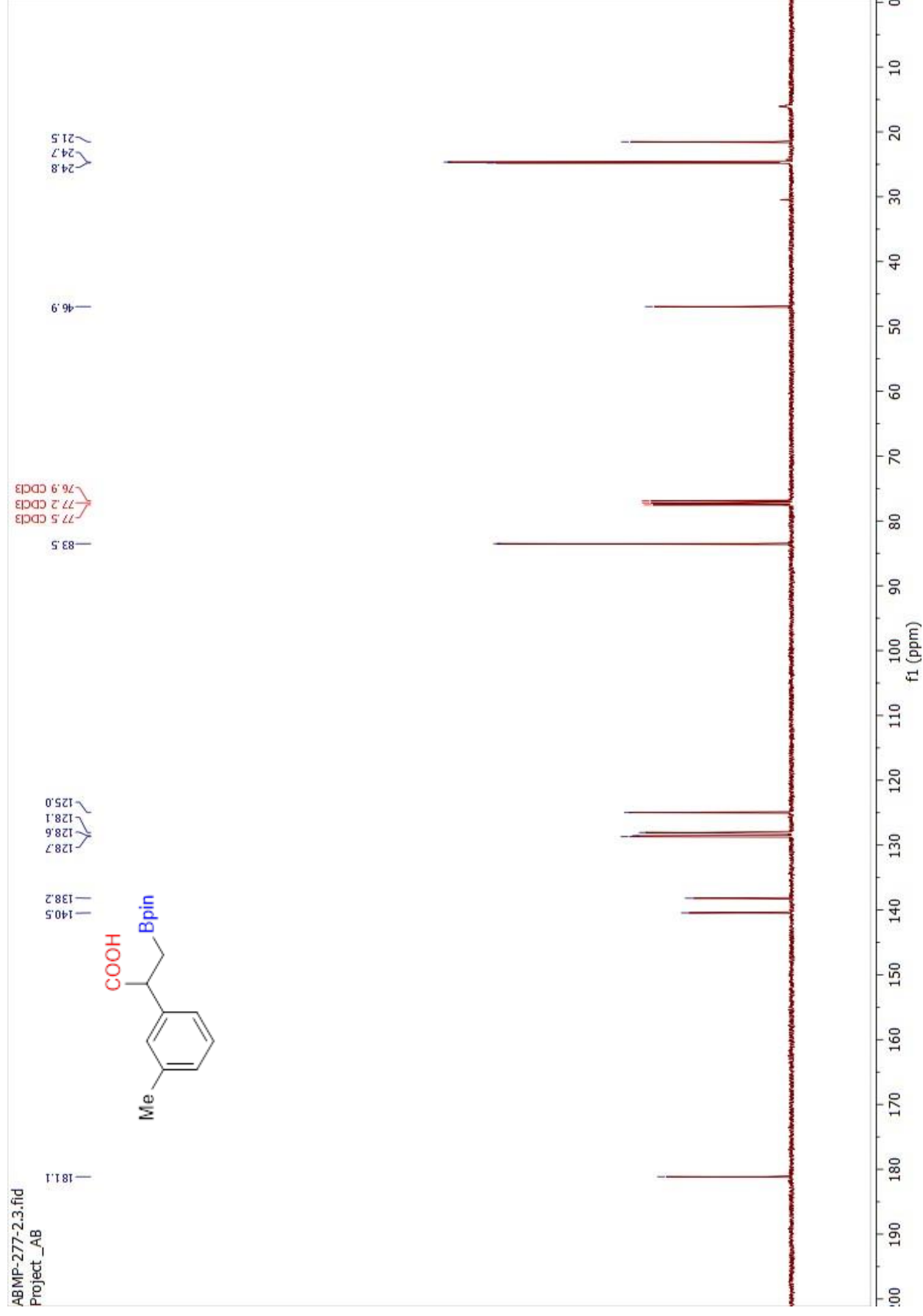


Spectrum S7. ¹H NMR of compound 2d in CDCl₃

ABMP-277-2.1.fid
Project_AB



Spectrum S8. ^{13}C NMR of compound **2d** in CDCl_3



Chromatogram S4. Compound 2d and its racemate.

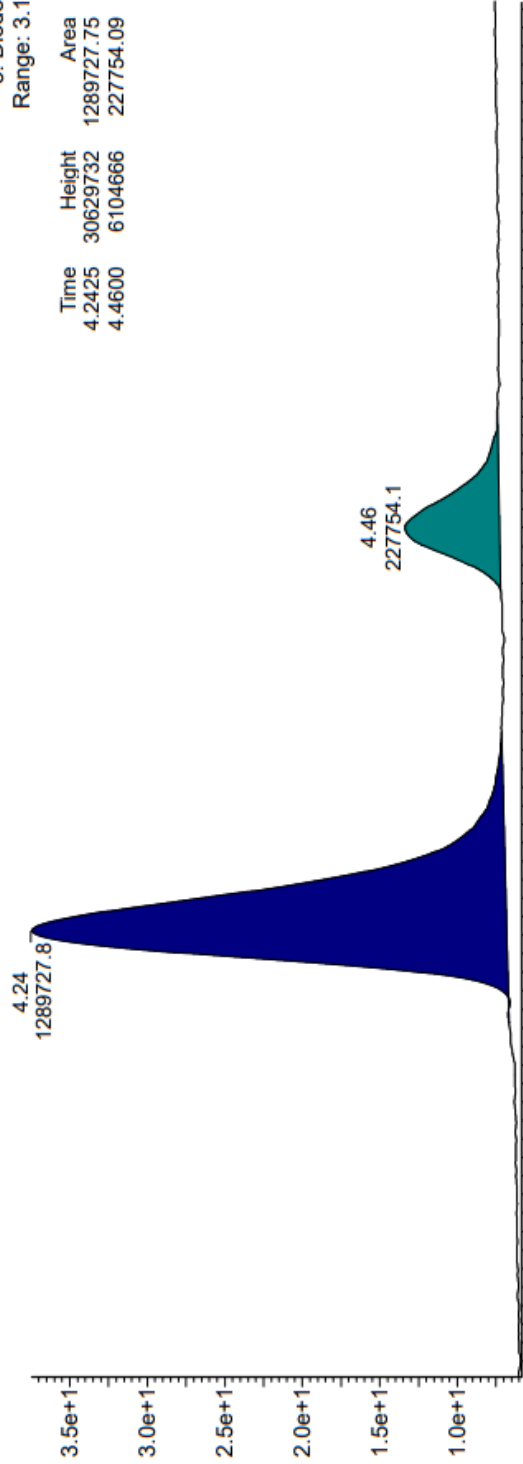
Cel2_iPrOH 0.2% TFA Chiral Separation

20-Jul-2022
14:38:38

UPC2

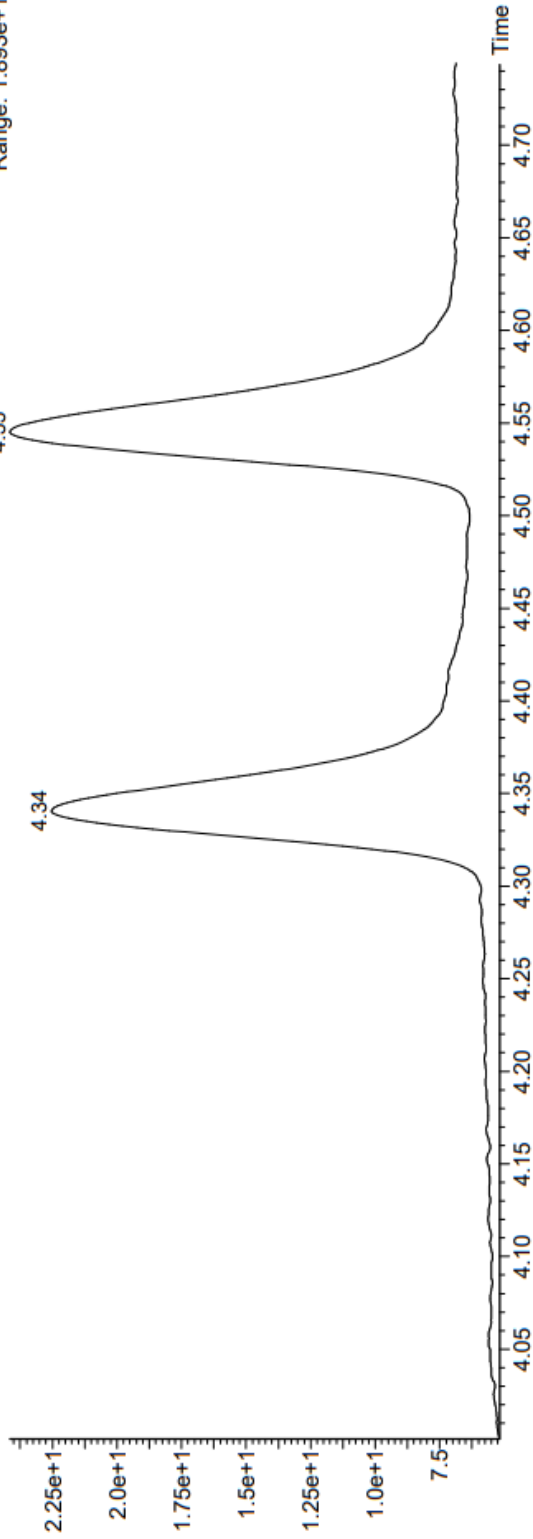
Time	Height	Area	Area%
4.2425	30629732	1289727.75	84.99
4.4600	6104666	227754.09	15.01

3: Diode Array
Range: 3.154e+1



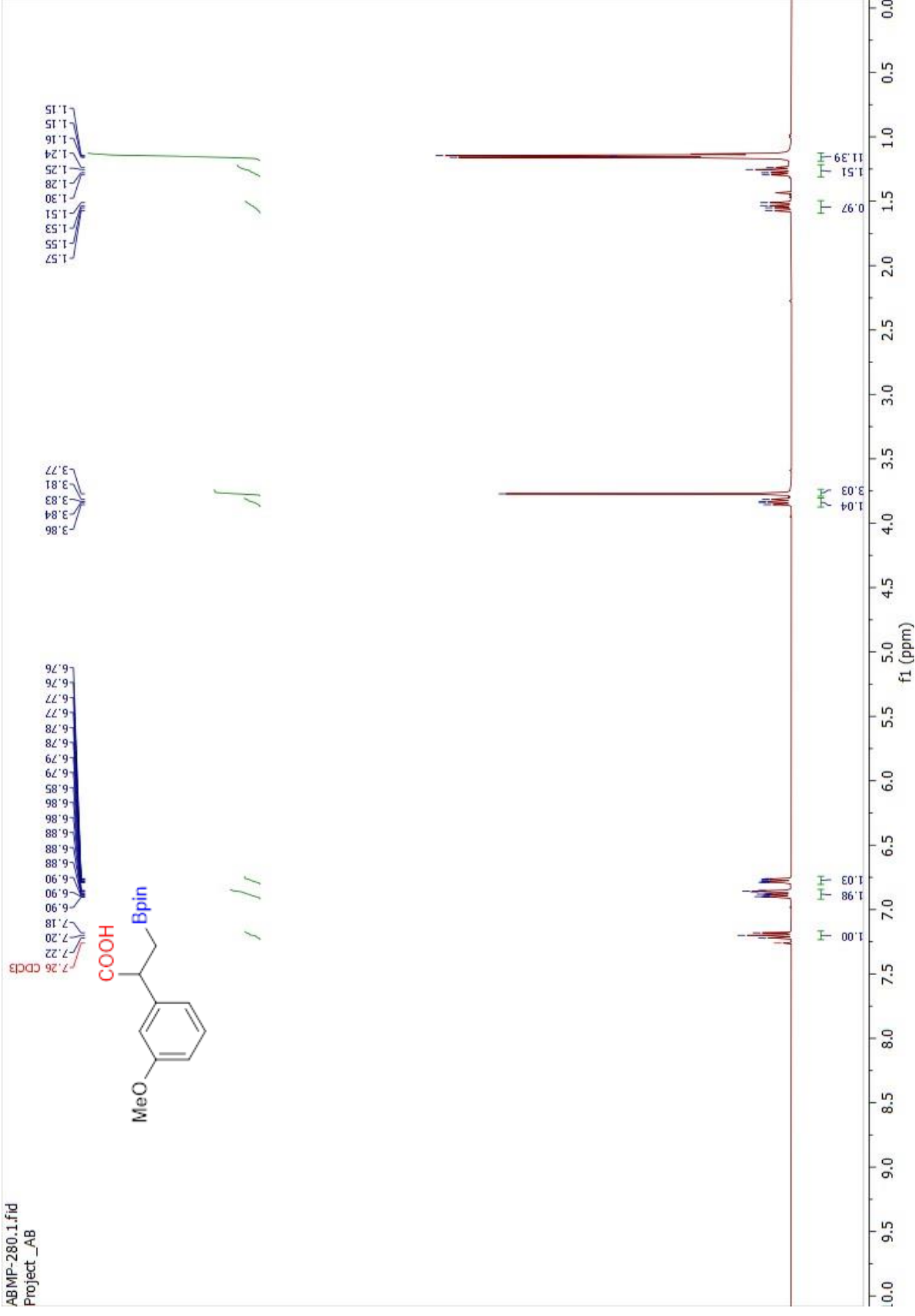
Time	Height	Area	Area%
4.3425	30629732	1289727.75	84.99
4.5500	6104666	227754.09	15.01

3: Diode Array
Range: 1.893e+1

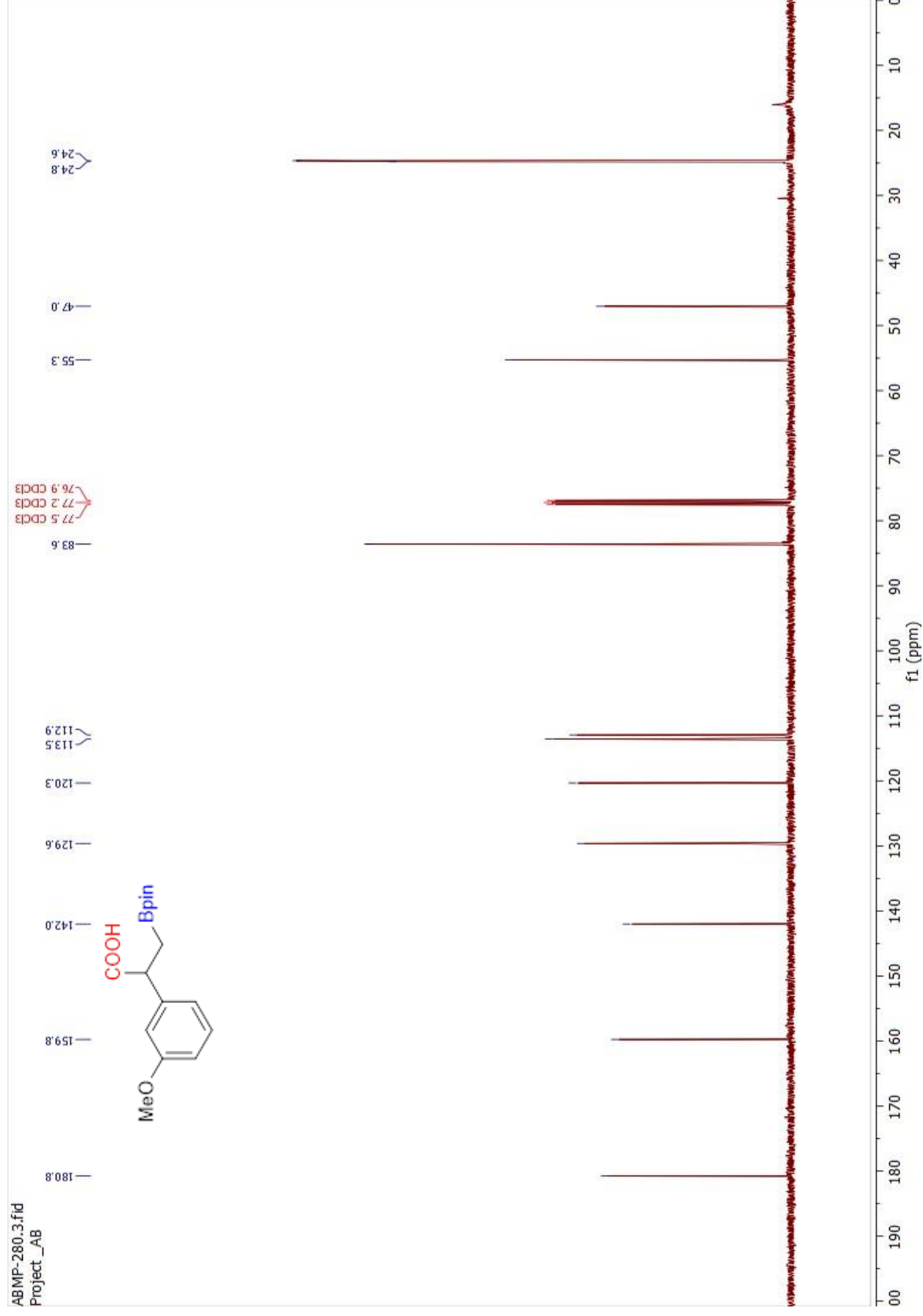


Spectrum S9. ¹H NMR of compound **2e** in CDCl₃

ABMP-280.1.fid
Project_AB



Spectrum S10. ¹³C NMR of compound **2e** in CDCl₃



Chromatogram S5. Compound **2e** and its racemate.

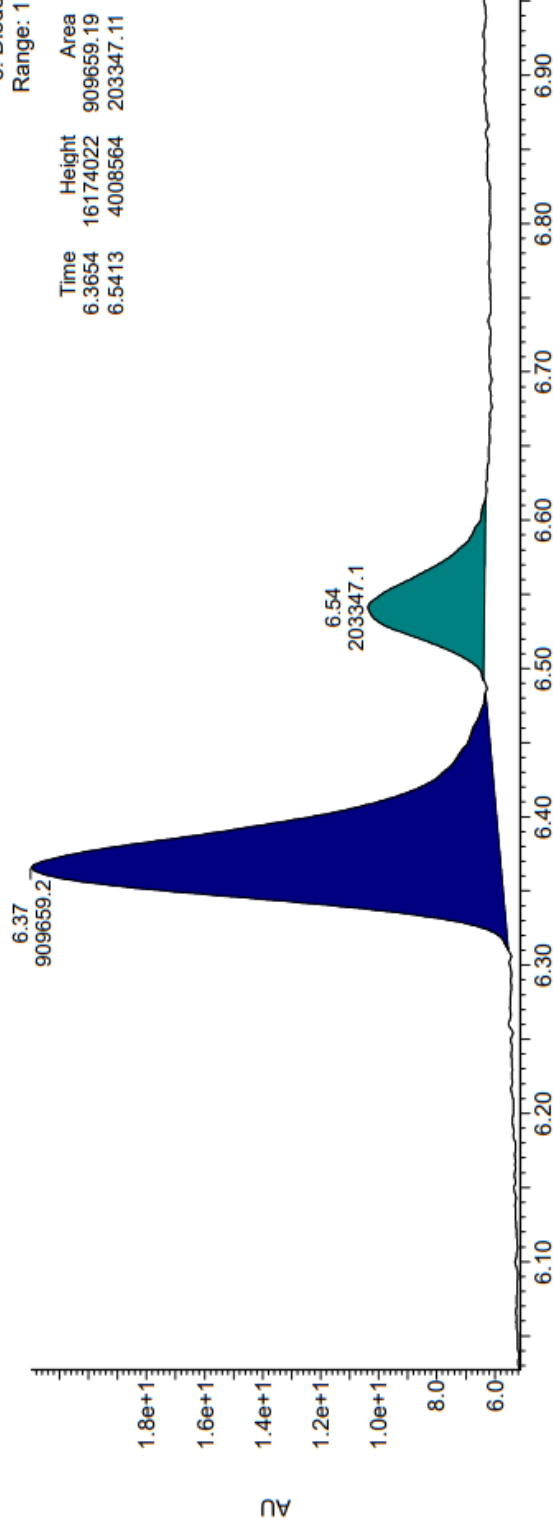
Cel2_iPrOH 0.2% TFA Chiral Separation

20-Jul-2022
16:20:56

UPC2

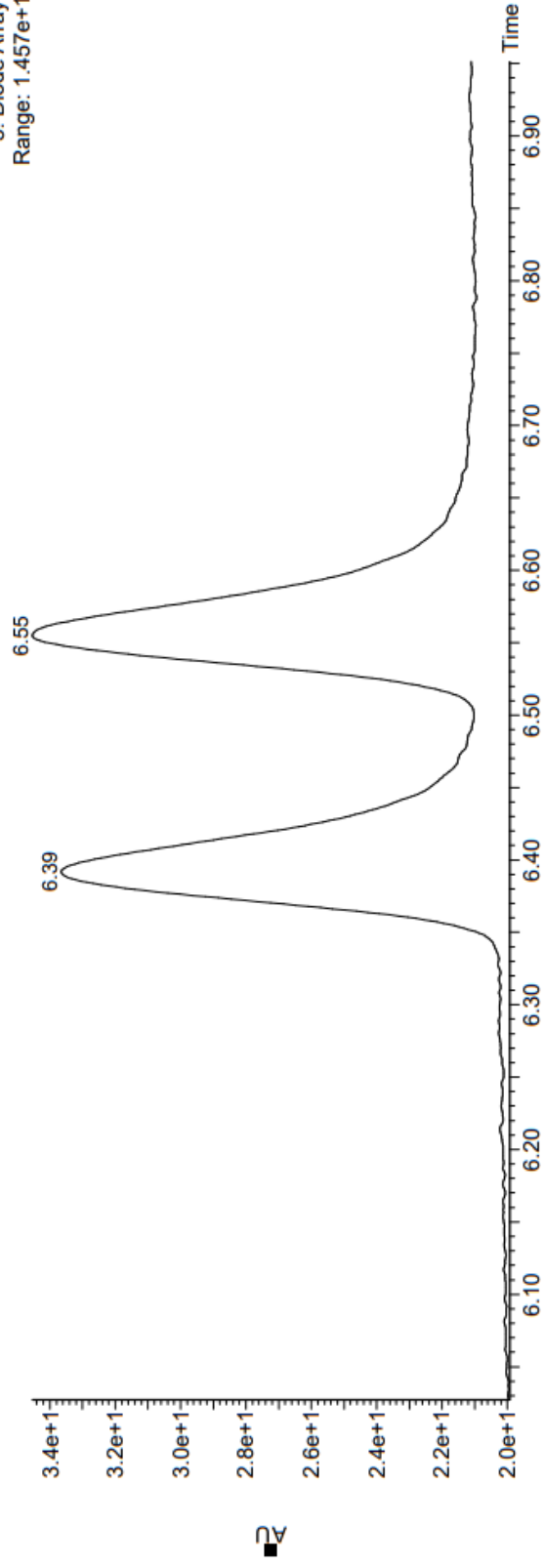
Time	Height	Area	Area%
6.3654	16174022	909659.19	81.73
6.5413	4008564	203347.11	18.27

3: Diode Array
Range: 1.68e+1



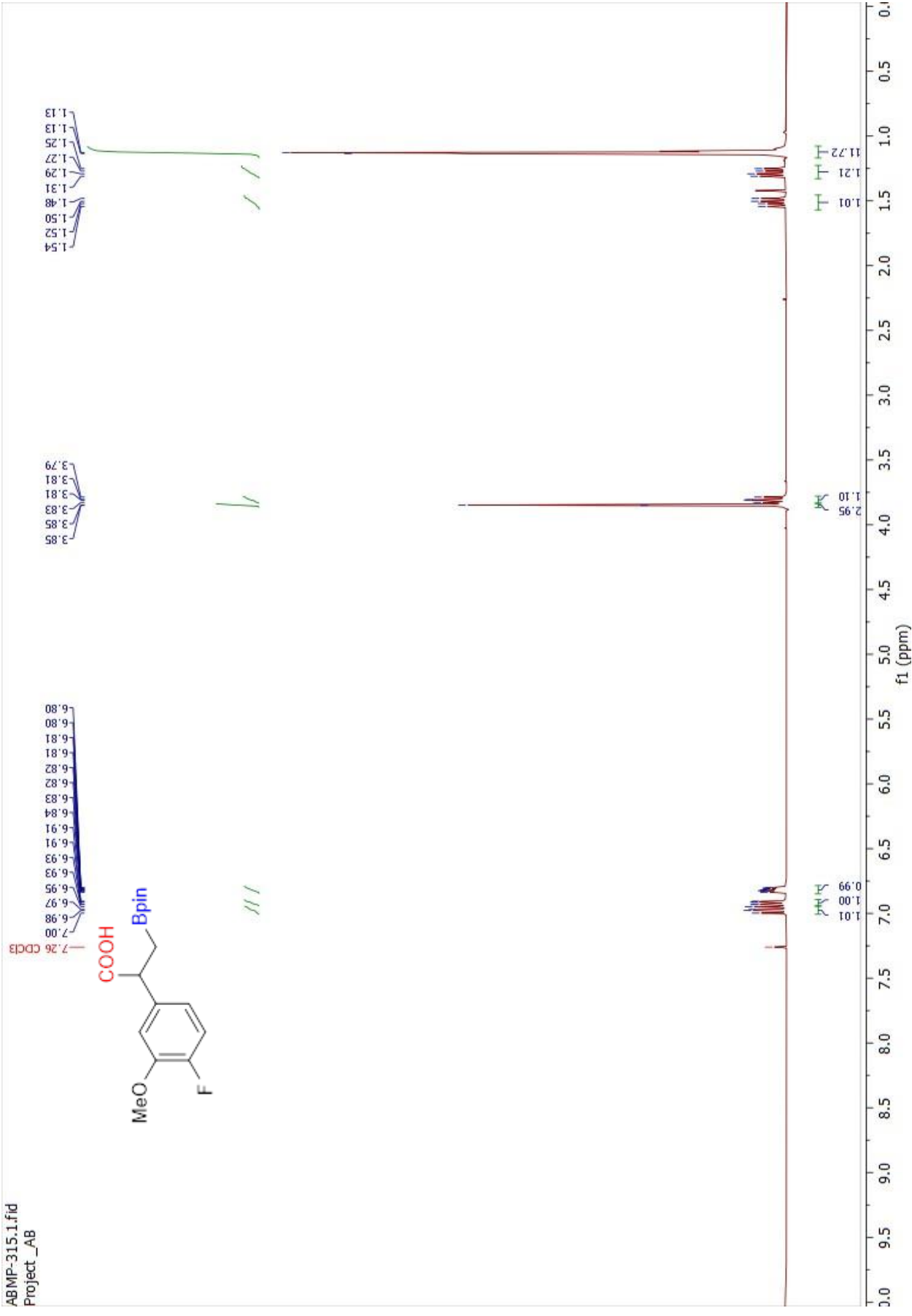
Time	Height	Area	Area%
6.3654	16174022	909659.19	81.73
6.5413	4008564	203347.11	18.27

3: Diode Array
Range: 1.457e+1



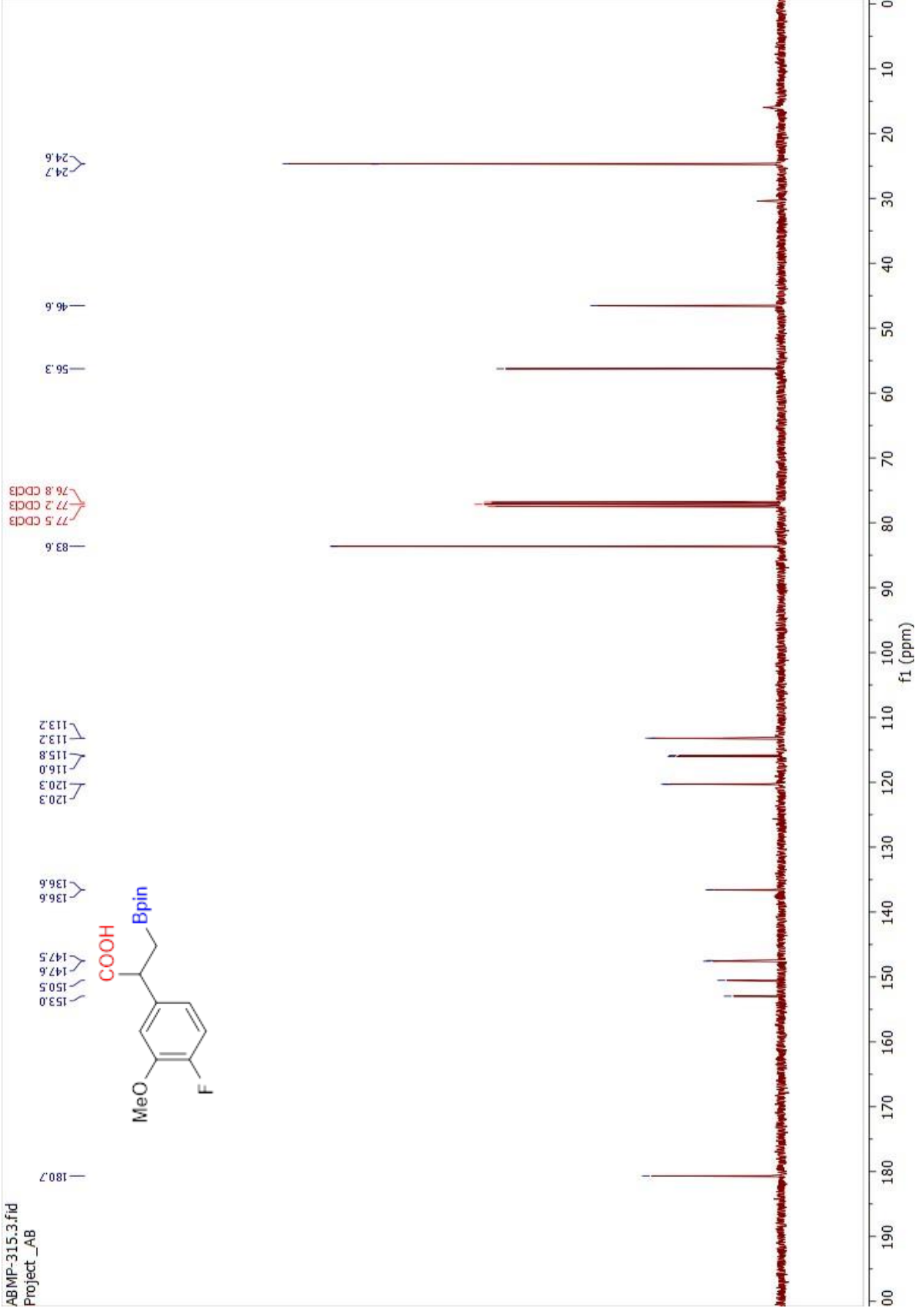
Spectrum S11. ¹H NMR of compound 2f in CDCl₃

ABMP-315.1.fid
Project_AB



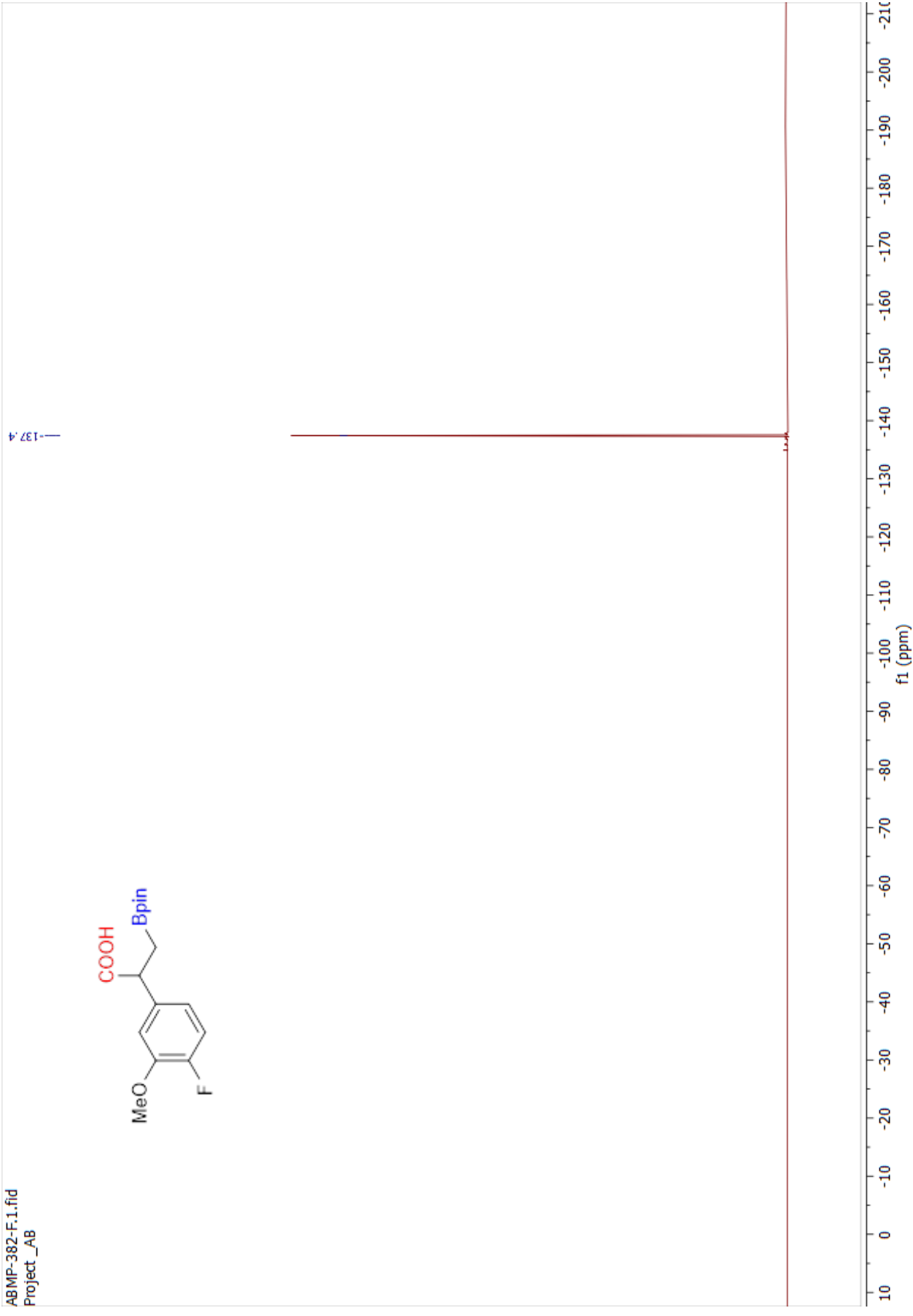
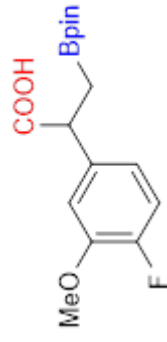
Spectrum S12. ¹³C NMR of compound **2f** in CDCl₃

ABMP-315.3.fid
Project_AB



Spectrum S13. ^{13}C NMR of compound **2f** in CDCl_3

ABMP-382-F.1.fid
Project_AB



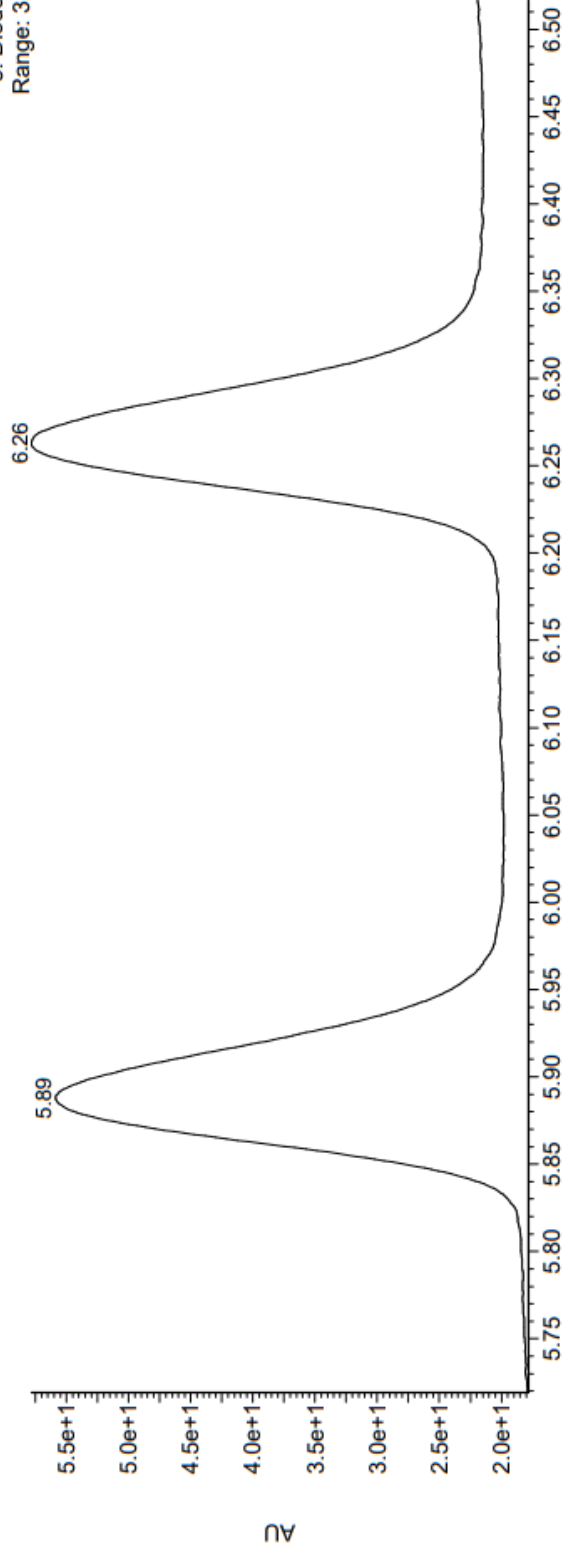
Chromatogram S6. Compound **2f** and its racemate.

Amy1_iPrOH 0.5% TFA Chiral Separation

30-Mar-2023
09:14:23

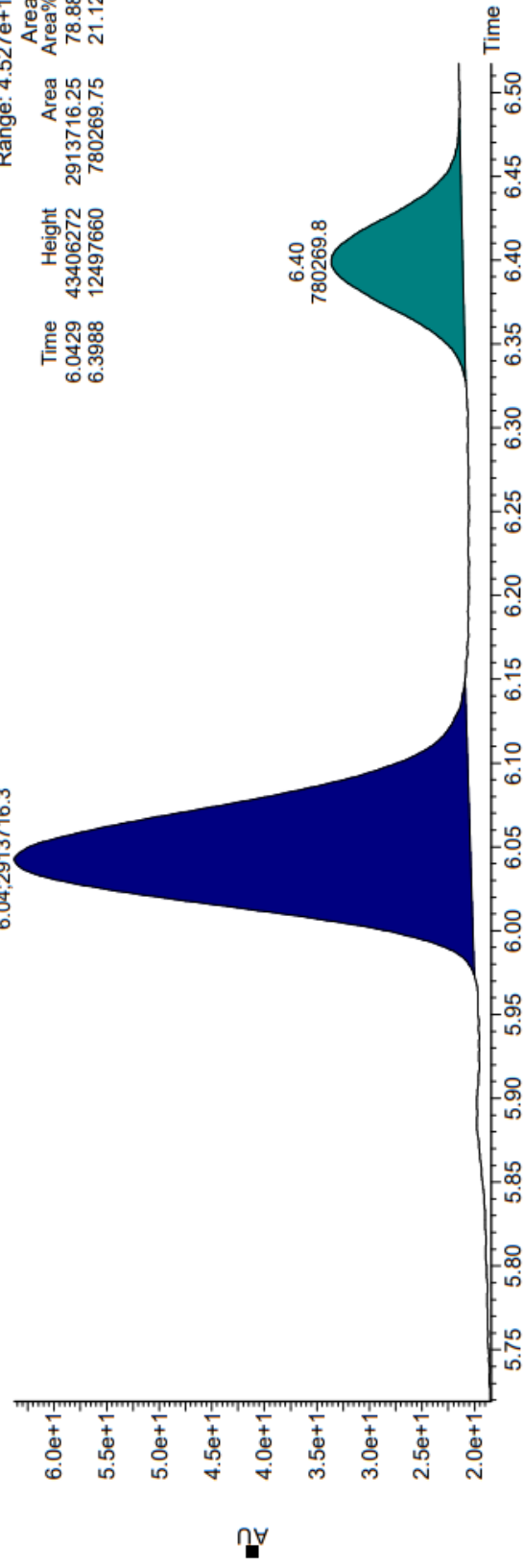
UPC2

3: Diode Array
Range: 3.99e+1



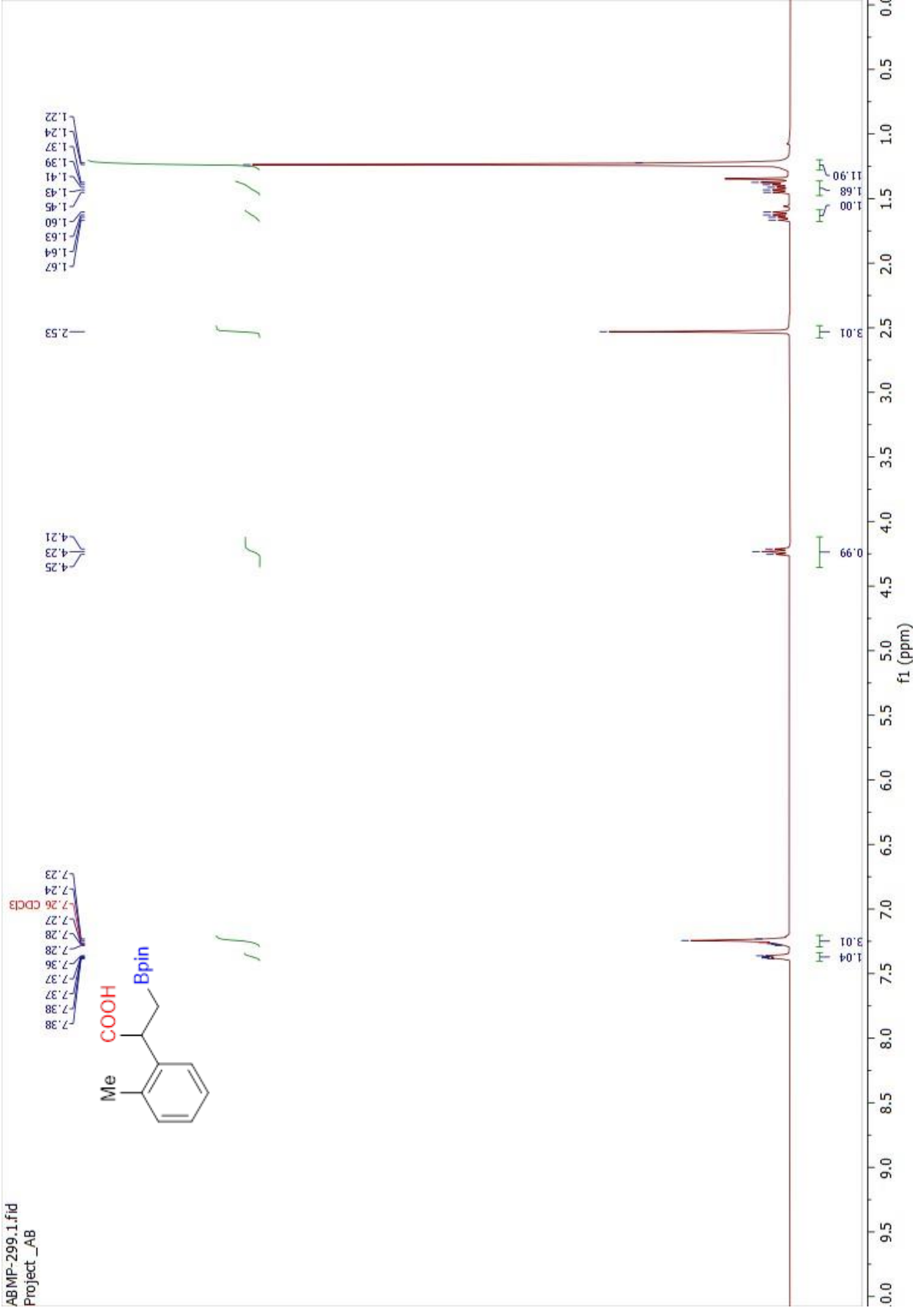
3: Diode Array
Range: 4.527e+1

Time	Height	Area	Area%
6.0429	43406272	2913716.25	78.88
6.3988	12497660	780269.75	21.12

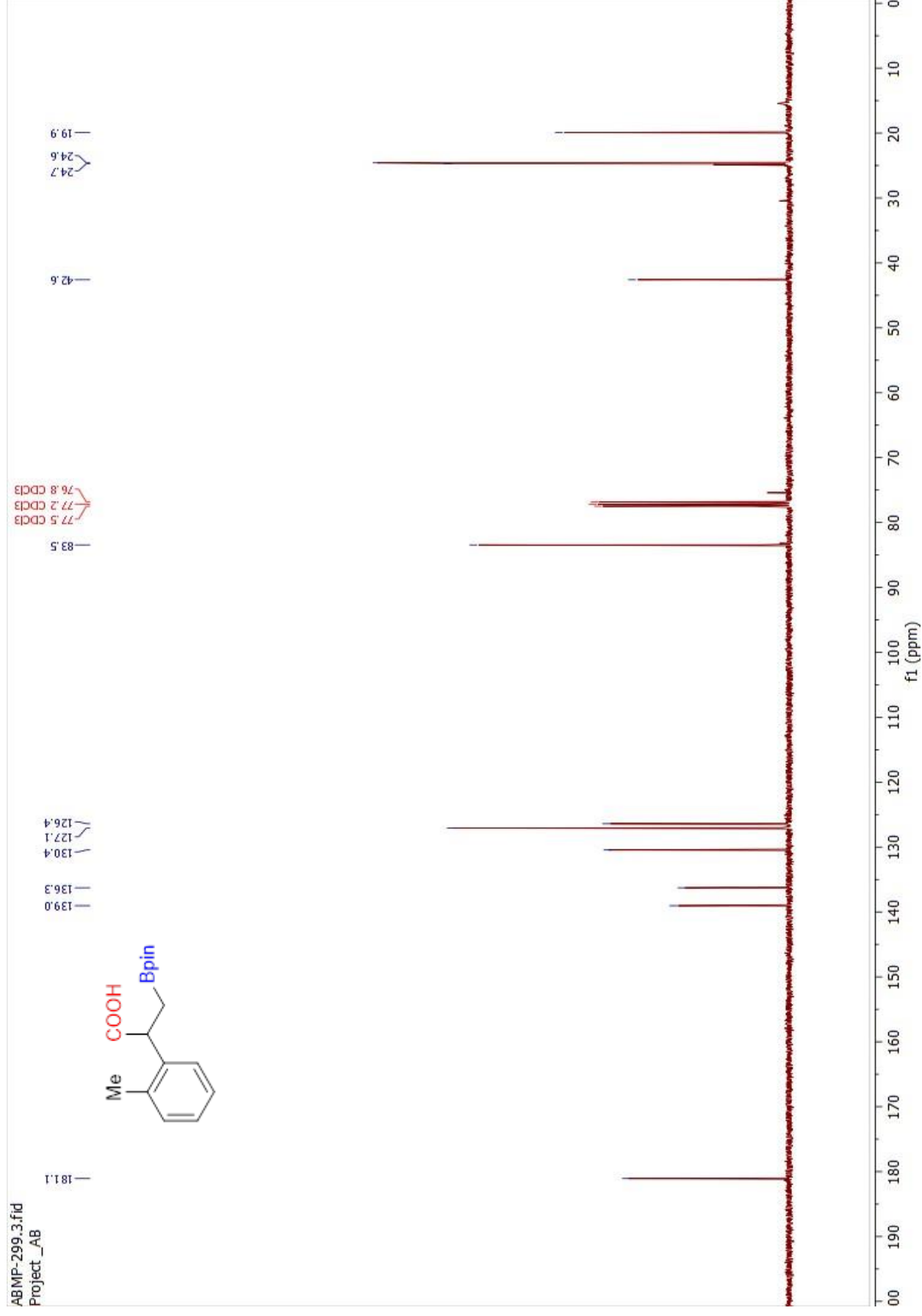


Spectrum S14. ¹H NMR of compound 2g in CDCl₃

ABMP-299.1.fid
Project_AB



Spectrum S15. ¹³C NMR of compound 2g in CDCl₃



Chromatogram S7. Compound **2g** and its racemate.

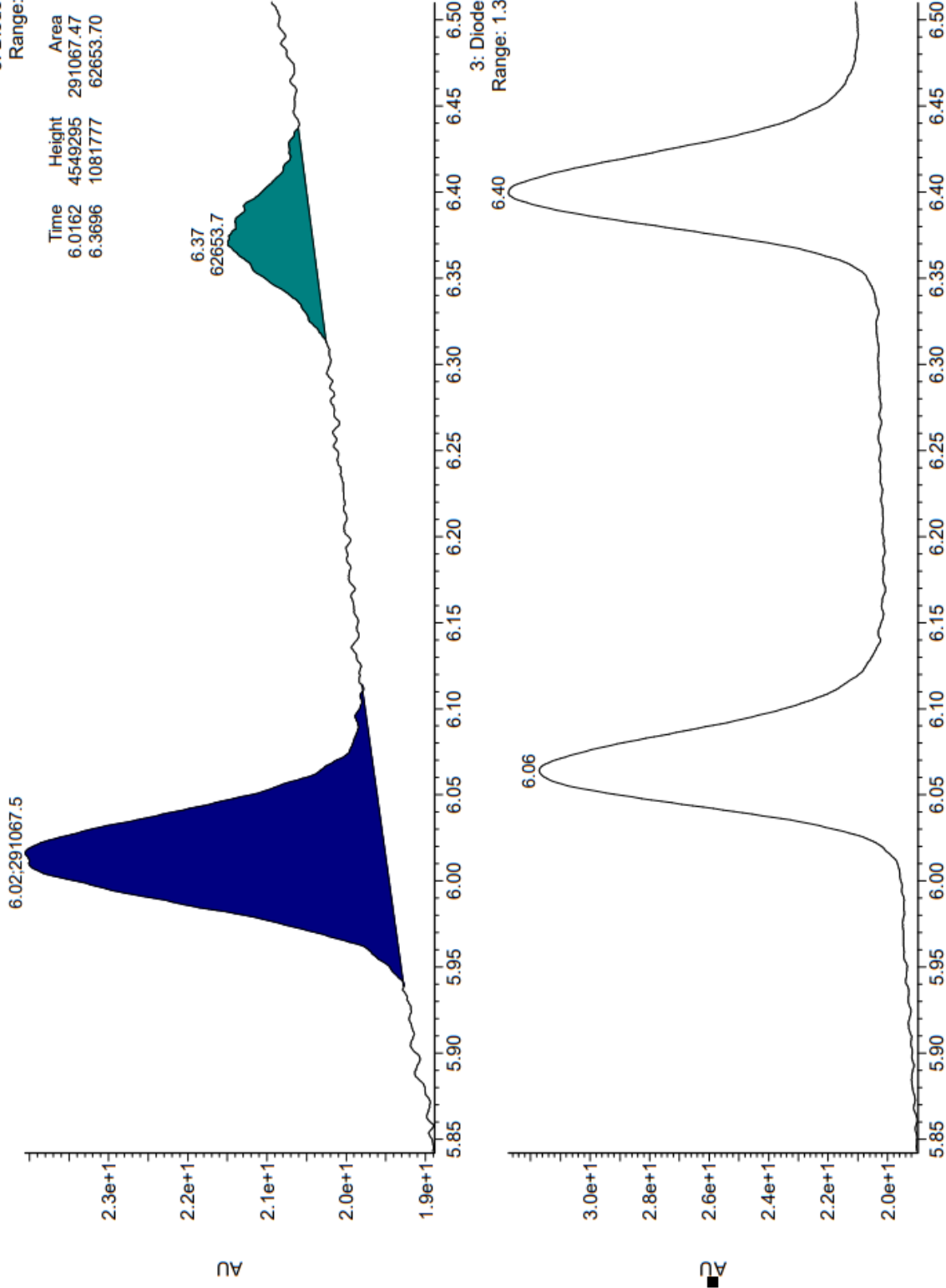
Amy1_iPrOH 0.5% TFA Chiral Separation

30-Mar-2023
09:33:17

UPC2

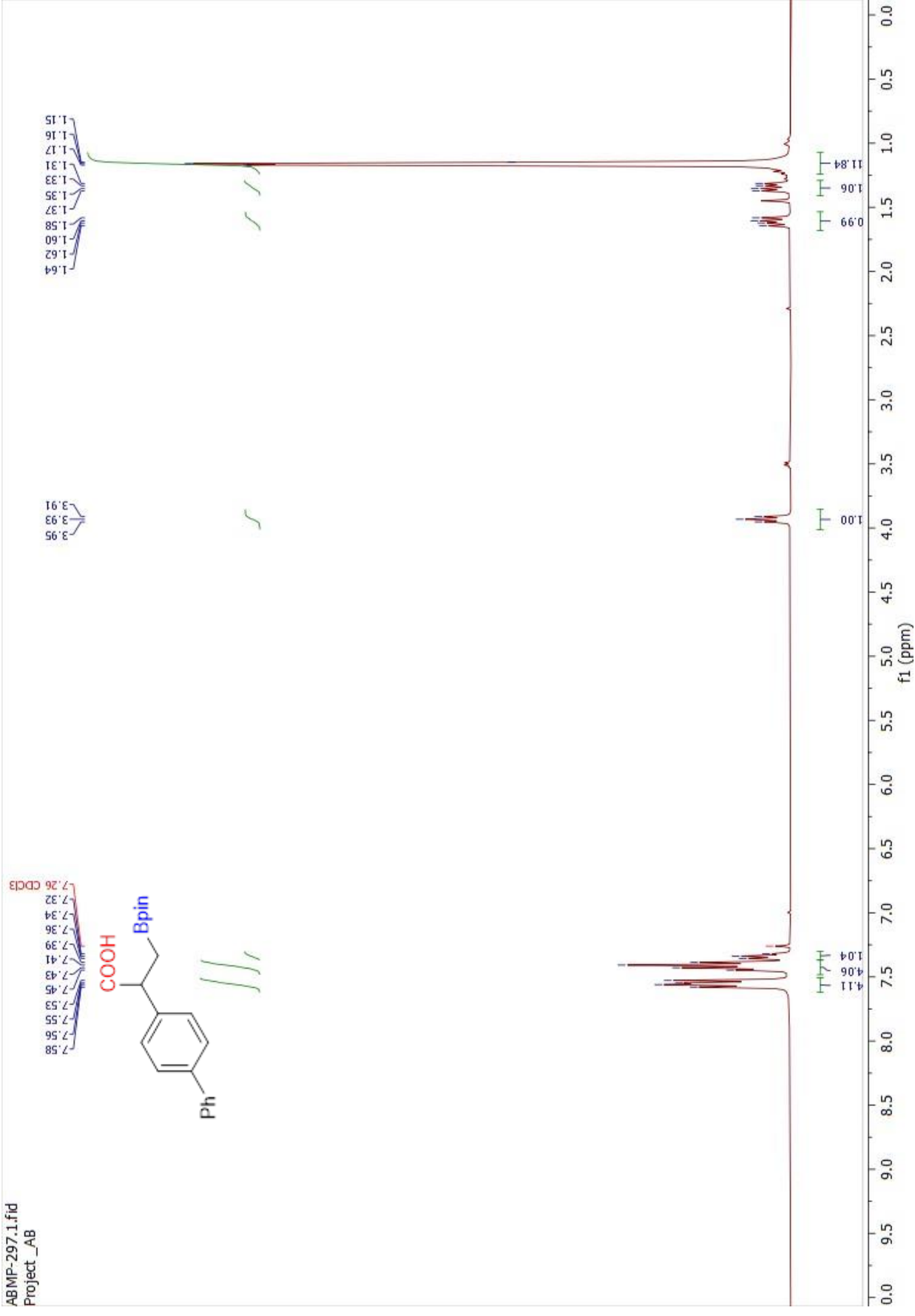
3: Diode Array
Range: 5.162

Time	Height	Area	Area%
6.0162	4549295	291067.47	82.29
6.3696	1081777	62653.70	17.71

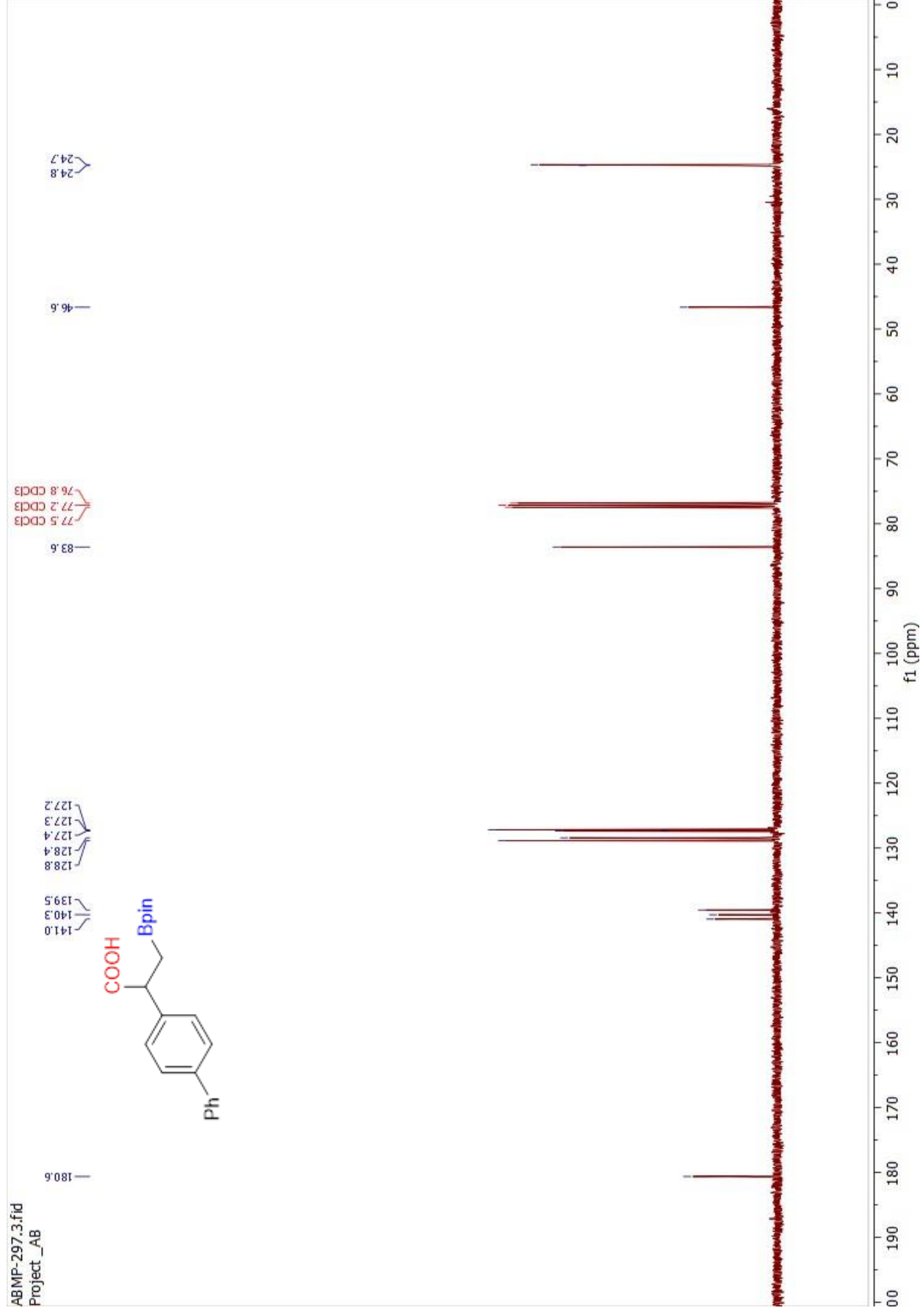


Spectrum S16. ¹H NMR of compound 2h in CDCl₃

ABMP-297.1.fid
Project_AB



Spectrum S17. ¹³C NMR of compound 2h in CDCl₃



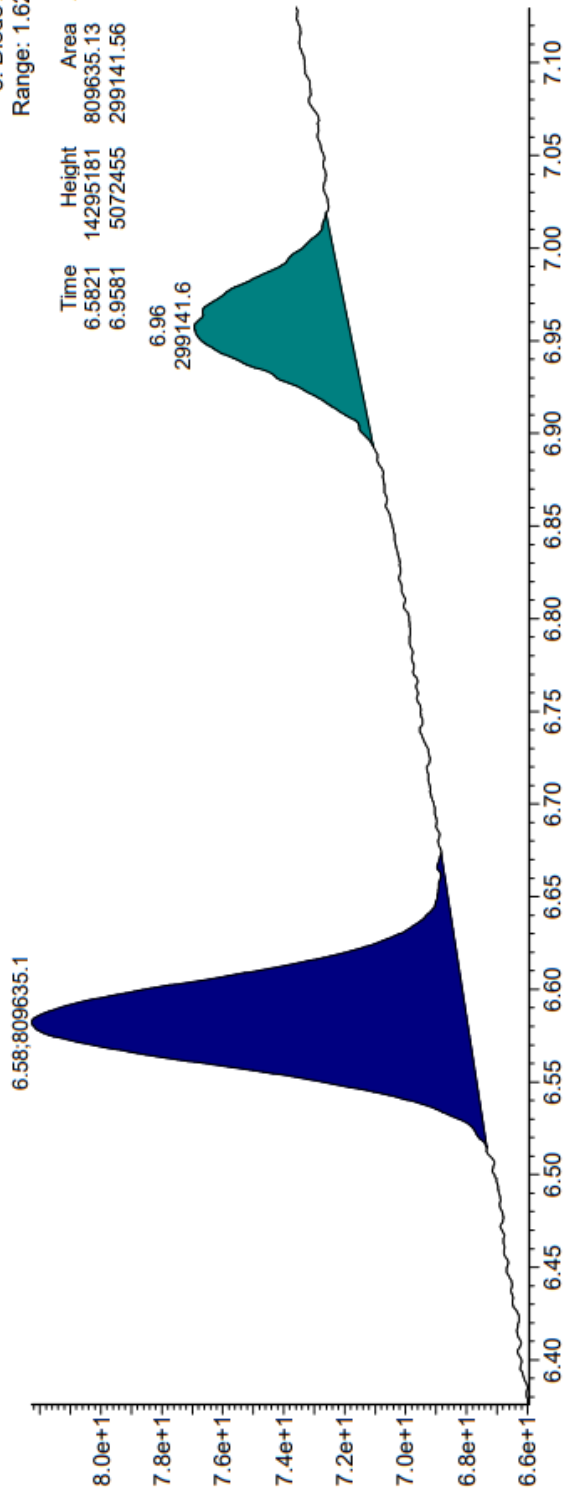
Chromatogram S8. Compound 2h and its racemate.

Amy1_iPrOH 0.5% TFA Chiral Separation

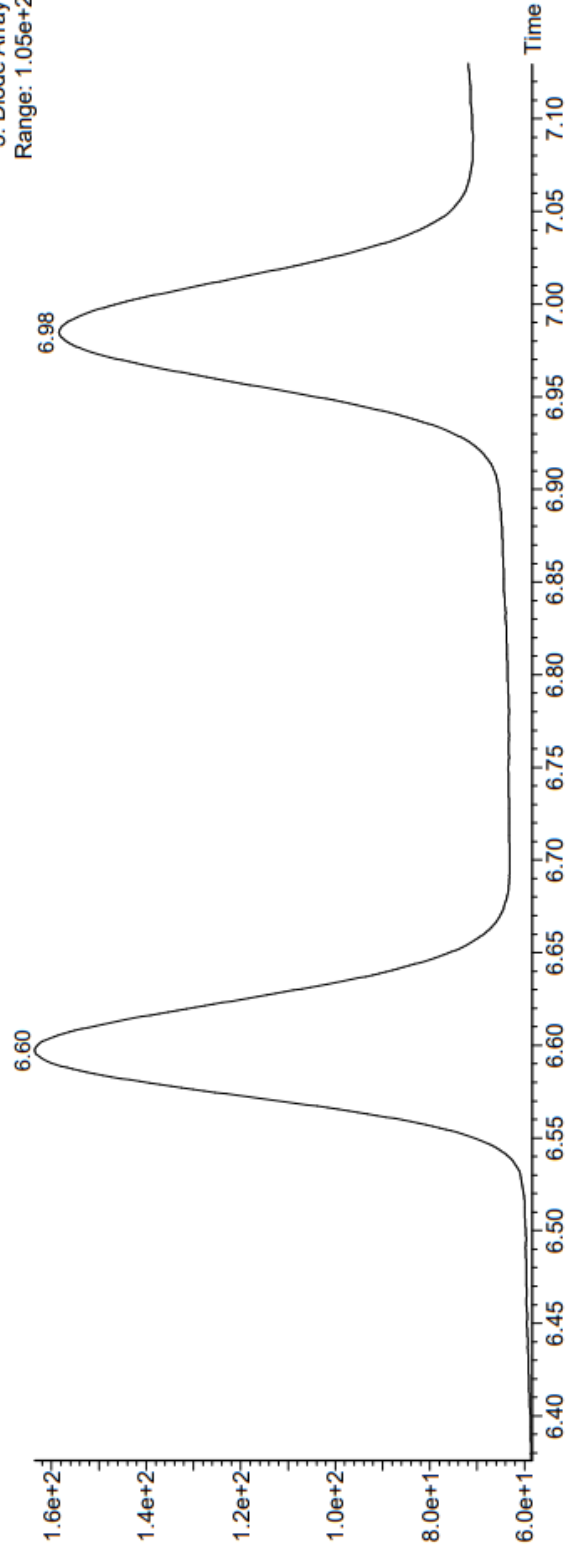
18-Apr-2023
13:41:19

UPC2

3: Diode Array
Range: 1.629e+1

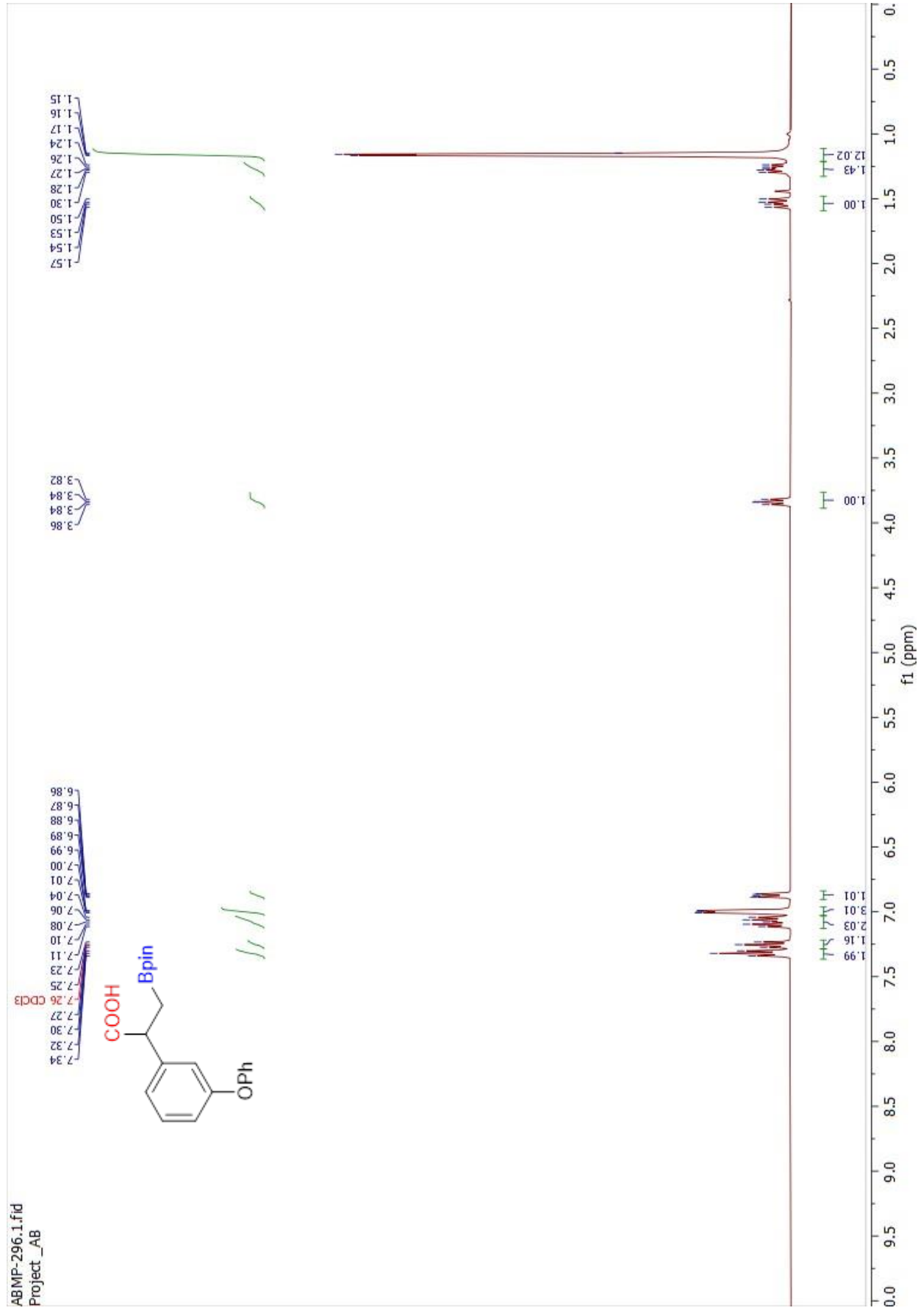


3: Diode Array
Range: 1.05e+2



Spectrum S18. ¹H NMR of compound 2i in CDCl₃

ABMP-296.1.fid
Project_AB



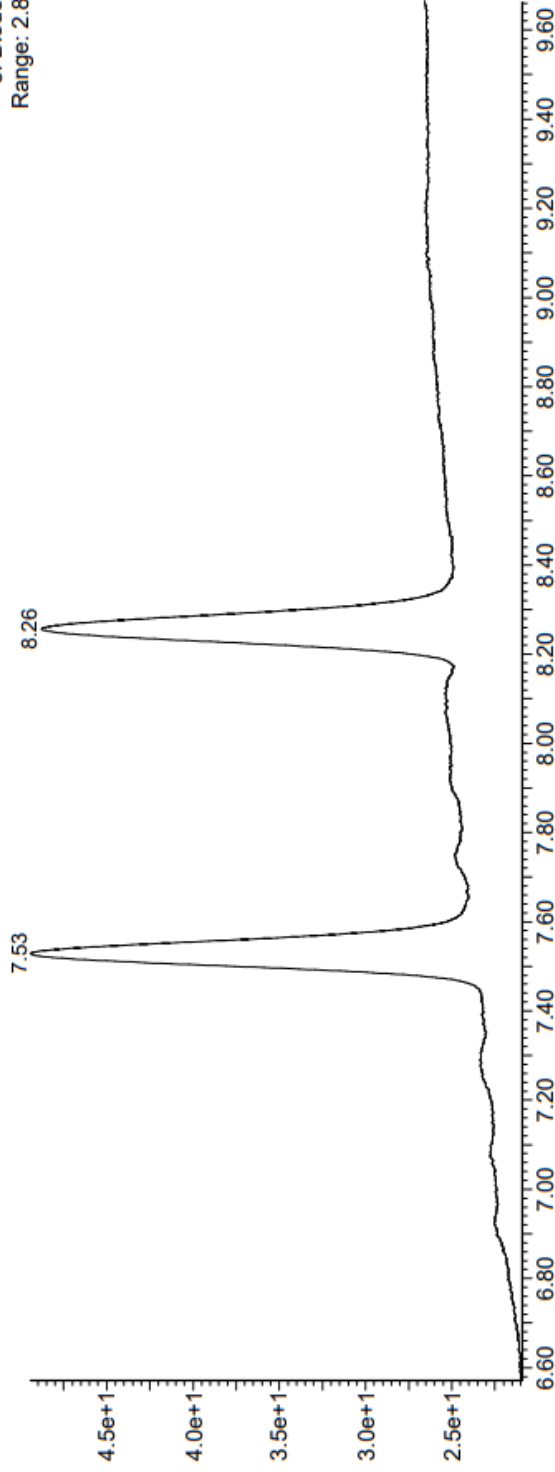
Chromatogram S9. Compound 2i and its racemate.

Cell1_iPrOH 0.5% TFA Chiral Separation

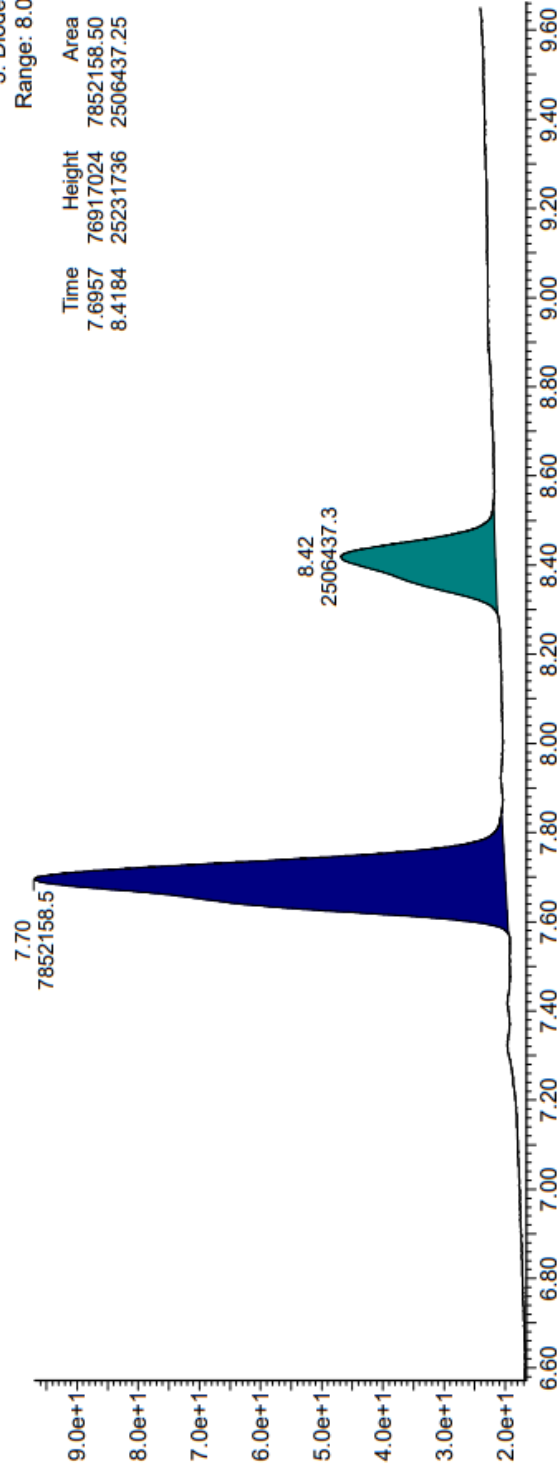
13-Mar-2023
13:28:42

UPC2

3: Diode Array
Range: 2.844e+1



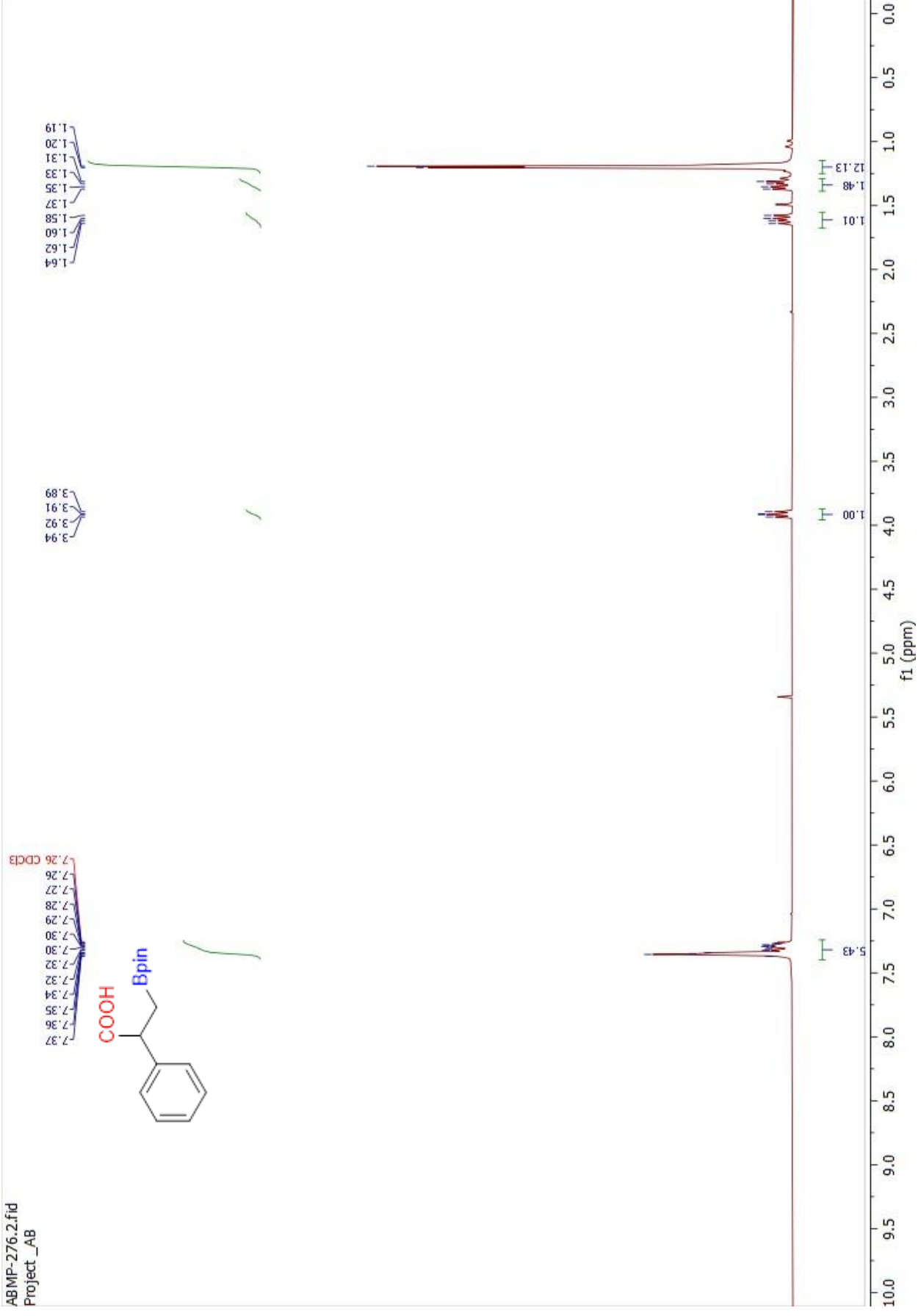
3: Diode Array
Range: 8.019e+1



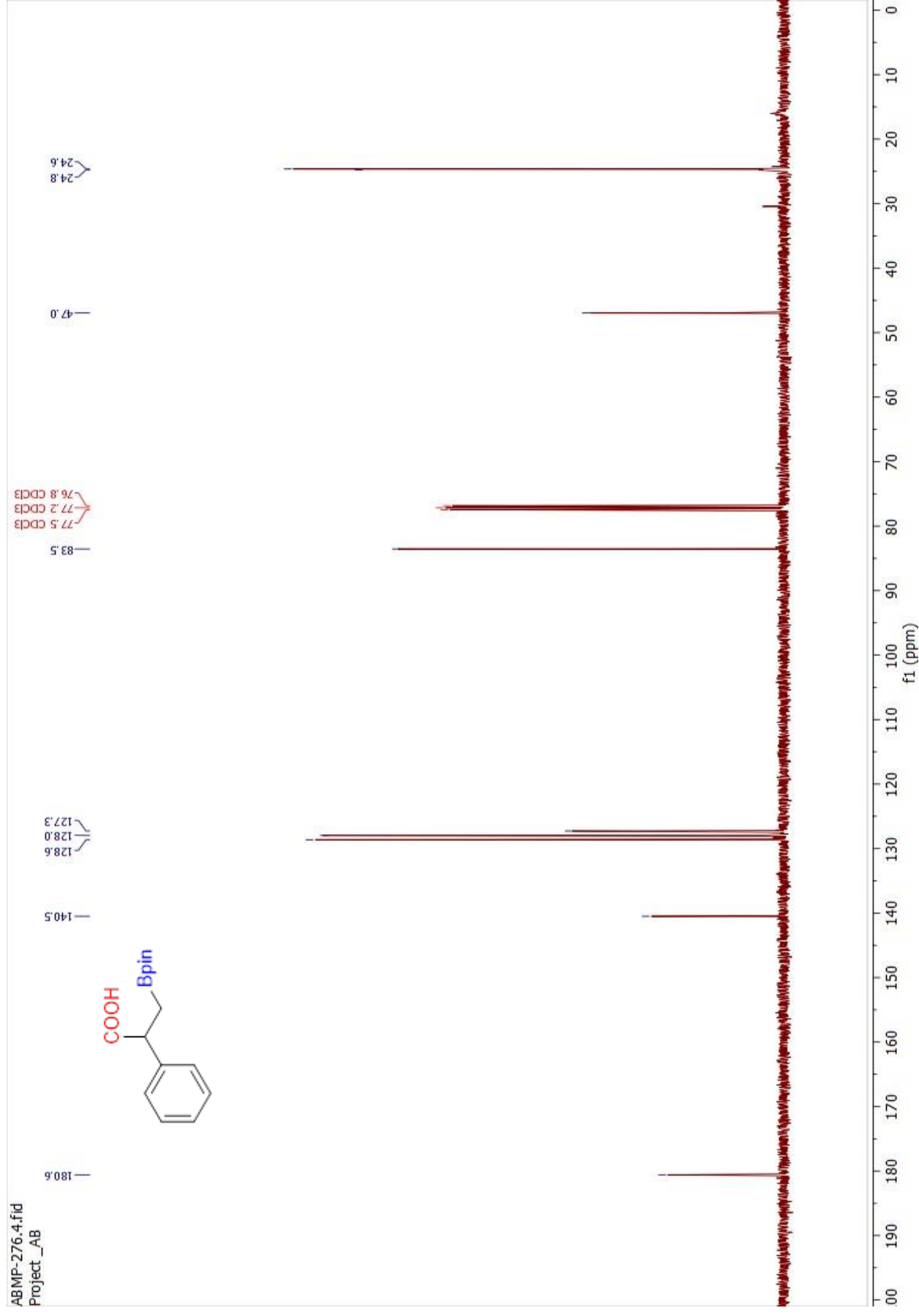
Time	Height	Area	Area%
7.6957	76917024	7852158.50	75.80
8.4184	25231736	2506437.25	24.20

Spectrum S20. ¹H NMR of compound 2j in CDCl₃

ABMP-276.2.fid
Project_AB



Spectrum S21. ¹³C NMR of compound 2j in CDCl₃



Chromatogram S10. Compound 2j and its racemate.

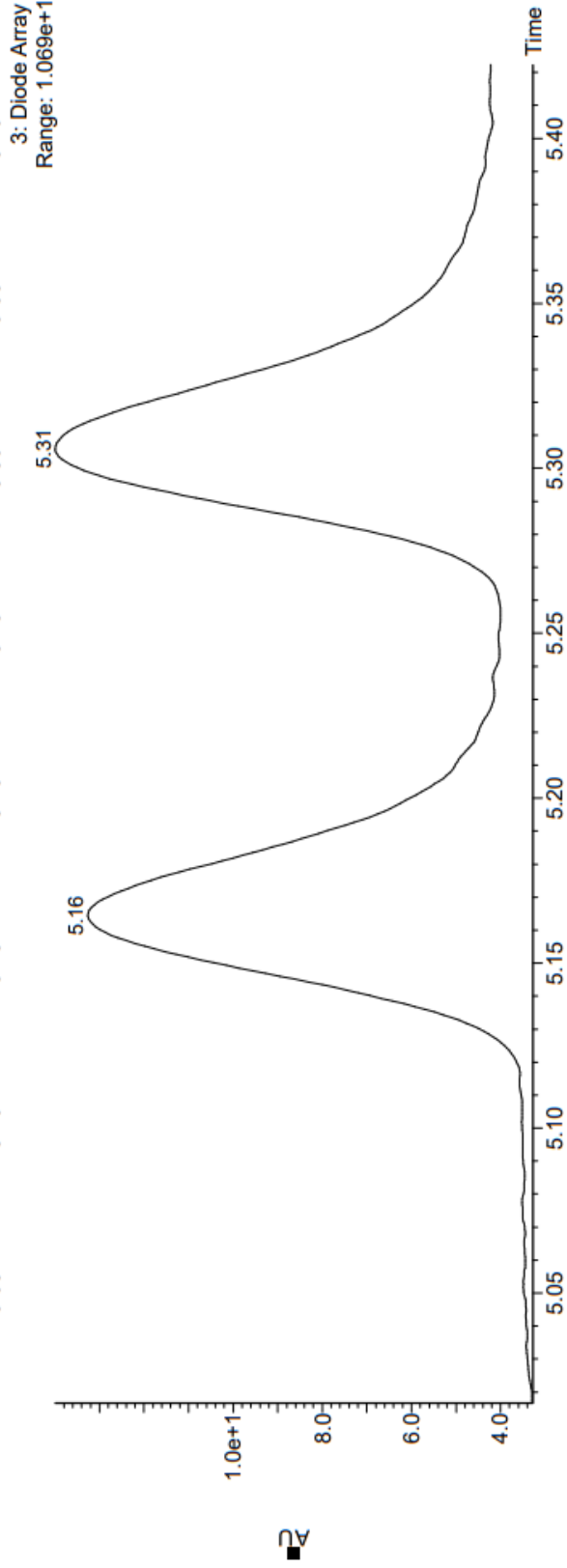
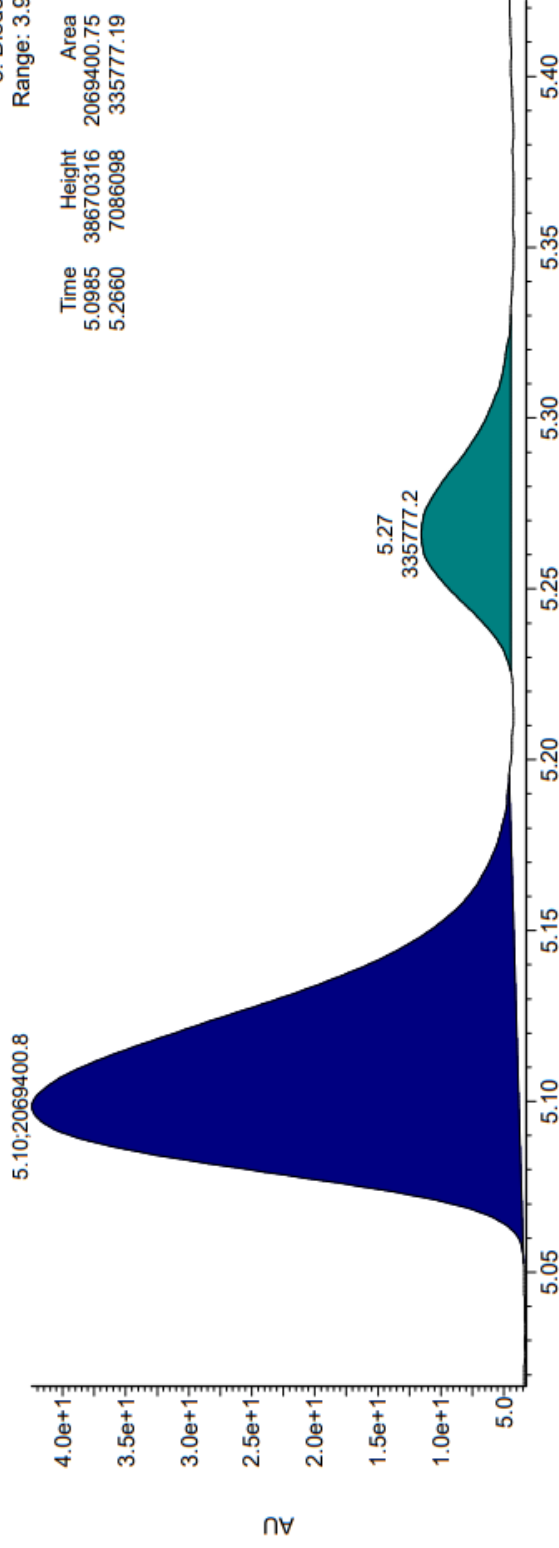
Cel2_iPrOH 0.2% TFA Chiral Separation

20-Jul-2022
12:40:34

UPC2

3: Diode Array
Range: 3.915e+1

Time	Height	Area	Area%
5.0985	38670316	2069400.75	86.04
5.2660	7086098	335777.19	13.96

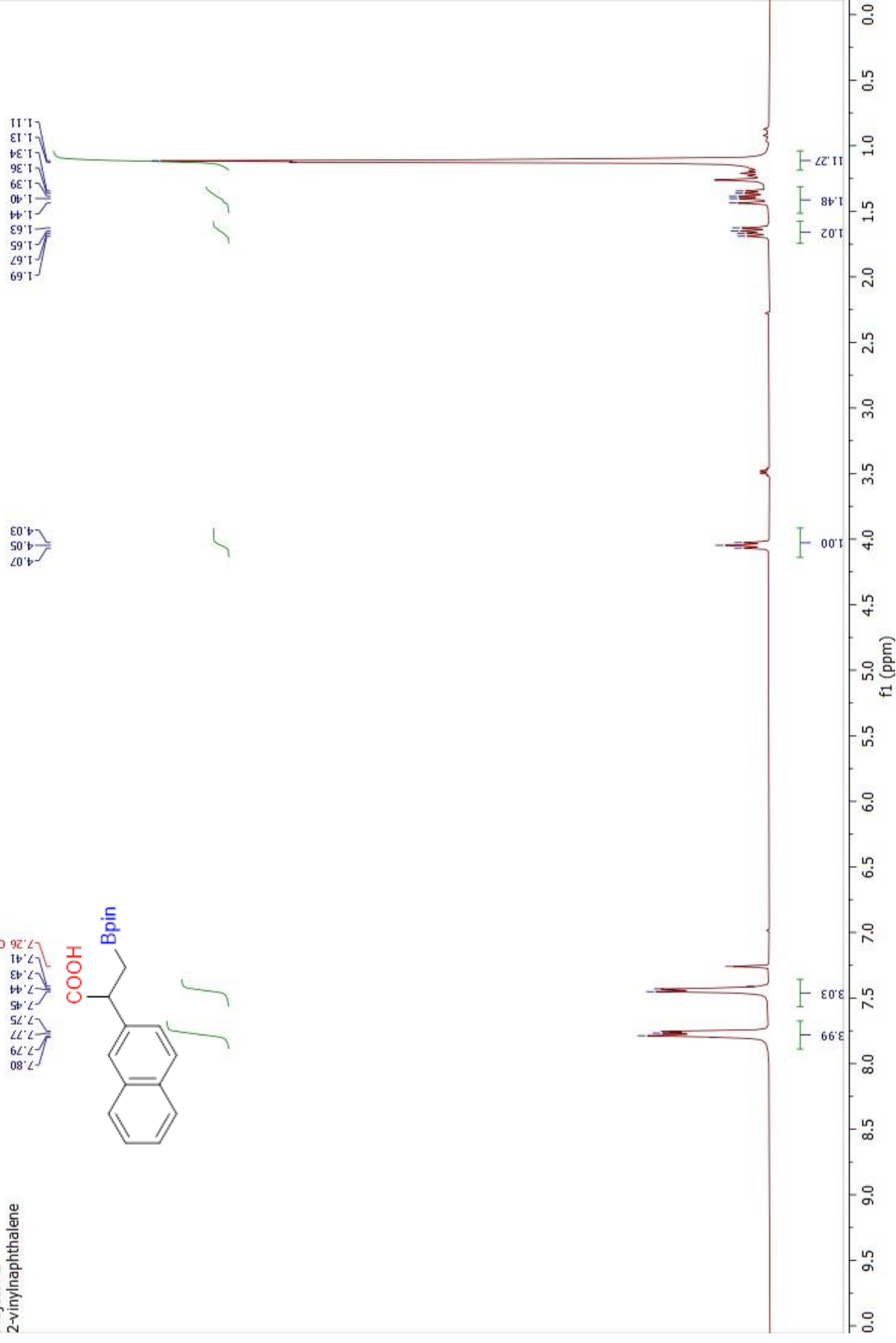
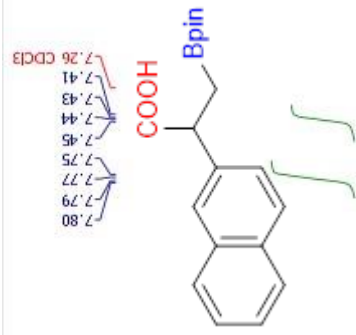


Spectrum S22. ¹H NMR of compound 2k in CDCl₃

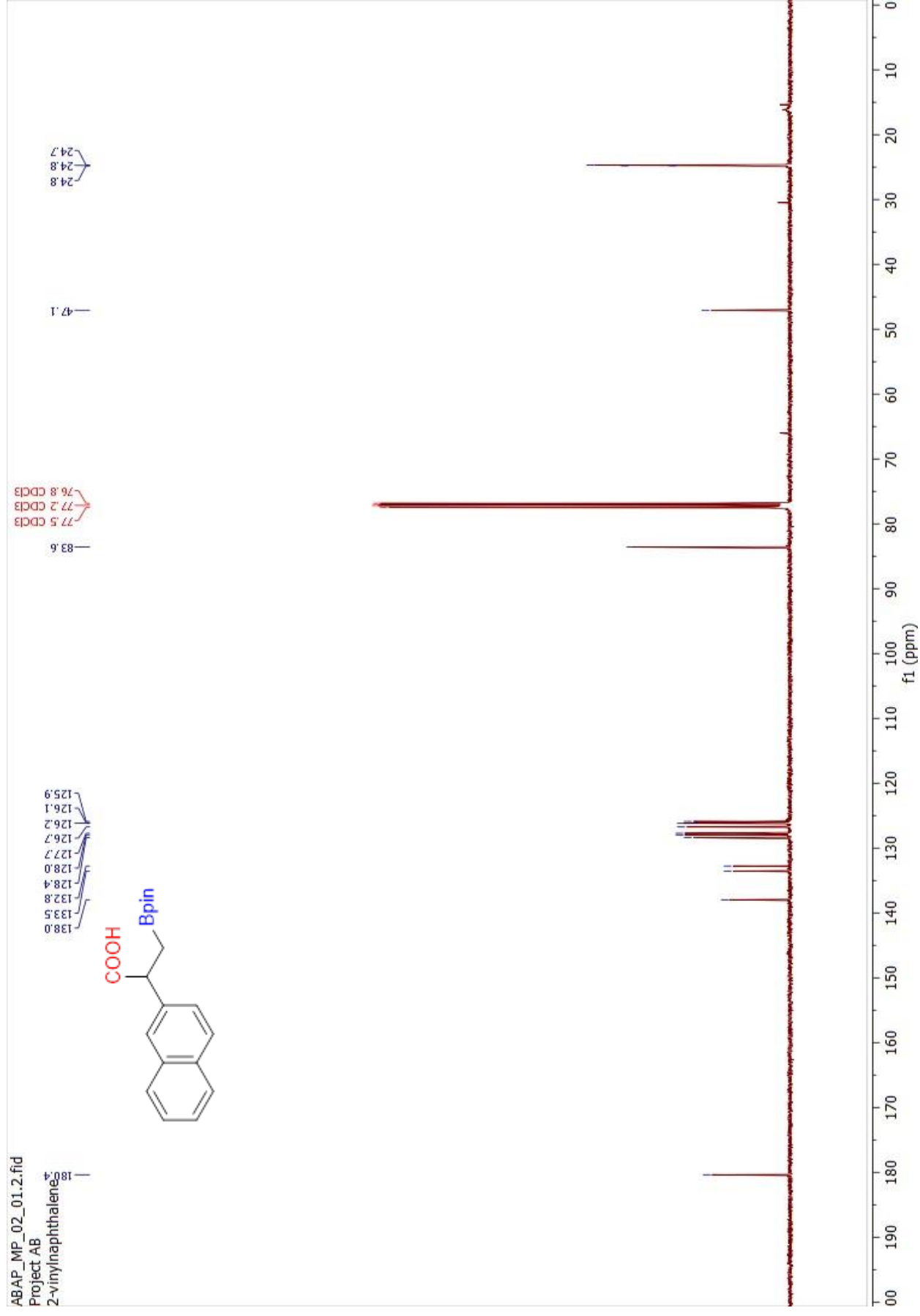
ABAP_MP_02_01.1.fid

Project AB

2-vinylnaphthalene



Spectrum S23. ^{13}C NMR of compound **2k** in CDCl_3



Chromatogram S11. Compound **2k** and its racemate.

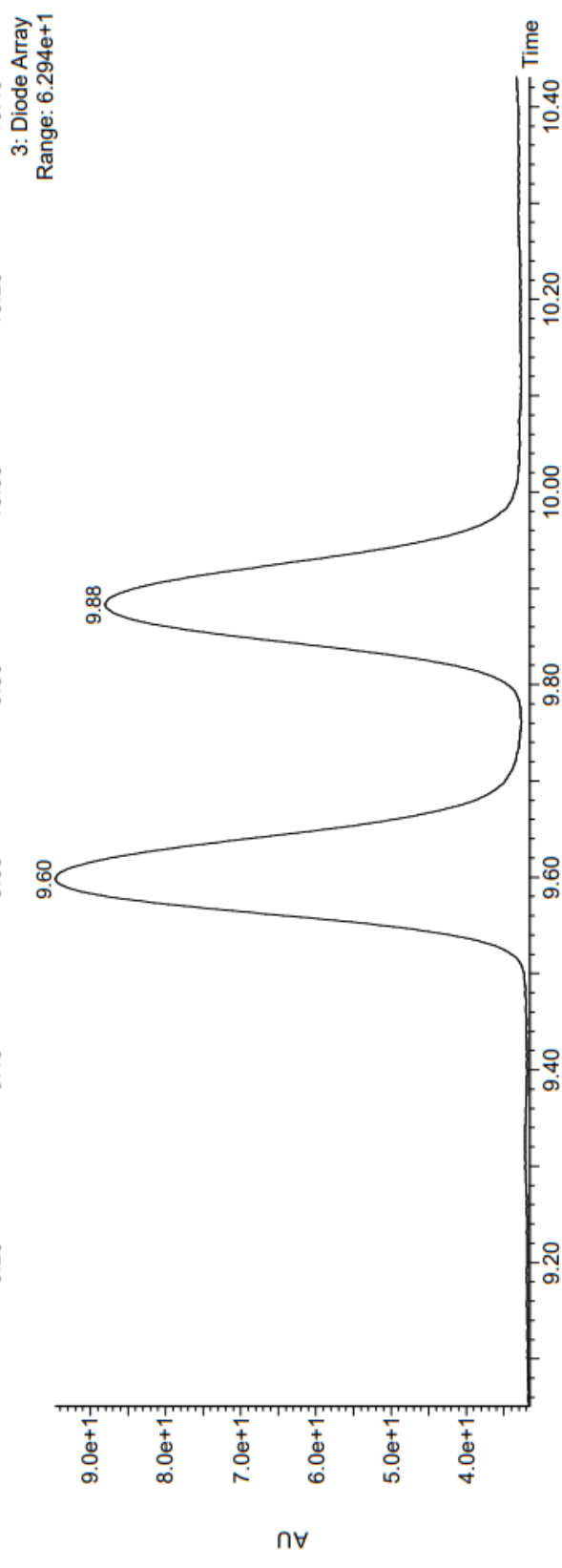
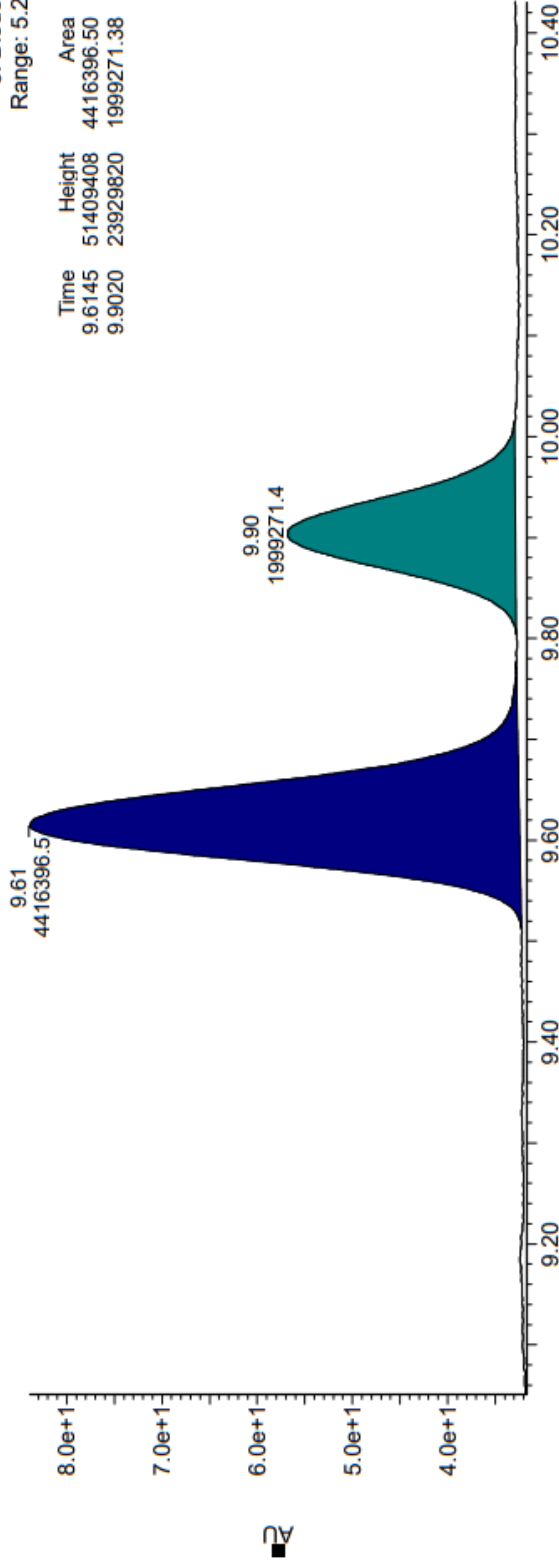
Amy1_iPrOH 0.5% TFA Chiral Separation

30-Mar-2023
12:03:55

UPC2

3: Diode Array
Range: 5.209e+1

Time	Height	Area	Area%
9.6145	51409408	4416396.50	68.84
9.9020	23929820	1999271.38	31.16

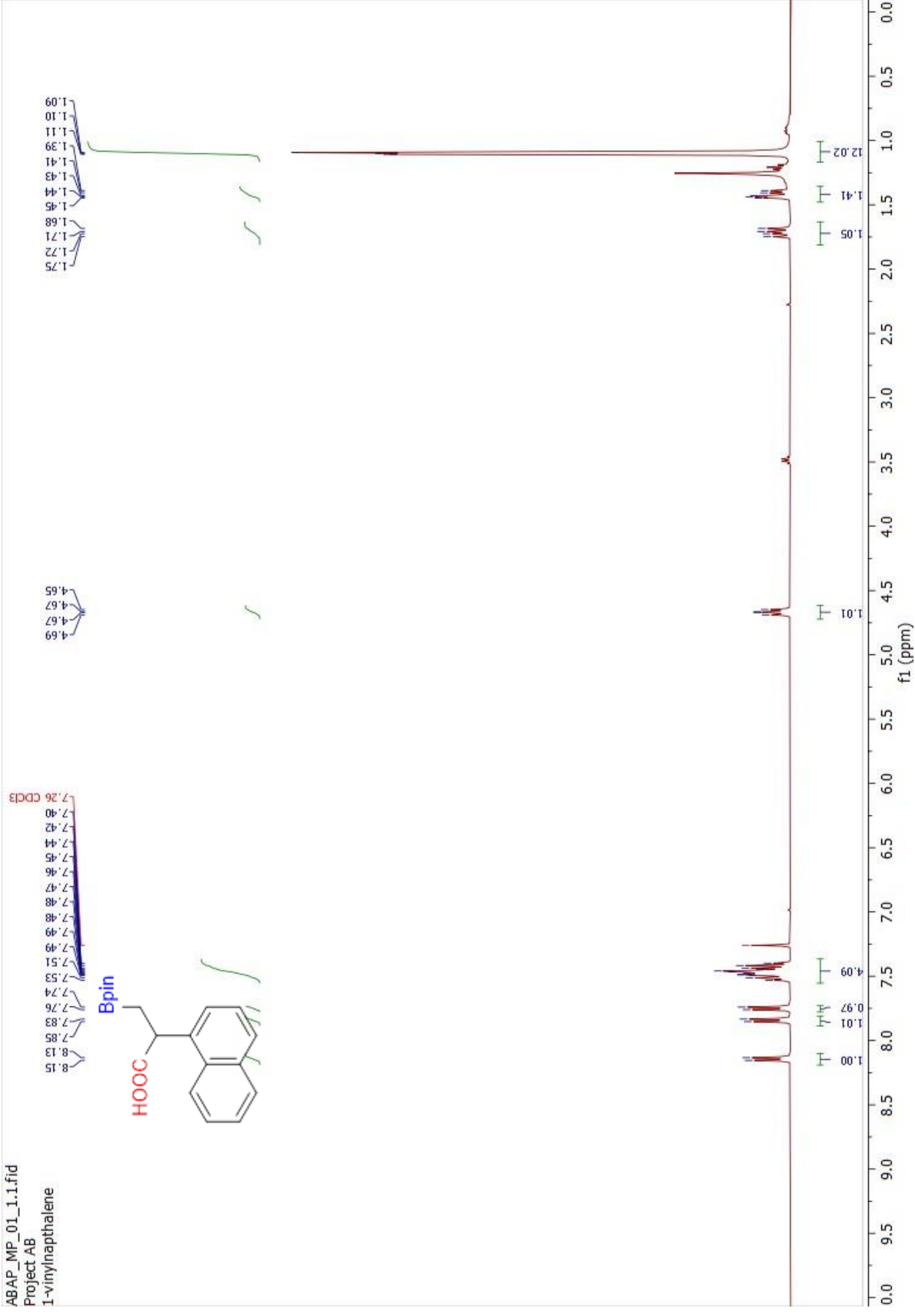


Spectrum S24. ¹H NMR of compound 2I in CDCl₃

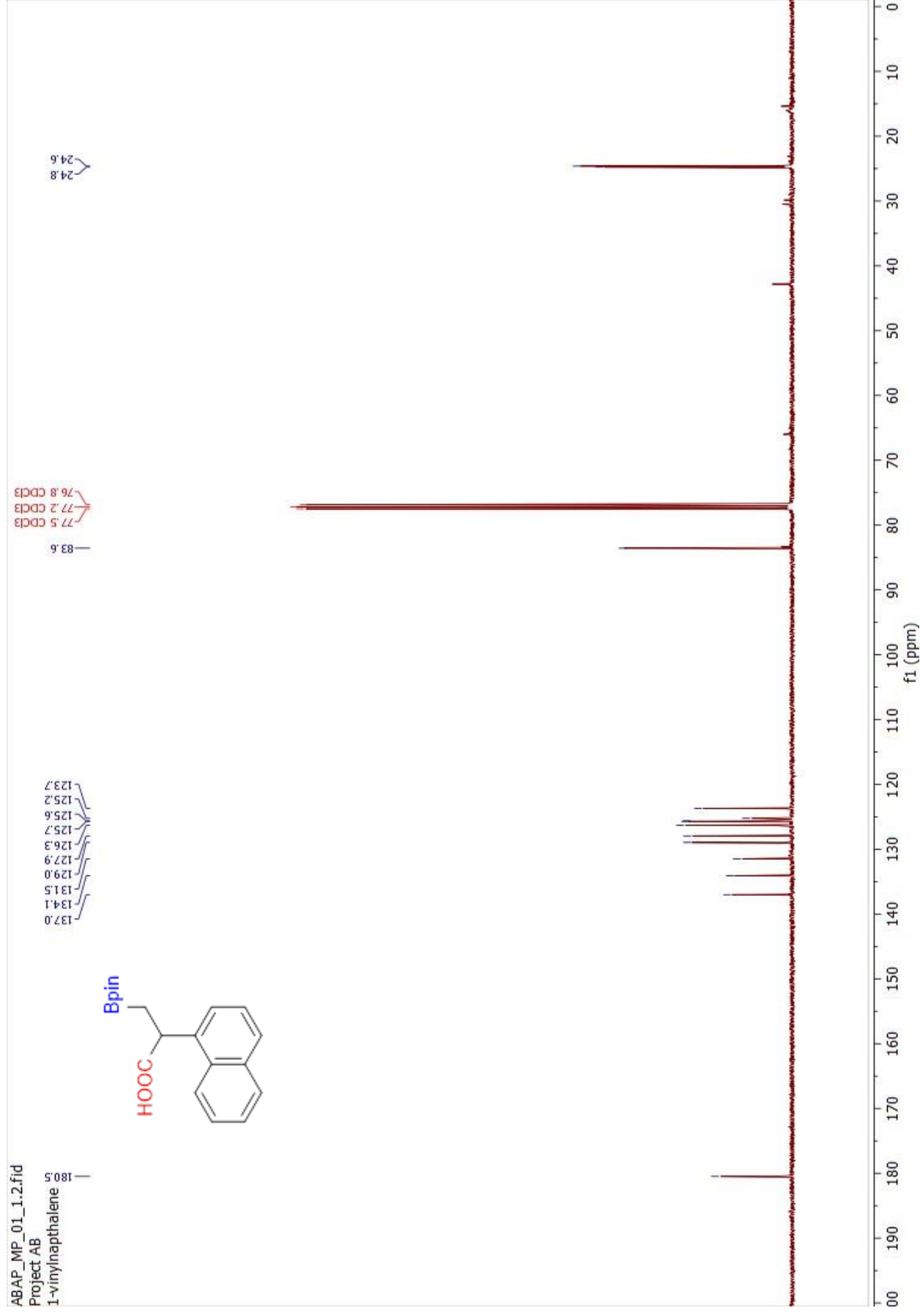
ABAP_MP_01_1_1.fid

Project AB

1-vinylnaphthalene



Spectrum S25. ¹³C NMR of compound 2I in CDCl₃



Chromatogram S12. Compound 2I and its racemate.

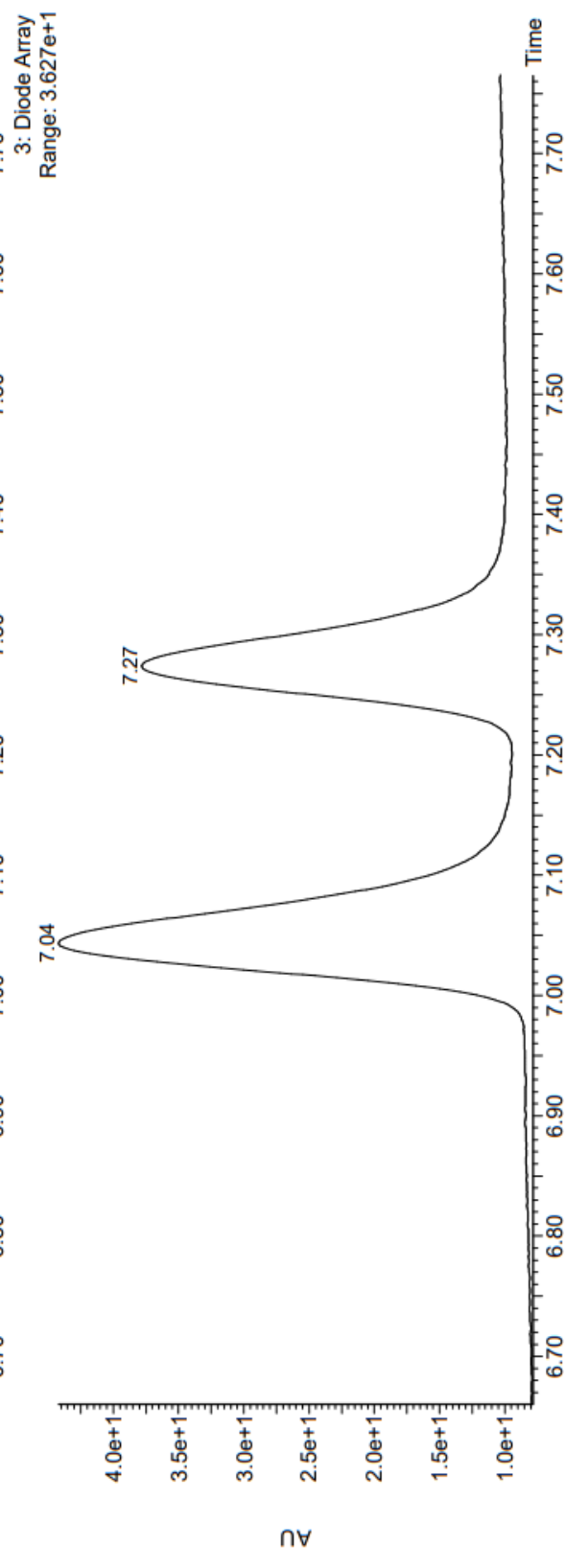
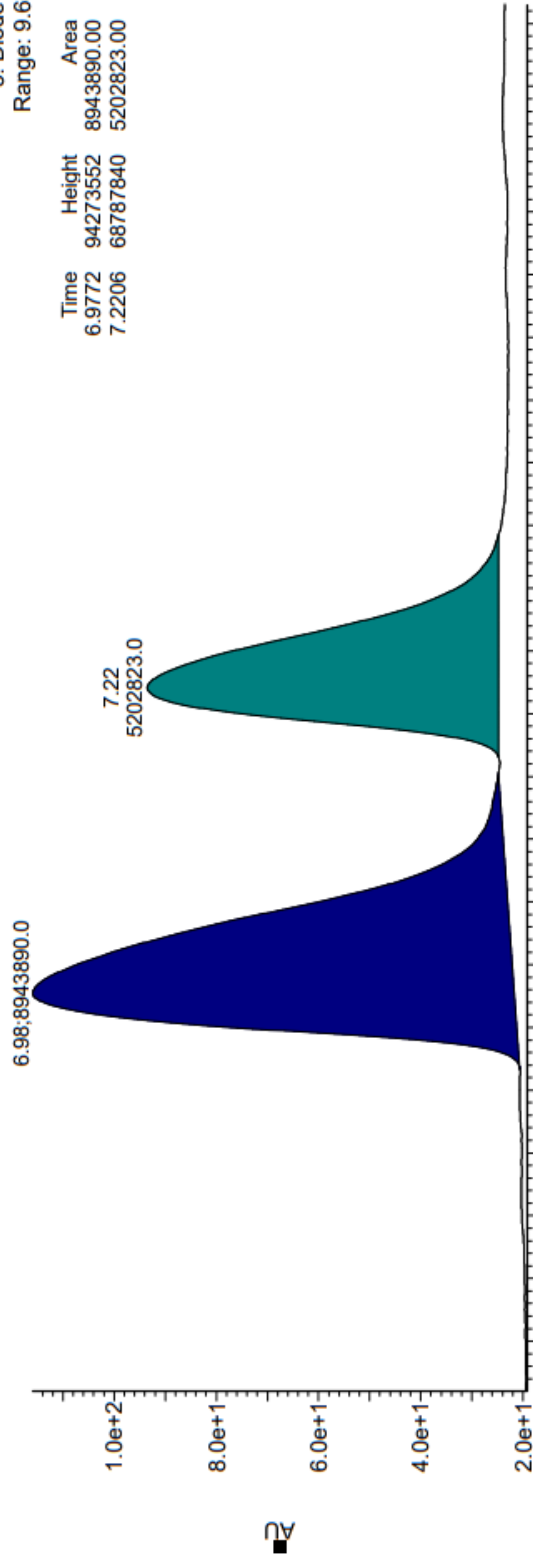
Cel1_iPrOH 0.5% TFA Chiral Separation

13-Mar-2023
12:48:09

UPC2

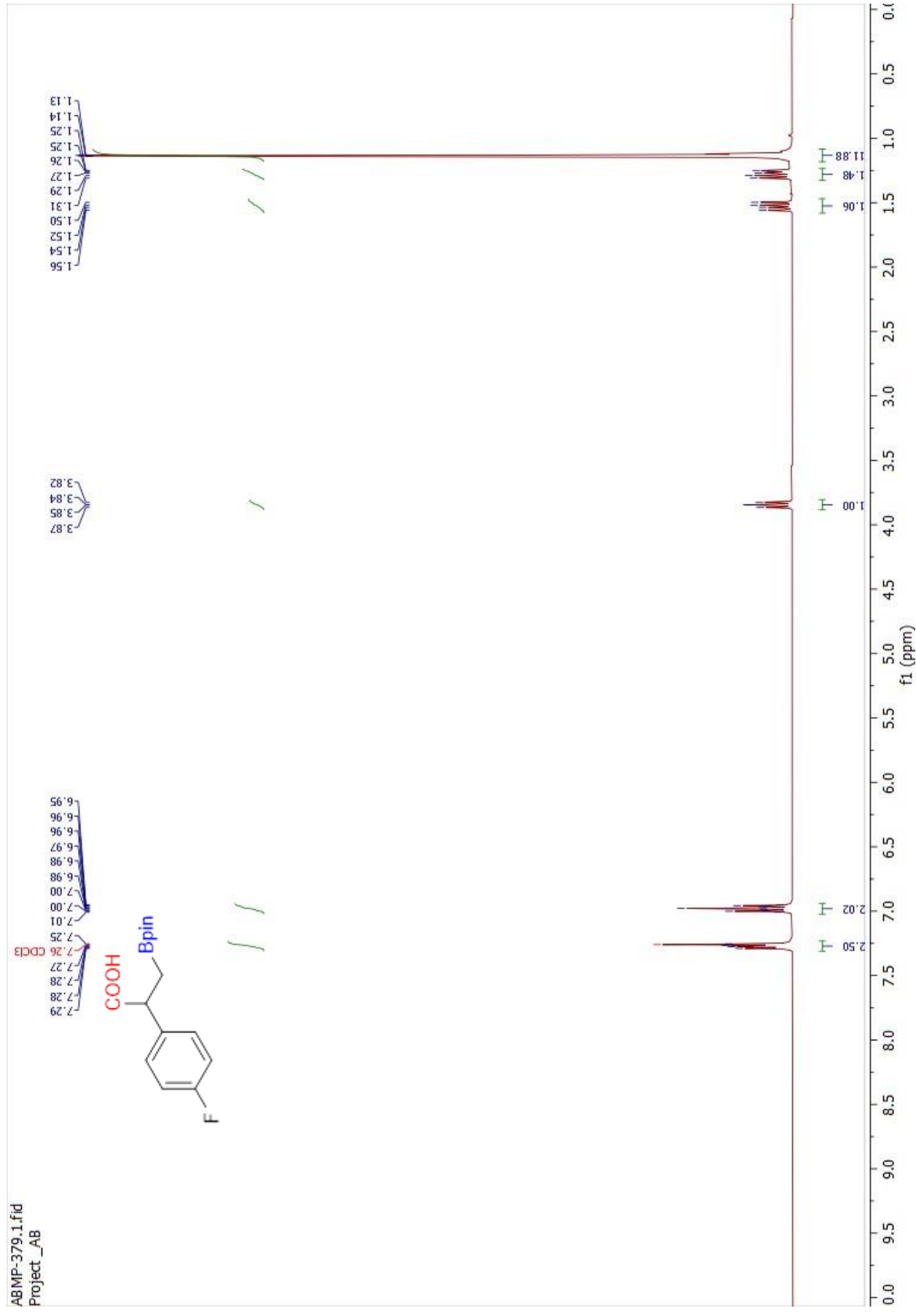
3: Diode Array
Range: 9.656e+1

Time	Height	Area	Area%
6.9772	94273552	8943890.00	63.22
7.2206	68787840	5202823.00	36.78

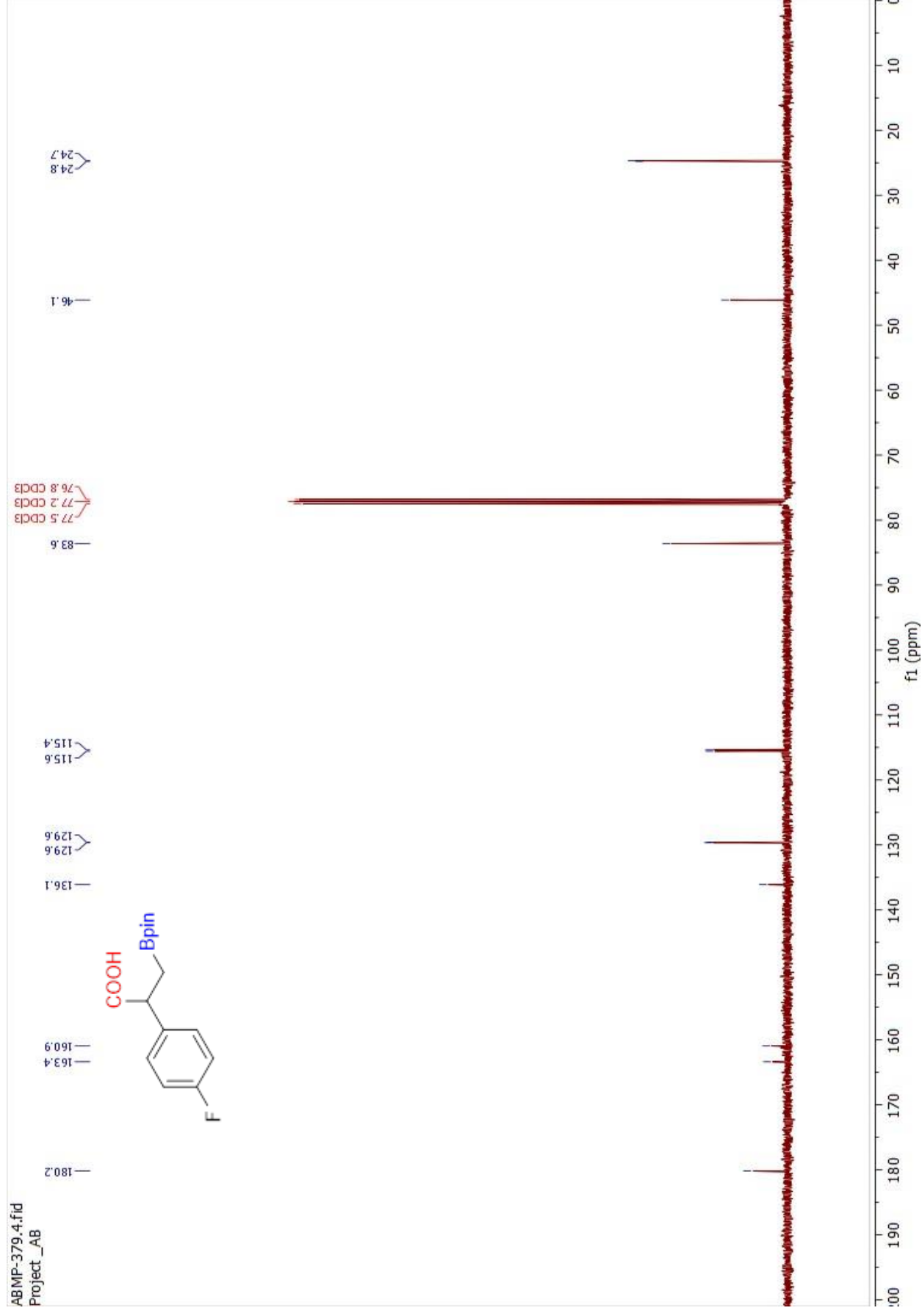


Spectrum S26. ¹H NMR of compound 2m in CDCl₃

ABMP-379.1.fid
Project_AB

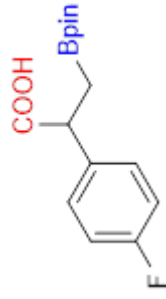


Spectrum S27. ¹³C NMR of compound 2m in CDCl₃

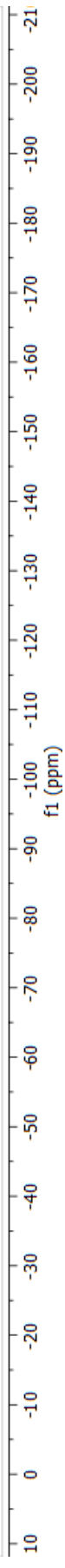


Spectrum S28. ^{19}F NMR of compound **2m** in CDCl_3

ABMP-386.2.fid
Project_AB



— -115.6



Chromatogram S13. Compound 2m and its racemate.

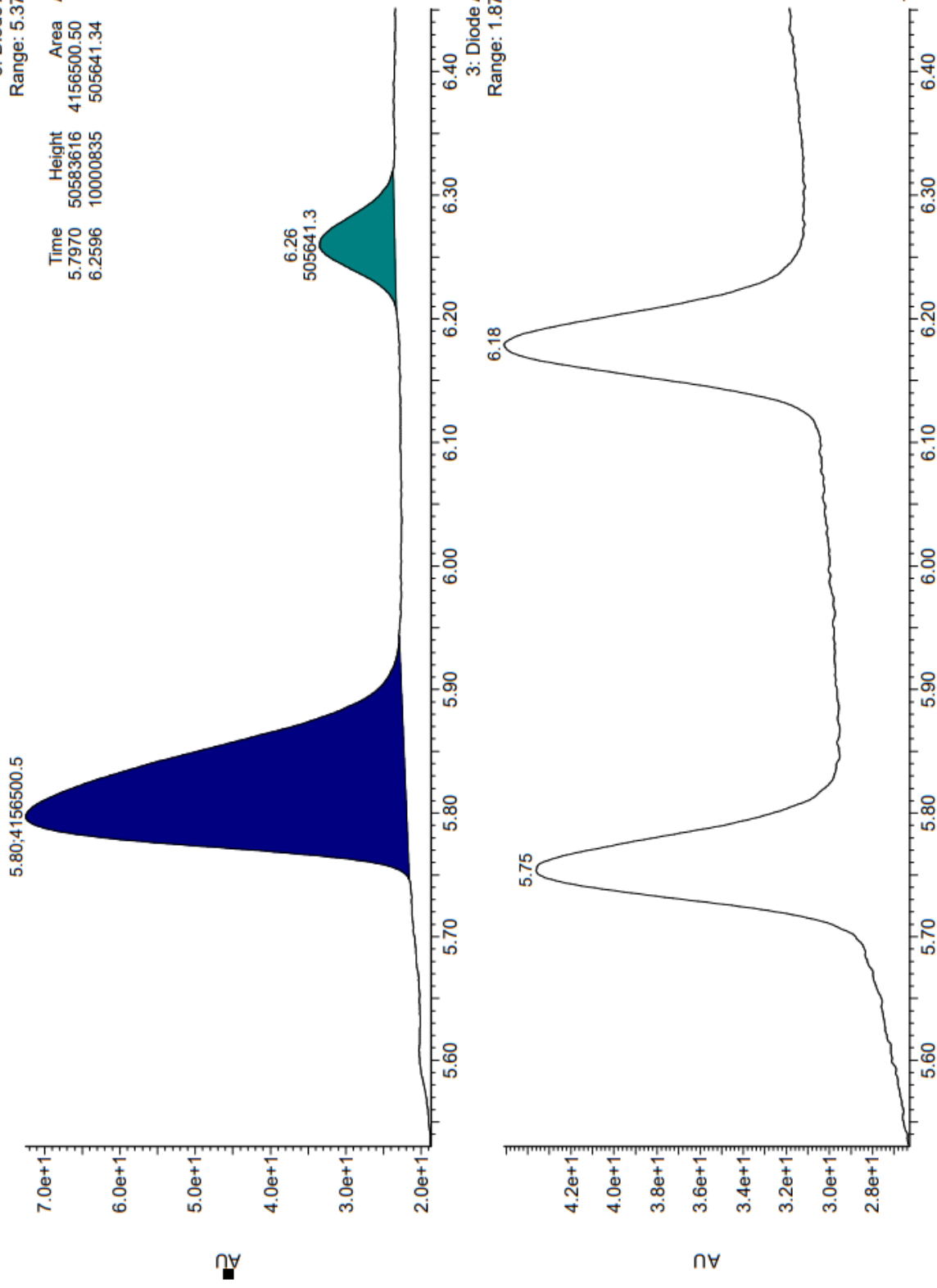
Amy1_iPrOH 0.5% TFA Chiral Separation

24-Mar-2023
15:12:02

UPC2

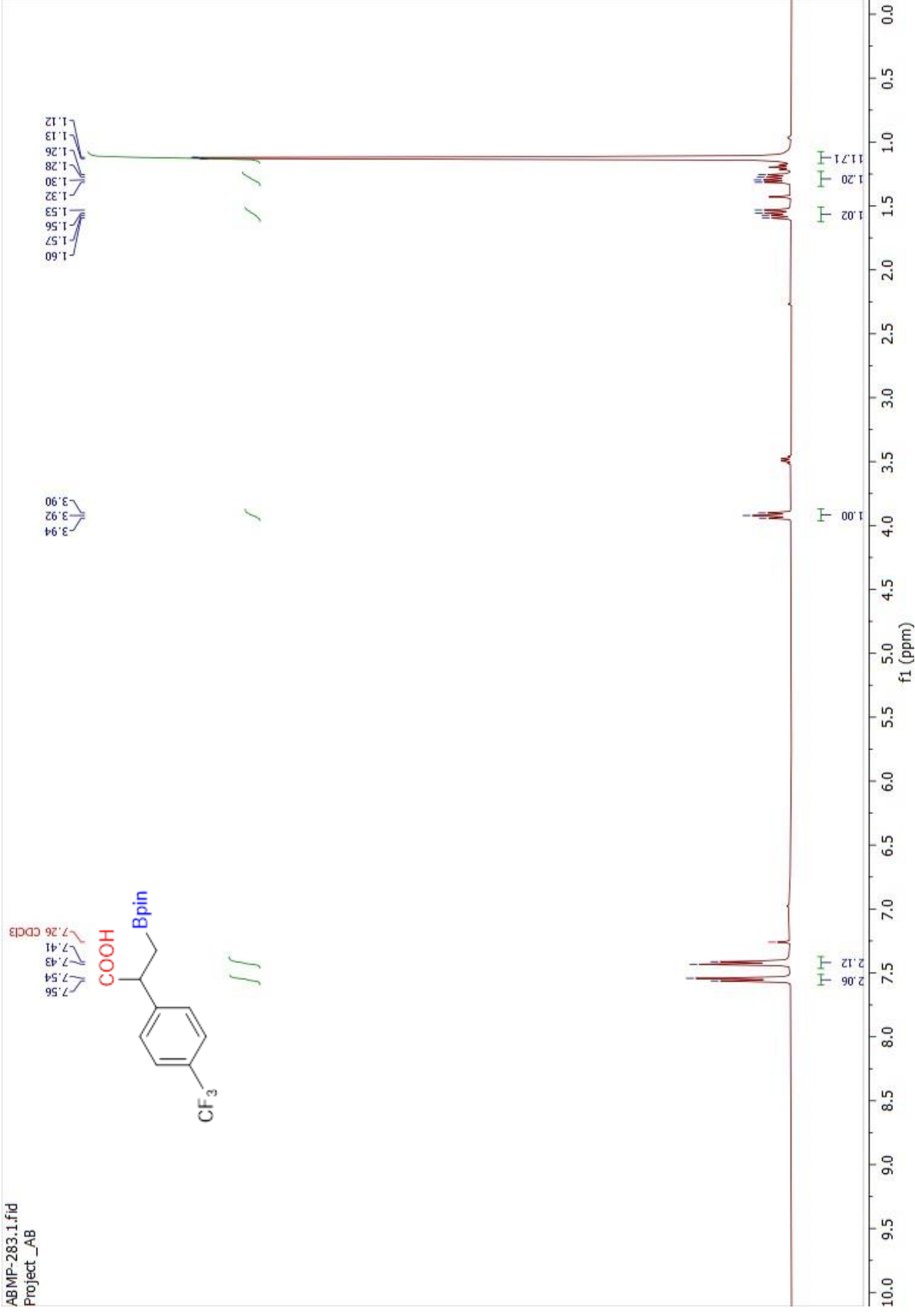
Time	Height	Area	Area%
5.7970	50583616	4156500.50	89.15
6.2596	10000835	505641.34	10.85

3: Diode Array
Range: 5.374e+1



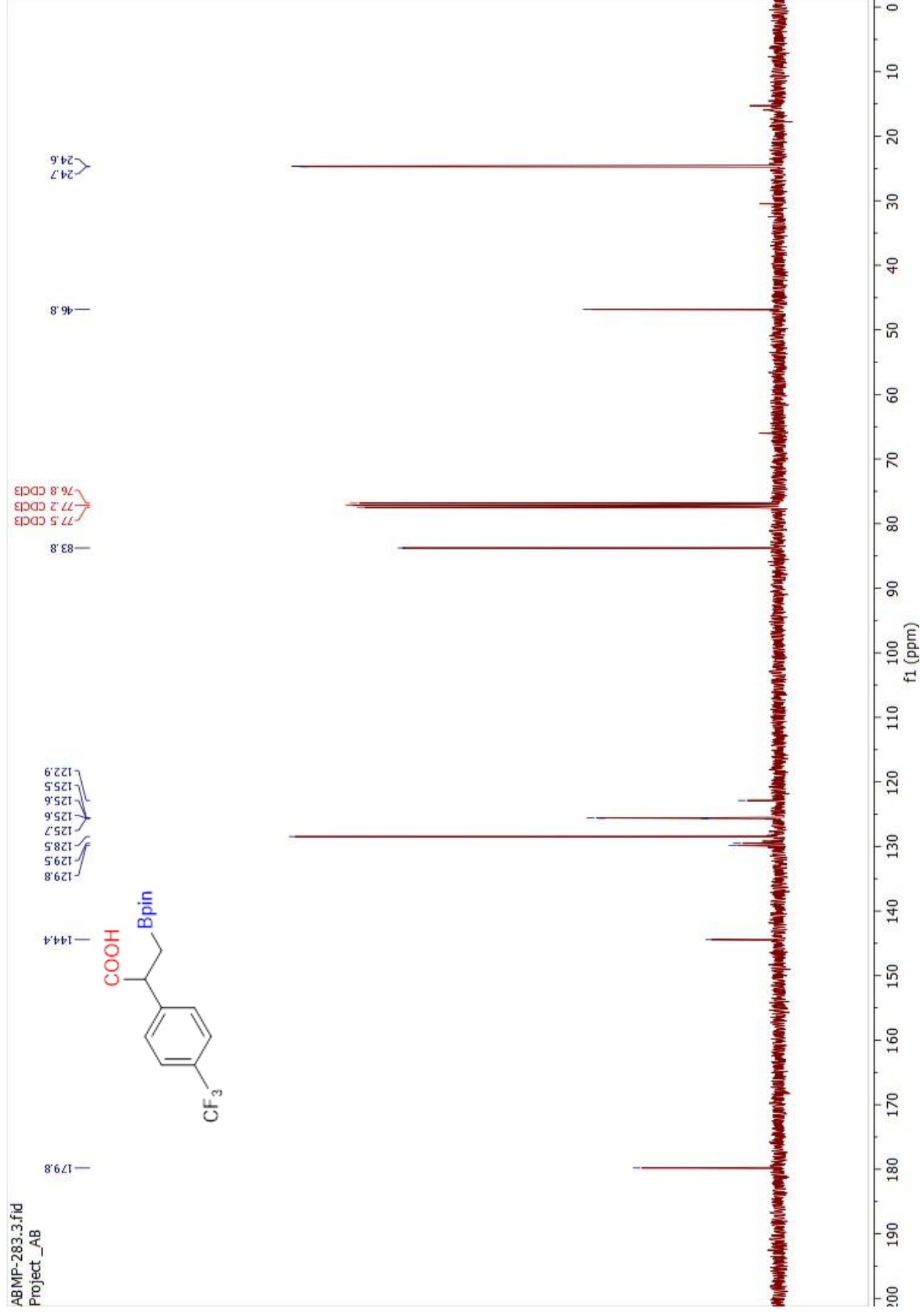
Spectrum S29. ¹H NMR of compound 2n in CDCl₃

ABMP-283.1.fid
Project_AB



Spectrum S30. ¹³C NMR of compound **2n** in CDCl₃

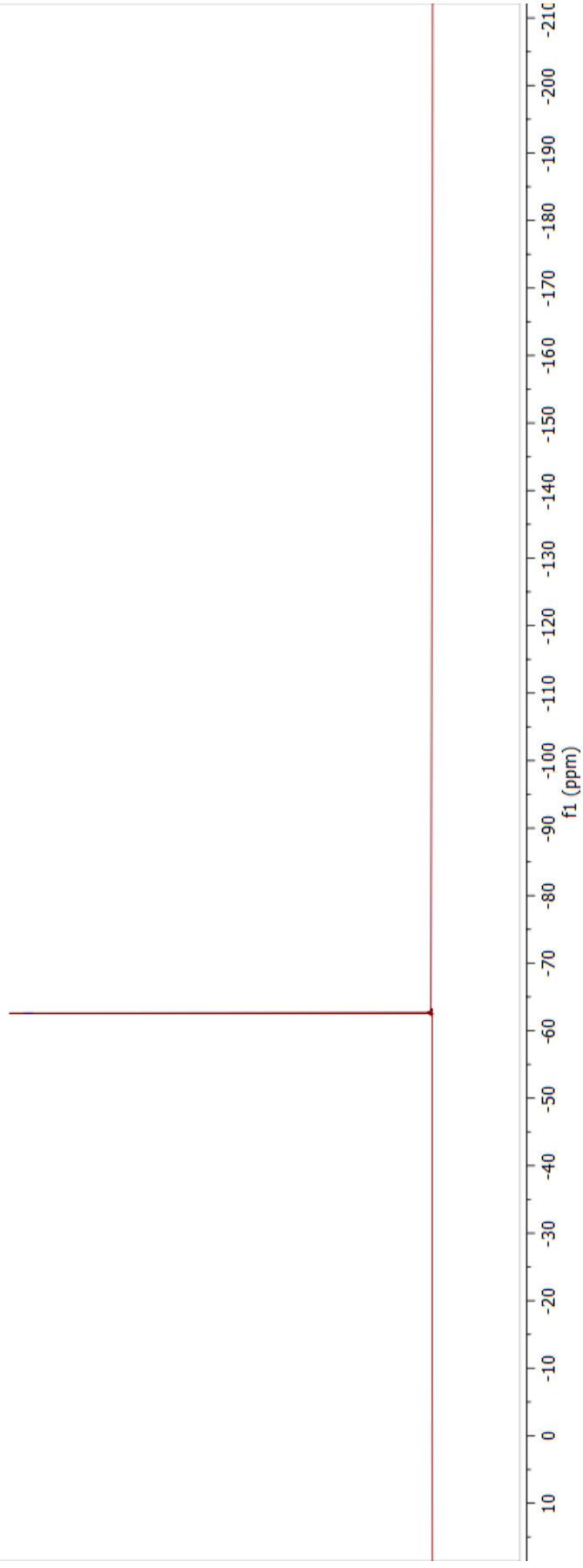
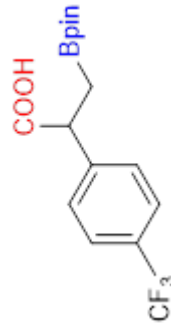
ABMP-283.3.fid
Project_AB



Spectrum S31. ^{19}F NMR of compound **2n** in CDCl_3

ABRD-028-F.1.fid
Project_AB

62.6

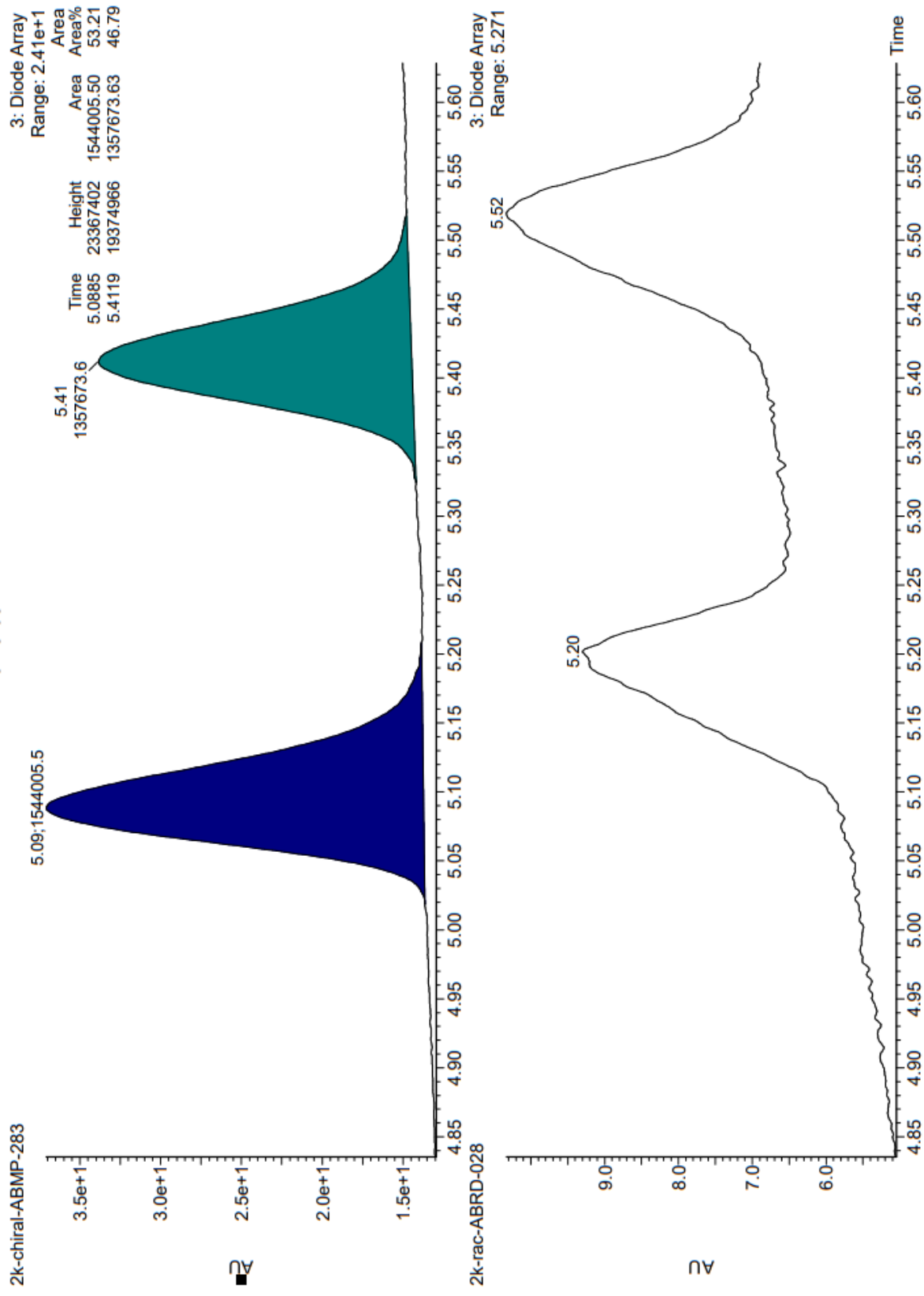


Chromatogram S14. Compound **2n** and its racemate.

Amy1_iPrOH 0.5% TFA Chiral Separation

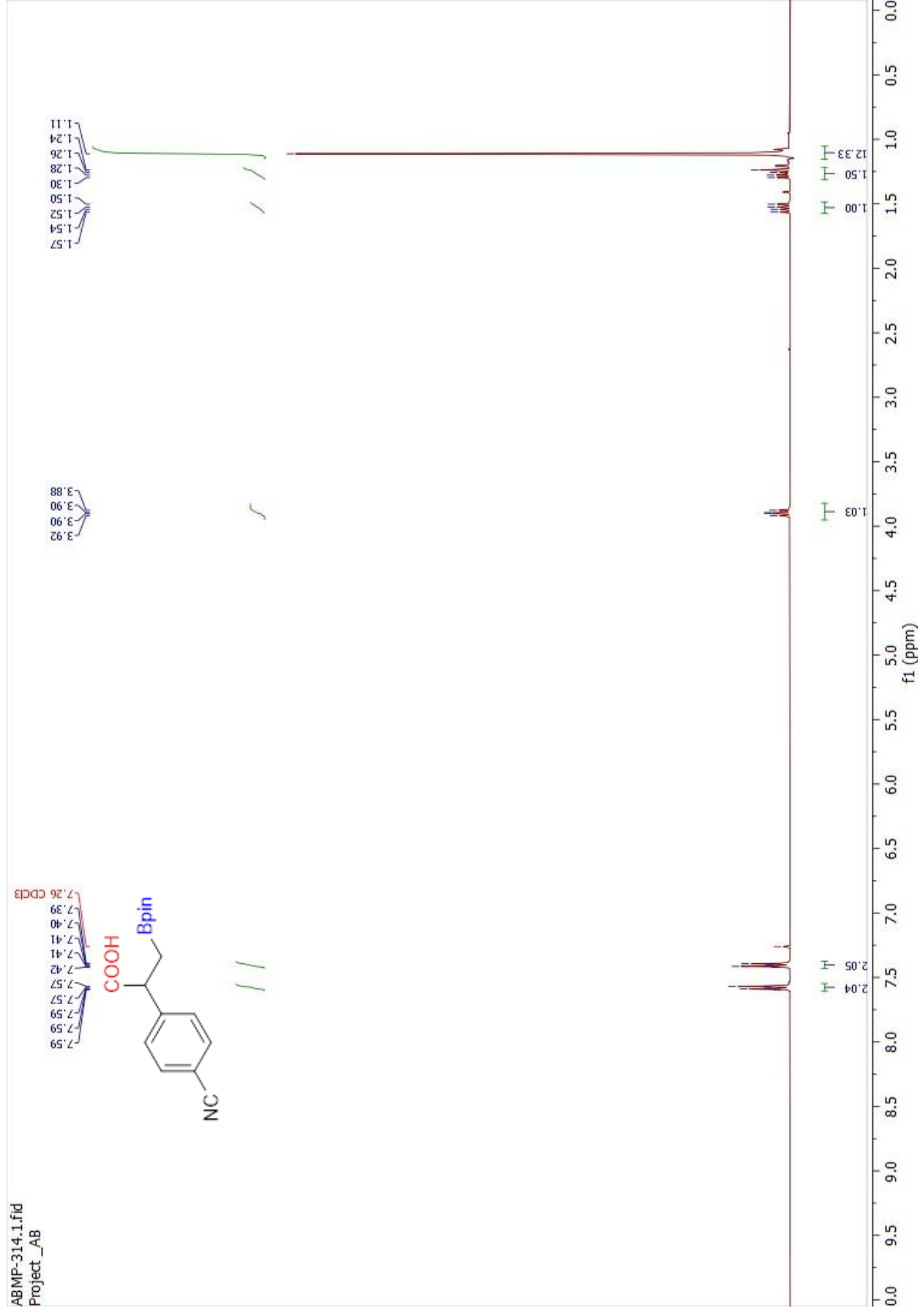
13-Mar-2023
15:28:08

UPC2

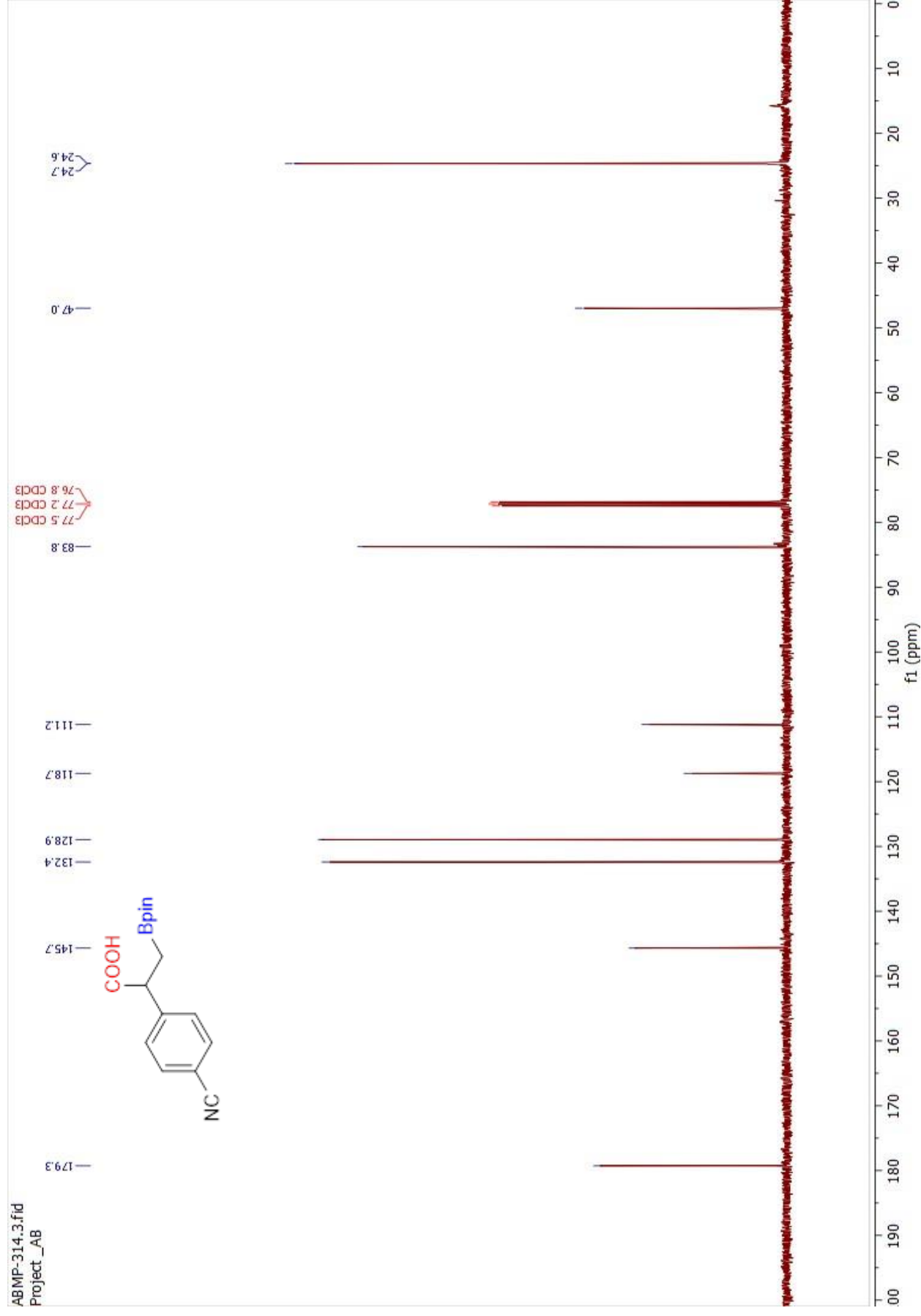


Spectrum S32. ¹H NMR of compound 2o in CDCl₃

ABMP-314.1.fid
Project_AB



Spectrum S33. ¹³C NMR of compound **2o** in CDCl₃



Chromatogram S15. Compound 2o and its racemate.

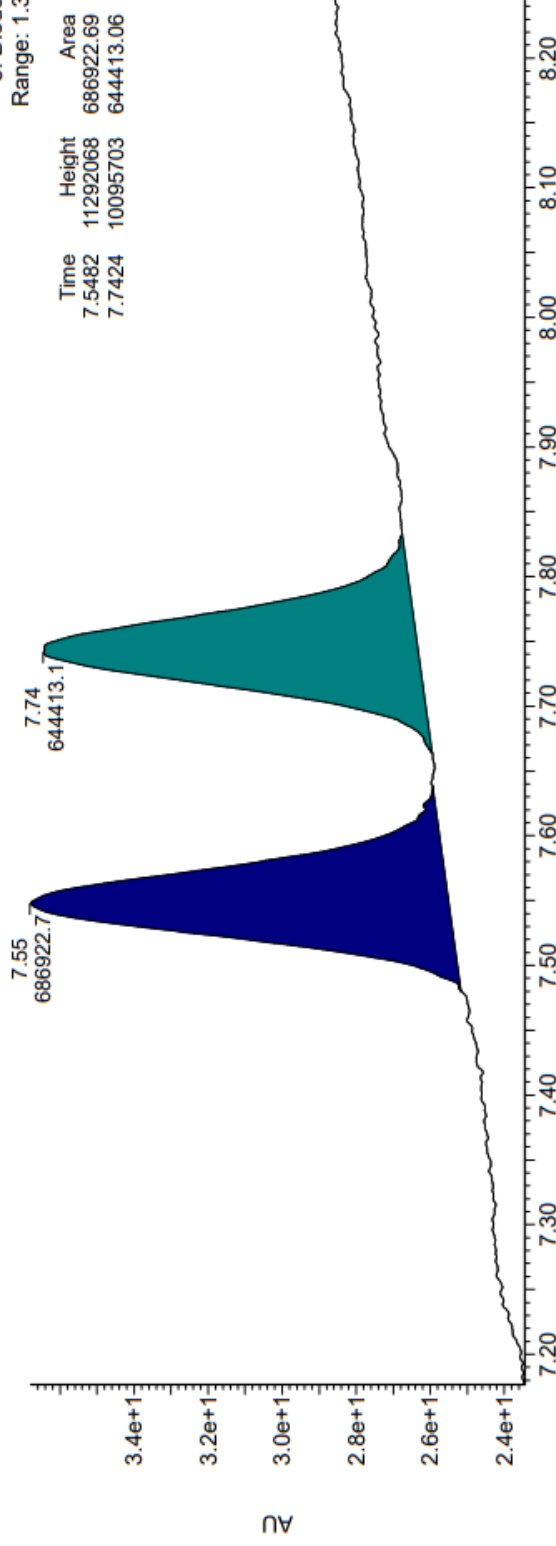
Amy1_iPrOH 0.5% TFA Chiral Separation

18-Apr-2023
12:16:08

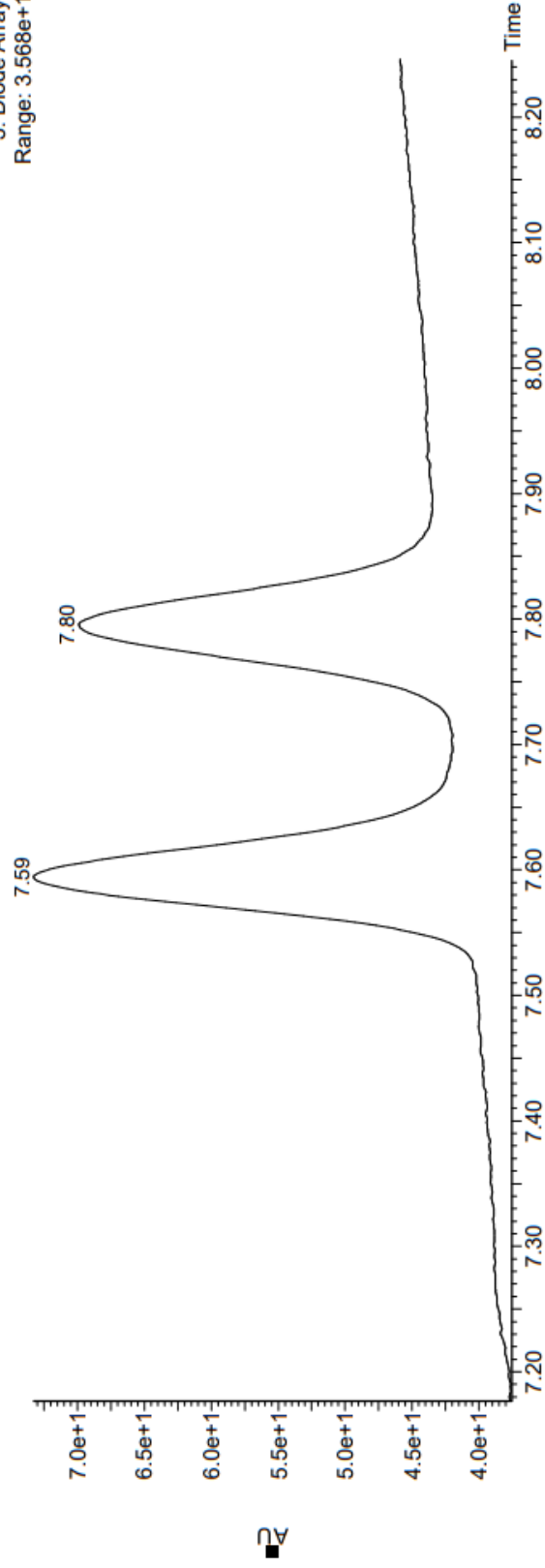
UPC2

Time	Height	Area	Area%
7.55	11292068	686922.69	51.60
7.74	10095703	644413.06	48.40

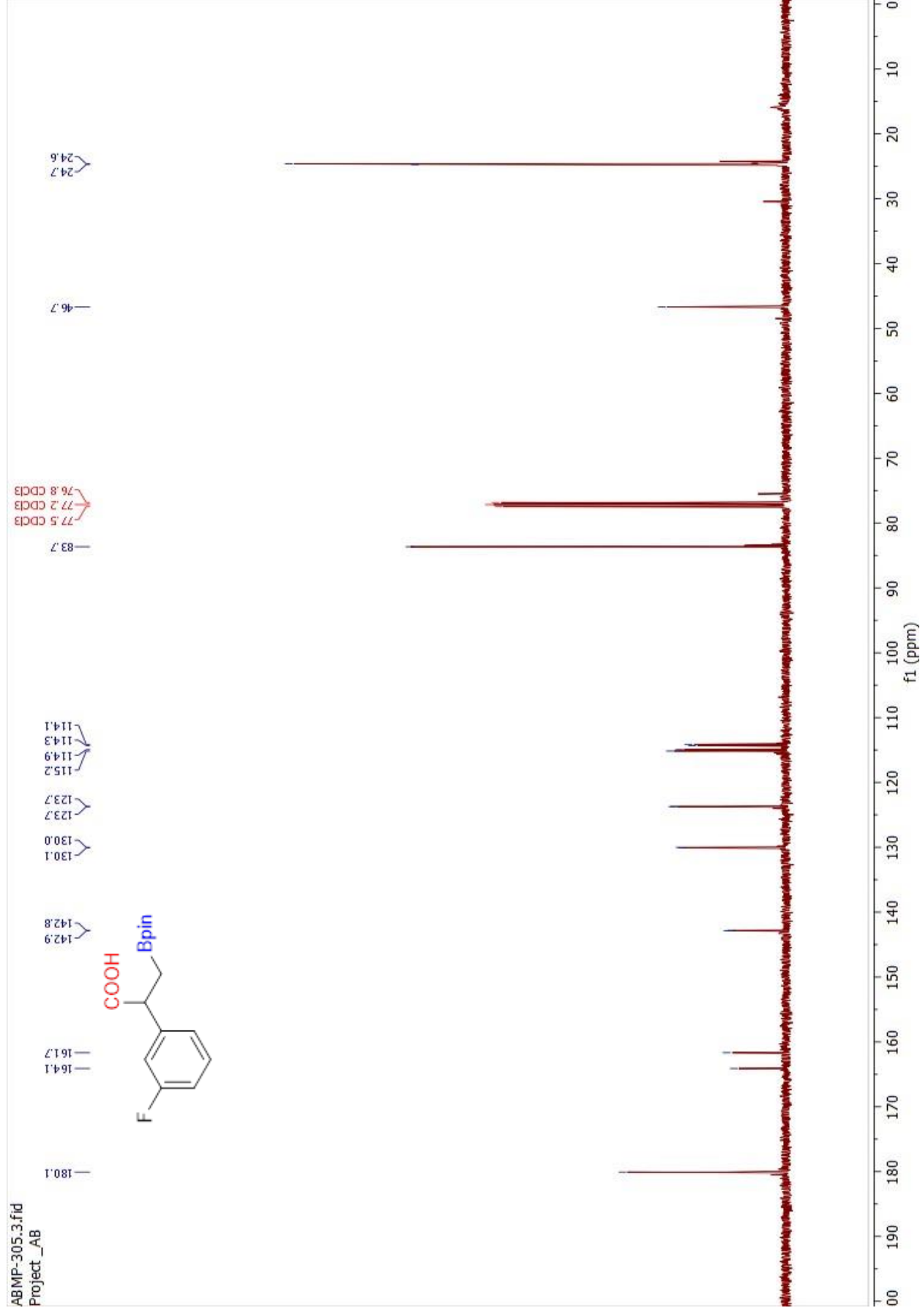
3: Diode Array
Range: 1.331e+1



3: Diode Array
Range: 3.568e+1

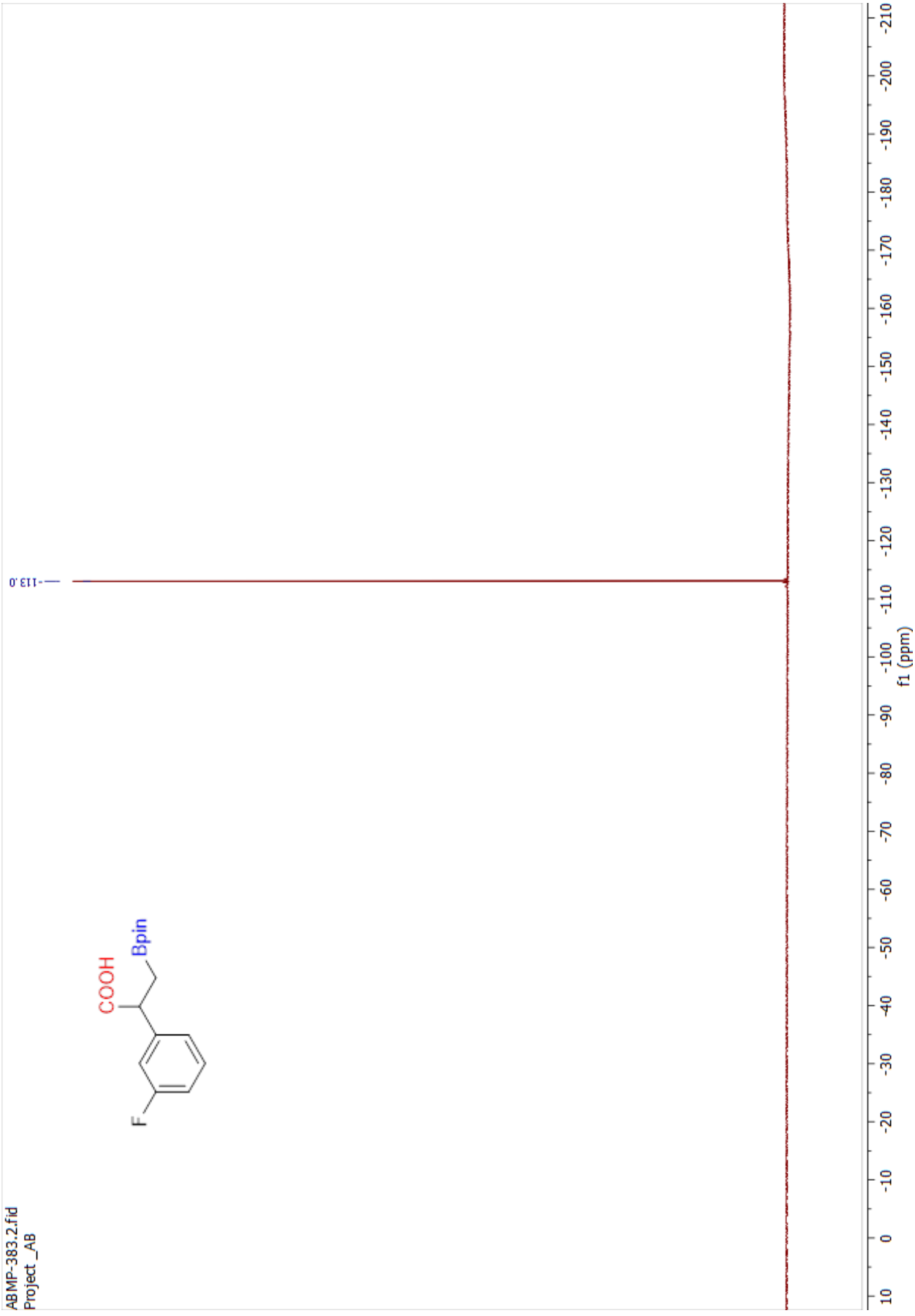
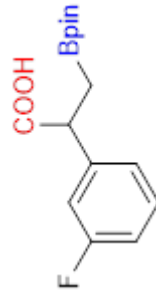


Spectrum S35. ¹³C NMR of compound 2p in CDCl₃



Spectrum S36. ^{19}F NMR of compound **2p** in CDCl_3

ABMP-383.2.fid
Project_AB



Chromatogram S16. Compound 2p and its racemate.

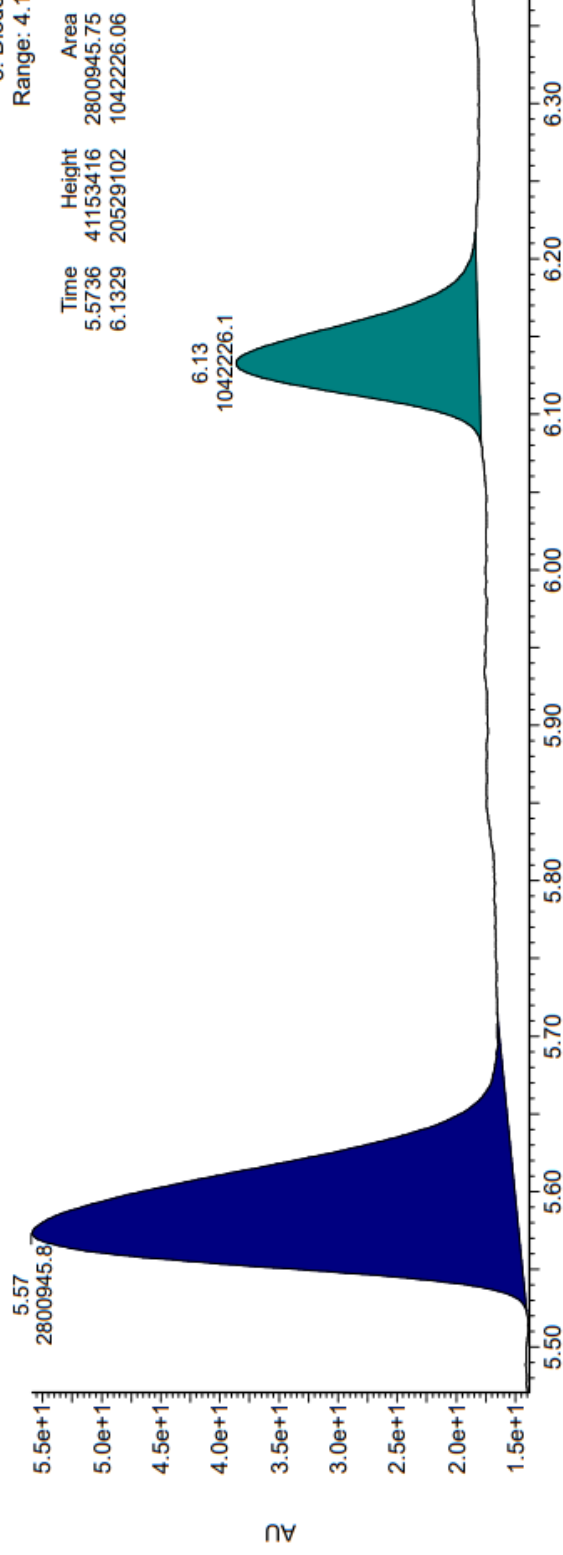
Amy1_iPrOH 0.5% TFA Chiral Separation

30-Mar-2023
15:28:35

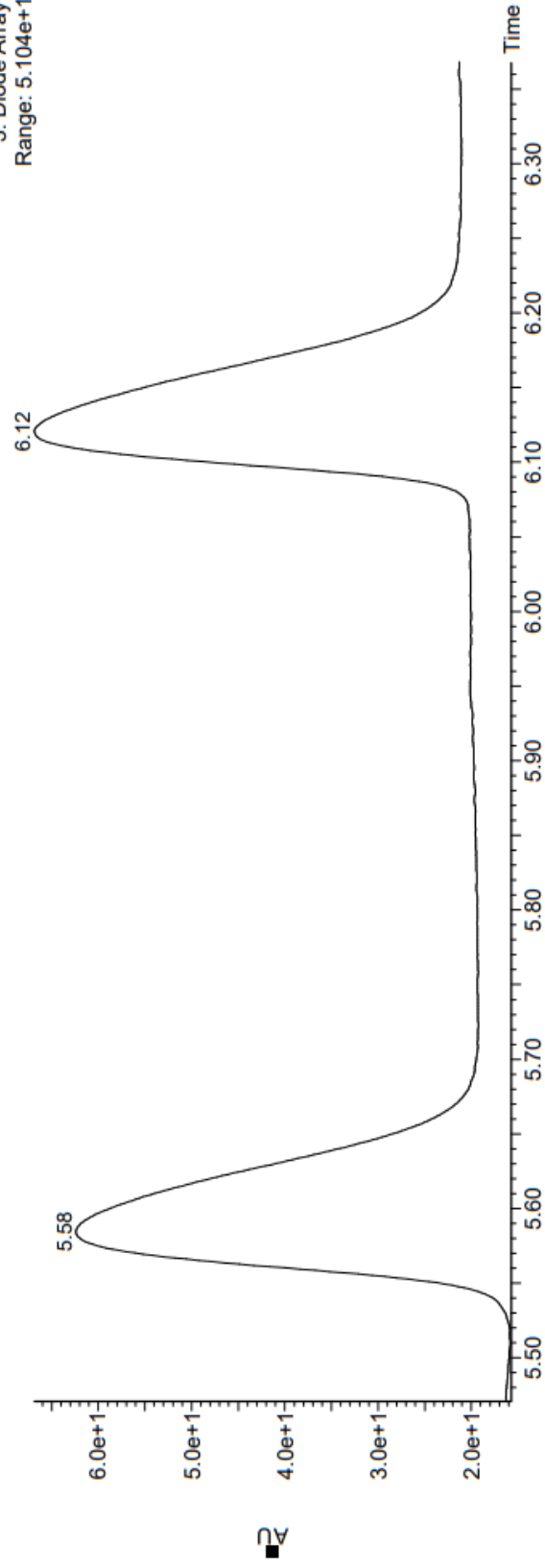
UPC2

3: Diode Array
Range: 4.196e+1

Time	Height	Area	Area%
5.5736	41153416	2800945.75	72.88
6.1329	20529102	1042226.06	27.12

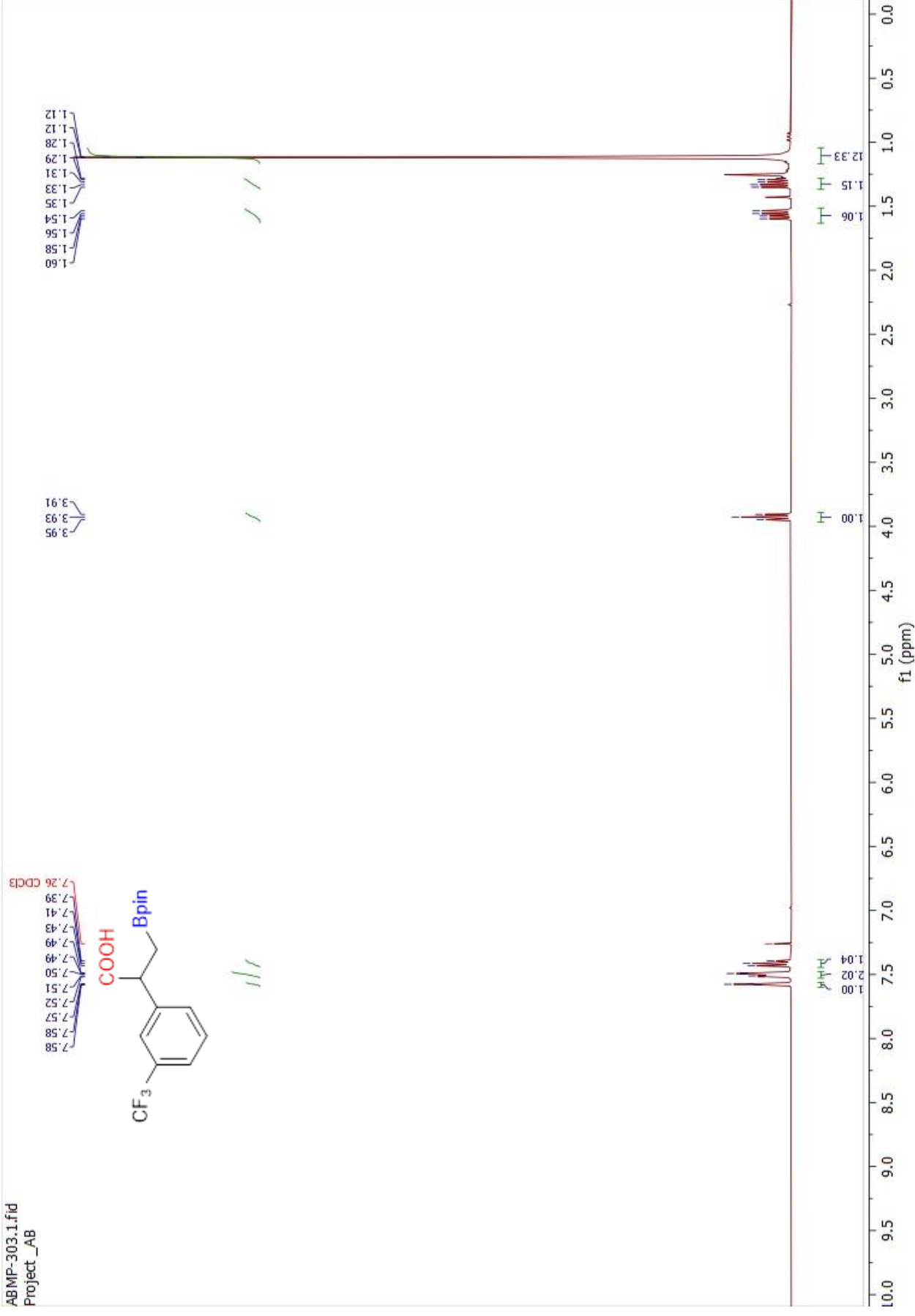


3: Diode Array
Range: 5.104e+1



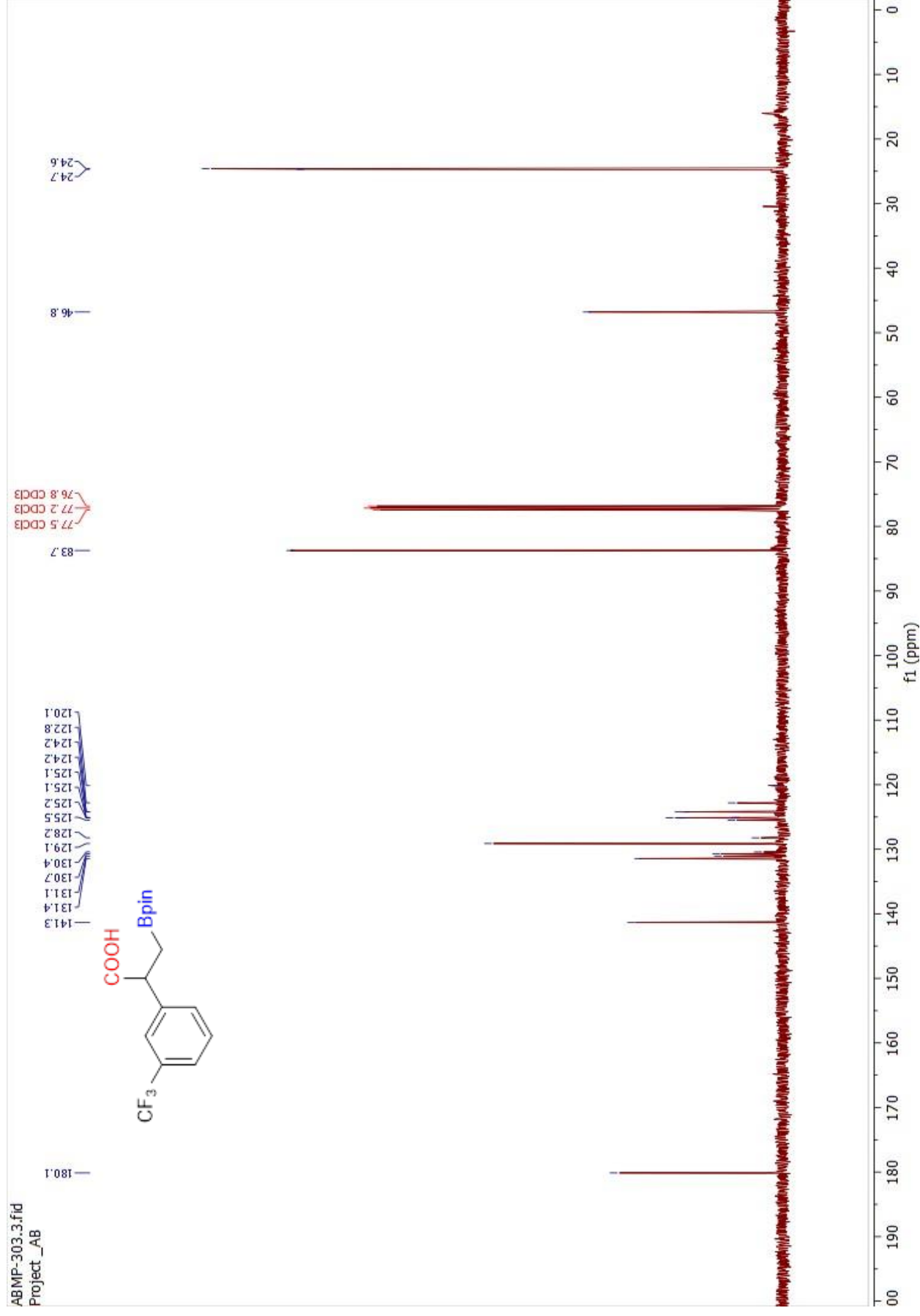
Spectrum S37. ¹H NMR of compound 2q in CDCl₃

ABMP-303.1.fid
Project_AB



Spectrum S38. ¹³C NMR of compound 2q in CDCl₃

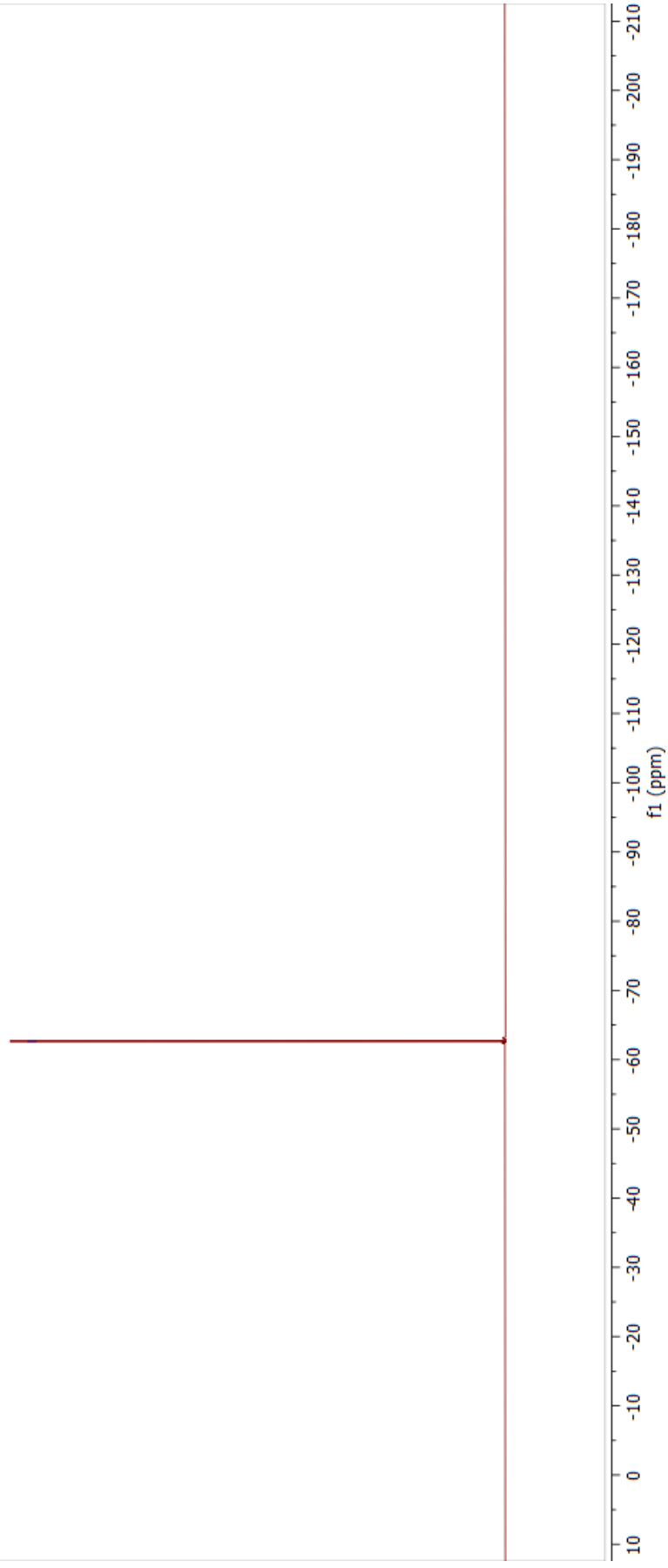
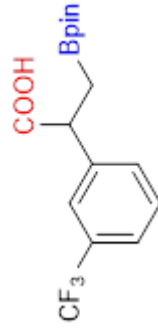
ABMP-303.3.fid
Project_AB



Spectrum S39. ^{19}F NMR of compound **2q** in CDCl_3

ABMP-384.2.fid
Project_AB

62.7



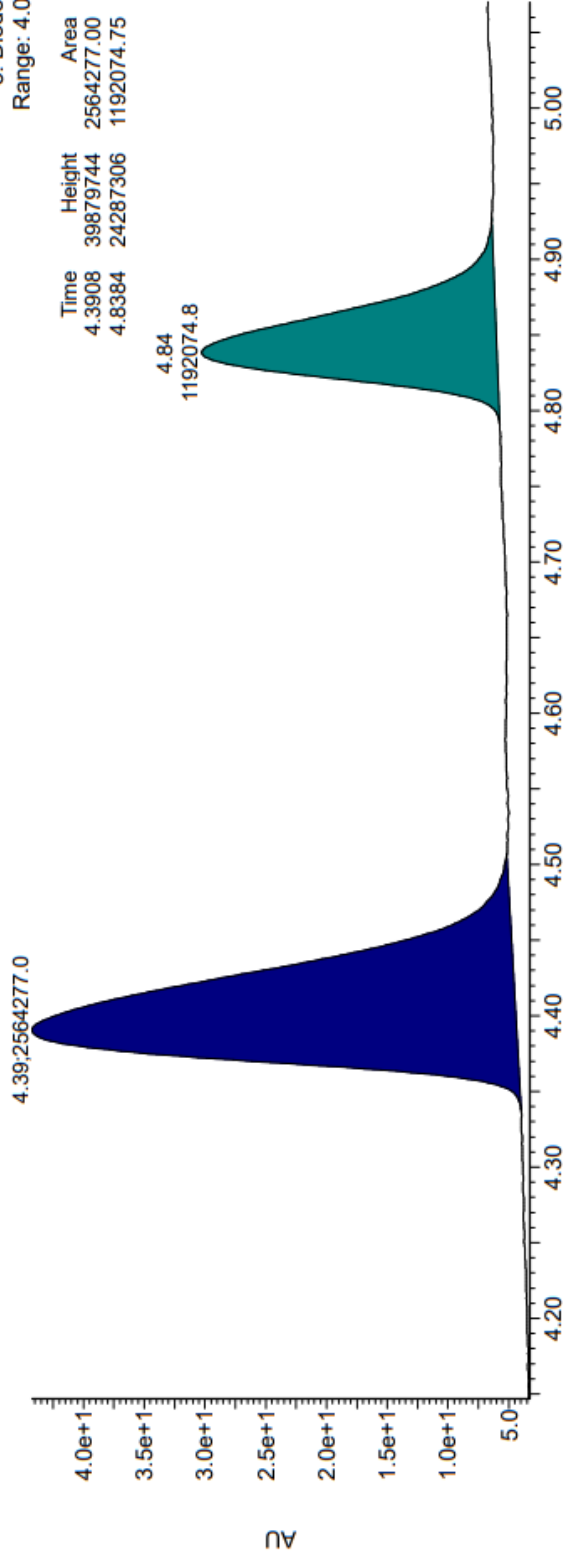
Chromatogram S17. Compound **2q** and its racemate.

Amy1_iPrOH 0.5% TFA Chiral Separation

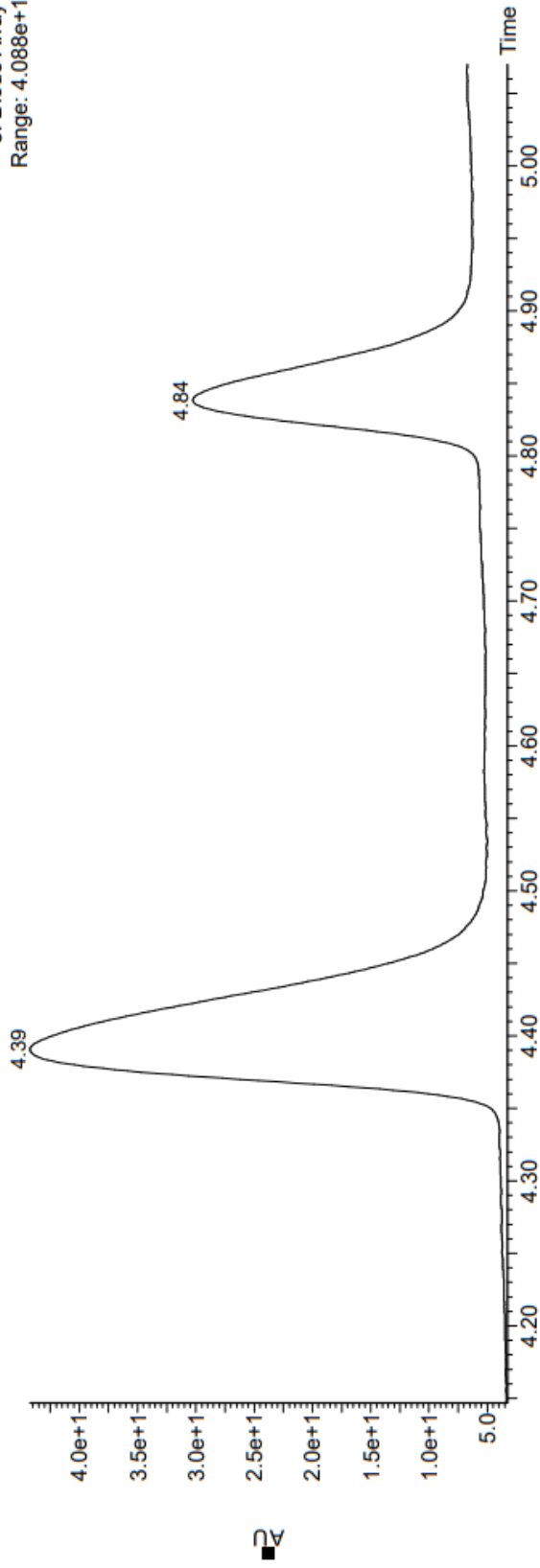
15-Mar-2023
11:39:54

UPC2

3: Diode Array
Range: 4.088e+1

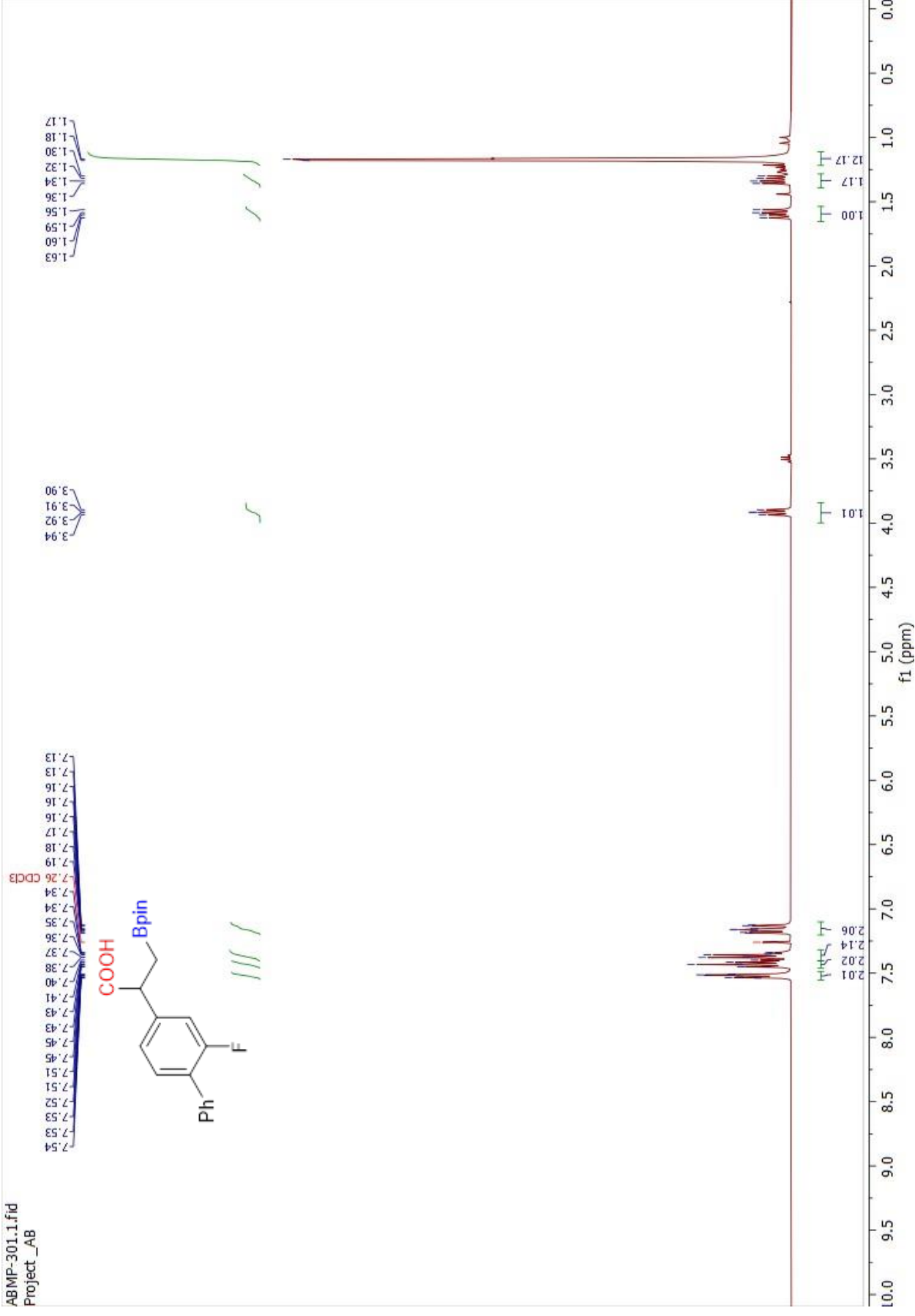


3: Diode Array
Range: 4.088e+1

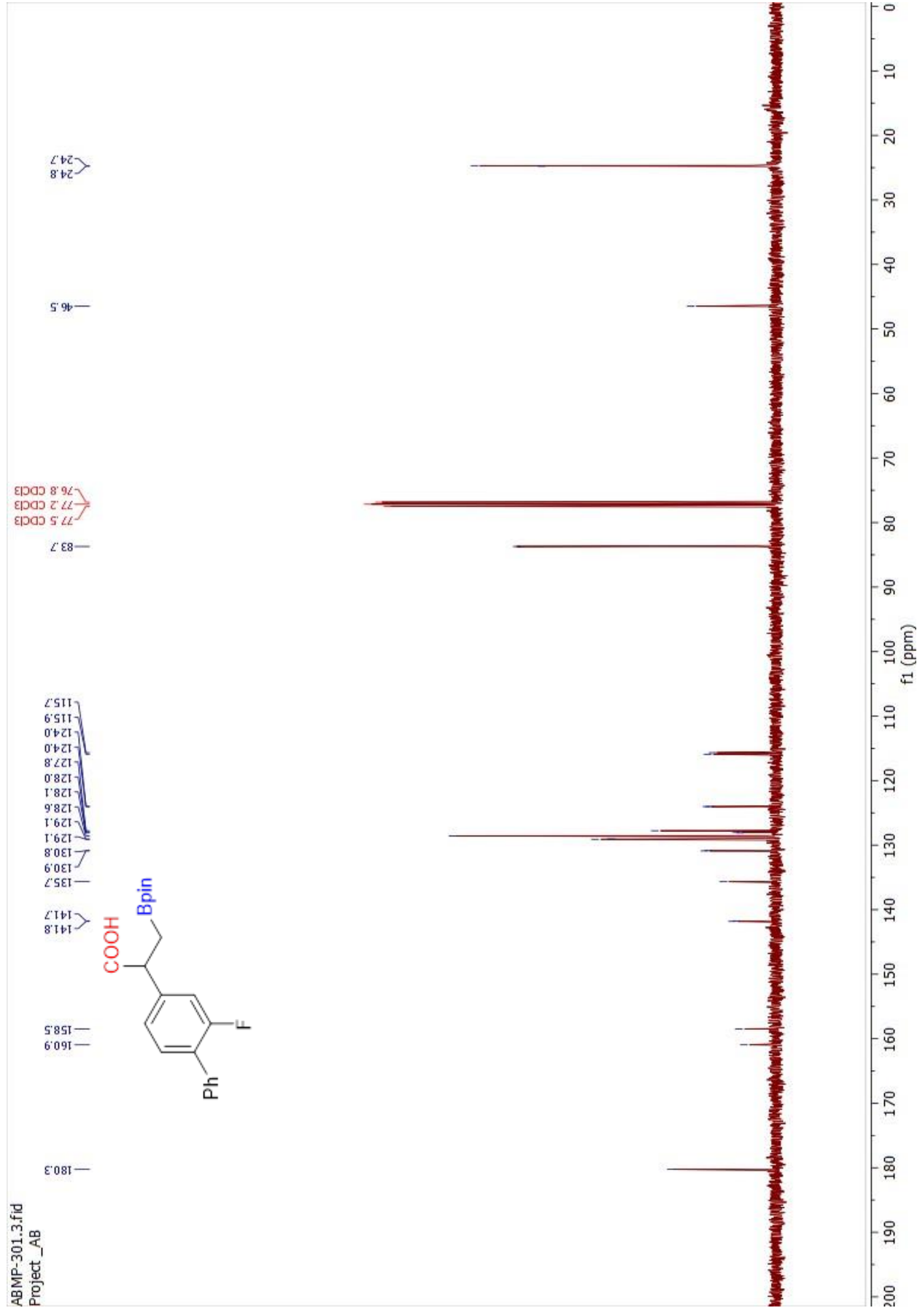


Spectrum S40. ¹H NMR of compound 2r in CDCl₃

ABMP-301.1.fid
Project_AB

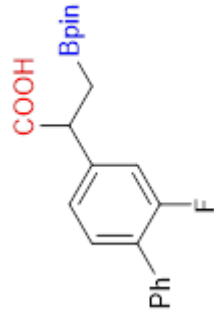


Spectrum S41. ¹³C NMR of compound 2r in CDCl₃

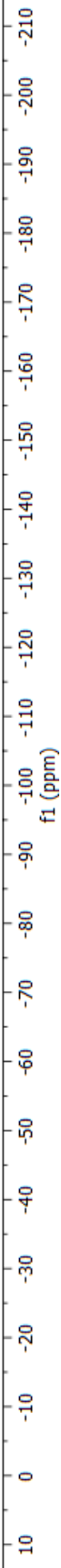


Spectrum S42. ^{19}F NMR of compound **2r** in CDCl_3

ABMP-301.4.fid
Project_AB



-117.70
-117.73
-117.75



Chromatogram S18. Compound **2r** and its racemate.

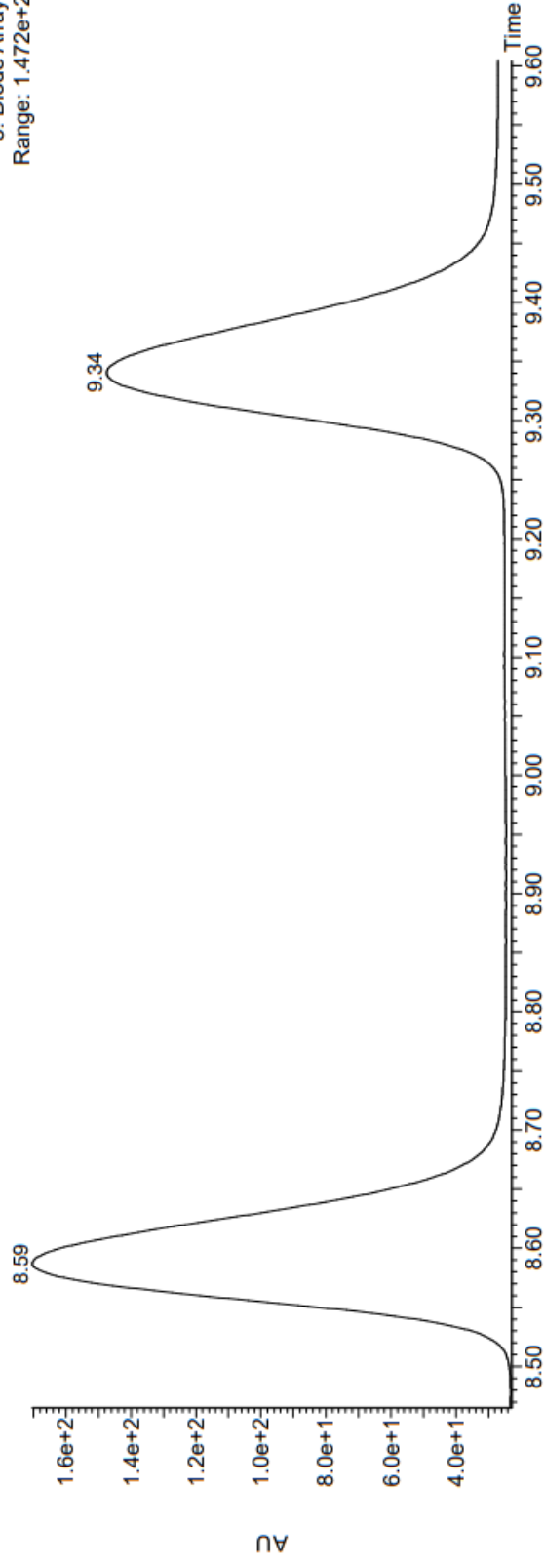
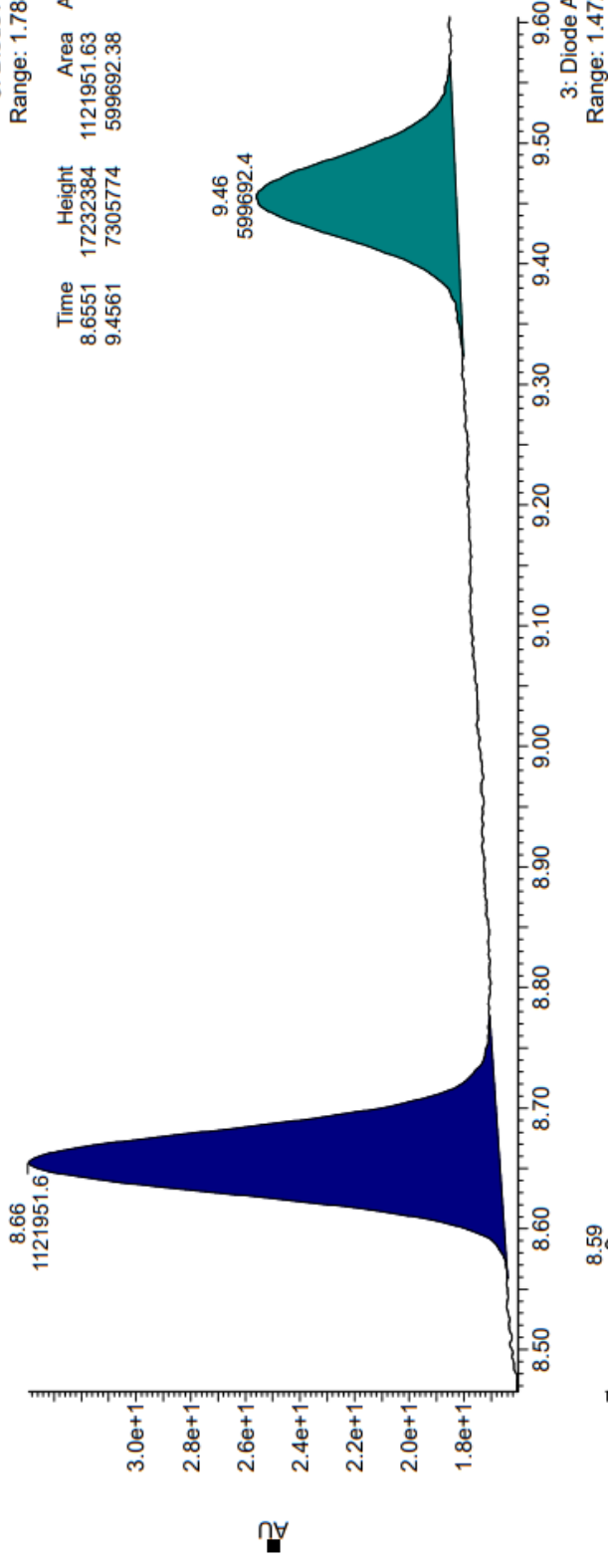
Cell1_iPrOH 0.5% TFA Chiral Separation

14-Mar-2023
12:52:36

UPC2

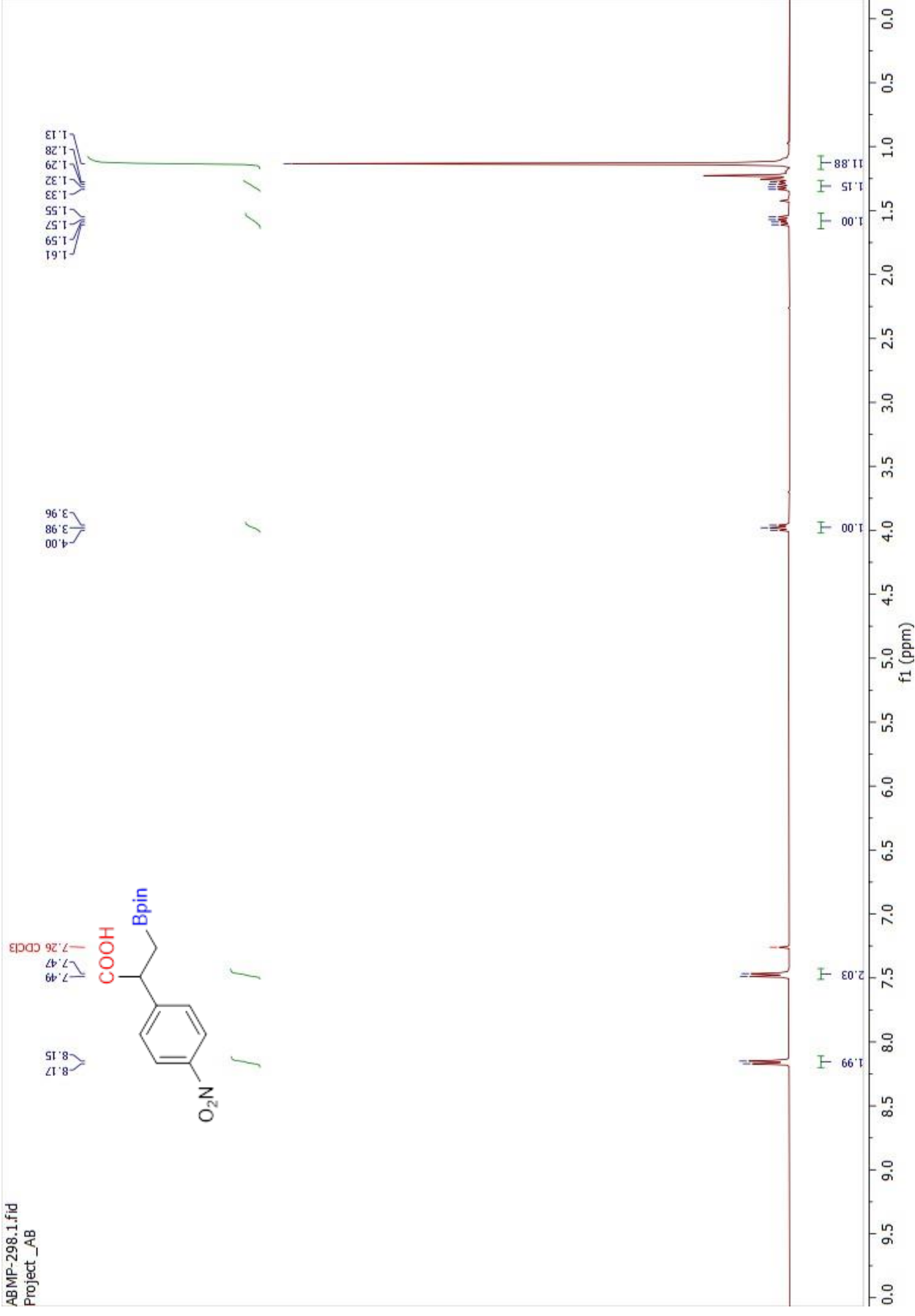
3: Diode Array
Range: 1.788e+1

Time	Height	Area	Area%
8.6551	17232384	1121951.63	65.17
9.4561	7305774	599692.38	34.83

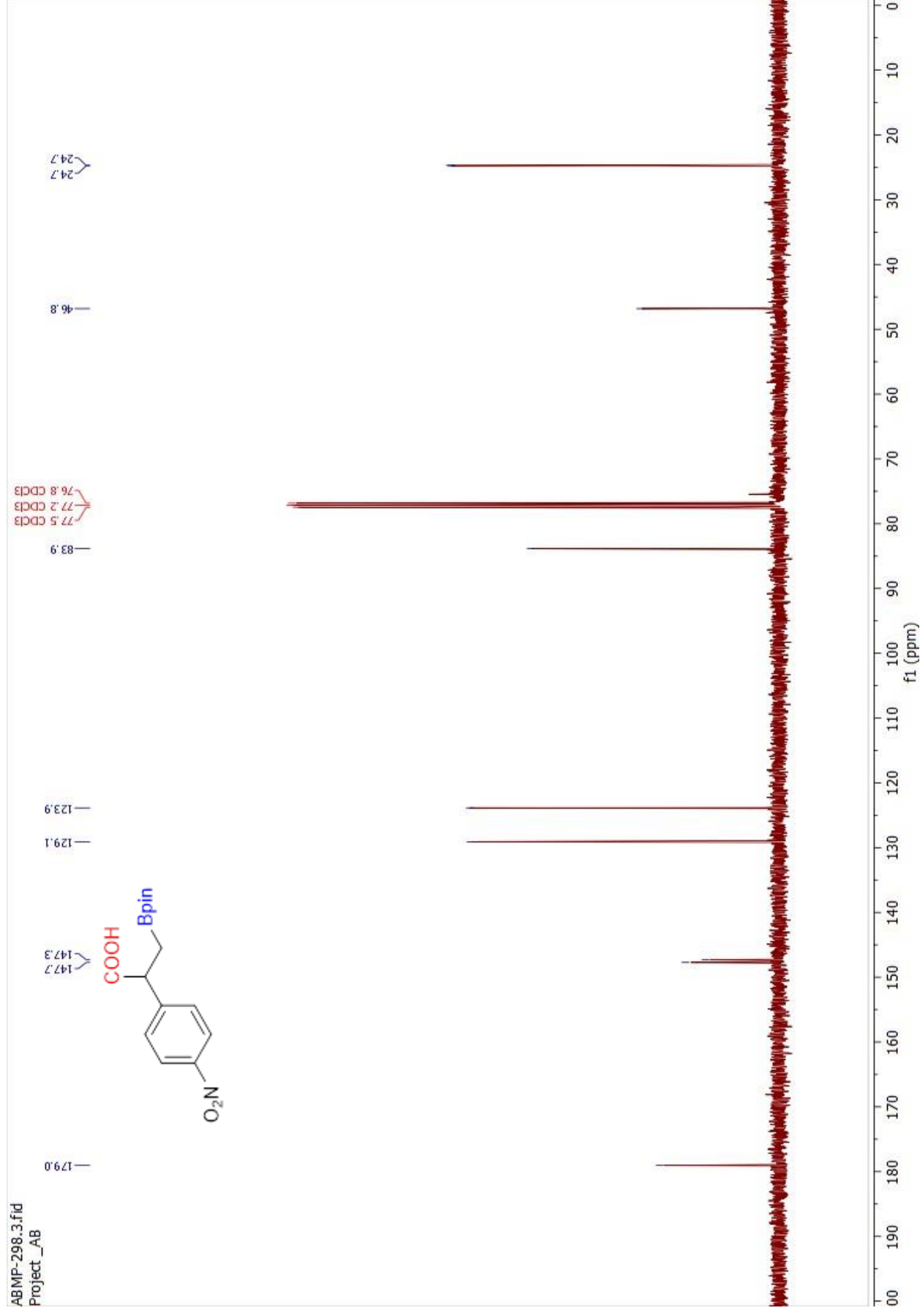


Spectrum S43. ^1H NMR of compound **2s** in CDCl_3

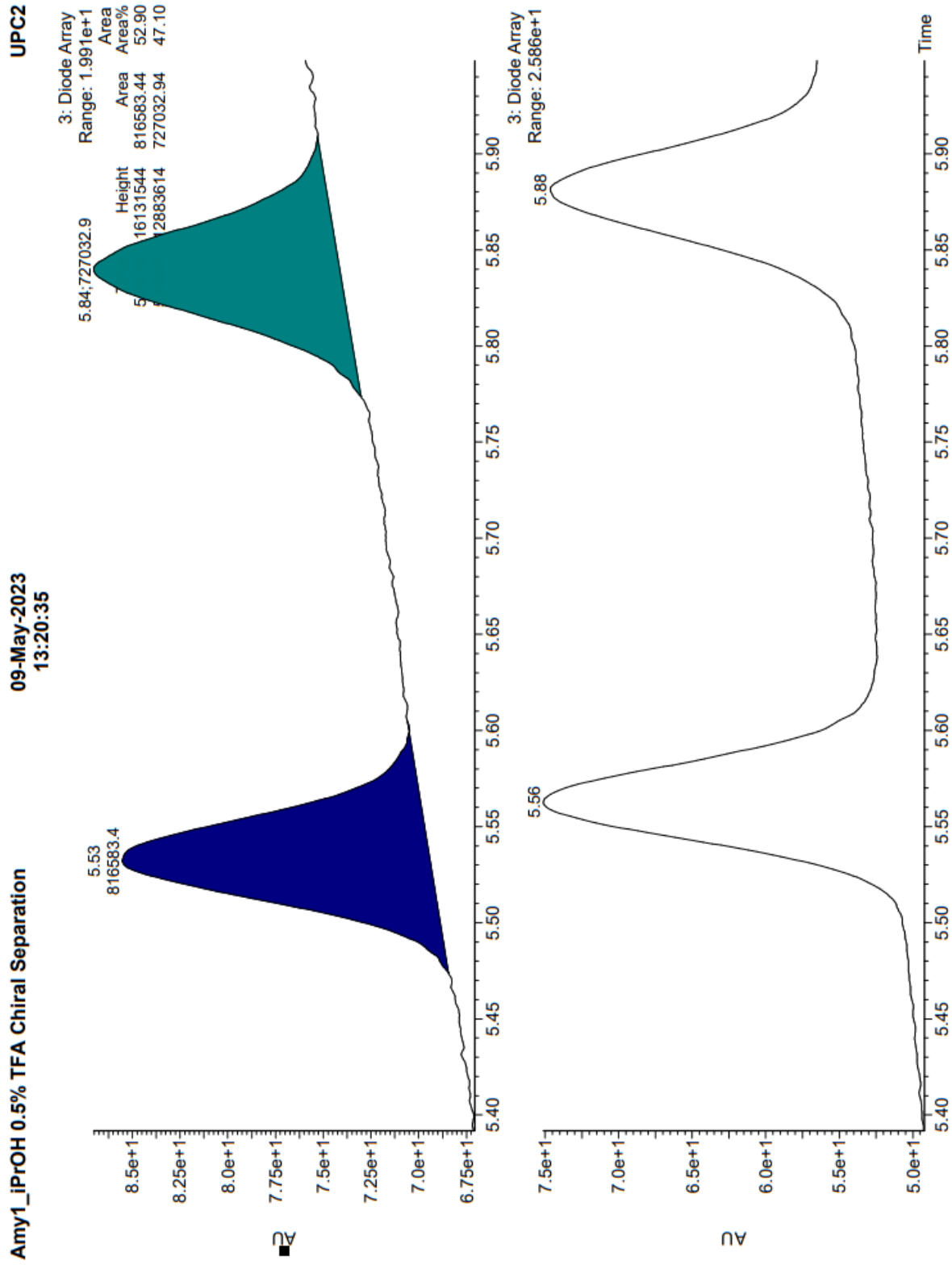
ABMP-298.1.fid
Project_AB



Spectrum S44. ^{13}C NMR of compound **2s** in CDCl_3



Chromatogram S19. Compound 2s and its racemate.

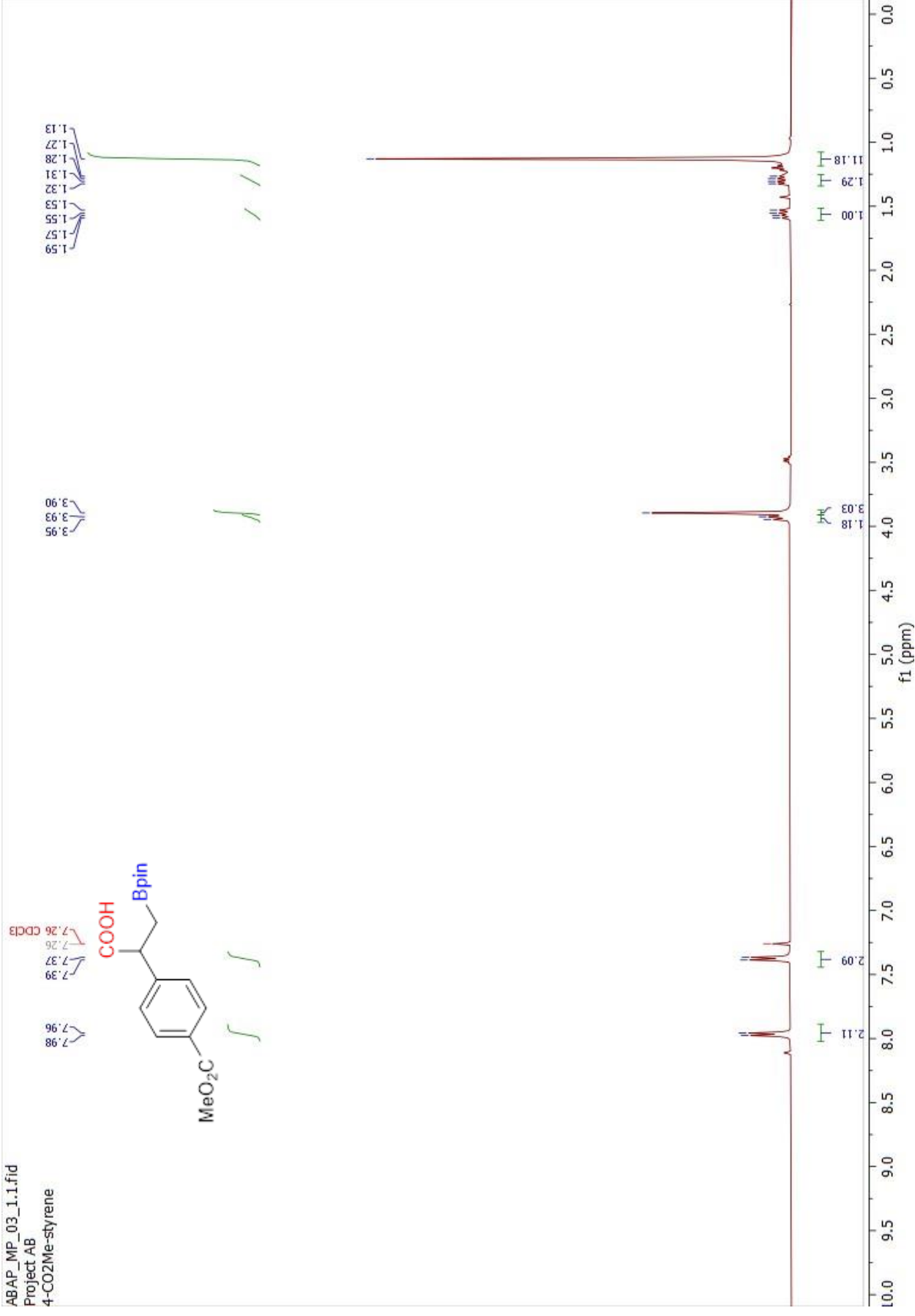


Spectrum S45. ^1H NMR of compound **2t** in CDCl_3

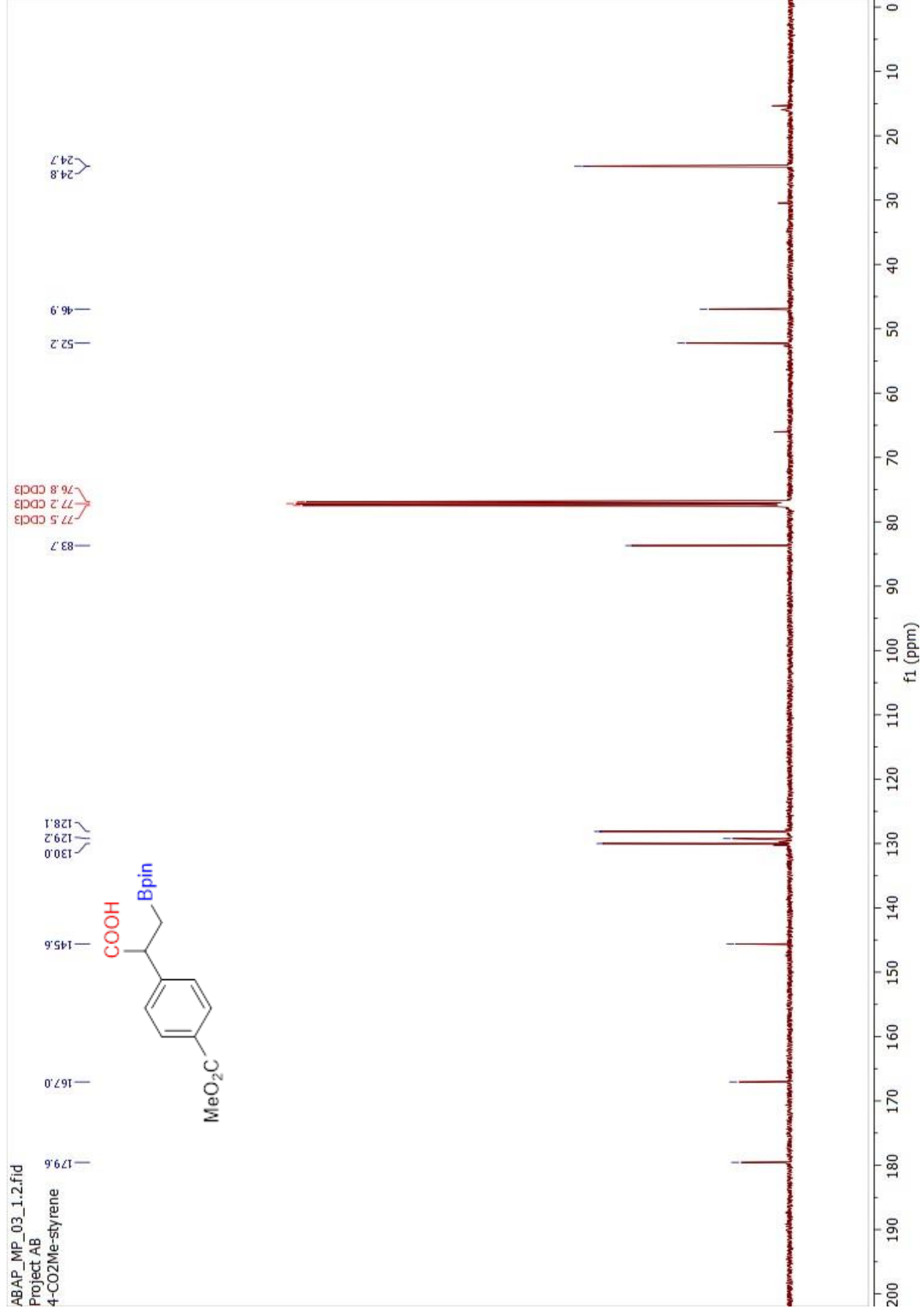
ABAP_MP_03_1_1.fid

Project AB

4-CO₂Me-styrene

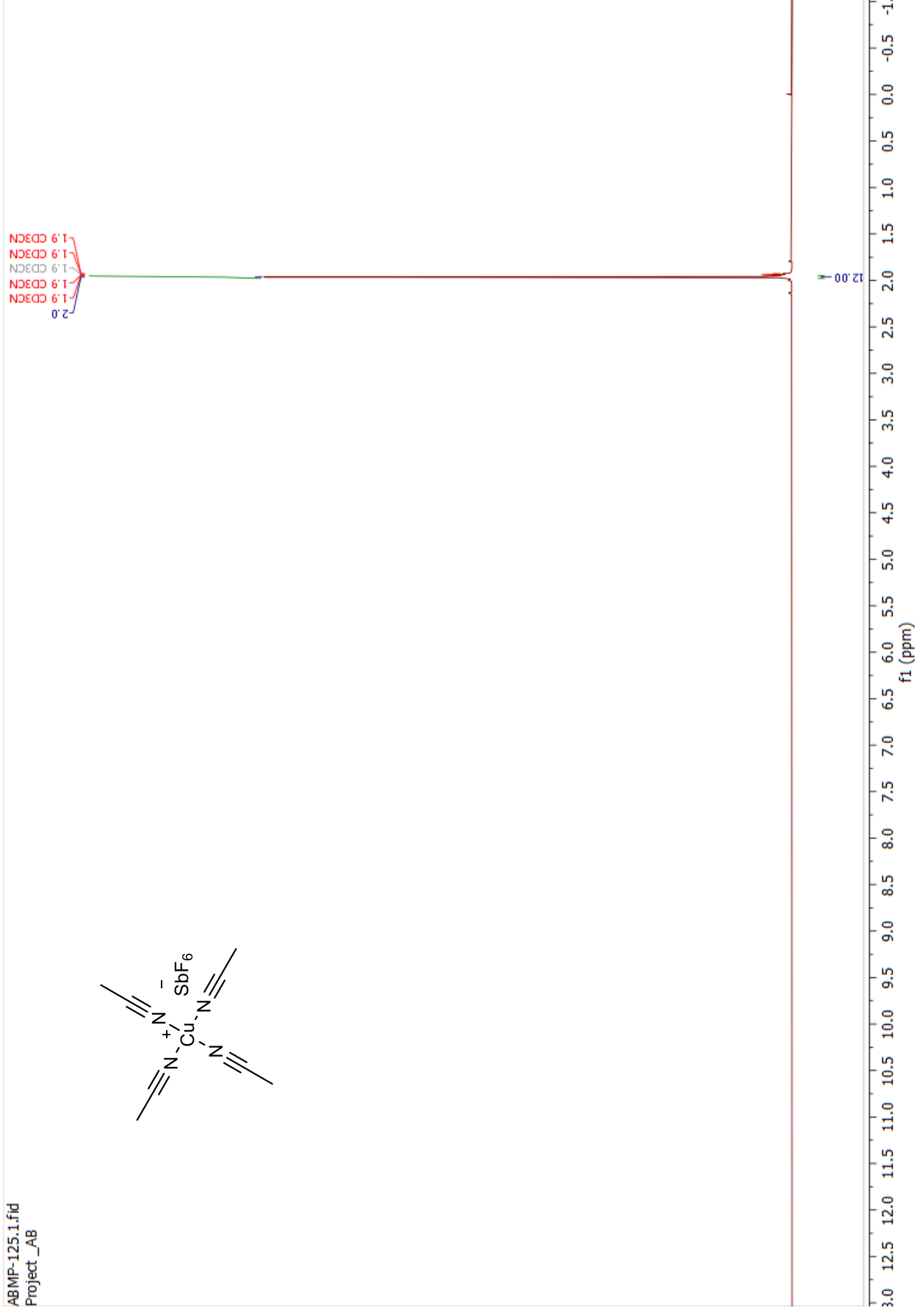
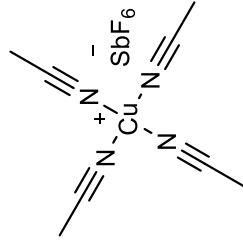


Spectrum S46. ^{13}C NMR of compound **2t** in CDCl_3



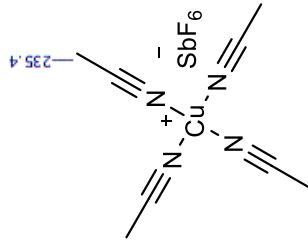
Spectrum S47. ¹H NMR of compound 2ab in CD₃CN

ABMP-125.1.fid
Project_AB

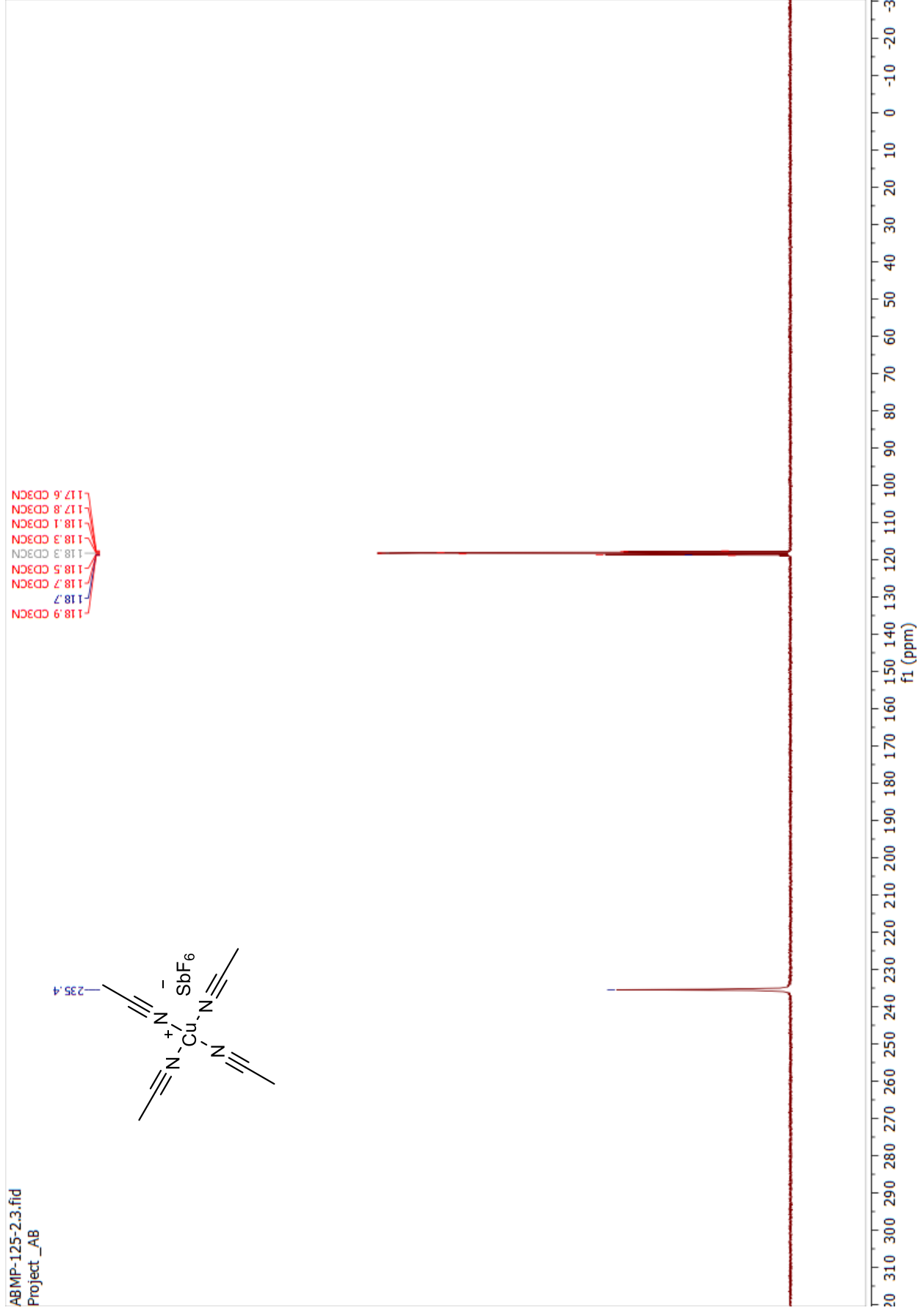


Spectrum S48. ^{13}C NMR of compound **2ab** in CD_3CN

ABMP-125-2.3.fid
Project_AB

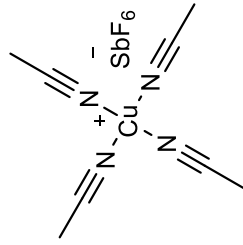


118.9 CD₃CN
118.7
118.7 CD₃CN
118.5 CD₃CN
118.3 CD₃CN
118.3 CD₃CN
118.1 CD₃CN
117.8 CD₃CN
117.6 CD₃CN

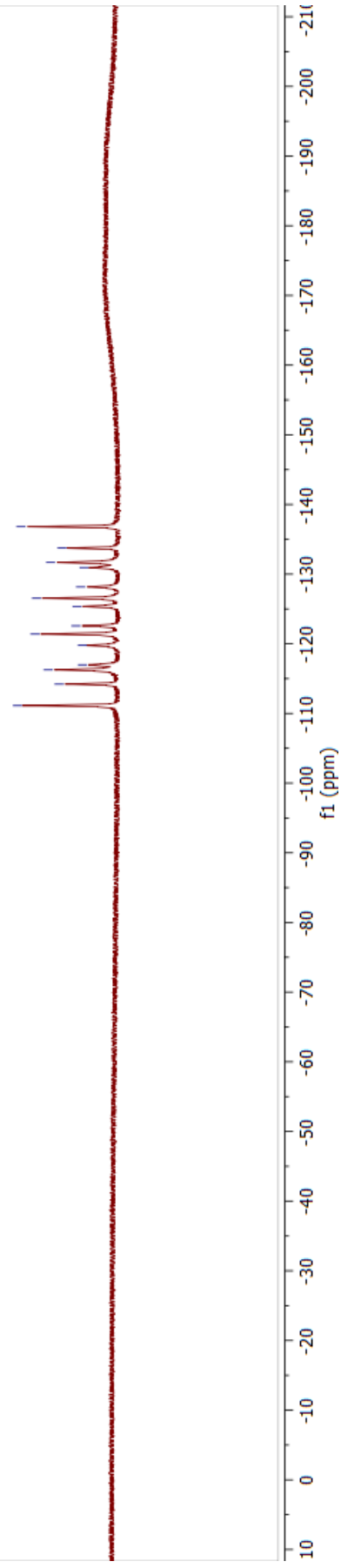


Spectrum S49. ^{19}F NMR of compound **2ab** in CD_3CN

ABMP-125.4.fid
Project_AB

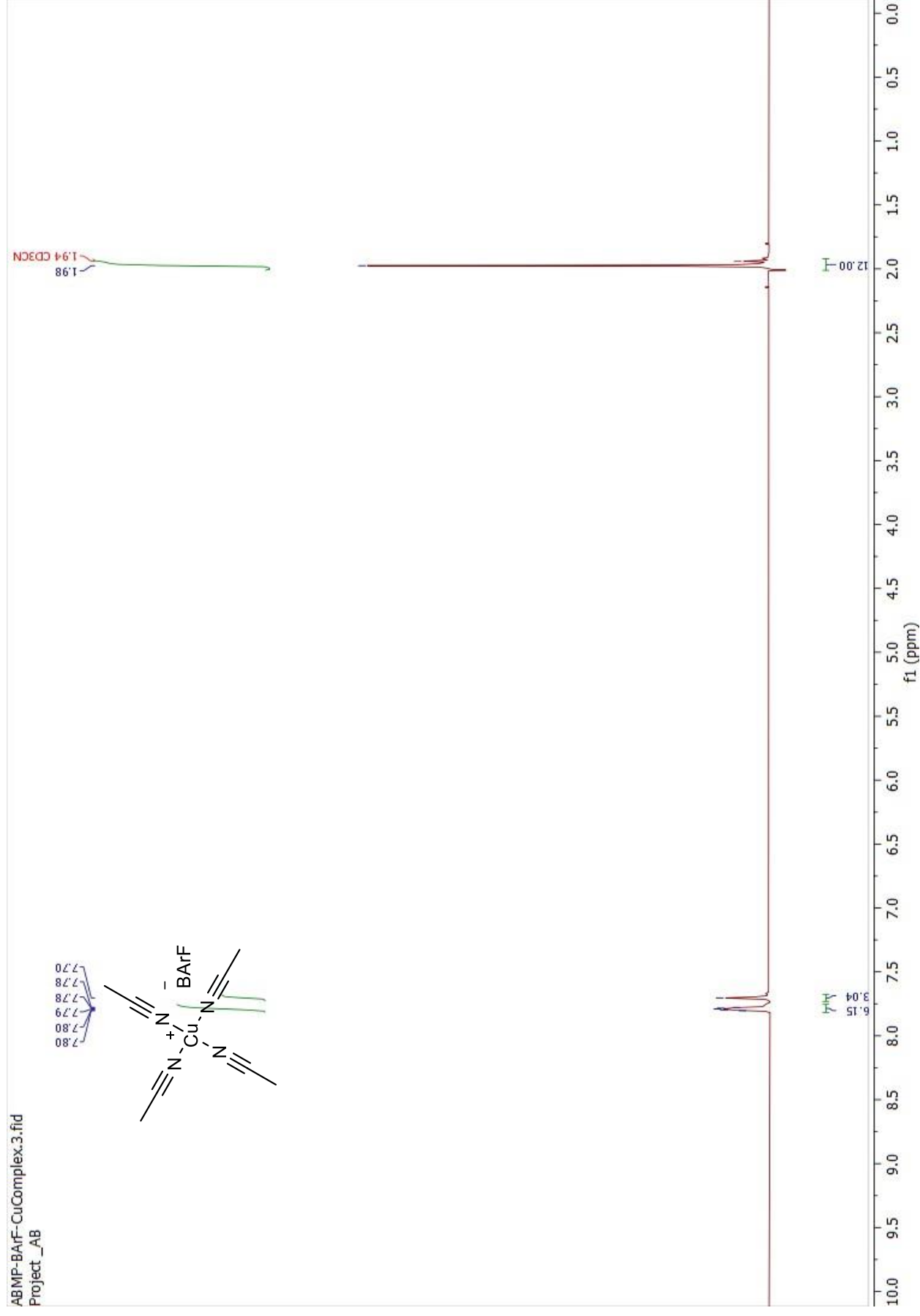


111.1
114.2
116.3
117.0
119.8
121.4
122.6
125.4
126.5
128.2
131.0
131.7
133.7
136.8



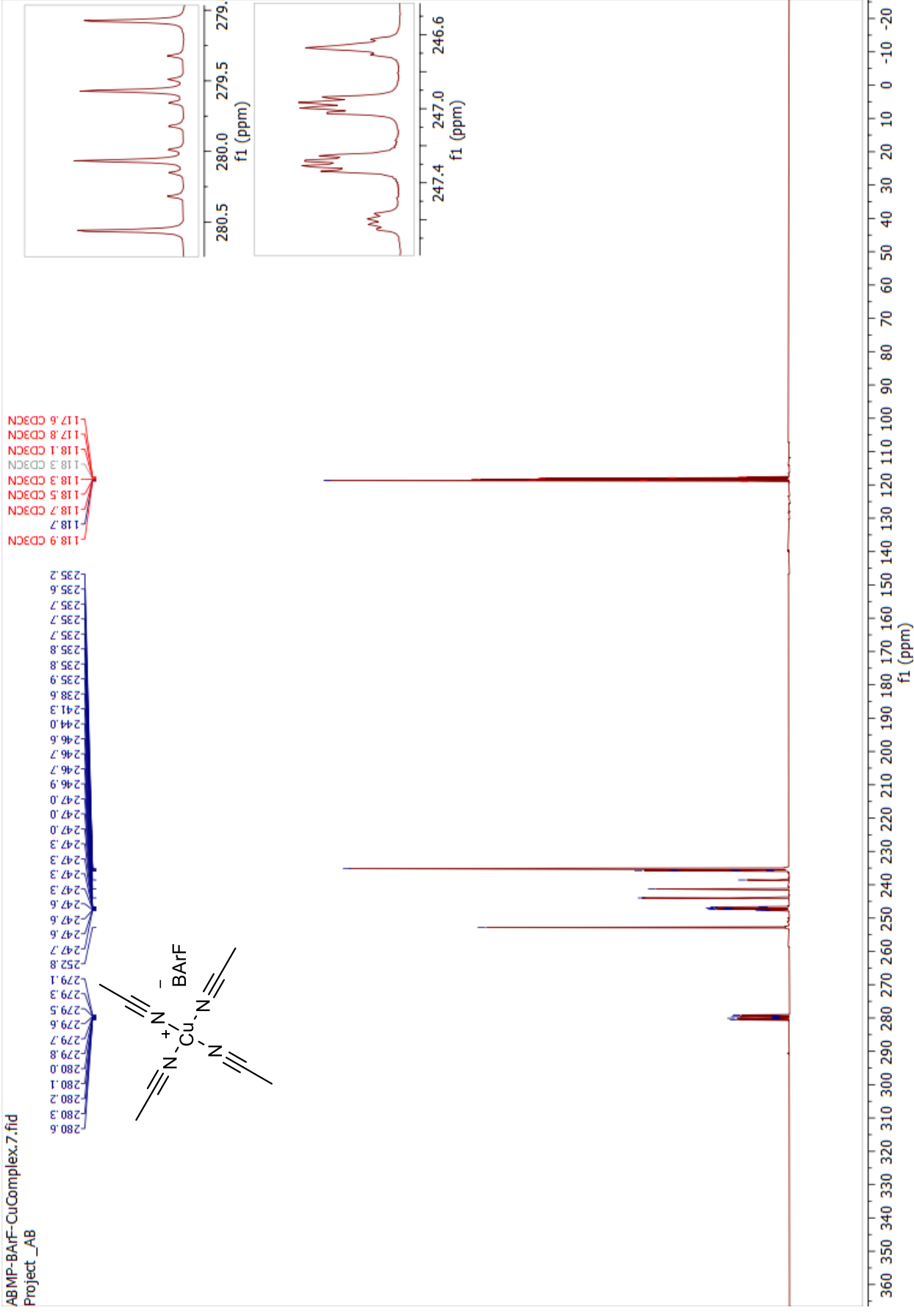
Spectrum S50. ^1H NMR of compound **2ac** in CD_3CN

ABMP-BArF-CuComplex.3.fid
Project_AB



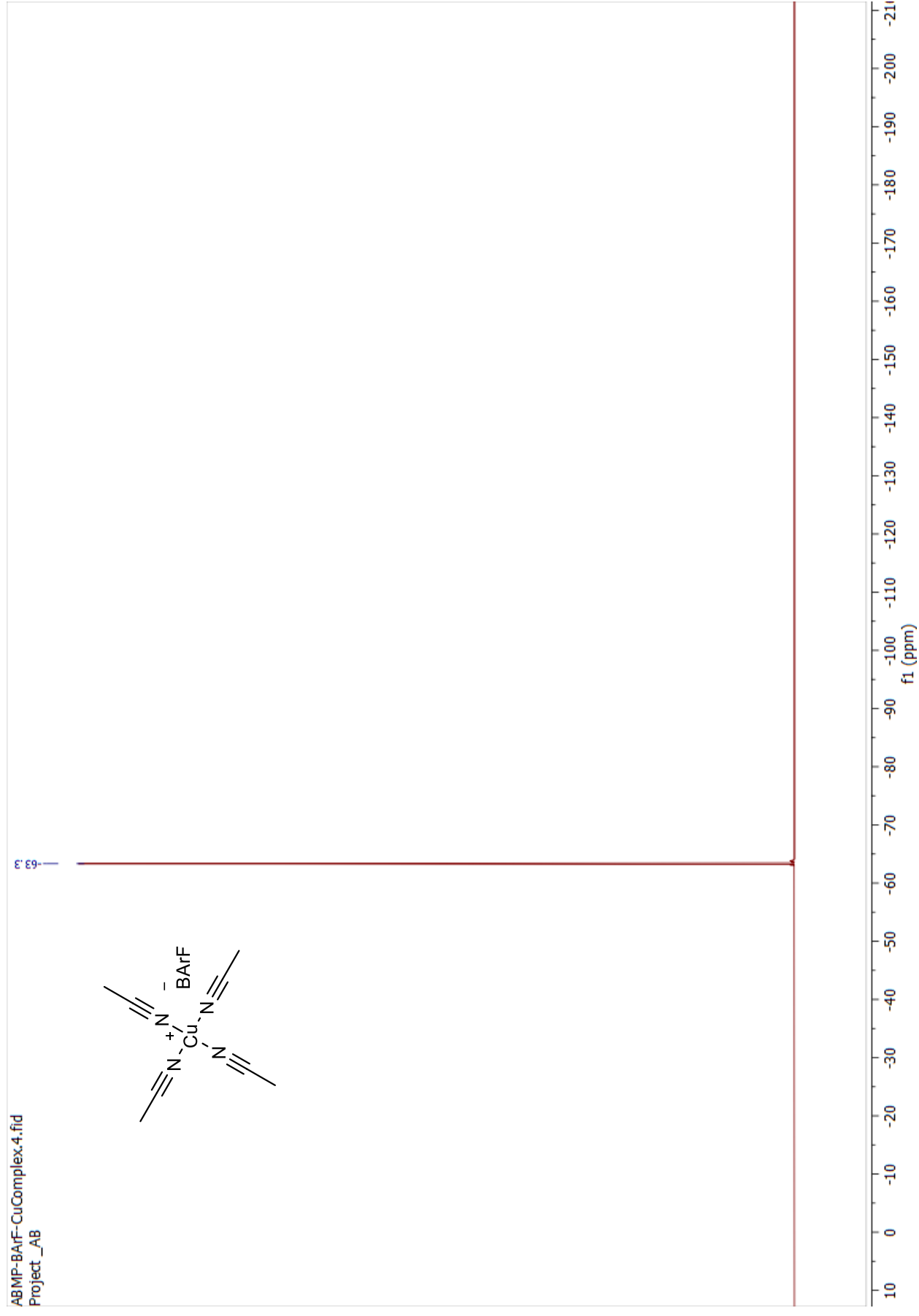
Spectrum S51. ¹³C NMR of compound 2ac in CD₃CN

ABMP-BArF-CuComplex.7.fid
Project_AB



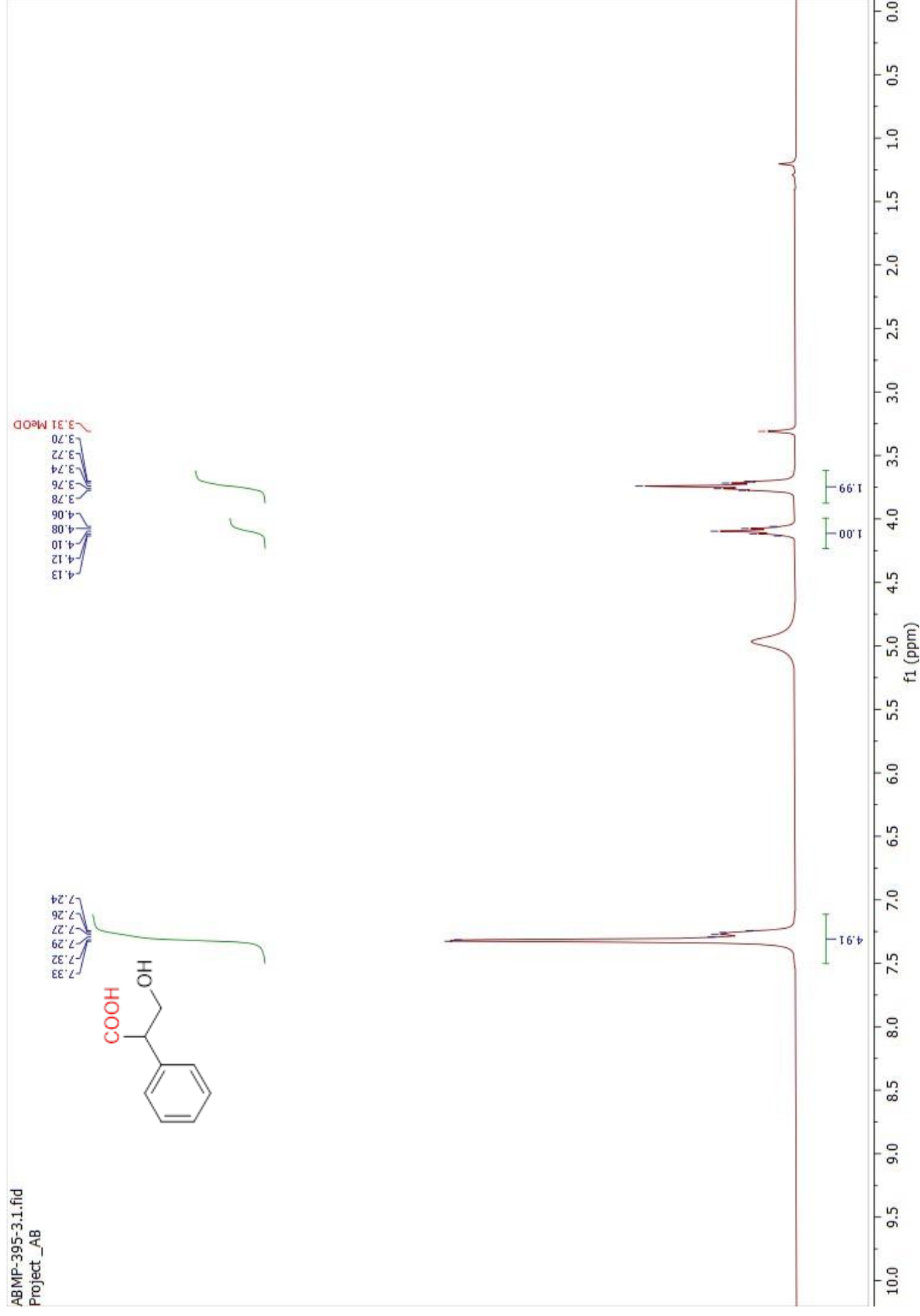
Spectrum S52. ^{19}F NMR of compound **2ac** in CD_3CN

ABMP-BArF-CuComplex.4.fid
Project_AB



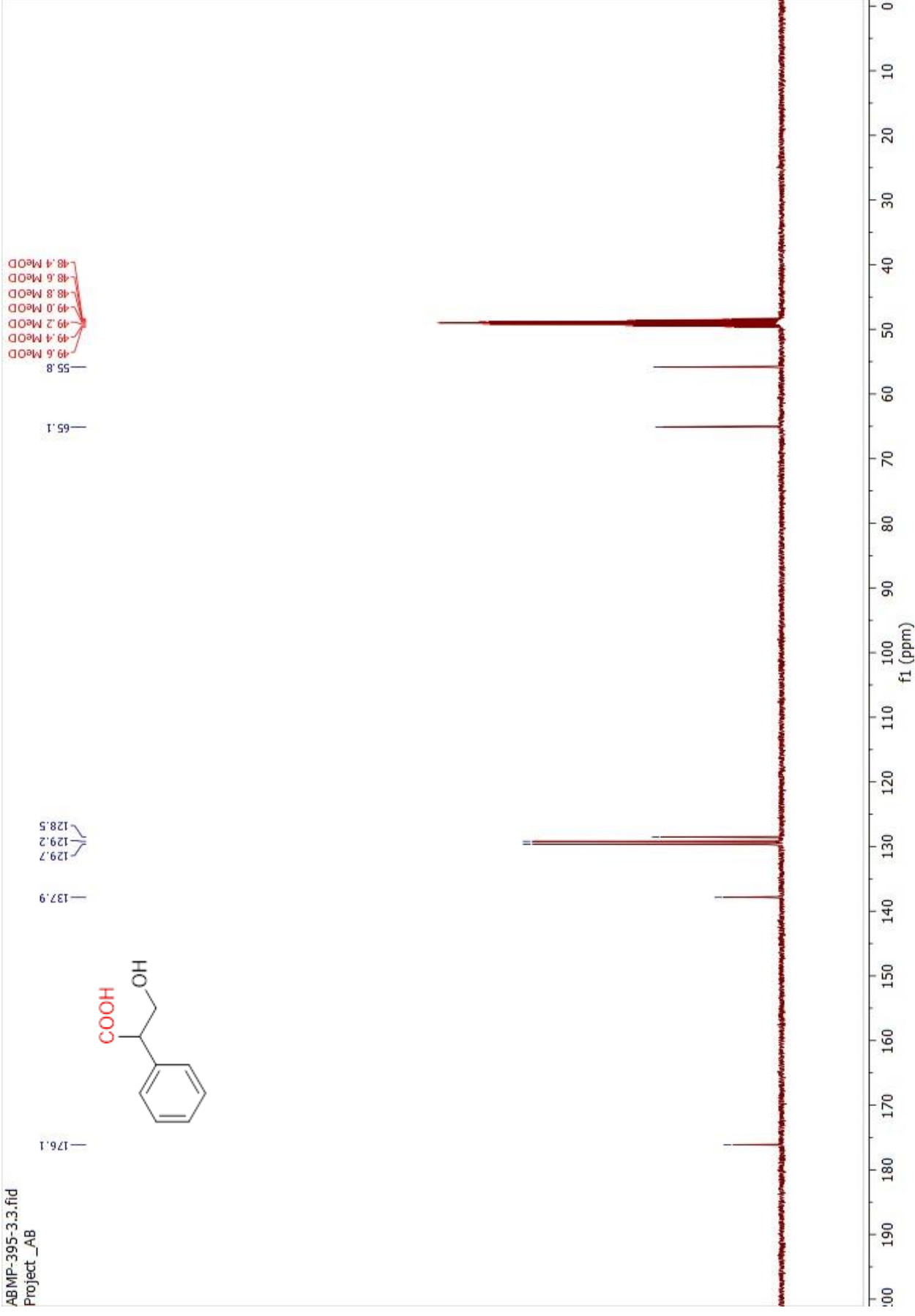
Spectrum S53. ¹H NMR of compound 3j in CD₃Cl

ABMP-395-3.1.fid
Project_AB



Spectrum S54. ¹³C NMR of compound **3j** in CD₃Cl

ABMP-395-3.3.fid
Project_AB



Chromatogram S21. a) Compound **3j**, b) commercially available (*R*)-tropic acid and c) the corresponding racemate

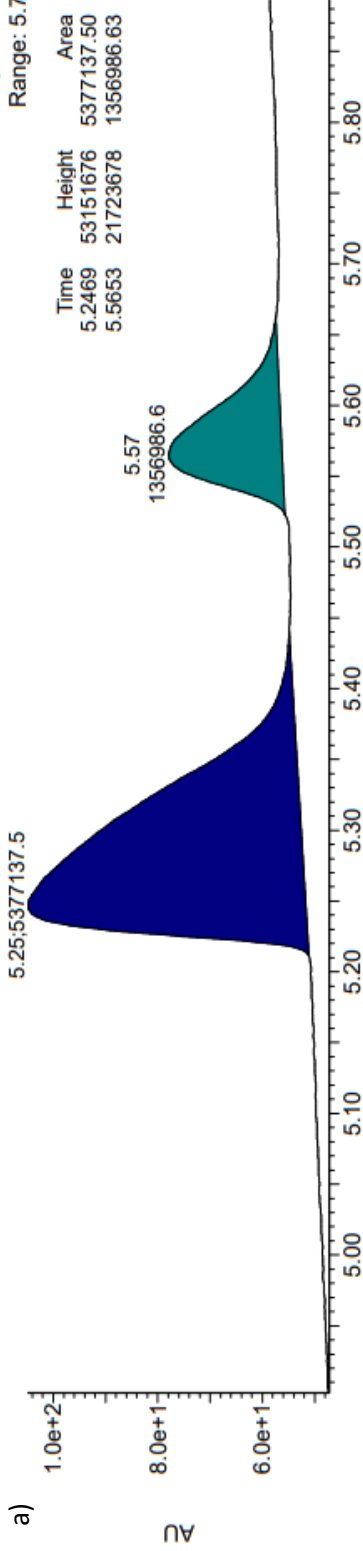
Amy1_iPrOH 0.5% TFA Chiral Separation

09-May-2023
13:53:02

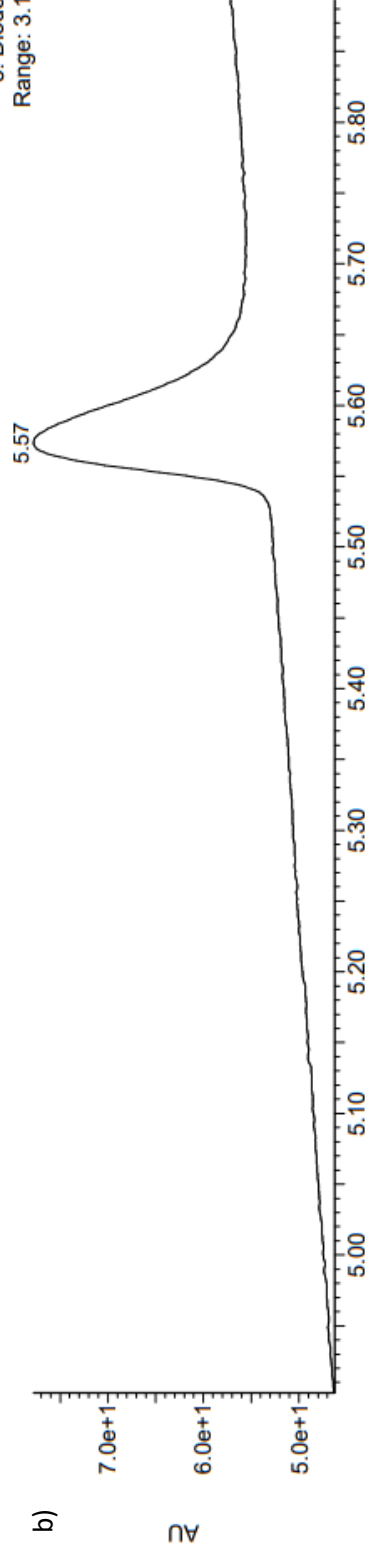
UPC2

Time	Height	Area	Area%
5.2469	53151676	5377137.50	79.85
5.5653	21723678	1356986.63	20.15

3: Diode Array
Range: 5.741e+1



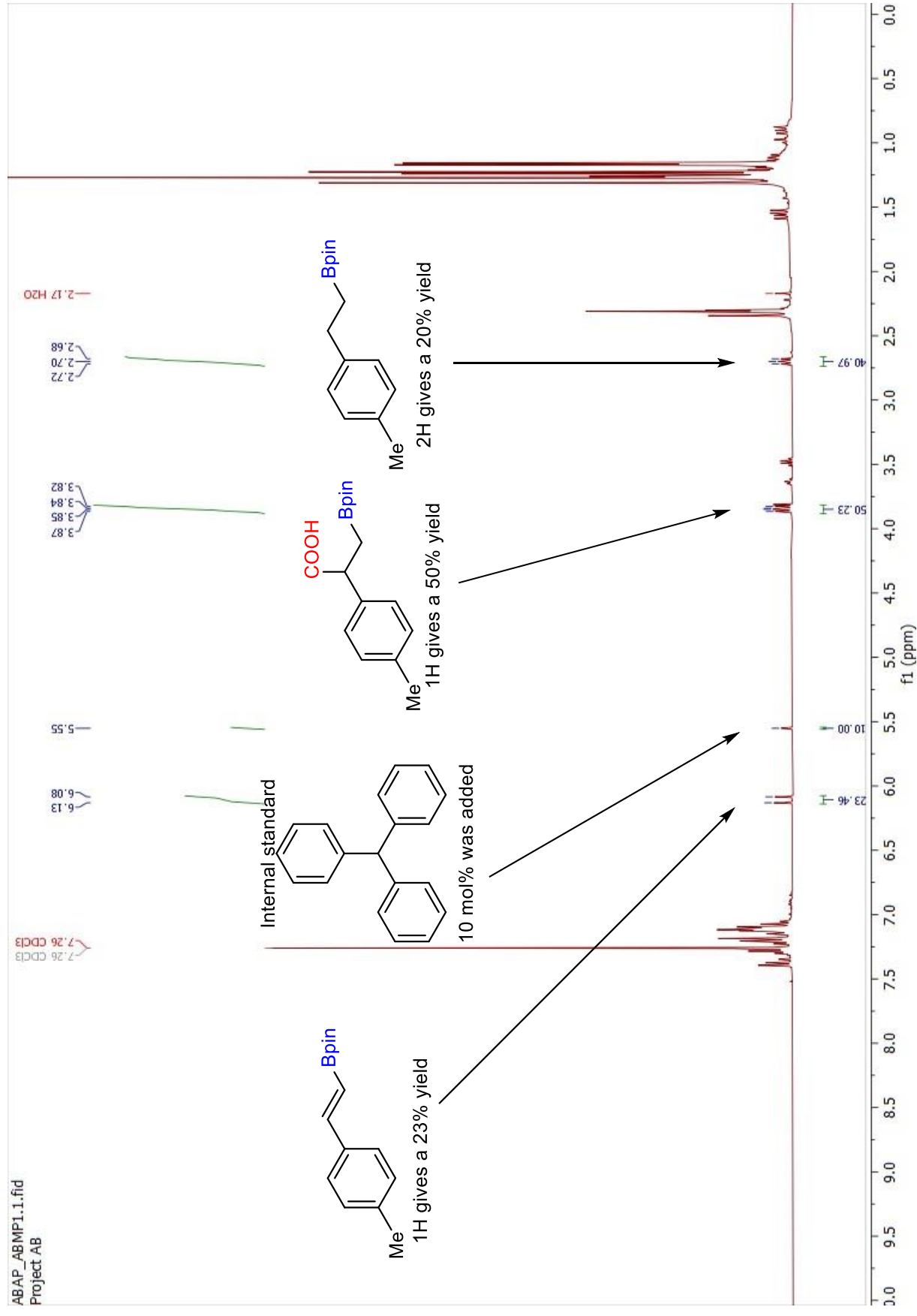
3: Diode Array
Range: 3.142e+1



3: Diode Array
Range: 3.795e+1



Spectrum S55. ^1H NMR of the crude reaction mixture from the borocarboxylation under the optimal conditions (Table S8, entry 3) for compound **3a** in CD_3Cl with mesitylene (10%) as internal standard.



4 References

- [1] T. W. Butcher, E. J. McClain, T. G. Hamilton, T. M. Perrone, K. M. Kroner, G. C. Donohoe, N. G. Akhmedov, J. L. Petersen, B. V. Popp, *Org. Lett.* **2016**, *18*, 6428-6431.
- [2] T. M. Perrone, A. S. Gregory, S. W. Knowlden, N. R. Ziemer, R. N. Alsulami, J. L. Petersen, B. V. Popp, *ChemCatChem* **2019**, *11*, 5814-5820.
- [3] Y. Zhang, W. Sun, C. Freund, A. M. Santos, E. Herdtweck, J. Mink, F. E. Kühn, *Inorg. Chim. Acta* **2006**, *359*, 4723-4729.
- [4] M. J. Frisch, G. W. Trucks, H. B. Schlegel, G. E. Scuseria, M. A. Robb, J. R. Cheeseman, G. Scalmani, V. Barone, G. A. Petersson, H. Nakatsuji, X. Li, M. Caricato, A. V. Marenich, J. Bloino, B. G. Janesko, R. Gomperts, B. Mennucci, H. P. Hratchian, J. V. Ortiz, A. F. Izmaylov, J. L. Sonnenberg, Williams, F. Ding, F. Lipparini, F. Egidi, J. Goings, B. Peng, A. Petrone, T. Henderson, D. Ranasinghe, V. G. Zakrzewski, J. Gao, N. Rega, G. Zheng, W. Liang, M. Hada, M. Ehara, K. Toyota, R. Fukuda, J. Hasegawa, M. Ishida, T. Nakajima, Y. Honda, O. Kitao, H. Nakai, T. Vreven, K. Throssell, J. A. Montgomery Jr., J. E. Peralta, F. Ogliaro, M. J. Bearpark, J. J. Heyd, E. N. Brothers, K. N. Kudin, V. N. Staroverov, T. A. Keith, R. Kobayashi, J. Normand, K. Raghavachari, A. P. Rendell, J. C. Burant, S. S. Iyengar, J. Tomasi, M. Cossi, J. M. Millam, M. Klene, C. Adamo, R. Cammi, J. W. Ochterski, R. L. Martin, K. Morokuma, O. Farkas, J. B. Foresman, D. J. Fox, in *Gaussian 16 Rev. B.01*, Wallingford, CT, **2016**.
- [5] J. P. Perdew, K. Burke, M. Ernzerhof, *Phys. Rev. Lett.* **1996**, *77*, 3865-3868.
- [6] a) G. A. Petersson, M. A. Al-Laham, *J. Chem. Phys.* **1991**, *94*, 6081-6090; b) G. A. Petersson, A. Bennett, T. G. Tensfeldt, M. A. Al-Laham, W. A. Shirley, J. Mantzaris, *J. Chem. Phys.* **1988**, *89*, 2193-2218; c) T. Clark, J. Chandrasekhar, G. W. Spitznagel, P. V. R. Schleyer, *J. Comput. Chem.* **1983**, *4*, 294-301.
- [7] S. Grimme, S. Ehrlich, L. Goerigk, *J. Comput. Chem.* **2011**, *32*, 1456-1465.
- [8] J. Tomasi, B. Mennucci, R. Cammi, *Chem. Rev.* **2005**, *105*, 2999-3094.
- [9] a) F. Jensen, *J. Chem. Phys.* **2013**, *138*, 014107; b) F. Jensen, *J. Chem. Phys.* **2001**, *115*, 9113-9125; c) F. Jensen, *J. Chem. Phys.* **2002**, *116*, 7372-7379; d) F. Jensen, *J. Phys. Chem. A* **2007**, *111*, 11198-11204; e) F. Jensen, T. Helgaker, *J. Chem. Phys.* **2004**, *121*, 3463-3470.
- [10] Q. Peng, F. Duarte, R. S. Paton, *Chem. Soc. Rev.* **2016**, *45*, 6093-6107.
- [11] a) K. Takahashi, T. Ishiyama, N. Miyaoura, *J. Organomet. Chem.* **2001**, *625*, 47-53; b) C. Pubill-Ulldemolins, A. Bonet, C. Bo, H. Gulyás, E. Fernández, *Chem. Eur. J.* **2012**, *18*, 1121-1126.

